

Catastrophe Theory, Symmetry Breaking and the pseudo Jahn-Teller Effect

Steven M Maley

Department of Chemistry

Lakehead University

Thunder Bay, Ontario, Canada

A dissertation submitted in partial fulfillment of the requirements for the degree of Doctor  
of Philosophy in Chemistry and Materials Science

© Steven M Maley, 2018

## ABSTRACT

This research focuses on the structural symmetry breaking observed in hypovalent silicon containing compounds. The structural symmetry breaking was studied from the perspective of the pseudo Jahn-Teller effect (pJTE). A density functional theory (DFT) based approach to assessing the pJTE parameters was developed to provide a computationally cost-effective alternative to the post Hartree-Fock procedures typically employed. Additionally, elementary catastrophe theory models were applied to gain a deeper insight into cases where the description of electronic structure by multiple quantum chemical methods are incongruous with one another.

The symmetry breaking of hypovalent silicon containing compounds was studied by examining Si-analogs of a series of a planar cyanocarbons: tetracyanoethylene (TCNE), tetracyanoquinodimethane (TCNQ), tetracyanodiphenylquinodimethane (TCNDQ) and tetracyanopyrenoquinodimethane (TCNP). Si-substitution generally resulted in structural symmetry breaking of both the neutral and anionic forms which enhanced their electron affinities. Moreover, Si-substitution was found to enhance the singlet and triplet diradical character of the  $\pi$ -conjugated systems.

The choice of density functional was found to have an impact on whether or not the pJTE was observed. This was studied in further detail by evaluating the effect of exact exchange on the description of the adiabatic potential energy surfaces (APESs) of disilene and 2Si TCNQ using the cusp catastrophe model. Functionals containing high amounts of exact exchange were found not to display the symmetry breaking effect.

The elliptic umbilic catastrophe was also applied to the study of the electronic structure of isothiirane. Furthermore, commonly used post analysis tools, the Quantum

Theory of Atoms in Molecules and Natural Resonance Theory, were critically assessed. The results of this study resolved an open question in the literature regarding the description of the electronic structure of isothiirane.

The pJTE parameters were evaluated using DFT by employing a model Hamiltonian that accounts for vibronic interactions. This model Hamiltonian was fit to cross-sections of the APES along the distorting mode. Best practices regarding the evaluation of pJTE parameters were also described. The procedure outlined in this thesis is applicable to the study of any pJTE problem where post Hartree-Fock methods are not feasible.

# TABLE OF CONTENTS

ABSTRACT.....	i
TABLE OF CONTENTS.....	iii
ACKNOWLEDGEMENTS.....	vi
LIST OF TABLES.....	viii
LIST OF FIGURES.....	x
STATEMENT OF CONTRIBUTIONS.....	xiii
CHAPTER ONE.....	1
Introduction.....	1
1.1 – References.....	8
CHAPTER TWO.....	10
Background Theory	
2.1 – Introduction.....	11
2.2 – The Schrödinger Equation.....	11
2.3 – The Born-Oppenheimer Approximation.....	12
2.4 – Potential Energy Surfaces.....	12
2.5 – Spin Orbitals and Slater Determinants.....	13
2.6 – The Variational Principle.....	14
2.7 – The Hartree-Fock Method.....	14
2.8 – Density Functional Theory.....	16
2.8.1 – Local Spin Density Approximation.....	20
2.8.2 – GGA Functionals.....	21
2.8.3 – meta-GGA (mGGA) Functionals.....	23
2.8.4 – Hybrid Functionals.....	25
2.8.5 – Range-Separated Hybrid Functionals.....	27
2.9 – Strengths and Weaknesses of the Hartree-Fock Method and Density Functional Theory.....	28
2.10 – Basis Sets.....	29
2.11 – Time-Dependent Density Functional Theory (TD-DFT).....	31
2.12 – Post Analysis Methods.....	32
2.12.1 – The Quantum Theory of Atoms in Molecules.....	32
2.12.2 – Natural Bond Orbital / Natural Resonance Theory Analysis.....	35
2.13 – Elementary Catastrophe Theory.....	38
2.13.1 – The Cusp Catastrophe.....	39
2.13.2 – The Elliptic Umbilic Catastrophe.....	40
2.14 – References.....	42
CHAPTER THREE.....	45
Isothiirane: <i>A Molecular Structure Dilemma Resolved</i>	
3.1 – Introduction.....	46
3.2 – Methodology.....	48
3.3 – Results and Discussion.....	48
3.3.1 – The Structure of Isothiirane.....	48
3.3.2 – Characteristics of the Electron Density.....	50

3.3.3 – The Elliptic Umbilic .....	54
3.3.4 – Natural Resonance Theory.....	56
3.3.5 – Substituent Effects.....	58
3.3.5.1 – Structural Changes .....	58
3.3.5.2 – Characteristics of the Electron Density Topology .....	61
3.3.5.3 – A Robust NRT Description .....	63
3.3.5.4 – NMR Shielding Tensor .....	64
3.3.5.5 – A Congruent Description of Electronic Structure.....	65
3.4 – Conclusions .....	67
3.5 – References .....	69
<b>CHAPTER FOUR.....</b>	<b>72</b>
<b>The Electron Affinities of TCNE and TCNQ: The Effect of Silicon Substitution</b>	
4.1 – Introduction .....	74
4.2 – Methodology .....	76
4.3 – Results and Discussion .....	77
4.3.1 – Part 1 – Assessment of Parent Compounds .....	77
4.3.1.1 – The Structure of TCNE and [TCNE] <sup>-</sup> .....	77
4.3.1.2 – The Structure of TCNQ and [TCNQ] <sup>-</sup> .....	79
4.3.1.3 – The Adiabatic Electron Affinities of TCNE and TCNQ .....	85
4.3.1.4 – Assessments of Relevant Silicon Containing Compounds .....	89
4.3.2 – Part 2 – Effect of Si-Substitution.....	90
4.3.2.1 – The Potential Energy Surfaces of the Si-Analogs of TCNE and TCNQ.....	90
4.3.2.2 – The Effect of Si-Substitution on Diradical Character .....	94
4.3.2.3 – The Effect of Si-Substitution on Electron Affinity .....	97
4.4 – Conclusions .....	101
4.5 – References .....	102
<b>CHAPTER FIVE .....</b>	<b>106</b>
<b>How the Amount of Hartree-Fock Exchange Affects the Observation of the Pseudo Jahn-Teller Effect</b>	
5.1 – Introduction .....	108
5.2 – Methodology .....	111
5.3 – Results and Discussion .....	112
5.3.1 – The Stationary Points of Disilene and 2Si TCNQ .....	112
5.3.2 – Insights from Catastrophe Theory .....	117
5.3.3 – The Impact of Exact Exchange on the pJTE .....	121
5.4 – Conclusions .....	124
5.5 – References .....	126
<b>CHAPTER SIX .....</b>	<b>130</b>
<b>Computational Insights into the Electronic Structure of TCNDQ and TCNP: The Effect of Si-Substitution</b>	
6.1 – Introduction .....	132
6.2 – Methodology .....	134
6.3 – Results and Discussion .....	135
6.3.1 – Assessments of Parent Compounds .....	135
6.3.2 – The Adiabatic Electron Affinities of TCNDQ and TCNP .....	139
6.3.3 – The Potential Energy Surfaces of the Si-Analogs.....	141
6.3.3.1 – 1Si TCNDQ and [1Si TCNDQ] <sup>-</sup> .....	141
6.3.3.2 – 2Si TCNDQ and [2Si TCNDQ] <sup>-</sup> .....	142
6.3.3.3 – 1Si TCNP and [1Si TCNP] <sup>-</sup> .....	147
6.3.3.4 – 2Si TCNP and [2Si TCNP] <sup>-</sup> .....	147

6.3.4 – The Effect of Si-Substitution on Diradical Character .....	154
6.3.5 – The Effect of Si-Substitution on the AEA's .....	157
6.4 – Conclusions .....	161
6.5 – References .....	163
<b>Chapter SEVEN.....</b>	<b>166</b>
<b>Using DFT to calculate Pseudo Jahn-Teller Effect Parameters: Understanding the Origin of Symmetry Breaking in Hypovalent Silicon</b>	
7.1 – Introduction .....	168
7.2 – Methodology .....	171
7.3 – Results and Discussion .....	172
7.3.1 – General Features of the Potential Energy Surfaces .....	172
7.3.1.1 – Disilene .....	172
7.3.1.2 – 2Si TCNE .....	173
7.3.1.3 – 2Si TCNQ .....	173
7.3.1.4 – 2Si TCNDQ .....	174
7.3.1.5 – 2Si TCNP .....	176
7.3.2 – Types of Pseudo Jahn-Teller Effect Responsible for Symmetry Breaking .....	178
7.3.3 – Evaluating the Pseudo Jahn-Teller Effect Parameters .....	179
7.3.4 – Suggested Best Practices in Assessing pJTE Problems .....	181
7.3.5 – Changes in the Topology of the Electron Density .....	184
7.4 – Conclusions .....	187
7.5 – References .....	189
<b>Chapter EIGHT .....</b>	<b>192</b>
<b>Summary, Future Work and Conclusions</b>	
8.1 – Overview .....	193
8.2 – Isothiirane: a molecular structure dilemma resolved .....	193
8.3 – The Electron Affinities of TCNE and TCNQ: <i>The Effect of Si-Substitution</i> .....	194
8.4 – How the Amount of Hartree-Fock Exchange Affects the Observation of the pseudo Jahn-Teller Effect .....	194
8.5 – Computational Insights in to the Electronic Structure of TCNDQ and TCNP: The Effect of Si-Substitution .....	196
8.6 – What is the Controlling Factor in the Symmetry Breaking of Hypovalent Silicon? ..	197
8.7 – Topics for Future Study .....	197
8.8 – General Conclusions .....	200
8.9 – References .....	202
<b>Appendices .....</b>	<b>204</b>
APPENDIX A .....	205
Supplementary Information for Chapter Three	
APPENDIX B .....	228
Supplemental Information for Chapter Four	
APPENDIX C .....	285
Supplementary Information for Chapter Five	
APPENDIX D .....	301
Supplementary Information for Chapter Six	
APPENDIX E .....	364
Supplemental Information for Chapter Seven	

## **ACKNOWLEDGEMENTS**

This work would not have been possible without the guidance of my supervisor Dr. Robert Mawhinney. Thank you for your support and encouragement over my years as a student. I am grateful for the opportunity to pursue my PhD in your lab. I must also express my gratitude to my committee members Dr. Craig MacKinnon and Dr. Hubert de Guise. Thank you for reviewing this thesis and providing your input, and for everything you have taught me over the years.

To my parents, Mike and Sandra. I could not have undertaken such a task without your love and support. You have taught me the value of working hard for the things I want in life. I also have to thank you for purchasing our first computer when I was small, I have been obsessed with them ever since. To the rest of my family, thank you for your support over the years.

*“There are only patterns, patterns on top of patterns,  
patterns that affect other patterns. Patterns hidden  
by patterns. Patterns within patterns. What we call  
chaos is just patterns we haven’t recognized. What  
we call random is just patterns we cannot decipher.  
What we can’t understand we call nonsense.  
What we can’t read we call gibberish.”*

**Chuck Palahniuk**

## LIST OF TABLES

<b>Table 2.1:</b> Rank and signature of the four stable critical points predicted by QTAIM ....	33
<b>Table 2.2:</b> The seven elementary catastrophes described by Thom .....	39
<b>Table 3.1:</b> Heavy atom geometrical parameters obtained at the CCSD(T)/aug-cc-pvNZ (N= D, T, Q) level and their CBS extrapolated values. Bond lengths (R) and perimeter (P) in Å, angles (A) in degrees. ....	49
<b>Table 3.2:</b> NRT Expansion weights (%) and natural bond orders for isothiirane obtained using all combinations of input. Calculated at B3PW91/BS2 level (Data for all other model chemistries available in Appendix A Table A.5) .....	57
<b>Table 3.3:</b> Interatomic distances (Å) and angles(°) for SC <sub>2</sub> C <sub>1</sub> backbone of substituted series.....	60
<b>Table 3.4:</b> Ellipticities of the RCPs, and S-C BCPs for the rings listed in Figure 6. Calculated at the B3PW91 / BS 2 level. ....	63
<b>Table 3.5:</b> Linear correlation coefficients for bond order-bond length relationships based on bond orders from NRT analysis of substituted series. <sup>1</sup> B3PW91/BS2 .....	64
<b>Table 4.1:</b> Mean percent deviation from average experimental structure of neutral TCNE. MIN, MAX, MIN x  and Standard Deviation (S.D) provided for each functional and basis set.....	80
<b>Table 4.2:</b> Mean percent deviation from average experimental structure of the [TCNE] <sup>-</sup> . MIN, MAX, MIN x  and standard deviation (S.D) provided for each functional and basis set. <S <sup>2</sup> > values: 0.75 – 0.76 (SI-Table 4).....	81
<b>Table 4.3:</b> Average percent deviation from experimental structure of neutral TCNQ. MIN, MAX, MIN x  and standard deviation (S.D) provided for each functional and basis set. <sup>1</sup> .....	83
<b>Table 4.4:</b> Average percent deviation from average experimental structure of [TCNQ] <sup>-</sup> . MIN, MAX, MIN x  and standard deviation (S.D) provided for each functional and basis set. <S <sup>2</sup> > values: 0.75 – 0.79 (SI-Table 8) <sup>1</sup> .....	84
<b>Table 4.5:</b> 2Si TCNQ representative relative energies (kcal/mol) of the three lowest neutral surface manifolds. <sup>1</sup> .....	97
<b>Table 5.1:</b> Disilene b <sub>2g</sub> mode wavenumber (cm <sup>-1</sup> ) calculated using HF and DFT/BS1-BS5. ....	113
<b>Table 5.2:</b> 2Si TCNQ b <sub>2g</sub> and b <sub>3u</sub> mode wavenumbers (cm <sup>-1</sup> ) calculated using HF and DFT/BS1-BS5.....	115
<b>Table 5.3:</b> Parameters for ( <sup>1</sup> A <sub>G</sub> + <sup>1</sup> B <sub>2G</sub> ) ⊗ b <sub>2g</sub> pJTE in disilene. K <sub>0</sub> , K <sub>v</sub> and K (eV/Å <sup>2</sup> ), Δ (eV), F (eV/Å) .....	122
<b>Table 5.4:</b> Parameters for ( <sup>1</sup> A <sub>G</sub> + <sup>1</sup> B <sub>2G</sub> ) ⊗ b <sub>2g</sub> pJTE in 2Si TCNQ. K <sub>0</sub> , K <sub>v</sub> and K (eV/Å <sup>2</sup> ), Δ (eV), F (eV/Å) .....	123
<b>Table 5.5:</b> Parameters for ( <sup>1</sup> A <sub>G</sub> + <sup>1</sup> B <sub>3U</sub> ) ⊗ b <sub>3u</sub> pJTE in 2Si TCNQ. K <sub>0</sub> , K <sub>v</sub> and K (eV/Å <sup>2</sup> ), Δ (eV), F (eV/Å) .....	123
<b>Table 6.1:</b> AEA's (eV) calculated for TCNDQ using chosen methods. Min, max, range and standard deviation (S.D.) of values for each functional and basis set also provided. ....	139
<b>Table 6.2:</b> AEA's (eV) calculated for TCNP using chosen methods. Min, max, range and standard deviation (S.D.) of values for each functional and basis set also provided. ....	140

<b>Table 6.3:</b> Experimental and calculated EA's (eV) for cyanocarbons .....	140
<b>Table 6.4:</b> B3LYP/BS4 predicted bond lengths (Å) for TCNDQ and [TCNDQ] <sup>-</sup> . Italicized values for Si-containing moiety. See Figure 6.1 for bond length labels. ....	144
<b>Table 6.5:</b> B3LYP/BS4 predicted bond lengths (Å) for TCNP and [TCNP] <sup>-</sup> . Italicized values for Si-containing moiety. See Figure 6.2 for bond length labels. ....	149
<b>Table 6.6:</b> Bond length alternation (BLA) values for TCNQ, TCNDQ and TCNP calculated using B3LYP/BS4. In the 1Si versions Ring A is attached to Si. Values for anion in italics. See Figures 6.1 and 6.2 for identity of ring. ....	153
<b>Table 6.7:</b> Delocalization index alternation (DIA) values for cyanocarbon series. B3LYP/BS4. In the 1Si versions Ring A is attached to Si. Values for anion in italics. See Figures 6.1 and 6.2 for identity of ring. ....	154
<b>Table 6.8:</b> AEA's (eV) of Si-substituted cyanocarbons .....	161
<b>Table 7.1:</b> pJTE parameters assessed using B3LYP/Def2TZVPP for planar 0 and 2Si molecules. ....	180

## LIST OF FIGURES

<b>Figure 2.1:</b> Representative adiabatic potential energy surface for a generic S <sub>N</sub> 2 reaction .....	13
<b>Figure 2.2:</b> Control parameter plane for cusp catastrophe .....	40
<b>Figure 2.3:</b> (A) Control parameter plane for elliptic umbilic catastrophe (B) view of hyperbolic region with number of critical points labelled. ....	41
<b>Figure 3.1:</b> Plot of SC <sub>2</sub> C <sub>1</sub> angle (degrees) and perimeter of the ring formed by the heavy atoms (Angstroms). Circles – RCP detected. X's – No RCP detected. Star – CCSD(T)/CBSExtrap value. Inset box: HF/BS1 (off scale). Above: Example molecular graphs for cyclic and acyclic structure. ....	51
<b>Figure 3.2:</b> Example MG's for a ring structure (centre), topologically unstable ring structures, and acyclic structures (outermost). Geometric parameters presented for B3PW91/BS2 and PBE0/BS1. Hydrogen atoms removed for clarity. ....	53
<b>Figure 3.3:</b> (A) Representation of the structure diagram of the S-C2-C1 system showing the possible cyclic (Region I) and acyclic structures (Regions II–IV). The hypocycloid shape defines the catastrophe set. Inset box: Catastrophe set described by Equation 1 and definition of axes. (B) Prediction of the unfolding the elliptic umbilic for motion along y-axis with v=0. ....	54
<b>Figure 3.4:</b> Possible resonance structures for (HS)(CH <sub>2</sub> )(CH) .....	56
<b>Figure 3.5:</b> Backbone structure obtained for each substituent at the B3PW91 / BS2 level of theory. Substituents listed in order of attachment to S and C <sub>1</sub> . Triangles – acyclic carbene MG. Circles – cyclic zwitterion MG. Squares – Ethenylthiol type MG. ....	62
<b>Figure 3.6:</b> $\sigma_{xx}$ component of the <sup>13</sup> C <sub>1</sub> NMR chemical shielding tensor as a function of the ring perimeter. Solid line: linear regression of all data points (R <sup>2</sup> :0.691). Dashed line: linear regression of dataset with outliers removed (R <sup>2</sup> : 0.916). Green markers – RCP detected. Red markers – No RCP Detected. Yellow marker – Unsubstituted value. Orange markers – outliers. B3PW91/BS 2. ....	65
<b>Figure 3.7:</b> A comparison between three key descriptors (Magnitude of C <sub>1</sub> VSCC, value of the $\sigma_{xx}$ component of the <sup>13</sup> C NMR chemical shielding tensor, and %RS-C obtained from the NRT RS-B,C analysis) of the electronic structure. Green markers – RCP detected. Red markers – No RCP Detected. Yellow marker – Unsubstituted value. Calculated at the B3PW91/BS 2 level. ....	66
<b>Figure 4.1:</b> Average experimental bond lengths and standard deviations (S.D.) (Å) for neutral and <i>reduced</i> TCNE. Black – carbon and blue – nitrogen. ....	78
<b>Figure 4.2:</b> Average experimental bond lengths (Å) for neutral and <i>reduced</i> TCNQ. Black – carbon, blue – nitrogen and white – hydrogen. ....	82
<b>Figure 4.3:</b> Deviation of chosen methods (dot w/ line for visualization purposes) from experimental AEA of TCNE. Experimental uncertainty visualized as two solid black lines. Deviation of Post-HF methods from references 4 and 5 visualized as dashed lines. ....	87
<b>Figure 4.4:</b> Deviation of chosen methods (dot w/ line for visualization purposes) from experimental AEA of TCNQ. Experimental uncertainty visualized as dashed lines. Deviation of Post-HF methods from references 6 and 7 visualized as solid lines. ....	88

<b>Figure 4.5:</b> Stationary points of the potential energy surfaces of TCNE analogs. $\nu$ indicates an imaginary frequency. Black – Carbon, Grey – Silicon, Blue – Nitrogen. ....	92
<b>Figure 4.6:</b> Stationary points of the potential energy surfaces of TCNQ analogs. $\nu$ indicates an imaginary frequency. Black – Carbon, Grey – Silicon, Blue – Nitrogen, White – Hydrogen .....	93
<b>Figure 4.7:</b> The adiabatic electron affinities (eV) using BS1 for (A) TCNE series and (B) TCNQ series. See Appendix B Figure B3 for BS6 values.....	100
<b>Figure 5.1:</b> Value of (A) $b_{2g}$ wavenumber (disilene) and (B) $b_{2g}$ and $b_{3u}$ wavenumbers (2Si TCNQ) for the BLYP and M06 family of functionals. ....	116
<b>Figure 5.2:</b> Visualization of the control parameter plane for the cusp catastrophe including the definitions of stabilization energy ( $\Delta E$ ), and vibrational modes $\omega$ (symmetry breaking) and $\omega'$ (symmetry restoring). ....	117
<b>Figure 5.4:</b> APES scans as %HFX is increased for (A) disilene (B) 2Si TCNQ $b_{2g}$ mode and (C) 2Si TCNQ $b_{3u}$ mode. Value of distorting mode, stabilization, pyramidalization and value of planarity restoring mode for each increment. ....	120
<b>Figure 5.5:</b> Change in a control parameter with increased exact exchange in BXLYPtest for (A) Disilene and (B) 2Si TCNQ $b_{2g}$ (blue) and $b_{3u}$ (red) vibrational modes. ....	121
<b>Figure 6.1:</b> <i>Top:</i> Structure of TCNDQ with bond length ranges and ring identity for neutral and <i>reduced</i> forms. <i>Bottom</i> – Stationary points on the potential energy surfaces of TCNDQ and [TCNDQ] $^-$ . $\nu$ indicates an imaginary frequency .....	136
<b>Figure 6.2:</b> <i>Top:</i> Structure of TCNP with bond length ranges and ring identity for neutral and <i>reduced</i> forms. <i>Bottom</i> – Stationary points on the potential energy surfaces of TCNP and [TCNP] $^-$ . $\nu$ indicates an imaginary frequency.....	138
<b>Figure 6.3:</b> Stationary points on the potential energy surfaces of 1Si TCNDQ and [1Si TCNDQ] $^-$ . $\nu$ indicates an imaginary frequency.....	143
<b>Figure 6.4:</b> Stationary points on the potential energy surfaces of 2Si TCNDQ and [2Si TCNDQ] $^-$ . On the anion surfaces the $C_1$ minima looks like the $C_2$ minima but with unequal pyramidalization of the Si-nuclei. $\nu$ indicates an imaginary frequency. ....	143
<b>Figure 6.5:</b> Stationary points on the potential energy surfaces of 1Si TCNP and [1Si TCNP] $^-$ . $\nu$ indicates an imaginary frequency.....	148
<b>Figure 6.6:</b> Stationary points on the potential energy surfaces of 2Si TCNP and [2Si TCNP] $^-$ . $\nu$ indicates an imaginary frequency.....	148
<b>Figure 6.7:</b> Adiabatic singlet-triplet gap ( $\Delta E_{S-T}$ in eV) calculated using BS4 for (A) TCNDQ and (B) TCNP series. ....	157
<b>Figure 6.8:</b> Adiabatic electron affinities (eV) calculated using BS4 for (A) TCNDQ series and (B) TCNP series. BS2 values available in Appendix D Figure D4A and D4B. ....	159
<b>Figure 7.1:</b> Representative PES for disilene with numbering of bond lengths. $\Delta\theta$ is the amount of Si-pyramidalization. Energy values are relative to the surface minimum. $\nu$ indicates an imaginary frequency.....	172
<b>Figure 7.2:</b> Representative PES for 2Si TCNE with numbering of bond lengths. $\Delta\theta$ is the amount of Si-pyramidalization. Energy values are relative to the surface minimum. $\nu$ indicates an imaginary frequency. ....	173

<b>Figure 7.3:</b> Representative PES for 2Si TCNQ with numbering of bond lengths (hydrogens omitted). $\Delta\theta$ is the amount of Si-pyramidalization. Energy values are relative to the surface minimum. ‡ on the M06 surface a $C_S$ (pseudo- $C_{2h}$ ) structure (not shown) is the lowest energy structure; the $C_{2h}$ structure is 0.004 kcal/mol higher in energy relative to the $C_S$ structure. $\nu$ indicates an imaginary frequency.	174
<b>Figure 7.4:</b> Representative PES for 2Si TCNDQ with numbering of bond lengths. M06 <sup>29</sup> data omitted. Inset box: CAM-B3LYP minimum. Energy values are relative to the surface minima. $\Delta\theta$ is the amount of Si-pyramidalization and $\Delta\phi$ is the amount of torsion around $R_1$ . $\nu$ indicates an imaginary frequency.....	175
<b>Figure 7.5:</b> Representative PES for 2Si TCNP with numbering of bond lengths. ‡ on the M06 surface the $C_{2v}$ structure is the lowest energy structure ( $\Delta E = 0.02$ kcal/mol). Inset box: CAM-B3LYP minimum. Energy values are relative to the surface minimum. $\Delta\theta$ is the amount of Si-pyramidalization. $\nu$ indicates an imaginary frequency. ....	177
<b>Figure 7.6:</b> The amount of pyramidalization as a function of the amount of stabilization (kcal/mol) at the global surface minima for the 2Si molecules. All functionals <sup>29a,b</sup> /Def2TZVPP. The outliers correspond to results obtained using CAM-B3LYP.....	178
<b>Figure 7.7:</b> Example scan along of APES of disilene. The red points correspond to geometries with energies greater than the planar geometry that are removed from the polynomial fit. ....	183
<b>Figure 7.8:</b> Changes in $\nabla^2\rho$ isosurface due to the ( $^1A_G + ^1B_{2G}$ ) $\otimes$ $b_{2g}$ pJTE in disilene <sup>38</sup> Only half the molecular graph is visualized for ease of viewing. Green – BCP, Pink – NNA. B3LYP/Def2TZVPP. ....	185
<b>Figure 7.9:</b> The amount of pyramidalization at Si-nuclei at the APES global minima as a function of the change in atomic energy calculated using QTAIM. Calculated using all functionals <sup>28</sup> in combination with Def2TZVPP.....	186
<b>Figure 7.10:</b> The change in atomic electron population (# electrons) as a function of the pyramidalization of the SI-nuclei at the APES global minima. Calculated using all functionals <sup>28</sup> in combination with Def2TZVPP.....	187

## STATEMENT OF CONTRIBUTIONS

The content of Chapter Three and Appendix A was previously published as:

S.M. Maley and R.C. Mawhinney *Isothiirane: a molecular structure dilemma resolved*, Journal of Computational Chemistry, 2018 doi: 10.1002/jcc.25758

### Author Contributions

The project was proposed by Robert Mawhinney

SMM performed the DFT calculations, and QTAIM and NBO/NRT analysis

Qadir Timerghazin performed the CCSD(T) calculations

SMM analyzed the data, prepared the figures and wrote the paper with input from Robert Mawhinney

The content of Chapter Four and Appendix B was previously published as:

S.M. Maley, C. Esau and R.C. Mawhinney *The electron affinities of TCNE and TCNQ: the effect of silicon substitution*, Structural Chemistry, 2018 doi: 10.1007/s11224-018-1186-1

### Author Contributions

The project was proposed by Robert Mawhinney

Crystal Esau performed the preliminary calculations

SMM performed the remaining DFT calculations

SMM analyzed the data, prepared the figures and wrote the paper with input from Robert Mawhinney

A paper based on the content of Chapter Five and Appendix C is in preparation at the time of writing

### Author Contributions

The project was proposed by SMM and Robert Mawhinney as a follow up to the results presented in Chapter 4.

SMM performed the DFT calculations

SMM developed the cusp catastrophe analysis model and vibronic Hamiltonian analysis with input from Robert Mawhinney

Qadir Timerghazin performed the CCSD(T) calculations

SMM analyzed the data, prepared the figures and wrote the paper with input from Robert Mawhinney

The content of Chapter Six and Appendix D was previously published as:

S.M. Maley and R.C. Mawhinney *Computational Insights into the Electronic Structure of TCNDQ and TCNP: the effect of silicon substitution*, Structural Chemistry, 2018 doi: 10.1008/s11224-018-1265-3

### **Author Contributions**

The project was proposed by SMM and Robert Mawhinney

SMM performed the DFT calculations

SMM analyzed the data, prepared the figures and wrote the paper with input from Robert Mawhinney

A paper based on the content of Chapter Seven and Appendix E is in preparation at the time of writing

### **Author Contributions**

The project was proposed by SMM and Robert Mawhinney

SMM performed the DFT calculations and QTAIM analysis

SMM analyzed the data, prepared the figures and wrote the paper with input from Robert Mawhinney

# **CHAPTER ONE**

## **Introduction**

This thesis focuses on two topics. The first is the observed symmetry breaking in hypovalent silicon-containing compounds. The second topic focuses on incongruous descriptions of electronic structure provided by modern quantum chemical methods. The two are linked through catastrophe theory.<sup>1</sup>

In contrast to molecules that contain a carbon-carbon double bond, which are typically planar, molecules containing silicon-silicon double bonds often take on *trans*-bent geometries.<sup>2</sup> Such geometries are commonly described as being pyramidalized at the Si-nuclei.

The first experimentally stable Si-Si double bond was reported by West *et. al.* who synthesized tetramesityldisilene via pyrolysis of 2,2-bis(mesityl)hexamethyltrisilane in a solution of hydrocarbons at -100°C.<sup>3</sup> X-ray diffraction of obtained crystals revealed a slightly pyramidalized geometry at the Si-nuclei.<sup>4</sup> Since this initial synthesis, over 70 disilenes have been experimentally prepared, exhibiting various amounts of pyramidalization.<sup>2</sup>

Despite this library of disilenes, the parent disilene ( $\text{Si}_2\text{H}_4$ ) has been experimentally elusive. Numerous computational studies have been reported in the literature however.<sup>5,6,7</sup> Early calculations with small (double-zeta) basis sets at the Hartree-Fock and configuration interaction levels of theory indicated a pyramidalized geometry was preferred.<sup>5,6</sup> These findings are consistent with recent fourth order Møller-Plesset perturbation theory and coupled cluster calculations performed with larger (triple-zeta) basis sets.<sup>7</sup>

There are also examples in the literature of molecules containing two hypovalent silicon centres not directly bonded, or multiple (more than two) hypovalent Si centres

bonded to one another. The Si-substituted *p*-quinodimethane prepared by Sekiguchi *et al.*<sup>8</sup> is an example of the former and silicene,<sup>9</sup> the silicon analog of graphene, is an example of the latter. Both of them are reported to have non-planar geometries.

A number of models have been put forth to rationalize the pyramidalized geometries of hypovalent Si containing molecules. The reluctance of the 3s orbitals of silicon to hybridize compared to the 2s orbitals of carbon is a commonly cited explanation of the pyramidalized geometry.<sup>4</sup> Another commonly discussed model is the one proposed by Carter, Goddard, Malrieu and Trinquier (CGMT model).<sup>10,11</sup>

The CGMT model relates the difference in energy between the singlet and triplet states in fragments formed from homolytic cleavage of the double bond with the observed geometry of the molecule. The model predicts a planar double bond if the triplet state is lower than the singlet state, as in the case of ethylene. Conversely, a more stable singlet state predicts a pyramidalized geometry, as in disilene.

A more general approach to understanding such molecular geometries is provided by the *pseudo* Jahn-Teller (pJT) effect. Whereas the Jahn-Teller effect describes symmetry breaking in electronically degenerate molecules, the pJT effect describes symmetry breaking in non-electronically degenerate molecules.<sup>12,13</sup>

The pJT effect describes the vibronic interaction between a ground state ( $\Psi_0$ ) and an electronically excited state ( $\Psi_n$ ) due to certain normal modes (Q). This interaction is quantified by the linear vibronic coupling constant (F).

$$F = \left\langle \Psi_0 \left| \left( \frac{\partial H}{\partial Q} \right)_0 \right| \Psi_n \right\rangle \quad (1.1)$$

Two electronic states can only interact if the product of their irreducible representations yields the irreducible representation of the vibrational mode. If the symmetry requirement is not satisfied the states cannot interact.<sup>12,13</sup>

The vibronic interaction reduces the primary curvature ( $K_0$ ) of the ground state potential energy surface

$$K_0 = \left\langle \Psi_0 \left| \left( \frac{\partial^2 H}{\partial Q^2} \right)_0 \right| \Psi_0 \right\rangle \quad (1.2)$$

according to

$$K = K_0 - K_V \quad (1.3)$$

where  $K_V$  is the vibronic contribution to the ground state curvature given by

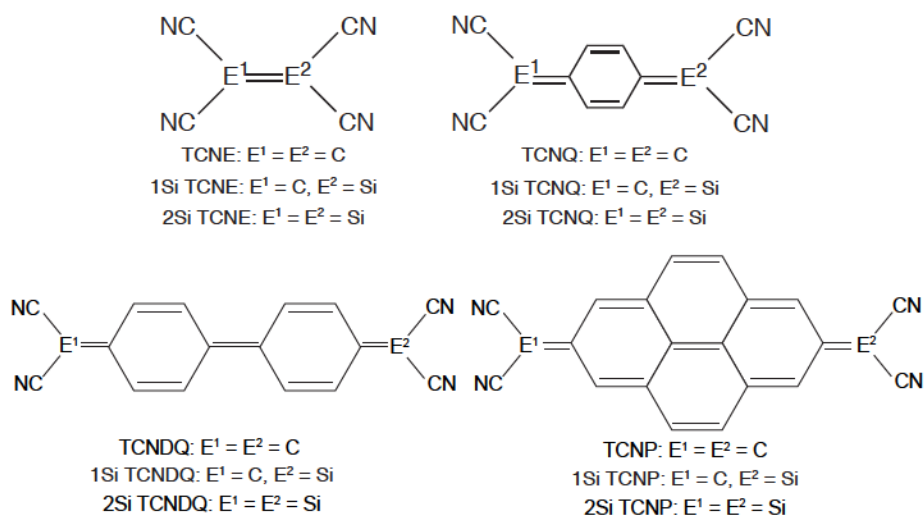
$$K_V = \frac{F^2}{\Delta} \quad (1.4)$$

where  $\Delta$  is the energy difference between the ground state and relevant excited state. If  $K_V > K_0$  at the high symmetry geometry, then symmetry breaking occurs. By evaluating the pJT parameters in (1.4) at the high symmetry geometry it is possible to rationalize the low symmetry geometry in terms of the vibronic interaction.

The direct calculation of the parameters relevant to the pJT effect is difficult. A common approach to obtain the pJT parameters is to fit a cross section of the potential energy surface along the normal mode to a model Hamiltonian that accounts for the vibronic interaction. This is best performed using multi-reference ab initio methods, but they are intractable for most systems of interest.<sup>14-16</sup> Recently Soto *et. al.* have reported on the pJT effect responsible for the buckling distortion in  $A_6H_6$  ( $A = \text{Si, Ge, Sn}$ ) using density functional theory (DFT) to generate the potential energy surface cross section

and excitation energy.<sup>17-19</sup> There are no other examples presented in the literature of this approach.

In the assessment of symmetry breaking effects in hypovalent silicon a series of planar cyanocarbons was chosen: Tetracyanoethylene (TCNE), tetracyanoquinodimethane (TCNQ), tetracyanodiphenoquinodimethane (TCNDQ) and tetracyanopyrenoquinodimethane (TCNP) (**Scheme 1.1**). These are convenient choices as they are planar with  $D_{2h}$  symmetry. Substitution of TCNE with Si-nuclei provides a model to study the symmetry breaking effects in two directly bonded Si-nuclei while the others provide opportunities to study symmetry breaking in cases where the Si-nuclei are not directly bonded, but are connected by an extended  $\pi$ -system.



**Scheme 1.1**

These cyanocarbons are also of interest due to their use in organic electronic applications. TCNE and TCNQ are both well known for their ability to form stable anions, leading to their inclusion in charge-transfer complexes (TCNQ)<sup>20, 21</sup> and magnetic materials (TCNE).<sup>22</sup> TCNDQ and TCNP are less well studied due to experimental limitations.<sup>23,24,25</sup>

Isovalent substitution (e.g. changing carbon for silicon) is one method of tuning electronic structure. This is often done in an effort to enhance the material properties of a molecule or gain deeper insight into the electronic structure of the parent compound. While the strategy of isovalent substitution has been used in other applications it has not been explored in the cyanocarbons.

Quantum chemical calculations provide a vast amount of information about the electronic structure of a molecule. Beyond routine data (energy, bond lengths, vibrational frequencies, etc.), further valuable information can be extracted from the wavefunction (or density) obtained from a calculation using a variety of post analysis tools.

Because all information about a molecule is contained in the wavefunction (or density), it would be expected that the description of the electronic structure obtained from post analysis methods be consistent with one another. While often in agreement with one another, there are a number of cases where conflicting descriptions occur. One example is the electronic structure of isothiirane, which despite being the subject of multiple studies, has only an ambiguous description.<sup>26</sup>

Moreover, when performing calculations using density functional theory (DFT) there are many methods (exchange-correlation functionals) to choose from and a consistent agreement between methods is not always obtained. The inconsistent characterization of spin states<sup>27</sup> and stationary points<sup>28,29</sup> by different exchange-correlation functionals are just a few examples.

In this thesis these topics are explored. Beginning with chapter 2 the methods commonly used throughout this work are described. In chapter 3 the electronic structure of isothiirane is studied and commonly-used post analysis tools are critically assessed. A

consistent interpretation of electronic structure of isothirane based on a catastrophe theory model is presented. In chapter 4 the ability of DFT to reproduce the experimental structures and electron affinities of TCNE and TCNQ is studied. Also in chapter 4 the effect of Si-substitution on the potential energy surfaces of TCNE and TCNQ and their electron affinities is explored. Chapter 5 discusses stationary points that are ambiguously characterized by DFT and the effect of Hartree-Fock exchange on the observation of the pJT effect is explored using a second catastrophe theory model. Also in chapter 5 a DFT approach to assessing pJT parameters is discussed. In chapter 6 the electronic structure of TCNDQ and TCNP is assessed and the effect of Si-substitution is studied. The DFT approach to assessing pJT parameters described in chapter 5 is applied to the parent and 2Si versions of all cyanocarbons in an attempt to understand the controlling factor in the symmetry breaking of hypovalent silicon containing compounds in chapter 7. Chapter 8 provides a summary of the research performed and suggests topics for further study. All energies reported are electronic energies with no zero-point vibrational correction.

## **1.1 – References**

- (1) Thom, R. *Structural Stability and Morphogenesis: An Outline of a General Theory of Models*. W. A. Benjamin, Inc. Massachusetts, **1975**
- (2) Fischer, R. C. and Power, P. P. *Chem. Rev.*, **2010**, 110, 3877-3923
- (3) West, R.; Fink, M. J. and Michl, J. *Science*, **1981**, 214(4527), 1343-1344
- (4) Fink, M. J.; Michalczyk, M. J.; Haller, K. J.; West, R. and Michl, J. *Organometallics*, **1984**, 3, 793-800
- (5) Snyder, L. C. and Wasserman, Z. R. *J. Am. Chem. Soc.* **1979**, 101(18), 5222-5223
- (6) Poirier, R. A. and Goddard, J. D. *Chem. Phys. Lett.* **1981**, 80(1), 37-41
- (7) Nori-Shargh, D.; Mousavi, S. N. and Boggs, J. E. *J. Phys. Chem. A.* **2013**, 117, 1621-1631
- (8) Nozawa, T.; Nagata, M.; Ichinohe, M. and Sekiguchi, A. *J. Am. Chem. Soc.* **2011**, 133, 5773-5775
- (9) Houssa, M.; Dimoulas, A. and Molle A. *J. Phys.: Condens. Matter* **2015**, 27, 253002
- (10) Carter, E. A. and Goddard, W. A. *J. Phys. Chem.* **1986**, 90(6), 998-1001
- (11) Trinquier, G. and Malrieu J.-P. *J. Am. Chem. Soc.* **1987**, 109, 5303-5315
- (12) Bersuker, I.B. *The Jahn-Teller Effect*. Cambridge University Press, Cambridge, UK. **2005**
- (13) Bersuker, I.B. *Chem. Rev.*, **2013**, 113 (3), 1351–1390
- (14) Liu, Y.; Bersuker, I.B., and Boggs, J.E. *Chemical Physics*, **2013**, 417, 26-29
- (15) Kayi H.; Garcia-Fernandez, P.; Bersuker, I.B.; and Boggs, J.E. *J. Phys. Chem. A.* **2013**, 117, 8671-8679
- (16) Kayi, H.; Bersuker, I.B., and Boggs, J.E. *J. Mol. Str.* **2012**, 1023, 108-114
- (17) Soto, J.R.; Molina, B. and Castro, J.J. *Phys. Chem. Chem. Phys.* **2015**, 17, 7624-7628
- (18) Soto, J.R.; Molina, B. and Castro, J.J. *MRS Advances*, **2016**, 1(22), 1591-1596

- (19) Soto, J.R.; Molina, B. and Castro, J.J. *MRS Advances*, **2017**, 2(29), 1563-1569
- (20) Ferraris, J.; Cowan, D. O.; Walatka V. and Perlstein, J.H. *J. Am. Chem. Soc.* **1973**, 95(3), 948-949
- (21) Anderson, P.W.; Lee, P.A. and Saitoh, M. *Solid State Comm.* **1973**, 13, 505-598
- (22) Miller, J. S.; Calabrese, J. C.; Rommelmann, H.; Chittipeddi, S. R.; Zhang, J. H.; Reiff, W. M. and Epstein A. J. *J. Am. Chem. Soc.* **1987**, 109, 769-781
- (23) Addison, A. W.; Dalal, N. S.; Hoyano, Y.; Huizinga, S. and Weiler, L. *Can. J. Chem.* **1977**, 55, 4191-4199
- (24) Maxfield, M.; Bloch, A. N. and Cowan, D. O. *J. Org. Chem.* **1985**, 50(11), 1789-1796
- (25) Gerson, F.; Heckendorn, R.; Cowan, D. O.; Kini, A. M. and Maxfield, M. *J. Am. Chem. Soc.* **1983**, 105(24), 7017-7023
- (26) Henn, J.; Leusser, D and Stalke, D. *J. Comp. Chem.* **2007**, 28(14), 2317-2324
- (27) Berryman, V. E. J.; Boyd, R. J. and Johnson, E. R. *J. Chem. Theory Comput.* **2015**, 11, 3022-3028
- (28) Oyeyemi, V. B.; Keith, J. A.; Pavone, M. and Carter, E. A. *J. Phys. Chem. Lett.* **2012**, 3, 289-293
- (29) Mawhinney, R.C. and Goddard, J. D. *J. Mol. Struc.* **2003**, 629(1), 263-27

## **CHAPTER TWO**

### **Background Theory**

## 2.1 – Introduction

The methods used throughout this thesis are outlined in this chapter. The majority of the electronic structure calculations performed are done using density functional theory (DFT) in combination with Pople style basis sets. Not all functionals (TPSS/TPSSh, BP86, and HCTH/407) are detailed in this chapter. The reader is encouraged to consult the references provided if further details are desired.

## 2.2 – The Schrödinger Equation

This thesis focuses on the determination of the electronic structure of molecules by computational quantum chemical methods. A natural starting point is the time-independent Schrödinger equation.

$$\hat{H}\psi(r, R) = E\psi(r, R) \quad (2.1)$$

It is an eigenvalue-eigenfunction equation where  $\hat{H}$  is the Hamiltonian, a linear Hermitian operator,  $E$  is an eigenvalue corresponding to the total energy of the system, and  $\psi$  is an element of an orthonormal set of eigenfunctions of the Hamiltonian called the wavefunction that depends on the position of the electrons ( $r$ ) and nuclei ( $R$ ).

The Hamiltonian operator (in atomic units) can be separated into its individual components:

$$\hat{H} = -\sum_{i=1}^N \frac{\nabla^2}{2} - \sum_{A=1}^M \frac{\nabla_A^2}{2M_A} - \sum_{i=1}^N \sum_{A=1}^M \frac{Z_A}{r_{iA}} + \sum_{i=1}^N \sum_{j>1}^N \frac{1}{r_{ij}} + \sum_{A=1}^M \sum_{B>A}^M \frac{Z_A Z_B}{R_{AB}} \quad (2.2)$$

The first two terms are the kinetic energy of the electrons and nuclei respectively. The third describes the attractive potential between the electrons and the nuclei. The last two terms describe the interelectronic and internuclear repulsive potentials, respectively.<sup>1</sup>

### 2.3 – The Born-Oppenheimer Approximation

Exact solutions to (2.1) are only possible for simple systems (e.g., hydrogen-like atoms) and to study more complex systems (molecules) the Born-Oppenheimer approximation is invoked. In the Born-Oppenheimer approximation the nuclei are regarded frozen relative to the motion of the electrons due to the disparity in their masses. As a result, the kinetic energy of the nuclei is ignored and repulsion between nuclei is a constant. The Hamiltonian is therefore parametric within the Born-Oppenheimer approximation as given by

$$\hat{H}(R_{AB}) = \left[ -\sum_{i=1}^N \frac{\nabla_i^2}{2} - \sum_{i=1}^N \sum_{j>i}^N \frac{1}{r_{ij}} - \sum_{i=1}^N \sum_{A=1}^M \frac{Z_A}{r_{iA}} \right] + \sum_{A=1}^M \sum_{B>A}^M \frac{Z_A Z_B}{R_{AB}} \quad (2.3)$$

The term in brackets is the *electronic* Hamiltonian which describes a system of N-electrons in a field of M-point charges, and it returns the electronic energy in the electronic Schrödinger equation.

$$\hat{H}_{el} \psi_{el} = E_{el} \psi_{el} \quad (2.4)$$

When combined with the nuclear-nuclear potential it yields the total energy within the Born-Oppenheimer approximation.<sup>1</sup>

$$E_{Total} = E_{el} + \sum_{A=1}^M \sum_{B>A}^M \frac{Z_A Z_B}{R_{AB}} \quad (2.5)$$

### 2.4 – Potential Energy Surfaces

By calculating (2.5) for multiple configurations of the nuclei (molecular geometries) an adiabatic potential energy surface (APES) is mapped out. The relationship between energy and molecular geometry can be understood by characterizing the stationary points on the surface. Stationary points are characterized as minima, transition structures

(maximum in one direction, minimum in all other directions) or saddle points (a maximum in more than one direction and minima in all other directions).<sup>5</sup> This characterization allows for a variety of chemical phenomena to be understood in terms of APESs.

An example APES describing an S<sub>N</sub>2 reaction is shown in **Figure 2.1**. The reactants correspond to a (local) minimum on the surface. As the reactants approach one another the energy increases until a maximum on the surface corresponding to the transition structure is reached. After the nucleophilic substitution occurs the energy decreases until the minimum corresponding to the products is reached.

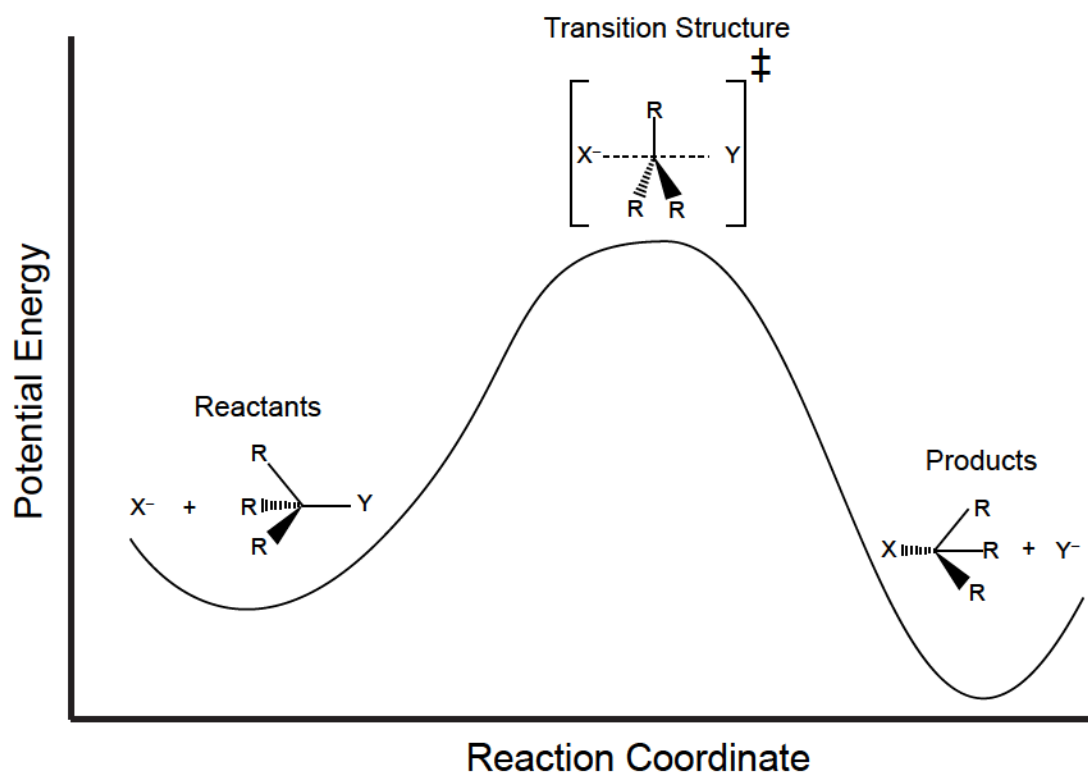


**Figure 2.1:** Representative adiabatic potential energy surface for a generic S<sub>N</sub>2 reaction

## 2.5 – Spin Orbitals and Slater Determinants

The wavefunction describes the spatial coordinates of the electrons. However, in order to fully describe an electron, it is necessary to specify its spatial coordinates and its spin. This is done by introducing two orthonormal spin functions denoted by  $\alpha$  (spin up,

$m_s = +1/2$ ) and  $\beta$  (spin down,  $m_s = -1/2$ ). Each electron is now described by the product of a spatial function  $\psi(r)$  and a spin function ( $\omega$ ) in a spin orbital  $\chi(x)$ .<sup>1</sup>

$$\chi(x) = \begin{cases} \psi(r)\alpha(\omega) \\ \psi(r)\beta(\omega) \end{cases} \quad (2.6)$$

The wavefunction must be anti-symmetric with respect to the exchange of any two electrons (the Pauli exclusion principle). This is conveniently enforced by writing the multi-electron wavefunction as a Slater determinant where  $\frac{1}{\sqrt{N!}}$  is a normalization factor.<sup>1</sup>

$$\psi = \frac{1}{\sqrt{N!}} \begin{bmatrix} \chi_1(x_1) & \cdots & \chi_N(x_1) \\ \vdots & \ddots & \vdots \\ \chi_1(x_N) & \cdots & \chi_N(x_N) \end{bmatrix} \quad (2.7)$$

## **2.6 – The Variational Principle**

The goal of solving the Schrödinger equation using a variational approach is to obtain the wavefunction that returns the lowest energy solution. Within the Born-Oppenheimer approximation this requires finding the distribution of electrons that minimizes  $E_{el}$  for a given nuclear configuration. The variational principle states that the energy of a trial wavefunction cannot be lower than the energy of the true wavefunction. This provides a means to improve the trial wavefunction in an iterative manner.<sup>1</sup>

$$E_0 < \hat{H}\psi \quad (2.8)$$

## **2.7 – The Hartree-Fock Method**

The Hartree-Fock method was developed to solve the electronic Schrödinger equation after the Born-Oppenheimer approximation has been invoked. It finds the best set of spin orbitals that describe the system of interest using a single Slater determinant. The best set of spin orbitals is the one that minimizes the electronic energy, in accordance with the variational principle.<sup>1</sup>

The expression for the best set of spin orbitals is the Hartree-Fock equation

$$\begin{aligned}
h(1)\chi_a(1) + \sum_{b \neq a} \left[ \int \frac{|\chi_b(2)|^2}{r_{12}} dx_2 \right] \chi_a(1) \\
- \sum_{b \neq a} \left[ \int \frac{\chi_b^*(2)\chi_a(2)}{r_{12}} dx_2 \right] \chi_b(1) = \varepsilon_a \chi_a(1)
\end{aligned} \tag{2.9}$$

where

$$h(1) = -\frac{\nabla_1^2}{2} - \sum_A \frac{Z_A}{r_{1A}} \tag{2.10}$$

is a one-electron Hamiltonian describing the kinetic energy and attractive potential for a single electron. The orbital energy of the spin orbital is  $\varepsilon_a$ .

The terms in square brackets describe electron-electron interactions. The first describes the coulombic interaction between electrons and the second describes the exchange interaction due to the anti-symmetry of the wavefunction.

The coulomb term in (2.9) describes the one-electron coulomb potential that the electron in  $\chi_a$  experiences due to a different electron in  $\chi_b$ . By summing over  $b \neq a$  the total average potential experienced by the electron in  $\chi_a$  due to the other N-1 electrons in the other spin orbitals is obtained. This is more conveniently expressed as the coulomb operator ( $\hat{J}_b$ ) which represents the average local potential at the position of electron one due to an electron in  $\chi_b$ .

$$\hat{J}_b(1) = \int \frac{|\chi_b(2)|^2}{r_{12}} dx_2 \tag{2.11}$$

The exchange interaction arises from the anti-symmetry requirement and does not have a classical interpretation like the coulomb term. Its effect can be understood by introducing the exchange operator ( $\hat{K}_b$ ) and applying it to spin orbital  $\chi_a(1)$ .

$$\hat{K}_b(1)\chi_a(1) = \left[ \int \frac{\chi_b^*(2)\chi_a(2)}{r_{12}} dx_2 \right] \chi_b(1) \quad (2.12)$$

The effect of the exchange operator is that it swaps electron one in  $\chi_a$  with electron two in  $\chi_b$ .

Using the definitions of the coulomb and exchange operator with the one electron Hamiltonian the Hartree-Fock equation becomes

$$\left[ \hat{h}(1) + \sum_{b \neq a} \hat{J}_b(1) - \sum_{b \neq a} \hat{K}_b(1) \right] \chi_a(1) = \varepsilon_a \chi_a(1) \quad (2.13)$$

Because the  $a=b$  case returns 0, the summations can be dropped and the Fock operator ( $\hat{f}(1)$ ) introduced as

$$\hat{f}(1) = h(1) + \sum_b \hat{J}_b(1) - \hat{K}_b(1) \quad (2.14)$$

and the Hartree-Fock equation is written as

$$\hat{f}(1)\chi_a(1) = \varepsilon_a \chi_a(1) \quad (2.15)$$

In Hartree-Fock theory electron correlation is described in only an average way. This results in a difference between the energy calculated using (2.15) and the exact energy of the non-relativistic Schrödinger equation. This difference in energy is referred to as the correlation energy. There are many *Post* Hartree-Fock methods that account for this difference. These methods are not focused on in this thesis so they will not be detailed,<sup>2</sup> but it will be briefly mentioned that they use multi-determinant wavefunctions to account for electron correlation.

## **2.8 – Density Functional Theory**

An alternative approach to the study of the electronic structure of atoms and molecules is density functional theory (DFT).<sup>3,4</sup> DFT is based on the two pioneering

theorems of Hohenberg and Kohn. The first theorem states that the ground state electron density ( $\rho(r)$ ) of a system of electrons determines the Hamiltonian and therefore all properties may be derived from it. In other words, the total electronic energy of the system is a *functional* of the density.

$$E = E[\rho] \quad (2.16)$$

The second theorem shows that the exact ground density and energy can be found by minimizing  $E[\rho]$  over all possible densities. While this may appear to be a straightforward approach to assessing electronic structure, there are some additional caveats that must be considered.<sup>3,4</sup>

The first is that the exact functional  $E[\rho]$  is unknown. The second is that even if the exact functional were known it is not explicit; the mapping of  $\rho$  to  $E$  cannot be written as a closed form expression (i.e.,  $E = \rho$ ). However, one is free to approximate  $E[\rho]$  in any manner they choose and the development of new approximations is at the core of current research in DFT.<sup>4</sup>

Kohn-Sham DFT (KS-DFT) is the formulation of DFT most commonly used in computational quantum chemistry and provides a good approximation to  $E[\rho]$ . In order to approximate the exact functional, Kohn and Sham proposed breaking it up into a sum of terms, identifying those that are known exactly and approximating those that are not. In KS-DFT the total energy functional is written as

$$E[\rho] = T_s[\rho] + V[\rho] + U[\rho] + E_{xc}[\rho] \quad (2.17)$$

where

$$T_s[\rho] = -\frac{1}{2} \sum_k^{\text{occupied}} \int \phi_k^* \nabla^2 \phi_k(r) dr \quad (2.18)$$

is the kinetic energy of a hypothetical reference system of non-interacting electrons whose total ground state density is exactly equal to  $\rho(r)$  and  $\phi_k(r)$  are the Kohn-Sham orbitals occupied by electrons which are related to the electron density by

$$\rho(r) = \sum_k^{\text{occupied}} |\phi_k(r)|^2 \quad (2.19)$$

$V[\rho]$  describes the electrostatic energy of the electron density interacting with an external potential  $v(r)$

$$V[\rho] = \int \rho(r)v(r)dr \quad (2.20)$$

and  $U[\rho]$  describes the electrostatic energy of one electron in the density interacting with another electron in the density.

$$U[\rho] = \frac{1}{2} \int \int \frac{\rho(r_1)\rho(r_2)}{|r_1 - r_2|} dr_1 dr_2 \quad (2.21)$$

The final term in (2.17),  $E_{xc}[\rho]$ , incorporates all other interactions and is called the *exchange-correlation* functional. It is the only unknown term.  $E_{xc}[\rho]$  can be broken into two parts called the *exchange* and *correlation* functionals:

$$E_{xc}[\rho] = E_x[\rho] + E_c[\rho] \quad (2.22)$$

The energy in KS-DFT is evaluated by introducing a basis set of orbitals (the Kohn-Sham orbitals) and minimizing the Kohn-Sham equation (2.23) in a self-consistent manner as in Hartree-Fock theory<sup>3, 5</sup>

$$\left[ -\frac{1}{2}\nabla^2\rho + V + U + E_{xc} \right] \phi_i = \varepsilon_i \phi_i \quad (2.23)$$

As stated, developing more accurate approximations to the exact  $E_{xc}[\rho]$  is the primary focus of research in DFT. Such approximations are typically written as integral expressions of the form<sup>4</sup>

$$E_{xc}[\rho] = \int e_{xc}(\rho, \nabla\rho, \nabla^2\rho, \tau, e_x^{exact}) dr \quad (2.24)$$

where  $e_{xc}$  is a function of the electron density and other quantities derived from it. Commonly used quantities include the modulus of the density gradient ( $|\nabla\rho|$ ), the Laplacian of the density ( $\nabla^2\rho$ ), the kinetic energy density ( $\tau$ )

$$\tau = \frac{1}{2} \sum_i^{occupied} |\nabla\phi_i|^2 \quad (2.25)$$

and the exact-exchange energy density

$$e_x^{exact}(r_1) = - \sum_{i,j=1}^{N/2} \int \frac{\phi_i(r_1)\phi_i^*(r_2)\phi_j^*(r_1)\phi_j(r_2)}{|r_1 - r_2|} dr_2 \quad (2.26)$$

Approximations to the exchange-correlation functional are ranked on a hypothetical “Jacob’s Ladder” proposed by Perdew.<sup>6</sup> In this ranking system approximations that depend only on  $\rho$  are on the lowest rung of the ladder and are referred to as local spin density approximations (LSDA). Approximations that depend on both  $\rho$  and  $|\nabla\rho|$  are rung 2 and are referred to as generalized-gradient approximations (GGA). Rung 3 of the ladder are functionals which also depend on  $\nabla^2\rho$  or  $\tau$  and are called meta-GGAs (mGGA). Functionals residing on rung 4 of the ladder have an additional dependence on the exact exchange energy density and are commonly known as hybrid functionals. There are also functionals that have an additional dependency on unoccupied Kohn-Sham orbitals called double-hybrid functionals, but they are not used in this work and will not be discussed. Below, some of the functionals that are most commonly used throughout this work are detailed.

### 2.8.1 – Local Spin Density Approximation

As mentioned the simplest approximation to the exchange-correlation functional is the LSDA. In this approximation it is assumed that the electron density varies so little it can be assumed to be uniform; this model is commonly referred to as the uniform electron gas (UEG) model. The exchange component of the LSDA is described by<sup>5</sup>

$$\begin{aligned}\varepsilon_X^{LSDA}[\rho] &= -\frac{3}{2}C_X \left[ \rho_\alpha^{1/3} - \rho_\beta^{1/3} \right] \\ C_X &= \frac{3}{4} \left( \frac{3}{\pi} \right)^{1/3}\end{aligned}\tag{2.27}$$

Analytical expressions for the low and high density limits of the UEG have been determined and Monte-Carlo methods used to determine the correlation energy of intermediate densities to a high degree of accuracy. Vosko, Wilk and Nusair (VWN) developed expressions that interpolate between the spin unpolarised ( $\zeta = 0$ ) and polarised ( $\zeta = 1$ ) limits, where  $\zeta$  is the normalized difference in spin densities.

$$\zeta = \frac{\rho_\alpha - \rho_\beta}{\rho_\alpha + \rho_\beta}\tag{2.28}$$

The correlation functional recommended by Vosko, Wilks and Nusair (Functional V) is given by<sup>6</sup>

$$\begin{aligned}\varepsilon_C^{VWN}(r_s, \zeta) &= \varepsilon_C(r_s, 0) + \varepsilon_a(r_s) \left[ \frac{f(\zeta)}{f(\zeta)} \right] [1 - \zeta^4] \\ &\quad + [\varepsilon_C(r_s, 1) - \varepsilon_C(r_s, 0)] f(\zeta) \zeta^4 \\ f(\zeta) &= \frac{(1 + \zeta)^{4/3} + (1 - \zeta)^{4/3} - 2}{2(2^{1/3} - 1)}\end{aligned}\tag{2.29}$$

The functions  $\varepsilon_C(r_s, \zeta)$  and  $\varepsilon_a(r_s)$  are parameterized using A,  $x_0$ , b and c as fitting constants

$$\begin{aligned}
\frac{\varepsilon_C}{a}(x) = A \left\{ \ln \frac{x^2}{X(x)} \right. \\
+ \frac{2b}{Q} \tan^{-1} \left( \frac{Q}{2x+b} \right) \\
- \frac{bx_0}{X(x_0)} \left[ \ln \frac{(x-x_0)^2}{X(x)} \right. \\
\left. \left. + \frac{2(b+2x_0)}{Q} \tan^{-1} \left( \frac{Q}{2x+b} \right) \right] \right\} \quad (2.30)
\end{aligned}$$

$$x = \sqrt{r_s}; X(x) = x^2 + bx + c; Q = \sqrt{4c - b^2}$$

Combining the Slater exchange functional with the VWN correlation functional yields the SVWN LSDA functional.

### 2.8.2 – GGA Functionals

LSDA functionals are deficient in so far as they describe the electron density as being a uniform quantity, an unphysical description. GGA functionals seek to improve this description by allowing the electron density to vary in space. As described above, GGA functionals are not only dependent on the value of  $\rho$  but also its gradient. As above the exchange and correlation components are separated and functionals are constructed for each.

One of the first GGA exchange functionals developed by Becke (B88) is still popular and is a correction to the LSDA exchange energy

$$\begin{aligned}
\varepsilon_X^{B88} &= \varepsilon_X^{LSDA} + \Delta\varepsilon_X^{B88} \\
\Delta\varepsilon_X^{B88} &= -\beta\rho^{1/3} \frac{m^2}{1 + 6\beta m \sinh^{-1} m} \quad (2.31) \\
m &= \frac{|\nabla\rho|}{\rho^{4/3}}
\end{aligned}$$

where  $\beta$  is determined by fitting to experimental data for rare gas atoms by varying the gradient variable,  $m$ .<sup>5,6</sup>

The B88 functional is commonly paired with the GGA correlation functional developed by Lee, Yang and Parr (LYP) described by<sup>5,7</sup>

$$\begin{aligned}
\varepsilon_C^{LYP} = & -4i \frac{\rho_\alpha \rho_\beta}{\rho^2 \left(1 + k\rho^{-\frac{1}{3}}\right)} \\
& - ij\omega \left\{ \frac{\rho_\alpha \rho_\beta}{18} \left[ 144(2^{2/3})C_F \left(\rho_\alpha^{8/3} + \rho_\beta^{8/3}\right) \right. \right. \\
& + (47 - 7\delta)|\nabla\rho|^2 - (45 - \delta) \left(|\nabla\rho_\alpha|^2 + |\nabla\rho_\beta|^2\right) \\
& + 2\rho^{-1}(11 - \delta) \left(\rho_\alpha|\nabla\rho_\alpha|^2 + \rho_\beta|\nabla\rho_\beta|^2\right) \left. \right] \\
& + \frac{2}{3}\rho^2 \left(|\nabla\rho_\alpha|^2 + |\nabla\rho_\beta|^2 - |\nabla\rho|^2\right) - \left(\rho_\alpha^2|\nabla\rho_\beta|^2 \right. \\
& \left. + \rho_\beta^2|\nabla\rho_\alpha|^2\right) \left. \right\} \\
\omega = & \frac{e^{-l\rho^{-1/3}}}{\rho^{14/3} \left(1 + k\rho^{-\frac{1}{3}}\right)} \\
\delta = & k\rho^{-1/3} + \frac{k\rho^{-\frac{1}{3}}}{\left(1 + k\rho^{-\frac{1}{3}}\right)}
\end{aligned} \tag{2.32}$$

where  $i, j, k$  and  $l$  are determined by fitting experimental data for the helium atom, to give the BLYP GGA functional.

Perdew *et. al.* also developed a GGA exchange functional based on a correction to the LSDA exchange energy given by<sup>5,9</sup>

$$\varepsilon_X^{PBE} = \varepsilon_X^{LSDA} F_X^{PBE} \tag{2.33}$$

$$F_X^{PBE} = 1 + q - \frac{q}{1 + rm^2}$$

where F is an *enhancement factor* with m as the same gradient variable defined in (2.31).

The corresponding correlation functional is written as an enhancement factor (H(t)) to the LSDA correlation functional and given by

$$\begin{aligned} \varepsilon_C^{PBE} &= \varepsilon_C^{LSDA} + H(t) \\ H(t) &= sf_3^3 \ln \left[ 1 + ut^2 \left( \frac{1 + At^2}{1 + At^2 + A^2t^4} \right) \right] \\ A &= u \left[ \exp \left( -\frac{\varepsilon_C^{LSDA}}{sf_3^3} \right) - 1 \right]^{-1} \\ f_3(\zeta) &= \frac{1}{2} [(1 + \zeta)^{2/3} + (1 - \zeta)^{2/3}] \\ t &= [2(3\pi)^{1/3} f_3]^{-1} m \end{aligned} \quad (2.34)$$

where q,r,s and u are non-empirical parameters derived from first principles.

### 2.8.3 – meta-GGA (mGGA) Functionals

A commonly used mGGA functional in this work is the one developed by Truhlar's group at the University of Minnesota, denoted M06-L. As described above, mGGA's depend on  $\rho$ ,  $|\nabla\rho|$  and  $\nabla^2\rho$  or  $\tau$ . The M06-L functional is based on a linear combination of PBE and the VSXC functional developed by Van-Voorhis and Scuseria. In this subsection  $r$  is the spatial coordinate of an electron. The M06 exchange functional is given by<sup>10</sup>

$$E_X^{M06} = \sum \int [F_X^{PBE}(\rho, \nabla\rho) f(w) + \varepsilon_X^{LSDA} h_X(r, z)] \quad (2.35)$$

where  $F_X^{PBE}$  is as defined in (2.33) and  $z$  is a working variable that depends on  $\tau$  defined by

$$z = \frac{2\tau}{\rho^{5/3}} - C_F \quad (2.36)$$

$$C_F = \frac{3}{5} (6\pi^2)^{2/3}$$

$h_x$  is a working function given by

$$h_x(r, z) = \left( \frac{d_0}{\gamma(r, z)} + \frac{d_1 r^2 + d_2 z}{\gamma^2(r, z)} + \frac{d_3 r^4 + d_4 r^2 z + d_5 z^2}{\gamma^3(r, z)} \right) \quad (2.37)$$

that depends on another working function  $\gamma$  described by

$$\gamma(r, z) = 1 + \alpha(r^2 + z) \quad (2.38)$$

$f(w)$  is referred to as the *kinetic-energy-density enhancement factor* defined by

$$f(w) = \sum_{i=0}^{11} a_i w^i \quad (2.39)$$

where  $w$  is a function of  $t$  which in turn is a function of both  $\rho$  and  $\tau$  given by

$$w^i = \frac{(n-1)}{(n+1)}$$

$$n = \frac{\tau^{LSDA}}{\tau} \quad (2.40)$$

$$\tau^{LSDA} = \frac{3}{10} (6\pi^2)^{2/3} \rho^{5/3}$$

The M06 correlation functional treats opposite-spin and same-spin correlation differently. The opposite-spin (denoted  $\alpha, \beta$ ) correlation is given by<sup>10</sup>

$$E_C^{M06} = \int e_{\alpha\beta}^{UE} [g(r_\alpha, r_\beta) + h_{\alpha\beta}(r_{\alpha\beta}, z_{\alpha\beta})] dr \quad (2.41)$$

where  $g_{\alpha\beta}(x_\alpha, x_\beta)$  is given by  $h(\alpha, \beta)$ .

$$g_{\alpha\beta}(r_\alpha, r_\beta) = \sum_{i=0}^n c_{C\alpha\beta, i} \left( \frac{\gamma c_{C\alpha\beta} (r_\alpha^2 + r_\beta^2)}{1 + \gamma c_{C\alpha\beta} (r_\alpha^2 + r)} \right)^i \quad (2.42)$$

$r$  describes position of the alpha and beta electrons ( $r^2 = r_\alpha^2 + r_\beta^2$ ) and  $z = z_\alpha + z_\beta$  is the working variable defined in (2.36) applied to the alpha and beta spin electrons separately.

The same-spin correlation is described by

$$E_C^{M06} = \int e^{UE} [g(r) + h(r, z)] dr \quad (2.43)$$

where  $g(r)$  is defined as

$$g(r) = \sum_{i=0}^n c_{C,i} \left( \frac{\gamma_C r^2}{1 + \gamma_C r^2} \right)^i \quad (2.44)$$

and  $h(x,z)$  is defined in (2.37).  $D$  is a self-interaction error correction factor given by

$$= 1 - \frac{r^2}{4(z + C_F)} \quad (2.45)$$

which vanishes for any one electron system. In (2.41) and (2.43)  $e^{UEG}$  is the correlation energy for opposite and same spin correlation and  $\gamma_{C\alpha\beta}$  and  $\gamma_C$  are two parameters from the M05 functionals previously developed by Truhlar's group. The total M06 correlation energy is the sum of the same and opposite spin correlation energies

$$E_C = E_C^{\alpha\beta} + E_C^{\alpha\alpha} + E_C^{\beta\beta} \quad (2.46)$$

#### 2.8.4 – Hybrid Functionals

The exchange-correlation energy can be connected to the potential that connects the non-interacting reference system to the actual system. This is done through the adiabatic connection formula (2.47).<sup>5</sup>

$$E_{XC} = \int_0^1 \langle \Psi_\lambda | V_{XC}(\lambda) | \Psi_\lambda \rangle d\lambda \quad (2.47)$$

In its simplest approximation  $V_{XC}(\lambda)$  is assumed to be linear and the integral is taken to be the average value of the two end points. In the  $V_{XC}(\lambda) = 0$  limit the electrons are non-

interacting and there is no correlation energy and the exchange energy is equal to that given by Hartree-Fock theory. If the actual system is approximated by the local functionals given by the LSDA then the exchange- correlation energy is given by the *half-and-half* (H+H) method

$$E_{XC}^{H+H} = \frac{1}{2} E_X^{Exact} + \frac{1}{2} (E_X^{LSDA} + E_C^{LSDA}) \quad (2.48)$$

A more accurate result can be obtained by writing the exchange energy as a combination of the LSDA exchange, exact exchange and a gradient correction term. The most popular hybrid functional is the Becke 3 parameter functional described by<sup>5,11</sup>

$$E_{XC} = (1 - n)E_X^{LSDA} + nE_X^{Exact} + o\Delta E_X^{B88} + (1 - p)E_C^{LSDA} + pE_C^{LYP} \quad (2.49)$$

where n, o and p are determined by fitting to experimental data to be 0.2, 0.7 and 0.8, respectively.

The hybrid M06 functionals (M06, M062X and M06-HF) are based on the following format<sup>10</sup>

$$E_{XC} = \frac{X}{100} E_X^{HF} + \left(1 - \frac{X}{100}\right) E_X^{M06} + E_C^{M06} \quad (2.50)$$

where X=28 (M06), 56 (M06-2X) or 100 (M06-HF). Similarly, the hybrid version of PBE (denoted PBE0) mixes 25% exact exchange and 75% DFT exchange.<sup>5,12</sup>

In most electronic structure packages, the amount of exact exchange a functional includes can be manually specified. This is done in this work using the Gaussian09 package<sup>13</sup> via the following keywords:

1. The BLYP functional is specified in the route section
2. The following I/Op codes are specified
  - a. IOp(3/76=10000xxxxx)

b. IOp(3/77=07200yyyyy)

c. IOp(3/77=081001000)

IOp(3/76) controls the amount of exact exchange. xxxxx = 00000 for 0% exact exchange and 10000 for 100%. Each increase of 1000 corresponds to a 10% increase and all leading zeroes must be specified. IOp(3/77) controls the amount of B88 exchange and is given by yyyyy=10000.

### 2.8.5 – Range-Separated Hybrid Functionals

The interaction of electrons with opposite spins occurring over a short distance is well described by DFT. On the other hand, the same interactions occurring over long distances are better described by exact exchange. This insight motivated the creation of range-separated (RS) hybrid functionals where short distance interactions are treated with DFT exchange while long distance interactions are treated with exact exchange.

In RS hybrids the operator describing the electron-electron Coulomb repulsion is split into a short and long range component<sup>4</sup>

$$\frac{1}{r_{12}} = \frac{1 - f(r_{12})}{r_{12}} + \frac{f(r_{12})}{r_{12}} \quad (2.51)$$

where  $f(r_{12})$  is a *screening function* that satisfies three criteria: 1) It ranges between 0 and 1. 2) as  $r_{12}$  approaches zero so does  $f$ , and 3) as  $r_{12}$  approaches infinity  $f$  approaches 1.

The most common choices for the screening function are the exponential function

$$f(r_{12}) = 1 - e^{-\omega r_{12}} \quad (2.52)$$

and the error function

$$f(r_{12}) = f(\omega r_{12}) = \frac{2}{\sqrt{\pi}} \int_0^{\omega r_{12}} e^{-t^2} dt \quad (2.53)$$

where  $\omega$  is a positive constant in both equations.

The CAM-B3LYP functional developed by Yanai *et. al.* has the short range exchange interaction described by<sup>15</sup>

$$E_X^{SR} = -\frac{1}{2} \sum \int \rho^{4/3} \nabla \rho \left\{ 1 - \frac{8}{3} a \left[ \sqrt{\pi} f\left(\frac{1}{2a}\right) + 2a(b-c) \right] \right\} dr \quad (2.54)$$

and the long range interaction by

$$E_X^{LR} = -\frac{1}{2} \sum_i^{occ} \sum_j^{occ} \int \int \phi_i^*(r_1) \phi_j^*(r_1) \frac{f(\mu r_{12})}{r_{12}} \phi_i(r_2) \phi_j(r_2) dr_1 dr_2 \quad (2.55)$$

where  $\mu$  is a parameter that determines the amount of DFT to HF exchange in cases of intermediate distances and  $\sigma$  can refer to either  $\alpha$  or  $\beta$  electrons. If  $\mu = 0$  then only DFT exchange is used, conversely if  $\mu = 1$  only exact exchange is used.

## **2.9 – Strengths and Weaknesses of the Hartree-Fock Method and Density Functional Theory**

While the Hartree-Fock method greatly simplifies that multi-electron problem and provides the best single determinant description of the electronic structure (in a complete basis set), it has some deficiencies.

The main drawback of the Hartree-Fock method is due to its description of electron correlation. As described in section 2.7 the electron correlation is described in only an average way. The correlation of electrons of the same spin is accounted for in Hartree-Fock theory by exchange operator, however, the correlation of electrons of opposite spin, due to Coulomb repulsion, is not accounted for. This leads to an improper description of chemically important effects (e.g. dispersion interactions). Electron correlation can be better accounted for using post Hartree-Fock methods.

The computational effort required for post Hartree-Fock methods limits their usage to small or medium sized molecules. On the other hand, DFT is able to account for electron correlation more accurately than the Hartree-Fock method at a computational effort approximately equal to the Hartree-Fock method. Results obtained from DFT are typically as accurate as those obtained from second order Møller-Plesset perturbation theory (MP2). However, there are many density functional approximations available and a variety of them should be tested to ensure a consistent result is obtained.

## **2.10 – Basis Sets**

Once a method (HF or DFT) has been chosen, a choice on how to represent the wavefunction or electron density must be made. This is done by using a basis set of functions to approximate the unknown molecular orbitals as a set of one electron functions. This is not an approximation if an infinite sized basis set is used (i.e., if the basis set is complete) but in practice this is not feasible and so finite sized basis sets of functions are used.<sup>1,5</sup>

There are two types of basis functions: Slater type and Gaussian type. Gaussian type are most commonly used for ease of integration. They are of the general form (in Cartesian coordinates)

$$\begin{aligned} \mathcal{F}_{\zeta,n,l,m}(x,y,z) &= Nx^n y^l z^m e^{-\zeta} \\ &= n + l + m \end{aligned} \tag{2.56}$$

where  $\zeta$  is a positive value and  $L$  is the orbital quantum number. To increase the efficiency of the calculation the basis functions are written as a linear combination of Gaussian functions called Contracted Gaussian Type basis functions (2.57).<sup>5</sup> The most commonly employed type of basis set used throughout this work will be described.

$$\phi = \sum_{i=1}^k a_i \mathcal{F}_i \quad (2.57)$$

The split valence Pople style basis sets represent the core electrons with one set of cGTOs and a different set of cGTOs to describe the valence electrons. For example, the 6-31G basis set is of double zeta quality where the core electrons are represented by 6 cGTOs and the valence by 3 cGTOs and 1 additional GTO. Similarly, the 6-311G basis set is of triple zeta quality where the core electrons are represented by 6 cGTOs and the valence is split into three functions of 3, 1 and 1 cGTO.<sup>1,5</sup>

These basis sets are commonly improved by adding additional *diffuse* or *polarization* functions. Diffuse functions are typically s or p type functions. They are denoted by + or ++ for a set of diffuse s and p functions on heavy atoms and an additional s function on hydrogen, respectively. Polarization functions add an additional function to atoms as well. For example, the 6-311++G(2df,pd) basis set has polarization functions on the heavy atoms as well as hydrogen, and 2 additional d functions and 1 additional f function on heavy atoms as well as one additional p and d function on hydrogen atoms. Diffuse and polarization functions are included in order to give the basis set more flexibility.<sup>5</sup>

Other basis sets used in this work are the Dunning style correlation consistent basis sets and the Def2 basis sets developed by Ahlrichs *et. al.* The Dunning basis sets are denoted cc-pvNZ where N=D,T,Q, 5, 6, denoting the quality of the basis set (double, triple, quadruple, quintuple, sextuple zeta), and are designed to converge to the complete basis set limit for post Hartree-Fock methods. They include an increasing number of

polarization functions and can be augmented with diffuse functions by attaching the aug- prefix to the basis set designation (e.g., aug-cc-pvDZ).

The Def2 family are split valence basis sets that can include varying amounts of polarization. For example, the Def2TZVP is a triple zeta quality basis set with polarization functions while Def2TZVPP is the same basis set with an increased amount polarization functions. In their original formulation they did not include diffuse functions. They have since been updated to include diffuse functions as in the Def2TZVPPD basis set.

## **2.11 – Time-Dependent Density Functional Theory (TD-DFT)**

DFT has become the method of choice for assessing the ground state electronic structure of large molecules. TD-DFT extends DFT to the time-dependent domain in order to study the excited states of molecules. In TD-DFT the variable of interest is the time-dependent density,

$$\rho(r, t) = N \int |\psi(r_1, r_2, \dots, r_N; t)|^2 dr_2 \dots dr_N \quad (2.58)$$

The Runge-Gross theorem forms the basis of TD-DFT. It states that densities  $n(r, t)$  and  $n'(r, t)$  which evolve from some initial state change under the influence of two different potentials  $v_{\text{ext}}(r, t)$  and  $v'_{\text{ext}}(r, t)$  are different if and only if the potentials differ by more than a time-dependent function. It establishes a one-to-one mapping between the time dependent density and the external potentials. Moreover, it establishes that there is a one-to-one mapping between the density and wavefunction for an initial state.<sup>16,17</sup>

Just like in ground state DFT, the interacting system of electrons is mapped onto a non-interacting system described by the potential  $v_{\text{ks}}(r, t)$  that yields the same density

as the interacting system. The non-interacting system is described by the time-dependent Kohn-Sham equation

$$i \frac{\partial}{\partial t} \psi_j(r, t) = \left[ -\frac{\nabla^2}{2} + v_{KS}(r, t) \right] \psi_j(r, t) \quad (2.59)$$

The excitation energies are determined from the Fourier transform of the first order response to the external potential.<sup>18</sup> Further technical details of TD-DFT are omitted but the reader is directed to the references at the end of this chapter.<sup>16-18</sup>

## **2.12 – Post Analysis Methods**

The electron density ( $\rho$ ) is obtained as a result of performing a calculation using one of the methods outlined above according to:<sup>5</sup>

$$|\psi|^2 = \rho(r) = N \int |\psi(r_1, r_2, \dots, r_N)|^2 dr_2 \dots dr_N \quad (2.60)$$

A variety of post-analysis schemes have been devised and are routinely used to extract further information about the system of interest. In this work the primary post-analysis tools used are the Quantum Theory of Atoms in Molecules (QTAIM) developed by Bader<sup>19, 20</sup> and Natural Bond Orbital / Natural Resonance Theory (NBO/NRT) analysis developed by Weinhold.<sup>21</sup>

### **2.12.1 – The Quantum Theory of Atoms in Molecules**

The Quantum Theory of Atoms in Molecules provides a topological analysis of  $\rho$ . The topology of  $\rho$  is dominated by large maxima at the position of the nuclei. Critical points (CPs) in  $\rho$  can be determined by examining its gradient<sup>19, 20</sup>

$$\nabla\rho = i \frac{d\rho}{dx} + j \frac{d\rho}{dy} + k \frac{d\rho}{dz} \begin{cases} = 0 & \text{at CP's and } \infty \\ \neq 0 & \text{elsewhere} \end{cases} \quad (2.61)$$

The maximum at the position of the nuclei is a type of CP called a nuclear critical point. The character of any other CP's can be determined by inspecting the 3x3 tensor corresponding to the nine second derivatives at the CP.<sup>19, 20</sup>

$$A = \begin{pmatrix} \frac{\partial^2 \rho}{\partial x^2} & \frac{\partial^2 \rho}{\partial x \partial y} & \frac{\partial^2 \rho}{\partial x \partial z} \\ \frac{\partial^2 \rho}{\partial y \partial x} & \frac{\partial^2 \rho}{\partial y^2} & \frac{\partial^2 \rho}{\partial y \partial z} \\ \frac{\partial^2 \rho}{\partial z \partial x} & \frac{\partial^2 \rho}{\partial z \partial y} & \frac{\partial^2 \rho}{\partial z^2} \end{pmatrix} \quad (2.62)$$

This matrix is diagonalizable because it is symmetric and real. Diagonalizing rotates the matrix to a principal axis system and returns three eigenvalues:  $\lambda_1 > \lambda_2 > \lambda_3$

$$\Lambda = \begin{bmatrix} 1 & 0 & 0 \\ 0 & 2 & 0 \\ 0 & 0 & 3 \end{bmatrix} \quad (2.63)$$

The CP can be further classified based on its rank (number) and signature (the algebraic sum of their signs). There are four stable CPs with a rank of 3 and a CP with a rank of less than 3 is said to be topologically unstable (see later). In Table 2.1 the rank and signature of the four types of stable CPs are presented.<sup>19,20</sup>

**Table 2.1:** Rank and signature of the four stable critical points predicted by QTAIM

	Rank	Signature
Nuclear Critical Point	3	-3
Bond Critical Point	3	-1
Ring Critical Point	3	+1
Cage Critical Point	3	+3

The nuclear critical point (NCP) is a (3,-3) CP indicating that  $\rho$  is a local maximum at this point. The bond critical point (BCP) is a (3,-1) CP that connects two atoms in a molecule where  $\rho$  is a maximum in two directions and a minimum in the direction perpendicular to the plane defined by the first two directions. A ring critical point (RCP) is a (3, +1) CP that connects three or more atoms where  $\rho$  is a minimum in the plane containing the ring and a maximum in the direction perpendicular to the ring. A cage critical point (CCP) is defined by three positive curvatures at the CP. The Poincaré-Hopf relationship relates the number and type of CPs that can co-exist in a molecule<sup>19, 20</sup>

$$n_{NCP} - n_{BCP} + n_{RCP} - n_{CCP} = 1 \quad (2.64)$$

As mentioned above, the topology of  $\rho$  is dominated by large maxima corresponding to the nuclei. This feature allows for the molecule to be partitioned into discrete nuclear regions called *atomic basins* (denoted by  $\Omega$ ). There is a surface that contains an atom within a molecule and it is required that the surface satisfy the boundary condition given by<sup>19,20</sup>

$$\nabla\rho \cdot n(r) = 0 \quad (2.65)$$

This is the *zero-flux condition* that states none of the gradient vectors of  $\rho$  may cross the surface bounding an atom. Such surfaces are called atomic basins and when two atomic basins touch there is a zero-flux interatomic surface that occurs between them.

Average properties (P) of individual atoms can be calculated by integrating over an atomic basin

$$P(\Omega) = \langle \hat{O} \rangle_{\Omega} = \frac{N}{2} \int_{\Omega} \int [\Psi^* \hat{O} \Psi + (\hat{O} \Psi)^* \Psi] dr d\tau \quad (2.66)$$

where  $\hat{O}$  is a one electron operator. Commonly calculated values include the atomic electron population, charge, volume and energy.<sup>19, 20</sup>

An additional topological feature called a *bond path* is found which links two atomic basins and is an indicator of a bonding interaction. The point along the bond path with the minimum electron density is where the BCP and interatomic surfaces are found. The network of bond paths and CPs that connect the nuclei in an equilibrium geometry is called a *molecular graph* (MG). The MG provides an unambiguous definition of molecular structure in QTAIM.<sup>19, 20</sup>

Earlier it was mentioned that a CP of rank  $< 3$  is an unstable critical point. If a MG contains such a CP, then a change in structure will occur; the unstable CP will be annihilated and a new MG corresponding to a new structure is obtained. A quantity relevant to structural change is the ellipticity ( $\varepsilon$ ) of a CP defined by

$$\varepsilon = \frac{1}{2} - 1 \quad (2.67)$$

$\varepsilon$  measures the relative accumulation of electron density in the plane of the bond path. Unstable CP's (those that are susceptible to annihilation) will have an  $\varepsilon > 1$ . The study of structural change of topologically unstable structures in QTAIM is performed using Thom's theory of elementary catastrophes (see 2.12).<sup>19</sup>

#### 2.12.2 – Natural Bond Orbital / Natural Resonance Theory Analysis

The NBO program developed by Weinhold *et. al.*<sup>21</sup> provides an analysis of the multi-electron wavefunction, calculated from a wavefunction method or DFT, in terms of localized electron pairs. It makes use of the first order reduced density matrix of the wavefunction ( $\gamma_1 - 1$ RDM)

$$\gamma_1(r_1, r_1') = N \int \Psi^*(r_1', r_2 \dots r_N) \Psi(r_1, r_2 \dots r_N) dr_2 \dots dr_N \quad (2.68)$$

where N is the number of electrons. The diagonal elements of (2.68) ( $r_1' = r_1$ ) return the electron density function

$$\rho_1 = \gamma_1(r_1, r_1) = N \int \Psi^*(r_1', r_2 \dots r_N) \Psi(r_1, r_2 \dots r_N) dr_2 \dots dr_N \quad (2.69)$$

where (2.69) represents the probability of finding an electron at position  $r_1$ . All of the information contained in the 1RDM can be obtained from the eigenvalue equation

$$\hat{\gamma} \theta_i = n_i \theta_i \quad (2.70)$$

where the eigenfunctions  $\theta_i$  are natural orbitals and the eigenvalues  $n_i$  is the occupancy of the orbital.<sup>22</sup>

NBO analysis focuses on searching the 1RDM for the highest occupancy orbitals associated with an atom A. By doing so the *natural atomic orbitals* (NAOs) corresponding to each atom are obtained. If the 1RDM is searched for the highest occupancy orbitals associated with a diatomic region (A–B) the set of *natural bond orbitals* (NBOs) is obtained. Algorithms for generating NBOs are implemented in the NBO 6.0 program and detailed in the references therein.<sup>21</sup>

The set of occupied NBOs is referred to as the set of *Lewis* NBOs and is accompanied by a set of *non-Lewis* NBOs. Any non-zero occupancy of the non-Lewis NBOs is said to correspond to electron delocalization. The NBO program generates a list of delocalization interactions between the Lewis and non-Lewis sets and uses them in the Natural Resonance Theory (NRT) module.<sup>22, 23, 24</sup>

The NRT module provides a resonance expansion description where the 1RDM is expanded as a series of candidate 1RDM operators

$$\hat{\Gamma} = \sum_{\alpha} w_{\alpha} \hat{\Gamma}_{\alpha} \quad (2.71)$$

and compares the candidate operators to the so-called true density matrix. The program attempts to minimize the difference between the two using a least squares variational functional,  $\delta_w$ , stated to be a measure of the irreducible error in describing the true 1RDM with the chosen candidate 1RDM operators (corresponding to resonance structures). It is stated to be an “internal criteria of accuracy”.<sup>22</sup>

$$\delta_w = \min \left\| \hat{\Gamma} - \sum_{\alpha} w_{\alpha} \hat{\Gamma}_{\alpha} \right\| \quad (2.72)$$

If the NRT expansion is an exact representation of the true 1RDM then  $\delta_w = 0$ . However, for expansions with  $\delta_w \neq 0$  the module calculates how much the expansion improves the description of the electronic structure over using only the first term in the 1RDM expansion ( $\delta_{ref}$ ). This is referred to as the *fractional improvement* ( $f_w$ ) and is given by

$$f_w = \frac{\delta_{ef} - \delta_w}{\delta_{ef}} \quad (2.73)$$

$f_w$  varies from 0 to 1 and approaches 1 as  $\delta_w$  approaches 0.<sup>22</sup>

The NRT analysis occurs in three steps.

1. A set of reference resonance structures is specified. This is either done automatically by the program or resonance structures of interest to the user are specified.
2. The set of NBOs is generated for each of the resonance structures specified and from the list of delocalization interactions a set of secondary resonance structures ( $\Gamma_{\alpha}$ ) are determined for each.

3. The resonance weights  $w_\alpha$  of each  $\Gamma_\alpha$  are determined.

### **2.13 – Elementary Catastrophe Theory**

The elementary catastrophe theory developed by Thom<sup>24</sup> provides an additional analysis tool that is used throughout this work. Briefly, it describes the sudden changes in the description of a state of a system under external perturbation. The most important points of the theory will be described.

The state of a system is described by two sets of variables, internal variables  $x = (x_1, \dots, x_m)$  and control variables  $c = (c_1, \dots, c_n)$  that are related by a *potential function*  $V(x, c)$ . When the control variables have fixed values the system will reach an equilibrium where the internal variables minimize the potential function. As the control variables are varied the potential function can suddenly jump and establish a new equilibrium.<sup>26</sup>

Whereas the potential function depends on internal and control variables, the eigenvalues of the stability matrix of any critical point in the potential function depend only on the values of the control variables. This means that there are values the control variables can take on that will cause zero eigenvalues in the stability matrix to be annihilated.<sup>26</sup>

There are seven elementary catastrophes originally described by Thom that contain either one or two internal variables and four or fewer control variables. They are compiled in **Table 2.2**. In this work the cusp and elliptic umbilic catastrophe are studied so they will be covered in further detail.<sup>26</sup>

**Table 2.2:** The seven elementary catastrophes described by Thom

Control Variables	1 Internal Variable	2 Internal Variables
1	Fold	–
2	Cusp	–
3	Swallowtail	Hyperbolic Umbilic Elliptic Umbilic
4	Butterfly	Parabolic Umbilic

### 2.13.1 – The Cusp Catastrophe

The cusp catastrophe describes the interrelationship between a two state system where one system has three critical points and the other has only one. It is given by

$$f(x; a, b) = \frac{1}{4}x^4 + \frac{1}{2}ax^2 + bx \quad (2.74)$$

where a and b are control variables and x is the internal variable. Its control parameter plane is visualized in **Figure 2.2**.<sup>27</sup>

Within the cusp shaped region of **Figure 2.2** the potential function has three critical points, while outside this region there is only one critical point. Inside the cusp the potential function is analogous to the potential energy surface shown in **Figure 2.1** Any change in the potential function requires the system to pass through the cusp shaped region whereby a doubly degenerate critical point, or in the case of the tip of the cusp a triply degenerate critical point, is formed. Beyond this point the degenerate critical point is annihilated and the system enters the larger region complementary to the cusp.<sup>27</sup>

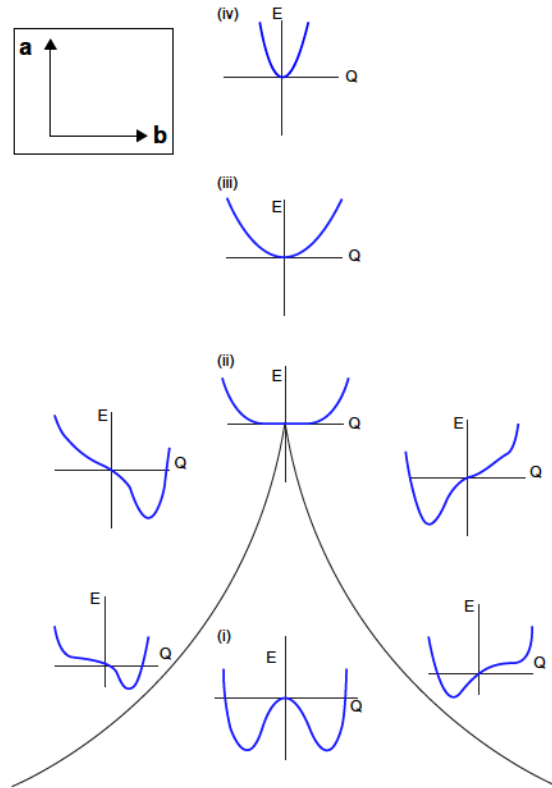


**Figure 2.2:** Control parameter plane for cusp catastrophe

### 2.13.2 – The Elliptic Umbilic Catastrophe

The elliptic umbilic catastrophe describes the interrelationship between a four state system where one state has four critical points while the other three states have only two. It is described by

$$f(y, z; u, v, w) = y^2z - \frac{z}{3}wy^3 + wy^2 - uy - vz \quad (2.75)$$

where  $u$ ,  $v$  and  $w$  are control variables and  $y$  and  $z$  are internal variables. Its control parameter plane is visualized in **Figure 2.3**.<sup>27</sup>

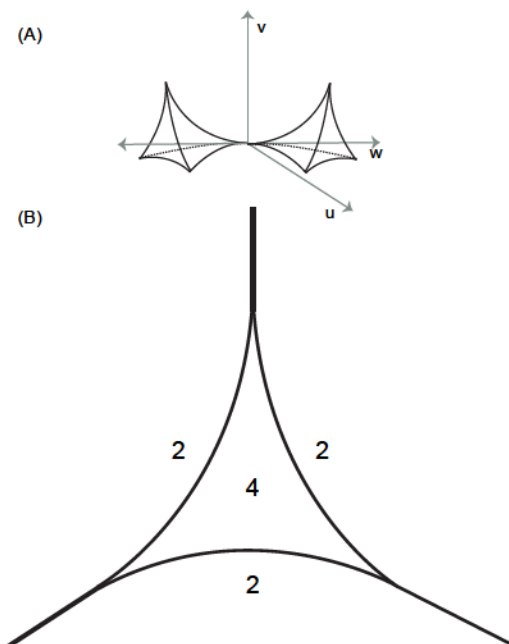


**Figure 2.3:** (A) Control parameter plane for elliptic umbilic catastrophe (B) view of hyperbolic region with number of critical points labelled.

Within the hyperbolic region of **Figure 2.3** the system has four critical points while outside there are only two. Passing through the hyperbolic region results in a doubly degenerate critical point forming and then annihilating as the system enters the region complementary to the hyperbolic region. This model has been previously applied to the study of structural changes in three-membered rings within QTAIM.<sup>19</sup>

## **2.14 – References**

- (1) Szabo, A. and Ostlund, N. *Modern Quantum Chemistry: An Introduction to Advanced Electronic Structure Theory*. McGraw-Hill, Inc. New York, New York (1996)
- (2) If the reader is interested references 1 and 5 of this chapter provide a good introduction to the Post Hartree-Fock methods commonly used in quantum chemistry.
- (3) Koch, W. and Holthausen, M.C. *A Chemist's Guide to Density Functional Theory*. John Wiley and Sons, New York, New York (2001)
- (4) Staroverov, V. *A Matter of Density: Exploring the Electron Density Concept in the Chemical, Biological, and Materials Sciences*. John Wiley and Sons, Hoboken, New Jersey (2013)
- (5) Jensen, F. *Introduction to Computational Chemistry 2<sup>nd</sup> Edition*. John Wiley and Sons, New York, New York (2007)
- (6) Vosko, S.H.; Wilk, L. and Nusair, M. *Can. J. Phys.*, **1980**, 58, 1200
- (7) Perdew, J.P. and Schmidt, K. *AIP Conf. Proc.*, **2001**, 577, 1
- (8) Becke, A.D. *Phys. Rev. A*. **1988**, 38, 3098
- (9) Lee, C.; Yang, W. and Parr, R.G. *Phys. Rev. B.*, **1988**, 37, 785
- (10) Perdew, J.P.; Burke, K. and Ernzerhof, M. *Phys. Rev. Lett.*, **1996**, 77, 3865
- (11) Zhao, Y. and Truhlar, D.G. *Theor. Chem. Acct.*, **2008**, 120, 215
- (12) Becke, A.D. *J. Chem. Phys.*, **1993**, 98, 5648
- (13) Ernzerhof, M. and Scuseria, G.E. *J. Chem. Phys.*, **1999**, 110, 5029

- (14) **Gaussian 09**, Revision D.01, Frisch, M. J.; Trucks, G. W.; Schlegel, H. B.; Scuseria, G. E.; Robb, M. A.; Cheeseman, J. R.; Scalmani, G.; Barone, V.; Mennucci, B.; Petersson, G. A.; Nakatsuji, H.; Caricato, M.; Li, X.; Hratchian, H. P.; Izmaylov, A. F.; Bloino, J.; Zheng, G.; Sonnenberg, J. L.; Hada, M.; Ehara, M.; Toyota, K.; Fukuda, R.; Hasegawa, J.; Ishida, M.; Nakajima, T.; Honda, Y.; Kitao, O.; Nakai, H.; Vreven, T.; Montgomery, J. A., Jr.; Peralta, J. E.; Ogliaro, F.; Bearpark, M.; Heyd, J. J.; Brothers, E.; Kudin, K. N.; Staroverov, V. N.; Kobayashi, R.; Normand, J.; Raghavachari, K.; Rendell, A.; Burant, J. C.; Iyengar, S. S.; Tomasi, J.; Cossi, M.; Rega, N.; Millam, J. M.; Klene, M.; Knox, J. E.; Cross, J. B.; Bakken, V.; Adamo, C.; Jaramillo, J.; Gomperts, R.; Stratmann, R. E.; Yazyev, O.; Austin, A. J.; Cammi, R.; Pomelli, C.; Ochterski, J. W.; Martin, R. L.; Morokuma, K.; Zakrzewski, V. G.; Voth, G. A.; Salvador, P.; Dannenberg, J. J.; Dapprich, S.; Daniels, A. D.; Farkas, Ö.; Foresman, J. B.; Ortiz, J. V.; Cioslowski, J.; Fox, D. J. Gaussian, Inc., Wallingford CT, 2009.
- (15) Yanai, T.; Tew, D.P. and Handy, N.C. *Chem. Phys. Lett.*, **2004**, 393, 51
- (16) Casida, M.E. and Hoix-Rotllant, M. *Annu. Rev. Phys. Chem.*, **2011**, 63, 1
- (17) Marques, M.A.L. and Gross, E.K.U. *Annu. Rev. Phys. Chem.*, **2004**, 55, 427
- (18) Maitra, N. T. *J. Chem. Phys.*, **2016**, 144, 220901
- (19) Bader, R.F.W. *Atoms in Molecules: A Quantum Theory*. Oxford University Press Inc. New York, New York (**2003**)
- (20) Matta, C.F. and Boyd, R.J. *The Quantum Theory of Atoms in Molecules: From Solid State to DNA and Drug Design*. Wiley-VCH, Weinheim, Germany (**2007**)
- (21) **NBO 6.0**. Glendening, E.D, Badenhoop, J.K, Reed A.E., Carpenter, J.E., Bohmann, J.A. Morales, C.M., Landis, C.R. and Weinhold, F. Theoretical Chemistry Institute, University of Wisconsin, Madison (**2013**).
- (22) Weinhold, F. and Landis, C. *Valency and Bonding: A Natural Bond Orbital Donor-Acceptor Perspective*. Cambridge University Press, Cambridge, United Kingdom (**2005**)
- (23) Glendening, E.D. and Weinhold, F. *J. Comp. Chem.*, **1998**, 19, 593
- (24) Glendening, E.D. and Weinhold, F. *J. Comp. Chem.*, **1998**, 19, 610
- (25) Glendening, E.D.; Badenhoop, J.K. and Weinhold, F. *J. Comp. Chem.*, **1998**, 19, 628

- (26) Thom, R. *Structural Stability and Morphogenesis: An Outline of a General Theory of Models*. W. A. Benjamin, Inc., Massachusetts. (1975)
- (27) Gilmore, R. *Catastrophe Theory for Scientists and Engineers*. Dover Publications, USA (1993).

## **CHAPTER THREE**

***Isothiirane: A Molecular Structure Dilemma Resolved***

This chapter has been published in the *Journal of Computational Chemistry*: S.M. Maley and R.C. Mawhinney, *J. Comput. Chem.*, 2018, doi: 10.1002/jcc.25758

## ABSTRACT

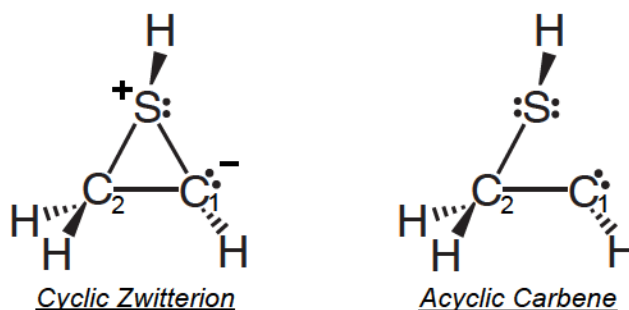
The electronic structure of molecules is routinely assessed using a number of methodologies including Bader's Quantum Theory of Atoms in Molecules (QTAIM) and Weinhold's Natural Bond Orbital/Natural Resonance Theory (NBO/NRT). Previously these methods were applied to the study of isothiirane, however, the results obtained were incongruous with one another: the QTAIM analysis suggested an acyclic structure while NRT indicated a cyclic structure. The previous results assume the NRT description to be correct despite limitations in the analysis, while Foroutan-Nejad et. al. employed a multiple molecular graph (MMG) analysis to resolve the QTAIM discrepancy. In this work we re-examine the electronic structure of isothiirane, employing a detailed NRT analysis and the catastrophe theory model originally described by Bader for the study of three-membered ring systems. Substituent effects are studied to obtain more detail about the electronic structure of the parent compound and gain insight into how its reactivity can be modified; additional analysis is performed using NMR tensor calculations. A congruous description of the electronic structure of isothiirane and the substituted versions is achieved using all modes of analysis. These results highlight how the careful application of commonly used methodologies can achieve a unified description of electronic structure, and the new view of bonding in isothiirane reveals that it may offer a means for incorporating sulfur in heterocycles.

### 3.1 – Introduction

The electronic structure of a molecule dictates its properties (geometry, reactivity, etc.) and its determination remains a busy field of study. Both theoreticians and experimentalists carry out electronic structure calculations in an effort to gain new information and chemical insight. Electronic structure calculations are routinely performed using *ab initio* wavefunction-based or Kohn-Sham density functional theory (DFT) methods.<sup>1</sup> According to the Hohenberg-Kohn theorems, all information about a chemical system is contained within its electron density.<sup>2</sup> Many methods for analyzing the electron density and extracting relevant information have been developed. They include such approaches as the *Quantum Theory of Atoms in Molecules* (QTAIM)<sup>3</sup>, *Natural Bond Orbital (NBO) and Natural Resonance Theory (NRT) Analysis*<sup>4</sup>, *Localized Orbital Locator (LOL) Method*<sup>5</sup>, and the *Electron Localization Function (ELF)*<sup>6</sup>. Methods for analyzing the electron density are expected to provide a congruent description of the electronic structure.

The electronic structure of (HS)(CH<sub>2</sub>)(CH) (isothiirane) was studied by Stalke *et. al.* in 2007<sup>7</sup>, Jacobsen in 2009<sup>8</sup> and Foroutan-Nejad *et. al.* in 2014.<sup>9</sup> Three analysis techniques were employed: QTAIM, NBO/NRT and LOL with varying degrees of agreement. NBO / NRT identified the structure of isothiirane as a ring (cyclic zwitterion – **Scheme 1**) with expansion weights of 78.4-87.8%. The QTAIM analysis varied with model chemistry, with the majority giving an acyclic structure and a Valence-Shell-Charge-Concentration (VSCC) on C<sub>1</sub> located in the H-C<sub>1</sub>-C<sub>2</sub> plane, consistent with an sp<sup>2</sup> type electronic structure and reminiscent of an acyclic carbene (**Scheme 3.1**). A few gave a ring structure, however, and it was noted that in these cases that the longer bond had a

lower electron density at the bond critical point (BCP) and hence a smaller bond order, contrary to the NBO/NRT results.<sup>10</sup> The LOL analysis provided a consistent description at all model chemistries and was congruent with the NBO / NRT analysis.



To account for the discrepancies in the QTAIM findings, Foroutan-Nejad *et. al.* presented a multiple molecular graph (MMG) approach as a means of accounting for the fact that the QTAIM picture is one where a structural change is occurring. However, the NBO / NRT results, which the previous authors assume to be correct based on chemical intuition, is still incongruent with the QTAIM results as no acyclic resonance structure was obtained. This discrepancy is the primary motivation behind the current study.

In this work we re-investigate the electronic structure of isothiirane to resolve the incongruous descriptions obtained previously. First, the structure of isothiirane is determined at the CCSD(T)/CBS<sub>Extrap</sub> level and the structures obtained previously using DFT and wavefunction based methods are compared. A QTAIM analysis is interpreted in the framework of catastrophe theory, originally applied by Bader to the understanding of the formation and destruction of three-membered ring systems.<sup>3,11</sup> NRT calculations are performed by manually specifying resonance structures for consideration to provide an unbiased assessment of electronic structure. NMR shielding tensor calculations are performed to gain additional insight into the local electronic structure of the C<sub>1</sub> nucleus.

Finally, substituent effects are explored to provide a more robust assessment of the electronic structure of the parent compound. It is shown that a congruous description of the electronic structure of isothiirane is possible with all modalities of analysis.

### **3.2 – Methodology**

The structure of (HS)(CH<sub>2</sub>)(CH) was optimized at the CCSD(T)/aug-cc-pvNZ (N = D, T, Q) level using Molpro<sup>12</sup> and a three-point extrapolation to the complete basis set (CBS) limit<sup>13</sup> was performed for the geometric parameters of the heavy atoms. Optimization, frequency, stability and NMR (GIAO) calculations were performed at the DFT level (B3LYP<sup>14</sup>, B3PW91<sup>15</sup>, PBE0<sup>16</sup>) with a triple-zeta Pople style basis set (6-311++g) with varying polarization functions (BS1: (d,p), BS2: (2d,2p), BS3: (2df,pd)) in Gaussian09 Rev. D.01.<sup>17</sup> The structure was also optimized at the MP2 / BS1 level of theory to re-assess one of the results of Stalke *et. al.*<sup>7</sup> Analysis of the electron density topology according to QTAIM was performed using AIMAll<sup>18</sup> and Multiwfn.<sup>19</sup> NBO and NRT calculations were performed using NBO 6.0.<sup>20</sup> Additional resonance structures are included in the NRT analysis using the \$NRTSTR keyword. Displaced geometries from the lowest vibrational mode were obtained using a step size (in Angstroms) of 0.1 with a refined step of 0.01 to locate the positions of the singularity.

### **3.3 – Results and Discussion**

#### **3.3.1 – The Structure of Isothiirane**

At the heart of the problem is the S-C<sub>1</sub> interaction, which is geometrically dictated by the size of the ring and the SC<sub>2</sub>C<sub>1</sub> angle. In order to obtain a high quality estimate of the true geometry of (HS)(CH<sub>2</sub>)(CH), optimizations were performed at the CCSD(T)/aug-cc-pvNZ (N = D, T, Q) levels of theory. The geometric parameters of the heavy atoms

were then extrapolated to the complete basis set (CBS) limit. These are compiled in Table 3.1 (values from all other model chemistries available in Table A1). Overall, the sum of the bond lengths in the ring are reduced by 0.159Å (3%) with extrapolation. S-C<sub>1</sub> decreases by 0.097Å (4.9%), S-C<sub>2</sub> by 0.046Å (2.4%), and C<sub>1</sub>-C<sub>2</sub> by only 0.016Å (1%). The final extrapolated structure has values of 1.898Å (S-C<sub>1</sub>), 1.838Å (S-C<sub>2</sub>), and 1.480Å (C<sub>1</sub>-C<sub>2</sub>). The SC<sub>2</sub>C<sub>1</sub> angle decreases from 71.4° to 68.9°, while the C<sub>2</sub>SC<sub>1</sub> and SC<sub>1</sub>C<sub>2</sub> angle increase slightly by 0.4° and 1.4°, respectively.

**Table 3.1:** Heavy atom geometrical parameters obtained at the CCSD(T)/aug-cc-pvNZ (N= D, T, Q) level and their CBS extrapolated values. Bond lengths (R) and perimeter (P) in Å, angles (A) in degrees.

	R(S-C <sub>1</sub> )	R(S-C <sub>2</sub> )	R(C <sub>1</sub> -C <sub>2</sub> )	P	A (SC <sub>2</sub> C <sub>1</sub> )	A(C <sub>2</sub> SC <sub>1</sub> )	A(SC <sub>1</sub> C <sub>2</sub> )
aug-cc-pvDZ	1.995	1.884	1.496	5.375	71.4	46.2	63.3
aug-cc-pvTZ	1.919	1.848	1.484	5.251	69.2	46.3	64.2
aug-cc-pvQZ	1.903	1.840	1.480	5.223	69.0	46.5	64.5
CBS <sub>Extrap</sub> <sup>1</sup>	1.898	1.838	1.480	5.216	68.9	46.6	64.7

1. Plots given in Appendix A Figures 1.1A–F

All of the methods tested by us and the previous authors overestimate S–C<sub>2</sub> and underestimate C<sub>1</sub>–C<sub>2</sub>, relative to the CCSD(T)/CBS<sub>Extrap</sub> structure. S–C<sub>1</sub> is overestimated by all methods used by both Stalke *et. al.* and Jacobsen, as well as most methods employed by us (exceptions are B3PW91 and PBE0 in combination with BS3 and PBE0 in combination with BS2). SC<sub>2</sub>C<sub>1</sub> is overestimated by B3LYP, B3PW91 and PBE in combination with BS1 as well as all the other model chemistries tested by Stalke *et. al.* and Jacobsen. The rest of the methods tested by us underestimate the angle. SC<sub>1</sub>C<sub>2</sub> is overestimated by all methods except HF and CISD in combination with BS1 and CCSD and B3PW91 in combination with TZVP. C<sub>2</sub>SC<sub>1</sub> is underestimated by all methods except B3PW91 in combination with BS2 and BS3 as well as PBE0 in combination with BS2 and BS3; PBE0 in combination with BS1 predicted the CBS value exactly. The methods that

best reproduce the CCSD(T)/CBS<sub>Extrap</sub> geometry are MP2 / BS1, B3PW91 / BS2 and PBE0 / BS1.

### 3.3.2 – Characteristics of the Electron Density

Isothiirane can exhibit two molecular graphs depending on model chemistry.<sup>7,8</sup> Whether a ring is observed is related to the amount of electron density brought to the area by its constituent atoms (a constant for a given molecule), the size of the triangle formed by the three atoms (perimeter and/or area), and the amount of the electron density along an edge (related to distance or opposite angle). In **Figure 3.1** the relationship between the SC<sub>2</sub>C<sub>1</sub> angle, ring perimeter and detection of a ring structure in isothiirane is visualized.

The majority of model chemistries fall in region 1 of **Figure 3.1**, where the SC<sub>2</sub>C<sub>1</sub> angle and perimeter are greater than the CBS<sub>Extrap</sub> values. With the exception of BP86/TZVP these model chemistries predict an acyclic structure.

A ring is predicted by 2 additional model chemistries (MP2/BS1<sup>21</sup> and PBE/TZVP) that fall in region 2 (smaller SC<sub>2</sub>C<sub>1</sub> angle but greater perimeter than CBS<sub>Extrap</sub>) and 4 model chemistries (B3PW91/BS2 or BS3 and PBE0/BS2 or BS3) that fall in region 3 (SC<sub>2</sub>C<sub>1</sub> angle and perimeter less than CBS<sub>Extrap</sub>) of **Figure 3.1**.

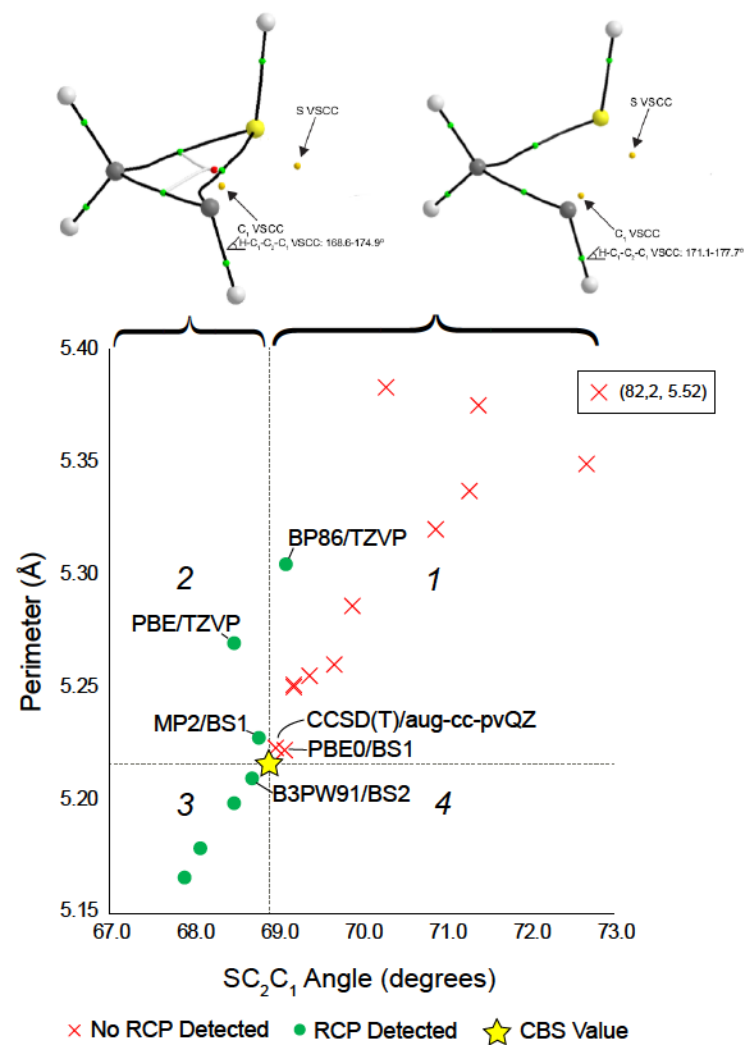
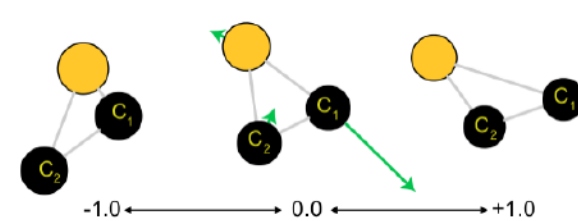


**Figure 3.1:** Plot of SC<sub>2</sub>C<sub>1</sub> angle (degrees) and perimeter of the ring formed by the heavy atoms (Angstroms). Circles – RCP detected. X's – No RCP detected. Star – CCSD(T)/CBSExtrap value. Inset box: HF/BS1 (off scale). Above: Example molecular graphs for cyclic and acyclic structure. Green circles – BCPs. Red circle – RCP

The CBS<sub>Extrap</sub> structure appears to be the boundary between the acyclic and cyclic structures. This is consistent with Jacobsen's conclusion regarding the geometry.<sup>8</sup> As shown in **Figure 3.1**, the ring critical point (RCP, green circle), when detected, lies close to the S-C<sub>1</sub> bond critical point (BCP, red circles) and the S-C<sub>1</sub> bond path is highly curved inward. This is an indicator of structural instability.

The stability of critical points (CPs) can be assessed by examining the second derivative matrix of  $\rho(r)$ , which when diagonalized returns three eigenvalues that reflect the curvature of the electron density at the CP. The extent to which the electron density is accumulated in a particular plane of the CP is determined by the ellipticity ( $\varepsilon$ ) of the CP. When detected, the ellipticity of the RCP ( $\varepsilon = 1.75$  to  $42.25$  – Appendix A Table A.3) is indicative of a topologically unstable structure susceptible to rupture via change in geometry,<sup>3,22</sup> while that for the more familiar tautomer, thiirane, suggests a topologically stable structure ( $\varepsilon = 0.50$  to  $0.76$ ). To examine this further, we have employed the approach of Foroutan-Nejad *et. al.*<sup>9</sup> for creating displaced geometries along the entirety of the lowest energy ring-opening mode (**Scheme 3.2** – wavenumbers available in Appendix A Table A.4).



**Scheme 3.2**

As the geometry is displaced in the -1.0 direction the S nucleus moves towards C<sub>1</sub>, decreasing the S-C<sub>1</sub> distance and perimeter. In the opposite (+1.0) direction the S nucleus moves away from C<sub>1</sub>, increasing the S-C<sub>1</sub> distance and perimeter. The S-C<sub>2</sub> distance

does not change significantly, however the  $SC_1C_2$  angle increases in  $-1.0$  direction and decreases in the  $+1.0$  direction. Analyzing the electron density at each step allows us to define the approximate region where the ring structure exists. The relevant data is presented in **Figure 3.2** for B3PW91/BS2 and PBE0/BS1, the model chemistries immediately surrounding the CCSD(T)/CBS<sub>Extrap</sub> value in **Figure 3.1**.

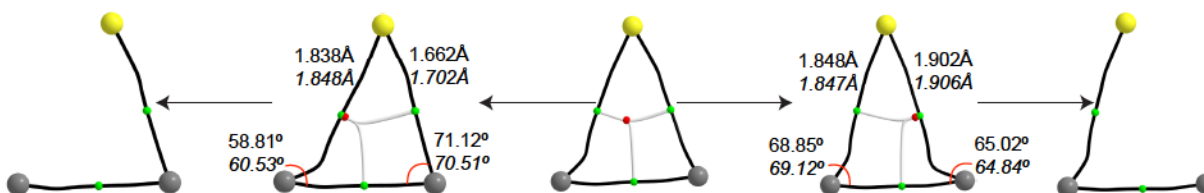


**Figure 3.2:** Example MG's for a ring structure (centre), topologically unstable ring structures, and acyclic structures (outermost). Geometric parameters presented for B3PW91/BS2 and PBE0/BS1. Hydrogen atoms removed for clarity.

As shown in **Figure 3.2**, there are more than 2 MG's for describing the topological features of isothirane. To understand this structural change in three-membered rings (3MR's) we use catastrophe theory as described almost forty years ago.<sup>11</sup>

As detailed by Bader et al, the structural stability of 3MR's can be described in terms of the unfolding of the elliptic umbilic (EU) catastrophe (Equation 1). In equation 1  $u$ ,  $v$  and  $w$  are control parameters describing how sensitive the topology is to configuration space ( $y, z$  nuclear motion) and the amount of electron density ( $w$ ). Here we provide an analysis of the ring structure region in both isothirane and thirane, the later chosen because of its structural similarity and because  $C_{2v}$  symmetry allows for analytical solutions.

$$f(y, z; w, y, v) = y^2z - \frac{z}{3} + wy^2 - uy - vz \quad (3.1)$$

### 3.3.3 – The Elliptic Umbilic

For thiirane, a singularity in  $\rho$  can be located by moving the S nucleus along the  $C_2$  ( $z$ ) axis. This point is referred to as the bifurcation point and the set of structures containing such a point is referred to as the catastrophe set. The singularity is chosen as the origin of both the molecular plane ( $y,z$ ) and the control space ( $u$  and  $v$  both equal 0) and the EU is unfolded from this point. The case of thiirane is similar to that of water ( $C_{2v}$ ,  $w \neq 0$ )<sup>11</sup> and we know that a ring exists for particular values of  $u$ ,  $v$  and  $w$ , as displayed in

**Figure 3.3.**

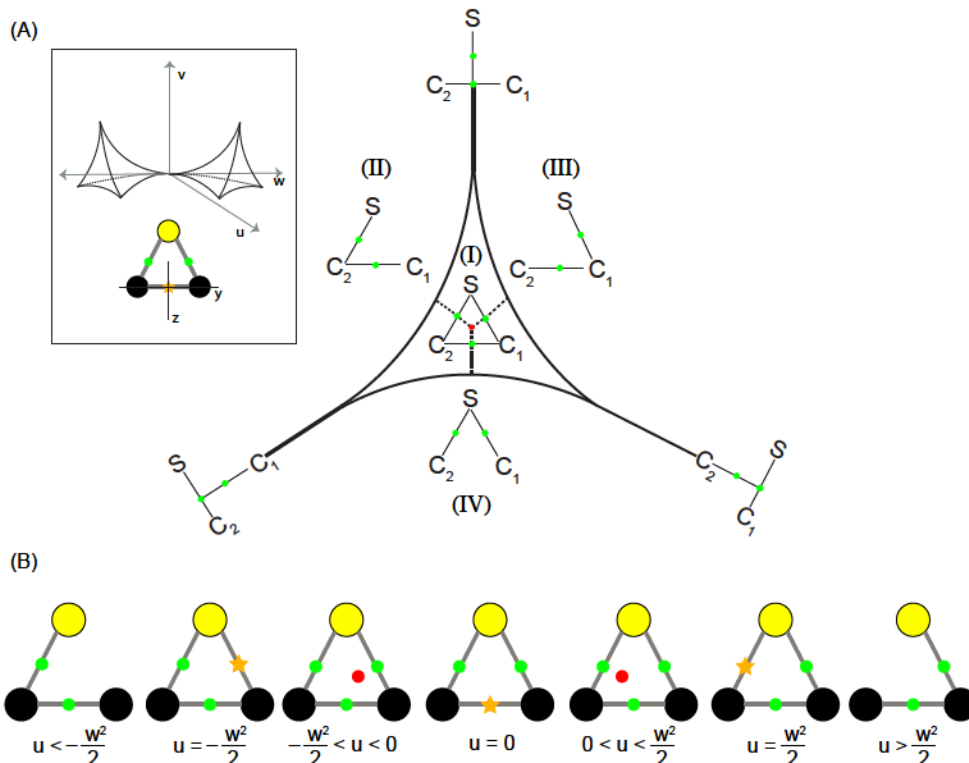


**Figure 3.3:** (A) Representation of the structure diagram of the S-C<sub>2</sub>-C<sub>1</sub> system showing the possible cyclic (Region I) and acyclic structures (Regions II–IV). The hypocycloid shape defines the catastrophe set. Inset box: Catastrophe set described by Equation 1 and definition of axes. (B) Prediction of the unfolding the elliptic umbilic for motion along  $y$ -axis with  $v=0$ .

The unfolding of the EU predicts four possible stable structures for the S-C<sub>2</sub>-C<sub>1</sub> system. Three corresponding to an acyclic structure (Regions II, III and IV) and one to a

cyclic structure (Region I). Specific values of  $y$ ,  $v$  and  $w$  define the size of the hypocycloid region of the structure diagram (**Figure 3.3**), which dictates when a ring structure is detected.

In the case of isothiirane the lack of a  $C_2$  symmetry axis makes an analytical description difficult. However, the general features of the EU are preserved. There are still three control variables that are affected by the nuclear motion in configuration space, and there are still three acyclic and one cyclic structure possible. Scans along the normal mode as described in **Figure 3.2** provide an approximate tracing of the EU, with the nuclear motion in configuration space combined in the vibrational mode.

As the structure is displaced in the +1.0 direction (**Scheme 3.2**) the RCP approaches the S-C<sub>1</sub> BCP (**Figure 3.3**:  $-w^2 / 2 < u < 0$ ) until the catastrophe point is reached (**Figure 3.2**: II or **Figure 3.3**:  $u = -w^2 / 2$ ). Beyond this point the acyclic MG that may be described as a carbene is obtained (**Figure 3.2** III or **Figure 3.3**:  $u < -w^2/2$ ). Conversely, as the structure is displaced in the -1.0 direction (**Scheme 3.2**) the RCP approaches the S-C<sub>2</sub> BCP (**Figure 3.3**:  $0 < u < w^2 / 2$ ) until the other catastrophe point is reached (**Figure 3.2**: IV or **Figure 3.3**:  $u = w^2 / 2$ ). Beyond this point another acyclic structure, corresponding to an ethenylthiol type structure, is obtained (**Figure 3.2**: V or **Figure 3.3**:  $u > w^2/2$ ). The third acyclic structure (Region IV) is not obtained in our analysis as this would require a different mode scan. The region the ring exists within for each model chemistry is bounded by the values obtained at the catastrophe points (**Figure 3.2**).

The model chemistries presented in **Figure 3.1** can be categorized using the EU model. Those displaying a cyclic structure fall in a region of the EU between  $-w^2 / 2 < u <$

0 and  $0 > u > w^2 / 2$ . The remaining model chemistries fall within the  $u < -w^2 / 2$  region of the EU. The application of the EU to understanding the topological features of isothiirane uncovers four possible structures, not just the two of Foroutan-Nejad *et. al.*<sup>9</sup>

### 3.3.4 – Natural Resonance Theory

The four resonance structures of isothiirane identified by Stalke *et. al.* along with the additional structure identified by us from unfolding the EU (RS-I) are presented in **Figure 3.4**. RS-B and RS-C are the most relevant equilibrium descriptors in light of the equilibrium QTAIM description.

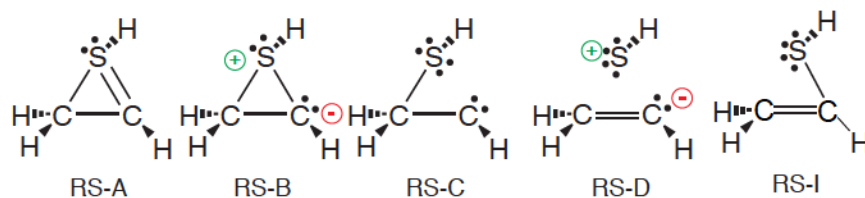


**Figure 3.4:** Possible resonance structures for (HS)(CH<sub>2</sub>)(CH)

Previous studies indicated that the electronic structure of isothiirane was primarily described by RS-B.<sup>7,8</sup> However, a greater bond order was assigned to the longer S-C<sub>1</sub> distance and RS-C was not detected when the default mode of the program was used. For a more accurate analysis, different RS descriptions that consider each of the resonance structures of interest are tested so that the best one is chosen.

In this study we varied the choice of NRT input structure, with all combinations of resonance structures tested at the B3PW91/BS2 level. The expansion weights and natural bond orders are collected in **Table 3.2** (results obtained for all other model chemistries using the default algorithm are available in Appendix A Table A.5). For comparison, thiirane was studied using the default mode. The NRT expansion of thiirane was dominated by a resonance structure corresponding to a cyclic species with identical

bond orders assigned to the S-C distances (Appendix A Table A.6). This description is congruent with the one provided by QTAIM.

Using RS-B as input yields the same NRT expansion as the default algorithm. With RS-C as input, the weights of RS-B and RS-D are reduced to 25.7% and 2.3%, respectively, and RS-C is now the leading structure with a weight of 55.7%. Interestingly, the resonance structure corresponding to an isomerized (ethenylthiol) species (RS-I) was identified with a weight of 15.3%, consistent with the EU picture. RS-D as input gives a resonance expansion where RS-C is the leading structure (48.1%) and RS-D and RS-I also contribute with weights of 21.8% and 28.0% respectively – RS-B is no longer a significant resonance contributor.

**Table 3.2:** NRT Expansion weights (%) and natural bond orders for isothirane obtained using all combinations of input. Calculated at B3PW91/BS2 level (Data for all other model chemistries available in Appendix A Table A.5)

	%B	%C	%D	%I	%O	S-C <sub>1</sub>	S-C <sub>2</sub>	C <sub>1</sub> -C <sub>2</sub>
Default	94.6	-	5.4	-	-	0.946	0.946	1.109
B	94.6	-	5.4	-	-	0.946	0.946	1.109
C	25.7	55.7	2.3	15.3	1.0	0.387	0.824	1.057
D	0.3	48.1	21.7	28	1.9	0.292	0.490	1.296
BC	85.1	7.9	7.0	-	-	0.872	0.930	1.102
BD	78.8	8.0	12.8	0.2	0.2	0.837	0.870	1.140
CD	17.2	56.3	7.5	18.9	0.1	0.362	0.735	1.120
BCD	78.8	8.1	12.9	-	0.2	0.837	0.870	1.140

Combining RS-B and RS-C (RS-B,C) gives an NRT expansion with the largest contribution from RS-B(85.1%), and smaller contributions from RS-C (8.0%) and RS-D (7.0%). RS-B,D yields an NRT expansion similar to RS-B,C with RS-B as the leading structure (78.8%), and RS-D and RS-C with weights of 12.8% and 8.0% respectively. RS-C,D is led by RS-C (56.3%), RS-I and RS-B have similar weights of 18.9% and 17.2%, respectively, while RS-D has a weight of 7.5%. Combining all three (RS-B,C,D) yields an almost identical results as the one obtained using RS-B,D.

As noted earlier (Section 3.3.1), at all levels of theory  $R_{SC1}$  is longer than  $R_{SC2}$ . At the B3PW91/BS2 level the difference is 0.041 Å, which equates roughly to a difference in bond order of 0.026 based on the Schomaker-Stevenson relationship<sup>23,24</sup> (Appendix A Table A.7) and a difference in delocalization index of 0.027 (Appendix A Table A.8).

The description of the S-C bond order in isothiirane provided by the default NRT calculation is poor, assigning identical values to both. The C/D/C,D descriptions over exaggerate the difference and underestimate the actual bond order. The  $\Delta BO_{NRT}$  obtained with RS-B,D or RS-B,C,D (0.033) are closest to the other measures, but RS-B,C also provides a close fit (0.058)

### 3.3.5 – Substituent Effects

The electronic structure of isothiirane at equilibrium can best be described as a hybrid of the acyclic carbene and cyclic zwitterion species, but it is a precarious balance. To further solidify this assessment, we have varied the substituents on S( $R^1$ ) and C<sub>1</sub>( $R^2$ ). Encouraging donation to the C<sub>1</sub> p-orbital should stabilize the carbene and enhance the acyclic structure, while encouraging sulfur to donate to C<sub>1</sub> or withdrawing density from C<sub>1</sub> should favour the cyclic structure. Here we explore this with a series of substituents chosen accordingly. In this section all geometries were optimized at the B3PW91 / BS2 level of theory as it reproduced the reference geometry most closely. Frequency calculations were performed on the optimized geometries to confirm they are minima.

#### *3.3.5.1 – Structural Changes*

The general effects of substitution on the geometric parameters (bond lengths and angles **Table 3.3**) of the parent compound are as follows: with only a few exceptions, electron donating groups on S result in a reduction in the SC<sub>2</sub>C<sub>1</sub> angle, a shortening of

the C<sub>1</sub>-C<sub>2</sub> distance and an increase in the S-C<sub>2</sub> distance, causing it to become larger than S-C<sub>1</sub>. The electron withdrawing substituents used can be separated into two groups: C-containing and halogens. The C-containing substituents result in S-C<sub>1</sub> distances and SC<sub>2</sub>C<sub>1</sub> angles that are similar to the parent compound. On the other hand, halogen substitution results in an increase in the S-C<sub>1</sub> distance and SC<sub>2</sub>C<sub>1</sub> angle and decrease in the S-C<sub>2</sub> distance. Electron donating substituents on C<sub>1</sub> generally resulted in the SC<sub>2</sub>C<sub>1</sub> angle and S-C<sub>1</sub> distance increasing.

Substituents that increase electron density on S also act to donate electron density to C<sub>1</sub>. When both the S and C<sub>1</sub> positions are substituted with the same substituent there is competition whether the S or C<sub>1</sub>-substituted structure is preferred. When the H on S is substituted with NC, NCS, OH, SCN and SeH the SC<sub>2</sub>C<sub>1</sub> angle decreases significantly and when placed in the C<sub>1</sub> position this angle greatly increased. When both positions are substituted with the same substituent the resulting structure of the SC<sub>2</sub>C<sub>1</sub> backbone is homologous to the C<sub>1</sub> substituted structure.

**Table 3.3:** Interatomic distances (Å) and angles(°) for SC<sub>2</sub>C<sub>1</sub> backbone of substituted series.

	S(R <sup>1</sup> )	C <sub>1</sub> (R <sup>2</sup> )	R(S-C <sub>1</sub> )	R(S-C <sub>2</sub> )	R(C <sub>1</sub> -C <sub>2</sub> )	Perimeter	A(SC <sub>2</sub> C <sub>1</sub> )	A(SC <sub>1</sub> C <sub>2</sub> )	A(C <sub>2</sub> SC <sub>1</sub> )
	H	H	1.890	1.849	1.470	5.209	68.7	46.2	65.1
S-EDG	CH <sub>3</sub>	H	1.850	1.831	1.478	5.159	67.0	66.6	47.3
	NH <sub>2</sub>	H	1.772	1.833	1.478	5.083	63.6	68.0	48.4
	NC	H	1.762	2.697	1.326	5.784	34.0	121.0	24.2
	NCS	H	1.770	2.710	1.330	5.810	33.7	121.6	24.7
	OH	H	1.748	2.707	1.330	5.786	33.0	122.5	24.5
	PH <sub>2</sub>	H	1.881	1.856	1.465	5.202	67.8	66.0	46.2
	SH	H	1.770	2.720	1.330	5.820	33.5	122.1	24.4
	SCN	H	1.765	2.696	1.327	5.788	34.2	120.7	25.0
	SeH	H	1.766	2.712	1.328	5.806	33.6	121.9	24.6
C <sub>1</sub> -EWG	H	CCl <sub>3</sub>	1.885	1.860	1.454	5.199	68.0	66.3	45.7
	H	CF <sub>3</sub>	1.874	1.856	1.459	5.189	67.6	66.3	46.1
	H	CN	1.901	1.856	1.461	5.218	68.7	65.5	45.7
	H	CHO	1.817	1.876	1.442	5.135	64.9	69.2	45.9
	H	SiH <sub>3</sub>	1.832	1.845	1.459	5.136	66.2	67.1	46.7
	H	CH <sub>3</sub>	1.978	1.853	1.461	5.291	63.1	72.2	44.7
	H	F	2.324	1.840	1.487	5.651	88.0	52.3	39.7
	H	Cl	2.115	1.846	1.475	5.436	78.2	58.7	43.0
	H	Br	2.043	1.847	1.474	5.364	75.0	60.8	44.2
C <sub>1</sub> -EDG	H	NH <sub>2</sub>	2.676	1.833	1.496	6.005	106.6	41.0	32.4
	H	NC	2.093	1.849	1.470	5.412	77.3	59.5	43.2
	H	NCS	2.518	1.838	1.488	5.844	97.8	46.3	35.8
	H	OH	2.579	1.834	1.495	5.908	101.1	44.2	34.7
	H	PH <sub>2</sub>	1.893	1.854	1.454	5.201	68.6	65.8	45.7
	H	SH	2.599	1.837	1.492	5.928	102.1	43.7	34.2
	H	SCN	2.511	1.841	1.467	5.819	98.2	46.5	35.3
	H	SeH	2.580	1.840	1.478	5.898	101.5	44.3	34.2
S-EDG + C <sub>1</sub> -EDG	CH <sub>3</sub>	CH <sub>3</sub>	1.901	1.836	1.468	5.205	69.2	64.6	46.2
	NH <sub>2</sub>	NH <sub>2</sub>	2.687	1.829	1.493	6.009	107.6	40.4	32.0
	NC	NC	1.954	1.856	1.467	5.277	70.9	63.9	45.2
	NCS	NCS	2.505	1.842	1.487	5.834	97.1	46.8	36.1
	OH	OH	2.444	1.827	1.488	5.759	94.4	48.2	37.4
	PH <sub>2</sub>	PH <sub>2</sub>	1.926	1.855	1.460	5.241	69.9	64.7	45.4
	SH	SH	1.779	2.682	1.334	5.794	35.7	118.3	26.0
	SCN	SCN	2.600	1.847	1.468	5.915	102.7	43.9	33.4
	SeH	SeH	2.582	1.850	1.475	5.907	101.3	44.6	34.1

### 3.3.5.2 – Characteristics of the Electron Density Topology

The type of MG obtained for each substituent pair is presented in **Figure 3.5**. Detection of a ring structure is related to the ring perimeter and amount of electron density along the S-C<sub>1</sub> distance (Appendix A Figure A.2). With the exception of CH<sub>3</sub>, NH<sub>2</sub> and PH<sub>2</sub>, which all exhibit the expected cyclic MG (**Figure 3.5** – Region I), all electron donating substituents on S result in isomerization (**Figure 3.5** – Region III, see SI-Figure 3 for a sample MG). All electron withdrawing substituents on C<sub>1</sub> result in a cyclic MG as expected. Electron donating substituents in the C<sub>1</sub> position result in the expected acyclic carbene molecular graph (**Figure 3.5** – Region II). Halogen substitution in the C<sub>1</sub> position also resulted in acyclic carbene MGs, contrary to what is expected for electron withdrawing substituents, but consistent with halogens acting as  $\pi$ -donors, thus stabilizing the carbene. The bisubstituted cases result in acyclic carbene MG's, with the exception of CH<sub>3</sub> and SH which resulted in cyclic and isomerized MG's, respectively. The VSCC adjacent to C<sub>1</sub> differentiates between Region I and II, with the latter situated closer to the nucleus and having a greater magnitude, while the former displays the opposite trend (Appendix A Figure A.4)

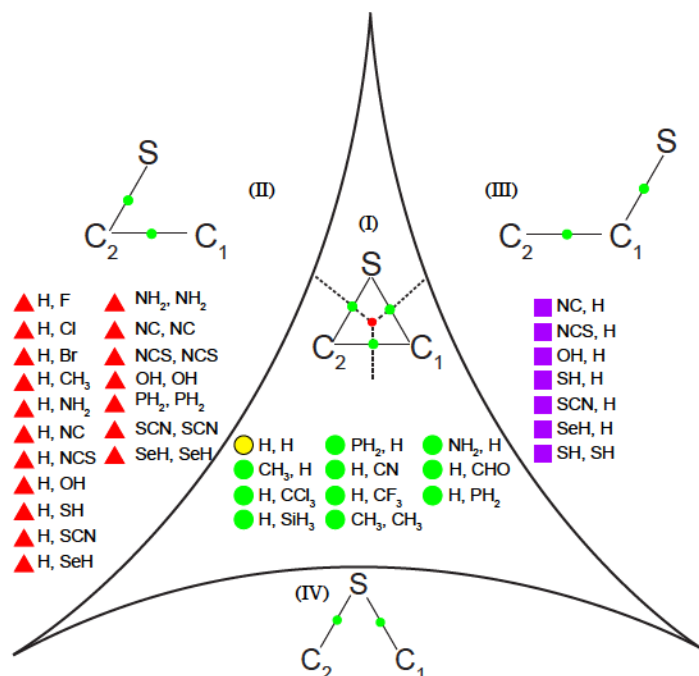


**Figure 3.5:** Backbone structure obtained for each substituent at the B3PW91 / BS2 level of theory. Substituents listed in order of attachment to S and C<sub>1</sub>. Triangles – acyclic carbene MG. Circles – cyclic zwitterion MG. Squares – Ethenylthiol type MG.

Ten cyclic MG's were obtained with substitution. The ellipticities of the RCP and S-C<sub>1</sub> and S-C<sub>2</sub> BCP's for these cases are collected in **Table 3.4**. With the exception of R<sup>1</sup>=NH<sub>2</sub>, the ellipticities are all greater than 1.0, indicating a topologically unstable structure. However, as expected, the ring structure is stabilized by the chosen substituents and the ellipticities of the RCP are lower than that of the parent compound. Furthermore, where the structure is located within the cyclic hypocycloid can be monitored by comparing the S-C<sub>1</sub> and S-C<sub>2</sub> BCP ellipticities. The ellipticities of the S-C<sub>2</sub> BCP's are greater than the S-C<sub>1</sub> BCP's for R<sup>1</sup>=CHO or SiH<sub>3</sub> and R<sup>2</sup>=NH<sub>2</sub>, while the opposite is true for the majority of other substituents. When  $\varepsilon_{S-C_1} > \varepsilon_{S-C_2}$  the structure exists in a region of the elliptic umbilic where  $0 < u < w^2 / 2$  and, conversely, when  $\varepsilon_{S-C_1} < \varepsilon_{S-C_2}$  the structure exists in the  $-w^2 / 2 < u < 0$  region (**Figure 3.3B**).

**Table 3.4:** Ellipticities of the RCPs, and S-C BCPs for the rings listed in Figure 6. Calculated at the B3PW91 / BS 2 level.

S, C <sub>1</sub>	$\epsilon$ S-C <sub>2</sub> BCP	$\epsilon$ SC <sub>2</sub> C <sub>1</sub> RCP	$\epsilon$ S-C <sub>1</sub> BCP
H, H	0.705	6.187	5.972
CH <sub>3</sub> , H	0.724	1.230	1.023
CH <sub>3</sub> , CH <sub>3</sub>	0.605	4.046	3.912
H, PH <sub>2</sub>	0.711	2.738	2.488
PH <sub>2</sub> , H	0.787	2.180	1.893
NH <sub>2</sub> , H	0.977	0.802	0.369
H, CN	0.679	2.650	2.436
H, CHO	1.303	1.351	0.485
H, SiH <sub>3</sub>	0.895	1.207	0.764
H, CF <sub>3</sub>	0.826	1.729	1.395
H, CCl <sub>3</sub>	0.775	1.854	1.553

### 3.3.5.3 – A Robust NRT Description

NRT calculations using various input structures according to **Figure 3.4** were performed for all 28 molecules characterized as either an acyclic carbene or cyclic zwitterion (**Figure 3.5**) and the expansion weights assessed (Appendix A Tables A.10-13). The resulting bond orders were analyzed to ensure the longer S-C distance was assigned a smaller bond order. Linear bond order – bond length relationships (Appendix A Figure A.5 for example based on RS-BC expansion) were tested for the datasets obtained using RS-BC, BS-BD and RS-BCD. The correlation coefficients for the bond order – bond length relationships are presented in **Table 3.5**.

All resonance expansions poorly describe S-C<sub>2</sub>, this is unsurprising given the small range of bond length values (1.827 to 1.876Å). The best overall description is obtained with RS-BC and the parent compound is best described as a hybrid of the cyclic structure (RS-B: 85.1%) and the acyclic structure (RS-C: 8.0%)

**Table 3.5:** Linear correlation coefficients for bond order-bond length relationships based on bond orders from NRT analysis of substituted series.<sup>1</sup> B3PW91/BS2

	S-C <sub>1</sub>	S-C <sub>2</sub>	S-C <sub>1</sub> +C <sub>2</sub>	C <sub>1</sub> -C <sub>2</sub>
RS-BC	0.925	0.190	0.947	0.604
RS-BD	0.722	0.162	0.657	0.394
RS-BCD	0.906	0.443	0.932	0.573

1. When structures are manually specified, the program first determines a set of corresponding NBO's. If NBO's corresponding to the given resonance structure cannot be found the calculation terminates. S-substituted with CH<sub>3</sub> and PH<sub>2</sub> and C<sub>1</sub>-substituted with Br had this error and are removed from the datasets.

The relationship between %RS-B, %RS-C and the ring perimeter (Appendix A Figure A.7) shows that substituents resulting in a cyclic MG have RS-B ranging from 82 to 95% and RS-C less than 10%. Conversely, substituents resulting in an acyclic MG have RS-B ranging from 1 to 79% and RS-C ranging from 13 to 96%. The acyclic MG is preferred once RS-C reaches ~10%. In the acyclic form, RS-B can be attributed to a 1,3-dipole, suggesting that isothirane may participate in cycloaddition reactions.

#### 3.3.5.4 – NMR Shielding Tensor

The <sup>13</sup>C NMR shielding tensors for the C<sub>1</sub> nuclei are available in Appendix A Table A.14. Substituents resulting in an acyclic MG have tensor components more consistent with a carbene (Details about shielding tensor analysis available in Appendix A). In these cases,  $\sigma_{xx}$  shows more (in some cases considerably more) deshielding than the unsubstituted parent. Halogen substituents on C<sub>1</sub> result in tensors consistent with a carbene, increasing in deshielding in the order of Br < Cl < F, confirming their activity as  $\pi$ -donors.

The amount of deshielding at the C<sub>1</sub> nucleus is roughly related to the perimeter of the ring (**Figure 3.6**), implying that the SC<sub>2</sub>C<sub>1</sub> angle, which controls the perimeter

(Appendix A Figure A.6), strongly influences the electronic structure. Four cases,  $R^1 = H$ ,  $R^2 = NCS$  and  $NH_2$  and  $R^1 = R^2 = NC$  and  $NH_2$  were found to be outliers. The large deshielding of  $\sigma_{xx}$  in the  $R^2 = NCS$  case is due to the small magnitude of the singlet-triplet gap ( $\Delta E_{ST}$ : +2.69kcal/mol). The  $R^1 = H$ ,  $R^2 = NH_2$ ,  $R^1 = R^2 = NH_2$ , and  $R^1 = R^2 = NC$  cases have %RS C of 96.25, 92.41, and 55.39 respectively. When the outliers are removed, the relationship between  $\sigma_{xx}$  deshielding and ring perimeter is strengthened.

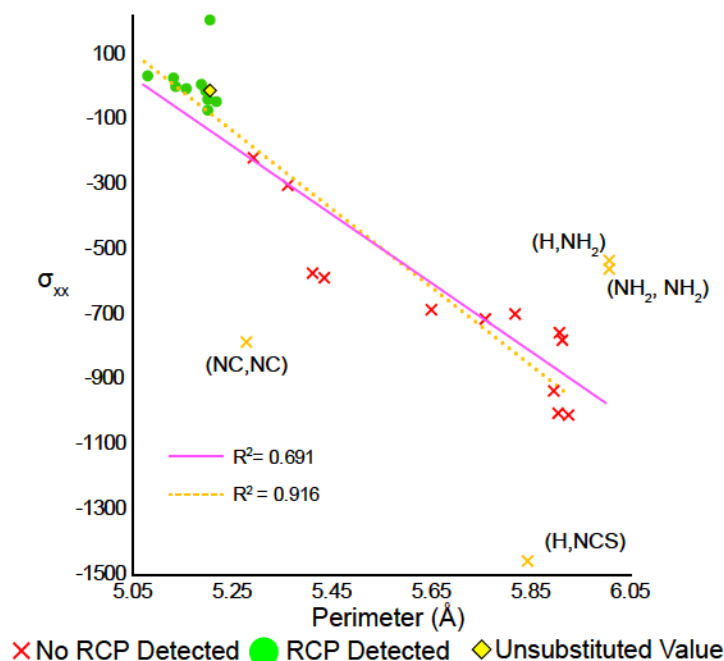


**Figure 3.6:**  $\sigma_{xx}$  component of the  $^{13}C_1$  NMR chemical shielding tensor as a function of the ring perimeter. Solid line: linear regression of all data points ( $R^2$ :0.691). Dashed line: linear regression of dataset with outliers removed ( $R^2$ : 0.916). Green markers – RCP detected. Red markers – No RCP Detected. Yellow marker – Unsubstituted value. Orange markers – outliers. B3PW91/BS 2.

### 3.3.5.5 – A Congruent Description of Electronic Structure

In **Figure 3.7**, the relationship between key descriptors from each modality is presented. Systems displaying acyclic MGs exhibit greater weights of RS-C, larger deshielding of  $\sigma_{xx}$  and a VSCC of lower magnitude. Conversely, systems having a cyclic MG have a lower weight of RS-C,  $\sigma_{xx}$  values close to zero and a VSCC of greater

magnitude. The cyclic structure is predicted to exist in only a small region by the unfolding of the elliptic umbilic, as reflected by the tight clustering of data points belonging to systems displaying cyclic MG's. On the other hand, the unfolding of the elliptic umbilic predicts a large region for the acyclic structure to exist in, and at the far end of this region the system is actually a stable singlet carbene. This allows for more variability in their description as demonstrated by the broad distribution of data points belonging to systems with acyclic MG's.

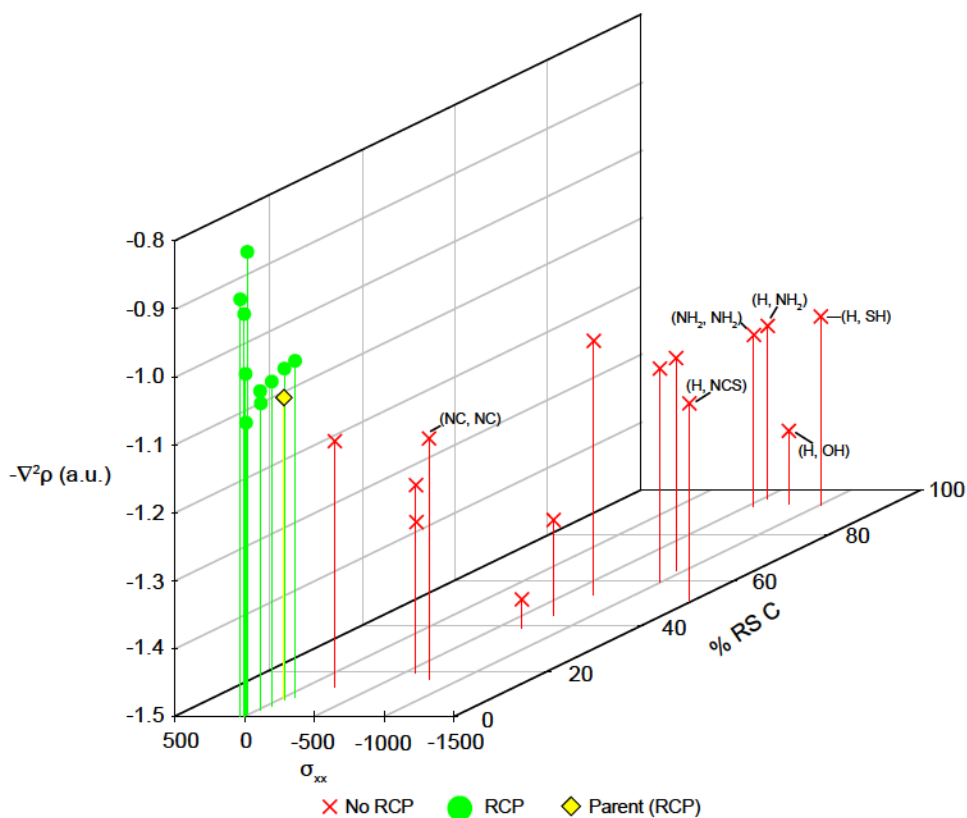


**Figure 3.7:** A comparison between three key descriptors (Magnitude of  $C_1$  VSCC, value of the  $\sigma_{xx}$  component of the  $^{13}\text{C}$  NMR chemical shielding tensor, and %RS-C obtained from the NRT RS-B,C analysis) of the electronic structure. Green markers – RCP detected. Red markers – No RCP Detected. Yellow marker – Unsubstituted value. Calculated at the B3PW91/BS 2 level.

As **Figure 3.7** details, the electronic structure of isothiirane can be tuned through substitution and modifying their donor/acceptor abilities may result in carbenic and/or 1,3-dipole reactivity. This makes isothiirane a molecule with potential value in [1+2] or [3+2] cycloadditions, similar to substituted cyclopropanes<sup>27,28</sup> and nitrilimines,<sup>29</sup> and would provide a new means of incorporating sulfur into a ring system.

### **3.4 – Conclusions**

The differing interpretation of “one and the same electron density” of isothiirane by two different methods of analysis was reinvestigated. A high level reference geometry was calculated at the CCSD(T) / CBS<sub>Extrap</sub> level, and methodologies used in this work and others were compared. Three methods, PBE and MP2 in combination with BS1 and B3PW91 / BS 2 reproduced the CCSD(T) / CBS<sub>Extrap</sub> geometry well. All methods of analysis indicate isothiirane has characteristics of both the acyclic and cyclic structures. The QTAIM analysis highlighted that the appearance of the ring is strongly related to the size of the ring, and the amount of electron density along the S-C<sub>1</sub> geometric line. The ring structure of isothiirane was shown to be topologically unstable, and when the influence of nuclear motion due to vibrational modes is considered in the context of the EU catastrophe, the best QTAIM description is obtained using four acyclic and one cyclic MG. A thorough NRT analysis highlighted that the acyclic carbene resonance structure (RS-C) is an important structure in the NRT-expansion. An analysis of the <sup>13</sup>C NMR chemical shielding tensor revealed some carbenic nature to the C<sub>1</sub> nuclei. Substituent effects provided a more detailed picture of the electronic structure of isothiirane, confirming its hybrid nature. Bond order – bond length relationships were built using the substituted series to assess the best NRT description for the unsubstituted parent. On the

basis of this NRT expansion the parent compound is best described as a hybrid of the cyclic structure (RS-B: 85.1%) and the acyclic structure (RS-C: 8.0%). A comparison of descriptors of the three modalities of analysis predict the cyclic and acyclic structure to exist in a narrow and large region, respectively, as predicted by the unfolding of the elliptic umbilic. This work demonstrates how the electronic structure of a molecule can be unambiguously characterized through a careful application of commonly used analysis tools. The electronic structure of isothiirane can be modified through substitution increasing its reactivity in [1+2] or [3+2] cycloadditions, which may offer a new method to form sulfur containing heterocycles.

### **3.5 – References**

- (1) Koch, W. and Holthausen M.C. *A Chemist's Guide to Density Functional Theory: Vol. 3.* Wiley-VCH (**2001**)
- (2) Hohenberg, P. and Kohn, W. *Phys. Rev.*, **1964**, 136
- (3) Bader, R.F.W *Atoms in Molecules: A Quantum Theory*; Oxford University Press (**1994**)
- (4) Weinhold, F. and Landis, C. *Valency and Bonding*; Cambridge University Press (**2005**)
- (5) Jacobsen, H. *Can. J. Chem.*, **2008**, 86, 695
- (6) Becke, A.D. and Edgecombe, K.E., *J. Chem. Phys.*, **1990**, 92, 5397
- (7) Henn, J.; Leusser, D. and Stalke, D. *J. Comp. Chem.*, **2007**, 28, 2317
- (8) Jacobsen, H. *J. Comp. Chem.*, **2009**, 30, 1093
- (9) Foroutan-Nejad, C.; Shahbazian, S. and Marek, R. *Chemistry Eur. J.*, **2014**, 20, 10140
- (10) Castillo N.; Robertson, K.N.; Choi, S.C.; Boyd, R.J. and Knop, O. *J. Comp. Chem.*, **2008**, 29, 367
- (11) Bader, R.F.W.; Nguyen-Dang, T.T. and Tal, Y.J. *J. Phys. Chem.*, **1979**, 70, 4316
- (12) MOLPRO, version 2010.1, a package of ab initio programs, Werner, H.-J.; Knowles, P. J.; Knizia, G.; Manby, F. R.; Schütz, M. and others, see <http://www.molpro.net>.
- (13) Peterson, K.; Woon, D. and Dunning, T. *J. Chem. Phys.*, **1993**, 100, 7410
- (14) A. D. Becke, *J. Chem. Phys.*, **1993**, 98, 5648
- (15) J. P. Perdew, Y. Wang, *Phys. Rev. B*, **1992**, 45, 13244
- (16) C. Adamo, V. Barone, *J. Chem. Phys.*, **1999**, 110, 6158

- (17) Gaussian 09, Revision **D.01**, Frisch, M. J.; Trucks, G. W.; Schlegel, H. B.; Scuseria, G. E.; Robb, M. A.; Cheeseman, J. R.; Scalmani, G.; Barone, V.; Mennucci, B.; Petersson, G. A.; Nakatsuji, H.; Caricato, M.; Li, X.; Hratchian, H. P.; Izmaylov, A. F.; Bloino, J.; Zheng, G.; Sonnenberg, J. L.; Hada, M.; Ehara, M.; Toyota, K.; Fukuda, R.; Hasegawa, J.; Ishida, M.; Nakajima, T.; Honda, Y.; Kitao, O.; Nakai, H.; Vreven, T.; Montgomery, J. A., Jr.; Peralta, J. E.; Ogliaro, F.; Bearpark, M.; Heyd, J. J.; Brothers, E.; Kudin, K. N.; Staroverov, V. N.; Kobayashi, R.; Normand, J.; Raghavachari, K.; Rendell, A.; Burant, J. C.; Iyengar, S. S.; Tomasi, J.; Cossi, M.; Rega, N.; Millam, J. M.; Klene, M.; Knox, J. E.; Cross, J. B.; Bakken, V.; Adamo, C.; Jaramillo, J.; Gomperts, R.; Stratmann, R. E.; Yazyev, O.; Austin, A. J.; Cammi, R.; Pomelli, C.; Ochterski, J. W.; Martin, R. L.; Morokuma, K.; Zakrzewski, V. G.; Voth, G. A.; Salvador, P.; Dannenberg, J. J.; Dapprich, S.; Daniels, A. D.; Farkas, Ö.; Foresman, J. B.; Ortiz, J. V.; Cioslowski, J.; Fox, D. J. Gaussian, Inc., Wallingford CT, 2009
- (18) AIMAll (Version 16.05.18), Todd A. Keith, TK Gristmill Software, Overland Park KS, USA, **2016** (aim.tkgristmill.com)
- (19) Tian, L. and Feiwu, C. *J. Comp. Chem.*, **2012**, 33, 580
- (20) *NBO 6.0*. E. D. Glendening, J. K. Badenhoop, A. E. Reed, J. E. Carpenter, J. A. Bohmann, C. M. Morales, C. R. Landis, and F. Weinhold, Theoretical Chemistry Institute, University of Wisconsin, Madison, **2013**.
- (21) In the work of Stalke *et. al.* usage of MP2/BS1 did not result in the detection of an RCP. In this work this method did result in the detection of an RCP despite the same optimized geometry as Stalke *et. al.* being obtained.
- (22) Bader, R.F.W and Matta, C.F. and Cortes-Guzman, F. *Organometallics*, **2004**, 23 6253
- (23) Peter, L. *J. Chem. Educ.*, **1986**, 63, 2
- (24) As suggested by Pauling and revised by Gordy and Paolini, a longer bond should have a smaller bond order. Based on the Schomaker-Stevenson relationship, the equation:

$$d_{ABn} = r_{A1} + r_{B1} - 10|\Delta\chi_{AB}| - (C_A + C_B - 17|\Delta\chi_{AB}|) \log n$$

was derived by Peter and used to calculate the lengths of a series of hetero and homodiatomic *p*-block element bonds. In this formulation,  $r_{A1}$  and  $r_{B1}$  are the single bond covalent radii of the elements;  $|\Delta\chi_{AB}|$  is the absolute difference in Allred-Rochow electronegativity of atoms A and B;  $C_A$  and  $C_B$  are a unitless multiple bond parameter and  $n$  is the bond order. Rearranging the above equation one can determine the bond order of an

experimental or calculated bond length:

$$n = 10^{-\left(\frac{d_{AB} - [r_A + r_B - 10|\chi_{AB}|]}{[C_A + C_B - 17|\chi_{AB}|]}\right)}$$

(25) Gordy, W. *J. Chem. Phys.*, **1947**, 15, 305

(26) Paolini, J.P. *J. Comp. Chem.*, **1990**, 11, 1160

(27) Grover, H.K.; Emmett, M.R. and Kerr, M.A. *Org. Biomol. Chem.*, **2015**, 13, 665

(28) Cavitt, M.A.; Phun, L.H. and France, S. *Chem. Soc. Rev.*, **2014**, 43, 804

(29) Mawhinney, R.C.; Muchall, H.M. and Pselherbe, G.H. *Can. J. Chem.*, **2005**, 83, 1615

## **CHAPTER FOUR**

### **The Electron Affinities of TCNE and TCNQ: The Effect of Silicon Substitution**

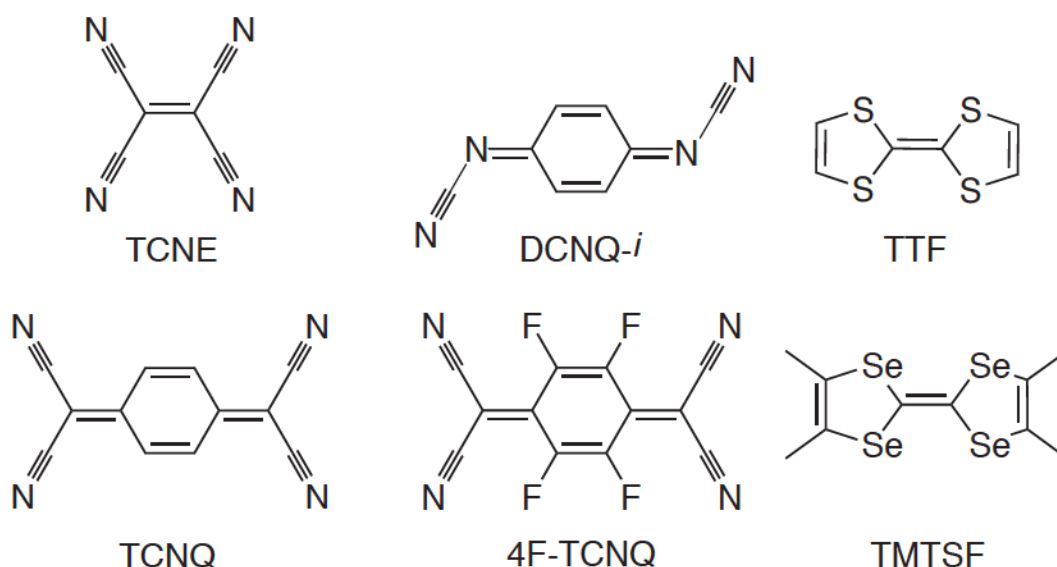
This chapter has been published in *Structural Chemistry*: S.M. Maley; C. Esau and R.C. Mawhinney, *Struct. Chem.*, 2018, doi: 10.1007/s11224-018-1186-1

## ABSTRACT

The cyanocarbons tetracyanoethylene (TCNE) and tetracyanoquinodimethane (TCNQ) are important electron acceptors used in organic electronic applications. A common approach to enhancing their performance is by structural modification with previous studies focusing on substituting the cyano ligands or annular moiety. In this work we assess the effect of hypovalent substitution, swapping carbon for silicon, on the potential energy surfaces and adiabatic electron affinities (AEAs). Si-substitution generally enhances AEA, and in the case of TCNQ stabilizes an open-shell singlet diradical state. Such findings may find value in the design of new materials based on the cyanocarbon platform.

## 4.1 – Introduction

The cyanocarbons tetracyanoethylene (TCNE) and tetracyanoquinodimethane (TCNQ) (**Scheme 4.1**) are experimentally and theoretically known to form stable anions.<sup>1-7</sup> The electron affinity (EA) of TCNE, measured using electron transfer equilibria, is 3.17eV (+/- 0.2eV),<sup>1</sup> while the EA of TCNQ has been recently revised by Zhu and Wang, using vibrationally resolved photoelectron spectroscopy, to be 3.343eV (+/- 0.001eV).<sup>3</sup>



**Scheme 4.1**

The ability of both molecules to form stable anions has led to their inclusion in a variety of novel materials applications. Perhaps the most well-known example is the charge transfer complex formed between TCNQ and tetrathiafulvalene (TTF – **Scheme 4.1**), where TCNQ acts as the electron acceptor and TTF the electron donor. The resulting complex has a conductivity of approximately  $10^4 \Omega^{-1} \text{ cm}^{-1}$  at 60K.<sup>8,9</sup> The first “organic” magnetic material combined TCNE with  $\text{FeCp}^*_2$  to yield  $[\text{TCNE}]^- [\text{FeCp}^*_2]^+$ , which displayed bulk ferromagnetic properties in accordance with the Curie-Weiss expression at temperatures above 60K.<sup>10</sup>

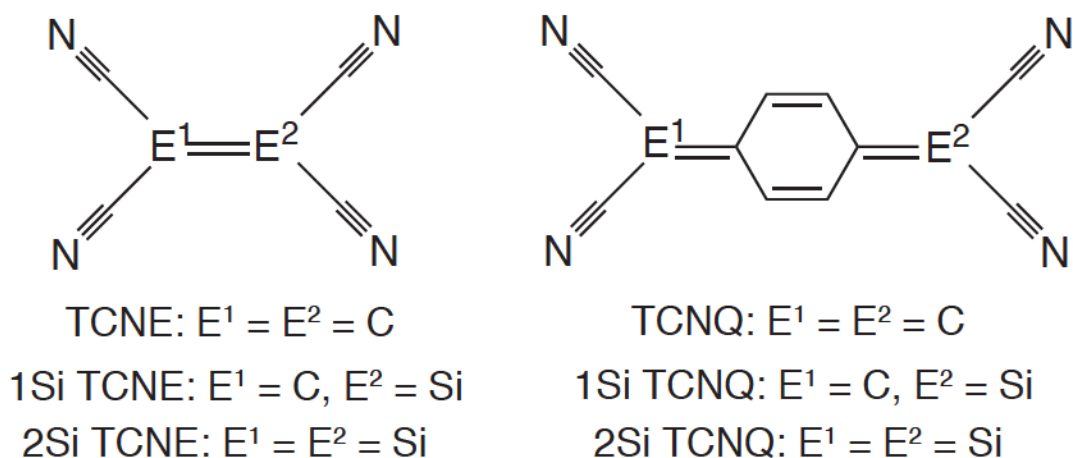
Electron donors, acceptors, and their substituted derivatives are commonly used to dope materials in an effort to increase performance.<sup>11</sup> The majority of strategies taken to modify TCNQ rely on modifying the annular portion. For example, the perfluoro-substituted derivative of TCNQ, 4F-TCNQ (**Scheme 4.1**), increases the conductivity in Zn- phthalocyanine based materials by orders of magnitude over the base material.<sup>12</sup>

An alternative approach to modifying the structure of TCNQ is to alter the backbone. However, doing so often results in the loss of a –CN group. For example, dicyano-*p*-quinone diamine (DCNQi – **Scheme 4.1**), has only two –CN groups. This is undesirable as the –CN groups are key to obtaining the essential electron accepting property,<sup>13</sup> and the electron affinities of such TCNQ derivatives are typically less than that of the parent compound.<sup>14</sup>

A promising strategy for tuning electronic structure is to substitute with an *isovalent* element, as has been done in modifying TTF. In the creation of superconducting Bechgaard salts, the sulfur atoms are substituted with selenium to form tetramethyltetraselenafulvalene (TMTSF – **Scheme 4.1**).<sup>15</sup> Taking this approach to tuning the electronic structure of TCNQ would allow for the retention of all four –CN ligands. Furthermore, Fukuda *et. al.*<sup>16</sup> have shown that substituting Si or Ge for C in *p*-quinodimethane enhances the singlet diradical character of the electronic structure, which may lead to other uses for TCNQ derivatives.

In this work we investigate the effect of step-wise substitution, changing C for Si, in the cyano positions (**Scheme 4.2**) on the structure and adiabatic electron affinities (AEAs) of TCNE and TCNQ. We first assess the performance of a variety of DFT functionals in combination with a selection of basis sets in determining the experimental

structure and EA of TCNE and TCNQ (Part 1). Following this, we focus on the silicon analogs (1Si TCNE, 2Si TCNE, 1Si TCNQ and 2Si TCNQ) by assessing and characterizing their potential energy surfaces from which the adiabatic electron affinities are obtained (Part 2).



**Scheme 4.2**

## **4.2 – Methodology**

The structures of all molecules (**Scheme 4.2**) were optimized with  $D_{2h}$  (TCNE, TCNQ, 2Si TCNE, 2Si TCNQ) or  $C_{2v}$  (1Si TCNE, 1Si TCNQ) symmetry. Six GGA functionals (BLYP,<sup>17</sup> BP86,<sup>18</sup> HCTH/407,<sup>19</sup> M06-L,<sup>20</sup> PBE<sup>21</sup> and TPSS<sup>22</sup>), seven hybrid functionals (B3LYP,<sup>23</sup> BH HLYP,<sup>24</sup> M06,<sup>20</sup> M06-2X,<sup>20</sup> M06-HF,<sup>20</sup> PBE0,<sup>25</sup> and TPSSH<sup>26</sup>), and a range separated hybrid (CAM-B3LYP<sup>27</sup>) were combined with six basis sets: three double-zeta (DZ) (**BS1**: cc-pvDZ, **BS2**: aug-cc-pvDZ, **BS3**: 6-31++g(d,p)) and three triple zeta (TZ) (**BS4**: cc-pvTZ, **BS5**: 6-311++g(d,p), **BS6**: 6-311++g(2df,pd). All calculations were performed using Gaussian09 Rev. D.01.<sup>28</sup> Results could not be obtained for TCNQ with BS2 due to SCF convergence problems. Frequency calculations were performed to

characterize all obtained stationary points on their respective potential energy surfaces (PESs) and, when necessary, displacement modes of imaginary frequencies were followed to locate minima. Wavefunctions were tested for lower energy solutions using the `stable=opt` keyword.<sup>29</sup> Spin projection methods were not used as there was no significant spin contamination noted (See SI Table 33-39, and 43-48).

## **4.3 – Results and Discussion**

### 4.3.1 – Part 1 – Assessment of Parent Compounds

We begin by assessing the performance of a variety of model chemistries in reproducing the average experimental structures of TCNE and TCNQ in their neutral and reduced forms. The average bond lengths and standard deviations of each bond length are assessed and the percent deviation of each model chemistry is calculated for each bond length and the mean deviation is computed. Following this, the deviation of the chosen model chemistries from the experimental EA values is computed.

#### *4.3.1.1 – The Structure of TCNE and [TCNE]<sup>-</sup>*

The structure of TCNE was determined by Becker *et. al.* using x-ray (XRD) and neutron diffraction (ND) spectroscopy and by Hope *et. al.* using gas phase electron diffraction (GED).<sup>30,31</sup> Based on their values, the average experimental structure (**Figure 4.1**) has bond lengths of  $1.352 \pm 0.006 \text{ \AA}$  ( $R_1$ ),  $1.435 \pm 0.003 \text{ \AA}$  ( $R_2$ ), and  $1.160 \pm 0.003 \text{ \AA}$  ( $R_3$ ).

[TCNE]<sup>-</sup> was characterized by both Miller *et. al.* and Bock *et. al.* using XRD<sup>10,32</sup> and using ND by Miller *et. al.*<sup>33</sup> In contrast to the neutral structure there was greater variation amongst the bond lengths, with  $R_1$  and  $R_3$  displaying the most variation (S.D.: 0.018 ( $R_1$ ) and 0.012 ( $R_3$ )), while  $R_2$  was almost identical for both XRD studies, with Miller *et. al.* reporting a value of  $1.417 \text{ \AA}$ , and Bock *et. al.*  $1.418 \text{ \AA}$ . The average experimental

structure (**Figure 4.1**) has bond lengths of  $1.418 \pm 0.018 \text{ \AA}$  ( $R_1$ ),  $1.414 \pm 0.005 \text{ \AA}$  ( $R_2$ ) and  $1.155 \pm 0.012 \text{ \AA}$  ( $R_3$ ).

To assess the accuracy in predicting the structure of both TCNE and  $[\text{TCNE}]^-$ , the percent deviation between predicted and average experimental value for each bond length was assessed (SI-Tables 2A-F) and the mean percent deviations are presented in **Table 4.1** for TCNE and **Table 4.2** for  $[\text{TCNE}]^-$ .

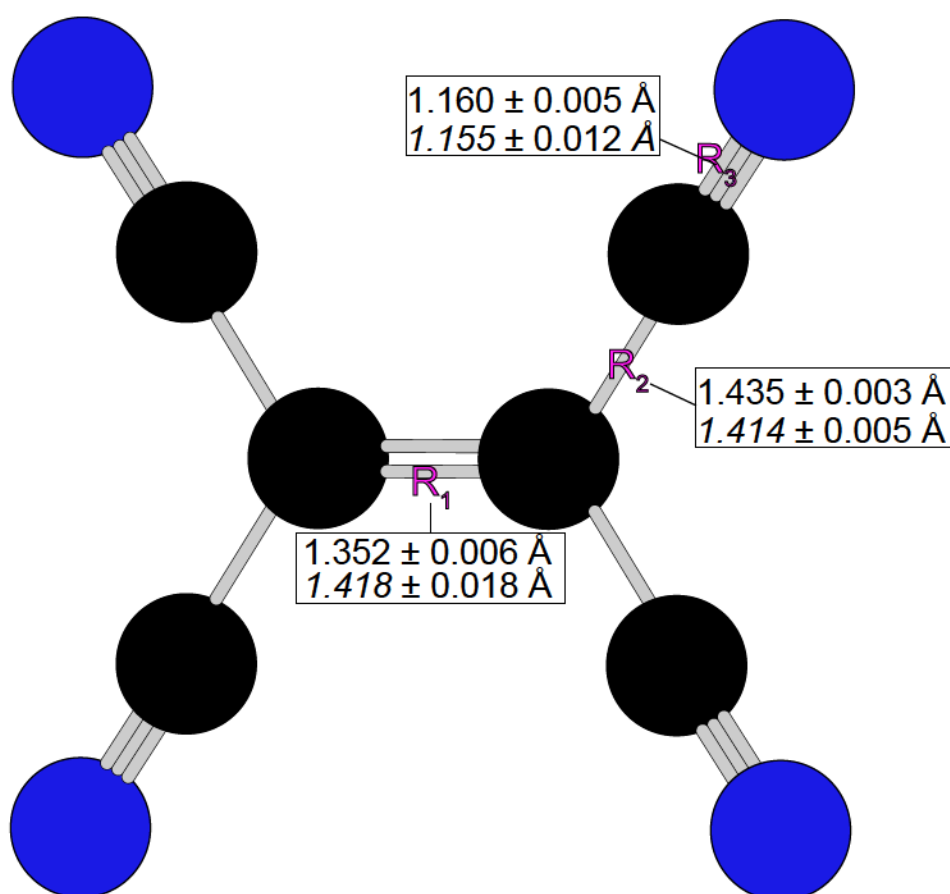


**Figure 4.1:** Average experimental bond lengths and standard deviations (S.D.) (Å) for neutral and *reduced* TCNE. Black – carbon and blue – nitrogen.

The average structure of TCNE was reproduced within 1.64%, and the average structure of  $[\text{TCNE}]^-$  was reproduced within 2.00%.  $R_1$  was typically overestimated in both  $[\text{TCNE}]$  and  $[\text{TCNE}]^-$ .  $R_2$  in TCNE was generally underestimated, while in  $[\text{TCNE}]^-$  it was

underestimated with TZ-basis sets and overestimated with DZ-basis sets.  $R_3$  in TCNE was generally overestimated by GGA's and underestimated by hybrids when combined with TZ-basis sets, but with DZ-basis sets it was typically overestimated. In  $[\text{TCNE}]^-$ ,  $R_3$  was overestimated by all methods. The overall error in the average structure prediction for both TCNE and  $[\text{TCNE}]^-$  was lowered by inclusion of exact exchange. This is primarily due to a decrease in the  $R_1$  and  $R_3$  error. The average experimental structure of TCNE was best reproduced by M06-2X/BS2 and M06-2X/BS4, while  $[\text{TCNE}]^-$  was best reproduced by CAM-B3LYP/BS4 and CAM-B3LYP/BS6.

#### 4.3.1.2 – The Structure of TCNQ and $[\text{TCNQ}]^-$

The structure of TCNQ was determined by Long *et. al.* to display a planar quinoid-type structure with  $R_1$  (1.346Å) and  $R_3$  (1.374Å) shorter than  $R_2$  (1.444Å) and  $R_4$  (1.441Å). The cyano bond ( $R_5$ ) had a distance of 1.140Å (**Figure 4.2**).<sup>34</sup>

The structure of  $[\text{TCNQ}]^-$  was determined by Hoekstra *et. al.*<sup>36</sup> and Kistenmacher *et. al.*<sup>37</sup> from XRD analysis of  $[\text{Rb}]^+$  and  $[\text{TTF}]^+$  crystals, respectively. Miller *et. al.* later obtained the structure of the isolated TCNQ radical anion via XRD.<sup>38</sup> In all cases, the structure was reported to be planar. The average experimental structure (**Figure 4.2**) has bond lengths of  $1.367 \pm 0.009 \text{Å}$  ( $R_1$ ),  $1.427 \pm 0.006 \text{Å}$  ( $R_2$ ),  $1.416 \pm 0.014 \text{Å}$  ( $R_3$ ),  $1.420 \pm 0.009 \text{Å}$  ( $R_4$ ) and  $1.154 \pm 0.005 \text{Å}$  ( $R_5$ ).

**Table 4.1:** Mean percent deviation from average experimental structure of neutral TCNE. MIN, MAX, MIN|x| and Standard Deviation (S.D) provided for each functional and basis set.

	BS1	BS2	BS3	BS4	BS5	BS6	MIN	MAX	MIN  x	S.D.
BLYP	-1.39	-1.64	-1.27	-0.88	-1.38	-1.23	-1.64	-0.88	0.88	0.23
BP86	-1.29	-1.53	-1.18	-0.81	-1.27	-1.14	-1.53	-0.81	0.81	0.21
HCTH	-0.73	-0.97	-0.66	-0.36	-0.75	-0.66	-0.97	-0.36	0.36	0.18
M06-L	-0.48	-0.72	-0.35	-0.04	-0.51	-0.39	-0.72	-0.04	0.04	0.20
PBE	-1.18	-1.42	-1.10	-0.75	-1.17	-1.06	-1.42	-0.75	0.75	0.20
TPSS	-1.04	-1.28	-0.92	-0.59	-1.03	-0.90	-1.28	-0.59	0.59	0.21
TPSSh	-0.63	-0.86	-0.56	-0.19	-0.63	-0.50	-0.86	-0.19	0.19	0.20
B3LYP	-0.43	-0.67	-0.31	0.05	-0.42	-0.28	-0.67	0.05	0.05	0.22
PBE0	-0.16	-0.40	-0.08	0.23	-0.16	-0.06	-0.40	0.23	0.06	0.19
M06	-0.12	-0.39	0.01	0.37	-0.13	0.01	-0.39	0.37	0.01	0.23
BH&HLYP	0.56	0.33	0.68	1.01	0.57	0.70	0.33	1.01	0.33	0.20
M06-2X	0.01	-0.22	0.09	0.43	0.01	0.12	-0.22	0.43	0.01	0.19
CAM-B3LYP	0.10	-0.15	0.21	0.57	0.11	0.25	-0.15	0.57	0.10	0.21
M06-HF	0.45	0.22	0.50	0.89	0.48	0.61	0.22	0.89	0.22	0.20
MIN	-1.39	-1.64	-1.27	-0.88	-1.38	-1.23				
MAX	0.56	0.33	0.68	1.01	0.57	0.70				
MIN x	0.01	0.15	0.01	0.04	0.01	0.01				
S.D.	0.60	0.61	0.60	0.60	0.61	0.61				

**Table 4.2:** Mean percent deviation from average experimental structure of the [TCNE]<sup>-</sup>. MIN, MAX, MIN|x| and standard deviation (S.D) provided for each functional and basis set. <S<sup>2</sup>> values: 0.75 – 0.76 (SI-Table 4)

	BS1	BS2	BS3	BS4	BS5	BS6	MIN	MAX	MIN x	S. D.
BLYP	-2.00	-1.92	-1.92	-1.26	-1.49	-1.28	-2.00	-1.26	1.26	0.31
BP86	-1.83	-1.75	-1.75	-1.12	-1.33	-1.13	-1.83	-1.12	1.12	0.30
HCTH	-1.21	-1.16	-1.15	-0.62	-0.79	-0.63	-1.21	-0.62	0.62	0.25
M06-L	-1.05	-0.97	-0.97	-0.40	-0.64	-0.43	-1.05	-0.40	0.40	0.27
PBE	-1.70	-1.63	-1.64	-1.03	-1.22	-1.03	-1.70	-1.03	1.03	0.29
TPSS	-1.63	-1.56	-1.55	-0.94	-1.15	-0.92	-1.63	-0.92	0.92	0.30
TPSSh	-1.26	-1.20	-1.19	-0.60	-0.80	-0.58	-1.26	-0.58	0.58	0.29
B3LYP	-1.12	-1.05	-1.04	-0.41	-0.63	-0.42	-1.12	-0.41	0.41	0.30
PBE0	-0.80	-0.74	-0.73	-0.18	-0.35	-0.17	-0.80	-0.17	0.17	0.27
M06	-0.84	-0.76	-0.76	-0.08	-0.30	-0.11	-0.84	-0.08	0.08	0.32
BH&HLYP	-0.25	-0.19	-0.15	0.42	0.21	0.43	-0.25	0.43	0.15	0.29
M06-2X	-0.67	-0.61	-0.60	-0.06	-0.25	-0.06	-0.67	-0.06	0.06	0.26
CAM-B3LYP	-0.67	-0.60	-0.59	0.03	-0.17	0.03	-0.67	0.03	0.03	0.30
M06-HF	-0.84	-0.76	-0.76	-0.08	-0.30	-0.11	-0.84	-0.08	0.08	0.32
MIN	-2.00	-1.92	-1.92	-1.26	-1.49	-1.28				
MAX	-0.25	-0.19	-0.15	0.42	0.21	0.43				
MIN x	0.25	0.19	0.15	0.03	0.17	0.03				
S. D.	0.49	0.48	0.49	0.48	0.48	0.48				

The percent deviation for each bond length was assessed (SI-Table: 6A-F and 7A-F) and the average deviation was computed. The structure of TCNQ reported by Long *et al.* was reproduced within 1.59% (**Table 4.3**), while the average structure of [TCNQ]<sup>-</sup> was reproduced within 1.50% (**Table 4.4**). R<sub>1</sub> and R<sub>3</sub> were overestimated by GGA's and hybrids, with the exception of those containing higher amounts of exact exchange. R<sub>2</sub> and R<sub>4</sub> were typically underestimated by all model chemistries. The R<sub>5</sub> distance is overestimated by most methods and typically shows the greatest deviation from the average experimental value (TCNQ: 0.12 to 3.52%, [TCNQ]<sup>-</sup>: 0.01 to 2.71%). The experimental structure of TCNQ was best reproduced by M06-L/BS4 while the average experimental structure of [TCNQ]<sup>-</sup> was best reproduced by B3LYP/BS5.

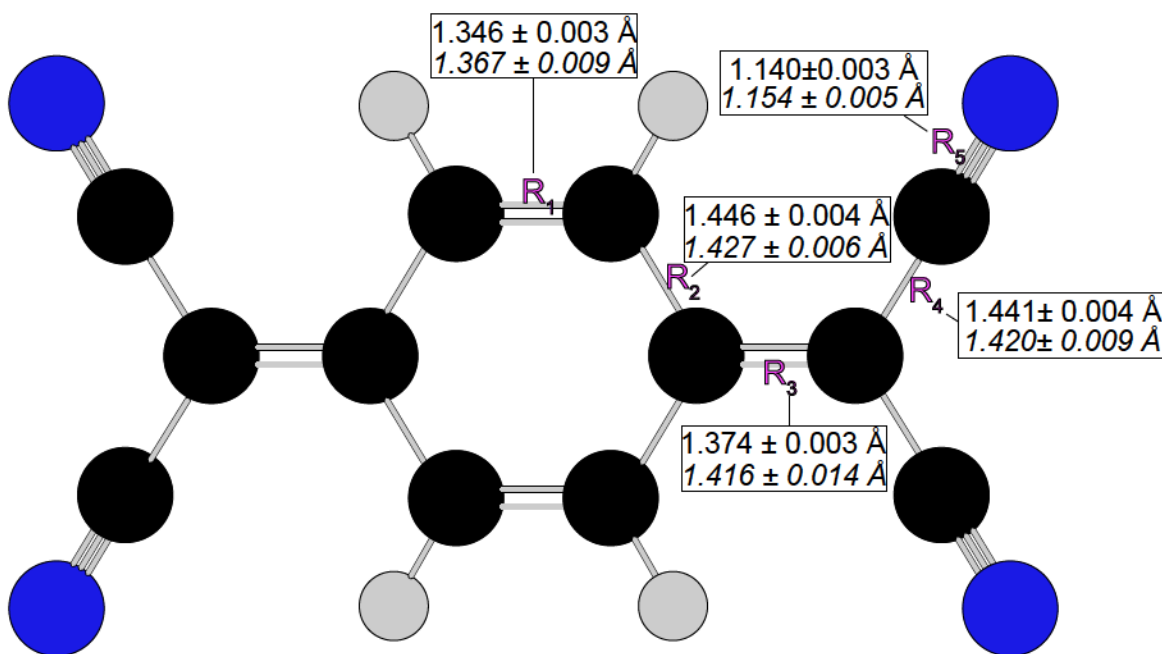


**Figure 4.2:** Average experimental bond lengths (Å) for neutral and *reduced* TCNQ. Black – carbon, blue – nitrogen and white – hydrogen.

**Table 4.3:** Average percent deviation from experimental structure of neutral TCNQ. MIN, MAX, MIN|x| and standard deviation (S.D) provided for each functional and basis set.<sup>1</sup>

	BS1	BS3	BS4	BS5	BS6	MIN	MAX	MIN x	S. D.
BLYP	1.59	1.52	0.89	1.14	0.90	0.89	1.59	0.89	0.30
BP86	1.43	1.37	0.23	1.01	0.78	0.23	1.43	0.23	0.44
HCTH	0.84	0.80	0.31	0.50	0.32	0.31	0.84	0.31	0.23
M06-L	0.62	0.54	0.00	0.27	0.04	0.00	0.62	0.00	0.25
PBE	1.31	1.26	0.69	0.90	0.70	0.69	1.31	0.69	0.27
TPSS	1.21	1.15	0.57	0.81	0.56	0.56	1.21	0.56	0.28
TPSSh	0.85	0.21	0.23	0.46	0.21	0.21	0.85	0.21	0.24
B3LYP	0.72	0.65	0.05	0.29	0.05	0.05	0.72	0.05	0.28
PBE0	0.41	0.36	-0.16	0.04	0.36	-0.16	0.41	0.04	0.23
M06	0.39	0.32	-0.32	-0.07	-0.29	-0.32	0.39	0.07	0.30
BH&HLYP	-0.16	-0.24	-0.78	-0.55	-0.78	-0.78	-0.16	0.16	0.26
M06-2X	0.34	0.30	-0.23	-0.02	-0.23	-0.23	0.34	0.02	0.25
CAM-B3LYP	0.23	0.16	-0.43	-0.20	-0.43	-0.43	0.23	0.16	0.28
M06-HF	0.12	0.10	-0.49	-0.31	-0.52	-0.52	0.12	0.10	0.28
MIN	-0.16	-0.24	-0.78	-0.55	-0.78				
MAX	1.59	1.52	0.89	1.14	0.90				
MIN x	0.12	2.12	3.12	4.12	5.12				
S. D.	0.51	0.52	0.46	0.50	0.50				

<sup>1</sup>. results could not be obtained for BS2

**Table 4.4:** Average percent deviation from average experimental structure of [TCNQ]<sup>-</sup> MIN, MAX, MIN|x| and standard deviation (S.D) provided for each functional and basis set. <S<sup>2</sup>> values: 0.75 – 0.79 (SI-Table 8)<sup>1</sup>

	BS1	BS3	BS4	BS5	BS6	MIN	MAX	MIN x	S. D.
BLYP	1.50	1.44	0.82	1.08	0.84	0.82	1.50	0.82	0.29
BP86	1.33	1.26	0.68	0.92	0.69	0.68	1.33	0.68	0.28
HCTH	0.72	0.69	0.20	0.39	0.21	0.20	0.72	0.20	0.23
M06-L	0.54	0.45	-0.07	0.20	-0.03	-0.07	0.54	0.03	0.24
PBE	1.20	1.15	0.59	0.81	0.60	0.59	1.20	0.59	0.26
TPSS	1.13	1.07	0.50	0.74	0.49	0.49	1.13	0.49	0.27
TPSSh	0.79	0.73	0.18	0.41	0.17	0.03	0.68	0.03	0.28
B3LYP	0.68	0.61	0.03	0.27	0.04	-0.75	-0.14	0.14	0.26
PBE0	0.37	0.31	-0.20	0.01	-0.20	-0.41	0.24	0.16	0.28
M06	0.36	0.28	-0.34	-0.09	-0.30	-0.34	0.36	0.09	0.29
BH&H	-0.14	-0.22	-0.75	-0.51	-0.75	-0.25	0.30	0.03	0.24
M06-2X	0.30	0.25	-0.25	-0.03	-0.24	-0.53	0.09	0.06	0.27
CAM-B3LYP	0.24	0.16	-0.41	-0.18	-0.41	-0.20	0.37	0.01	0.25
M06-HF	0.09	0.06	-0.50	-0.31	-0.53	0.17	0.79	0.17	0.26
MIN	-0.14	-0.22	-0.75	-0.51	-0.75				
MAX	1.50	1.44	0.82	1.08	0.84				
MIN x	0.09	0.06	0.03	0.03	0.04				
S. D.	0.47	0.48	0.46	0.47	0.47				

1. results could not be obtained for BS2

#### 4.3.1.3 – The Adiabatic Electron Affinities of TCNE and TCNQ

The experimental EA's of TCNE and TCNQ were reported to be 3.17eV ( $\pm 0.2\text{eV}$ )<sup>1</sup> and 3.343eV ( $\pm 0.001\text{ eV}$ ),<sup>3</sup> respectively. Our calculated AEA's for TCNE and TCNQ along with their percent deviations from experimental values are compiled in SI-Tables 9–12. Also in supplemental information (SI-Table 12) are the AEA's of Post-HF methods tested by Milian *et. al.*<sup>4-7</sup> The percent deviation of our chosen methods and select<sup>39</sup> Post-HF values from the experimental EA are visualized in **Figure 4.3** for TCNE and **Figure 4.4** for TCNQ.

The magnitude of the deviation of all functionals is typically lower when Dunning style basis sets (BS1, BS2 and BS4) are used. The Pople style basis sets (BS3, BS5 and BS6) generally show similar performance (See Table S10 and S12). However, contrary to expectations, the deviation is greater when diffuse functions are included in the basis set. BLYP shows the lowest deviation at all basis sets except BS1, consistent with previous findings of Curtiss *et. al.* regarding the calculation of AEA's of the G2 ion test set.<sup>40</sup> The AEAs do not show a pattern with respect to the choice of functional. Vikramaditya and Lin showed increasing the amount of exact exchange causes the vertical EA to decrease.<sup>41</sup> However we find the AEA increases as the amount of exchange is increased (SI-Figure 5 and 6).

Most model chemistries predict a bound anion for TCNE, with AEA's ranging from 2.781 to 3.571eV, and all model chemistries predict a bound anion for TCNQ, with AEA's ranging from 3.099 to 3.898eV. M06-HF in combination with all basis sets predict the TCNE anion to be unbound, with AEA's ranging from -1.397 to -3.189eV (not visualized). In general, the magnitudes of both AEA's are larger when hybrid functionals or TZ basis

sets are used. In both TCNE and TCNQ, BLYP reported the lowest value. For TCNE the highest values are predicted by M06 (BS1 and BS2), HCTH (BS3 and BS6) and CAM-B3LYP (BS4 and BS5). For TCNQ the highest values are predicted by M06(BS1), CAM-B3LYP (BS3) and M06-HF (BS4-BS6). In most cases DFT outperformed the Post-HF methods.

The majority of the model chemistries overestimated the AEA of both TCNE and TCNQ, with none reproducing the value within experimental uncertainty. The AEA of TCNE was underestimated by 19 of 93 model chemistries, including 10 functionals (BLYP, BP86, HCTH, PBE, TPSS, TPSSh, B3LYP, BH&HYLP, M06-2X and CAM-B3LYP) in combination with BS1 and 8 Post-HF methods. BLYP in combination with BS4 also underestimates the AEA, while M06-L in combination with BS1 best reproduced the experimental value (3.180eV, 0.32% dev.). This is slightly better than the best Post-HF method, CASPT-2/ANO[4s3p1d] (3.19eV, 0.64% dev.).<sup>5</sup>

Similarly, the AEA of TCNQ was underestimated by 13 of 81 model chemistries: 3 functionals (BLYP, PBE and TPSS) in combination with BS1 and 6 Post-HF methods. The closest value was obtained by PBE in combination with BS1 (3.338eV, 0.15% dev.). This method performed better than PMP2 in combination with BS2, which was the best Post-HF method (3.37eV, 0.81%).<sup>6</sup>

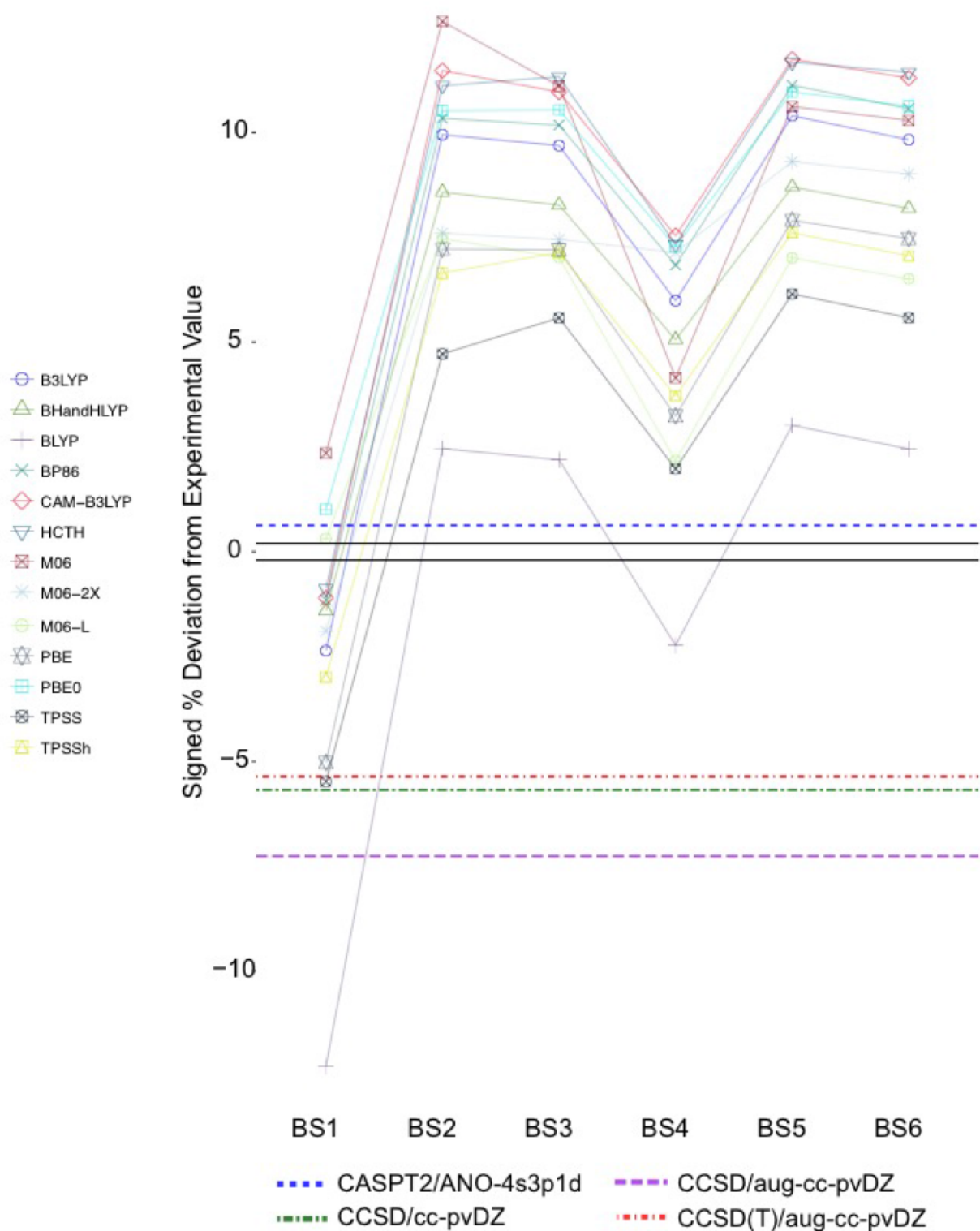


**Figure 4.3:** Deviation of chosen methods (dot w/ line for visualization purposes) from experimental AEA of TCNE. Experimental uncertainty range visualized as two solid black lines. Deviation of Post-HF methods from references 4 and 5 visualized as dashed lines.

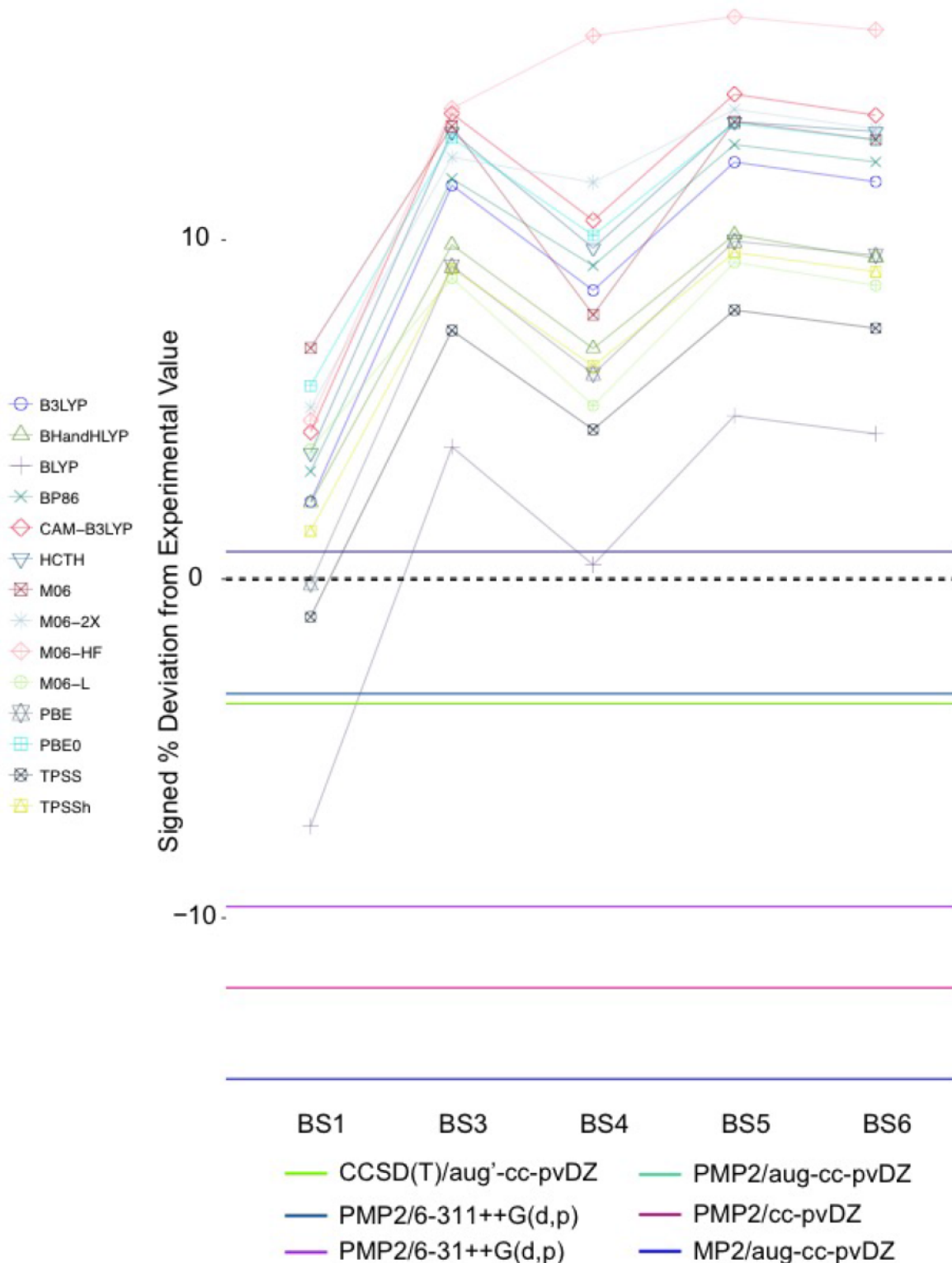
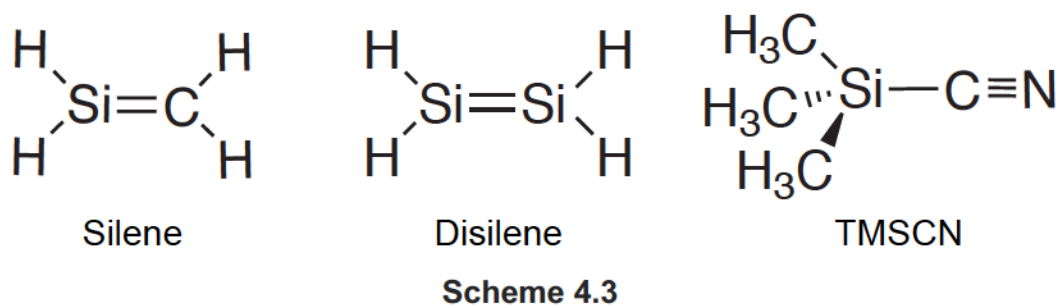


**Figure 4.4:** Deviation of chosen methods (dot w/ line for visualization purposes) from experimental AEA of TCNQ. Experimental uncertainty range visualized as dashed lines. Deviation of Post-HF methods from references 6 and 7 visualized as solid lines.

#### 4.3.1.4 – Assessments of Relevant Silicon Containing Compounds

Prior to examining the silicon analogs of TCNE and TCNQ (**Scheme 2**), we first assessed the error in determining Si=C and Si-CN bonds common to most analogs, as well as the Si=Si moiety. The Si=C bond in silene (**Scheme 3**) was determined to have a length of  $1.703 \pm 0.002 \text{ \AA}$  by Bailleux *et. al.* using submillimeter wave spectroscopy.<sup>42,43</sup> Our chosen methods overestimate the distance by less than 1.65% and underestimate by less than 0.85% (Appendix B Table B13). GGA functionals overestimated this length with the exception of M06-L in combination with TZ basis sets. The hybrid functionals typically underestimated the value when combined with TZ basis sets, and overestimated with DZ basis sets.



The Si=Si bond of disilene has not been characterized experimentally. A number of related disilenes have been prepared and, based on a sample of available experimental bond lengths compiled by Fischer and Power<sup>44</sup> (Appendix B Table B14), we assigned an average length of  $2.163 \pm 0.019 \text{ \AA}$  to the Si=Si moiety. The Si=Si bond in disilene (**Scheme 4.3**) is  $2.169 \text{ \AA}$  at the CCSD(T)-F12/aug-cc-pv(t+dz) level of theory,<sup>45</sup> in agreement with the average length from Fischer and Power, and will serve as our benchmark. The DFT optimized  $D_{2h}$  structures of disilene underestimate the benchmark value by no more than 2.35%. The deviation is greatly reduced when GGA functionals are used (Appendix B

Table B15) while the deviation is typically greater when hybrid functionals and TZ-basis sets are used.

Trimethylsilylcyanide (TMSCN – **Scheme 4.3**) has been characterized using gas phase electron diffraction by Dakkouri and Obberhammer<sup>46</sup> and was our benchmark for this fragment. The Si-CN bond was  $1.844\text{\AA} \pm 0.022\text{\AA}$  and the cyano bond was  $1.170\text{\AA} \pm 0.007\text{\AA}$ . Our optimized structures of TMSCN overestimate the experimental Si-CN bond by less than 2.94% (Appendix B Table B16) with the deviation typically reduced when hybrid functionals and TZ basis sets are used. The cyano bond is underestimated (-0.03 to -2.66%) by all non-GGA methods, with the exception of M06-L in combination with DZ basis sets (0.03 to 0.68%). GGA functionals typically performed better than the hybrid functionals, which showed larger deviations when TZ basis sets were used (Appendix B Table B18).

#### 4.3.2 – Part 2 – Effect of Si-Substitution

Structurally, the choice of functional or basis set is not a major issue as all benchmark structures were reproduced within 3%. The EA of TCNE and TCNQ however, showed both functional and basis set dependencies with the basis sets in particular displaying repeatable patterns. As such, we have limited the number of basis sets to two for assessing the Si-analogs of TCNE and TCNQ: the smallest (BS1) and the largest (BS6). However, to confirm that patterns were similar, a limited study was performed using BS3 and BS4 (See Appendix B Figure B8).

##### *4.3.2.1 – The Potential Energy Surfaces of the Si-Analogs of TCNE and TCNQ*

Stationary points on the potential energy surfaces of TCNE and TCNQ are given in **Figures 4.4** and **4.5**, respectively. The relative energies and vibrational wavenumbers

of all imaginary modes can be found Table SI19-32. As described earlier, the parent compounds have planar minima. For 1Si analogs, the neutral species maintain planarity ( $360.0^\circ - \sum \angle \text{Si} = 0^\circ$ ), but the planar  $C_{2v}$  anions are characterized as transition states, relaxing to non-planar  $C_s$  minima. Symmetry breaking occurs only at the silicon centre, with the carbon centre remaining planar. Si pyramidalization ( $360.0^\circ - \sum \angle \text{Si} \neq 0^\circ$ ) in  $[1\text{Si TCNE}]^-$  ranges from 39.0 to 47.7° (BS1) and 34.0 to 40.0° (BS6) and in  $[1\text{Si TCNQ}]^-$  from 37.5 to 48.9° (BS1) and 29.6 to 41.2° (BS6). The 2Si analogs exhibit more complex surfaces with all planar structures characterized as saddle points leading to non-planar minima.

Neutral  $D_{2h}$  2Si TCNE is a transition structure that relaxes to a *trans*-bent  $C_{2h}$  minimum with both Si nuclei equally pyramidalized (17.2 to 24.1° (BS1) and 15.4 to 21.5° (BS6)).  $D_{2h}$   $[2\text{Si TCNE}]^-$  is a third order saddle point on all surfaces, relaxing to *trans*-bent ( $C_{2h}$ ), *cis*-bent ( $C_{2v}$ ) and twisted ( $D_2$ ) structures. The  $C_{2v}$  and  $D_2$  structures further relax to quasi-degenerate  $C_s$ ,  $C_2$  and  $C_1$  structures, all strongly resembling the  $C_{2h}$  structure, with the lowest energy structure model chemistry dependent.

When BS1 is used, all GGA's except M06-L predict the  $C_2$  structure to be the lowest energy structure. PBE0 and M06-L predict a  $C_s$  lowest energy structure and the hybrid M06 functionals predict a  $C_1$  lowest energy structure. The remaining functionals predict the  $C_{2h}$  structure to be the lowest energy structure. When BS6 is used, the majority of functionals predict the  $C_{2h}$  structure as the lowest energy structure. The  $C_s$  structure is the minimum on the M06-L and M06 surfaces, while the  $C_2$  structure is the minimum on the HCTH, TPSSh and PBE0 surfaces. M06-2X again predicts a  $C_1$  lowest energy structure.

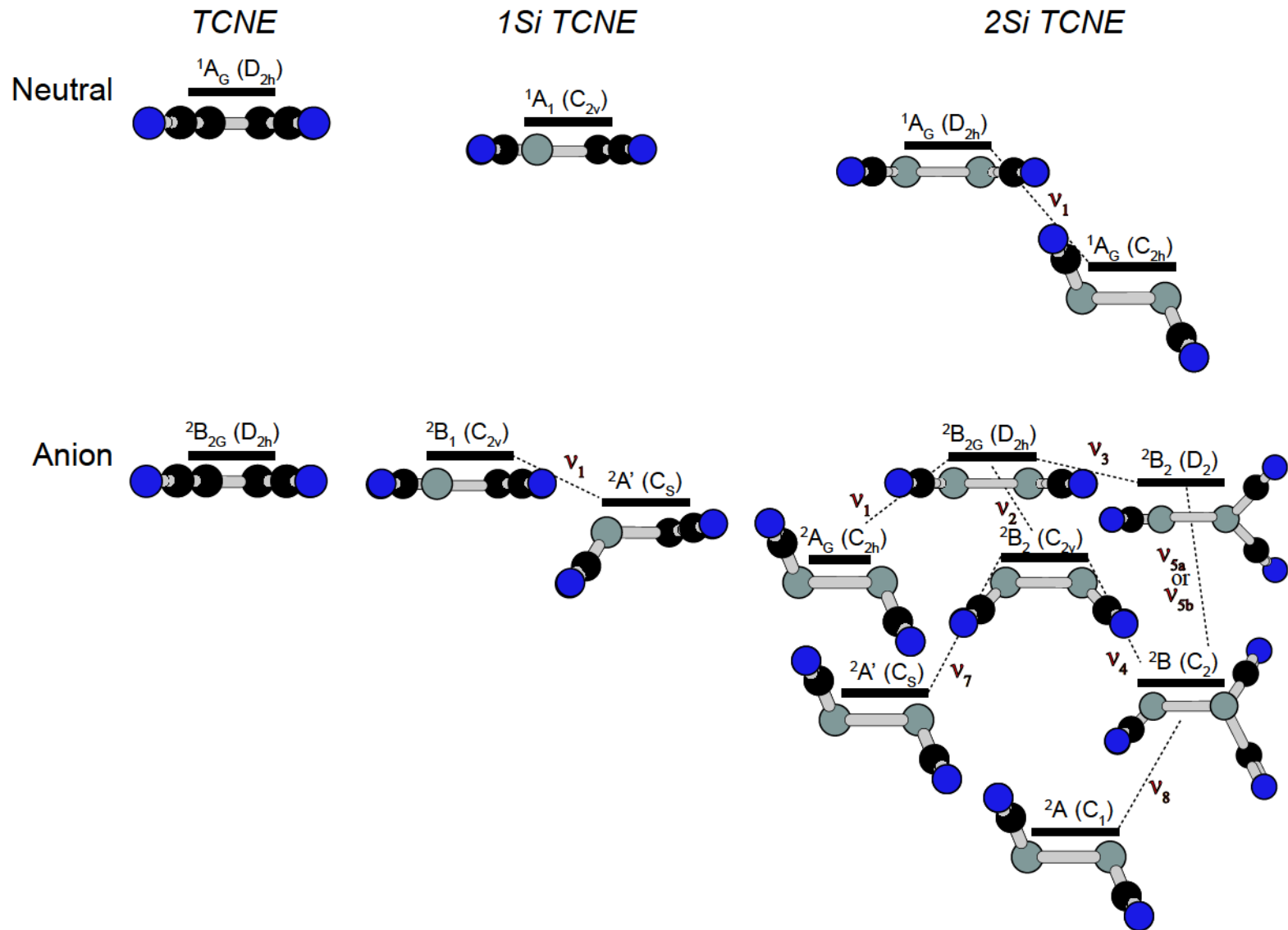


**Figure 4.5:** Stationary points of the potential energy surfaces of TCNE analogs.  $\nu$  indicates an imaginary frequency. Black – Carbon, Grey – Silicon, Blue – Nitrogen.

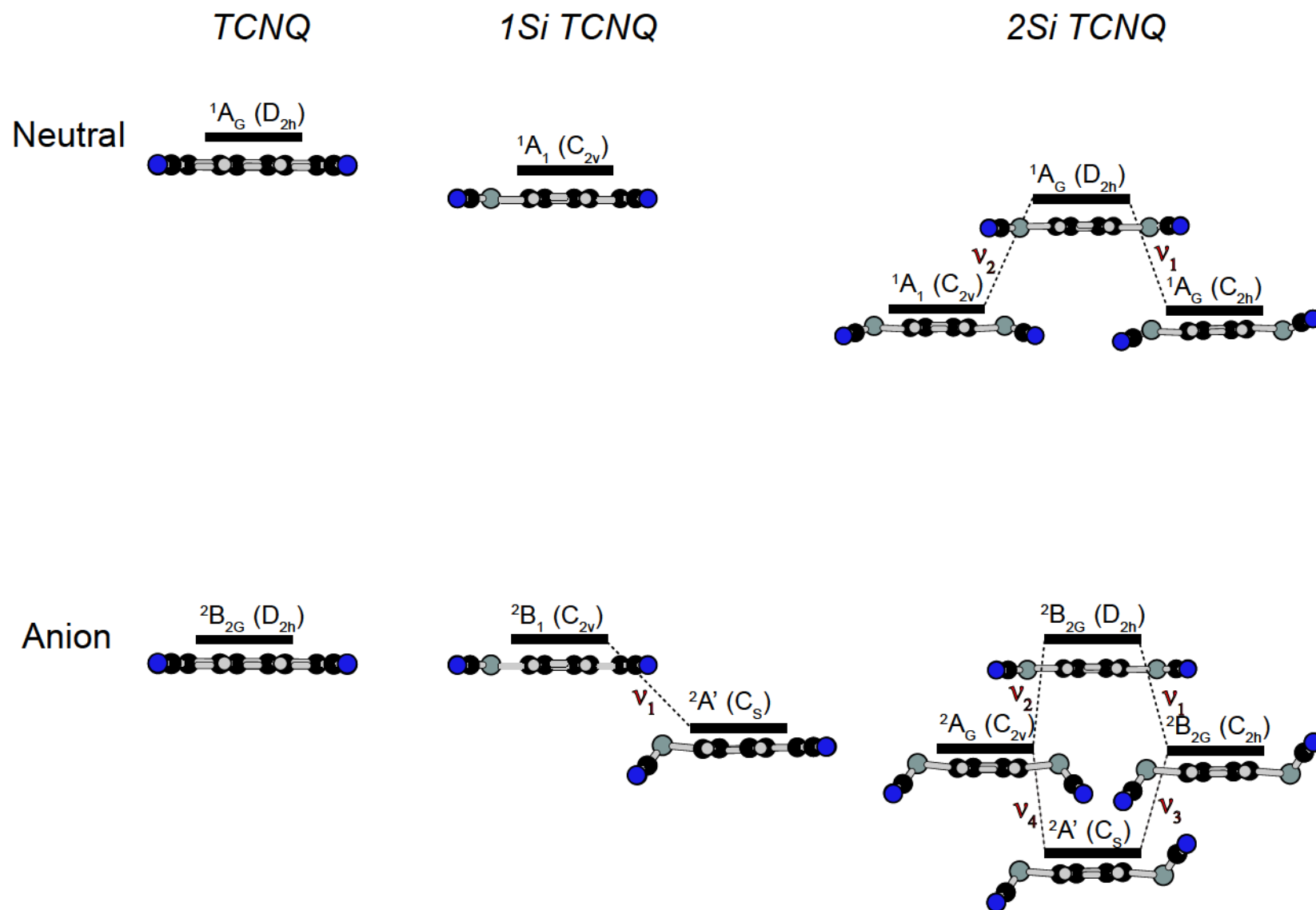


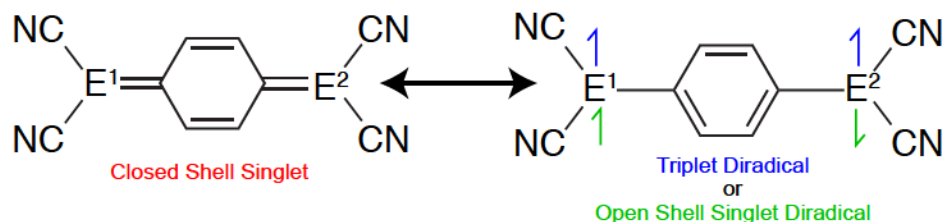
**Figure 4.6:** Stationary points of the potential energy surfaces of TCNQ analogs.  $\nu$  indicates an imaginary frequency. Black – Carbon, Grey – Silicon, Blue – Nitrogen, White – Hydrogen

The 2Si TCNQ second order saddle point relaxes to *trans*-bent  $C_{2h}$  and *cis*-bent  $C_{2v}$  structures at most levels of theory. Four functionals (BHandHLYP, M06-2X, CAM-B3LYP and M06-HF) predict a planar  $D_{2h}$  minimum. The remaining functionals predict the  $C_{2h}$  structure to be the lowest energy structure. This is consistent with the findings of Fukuda *et. al.* who reported the Si and Ge substituted *p*-quinodimethanes to be non-planar.<sup>16</sup>

$[2Si\ TCNQ]^-$  is predicted to be a second order saddle point with all functionals, except M06, BHandHLYP, M06-2X, CAM-B3LYP and M06-HF, predicting the *trans*-bent  $C_{2h}$  structure as the lowest energy structure. The exceptions further relax to a  $C_s$  (*pseudo*- $C_{2h}$ ) structure and display the same type of pyramidalization as the  $C_{2h}$  structure, although the magnitude of pyramidalization is larger for one of the Si nuclei. (e.g., BH&HLYP/BS6: 63.1° v. 27.2°)

#### 4.3.2.2 – The Effect of Si-Substitution on Diradical Character

Two resonance structures can be drawn to describe the electronic structure of neutral TCNQ analogs: one corresponding to the traditional quinoidal (closed-shell) species and another with a benzenoid (open-shell diradical) structure (**Scheme 4.4**), which can exist in either a triplet ( $T$ ,  $M_S=1$ ) or singlet (OSS,  $M_S=0$ ) electron configuration. Fukuda *et. al.* showed that exocyclic substitution with Si or Ge in the related *p*-quinodimethanes led to an enhancement of the OSS character.<sup>16</sup>



$E^1$  and  $E^2 = C$  or  $Si$

**Scheme 4.4**

The wavefunctions of the optimized closed shell planar structures were tested for instability by searching for lower energy electronic configurations. RKS→UKS instabilities were detected for 2Si TCNQ with all functionals except BLYP. Only BHandHLYP/BS1 gave an instability for 1Si TCNQ and no such instabilities were detected for TCNQ. To explore how Si-substitution effects the magnitude of the singlet-triplet gap ( $\Delta E_{S-T}$ ), the lowest diradical states were assessed. For TCNQ and 1Si TCNQ the triplet state was examined, while for 2Si TCNQ the lowest triplet and open shell singlet states were evaluated.

The planar 2Si TCNQ OSS is predicted to be a second order saddle point that relaxes to *trans*-bent  $C_{2h}$  and *cis*-bent  $C_{2v}$  minima, with a few exceptions. With BS6, HCTH, M06-L, TPSSh, B3LYP, PBE0, M06-2X and M06-HF relax to a  $C_s$ -symmetry *trans*-bent (*pseudo*- $C_{2h}$ ) minima with the amount of pyramidalization slightly greater for one Si nucleus (e.g., B3LYP: 21.78° v. 21.79°).

In all cases the “*trans*-bent” structure is the minimum on the OSS surface and the lowest energy structure for the neutral manifold (**Table 4.5**) with Si-pyramidalization ranging from 19.4 to 30.6 (BS1) and 18.5 to 29.7 (BS6) (BS1 > BS6 in all cases). The amount of pyramidalization in the OSS case is greater than that in the corresponding CSS structure.

On the triplet surface,  $D_{2h}$  2Si TCNQ is characterized as a second order saddle point that relaxes to *trans*-bent  $C_{2h}$  and *cis*-bent  $C_{2v}$  minima. GGA functionals predict the  $C_{2v}$  structure to be the lowest energy structure, with pyramidalization ranging from 22.8 to 25.1° (BS1) and 21.4 to 24.6° (BS6). Hybrid functionals, however, predict a  $C_{2h}$  lowest

energy structure, with pyramidalization ranging from 23.9 to 31.4° (BS1) and 22.9 to 30.7° (BS6). Again, pyramidalization is larger than in the CSS state.

$\langle S^2 \rangle$  for an OSS state is expected to range from 0 to 1, depending on the diradical character, while that of a triplet is expected to be 2.<sup>47</sup> For 2Si TCNQ  $\langle S^2 \rangle_{\text{OSS}}$  is generally less than one (Appendix B Table B43), indicating some degree of singlet diradical character to the ground state.<sup>48,49</sup> It is lower in planar structures (hybrid functionals containing higher amounts of exact exchange predict larger values) and structural symmetry breaking increases it, indicating an enhancement of the singlet diradical. The triplet diradicals have  $\langle S^2 \rangle$  approximately equal to 2 indicating no spin contamination (Appendix B Tables B44-B48). Therefore,  $\Delta E_{\text{S-T}}$  was not corrected.

In the planar structure  $\Delta E_{\text{S-T}}$  decreases in the order: 0Si > 1Si > 2Si. BHandHLYP, M06-2X, CAM-B3LYP and M06-HF predict planar triplet 2Si TCNQ to be more stable than the CSS state, but all functionals predict the OSS to be most stable. Upon structural symmetry breaking, with the exception of BP86, BLYP and PBE, the triplet  $C_{2h}$  and  $C_{2v}$  structures are more stable than the CSS  $C_{2h}$  and  $C_{2v}$  structures and as noted the *trans*-bent OSS structure is the lowest energy structure for the neutral manifold. The ordering of neutral states is important when determining AEAs because the stabilization of the neutral state will result in a decrease of the AEA.

**Table 4.5:** 2Si TCNQ representative relative energies (kcal/mol) of the three lowest neutral surface manifolds.<sup>1</sup>

BS1		CSS	T	OSS
BP86	D <sub>2h</sub>	2.67	10.04	– <sup>3</sup>
	C <sub>2h</sub>	2.07	3.10	<b>0.00</b>
	C <sub>2v</sub>	2.29	3.07	0.28
B3LYP	D <sub>2h</sub>	8.42	11.82	6.12
	C <sub>2h</sub>	8.04	2.20	<b>0.00</b>
	C <sub>2v</sub>	8.17	2.21	0.24
BHandHLYP	D <sub>2h</sub>	18.96	14.88	9.56
	C <sub>2h</sub>	– <sup>2</sup>	1.97	<b>0.00</b>
	C <sub>2v</sub>	– <sup>2</sup>	2.02	0.20
BS6		CSS	T	OSS
BP86	D <sub>2h</sub>	2.70	9.80	2.60
	C <sub>2h</sub>	2.20	3.13	<b>0.00</b>
	C <sub>2v</sub>	2.39	3.11	0.26
B3LYP	D <sub>2h</sub>	8.11	11.52	5.84
	C <sub>2h</sub>	7.77	1.99	<b>0.00</b>
	C <sub>2v</sub>	7.88	2.01	<b>0.00</b>
BHandHLYP	D <sub>2h</sub>	18.85	15.14	9.90
	C <sub>2h</sub>	– <sup>2</sup>	1.93	<b>0.00</b>
	C <sub>2v</sub>	– <sup>2</sup>	1.99	0.20

1. The remaining model chemistries are available in SI Tables 40 and 41

2. Planar D<sub>2h</sub> 2Si TCNQ minimum predicted

3. Attempts to calculate OSS returned CSS result

#### 4.3.2.3 – The Effect of Si-Substitution on Electron Affinity

All AEA's were determined from the global surface minima and are visualized in **Figure 4.6A** for TCNE and **Figure 4.6B** for TCNQ. The AEA of TCNE ranges from 2.781 to 3.245eV (BS1) and 3.248 to 3.533eV (BS6). As described earlier, M06-HF predicts an unstable anion: -2.984eV (BS1) and -2.311eV (BS6). For 1Si TCNE, with the exception of M06-HF, which predicts an unstable anion when combined with BS1, the AEA ranges from 3.122 to 3.498eV (BS1) and 3.437 to 3.928eV (BS6). The AEA's of 2Si TCNE range from 3.434eV to 4.186eV (BS1) and 3.371 to 4.448eV (BS6). In TCNE the average increase in AEA for the first Si-substitution is 0.301eV (BS1) and 0.224eV (BS6) and for

the second Si-substitution 0.362 (BS1) and 0.295 eV (BS6). All model chemistries, except CAM-B3LYP/BS6, predict AEA to increase in the order of  $0 < 1 < 2\text{Si}$ .

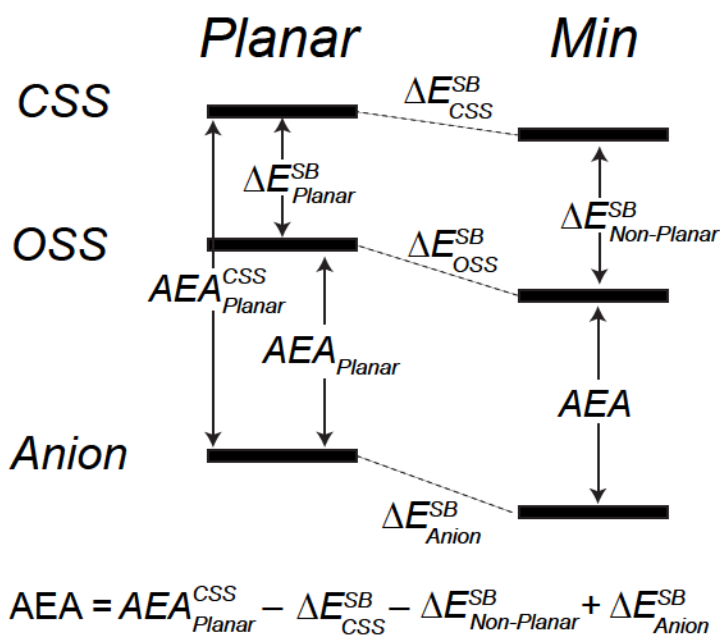
The AEA of TCNQ ranges from 3.099 to 3.571eV (BS1) and 3.486 to 3.885eV (BS6). M06-HF predicts an unstable anion when combined with BS1 (-5.845eV). For 1Si TCNQ, with the exception of M06-HF, the AEA ranges from 3.297 to 3.733eV (BS1) and 3.596 to 4.207eV (BS6). The AEA of 2Si TCNQ ranges from 2.986 to 3.684eV (BS1) and 3.419 to 3.893eV (BS6). The average increase in AEA for the first Si-substitution is 0.180eV (BS1) and 0.131eV (BS6). For the second Si-substitution all GGA's except BP86 and HCTH predict an average increase of 0.145eV and the remaining functionals predict a decrease of 0.097eV (BS1). When BS6 is used an average decrease of 0.201eV is predicted for all functionals except BLYP, BP86 and PBE which predict an average increase of 0.092eV.

The changes in the AEA of TCNQ are more dependent on model chemistry choice than TCNE. When combined with BS1 there are three scenarios. All GGA's except HCTH predict the AEA to increase in the order of  $0 < 1 < 2\text{Si}$ ; HCTH, TPSSh, B3LYP and M06 predict it to increase in the order  $0 < 2 < 1\text{Si}$ ; PBE0, BHandHLYP, M06-2X and CAM-B3LYP predict it to increase in the order  $2 < 0 < 1\text{Si}$ . BS6 has the same three scenarios. BLYP, BP86 and PBE predict the AEA to increase in the order of  $0 < 1 < 2\text{Si}$ ; M06-L, TPSS, TPSSh, B3LYP and M06 predict it to increase in the order of  $0 < 2 < 1\text{Si}$ ; and all other functionals predict it to increase in the order of  $2 < 0 < 1\text{Si}$ .

The effect of basis set was also tested by calculating the AEA's using BS3 and BS4 with a sample of functionals. These PESs have the same general features as those

calculated using BS1 and BS6. Generally, the AEA's of the Si-analogs display the same basis set trends as the unsubstituted compounds (Figure S8).

The AEAs typically increase upon going from the 0 to 1Si analog. This increase is primarily due to an increase in stability of the anion that results from symmetry breaking. The further increase in AEA in the 2Si analog is due to the fact that both the neutral and anion structures exhibit symmetry breaking which increases their stability. However, in the case of 2Si TCNQ electronic symmetry breaking also occurs. This results in a further increase in stability of the neutral form relative to the anion and results in a decrease in AEA (**Scheme 4.5**). Functionals containing higher amounts of exact exchange typically predict greater stability of the OSS (relative to the CSS) which causes the 2Si AEA to be less than the 0 or 1Si AEA.

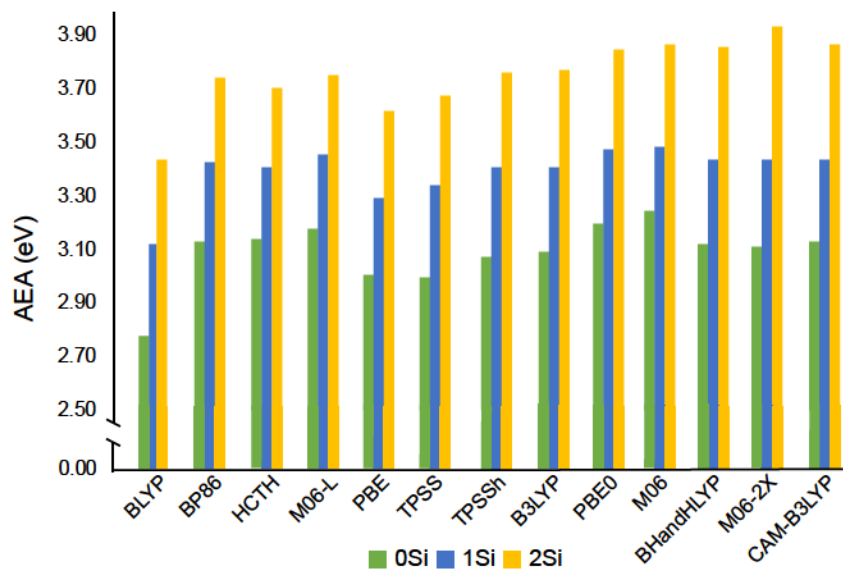


**Scheme 4.5**

The best estimate of the AEA of TCNE was obtained by M06-L/BS1 (3.180eV, 0.32% dev.). The AEA's of 1Si TCNE and 2Si TCNE calculated with this model chemistry

are 3.452eV and 3.754eV, increases of 8.6% and 18.1%, respectively. PBE/BS1 best reproduced the AEA of TCNQ (3.338eV, 0.15% dev.). The AEA's of 1Si TCNQ and 2Si TCNQ calculated using PBE/BS1 are 3.297eV and 3.581eV, a 1.28% decrease and 7.28% increase, respectively.

(A)



(B)

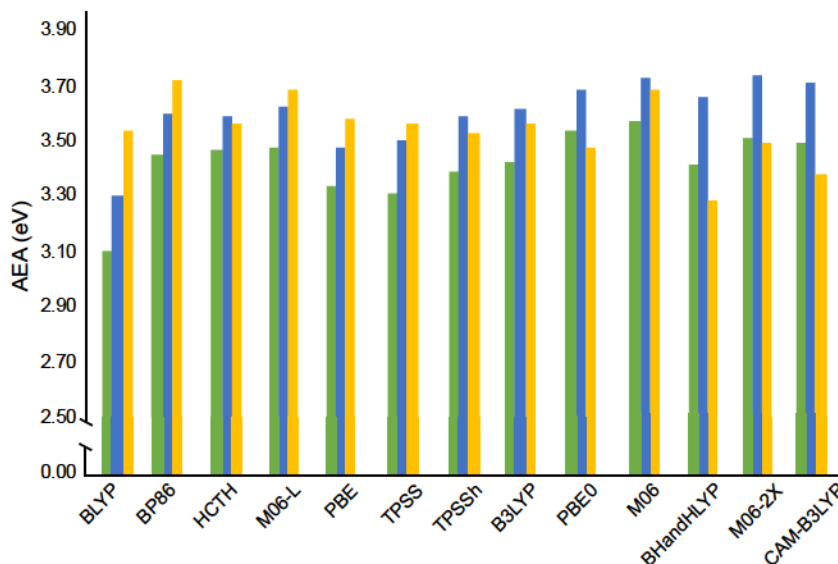


**Figure 4.7:** The adiabatic electron affinities (eV) using BS1 for (A) TCNE series and (B) TCNQ series. See Appendix B Figure B3 for BS6 values.

#### **4.4 – Conclusions**

A large sample of model chemistries were tested for their ability to reproduce the experimental structures of both neutral and reduced TCNE and TCNQ, as well as their adiabatic electron affinities. Both the structures and AEA's were reproduced with reasonable accuracy, however, none of the chosen methods reproduced the values of the EA within experimental uncertainty. Additionally, the structures of relevant Si-containing compounds were also reproduced with reasonable accuracy by the chosen methods.

Si-substitution was shown to consistently have a positive increase on the AEA of both TCNE and TCNQ. Si-substitution also resulted in the stabilization of the triplet and singlet diradical states in some cases. The increase in stability of the singlet diradical state in 2Si TCNQ causes the AEA to decrease. The neutral 1Si analogs were reported to be planar minima on their respective PES, while the reduced 1Si analogs displayed a non-planar geometry with pyramidalization at the Si-nuclei. The neutral and reduced 2Si analogs were also non-planar, exhibiting a *trans-bent* lowest energy structure structure with pyramidalization of both Si-nuclei.

The potential to create a stable singlet or triplet diradical using the TCNQ platform may have numerous applications in organic electronics including the design of new organic field effect transistors (OFETs)<sup>50</sup> and energy storage materials.<sup>51</sup> There is also the possibility that such molecules could exhibit singlet fission properties useful in the design of efficient organic photovoltaics.<sup>52</sup> These findings may be of value in the rational design and characterization of novel organic electronic materials based on cyanocarbons.

## **4.5 – References**

- (1) Chowdhury, S. and Kebarle, P. *J. Am. Chem. Soc.*, **1986**, 108, 5453
- (2) Compton R.N. and Cooper, C.D., *J. Chem. Phys.*, **1977**, 66, 4325
- (3) Zhu, G. and Wang, L. *J. Chem. Phys.*, **2015**, 143, 221102
- (4) Milián, B.; Pou-Amérigo, R.; Viruela, R. and Ortí, E. *Chem. Phys. Lett.*, **2003**, 375, 376
- (5) Milián, B.; Pou-Amérigo, R.; Merchán, M. and Ortí, E. *Chem. Phys. Chem.*, **2005**, 6, 503
- (6) Milián, B.; Pou-Amérigo, R.; Merchán, M. and Ortí, E. *J. Mol. Structure. (THEOCHEM)*, **2004**, 709, 97
- (7) Milián, B.; Pou-Amérigo, R.; Merchán, M. and Ortí, E. *Chem. Phys. Lett.*, **2004**, 391, 148
- (8) Ferraris, J.; Cowan, D.O.; Walatka, V. and Perlstein J.H. *J. Am. Chem. Soc.*, **1973**, 95(3), 948
- (9) Anderson, P.W. and Lee, P.A., *Solid State Comm.* **1973**, 13(5), 595
- (10) Miller, J.S.; Zhang, J.H.; Reiff, W.M.; Dixon, D.A.; Preston, L.D.; Reis, A.H.; Gebert, E.; Extine, M.; Troup, J.; Epstein A.J. and Ward, M.D. *J. Am. Chem. Soc.*, **1987**, 109, 769
- (11) Walzer, K.; Maennig, B.; Pfeiffer, M. and Leo, K., *Chem. Rev.* **2007**, 1233
- (12) Maennig, B.; Pfeiffer, M.; Nollau, A.; Zhou, X.; Leo, K. and Simon, P. *Phys. Rev. B.* **2001**, 64 195208
- (13) Brinkmann, N.R.; Rienstra-Kiracofe, J.C. and Schaefer III, H.F. *Molecular Physics*, **2001**, 99(8), 663
- (14) Martín, N.; Segura, J.L. and Seoane, C. *J. Mater. Chem.*, **1997**, 7(9) 1661
- (15) Parkin, S.S.P.; Ribault, M.; Jerome, D. and Bechgaard, K. *Phys. C: Solid State Phys.*, **1981**, 14, 5305
- (16) Fukuda, K.; Nozawa, T.; Yotsuyanagi, H.; Ichinohe, M.; Sekiguchi, A. and Nakano, M. *J. Phys. Chem. C.*, **2015**, 119(2), 1188

- (17) a) Becke, A.D., *Phys. Rev. A.*, **1988**, 38, 3098  
b) Lee, C.; Yang, W. and Parr, R.G. *Phys. Rev. B.*, **1988**, 37, 785
- (18) Hamprecht, F.A.; Cohen, A.J.; Tozer, D.J. and Handy, N.C. *J. Chem. Phys.*, **1998**, 109, 6264
- (19) Zhao, Y. and Truhlar, D.G., *Theor. Chem. Acc.*, **2008**, 120 , 215
- (20) Perdew, J.P. *Phys. Rev. B.* **1986**, 33, 8822
- (21) Perdew, J.P.; Burke, K. and Ernzerhof, M. *Phys. Rev. Lett.*, **1996**, 77, 3865
- (22) Tao, J.M.; Perdew, J.P.; Staroverov, V.N. and Scuseria, G.E. *Phys. Rev. Lett.*, **2003**, 91, 146401
- (23) Becke, A.D. *J. Chem. Phys.*, **1993**, 98, 5648
- (24) Becke, A.D. *J. Chem. Phys.*, **1993**, 98, 1372
- (25) Adamo, C. and Barone, V. *J. Chem. Phys.* **1999**, 110, 6158
- (26) Staroverov, V.N.; Scuseria, G.E.; Tao, J. and Perdew, J.P. *J. Chem. Phys.*, **2003**, 119, 12129
- (27) Yanai, T.; Tew, D.P. and Handy, N.C. *Chem. Phys. Lett.*, **2004**, 393, 51
- (28) **Gaussian 09**, Revision D.01, Frisch, M. J.; Trucks, G. W.; Schlegel, H. B.; Scuseria, G. E.; Robb, M. A.; Cheeseman, J. R.; Scalmani, G.; Barone, V.; Mennucci, B.; Petersson, G. A.; Nakatsuji, H.; Caricato, M.; Li, X.; Hratchian, H. P.; Izmaylov, A. F.; Bloino, J.; Zheng, G.; Sonnenberg, J. L.; Hada, M.; Ehara, M.; Toyota, K.; Fukuda, R.; Hasegawa, J.; Ishida, M.; Nakajima, T.; Honda, Y.; Kitao, O.; Nakai, H.; Vreven, T.; Montgomery, J. A., Jr.; Peralta, J. E.; Ogliaro, F.; Bearpark, M.; Heyd, J. J.; Brothers, E.; Kudin, K. N.; Staroverov, V. N.; Kobayashi, R.; Normand, J.; Raghavachari, K.; Rendell, A.; Burant, J. C.; Iyengar, S. S.; Tomasi, J.; Cossi, M.; Rega, N.; Millam, J. M.; Klene, M.; Knox, J. E.; Cross, J. B.; Bakken, V.; Adamo, C.; Jaramillo, J.; Gomperts, R.; Stratmann, R. E.; Yazyev, O.; Austin, A. J.; Cammi, R.; Pomelli, C.; Ochterski, J. W.; Martin, R. L.; Morokuma, K.; Zakrzewski, V. G.; Voth, G. A.; Salvador, P.; Dannenberg, J. J.; Dapprich, S.; Daniels, A. D.; Farkas, Ö.; Foresman, J. B.; Ortiz, J. V.; Cioslowski, J.; Fox, D. J. Gaussian, Inc., Wallingford CT, 2009.
- (29) Baurenschmidt, R. and Ahlrics, R. *J. Chem. Phys.*, **1996**, 104, 9047
- (30) Becker, P.; Coppens, P. and Ross, F.K. *J. Am. Chem. Soc.* **1973**, 95(23), 7604

- (31) Hope, H. *Acta. Chem. Scand.* **1968**, 22(3), 1057
- (32) Bock, H.; Näther, C. and Ruppert, K. *Anorg. Allg. Chem.* **1992**, 614, 109
- (33) Zheludev, A.; Grand, A.; Ressouche, E.; Schweizer, J.; Morin, B.; Epstein, A.J.; Dixon, D.A. and Miller, J.S. *J. Am. Chem. Soc.* **1993**, 116, 7243
- (34) Long, R.E.; Sparks, R.A. and Trueblood, K. N. *Acta. Cryst.* **1965**, 18, 932
- (35) Herbstein F. H., *Perspectives in Structural Chemistry*, Vol. IV, 166, New York: Wiley, **1971**
- (36) Hoekstra, A.; Spoelder, T. and Vos, A. *Acta. Cryst. B*, **1972**, 14
- (37) Kistenmacher, B.; Phillips, T.E. and Cowan, D.O. *Acta. Cryst. B*, **1974**, 30, 763
- (38) Miller, J.; Zhang, J.H.; Reiff, W.M.; Dixon, D.A.; Preston, L.D.; Reis, A.H.; Gebert, E.; Extine, M. Troup, J.; Epstein, A.J. and Ward, M.D. *J. Chem. Phys.*, **1987**, 91, 4344
- (39) The Post-HF methods selected for visualization in Figure 3 and Figure 4 are those that deviated the least from the experimental value. The remaining methods plot off-scale.
- (40) Curtiss, L.A.; Redfem, P.C.; Raghavachari, K. and Pople, J.A. *J. Chem. Phys.*, **1998**, 109, 42
- (41) Vikramaditya, T. and Lin, S. *J. Comp. Chem.*, **2017**, 38(21), 1844
- (42) Bailleux, S.; Bogey, M.; Breidung, J.; Bürger, H.; Fajgar, R.; Liu, Y.; Pola, J.; Senzlober, M. and Thiel W. *Angew. Chem. Int. Ed.*, **1996**, 35, 2513
- (43) Bailleux, S.; Bogey, M.; Demaison, J.; Bürger, H.; Senzlober, M.; Breidun, J.; Thiel, W.; Fajgar, R. and Pola, J. *J. Chem. Phys.*, **1997**, 106, 10016
- (44) Fischer, R. and Power, P. *Chem. Rev.* **2010**, 110(7), 3877
- (45) MOLPRO. Optimization and Frequency calculation performed at CCSD(T)-F12/aug-cc-pV(T+d)Z level of theory using numerical gradients
- (46) Dakkouri, M. and Oberhammer, H. *Zeitschrift Für Naturforschung: A*, **1974**, 29(3), 513
- (47) Gräfenstein, J. and Cremer D. *Molecular Physics*, **2001**, 99(11), 981

- (48) Ortiz, R. P.; Casado, J.; Hernández, V.; López Navarrete, J.T.; Viruela, P.M.; Ortí, E.; Takimiya, K. and Otsubo, T. *Angew. Chem. Int. Ed.* **2007**, 46, 9057
- (49) Trinquier, G. and Malrieu, J. *Chem. Eur. J.* **2014**, 20, 814
- (50) Chikamatsu, M.; Mikami, T.; Chisaka, J.; Yoshida, Y.; Azumi, R. and Yase, K. *Appl. Phys. Lett.*, **2007**, 119(2), 1188
- (51) Morita, Y.; Nishida, S.; Murata, T.; Moriguchi, M.; Ueda, A.; Satoh, M.; Arifuku, K.; Sato, K. and Takui, T. *Nat. Mater.*, **2011**, 10, 947
- (52) Lee, J.; Jadhav, P.; Reuswig, P.D.; Yost, S.R.; Thompson, N.J.; Congreve, D.N.; Hontz, E., Van Voorhis, T. and Baldo M.A. *Acc. Chem. Res.*, **2013**, 46, 3544

## **CHAPTER FIVE**

**How the Amount of Hartree-Fock Exchange Affects the Observation of  
the Pseudo Jahn-Teller Effect**

## **Overview**

Potential energy surfaces are a concept at the heart of computational chemistry. Previous studies have detailed the effect of both integration grid size and exact exchange on various properties including the nature of stationary points (i.e., transition structure v. minimum) on potential energy surfaces but none have addressed the root cause of such discrepancies. In this work we introduce a catastrophe theory approach to the problem and examine two contentious stationary points belonging to planar disilene and 2Si TCNQ from the perspective of the pseudo Jahn-Teller effect (pJTE) using DFT methods. First the planar stationary points are characterized using a variety of model chemistries and integration grids. The effect of the amount of Hartree-Fock exchange is then studied and the usage of DFT for assessing pJTE parameters is explored.

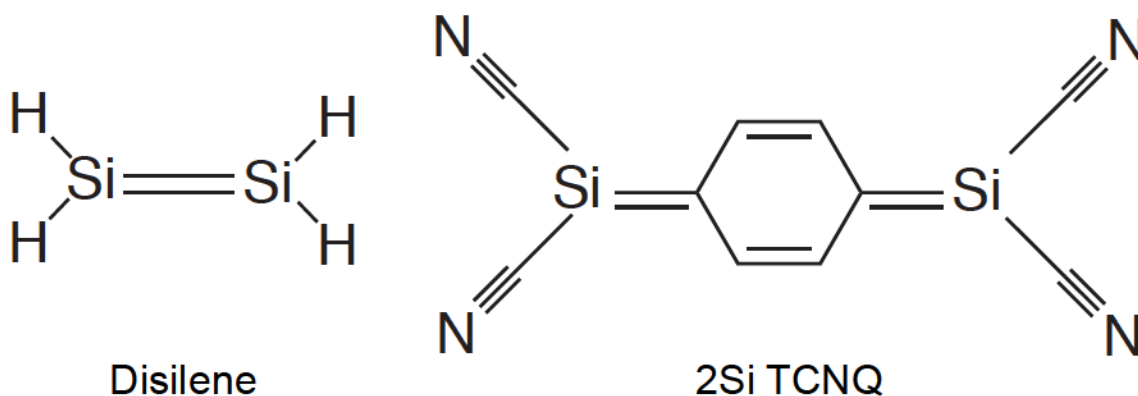
## **5.1 – Introduction**

The potential energy surface (PES) is a concept at the heart of chemistry. The relationship between a molecule's structure and energy can be understood in an intuitive way using a PES, with the PES characterized in terms of minima and maxima (transition structures and/or higher order saddle points) allowing for a variety of phenomena (spectroscopy, photochemistry, chemical kinetics) to be understood and studied within the Born-Oppenheimer approximation on adiabatic potential energy surfaces (APES).<sup>1,2,3</sup>

The energy and structure of a molecule can be determined using Hartree-Fock theory and, to greater accuracy, by including electron correlation using Post-HF methods (e.g., MP2, CCSD, etc.). In the case of the latter, the increase in computational complexity limits their usage to relatively small molecules.<sup>3,4</sup> Moreover, the cost for calculating gradients is (depending on package, algorithms, etc.) approximately six times the cost of one single point calculation at the same level of theory,<sup>4</sup> making optimizations and frequency calculations (which have an even higher cost than a gradient calculation) at these levels of theory intractable for even medium sized molecules. Fortunately, density functional theory (DFT) has advanced greatly and the Kohn-Sham implementation of DFT (KS-DFT) allows for the determination of a molecule's electronic structure at a cost of  $N^{3-4}$  with relatively high accuracy.<sup>5,6</sup>

Previously we studied the APESs of disilene and 2Si TCNQ (**Scheme 5.1**) and found that the character of the  $D_{2h}$  planar stationary points varied with choice of functional.<sup>7</sup> Hybrid functionals containing higher amounts of exact (Hartree-Fock) exchange (HFX) predicted planar minima, while most others predicted transition

structures. Resolving this discrepancy in stationary point characterization is the motivation behind the current study.



**Scheme 5.1**

The pseudo Jahn-Teller effect (pJTE) is the only source of structural instability (symmetry breaking) in electronically non-degenerate polyatomics.<sup>8</sup> It describes how vibronic interactions between the ground and excited states in a diabatic formulation affect the curvature of the ground state. In this approach, the curvature of the diabatic ground state ( $\psi_0$ ) is given by the primary force constant ( $K_0$ )

$$K_0 = \left\langle \psi_0 \left| \left( \frac{\partial^2 H}{\partial Q^2} \right)_0 \right| \psi_0 \right\rangle \quad (5.1)$$

and the magnitude of the vibronic interaction is measured by the non-adiabatic coupling constant ( $F$ ), given by the matrix element

$$F = \left\langle \psi_0 \left| \left( \frac{\partial H}{\partial Q} \right)_0 \right| \psi_n \right\rangle \quad (5.2)$$

where  $\psi_n$  is a diabatic excited electronic state. The extent to which vibronic interactions affect the curvature of the ground state is defined by the vibronic contribution to the curvature of the ground state given by

$$K_v = \frac{F^2}{\Delta} \quad (5.3)$$

where  $\Delta$  is the vertical excitation energy from the ground to the excited state. The total curvature exhibited on the APES is given by

$$K = K_0 - K_v \quad (5.4)$$

This curvature, defined in terms of the force constant, characterizes stationary points. It is known that  $K_0$  can only be positive,<sup>9</sup> therefore,  $K$  can only be negative if  $K_v > K_0$ . The stationary point in this case is a maximum (saddle point) on the PES. Otherwise a minimum is observed. Manipulations of Equations 3 and 4 leads to the *condition for instability* (Equation 5)<sup>8</sup>

$$K_0 < \frac{F^2}{\Delta} \quad (5.5)$$

The direct evaluation of pJTE parameters using a diabatic model is difficult and often not computationally feasible for many systems of interest.<sup>8,10</sup> A common alternative approach is to fit a model Hamiltonian which accounts for the vibronic interaction to a cross-section of the APES along the coordinate of the distorting mode.<sup>10-12</sup> While post-HF methods are typically employed, it is also possible to use DFT as discussed by Soto *et. al.*<sup>14-16</sup>

In this chapter we characterize the planar stationary points of disilene and 2Si TCNQ using DFT, exploring the impact of increased HF exchange. Following this a catastrophe theory model is introduced to explore how double minimum parameters vary with exact exchange. Finally, a model vibronic Hamiltonian is employed and fit to cross-sections of the APES's of both molecules in order to further clarify the impact of increased exact exchange on pJTE parameters. It will be shown that increasing the amount of HFX

affects the description of the APES from the perspective of both catastrophe theory and the pJTE.

## **5.2 – Methodology**

Disilene and 2Si TCNQ were optimized in  $D_{2h}$  symmetry using DFT. Thirteen functionals were used: one LSDA (SVWN<sup>17</sup>), four GGA's/meta-GGA's (BLYP,<sup>18</sup> PBE,<sup>19</sup> M06-L<sup>20</sup> and TPSS<sup>21</sup>), seven hybrids (TPSSh (HFX:10%),<sup>22</sup> B3LYP (HFX: 21%),<sup>23</sup> PBE0 (HFX: 25%),<sup>24</sup> M06 (HFX: 28%),<sup>20</sup> BHandHLYP (HFX: 50%),<sup>25</sup> M06-2X (HFX: 56%) and M06-HF (HFX: 100%),<sup>20</sup> and two range-separated (RS) hybrids (CAM-B3LYP (HFX: 20%(short), 65%(long))<sup>26</sup> and w-B97XD (HFX: 22%(short), 100%(long))<sup>27</sup> were combined with five basis sets: a triple-zeta Pople style basis set with increasing polarization functions (6-311++g **BS1**: (d,p), **BS2**: (2d,2p), **BS3** (2df,pd)), the Def2TZVPP (**BS4**) basis set developed by Ahlrich's group and the Dunning-Huzinaga full double-zeta (D95) basis set (**BS5**). Stationary points were characterized by frequency calculations and the displacement modes of imaginary frequencies followed to locate minima. Time-Dependent (TD) DFT calculations were performed to calculate the vertical excitation energies. All calculations were performed using Gaussian09 Rev. D.01.<sup>28</sup>

To study the effect of exact exchange the BLYP functional is combined with the appropriate keywords in G09 to vary the A parameter in Equation 6. We refer to this functional as BXLYPTest throughout.<sup>29</sup>

$$A \cdot E_X^{Slater} + (1 - A) \cdot E_X^{HF} + B \cdot \Delta_X^{Becke} + C \cdot E_C^{LYP} + (1 - C) \cdot E_C^{VWN} \quad (5.6)$$

The effect of the integration grid size was tested by using the three most common grid sizes in G09: Fine, Ultrafine and Superfine. Additionally, the spherical product grid referred to as SG-1 was also tested. The effect of optimization criteria (tight and very tight)

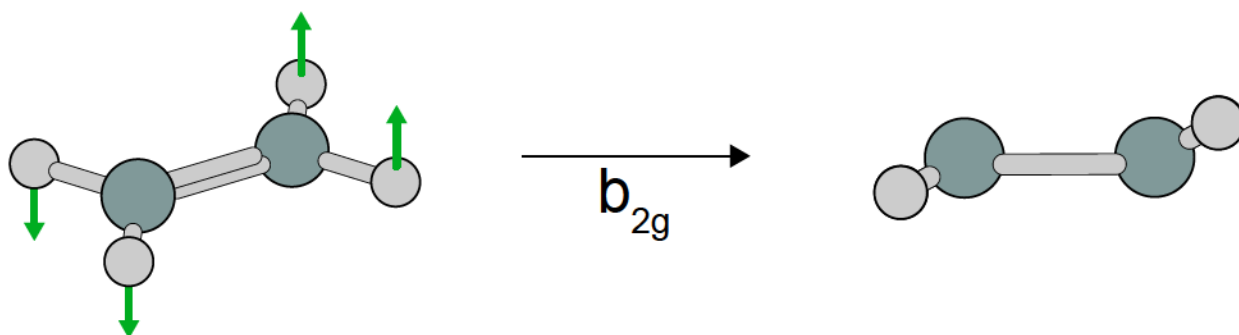
was also examined. No significant effects were observed (See Appendix C Tables C1-3 for sample data).

In the generation of the APES cross-sections, displaced geometries were created by subtracting the coordinates of the low and high symmetry geometries and adding the difference to the high symmetry coordinates in 0.1 increments. The resulting surfaces were fit to the model vibronic Hamiltonian described below using Prism 7.0.<sup>30,31</sup>

### **5.3 – Results and Discussion**

#### **5.3.1 – The Stationary Points of Disilene and 2Si TCNQ**

We begin by establishing reference data for the planar  $D_{2h}$  structure of disilene by optimizing its structure at the CCSD(T)-F12/aug-cc-pv(d+t)Z level of theory.<sup>32</sup> The planar stationary point is characterized as a transition structure (TS) unstable with respect to a  $b_{2g}$ -bending mode ( $221i\text{ cm}^{-1}$  – **Scheme 5.2**). The TS relaxes to a *trans*-bent  $C_{2h}$  structure that is 0.50kcal/mol more stable and equally pyramidalized ( $360^\circ - \sum\angle_{\text{Si}} = 8.6^\circ$ ) at the Si-nuclei, in agreement with Post-HF results obtained by Nori-Shargh *et. al.*<sup>33</sup> The planar stationary point of disilene was characterized using the chosen methods and the wavenumbers of the  $b_{2g}$  bending mode are compiled in **Table 5.1**.



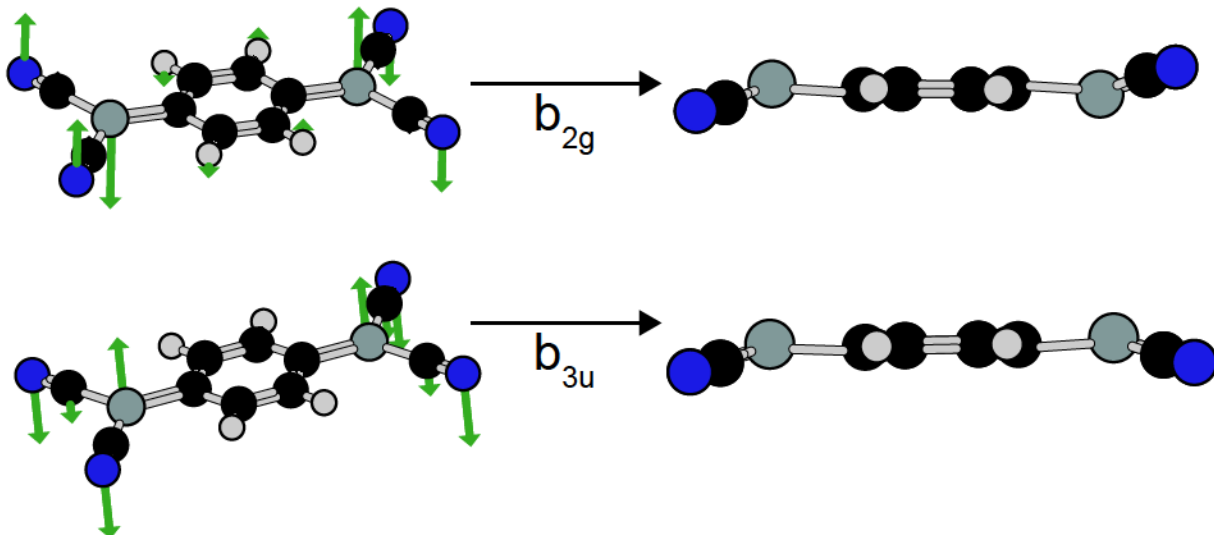
**Scheme 5.2**

**Table 5.1:** Disilene  $b_{2g}$  mode wavenumber ( $\text{cm}^{-1}$ ) calculated using HF and DFT/BS1-BS5.

	BS1	BS2	BS3	BS4	BS5
HF	14 <i>i</i>	178	174	188	161 <i>i</i>
SVWN	216 <i>i</i>	207 <i>i</i>	200 <i>i</i>	195 <i>i</i>	180 <i>i</i>
BLYP	293 <i>i</i>	281 <i>i</i>	280 <i>i</i>	273 <i>i</i>	283 <i>i</i>
M06-L	292 <i>i</i>	259 <i>i</i>	251 <i>i</i>	258 <i>i</i>	306 <i>i</i>
PBE	256 <i>i</i>	245 <i>i</i>	241 <i>i</i>	236 <i>i</i>	235 <i>i</i>
TPSS	259 <i>i</i>	245 <i>i</i>	247 <i>i</i>	239 <i>i</i>	258 <i>i</i>
TPSSh	238 <i>i</i>	216 <i>i</i>	219 <i>i</i>	210 <i>i</i>	237 <i>i</i>
B3LYP	244 <i>i</i>	221 <i>i</i>	224 <i>i</i>	214 <i>i</i>	239 <i>i</i>
PBE0	193 <i>i</i>	168 <i>i</i>	167 <i>i</i>	158 <i>i</i>	178 <i>i</i>
M06	286 <i>i</i>	262 <i>i</i>	262 <i>i</i>	276 <i>i</i>	296 <i>i</i>
BH&HLYP	169 <i>i</i>	107 <i>i</i>	107 <i>i</i>	88 <i>i</i>	185 <i>i</i>
M06-2X	23 <i>i</i>	46	72	60	150
M06-HF	235	192	171	165	325
CAM-B3LYP	156 <i>i</i>	121 <i>i</i>	118 <i>i</i>	102 <i>i</i>	149 <i>i</i>
w-B97XD	170 <i>i</i>	117 <i>i</i>	112 <i>i</i>	91 <i>i</i>	134 <i>i</i>

HF / BS2-BS4, M06-2X / BS2-BS5 and M06-HF/BS1-BS5 predict the planar stationary point to be a minimum. HF and M06-2X with BS1 predict a transition structure, but deviate severely from the reference value. All remaining model chemistries predicted a transition structure.

A high level reference value could not be obtained for 2Si TCNQ due to size. The majority of DFT methods predict the planar 2Si TCNQ stationary point to be a second-order saddle point unstable with respect to  $b_{2g}$  and  $b_{3u}$  bending modes (**Scheme 5.2** and **Table 5.2**). M06-2X, M06-HF, CAM-B3LYP and w-B97XD predict planar minima with all basis sets, as does BH&HLYP when combined with BS2-BS4 and HF combined with BS1-BS3 and BS5. PBE0/BS2 and HF/BS4 predict a planar TS unstable with respect to the  $b_{2g}$  mode only. BLYP predicts the greatest imaginary wavenumber, with the exception of 2Si TCNQ  $b_{3u}$  mode when combined with BS2 (PBE) and BS5 (M06-L), and M06-HF predicts the greatest real wavenumber.



**Scheme 5.3**

For disilene and 2Si TCNQ most functionals predict the lowest wavenumber when combined with BS1 and increasing the polarization functions (BS1 to BS3) generally causes a decrease in the wavenumber; the values obtained using BS2 and BS3 are similar. BS4 predicts the lowest wavenumber of all TZ basis sets except when combined with the M06 suite, with the exception of M06-HF. The other M06 functionals predict the largest wavenumber when combined with BS5.

**Table 5.2:** 2Si TCNQ  $b_{2g}$  and  $b_{3u}$  mode wavenumbers ( $\text{cm}^{-1}$ ) calculated using HF and DFT/BS1-BS5.

	BS1		BS2		BS3		BS4		BS5	
	$b_{2g}$	$b_{3u}$								
HF	59	34	70	37	66	88	66 <i>i</i>	36	49	32
SVWN	35 <i>i</i>	18 <i>i</i>	21 <i>i</i>	7	26 <i>i</i>	6 <i>i</i>	27 <i>i</i>	8 <i>i</i>	23 <i>i</i>	2 <i>i</i>
BLYP	80 <i>i</i>	73 <i>i</i>	75 <i>i</i>	66 <i>i</i>	74 <i>i</i>	65 <i>i</i>	74 <i>i</i>	65 <i>i</i>	78 <i>i</i>	69 <i>i</i>
M06-L	67 <i>i</i>	55 <i>i</i>	66 <i>i</i>	54 <i>i</i>	52 <i>i</i>	35 <i>i</i>	59 <i>i</i>	44 <i>i</i>	82 <i>i</i>	71 <i>i</i>
PBE	60 <i>i</i>	48 <i>i</i>	51 <i>i</i>	68 <i>i</i>	53 <i>i</i>	40 <i>i</i>	54 <i>i</i>	40 <i>i</i>	57 <i>i</i>	44 <i>i</i>
TPSS	69 <i>i</i>	60 <i>i</i>	62 <i>i</i>	52 <i>i</i>	64 <i>i</i>	54 <i>i</i>	66 <i>i</i>	56 <i>i</i>	68 <i>i</i>	57 <i>i</i>
TPSSh	60 <i>i</i>	50 <i>i</i>	52 <i>i</i>	41 <i>i</i>	55 <i>i</i>	44 <i>i</i>	57 <i>i</i>	47 <i>i</i>	59 <i>i</i>	47 <i>i</i>
B3LYP	60 <i>i</i>	52 <i>i</i>	53 <i>i</i>	43 <i>i</i>	54 <i>i</i>	44 <i>i</i>	55 <i>i</i>	45 <i>i</i>	59 <i>i</i>	48 <i>i</i>
PBE0	34 <i>i</i>	21 <i>i</i>	16 <i>i</i>	9	25 <i>i</i>	11 <i>i</i>	27 <i>i</i>	13 <i>i</i>	31 <i>i</i>	17 <i>i</i>
M06	72 <i>i</i>	66 <i>i</i>	70 <i>i</i>	63 <i>i</i>	60 <i>i</i>	50 <i>i</i>	58 <i>i</i>	48 <i>i</i>	74 <i>i</i>	66 <i>i</i>
BH&HLYP	21 <i>i</i>	12 <i>i</i>	20	23	14	16	9	15	22 <i>i</i>	8 <i>i</i>
M06-2X	33	66	31	38	42	31	39	29	49	33
M06-HF	84	105	86	108	84	45	84	45	94	45
CAM-B3LYP	26	22	38	27	35	26	37	27	26	22
w-B97XD	37	30	46	31	44	69	44	31	32	25

The inclusion of exact exchange causes a decrease in all wavenumbers. In **Figure 5.1A** and **5.1B** the wavenumbers of the bending modes of interest are plotted against the amount of exact exchange for the BLYP family and the M06 suite of functionals. In the case of disilene, all Becke type functionals, M06-L and M06 predict a TS while the higher exchange M06 functionals predict a planar minimum. A similar trend is observed for 2Si TCNQ, but with BHandHLYP predicting a planar minimum.

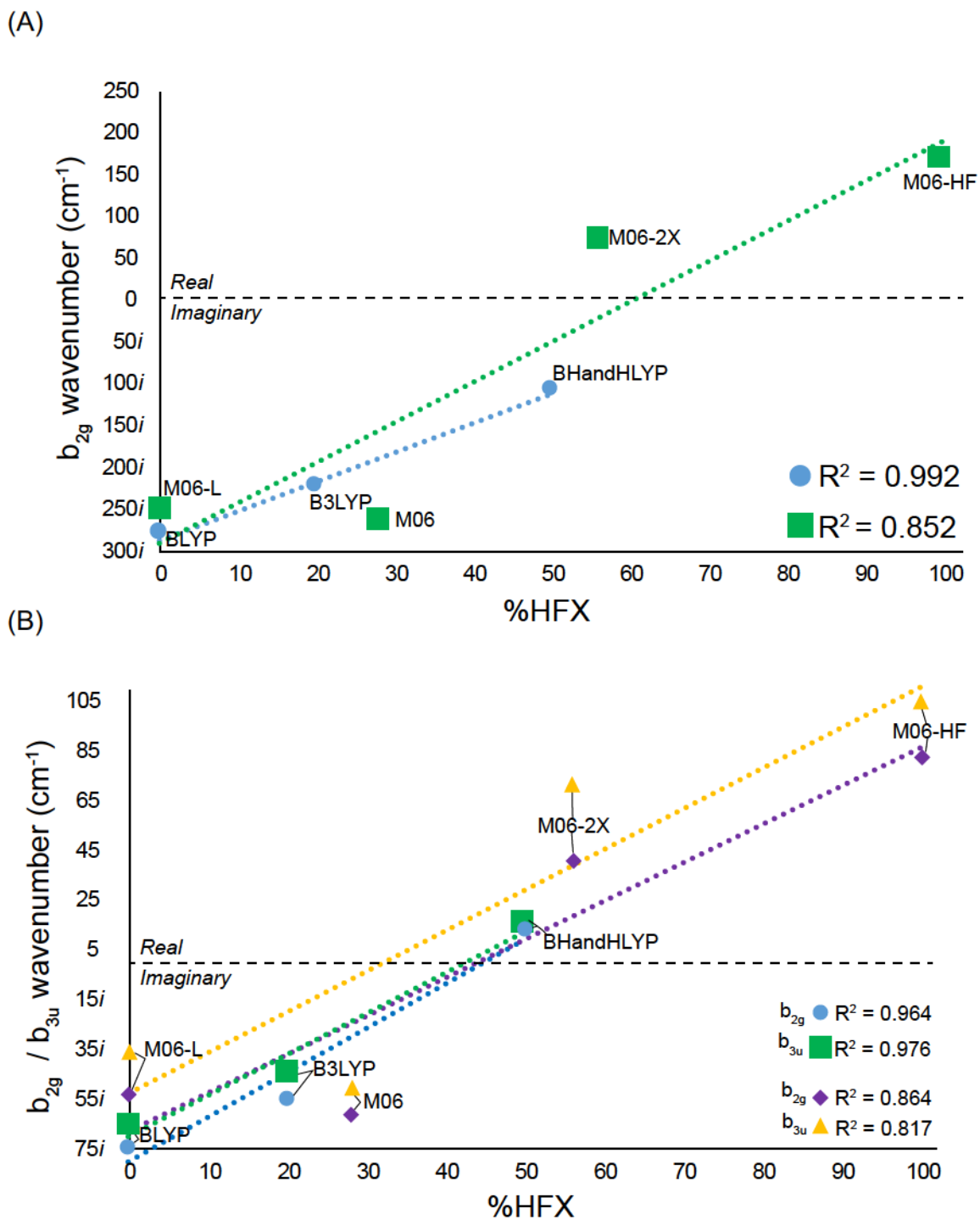


**Figure 5.1:** Value of (A)  $b_{2g}$  wavenumber (disilene) and (B)  $b_{2g}$  and  $b_{3u}$  wavenumbers (2Si TCNQ) for the BLYP and M06 family of functionals.

### 5.3.2 – Insights from Catastrophe Theory

To examine the discrepancies in stationary points we make use of the cusp catastrophe presented by Thom.<sup>34,35</sup> It describes two different states of behaviour in a system: one characterized by two isolated minima separated by a local maximum (a double-well APES) and another characterized by a single minimum (a single-well APES). It is described by Equation 5.7 and has two control parameters, **a** and **b**,

$$f(x; a, b) = \frac{1}{4}x^4 + \frac{1}{2}ax^2 + bx \quad (5.7)$$

where **a** is related to the bifurcation of the critical points and **b** is related to the shape of the APES. The control parameter plane is visualized in **Figure 5.2**. In all cases studied here, **b=0** due to symmetry.

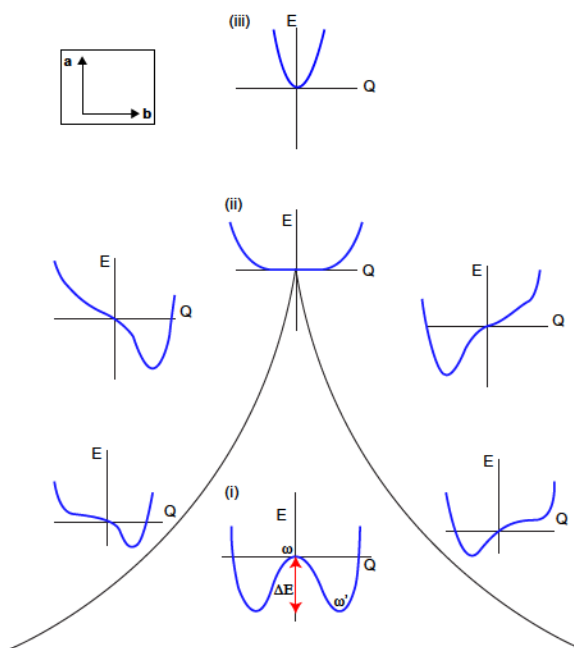


**Figure 5.2:** Visualization of the control parameter plane for the cusp catastrophe including the definitions of stabilization energy ( $\Delta E$ ), and vibrational modes  $\omega$  (symmetry breaking) and  $\omega'$  (symmetry restoring).

Within the cusp shaped region (**Figure 5.2 (i)**)  $a < 0$  and a double well exists, with three critical points corresponding to the geometries observed: one for the high symmetry

( $D_{2h}$ ) geometry and two for equivalent, low symmetry  $C_{2h}$  /  $C_{2v}$  configurations. Outside of the cusp,  $a > 0$  and the APES is a single-well (**Figure 5.2 Region (iii)**). To move from **Region (i)** to **Region (iii)** a bifurcation of critical points occurs when they coalesce at the top of the cusp (**Figure 5.2 Region (ii)**).

In the systems studied, the stabilization ( $\Delta E_{SB}$ ) achieved through symmetry breaking is commensurate with the degree of pyramidalization at the Si-nuclei (SI Figure 1A–C). Additionally, the wavenumbers of the symmetry breaking mode ( $\omega$ ) (**Table 5.1** and **5.2**) and the mode that restores planarity in the low symmetry geometry ( $\omega'$ ) are proportional (Appendix C Tables C7-11).

For both molecules, GGA functionals typically report greater magnitudes of pyramidalization, stabilization and vibrational wavenumbers indicating the surface is a well-defined double-well potential and therefore occur lower on the  $a$ -axis. Conversely, hybrid functionals that predict symmetry breaking typically predict lower magnitudes of pyramidalization, stabilization and vibrational modes. While these cases still fall within the cusp region, they occur higher on the  $a$ -axis than the GGA functionals and are described by less well defined double-well potentials.

In both disilene and 2Si TCNQ the functionals containing higher amounts of exact exchange, and in the case of 2Si TCNQ, range separated functionals, fall outside the cusp region and describe the APES as a single-well potential. Thus, the amount of exact exchange is related to the  $a$  control parameter, dictating where along the  $a$ -axis in **Figure 5.2** the system occurs.

To examine how exact exchange impacts the  $a$  control parameter we use the BXLYPTest functional described in the methodology section, and increase the amount of

exact exchange from 0 to 100% in 10% increments. The  $D_{2h}$  structures of disilene and 2Si TCNQ are optimized at each increment and the obtained stationary points characterized for each increase. All imaginary modes are followed to the APES minima. The APESs are mapped out along the modes of interest for each increment in BXLYPTest in **Figure 5.4**.

In **Figure 5.4** the APESs are well-defined double-wells when  $X=0\%$ . As the amount of exact exchange is increased the surfaces become flatter and the three stationary points approach one another. The effects of symmetry breaking are diminished as indicated by the reduction in stabilization and pyramidalization. When  $X$  is greater than 70% (disilene) and 50% (2Si TCNQ) the systems enter the region outside the cusp and symmetry breaking is no longer observed. The single-well potentials become more well defined as  $X$  approaches 100%.

The value of the **a** control parameter is obtained by fitting each APES in **Figure 5.4** to a fourth order polynomial.<sup>36</sup> As expected, the value of **a** is  $< 0$  when symmetry breaking is detected, and increases with %HFX. Conversely, the value of **a** is  $> 0$  when symmetry breaking is not observed and increases with %HFX (See SI-Table 12-14). In **Figure 5a** (Disilene) and **5b** (2Si TCNQ) the value of **a** is plotted as a function of %HFX.<sup>37</sup> The polynomial regressions presented in **Figure 5.5a** and **5.5b** describe how the **a** control parameter varies with %HFX. Disilene and 2Si TCNQ are predicted to exist within the cusp region when %HFX is less than 74.5% and 56.5%, respectively.

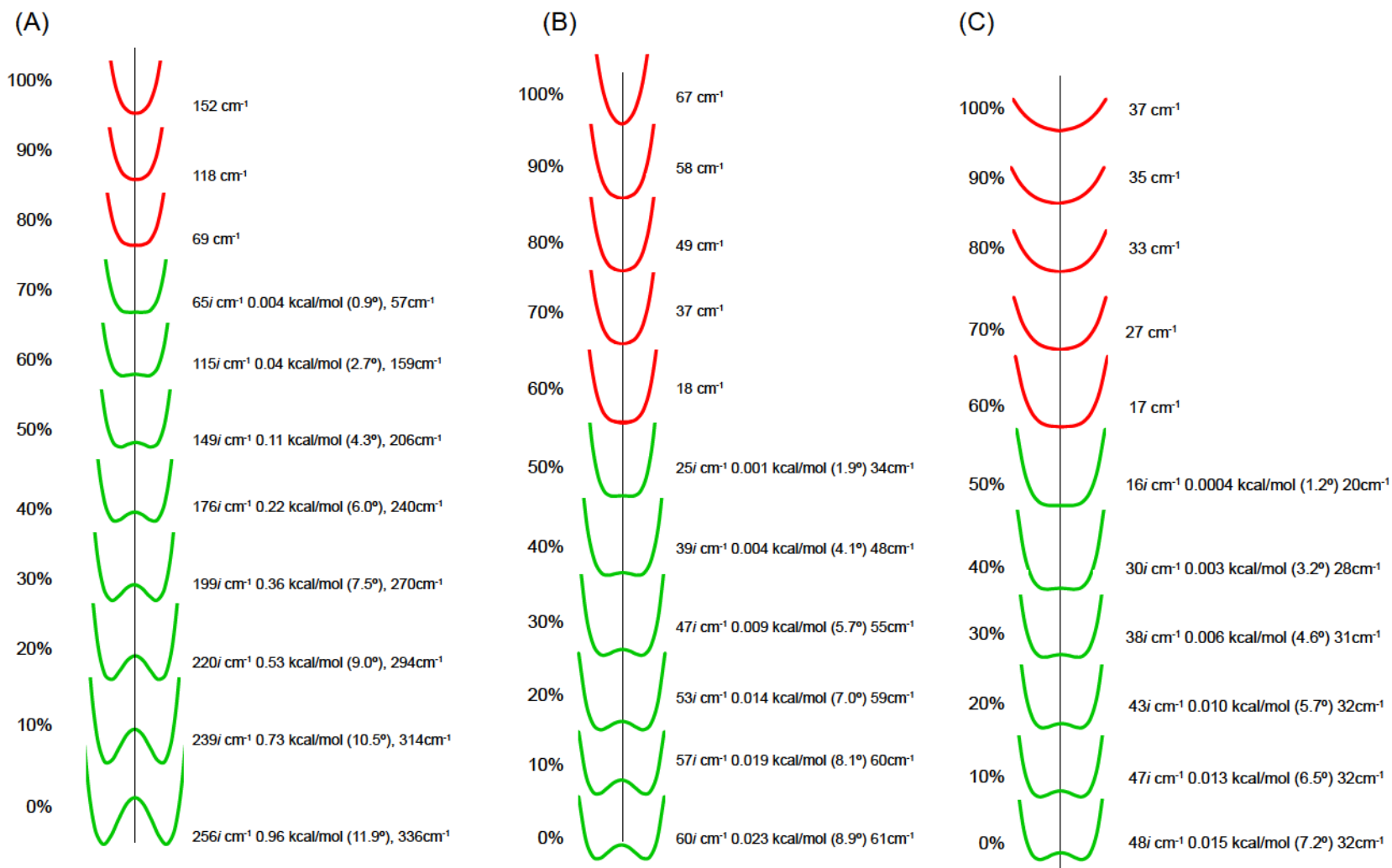


**Figure 5.4:** APES scans as %HFX is increased for (A) disilene (B) 2Si TCNQ  $b_{2g}$  mode and (C) 2Si TCNQ  $b_{3u}$  mode. Value of distorting mode, stabilization, pyramidalization and value of planarity restoring mode for each increment.

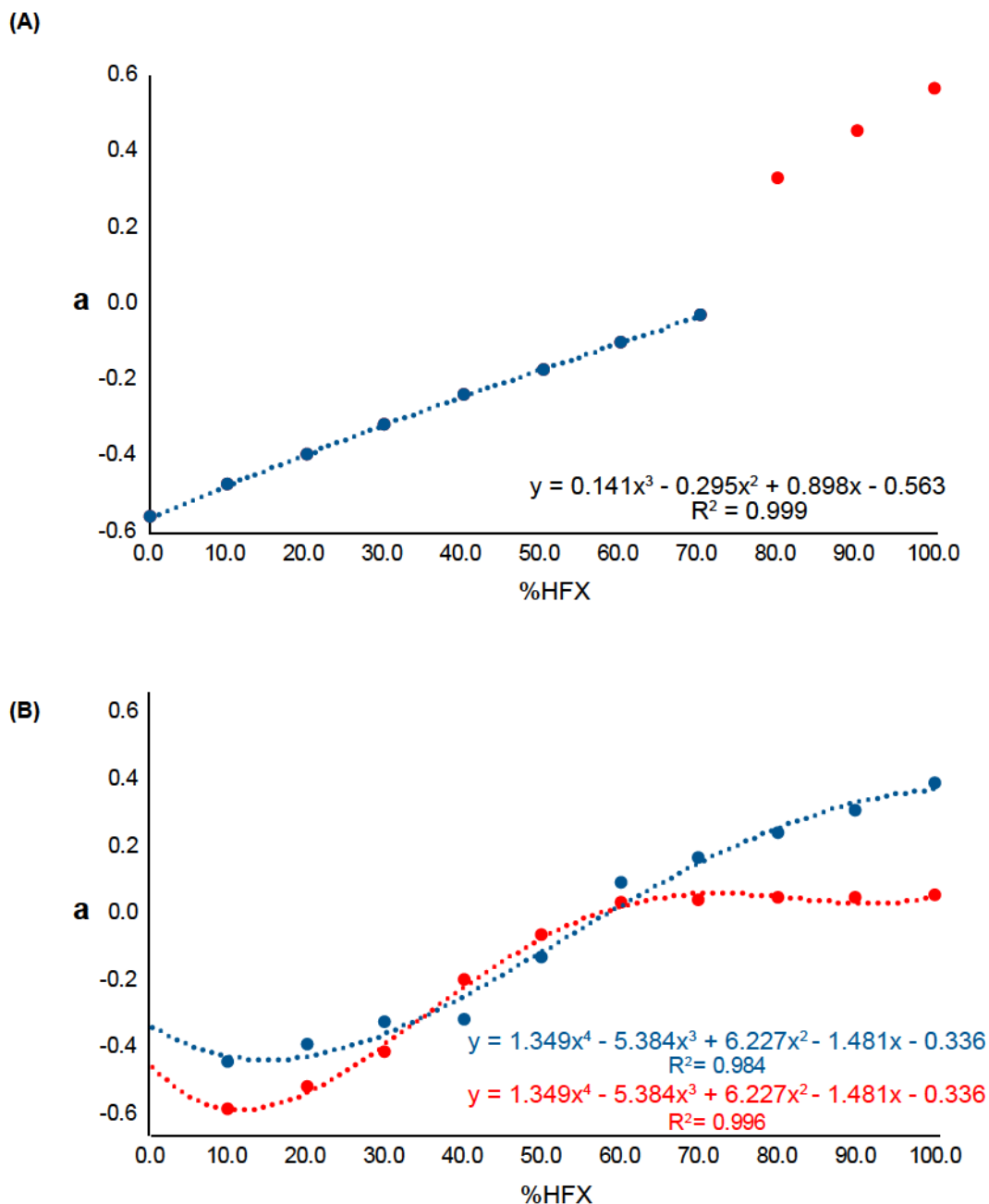


**Figure 5.5:** Change in **a** control parameter with increased exact exchange in BXLYPTest for (A) Disilene and (B) 2Si TCNQ  $b_{2g}$  (blue) and  $b_{3u}$  (red) vibrational modes.

### 5.3.3 – The Impact of Exact Exchange on the pJTE

In the pJTE the vibronic interaction between the ground and excited state can only be non-zero if the symmetry requirement is satisfied: the direct product of the irreducible representations of the coupling states must produce the irreducible representation of the

vibrational mode.<sup>8,10</sup> Based on this requirement two different pJTEs are identified: (<sup>1</sup>A<sub>G</sub> + <sup>1</sup>B<sub>2G</sub>) ⊗ b<sub>2g</sub> *trans*-bending in disilene and 2Si TCNQ; and (<sup>1</sup>A<sub>G</sub> + <sup>1</sup>B<sub>3U</sub>) ⊗ b<sub>3u</sub> *cis*-bending in 2Si TCNQ.

The cross-sections of the APESs shown in **Figure 5.5** are fit to a model vibronic Hamiltonian described by<sup>10</sup>

$$E(Q) = \frac{1}{2} \left[ K_0 - \frac{F^2}{\Delta} \right] Q^2 - \frac{1}{4} \left[ \frac{F^4}{\Delta^3} \right] Q^4 + \Delta E_{SB} \quad (5.6)$$

where  $Q$  is the coordinate along the APES. All excitation values ( $\Delta$ ) are obtained by TD-DFT calculations on the high symmetry geometry while  $F$  and  $K_0$  are obtained from the fitting. Relevant values are presented in **Table 5.4** (disilene), **Table 5.5** (2Si TCNQ b<sub>2g</sub>) and **Table 5.6** (TCNQ b<sub>3u</sub>)

**Table 5.3:** Parameters for (<sup>1</sup>A<sub>G</sub> + <sup>1</sup>B<sub>2G</sub>) ⊗ b<sub>2g</sub> pJTE in disilene.  $K_0$ ,  $K_v$  and  $K$  (eV/Å<sup>2</sup>),  $\Delta$  (eV),  $F$  (eV/Å)

%HFX	$\Delta$	$K_0$	$F$	$K_v$	$K$
0%	4.779	2.330	3.718	2.893	-0.562
10%	4.882	2.347	3.714	2.826	-0.478
20%	4.989	2.348	3.700	2.744	-0.396
30%	5.080	2.321	3.660	2.637	-0.316
40%	5.177	2.271	3.604	2.509	-0.238
50%	5.271	2.501	3.756	2.676	-0.175
60%	5.365	2.411	3.671	2.512	-0.101
70%	5.455	2.226	3.508	2.256	-0.031
80%	5.546	8.846	6.873	8.516	0.330
90%	5.637	9.096	6.981	8.645	0.451
100%	5.726	9.403	7.113	8.837	0.567

**Table 5.4:** Parameters for ( $^1A_G + ^1B_{2G}$ )  $\otimes$   $b_{2g}$  pJTE in 2Si TCNQ.  $K_0$ ,  $K_V$  and  $K$  (eV/Å<sup>2</sup>),  $\Delta$  (eV),  $F$  (eV/Å)

%HFX	$\Delta$	$K_0$	$F$	$K_V$	$K$
0%	2.769	4.176	3.764	5.117	-0.941
10%	2.979	2.347	2.884	2.792	-0.445
20%	3.191	2.556	3.068	2.950	-0.394
30%	3.408	2.770	3.246	3.092	-0.321
40%	3.630	4.199	4.049	4.518	-0.319
50%	3.855	4.237	4.105	4.371	-0.134
60%	4.085	2.967	3.427	2.876	0.091
70%	4.317	3.179	3.605	3.011	0.168
80%	4.547	3.341	3.754	3.099	0.241
90%	4.771	3.520	3.913	3.210	0.310
100%	4.981	3.737	4.085	3.351	0.386

**Table 5.5:** Parameters for ( $^1A_G + ^1B_{3U}$ )  $\otimes$   $b_{3u}$  pJTE in 2Si TCNQ.  $K_0$ ,  $K_V$  and  $K$  (eV/Å<sup>2</sup>),  $\Delta$  (eV),  $F$  (eV/Å)

%HFX	$\Delta$	$K_0$	$F$	$K_V$	$K$
0%	2.670	2.485	2.874	3.094	-0.610
10%	2.874	2.987	3.204	3.572	-0.585
20%	3.080	3.381	3.466	3.901	-0.520
30%	3.291	3.668	3.665	4.081	-0.413
40%	3.505	3.051	3.375	3.249	-0.198
50%	3.722	3.530	3.657	3.593	-0.063
60%	3.940	1.698	2.564	1.668	0.030
70%	4.154	1.357	2.338	1.316	0.041
80%	4.359	1.075	2.118	1.029	0.046
90%	4.543	0.909	1.978	0.861	0.048
100%	4.699	0.752	1.815	0.701	0.051

In all cases,  $\Delta$  increases and  $K$  decreases as %HFX is increased. The other values ( $K_0$ ,  $F$  and  $K_V$ ) display additional trends. The changes in  $K$  are consistent with those described by the cusp catastrophe and also with the scans along the APES presented in

**Figure 5.5.**

When symmetry breaking is observed in disilene,  $K_0$  and  $F$  increase from 0 to 20% HFX then decrease;  $K_V$  decreases from 0 to 70%. When symmetry breaking is not observed all values increase.

When the  $(^1A_G + ^1B_{2G}) \otimes b_{2g}$  pJTE in 2Si TCNQ is observed,  $K_0$ ,  $F$  and  $K_V$  decrease from 0 to 10%, but otherwise they typically increase. The difference in trend from 0 to 10% is likely due to the 0% being an outlier; the magnitude in all values obtained at this point is greater than the other entries in **Table 5.5**. When symmetry breaking is not observed all values increase.

When the  $(^1A_G + ^1B_{3U}) \otimes b_{3u}$  pJTE in 2Si TCNQ is observed all values increase with the exception of the 40% entry in **Table 5.6**. When symmetry breaking is not observed all values decrease.

The effect of increased exact exchange on TD-DFT excitation energies has been discussed in the literature before in charge-transfer states<sup>38</sup> and is the result of delocalization error.<sup>40</sup> The excitation energies of 2Si TCNQ are affected more by the increase in exact exchange than disilene as indicated by slopes from linear regressions (Appendix C C4A and C4B). 2Si TCNQ is a delocalized system and can potentially exist as a zwitterion (an intra-molecular charge transfer state), so it is more susceptible to the delocalization error.

## **5.4 – Conclusions**

This work demonstrates the effect of increased exact exchange on the characterization of two contentious stationary points. While GGA functions and lower exchange containing hybrids predict symmetry breaking, those with higher fractions of

exact exchange (BHandHLYP, M06-2X and M06-HF) and range-separated hybrids (CAM-B3LYP and wB97-XD) do not.

Additionally, a simple approach to the evaluation of pJTE parameters using DFT was presented. The model vibronic Hamiltonian described was able to account for the changes in the APES that occur with increased exact exchange with some limitations. It may be a viable method to study the pJTE in systems for which post-HF are not feasible. Finally, the increase in excitation energies with increased amounts of exact exchange is the result of delocalization error.

The effect of increased exacted exchange was studied using an application of catastrophe theory previously unexplored. The cusp catastrophe model described here has further reaching applications to a variety of quantum chemical problems to be addressed by our group in later work.

## **5.5 – References**

- (1) Lewars, E.G. *Computational Chemistry*. Springer, **2003** DOI: 10.1007/987-90-481-3862-3\_2,
- (2) Simons, J. *Introduction to Theoretical Chemistry, Second Edition*. Available free of charge from: <https://simons.hec.utah.edu/ITCSecondEdition/>
- (3) Mustroph, H. *Chem. Phys. Chem.*, **2016**, 17, 1
- (4) Szabo, A. and Ostlund, N.S. *Modern Quantum Chemistry: An Introduction to Advanced Electronic Structure Theory*. Macmillan Publishing Co. Inc., New York, (**1982**)
- (5) Jensen, F. *Introduction to Computational Chemistry*, Wiley, Chichester, UK, (**2007**)
- (6) Koch, W. and Holthausen, K.C. *A Chemist's Guide to Density Functional Theory*. Wiley-VHC, (**2001**)
- (7) Maley, S.M.; Esau, C. and Mawhinney, R.C. *Struct. Chem.*, **2018** doi: 10.1007/s11224-018-1186-1
- (8) Bersuker, I.B. *Chem. Rev.*, **2013**, 113(3) 1351
- (9) Bersuker, I.B. *Teor. Ekip. Khim.*, **1980**, 66, 161
- (10) Bersuker, I.B. *The Jahn-Teller Effect*. Cambridge University Press, Cambridge, UK. (**2005**)
- (11) Liu, Y.; Bersuker, I.B. and Boggs, J.E. *Chemical Physics*, **2013**, 417, 26
- (12) Kayi H.; Garcia-Fernandez, P.; Bersuker, I.B. and Boggs, J.E. *J. Phys. Chem. A.*, **2013**, 117, 8671
- (13) Kayi, H.; Bersuker, I.B. and Boggs, J.E. *J. Mol. Str.* **2012**, 1023, 108
- (14) Soto, J.R.; Molina, B. and Castro, J.J. *Phys. Chem. Chem. Phys.*, **2015**, 17 7624
- (15) Soto, J.R.; Molina, B. and Castro, J.J. *MRS Advances*, **2016**, 1(22) 1591

- (16) Soto, J.R.; Molina, B. and Castro, J.J. *MRS Advances*, **2017**, 2(29) 1563
- (17) a) Hohenberg, P. and Kohn, W. *Phys. Rev.*, **1964**, 136, B864-B71  
b) Vosko, S.H.; Wilk, L and Nusair, M. *Can. J. Phys.*, **1980**, 58, 1200
- (18) a) Becke, A.D. *Phys. Rev. A.*, **1988**, 38, 3098  
b) Lee, C., Yang, W. and Parr, R.G. *Phys. Rev. B*, **1988**, 37, 785
- (19) Perdew, J.P.; Burke, K. and Ernzerhof, M. *Phys. Rev. Lett.*, **77** 3865-3868 (1996)
- (20) Zhao, Y. and Truhlar, D.G. *Theor. Chem. Acct.*, **120** 215 (2008)
- (21) Tao, J.M.; Perdew, J.P.; Staroverov, V.N. and Scuseria, G.E. *Phys. Rev. Lett.* **91** 146401 (2003)
- (22) Staroverov, V.N.; Scuseria, G.E.; Tao, J. and Perdew, J.P. *J. Chem. Phys.*, **2003**, 119, 12129
- (23) Becke, A.D. *J. Chem. Phys.*, **1993**, 98, 5648
- (24) Adamo, C. and Barone, V. *J. Chem. Phys.*, **1999**, 110, 6158
- (25) Becke, A.D. *J. Chem. Phys.*, **1993**, 98, 1372
- (26) Yanai, T.; Tew, D. and Handy, N. *Chem. Phys. Lett.*, **2004**, 393, 51
- (27) Chai, J.D. and Head-Gordon, M. *Phys. Chem. Chem. Phys.* **2008**, 10, 6615

- (28) **Gaussian 09, Revision D.01**, Frisch, M. J.; Trucks, G. W.; Schlegel, H. B.; Scuseria, G. E.; Robb, M. A.; Cheeseman, J. R.; Scalmani, G.; Barone, V.; Mennucci, B.; Petersson, G. A.; Nakatsuji, H.; Caricato, M.; Li, X.; Hratchian, H. P.; Izmaylov, A. F.; Bloino, J.; Zheng, G.; Sonnenberg, J. L.; Hada, M.; Ehara, M.; Toyota, K.; Fukuda, R.; Hasegawa, J.; Ishida, M.; Nakajima, T.; Honda, Y.; Kitao, O.; Nakai, H.; Vreven, T.; Montgomery, J. A., Jr.; Peralta, J. E.; Ogliaro, F.; Bearpark, M.; Heyd, J. J.; Brothers, E.; Kudin, K. N.; Staroverov, V. N.; Kobayashi, R.; Normand, J.; Raghavachari, K.; Rendell, A.; Burant, J. C.; Iyengar, S. S.; Tomasi, J.; Cossi, M.; Rega, N.; Millam, J. M.; Klene, M.; Knox, J. E.; Cross, J. B.; Bakken, V.; Adamo, C.; Jaramillo, J.; Gomperts, R.; Stratmann, R. E.; Yazyev, O.; Austin, A. J.; Cammi, R.; Pomelli, C.; Ochterski, J. W.; Martin, R. L.; Morokuma, K.; Zakrzewski, V. G.; Voth, G. A.; Salvador, P.; Dannenberg, J. J.; Dapprich, S.; Daniels, A. D.; Farkas, Ö.; Foresman, J. B.; Ortiz, J. V.; Cioslowski, J.; Fox, D. J. Gaussian, Inc., Wallingford CT, 2009.
- (29) The IOps used to manually vary the amount of exact exchange are IOp(3/76), IOp(3/77) and IOp(3/78). See the Gaussian09 users guide for additional details.
- (30) Non-linear regression performed to fit the model vibronic Hamiltonian (Equation 7) using GraphPad Prism version 7.00 for Macintosh, GraphPad Software, La Jolla California, USA. [www.graphpad.com](http://www.graphpad.com)
- (31) The polynomial coefficients and  $r^2$  value for the curve fitting are available in Appendix C Tables C13-14.
- (32) CCSD(T)-F12/aug-cc-pv(d+t)Z calculations performed in Molpro Version 2015.1
- (33) Nori-Shargh, D.; Mousavi, S.N., and Boggs, J.E. *J. Phys. Chem. A*, **2013**, 117(7), 1621
- (34) Thom, R. *Structural Stability and Morphogenesis: An Outline of a General Theory of Models*. W. A. Benjamin, Inc. Massachusetts, (1975)
- (35) Gilmore, R. *Catastrophe Theory*. Encyclopedia of Applied Physics, Vol. 3. VCH Publishers, Inc. (1992)
- (36) The value of the **a** control parameter is obtained by multiplying the  $a_2$  coefficient obtained by the polynomial fit by 2.
- (37) a) The polynomial fits presented in Figure 5a and 5b were chosen so that their roots correspond to the value of %HFX where symmetry breaking is no longer observed based on regression of the force constants of G09. This discrepancy in

the two plots is due to the fitting procedure employed to obtain the a control parameter.

b) In the case of disilene it was only possible to obtain the correct value if the 80-100% points were not included in the regression. Including all points in the polynomial regression returned a root that corresponded to 68% exact exchange where is still predicted. For 2Si TCNQ the regressions the data point at 0% exchange is removed. This is done to increase the agreement with the G09 force constant analysis (See Appendix C Figures C2 and C3)

(38) Huang, S.; Zhang, Q.; Shiota, Y.; Nakagawa, T.; Kuwabara, K.; Yoshizawa, K. and Adachi, C. *J. Chem. Theory Comput.*, **2013**, 9, 3872

(39) Cohen, A.J.; Mori-Sanchez, P. and Yang, W. *Chem Rev.*, 2012, 112, 289

## **CHAPTER SIX**

### **Computational Insights into the Electronic Structure of TCNDQ and TCNP: The Effect of Si-Substitution**

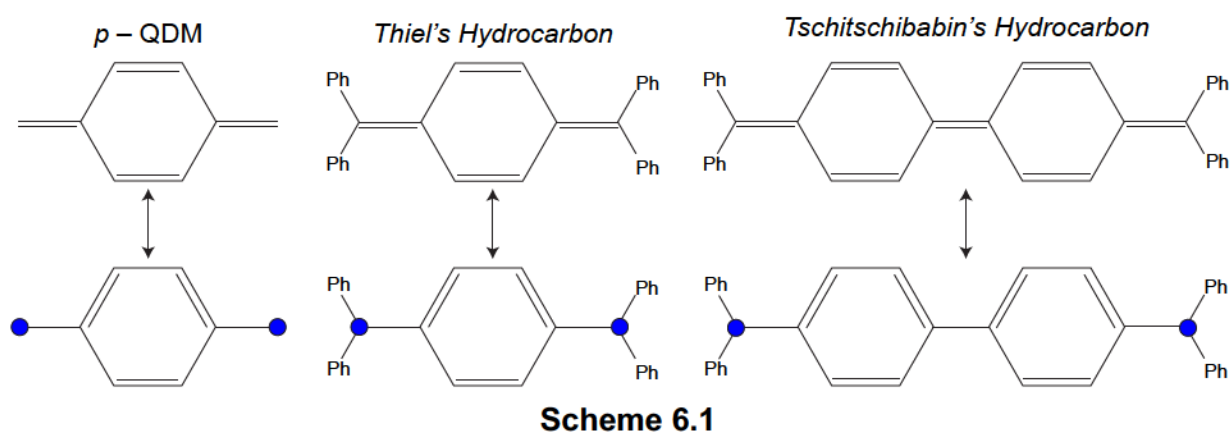
This chapter has been previously published in *Structural Chemistry*: S.M. Maley and R.C. Mawhinney, *Struct. Chem.*, 2018 doi: 10.1007/s11224-018-1265-3

### **Abstract**

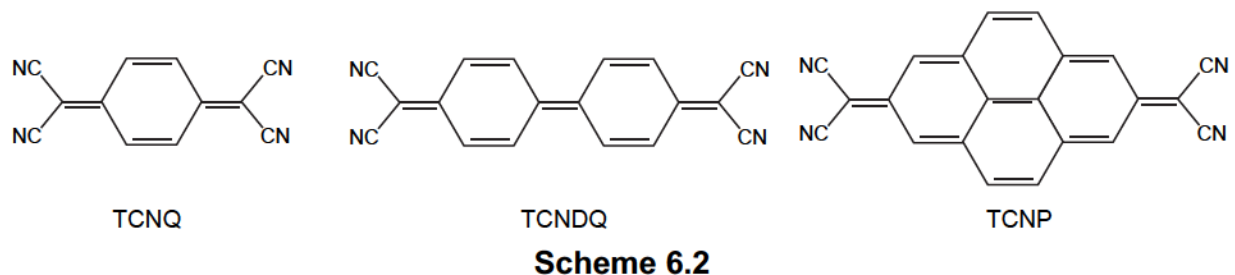
Tetracyanodiphenoquinodimethane (TCNDQ) and tetracyanopyrenoquinodimethane (TCNP) are larger cyanocarbons related to tetracyanoethylene (TCNE) and tetracyanoquinodimethane (TCNQ). In contrast to TCNE and TCNQ there are limited studies detailing the electronic structure of TCNDQ and TCNP. In this work we provide structural characterization and adiabatic electron affinities (AEAs) of TCNDQ and TCNP. The isovalent substitution strategy (swapping C for Si) discussed previously by our group is also applied and the effect of Si-substitution on the potential energy surfaces and AEAs of the parent compounds is assessed. Si-substitution enhances the AEAs and stabilizes the triplet diradical ground state of both compounds. These findings provide missing information regarding the electronic structure of TCNDQ and TCNP and further demonstrate the effectiveness of the isovalent substitution strategy.

## 6.1 – Introduction

*p*-quinodimethane (*p*-QDM – **Scheme 6.1**), a derivative of quinone, exhibits diradical character in its neutral ground state resulting in high reactivity. Attempts to stabilize the diradical by terminal substitution with phenyl groups resulted in Thiel and Tschitchibabin hydrocarbons (**Scheme 6.1**).<sup>1,2</sup> Thiel's hydrocarbon exhibits a closed shell ground state, while the ground state of Tschitchibabin's hydrocarbon has a large amount of diradical character.<sup>3</sup> Molecules exhibiting diradical character are of interest due to their potential applications in organic electronic materials.<sup>4-7</sup>



Terminal substitution of the *p*-QDM units with strongly electron withdrawing cyano groups is another stabilization option. This substitution strategy results in the formation of the well-studied cyanocarbon tetracyanoquinodimethane (TCNQ), and the related tetracyanodiphenylquinodimethane (TCNDQ) and tetracyanopyrenoquinodimethane (TCNP) (**Scheme 6.2**).



TCNQ and [TCNQ]<sup>-</sup> are well studied experimentally and computationally.<sup>8-14</sup> Their structures are well characterized by X-ray and neutron diffraction studies, showing planar D<sub>2h</sub> symmetry.<sup>8-11</sup> Zhu and Wang reported the electron affinity (EA) of TCNQ to be 3.343±0.001eV.<sup>15</sup> For TCNDQ and TCNP, on the other hand, there is limited information available in the literature.<sup>16-18</sup>

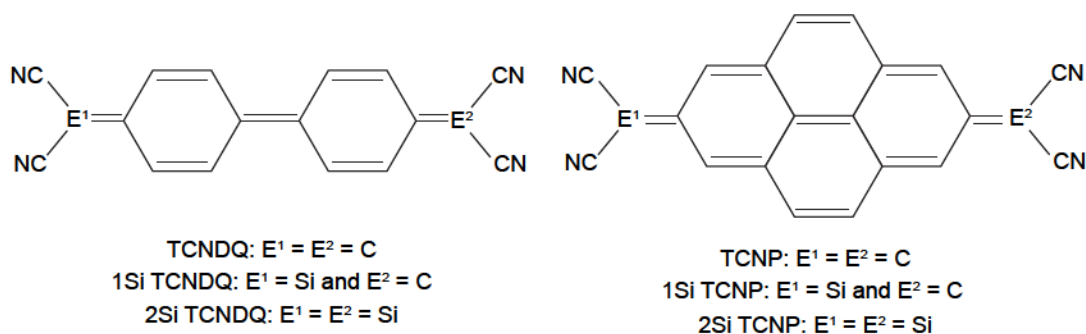
Attempts to synthesize both TCNDQ and TCNP have been unsuccessful due to polymerization. The dianions of both however have been prepared by deprotonating their dihydro analogs,<sup>16-18</sup> and the monoanion has been obtained by electrochemical oxidation. Addison *et. al.* assigned a twisted structure to [TCNDQ]<sup>-</sup> based on a UV-vis analysis of the electrochemical oxidation<sup>16</sup> while Maxfield *et. al.* reported an EA of 2.9eV for TCNP.<sup>17</sup>

Gerson *et. al.* determined the electron spin resonance (ESR) spectra of both monoanions and performed semi-empirical calculations, finding that the π-spin populations were consistent with the ESR spectra.<sup>18</sup> Despite these studies, the structures of the neutral and anionic forms have not been definitively characterized.

Previously, we reported that Si-substitution of tetracyanoethylene (TCNE) and TCNQ enhanced the adiabatic electron affinities (AEAs) of both molecules and increased open-shell singlet diradical character of 2Si TCNQ.<sup>14</sup> This may be a viable strategy to enhance the diradical character in TCNDQ and TCNP. Si-substitution also resulted in non-planar minima for both neutral and anionic species.

In this work we focus on the neutral and monoanionic (reduced) states of TCNDQ and TCNP to provide structural information and adiabatic electron affinities for both. The ability of commonly used density functionals to reproduce the ESR coupling constants of Gerson *et. al.* is also tested. The potential energy surfaces (PESs) of the 1 and 2Si

analogs of TCNDQ and TCNP (**Scheme 6.3**) in neutral and reduced forms are assessed and contrasted with those of the Si analogs of TCNQ to understand how extending the backbone affects symmetry breaking effects. Finally, the effect of Si-substitution on the stability of the diradical ground state and AEAs of both TCNDQ and TCNP is assessed.



**Scheme 6.3**

## **6.2 – Methodology**

All structures were optimized in  $D_{2h}$  (TCNDQ, TCNP, 2Si TCNDQ and 2Si TCNP) or  $C_{2v}$  (1Si TCNDQ and 1Si TCNP) symmetry. All stationary points were characterized by frequency analysis and when required imaginary frequencies were followed to the global surface minima. All calculations were performed using DFT in Gaussian09 Rev. D.01.<sup>19</sup> 9 functionals including 3 GGA's (BLYP,<sup>20</sup> PBE<sup>21</sup> and M06-L<sup>22</sup>), 5 hybrids (B3LYP,<sup>23</sup> PBE0,<sup>24</sup> M06, M06-2X and M06-HF<sup>22</sup>) and 1 range-separated hybrid (CAM-B3LYP<sup>25</sup>) were combined with 2 double zeta (**BS1**: Def2SVPP and **BS2**: cc-pvDZ) and 2 triple zeta (**BS3**: 6-311++g(d,p) and **BS4**: Def2TZVPP) basis sets. Stability calculations were performed to test for any lower energy solutions to the wavefunction.<sup>26</sup> With the exception of M06-2X, M06-HF and CAM-B3LYP the  $\langle S^2 \rangle$  values of the anions do not indicate spin-contamination (Appendix D Tables D7-D9 and D48-D54). The spin contamination annihilated  $\langle S^2 \rangle$  values of the exceptions are closer to the expected value of 0.75 (Appendix D Table D10-D12, D55-D62). AIMAll<sup>27</sup> was used to provide further insight into

the electronic structure based on the Quantum Theory of Atoms in Molecules (QTAIM).<sup>28</sup> Anisotropic ESR hyperfine coupling constants were calculated and compared to the experimental values of Gerson *et. al.* in an effort to assess model chemistry performance. While no methods were found to perform well for all nuclei the deviation from experiment is typically less than one Gauss.<sup>29</sup>

## **6.3 – Results and Discussion**

### 6.3.1 – Assessments of Parent Compounds

Most model chemistries report TCNDQ (**Figure 6.1**) to exhibit a planar  $D_{2h}$  structure, in line with TCNQ.<sup>8,12-14</sup> Five model chemistries (BLYP and PBE in combination with BS3 and BS4 and M06-HF/BS3) predict a planar transition structure (TS) that relaxes to a  $D_2$  symmetry TS<sup>30</sup> that is twisted about the central C–C bond (0.01 to 5.28°) but otherwise planar; the bond lengths do not change appreciably in these cases.

Unlike  $[TCNQ]^-$ ,<sup>9-14</sup>  $D_{2h}$   $[TCNDQ]^-$  (**Figure 6.1**) does not maintain planarity and is predicted to be a TS that relaxes to a  $D_2$  structure twisted around the central C–C bond. The degree of twist ranges are 1.5-18.5° (BS1), 9.6-19.0° (BS2), 15.5-21.8° (BS3) and 12.3-19.9° (BS4). M06 in combination with BS1 or BS2 predicts only small amounts of twisting (0.0002 and 0.015°, respectively). The twist angle increases in the order BS1 < BS2 < BS4 < BS3 for all functionals except M06-L<sup>31</sup> and is typically smaller when functionals with large amounts of Hartree-Fock exchange are used. This is more pronounced with DZ basis sets. The degree of twist in  $[TCNDQ]^-$  is less than neutral and substituted biphenyl, but greater than that reported for reduced substituted biphenyl.<sup>32-34</sup> The bond lengths do not change significantly upon twisting.

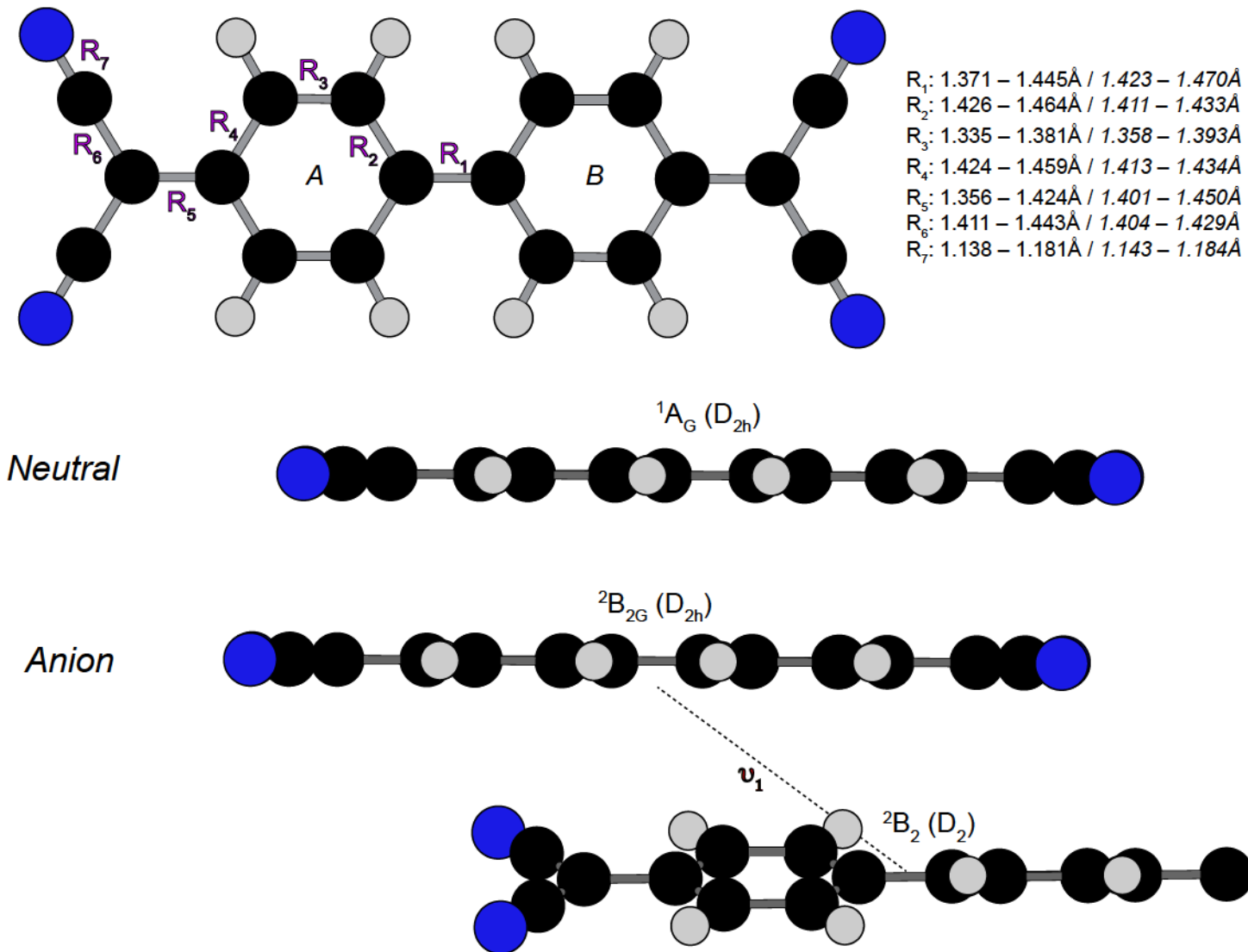


**Figure 6.1:** Top: Structure of TCNDQ with bond length ranges and ring identity for neutral and reduced forms. Bottom – Stationary points on the potential energy surfaces of TCNDQ and [TCNDQ]<sup>-</sup>.  $\nu$  indicates an imaginary frequency

In comparison to TCNDQ, TCNP has two additional ethylene units linking the biphenyl moiety helping enforce planarity. TCNP and [TCNP]<sup>-</sup> (**Figure 6.2**) are predicted to be planar D<sub>2h</sub> minima by all model chemistries.

Both TCNDQ and TCNP exhibit quinoidal character (alternating single and double bonds), like TCNQ. In TCNDQ R<sub>2</sub>, R<sub>4</sub> and R<sub>6</sub> are longer than R<sub>1</sub>, R<sub>3</sub>, R<sub>5</sub> and R<sub>7</sub>, while in TCNP R<sub>2</sub>, R<sub>4</sub>, R<sub>5</sub>, R<sub>6</sub> and R<sub>8</sub> are greater than R<sub>1</sub>, R<sub>1</sub>', R<sub>3</sub> R<sub>5</sub> and R<sub>7</sub>.

Upon reduction, the bond lengths equalize slightly, thus decreasing the quinoidal character. These changes in bond length can be rationalized by examining the LUMO (Appendix D Figure D1A and D1B) of the neutral compound which displays bonding character over the distances that decrease and anti-bonding character over those that increase.

A more generic measure of the quinoidal character is given by the bond length alternation (BLA).<sup>35</sup> BLA is a geometrical parameter defined as the difference in the average single and double bond length in  $\pi$ -conjugated systems. A similar quantity, the delocalization index alternation (DIA),<sup>36</sup> can be calculated using QTAIM delocalization index values. Both values approach zero as the system becomes fully delocalized.

The BLA and DIA of the ring common to all  $\pi$ -conjugated cyanocarbons decreases in the order TCNQ (BLA: 0.094, DIA: 0.467) > TCNDQ (0.079, 0.393) > TCNP (0.067, 0.295). Similarly, upon reduction, BLA and DIA decrease but maintain the same ordering: TCNQ (0.043, 0.197) > TCNDQ (0.037, 0.154) > TCNP (0.028, 0.121) reflecting the decrease in quinoidal character. The effect is diminished with conjugation.

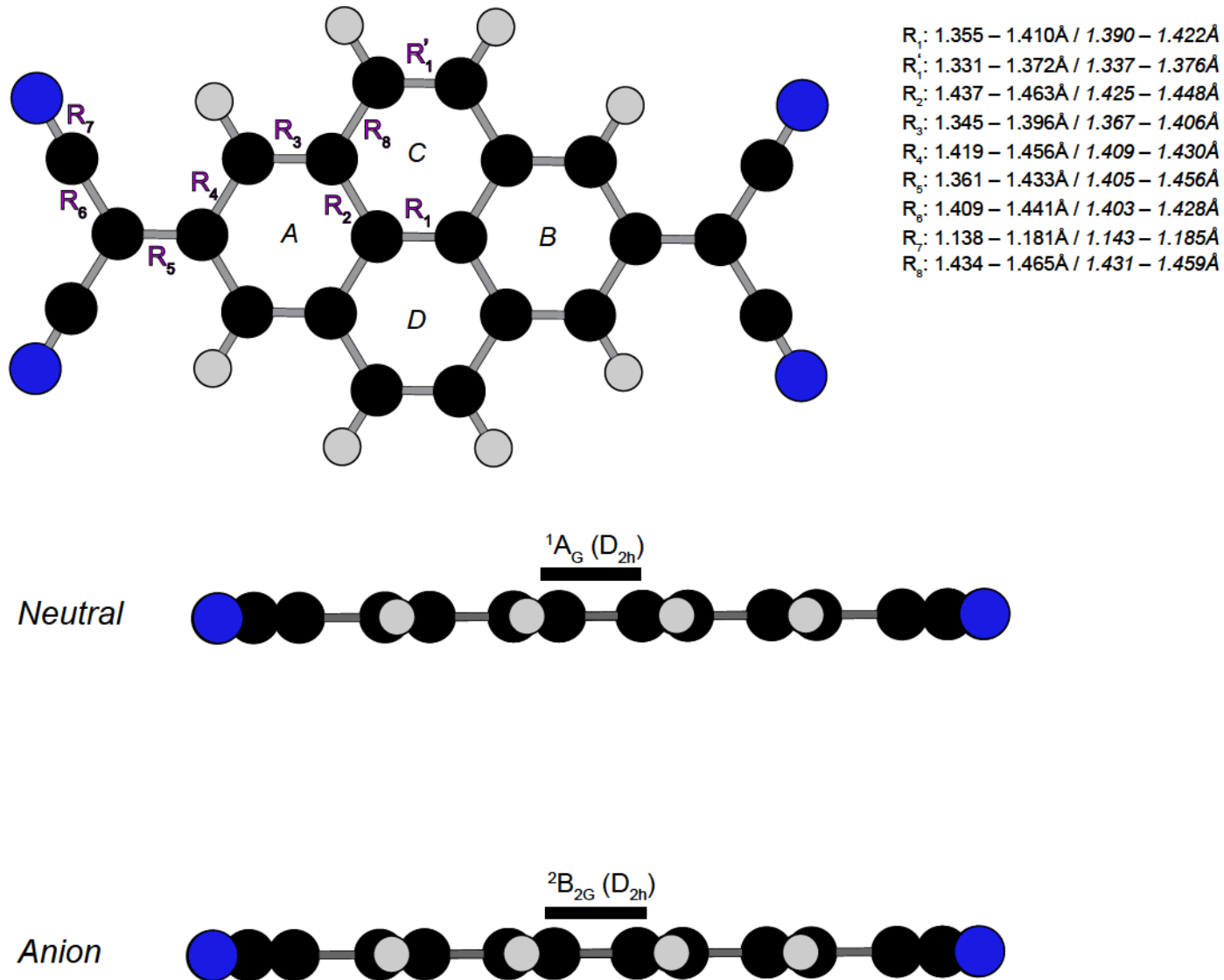


**Figure 6.2:** Top: Structure of TCNP with bond length ranges and ring identity for neutral and reduced forms. Bottom – Stationary points on the potential energy surfaces of TCNP and  $[TCNP]^-$ .  $\nu$  indicates an imaginary frequency.

### 6.3.2 – The Adiabatic Electron Affinities of TCNDQ and TCNP

The EA's of the related compounds TCNE and TCNQ are well studied experimentally, with values of 3.170eV and 3.343eV, respectively.<sup>37,15</sup> By comparing electrical resistivity measurements on a series of charge-transfer complexes involving [TCNQ]<sup>-</sup> and [TCNDQ]<sup>-</sup>, Morinaga *et. al.* proposed that the EA of TCNDQ is less than that of TCNQ.<sup>38</sup> However, no definitive EA value has ever been reported. For TCNP Maxfield *et. al.* reported an EA of 2.9eV.<sup>17</sup> Using the minimum energy structures of the neutral and anion species we present the AEA's of TCNDQ and TCNP in **Table 6.1** (TCNDQ) and **Table 6.2** (TCNP).

**Table 6.1:** AEA's (eV) calculated for TCNDQ using chosen methods. Min, max, range and standard deviation (S.D.) of values for each functional and basis set also provided.

	BS1	BS2	BS3	BS4	Min	Max	Range	S. D.
BLYP	3.397	3.311	3.680	3.608	3.311	3.680	0.369	0.150
M06L	3.777	3.674	3.843	3.699	3.674	3.843	0.169	0.067
PBE	3.650	3.553	3.860	3.794	3.553	3.860	0.307	0.120
B3LYP	3.772	3.674	3.978	3.913	3.674	3.978	0.304	0.119
PBE0	3.912	3.803	4.036	3.975	3.803	4.036	0.233	0.086
M06	3.914	3.831	4.038	3.910	3.831	4.038	0.207	0.074
M062X	3.971	3.855	4.125	4.050	3.855	4.125	0.270	0.100
M06-HF	4.007	3.883	4.252	4.196	3.883	4.252	0.368	0.147
CAM-B3LYP	3.913	3.811	4.107	4.042	3.811	4.107	0.297	0.115
Min	3.397	3.311	3.680	3.608				
Max	4.007	3.883	4.252	4.196				
Range	0.610	0.572	0.572	0.587				
S. D.	0.181	0.173	0.163	0.174				

**Table 6.2:** AEA's (eV) calculated for TCNP using chosen methods. Min, max, range and standard deviation (S.D.) of values for each functional and basis set also provided.

	BS1	BS2	BS3	BS4	Min	Max	Range	S.D
BLYP	3.498	3.411	3.765	3.694	3.411	3.765	0.353	0.143
M06L	3.896	3.790	3.949	3.805	3.790	3.949	0.159	0.065
PBE	3.757	3.660	3.950	3.884	3.660	3.950	0.290	0.112
B3LYP	3.911	3.812	4.101	4.036	3.812	4.101	0.289	0.112
PBE0	4.064	3.954	4.172	4.111	3.954	4.172	0.218	0.080
M06	4.067	3.985	4.179	4.049	3.985	4.179	0.194	0.070
M062X	4.155	4.038	4.290	4.218	4.038	4.290	0.252	0.093
M06-HF	4.247	4.121	4.467	4.418	4.121	4.467	0.346	0.138
CAM-B3LYP	4.099	3.997	4.280	4.213	3.997	4.280	0.283	0.108
Min	3.498	3.411	3.765	3.694				
Max	4.247	4.121	4.467	4.418				
Range	0.750	0.709	0.702	0.724				
S.D	0.217	0.208	0.201	0.213				

The AEA ranges from 3.311 to 4.252eV for TCNDQ and from 3.411 to 4.467eV for TCNP. AEA's are greater when functionals with higher amounts of Hartree-Fock exchange are used (e.g., BLYP predicts the lowest value and M06-HF the highest). Additionally, AEA's are greater when TZ-basis sets are used with BS3 predicting the largest value for all functionals.

All model chemistries predict TCNE < TCNQ < TCNDQ < TCNP. In our previous work, the experimental EA's of TCNE and TCNQ were best reproduced by M06-L/BS2 and PBE/BS2, respectively.<sup>14</sup> At these model chemistries the AEA of TCNDQ is 3.674eV (M06-L) and 3.553eV (PBE) and for TCNP it is 3.790eV (M06-L) and 3.660eV (PBE) (Table 6.3).

**Table 6.3:** Experimental and calculated EA's (eV) for cyanocarbons

	TCNE	TCNQ	TCNDQ	TCNP
Experiment	3.17 <sup>37</sup>	3.383 <sup>15</sup>	< 2.8eV <sup>17</sup>	2.9eV <sup>17</sup>
PBE/BS2	3.010 <sup>14</sup>	3.338 <sup>14</sup>	3.553	3.660
M06-L/BS2	3.180 <sup>14</sup>	3.471 <sup>14</sup>	3.674	3.790

AEA's calculated for TCNP are significantly greater (15-35%) than the experimental value reported by Maxfield *et. al.* (2.9eV).<sup>17</sup> This experimental value, as well as the EA they report for TCNQ (2.8eV) are suspiciously low. Moreover, as our results reveal, AEA should increase as the conjugation network is extended. On this basis, the experimental EA of TCNP should be re-assessed if possible.

### 6.3.3 – The Potential Energy Surfaces of the Si-Analogs

With the exception of [TCNDQ]<sup>-</sup> all parent compounds have planar minima (**Figures 6.1** and **6.2**). The Si analogs, however, have more complicated PESs and often depend on model chemistry. The PESs of the Si analogs were assessed using BS2 and BS4. A limited number of functionals were used to assess the PESs using BS1 and BS3 in order to test for basis set effects. Representative PESs are presented in **Figures 6.3-6.6**. Energetics and vibrational frequencies are available in Appendix D Tables D15-D46. Representative bond lengths, calculated at the B3LYP/BS4 level, are compiled in **Tables 6.4** and **6.5** (remaining model chemistry data available in Appendix D Tables D63-D78). In all cases, M06-HF predicts planar minima, the other functional dependencies are now discussed.

#### 6.3.3.1 – 1Si TCNDQ and [1Si TCNDQ]<sup>-</sup>

The character of the neutral planar stationary point varies with functional. For convenience, the results obtained for each model chemistry is compiled below.

*Minimum:* M06/BS4, PBE0/BS2 and BS4, M06-HF/ BS2 and BS4  
CAM-B3LYP/BS2 and BS4

*Transition Structure:* PBE/BS2, M06-L/BS2 and BS4, B3LYP/BS2,  
M06/BS2, M06-2X/BS2 and BS4

*Second Order Saddle Point:* BLYP/BS2 and BS4, PBE/BS4, B3LYP/BS4

Seven model chemistries predict the planar neutral structure to be a minimum and another seven predict a TS. On the PBE, B3LYP and M06/BS2 and M06-L/BS2 or BS4 surfaces the TS relaxes to a  $C_s$  symmetry structure that is pyramidalized (3.6 to 7.2°)<sup>39</sup> at the Si-nucleus but otherwise planar (**Figure 6.4**). On the M06-2X/BS2 and BS4 surfaces the TS relaxes to a twisted (BS2: 1.2; BS4: 2.7°)  $C_2$ -structure like that observed for [TCNDQ]<sup>-</sup> where the Si-nucleus is not pyramidalized. The second order saddle points (SOSP) relax to  $C_s$  and  $C_2$  transition structures that further relax to a  $C_1$  structure that is both twisted around the central C–C bond (0.1 to 13.8°) and pyramidalized (0.3 to 13.8°) at the Si-nucleus.

All model chemistries predict planar [1Si TCNDQ]<sup>-</sup> to be a SOSP (**Figure 6.4**) that relaxes to  $C_2$  and  $C_s$  TSs. Both converge on the  $C_1$  minimum that is both twisted around the central C–C bond (BS2: 0.1 to 0.2°; BS4: 19.1 to 28.4°) and pyramidalized at the Si-nucleus (BS2: 29.7 to 62.5°; BS4: 25.7 to 46.0°). The amount of torsion around the central C–C bond is greater than in [TCNDQ]<sup>-</sup>.

#### 6.3.3.2 – 2Si TCNDQ and [2Si TCNDQ]<sup>-</sup>

The character of the neutral planar stationary point varies with functional, as shown below.

*Minimum:* M06-HF/ BS2 and BS4

*Second Order Saddle Point:* M06-L/BS2, M06/BS2, CAM-B3LYP/BS2 and BS4

*Third Order Saddle Point:* BLYP/BS2 and BS4, M06-L/BS4, PBE/BS2 and BS4, B3LYP/BS2 and BS4, M06/BS4,<sup>40</sup> M06-2X/BS2 and BS4, PBE0/BS2 and BS4

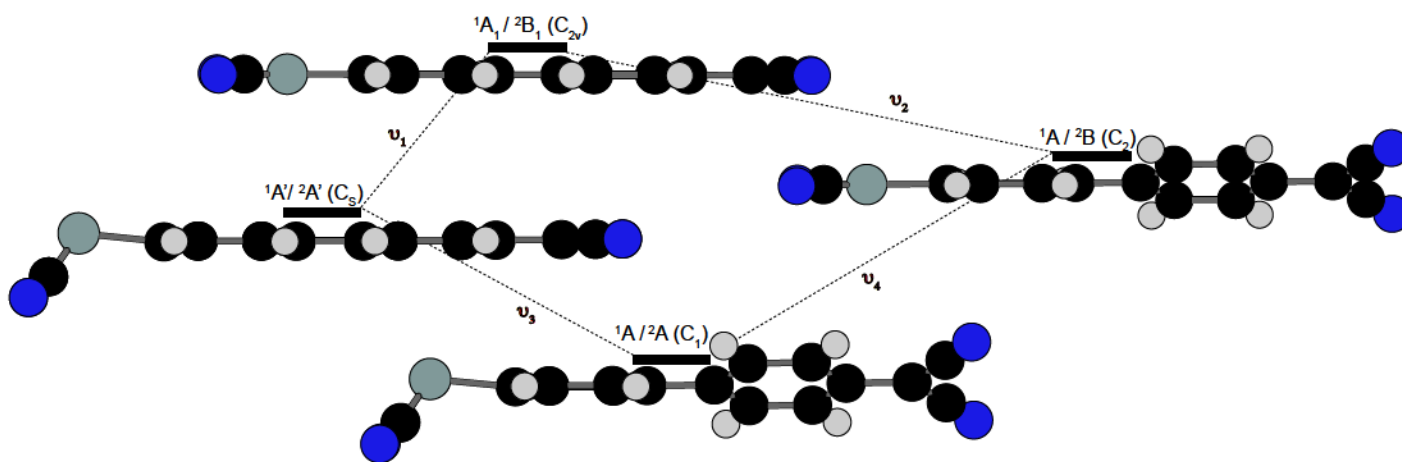


**Figure 6.3:** Stationary points on the potential energy surfaces of 1Si TCNDQ and [1Si TCNDQ]<sup>-</sup>.  $\nu$  indicates an imaginary frequency

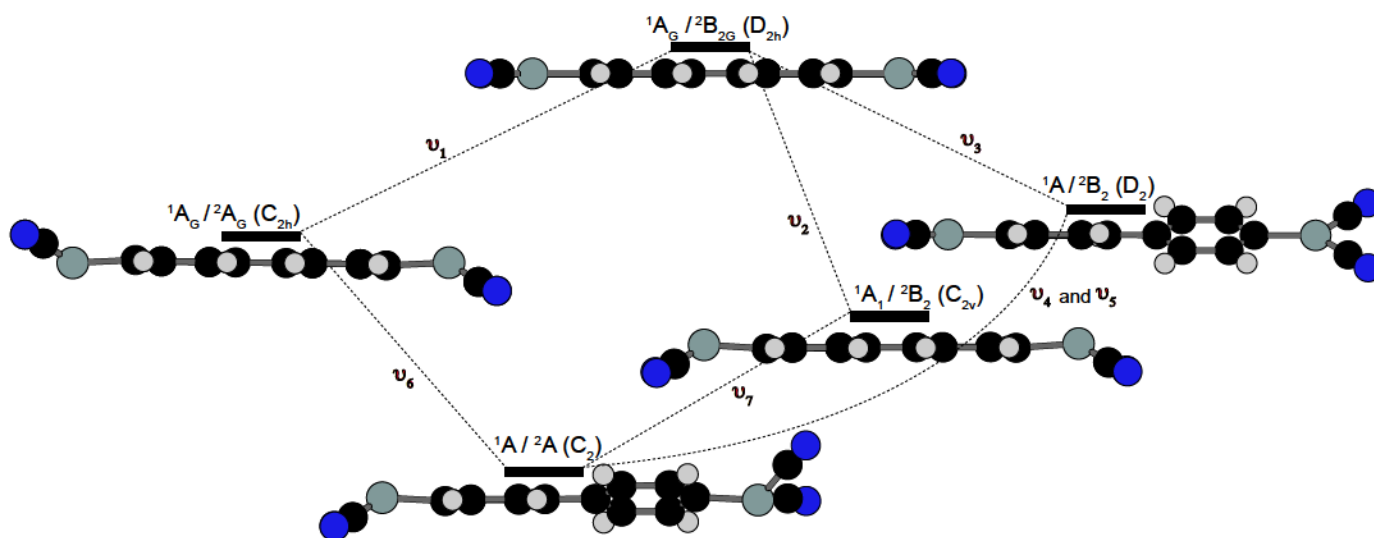


**Figure 6.4:** Stationary points on the potential energy surfaces of 2Si TCNDQ and [2Si TCNDQ]<sup>-</sup>. On the anion surfaces the C<sub>1</sub> minima looks like the C<sub>2</sub> minima but with unequal pyramidalization of the Si-nuclei.  $\nu$  indicates an imaginary frequency.

The SOSPs relax to *trans*-bent  $C_{2h}$  and *cis*-bent  $C_{2v}$  structures where both Si are equally pyramidalized. On the M06/BS2 surface  $C_{2h}$  and  $C_{2v}$  structures are minima, with  $C_{2v}$  the lowest energy structure having a pyramidalization of  $17.0^\circ$ . On the M06-L/BS2 surface the  $C_{2h}$  and  $C_{2v}$  structures are TSs that further relax to a  $C_2$  minimum that is equally pyramidalized at the Si-nuclei ( $17.1^\circ$ ) and twisted ( $16.2^\circ$ ). The CAM-B3LYP PES varies with basis set. On the BS2 surface the  $C_{2h}$  and  $C_{2v}$  structures again relax to a  $C_2$  structure, but it is now characterized as a TS and further relaxes to a  $C_1$  structure that is pyramidalized at only one Si-nucleus ( $20.2^\circ$ ) but otherwise planar. On the CAM-B3LYP/BS4 surface the  $C_{2h}$  and  $C_{2v}$  structures relax to a  $C_s$  structure that is also pyramidalized at one Si-nucleus ( $14.3^\circ$ ) and otherwise planar.

The third order saddle point (TOSP) relaxes to *trans*-bent  $C_{2h}$ , *cis*-bent  $C_{2v}$  and twisted  $D_2$  TSs, which further relax to a  $C_2$  structure that is pyramidalized (BS2:  $9.3$  to  $19.0^\circ$ ; BS4:  $8.2$  to  $16.7^\circ$ ) and twisted (BS2:  $8.9$  to  $19.6^\circ$ ; BS4:  $10.1$  to  $20.8^\circ$ ) (**Figure 6.5**).

The planar anion is predicted to be a TOSP by all model chemistries. Like the neutral case, it relaxes to a  $C_2$  structure that is the lowest energy structure on all surfaces except CAM-B3LYP, M06-2X and M06-HF surfaces. The exceptions further relax to a  $C_1$  lowest energy structure. The  $C_2$  minima are equally pyramidalized at the Si-nuclei (BS2:  $43.3$  to  $47.7^\circ$ ;  $41.2$  to  $42.9^\circ$  BS4) and twisted around the central C–C bond (BS2:  $23.0$  to  $27.2^\circ$ ; BS4:  $27.2$  to  $28.9^\circ$ ). The  $C_1$  minima have unequally pyramidalized Si-nuclei (e.g.,  $26.3$  v.  $68.0^\circ$  CAM-B3LYP/BS4) and are also twisted around the central C–C bond (BS2:  $30.3$  to  $39.8^\circ$ ; BS4:  $27.7$  to  $31.7^\circ$ ).

At the planar geometry  $R_1$ ,  $R_3$ ,  $R_5$  and  $R_7$  increase while the remaining bonds decrease with Si-substitution (**Table 4**).  $R_1$  shows the greatest increased followed by  $R_5$

and  $R_3$ .  $R_7$  does not change significantly ( $0.001\text{\AA}$  with each Si-substitution).  $R_2$  decreases most followed by  $R_4$  and  $R_6$ . In the 1Si cases the substituted half typically exhibits a greater change. The change in bond length is typically greater upon second Si-substitution. In the reduced version the changes in bond lengths show a similar pattern, however, the magnitude of change is decreased.

**Table 6.4:** B3LYP/BS4 predicted bond lengths (Å) for TCNDQ and [TCNDQ]<sup>-</sup>. Italicized values for Si-containing moiety. See **Figure 6.1** for bond length labels.

Neutral		R <sub>1</sub>	R <sub>2</sub> / R <sub>2</sub> '	R <sub>3</sub> / R <sub>3</sub> '	R <sub>4</sub> / R <sub>4</sub> '	R <sub>5</sub> / R <sub>5</sub> '	R <sub>6</sub> / R <sub>6</sub> '	R <sub>7</sub> / R <sub>7</sub> '
0Si	D <sub>2h</sub>	1.414	1.436	1.356	1.434	1.392	1.420	1.155
1Si	C <sub>2v</sub>	1.426	1.429 / 1.429	1.360 / 1.363	1.430 / 1.426	1.399 / 1.764	1.417 / 1.800	1.156 / 1.156
	C <sub>s</sub>	1.426	1.429 / 1.429	1.360 / 1.363	1.430 / 1.426	1.399 / 1.764	1.417 / 1.801	1.156 / 1.156
	C <sub>2</sub>	1.426	1.429 / 1.429	1.360 / 1.363	1.430 / 1.426	1.399 / 1.764	1.417 / 1.801	1.156 / 1.156
2Si	D <sub>2h</sub>	1.438	1.423	1.367	1.422	1.773	1.799	1.157
	C <sub>2h</sub>	1.445	1.420	1.369	1.418	1.796	1.816	1.156
	C <sub>2v</sub>	1.445	1.420	1.370	1.418	1.797	1.816	1.156
	D <sub>2</sub>	1.438	1.423	1.367	1.422	1.773	1.799	1.157
	C <sub>2</sub>	1.445	1.418	1.370	1.418	1.798	1.816	1.156
Anion		R <sub>1</sub>	R <sub>2</sub> / R <sub>2</sub> '	R <sub>3</sub> / R <sub>3</sub> '	R <sub>4</sub> / R <sub>4</sub> '	R <sub>5</sub> / R <sub>5</sub> '	R <sub>6</sub> / R <sub>6</sub> '	R <sub>7</sub> / R <sub>7</sub> '
0Si	D <sub>2h</sub>	1.452	1.417	1.372	1.418	1.425	1.411	1.159
	D <sub>2</sub>	1.451	1.416	1.372	1.418	1.426	1.411	1.159
1Si	C <sub>2v</sub>	1.456	1.415 / 1.416	1.373 / 1.376	1.418 / 1.412	1.427 / 1.802	1.410 / 1.800	1.160 / 1.160
	C <sub>s</sub>	1.460	1.414 / 1.413	1.373 / 1.378	1.417 / 1.409	1.427 / 1.855	1.410 / 1.862	1.159 / 1.157
	C <sub>2</sub>	1.455	1.413 / 1.414	1.374 / 1.377	1.418 / 1.412	1.428 / 1.803	1.409 / 1.799	1.160 / 1.160
	C <sub>1</sub>	1.458	1.412 / 1.411	1.374 / 1.379	1.417 / 1.409	1.429 / 1.858	1.410 / 1.862	1.159 / 1.157
2Si	D <sub>2h</sub>	1.459	1.414	1.376	1.414	1.805	1.799	1.161
	C <sub>2h</sub>	1.471	1.409	1.381	1.406	1.862	1.862	1.157
	C <sub>2v</sub>	1.471	1.409	1.381	1.406	1.863	1.862	1.157
	D <sub>2</sub>	1.458	1.412	1.377	1.414	1.806	1.799	1.161
	C <sub>2</sub>	1.468	1.407	1.381	1.407	1.865	1.863	1.157

#### 6.3.3.3 – 1Si TCNP and [1Si TCNP]<sup>-</sup>

Planar 1Si TCNP is predicted to be a TS by B3LYP, BLYP, M06-L and PBE in combination with BS2 or BS4 and M06/BS2 (**Figure 6.5**). The remaining model chemistries predict planar minima, similar to observations in 1Si TCNE and 1Si TCNQ.<sup>14</sup> The TSs relax to a C<sub>s</sub> minima that is pyramidalized at the Si-nucleus (BS2: 0.4 to 15.3°; BS4: 3.6 to 11.5°) but otherwise planar.

The anion is predicted to be a TS by all methods, relaxing to a C<sub>s</sub> structure that is pyramidalized at the Si-nuclei (BS2: 29.3 to 66.8°; BS4: 25.4 to 45.1°) but otherwise planar, similar to those observed in [1Si TCNE]<sup>-</sup> and [1Si TCNQ]<sup>-</sup>.<sup>14</sup>

#### 6.3.3.4 – 2Si TCNP and [2Si TCNP]<sup>-</sup>

Planar 2Si TCNP is predicted to be a SOSF by all functionals except M06-HF. The SOSFs relax to *trans*-bent C<sub>2h</sub> and *cis*-bent C<sub>2v</sub> structures which are minima on all surfaces except CAM-B3LYP/BS2 or BS4 and M06-2X/BS2 (**Figure 6.6**). On these surfaces the C<sub>2h</sub> and C<sub>2v</sub> structures are TSs that further relax to a C<sub>s</sub> minimum that is pyramidalized at only one Si-nucleus (e.g. M06-2X/BS2: 28.7°). With the exception of M06/BS4, the remaining surfaces have a C<sub>2h</sub> lowest energy structure, equally pyramidalized at the Si-nuclei (BS2: 14.3 to 19.8°; BS4: 11.3 to 17.6°); the C<sub>2v</sub> structure (16.4° pyramidalization) is the lowest energy structure on the M06/BS4 surface. These symmetry breaking effects are similar to those in 2Si TCNQ.<sup>14</sup>

Planar [2Si TCNP]<sup>-</sup> is predicted to be a SOSF by all functionals, relaxing to *trans*-bent C<sub>2h</sub> and *cis*-bent C<sub>2v</sub> structures. The C<sub>2h</sub> structure is equally pyramidalized at the Si-nuclei (BS2: 43.6 to 45.6°; BS4: 41.5 to 48.3°) and is the global minima on most surfaces. On the M06, M06-2X, M06-HF and CAM-B3LYP surfaces, however, the C<sub>2h</sub>

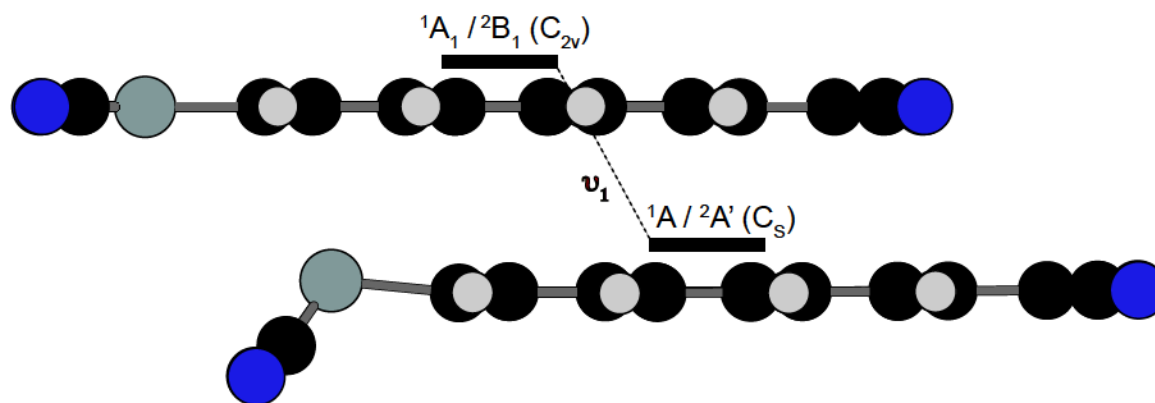


**Figure 6.5:** Stationary points on the potential energy surfaces of 1Si TCNP and [1Si TCNP]<sup>-</sup>.  $\nu$  indicates an imaginary frequency

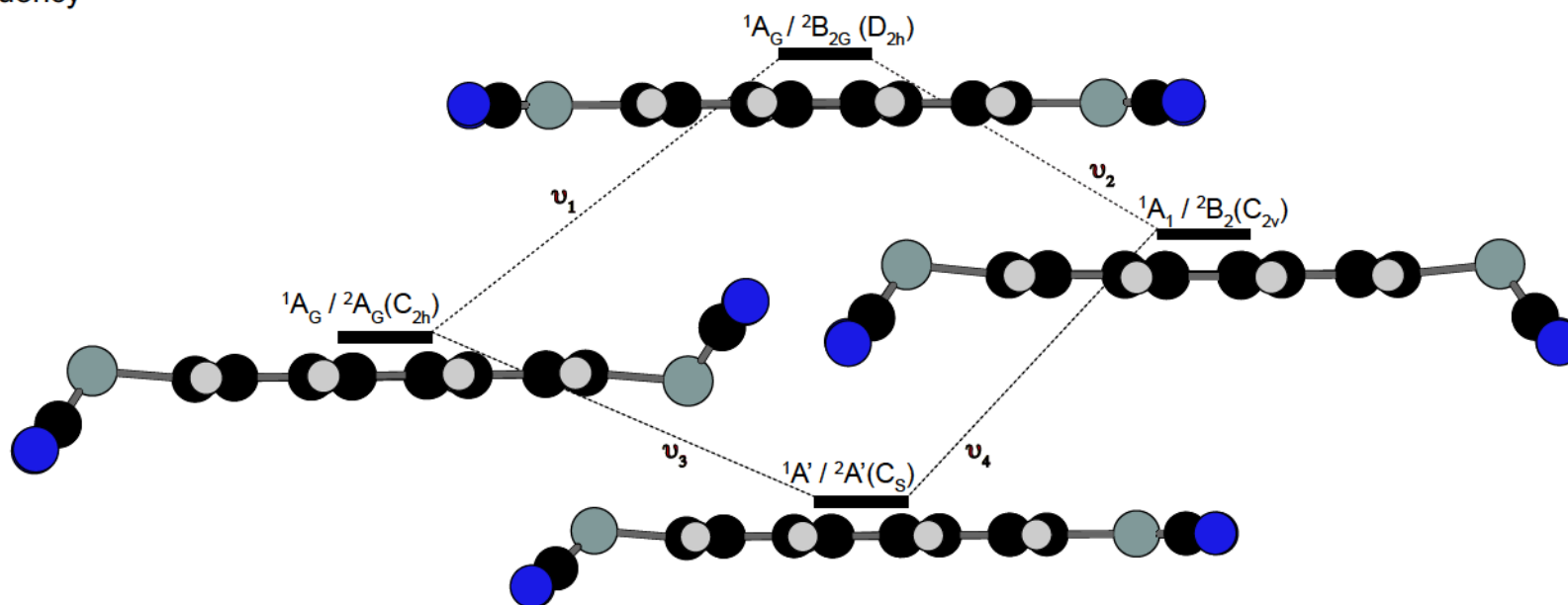


**Figure 6.6:** Stationary points on the potential energy surfaces of 2Si TCNP and [2Si TCNP]<sup>-</sup>.  $\nu$  indicates an imaginary frequency

and  $C_{2v}$  structures further relax to a  $C_s$  structure that is *pseudo*- $C_{2h}$ , but with the Si-nuclei unequally pyramidalized (M06-2X/BS2: 39.1° and 71.6°). These symmetry breaking effects are similar to those observed in  $[2Si\ TCNQ]^-$  (M06-2X/BS2: 28.2° and 69.1°).<sup>14</sup>

At the planar geometry  $R_1$ ,  $R_1'$ ,  $R_3$ ,  $R_5$  and  $R_7$  increase in length while the remaining bond lengths decrease with Si-substitution. In the pyrene moiety,  $R_1$  shows the greatest increase followed by  $R_3$ .  $R_1'$  and  $R_7$  do not change significantly.  $R_2$  decreases the most followed by  $R_4$ . The remaining bonds decrease by a similar amount. The magnitude of change is greater for the first substitution for the bonds furthest away from the substitution (i.e.,  $R_1$ ,  $R_1'$ ,  $R_2$  and  $R_2'$ ), but the opposite is true of the bonds closest to the substitution. In the 1Si versions the substituted half typically displays a greater change. The reduced version shows similar patterns. However, some bond lengths ( $R_2$ ,  $R_2'$ ,  $R_3$  and  $R_4$ ) increase/decrease with the first substitution but show the opposite trend upon second substitution.

**Table 6.5:** B3LYP/BS4 predicted bond lengths (Å) for TCNP and [TCNP]<sup>-</sup>. Italicized values for Si-containing moiety. See **Figure 6.2** for bond length labels.

Neutral		R <sub>1</sub>	R <sub>1</sub> '	R <sub>2</sub> / R <sub>2</sub> '	R <sub>3</sub> / R <sub>3</sub> '	R <sub>4</sub> / R <sub>4</sub> '	R <sub>5</sub> / R <sub>5</sub> '	R <sub>6</sub> / R <sub>6</sub> '	R <sub>7</sub> / R <sub>7</sub> '	R <sub>8</sub> / R <sub>8</sub> '
0Si	D <sub>2h</sub>	1.348	1.348	1.444	1.370	1.429	1.400	1.418	1.155	1.443
1Si	C <sub>2v</sub>	1.392	1.350	1.438 / 1.439	1.375 / 1.378	1.424 / 1.421	1.409 / 1.772	1.415 / 1.799	1.156 / 1.156	1.441 / 1.440
	C <sub>s</sub>	1.392	1.350	1.438 / 1.439	1.375 / 1.378	1.424 / 1.420	1.408 / 1.778	1.415 / 1.803	1.156 / 1.156	1.350 / 1.440
2Si	D <sub>2h</sub>	1.399	1.351	1.435	1.382	1.417	1.784	1.798	1.157	1.439
	C <sub>2h</sub>	1.401	1.352	1.433	1.384	1.413	1.808	1.817	1.156	1.438
	C <sub>2v</sub>	1.401	1.351	1.433	1.384	1.413	1.808	1.817	1.156	1.438
Anion		R <sub>1</sub>	R <sub>1</sub> '	R <sub>2</sub> / R <sub>2</sub> '	R <sub>3</sub> / R <sub>3</sub> '	R <sub>4</sub> / R <sub>4</sub> '	R <sub>5</sub> / R <sub>5</sub> '	R <sub>6</sub> / R <sub>6</sub> '	R <sub>7</sub> / R <sub>7</sub> '	R <sub>8</sub> / R <sub>8</sub> '
0Si	D <sub>2h</sub>	1.403	1.353	1.431	1.384	1.415	1.430	1.410	1.160	1.439
1Si	C <sub>2v</sub>	1.406	1.355	1.428 / 1.431	1.386 / 1.390	1.415 / 1.409	1.433 / 1.809	1.408 / 1.799	1.161 / 1.160	1.438 / 1.437
	C <sub>s</sub>	1.408	1.354	1.429 / 1.428	1.386 / 1.391	1.414 / 1.406	1.435 / 1.860	1.409 / 1.861	1.160 / 1.157	1.439 / 1.437
2Si	D <sub>2h</sub>	1.408	1.354	1.429	1.389	1.411	1.812	1.798	1.161	1.438
	C <sub>2h</sub>	1.413	1.355	1.426	1.393	1.404	1.869	1.863	1.157	1.436
	C <sub>2v</sub>	1.413	1.355	1.426	1.393	1.404	1.868	1.863	1.157	1.436

The bond lengths (**Tables 6.4** and **6.5**) and delocalization indices (Appendix D Tables D79-D82) of both compounds decrease upon Si-substitution, reduction and structural symmetry breaking. These changes are reflected in the BLA and DIA analyses (**Tables 6.6** and **6.7**).

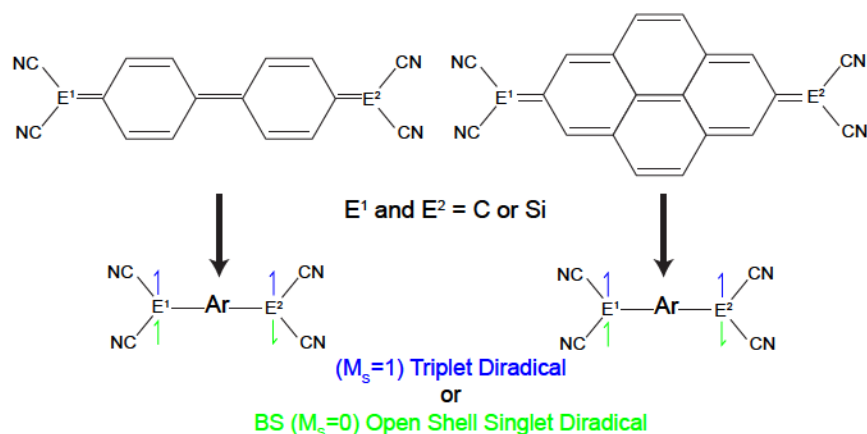
BLA in planar TCNDQ decreases with Si-substitution in the order 0Si (0.079) > 1Si (0.064) > 2Si (0.054), and in planar TCNP in the order 0Si (0.067) > 2Si (0.044) > 1Si (0.042). The additional rings (C and D) in TCNP also display this pattern. In the 1Si versions the substituted ring has a smaller BLA. All BLAs decrease upon reduction with the largest change observed in the 0Si versions. BLA follows the same pattern with Si substitution for [TCNP]<sup>-</sup> but for [TCNDQ]<sup>-</sup> decreases in the order 1Si (0.043) > 0Si (0.042) > 2Si (0.038). BLA decreases upon symmetry breaking with a greater decrease in the anions.

The DIAs of planar TCNDQ and TCNP decrease in the order 0Si (TCNDQ: 0.295, TCNP: 0.393) > 1Si (0.190, 0.284) > 2Si (0.160, 0.246). The additional rings in TCNP also decrease in the order 0Si (0.359) > 1Si (0.320) > 2Si (0.293). In the 1Si versions DIA is smaller for the substituted ring. All DIAs decrease upon reduction with the largest change observed in the 0Si versions. The DIA of [TCNP]<sup>-</sup> follows the same pattern with Si-substitution but decreases in the order 0Si (0.239) > 2Si (0.165) > 1Si (0.164) for [TCNDQ]<sup>-</sup>. DIA decreases upon symmetry breaking with a greater decrease in the anions.

Using DI's, we can compute the alternation along the entirety of the conjugation network, allowing us to assign one overall DIA value to each molecule. The overall DIA decreases as the  $\pi$ -conjugation network is increased, TCNQ (0.345) > TCNDQ (0.295) > TCNP (0.249). It also decreases with Si-substitution. For TCNDQ it decreases in the order

0Si (0.249) > 1Si (0.201) > 2Si (0.145) and for TCNP 0Si (0.295) > 2Si (0.22) > 1Si (0.213). The overall DIA decreases upon reduction. For both [TCNDQ]<sup>-</sup> and [TCNP]<sup>-</sup> it decreases in the order 0Si (TCNDQ: 0.173, TCNP: 0.114) > 1Si (0.136, 0.091) > 2Si (0.098, 0.059). The overall DIA decreases upon symmetry breaking with a larger decrease noted in the anion cases.

The reduction in quinoidal character revealed by the BLA and DIA analysis implies that the electronic structure of the ground state is becoming more aromatic. This is normally attributed to an increase in diradical character (**Scheme 6.4**).



**Scheme 6.4**

**Table 6.6:** Bond length alternation (BLA) values for TCNQ, TCNDQ and TCNP calculated using B3LYP/BS4. In the 1Si versions Ring A is attached to Si. Values for anion in italics. See Figures 6.1 and 6.2 for identity of ring.

			Ring A	Ring B	Ring C = D
TCNP	0Si	D <sub>2h</sub>	0.067 / 0.039	–	0.095 / 0.057
		C <sub>2v</sub>	0.042 / 0.030	0.047 / 0.036	0.060 / 0.053
	1Si	C <sub>s</sub>	0.051 / 0.026	0.057 / 0.036	0.046 / 0.052
		D <sub>2h</sub>	0.044 / 0.031	–	0.062 / 0.052
	2Si	C <sub>2h</sub>	0.039 / 0.022	–	0.059 / 0.047
		C <sub>2v</sub>	0.039 / 0.022	–	0.059 / 0.047
TCNDQ	0Si	D <sub>2h</sub>	0.079 / 0.042	–	–
		D <sub>2</sub>	– / 0.045	–	–
	1Si	C <sub>2v</sub>	0.064 / 0.043	0.069 / 0.038	–
		C <sub>s</sub>	0.064 / 0.043	0.069 / 0.032	–
		C <sub>2</sub>	0.064 / 0.042	0.069 / 0.037	–
		C <sub>1</sub>	0.064 / 0.041	0.069 / 0.031	–
	2Si	D <sub>2h</sub>	0.056 / 0.038	–	–
		C <sub>2h</sub>	0.050 / 0.027	–	–
		C <sub>2v</sub>	0.049 / 0.027	–	–
		D <sub>2</sub>	0.056 / 0.036	–	–
		C <sub>2</sub>	0.048 / 0.025	–	–
	TCNQ	0Si	D <sub>2h</sub>	0.094 / 0.051	–
1Si		C <sub>2v</sub>	0.080 / 0.046	–	–
		C <sub>s</sub>	– / 0.044	–	–
2Si		D <sub>2h</sub>	0.068 / 0.044	–	–
		C <sub>2h</sub>	0.063 / 0.028	–	–
		C <sub>2v</sub>	0.065 / 0.031	–	–

**Table 6.7:** Delocalization index alternation (DIA) values for cyanocarbon series. B3LYP/BS4. In the 1Si versions Ring A is attached to Si. Values for anion in italics. See Figures 6.1 and 6.2 for identity of ring.

			Ring A	Ring B	Ring C = Ring D	Overall
TCNP	0Si	D <sub>2h</sub>	0.295 / 0.174	–	0.359 / 0.274	0.295 / 0.181
		1Si	C <sub>2v</sub>	0.190 / 0.097	0.252 / 0.162	0.320 / 0.255
		C <sub>s</sub>	0.186 / 0.086	0.252 / 0.159	0.318 / 0.252	0.211 / 0.114
	2Si	D <sub>2h</sub>	0.160 / 0.106	–	0.293 / 0.254	0.222 / 0.163
		C <sub>2h</sub>	0.137 / 0.066	–	0.280 / 0.232	0.202 / 0.136
		C <sub>2v</sub>	0.137 / 0.066	–	0.280 / 0.233	0.202 / 0.136
TCNDQ	0Si	D <sub>2h</sub>	0.393 / 0.239	–	–	0.249 / 0.076
		D <sub>2</sub>	– / 0.234	–	–	– / 0.069
	1Si	C <sub>2v</sub>	0.284 / 0.164	0.348 / 0.225	–	0.201 / 0.065
		C <sub>s</sub>	0.283 / 0.140	0.348 / 0.223	–	0.200 / 0.052
		C <sub>2</sub>	0.284 / 0.157	0.348 / 0.218	–	0.201 / 0.058
		C <sub>1</sub>	0.283 / 0.133	0.348 / 0.213	–	0.200 / 0.044
	2Si	D <sub>2h</sub>	0.246 / 0.165	–	–	0.145 / 0.047
		C <sub>2h</sub>	0.216 / 0.115	–	–	0.113 / 0.002
		C <sub>2v</sub>	0.215 / 0.114	–	–	0.112 / 0.002
		D <sub>2</sub>	0.246 / 0.156	–	–	0.145 / 0.038
		C <sub>2</sub>	0.208 / 0.105	–	–	0.104 / -0.009
	TCNQ	0Si	D <sub>2h</sub>	0.467 / 0.270	–	–
1Si		C <sub>2v</sub>	0.360 / 0.207	–	–	0.245 / 0.076
		C <sub>s</sub>	– / 0.199	–	–	– / 0.072
2Si		D <sub>2h</sub>	0.270 / 0.165	–	–	0.166 / 0.047
		C <sub>2h</sub>	0.246 / 0.097	–	–	0.145 / -0.013
		C <sub>2v</sub>	0.252 / 0.103	–	–	0.150 / -0.009

#### 6.3.4 – The Effect of Si-Substitution on Diradical Character

There are two classes of resonance structures that can be drawn to describe the electronic structure of TCNDQ and TCNP (**Scheme 6.4**). One class corresponds to a closed shell singlet configuration, and the other to an open shell diradical, which can exist in either a triplet (T – M<sub>S</sub>=1) or singlet (OSS – M<sub>S</sub>=0) electron configuration.

The related Tschitchitbabin's hydrocarbon displays some diradical character in its ground state, and Fukuda *et. al.* showed that substituting Si or Ge in the exocyclic position of *p*-QDM resulted in stabilization of the OSS state.<sup>40</sup> Moreover, we showed that Si-substitution enhanced the OSS and triplet diradical character of TCNQ.<sup>14</sup> Unlike the previous examples, stability calculations did not reveal a stable singlet diradical.<sup>41</sup> We focus here on the triplet surface. In all cases,  $\langle S^2 \rangle$  values are approximately 2 indicating no spin contamination (Appendix D Tables D83-D94).

Triplet  $D_{2h}$  TCNDQ is predicted by all functionals to be a TS that relaxes to a twisted  $D_2$  minimum (akin to [TCNDQ]<sup>-</sup> **Figure 6.1**). Torsion around the central C–C bond ranges from 31.1 to 45.2°(BS2) and 31.0 to 43.0°(BS4).

Planar 1Si TCNDQ is predicted to be a SOSP by all functionals, relaxing to a  $C_s$  pyramidalized TS, and a  $C_2$  twisted TS. Both further relax to a twisted and pyramidalized  $C_1$  minimum, similar to [1Si TCNDQ]<sup>-</sup> (**Figure 6.3**). The amount of torsion ranges from 30.5 to 41.7°(BS2) and 30.8 to 44.5°(BS4) and the pyramidalization ranges from 23.5 to 31.4°(BS2) and 22.5 to 30.9°(BS4).

All functionals predict planar triplet 2Si TCNDQ to be a TOSP that relaxes to *trans*-bent  $C_{2h}$ , *cis*-bent  $C_{2v}$  and twisted  $D_2$  TSs. These further relax to a  $C_2$  global minima that is twisted and equally pyramidalized at Si-nuclei similar to CSS 2Si TCNDQ (**Figure 6.4**). The pyramidalization ranges from 23.3 to 30.7°(BS2) and 22.3 to 30.7°(BS4). The amount of torsion around the central C–C bond ranges from 25.8 to 46.7°(BS2) and 31.8 to 43.1°(BS4). The magnitude of the pyramidalization and torsion are greater in the triplet than the CSS.

Planar triplet TCNP is predicted to be a minimum and planar 1Si TCNP is predicted to be a TS by all functionals, the latter relaxing to a  $C_s$  symmetry minimum that is pyramidalized at the Si-nucleus. The amount of pyramidalization ranges from 23.7 to 31.4° (BS2) and 22.2 to 30.9° (BS4). These findings are similar to what is observed on the triplet surfaces of TCNQ and 1Si TCNQ.<sup>14</sup>

Planar triplet 2Si TCNP is a SOSP that relaxes to *trans*-bent  $C_{2h}$  and *cis*-bent  $C_{2v}$  structures, consistent with observations on the triplet 2Si TCNQ surface. On the BS2 surfaces, all functionals except M06-HF predict a  $C_{2h}$  lowest energy structure; M06-HF predicts a  $C_{2v}$  minimum. The pyramidalization of the  $C_{2h}$  structure ranges from 23.5 to 38.4° and the pyramidalization of the  $C_{2v}$  minimum is 31.0°.

On the BS4 surfaces the  $C_{2h}$  structure is predicted to be the lowest energy structure by all functional except hybrid M06 functionals, which predict a  $C_{2v}$  lowest energy structure. The pyramidalization of the  $C_{2h}$  minima from 22.4 to 25.7° and that of the  $C_{2v}$  minima ranges from 24.5 to 30.5°. The amount of pyramidalization is greater in the triplet than the CSS for both BS2 and BS4.

The adiabatic single-triplet gap ( $\Delta E_{S-T}$ ) increases with Si-substitution, with a further increase due to structural symmetry breaking (**Figure 6.7**). Most model chemistries predict TCNDQ to be a CSS, while all model chemistries except BLYP and PBE (BS2 and BS4) predict a triplet ground state for the 1Si analog. For 2Si TCNDQ all model chemistries predict a triplet ground state. With the exception of the GGA functionals and B3LYP/BS4, TCNP is predicted to have a triplet ground state and all model chemistries predict a triplet ground state for the 1 and 2Si analogs.

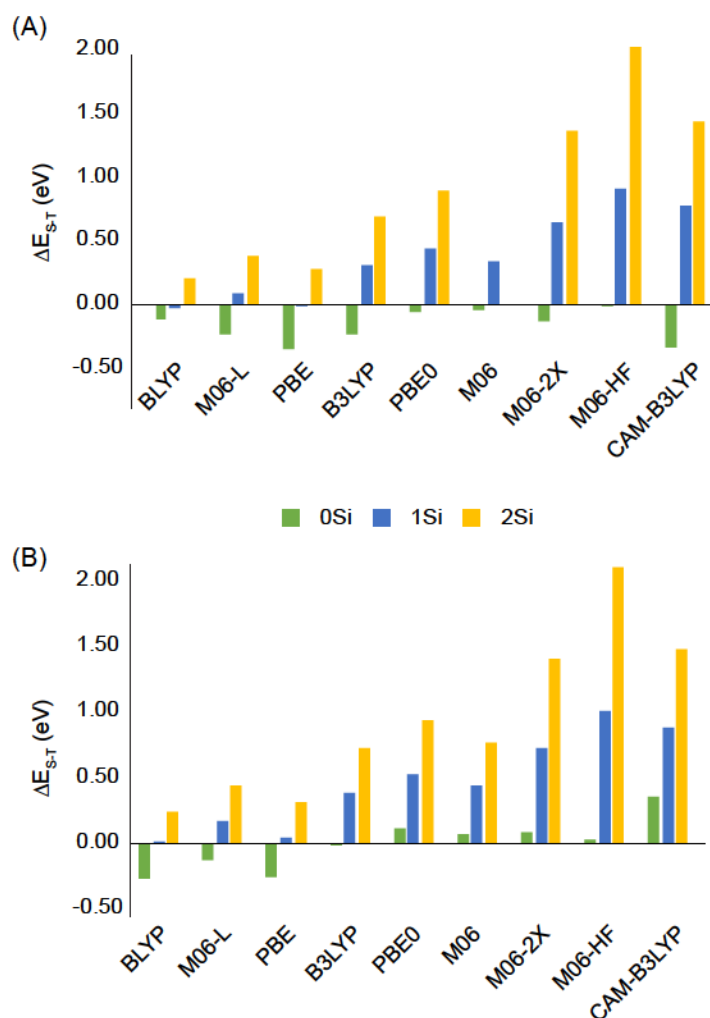


**Figure 6.7:** Adiabatic singlet-triplet gap ( $\Delta E_{S-T}$  in eV) calculated using BS4 for (A) TCNDQ and (B) TCNP series.

### 6.3.5 – The Effect of Si-Substitution on the AEA's

The orbital picture (Appendix D Figures D2 and D3) reveals that removing a single electron from the anion produces the closed shell singlet state and we will focus on these AEAs here. However, above we determined that many model chemistries predict a triplet ground state. Therefore, the CSS may be unstable and would likely only be transiently observed before the molecule relaxed to the triplet surface and underwent polymerization (as observed experimentally).<sup>16-18</sup>

The AEA's of TCNDQ range from 3.311 to 3.883eV (BS2) and 3.607 to 4.196eV (BS4) (**Figure 6.8A**). For 1Si TCNDQ the AEA's range from 3.530 to 4.395eV (BS2) and 3.745 to 4.749eV (BS4). 2Si TCNDQ has AEA's ranging from 3.672 to 5.367eV (BS2) and 3.836eV to 5.584eV (BS4). The average increase in AEA for the first Si-substitution is 0.256eV (BS2) and 0.335eV (BS4) and for the second Si-substitution is 0.335eV (BS2) and 0.291eV (BS4).

The AEA's of TCNP range from 3.411 to 4.121eV (BS2) and 3.694 to 4.418eV (BS4) (**Figure 6.8B**). For 1Si TCNP the AEA's range from 3.607 to 4.653eV (BS2) and 3.806 to 4.983eV (BS4). The AEA's of 2Si TCNP range from 3.724 to 5.572eV (BS2) and 3.879 to 5.171eV (BS4). The average increase in AEA for the first Si-substitution is 0.233eV (BS2) and 0.184eV (BS4) and for the second Si-substitution is 0.303eV (BS2) and 0.191eV (BS4).

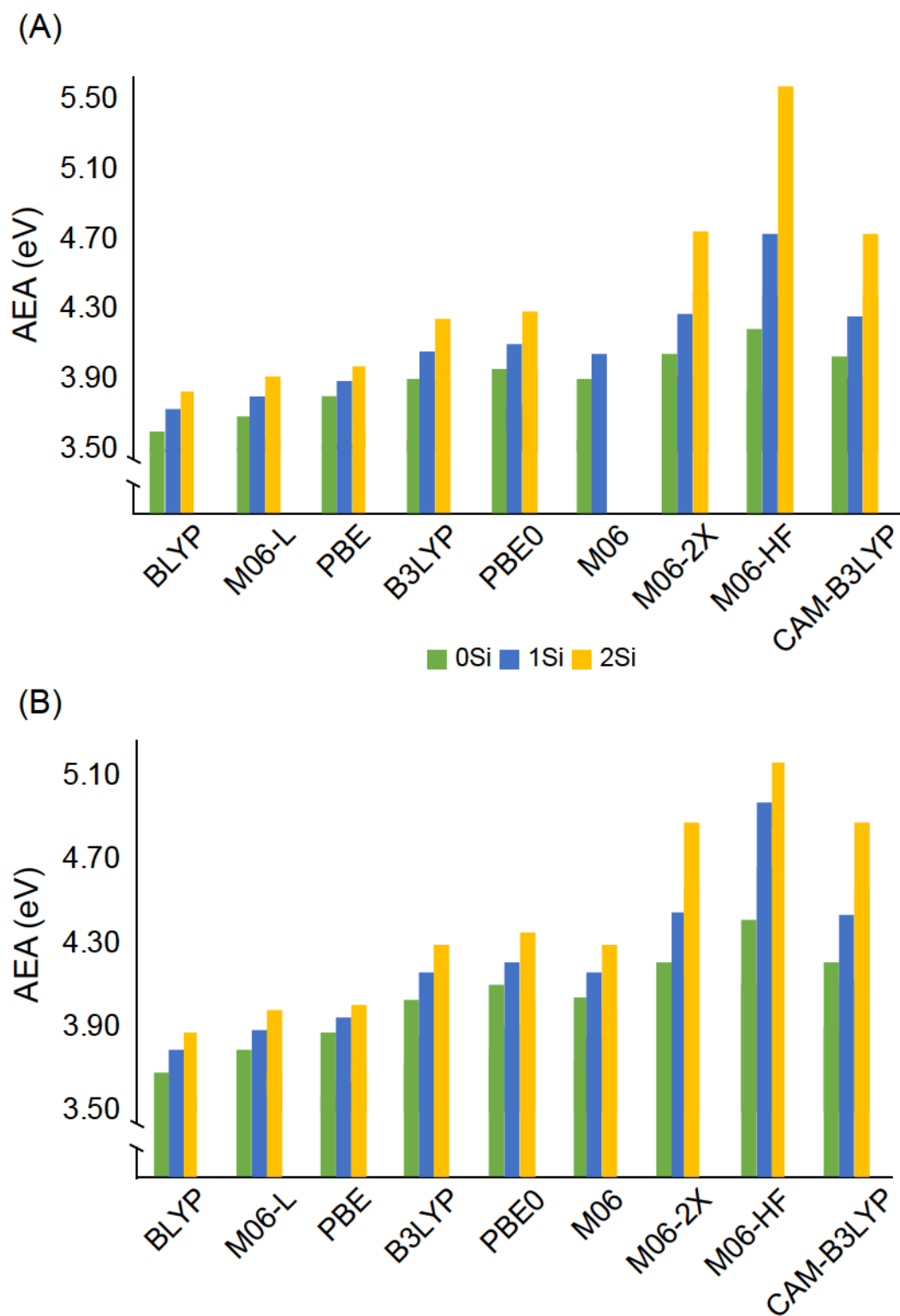
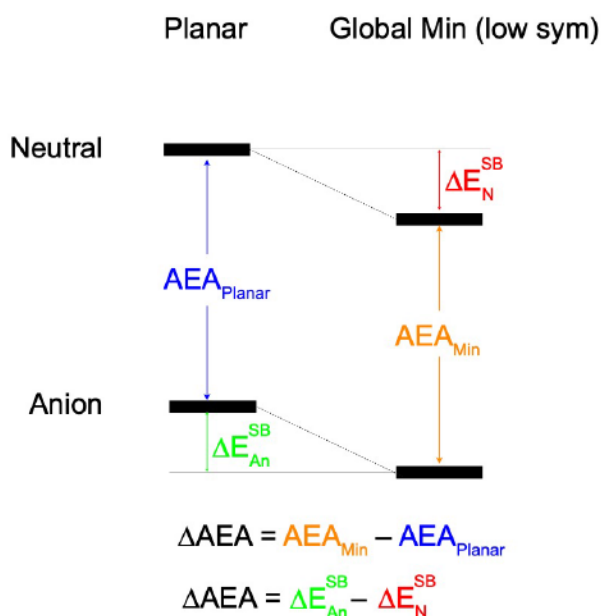


**Figure 6.8:** Adiabatic electron affinities (eV) calculated using BS4 for (A) TCNDQ series and (B) TCNP series. BS2 values available in Appendix D Figure D4A and D4B.

BLYP predicts the smallest AEA in all cases and M06-HF predicts the greatest. The large increase observed for M06-HF is due to absence of structural symmetry breaking in the neutral cases. Si-substitution causes a decrease in the AEA of the planar geometry (Appendix D Tables D99-D102). Structural symmetry breaking results in (unequal) stabilization of both states. The difference in AEA's calculated using the planar and minimum energy structures is equal to the difference in stabilization resulting from symmetry breaking (**Scheme 6.5**). Therefore, the enhancement of the AEA is a geometric effect. These findings are similar to those previously reported for the Si-analogs of TCNE and TCNQ.<sup>14</sup>



**Scheme 6.5**

Using PBE and M06-L in combination with BS2, we provide our best estimate of the AEA's of the Si-analogs of TCNDQ and TCNP along with those for TCNE and TCNQ (**Table 6.8**). The increase in AEA of TCNE is greater in the 2Si version than the 1Si version while the opposite is true of the other molecules. The smallest increase in AEA is noted for 2Si TCNQ, which is due to electronic symmetry breaking (i.e., formation of a

singlet diradical) stabilizing the neutral state relative to the anion.<sup>14</sup> The AEA's of the Si-analogs of TCNDQ and TCNP are greater than those of the Si-analogs of TCNE and TCNQ.

**Table 6.8:** AEA's (eV) of Si-substituted cyanocarbons

	#Si	TCNE	TCNQ	TCNDQ	TCNP
PBE/BS2	0	3.010	3.338	3.553	3.660
	1	3.297	3.475	3.708	3.789
	2	3.618	3.581	3.840	3.900
M06-L/BS2	0	3.180	3.471	3.674	3.790
	1	3.452	3.620	3.857	3.947
	2	3.754	3.684	4.001	4.068

#### **6.4 – Conclusions**

The structures of TCNDQ and TCNP as well as their 1 and 2Si analogs were assessed using DFT. TCNDQ, TCNP and [TCNP]<sup>-</sup> were predicted to be planar minima, consistent with TCNE and TCNQ. [TCNDQ]<sup>-</sup> was reported to be a twisted structure, in accordance with experimental findings. The neutral 1Si analogs were generally planar minima while the reduced 1Si analogs were pyramidalized at the Si-nuclei. The neutral and reduced 2Si analogs were also non planar, exhibiting pyramidalized geometries at the global surface minima. The structural symmetry breaking effects are congruous with those observed in the Si-analogs of TCNE and TCNQ.

TCNDQ and TCNP possess quinoidal type structures. The quinoidal character was quantified using BLA and DIA analysis. The quinoidal character was found to decrease as the  $\pi$ -conjugation network was extended and upon forming the anion. It was also found to decrease with Si-substitution and structural symmetry breaking. The singlet-triplet gap was found to decrease upon Si-substitution and a triplet diradical ground state predicted for the 2Si analogs.

The AEA's of TCNDQ and TCNP were assessed and the AEA's of the cyanocarbons are expected to increase as the  $\pi$ -conjugation network increases in size. Si-substitution consistently enhanced the AEA of both TCNDQ and TCNP, consistent with our previous findings regarding the AEA's of TCNE and TCNQ. These findings further demonstrate the efficacy of isovalent substitution as a strategy to enhance the performance of electron acceptors. Furthermore, the ability to form a stable triplet diradical ground state is of potential value in the creation of triplet fusion materials for organic light emitting diode technologies.<sup>43,44</sup>

## **6.5 – References**

- (1) Thiele, J. and Balhorn, H. *Chem. Ber.*, **1904**, 37, 1756
- (2) Tschitchitbabin, A.E. *Chem. Ber.*, **1907**, 40, 1810
- (3) Ravat, P. and Baumgarten, M. *Phys. Chem. Chem. Phys.*, **2014**, 17(2) 983
- (4) Kamada, K.; Ohta K.; Kubo, T.; Shimizu, A.; Morita, Y.; Nakasuji, K.; Kishi, R.; Ohta, S.; Furukawa, S. I.; Takahasi, H. and Nakano, M. *Angew. Chem. Int. Ed.*, **2007**, 46, 3544
- (5) Chikamatsu, M.; Mikami, T.; Chisaka, J.; Yoshida, Y.; Azumi, R. and Yase, K. *Appl. Phys. Lett.* **2007**, 91, 043506
- (6) Son, Y.; Cohen, M. L., Louie, S. G., *Phys. Rev. Lett.*, **2006**, 97 216803
- (7) Morita, Y.; Nishida, S.; Murata, T.; Moriguchi, M.; Ueda, A.; Satoh, M.; Arifuku, K.; Soto, K. and Takui, T. *Nat. Mater.* **2011**, 10, 947
- (8) Long R. E.; Sparks, R. A. and Trueblood, K. N., *Acta. Cryst.*, **1965**, 18, 932
- (9) Hoekstra, A.; Spoelder, T. and Vos, A., *Acta. Cryst.* **1972**, B28, 14
- (10) Kistenmacher, T. J.; Phillips, T. E. and Cowan, D. O., *Acta. Cryst.*, **1974**, B30 763
- (11) Miller, J. S.; Zhang, J. H.; Reiff, W. M.; Dixon, D. A.; Preston, L. D.; Reis Jr., A. H.; Gebert, E.; Extine, M.; Troup, J.; Epstein, A. J. and Ward, M. D., *J. Phys Chem.*, **1987**, 91, 4344
- (12) Milian, B.; Pou-Amerigo, R.; Viruela, R. and Orti, E. *J. Mol. Str. (Theochem)*, **2004**, 709, 97
- (13) Milian, B.; Pou-Amerigo, R.; Viruela, R. and Orti, E. *Chem. Phys. Lett.*, **2004**, 391, 148
- (14) Maley, S.M.; Esau, C. and Mawhinney, R.C. *Struct. Chem.*, **2018**, doi: 10.1007/s11224-018-1186-1
- (15) Zhu, G.-Z. and Wang, L.-S. *J. Chem. Phys.*, **2015**, 143, 221102
- (16) Addison, A. W.; Dalal, N. S.; Hoyano, Y.; Huizinga, S. and Weiler, L. *Can. J. Chem.* **1977**, 55, 4191

- (17) Maxfield, M.; Bloch, A. N. and Cowan, D. O. *J. Org. Chem.* **1985**, 50(11), 1789
- (18) Gerson, F.; Heckendorn, R.; Cowan, D. O.; Kini, A. M. and Maxfield, M. *J. Am. Chem. Soc.*, **1983**, 105(24), 7017
- (19) **Gaussian 09, Revision D.01**, Frisch, M. J.; Trucks, G. W.; Schlegel, H. B.; Scuseria, G. E.; Robb, M. A.; Cheeseman, J. R.; Scalmani, G.; Barone, V.; Mennucci, B.; Petersson, G. A.; Nakatsuji, H.; Caricato, M.; Li, X.; Hratchian, H. P.; Izmaylov, A. F.; Bloino, J.; Zheng, G.; Sonnenberg, J. L.; Hada, M.; Ehara, M.; Toyota, K.; Fukuda, R.; Hasegawa, J.; Ishida, M.; Nakajima, T.; Honda, Y.; Kitao, O.; Nakai, H.; Vreven, T.; Montgomery, J. A., Jr.; Peralta, J. E.; Ogliaro, F.; Bearpark, M.; Heyd, J. J.; Brothers, E.; Kudin, K. N.; Staroverov, V. N.; Kobayashi, R.; Normand, J.; Raghavachari, K.; Rendell, A.; Burant, J. C.; Iyengar, S. S.; Tomasi, J.; Cossi, M.; Rega, N.; Millam, J. M.; Klene, M.; Knox, J. E.; Cross, J. B.; Bakken, V.; Adamo, C.; Jaramillo, J.; Gomperts, R.; Stratmann, R. E.; Yazyev, O.; Austin, A. J.; Cammi, R.; Pomelli, C.; Ochterski, J. W.; Martin, R. L.; Morokuma, K.; Zakrzewski, V. G.; Voth, G. A.; Salvador, P.; Dannenberg, J. J.; Dapprich, S.; Daniels, A. D.; Farkas, Ö.; Foresman, J. B.; Ortiz, J. V.; Cioslowski, J.; Fox, D. J. Gaussian, Inc., Wallingford CT, 2009.
- (20) a) Becke, A.D. *Phys. Rev. A.*, **1988**, 38, 3098  
b) Lee, C., Yang, W. and Parr, R.G. *Phys. Rev. B*, **1988**, 37, 785
- (21) Perdew, J.P.; Burke, K., and Ernzerhof, M. *Phys. Rev. Lett.*, **1996**, 77, 3865
- (22) Zhao, Y. and Truhlar, D.G. *Theor. Chem. Acct.*, **2008**, 120, 215
- (23) Becke, A.D. *J. Chem. Phys.*, **1993**, 98, 5648
- (24) Adamo, C. and Barone, V. *J. Chem. Phys.*, **1999**, 110, 6158
- (25) Yanai, T., Tew, D. and Handy, N. *Chem. Phys. Lett.*, **2004**, 393, 51
- (26) Baurenschmidt, R. and Ahlrics, R. *J. Chem. Phys.*, **1996**, 104, 9047
- (27) AIMAll (Version 17.11.14), Todd A. Keith, TK Gristmill Software, Overland Park KS, USA (**2017**) (aim.tkgristmill.com)
- (28) Bader, R. F. W., *Atoms in Molecules: A Quantum Theory*. Oxford University Press, New York, USA (**2003**)
- (29) The deviation in calculated ESR constants is available in Appendix D Tables D13 and D14.

- (30) Imaginary frequencies could not be removed in these cases. They lead back to the twisted  $D_2$  structure described.
- (31) M06-L increases in the order BS4 < BS1 < BS2 < BS3
- (32) Grein, F. *J. Mol. Str. (Theochem)*, **2003**, 624, 23-28
- (33) Choi, J.; Cho D.W.; Tojo, S.; Fujitsuka, M. and Majima, T. *J. Phys. Chem. A*, **2015**, 119, 851
- (34) Campanelli, A.R. and Domenciano, A. *Struct. Chem.*, **2013**, 24 867
- (35) Casado, J.; Burrezo, P.M.; Zafra, J.L. and Navattete, J.T.L. *Angew. Chem. Int. Ed.*, **2017**, 56(9), 2250
- (36) The DIA values are computed as the difference between the average double bond DI and average single bond DI. This is done so that DIA carries the same sign as BLA.
- (37) Chowdhury, S. and Kebarle, P. *J. Am. Chem. Soc.*, **1986**, 108, 5423
- (38) Morinaga, M., Nogami, T. and Mikawa, H. *Bull. Chem. Soc. Japan*, **1979**, 52(12), 3739
- (39) M06/BS2 is  $C_s$  symmetry but displays no pyramidalization.
- (40) The 2Si TCNDQ PES could not be mapped out with M06/BS4 due to integration grid errors
- (41) Fukuda, K.; Nozawa, T.; Yotsuyanagi, H.; Ichinohe, M.; Sekiguchi, A. and Masayoshi, N. *J. Phys. Chem. C*, **2015**, 119(2), 1188
- (42) Further attempts to calculate the energy of the OSS by using the triplet wavefunction and permuting the orbitals resulted in the CSS solution being obtained.
- (43) Wakasa, M.; Yago, T.; Sonoda, Y. and Katoh, R. *Comm. Chem.* **2018**, 1(9)
- (44) Tang, X.; Hu, Y.; Jia, W.; Pan, R.; Deng, J.; Deng, J.; He, Z. and Xiong, Z. *ACS Appl. Mater. Interfaces*, **2018**, 10(2), 1948

## **Chapter SEVEN**

**Using DFT to calculate Pseudo Jahn-Teller Effect Parameters:  
Understanding the Origin of Symmetry Breaking in Hypovalent Silicon**

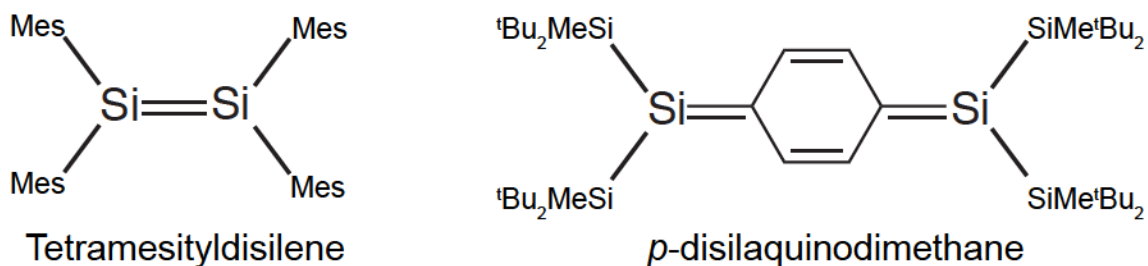
## **Overview**

Heavy group 14 analogs of planar carbon molecules are well known to prefer bent or pyramidalized geometries. The pseudo Jahn-Teller effect (pJTE) is a general approach to understanding the origin of such molecular geometries. Computationally intensive multi-reference post Hartree-Fock methods are generally required to obtain values relevant to the pJTE. However, an alternative approach, using more computationally efficient density functional theory (DFT) and fitting a model vibronic Hamiltonian, can account for the pJTE parameters. It is shown that the DFT approach is a viable alternative for determining values relevant to the pJTE. Difficulties associated the DFT based approach to the study of the pJTE are discussed and changes in the electronic structure are explored using the Quantum Theory of Atoms in Molecules.

## 7.1 – Introduction

In contrast to hypovalent carbon-carbon bonds, which display a planar geometry, their heavy group 14 analogs (Si, Ge, Sn, Pb) typically display bent or pyramidalized geometries.<sup>1</sup> The first example of a stable Si–Si double bond was synthesized by West *et. al.* when they prepared tetramesityldisilene (**Scheme 7.1**).<sup>2</sup> X-ray diffraction of obtained crystals indicated slightly pyramidalized Si-nuclei ( $3.7^\circ$ ).<sup>3</sup> Since then, more than 70 molecules containing Si–Si double bonds have been prepared, many displaying pyramidalized geometries.<sup>1</sup>

A related compound is *p*-disilaquinodimethane prepared by Sekiguchi *et. al.* (**Scheme 7.1**).<sup>4</sup> To the best of our knowledge this is the only example of a molecule containing two hypovalent Si not directly bonded. Despite the hypovalent Si-nuclei being separated by a phenyl unit, the structure shows a slight pyramidalization at the Si-nuclei ( $0.4^\circ$ ).



**Scheme 7.1**

While there have been models put forth to explain the non-planarity of the heavy group 14 analogs, such as the CGMT model,<sup>5,6</sup> the pseudo Jahn-Teller effect (pJTE) is a more general approach that can be used to rationalize the structures of non-electronically degenerate molecules on the basis of vibronic interactions.<sup>7,8</sup> It describes how vibronic interaction between ground and excited states affects the curvature of the ground state

adiabatic potential energy surface (APES). The strength of the vibronic interaction is given by a non-adiabatic coupling constant ( $F$ ):

$$F = \left\langle \Psi_0 \left| \left( \frac{\partial H}{\partial Q} \right)_0 \right| \Psi_n \right\rangle \quad (7.1)$$

and the curvature of the ground state surface ( $K_0 > 0$ )<sup>9</sup> is defined by

$$K_0 = \left\langle \Psi_0 \left| \left( \frac{\partial^2 H}{\partial Q^2} \right)_0 \right| \Psi_0 \right\rangle \quad (7.2)$$

The vibronic interaction reduces the curvature of the ground state surface according to

$$K_V = \frac{F^2}{\Delta} \quad (7.3)$$

where  $\Delta$  is the vertical excitation energy from the ground to the excited state. The total curvature of the ground state surface ( $K$ ) is then given by

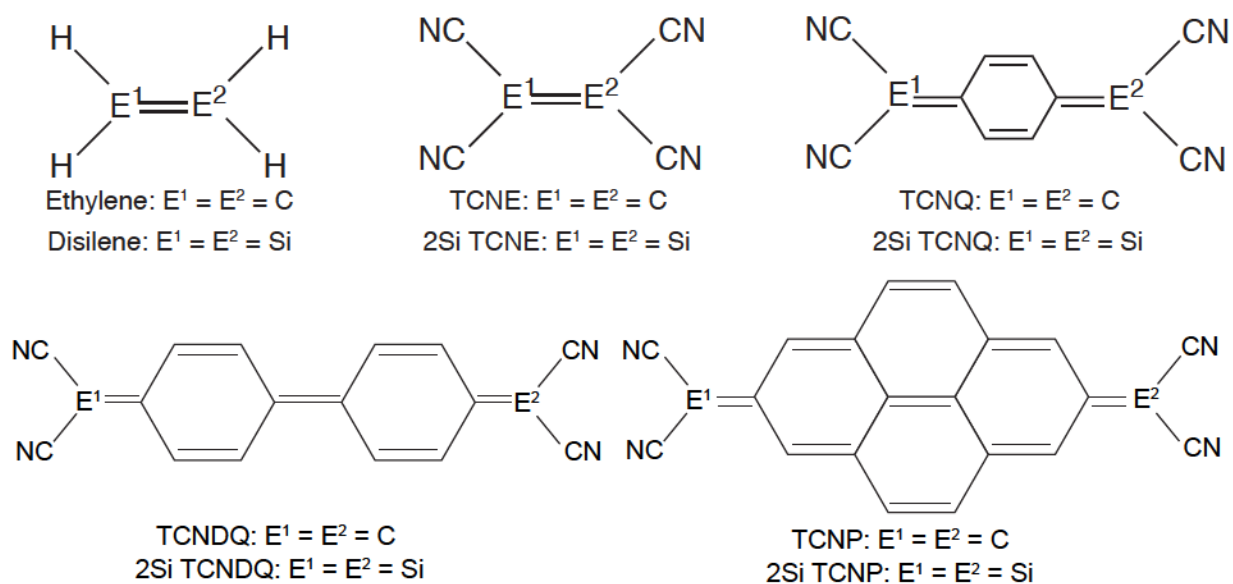
$$K = K_0 - K_V \quad (7.4)$$

When  $K_V > K_0$  the stationary point of the high symmetry (planar) geometry is characterized as a saddle point on the APES and symmetry breaking is observed.

The direct evaluation of pJTE parameters is challenging.<sup>7,8</sup> Multi-reference ab initio methods are the preferred method as they offer an accurate description of all relevant electronic states.<sup>10-12</sup> However, they are intractable for many systems including the molecules discussed in this work. Therefore, values are obtained by fitting cross-sections of the APES along the distorting mode to a model vibronic Hamiltonian (Equation 7.5).<sup>7,8</sup> A similar approach has also been used by Soto *et. al.* to evaluate the pJTE parameters relevant to the buckling distortion in the heavy analogs (Si, Ge, Sn) of graphene.<sup>13-15</sup>

$$E(Q) = \frac{1}{2} \left[ K_0 - \frac{F^2}{\Delta} \right] Q^2 - \frac{1}{4} \left[ \frac{F^4}{\Delta^3} \right] Q^4 + \Delta E_{SB} \quad (7.5)$$

In chapter 5 a model vibronic Hamiltonian was fit to cross-sections of the APES of disilene and 2SiTCNQ calculated using density functional theory (DFT). Here we apply the same method to the 2Si analogs of all cyanocarbons introduced from our earlier chapters along with the parent (carbon) versions (**Scheme 7.2**) in an effort to understand the controlling factors in the symmetry breaking of hypovalent silicon containing molecules.



**Scheme 7.2**

The pJTE causes changes in a molecule's electronic structure. According to Berusker "... *molecular shapes are formed by the equilibrium configuration of the nuclei in the mean field of the electronic cloud. Obviously any change of the latter influences the former*".<sup>7,8</sup> The Quantum Theory of Atoms in Molecules (QTAIM)<sup>16,17</sup> allows areas of electron density concentration and depletion (the electronic cloud) to be identified by examining the Laplacian of the electron density ( $\nabla^2\rho$ ). Furthermore, changes in the atomic

properties due to symmetry breaking (for example, the atomic energy or electron population) can be quantified using QTAIM.

In this chapter, the APESs of the 2Si-analogs of ethylene and the cyanocarbon series are briefly contrasted with those of the parent versions and pJTEs common to 2Si-analogs are identified. A model vibronic Hamiltonian is fit to cross-sections of the DFT APES in order to assess the pJTE parameters. These parameters are then contrasted in an effort to elucidate the controlling factor in the symmetry breaking of hypovalent silicon. Challenges associated with the fitting procedure are discussed. Changes in  $\nabla^2\rho$  along with quantitative changes in the atomic properties due to symmetry breaking are studied to gain additional insight in to how the pJTE affects electronic structure.

## **7.2 – Methodology**

All structures were optimized in  $D_{2h}$  symmetry using DFT. 9 functionals including 3 GGA's (BLYP,<sup>18</sup> M06-L<sup>19</sup> and PBE<sup>20</sup>), 5 hybrids (B3LYP,<sup>21</sup> PBE0,<sup>22</sup> M06,<sup>19</sup> M06-2X<sup>19</sup> and M06-HF<sup>19</sup>) and CAM-B3LYP<sup>23</sup> were combined with the Def2TZVPP basis set. All stationary points were characterized by frequency calculations and, when required, imaginary frequencies were followed to the surface minima. All vertical excitation energies were determined using Time-Dependent (TD) DFT. To generate scans along the APES the coordinates of the low and high symmetry geometries are subtracted from one another and the scaled difference is added (in 0.1 increments) to the high symmetry geometry. All DFT calculations were performed using Gaussian 09 Rev. D.01.<sup>24</sup> The fitting of the model Hamiltonian to the APES cross sections was performed using Prism 7.0<sup>25</sup> and the cross-sections were generated at the B3LYP/Def2TZVPP level of theory, as used by Soto *et. al.*<sup>13-15</sup> QTAIM analysis was performed using the AIMAll package.<sup>26</sup>

## 7.3 – Results and Discussion

### 7.3.1 – General Features of the Potential Energy Surfaces

The parent compounds are characterized as  $D_{2h}$  planar minima with  $^1A_G$  ground states by all functionals. On the other hand, all planar 2Si analogs have  $^1A_G$  ground states, but are generally predicted to be saddle points on their PESs. The general features of the 2Si PESs (see **Figures 7.1-7.5** for representative PES diagrams) are described along with changes in geometry that occur upon symmetry breaking.

#### 7.3.1.1 – Disilene

All functionals except M06-2X and M06-HF predict  $D_{2h}$  disilene to be a transition structure unstable with respect to a  $b_{2g}$  bending mode. The transition structure relaxes to a *trans*-bent  $C_{2h}$  minimum that is 0.003 to 1.21 kcal/mol more stable than the planar configuration (**Figure 7.1**). Upon symmetry breaking the Si nuclei pyramidalize  $0.2^\circ$  to  $13.0^\circ$  and  $R_1$  (0.61 to 1.84%) and  $R_2$  (0.18 to 0.5%) increase in length.

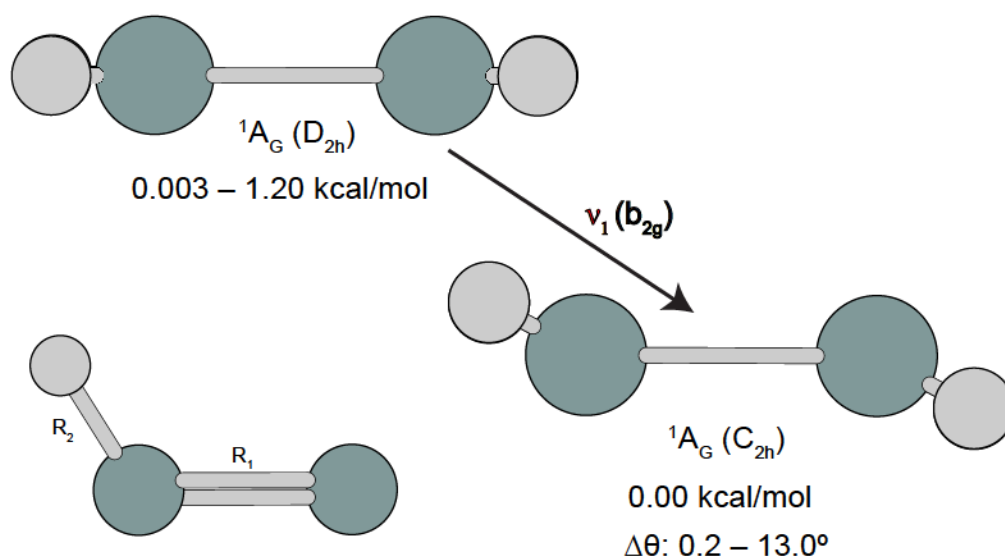


**Figure 7.1:** Representative PES for disilene with numbering of bond lengths.  $\Delta\theta$  is the amount of Si-pyramidalization. Energy values are relative to the surface minimum.  $\nu$  indicates an imaginary frequency.

### 7.3.1.2 – 2Si TCNE

All functionals predict planar 2Si TCNE to be a transition structure unstable with respect to a  $b_{2g}$  bending mode. The transition structure relaxes to a *trans*-bent  $C_{2h}$  minimum that is 0.02 to 3.37 kcal/mol more stable than the planar configuration (**Figure 7.2**). All functionals predict the stabilization to be greater in the case of 2Si TCNE than disilene. This is in line with the suggestion that electronegative substituents cause greater distortions in disilenes.<sup>27</sup> Upon symmetry breaking the Si-nuclei pyramidalize  $6.8^\circ$  to  $21.0^\circ$ ,  $R_1$  and  $R_2$  increase by 1.13 to 3.99% and 0.27 to 1.24%, respectively. The cyano bond length ( $R_3$ ) changes only slightly -0.03% to +0.04%.

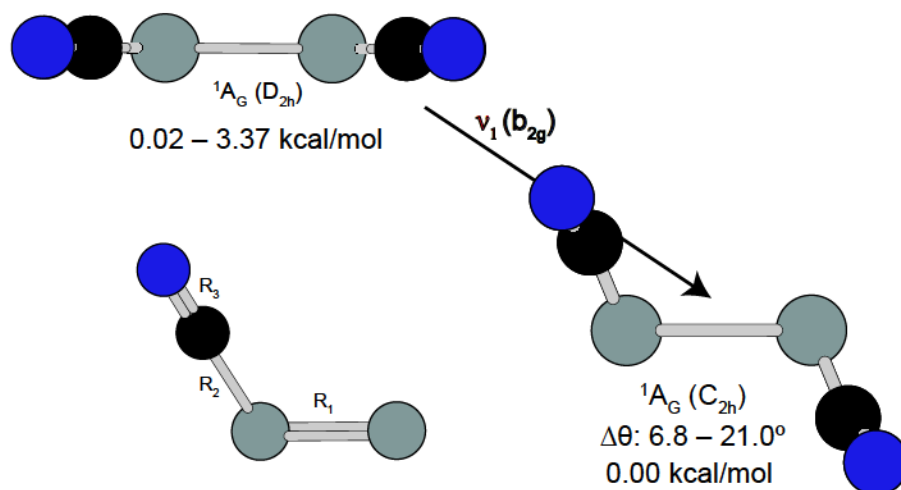


**Figure 7.2:** Representative PES for 2Si TCNE with numbering of bond lengths.  $\Delta\theta$  is the amount of Si-pyramidalization. Energy values are relative to the surface minimum.  $\nu$  indicates an imaginary frequency.

### 7.3.1.3 – 2Si TCNQ

All functionals except, M06-2X, M06-HF and CAM-B3LYP, predict the  $D_{2h}$  structure to be a second order saddle point unstable with respect to  $b_{2g}$  *trans* and  $b_{3u}$  *cis* bending modes. The exceptions predict a planar minimum. The saddle point relaxes to *trans*-bent  $C_{2h}$  and *cis*-bent  $C_{2v}$  minima with the  $C_{2h}$  structure as the lowest energy structure on all

surfaces except M06 (**Figure 7.3**). On the M06 surface the  $C_{2h}$  and  $C_{2v}$  structures further relax to a  $C_S$  (*pseudo*  $C_{2h}$ ) symmetry minima; the  $C_{2h}$  and  $C_S$  structures are quasi-degenerate ( $\Delta E = 0.001$  kcal/mol). On the M06-L and PBE0 surfaces the  $C_{2v}$  structure further relaxes to the  $C_S$  structure.

Upon symmetry breaking the Si-nuclei are pyramidalized  $6.8$  to  $10.7^\circ$  at the global minima; on the M06 surface, the lowest energy structure pyramidalization is  $6.4^\circ$ .<sup>28</sup>  $R_1$  (0.05 to 0.26%),  $R_3$  (0.23 to 1.05%) and  $R_4$  (0.13 to 0.73%) increase while  $R_2$  (0.08 to 0.30%) and  $R_5$  (0.01 to 0.04%) decrease.

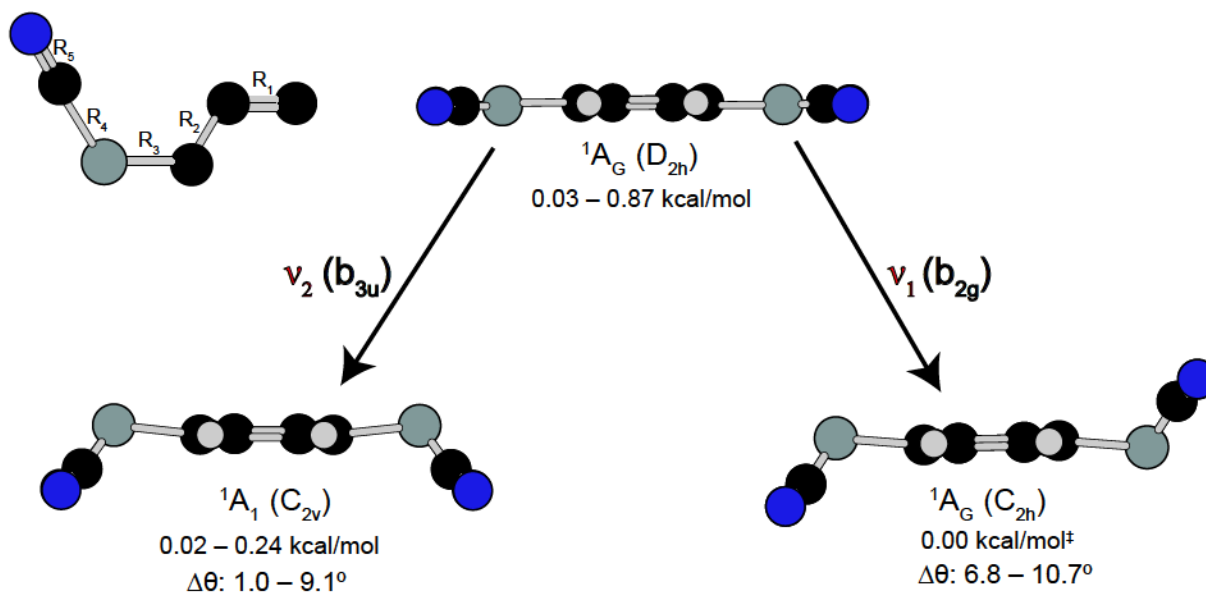


**Figure 7.3:** Representative PES for 2Si TCNQ with numbering of bond lengths (hydrogens omitted).  $\Delta\theta$  is the amount of Si-pyramidalization. Energy values are relative to the surface minimum. † on the M06 surface a  $C_S$  (*pseudo*- $C_{2h}$ ) structure (not shown) is the lowest energy structure; the  $C_{2h}$  structure is 0.004 kcal/mol higher in energy relative to the  $C_S$  structure.  $\nu$  indicates an imaginary frequency.

#### 7.3.1.4 – 2Si TCNDQ

All functionals,<sup>29</sup> except M06-HF, predict the  $D_{2h}$  structure to be a saddle point unstable with respect to  $b_{2g}$  *trans*-bending,  $b_{3u}$  *cis*-bending, and  $a_u$  twisting modes (except

CAM-B3LYP). The saddle point relaxes to *trans*-bent  $C_{2h}$ , *cis*-bent  $C_{2v}$  and twisted  $D_2$  transition structures that further relax to a  $C_2$  symmetry minimum that is twisted around  $R_1$  and equally pyramidalized at both Si nuclei (**Figure 7.4**). On the CAM-B3LYP surface the planar structure relaxes to  $C_{2h}$  and  $C_{2v}$  transition structures that further relax to a  $C_s$  symmetry structure that is pyramidalized ( $14.6^\circ$ ) at one Si-nuclei but otherwise planar.

The  $C_2$  structure is the lowest energy structure and is 0.43 to 2.44 kcal/mol more stable than the planar structure. The amount of torsion around  $R_1$  ranges from  $11.2$  to  $21.4^\circ$  and the pyramidalization ranges from  $8.4$  to  $16.5^\circ$ .  $R_1$  (0.21 to 1.89%),  $R_3$  (0.04 to 0.78%),  $R_5$  (0.28 to 0.84%), and  $R_6$  (0.10 to 1.20%) increase and  $R_2$  (0.06 to 1.22%),  $R_4$  (0.06 to 1.02%) and  $R_7$  (0.07 to 0.59%) decrease. The  $C_{2h}$  and  $C_{2v}$  ranges include the CAM-B3LYP minima.

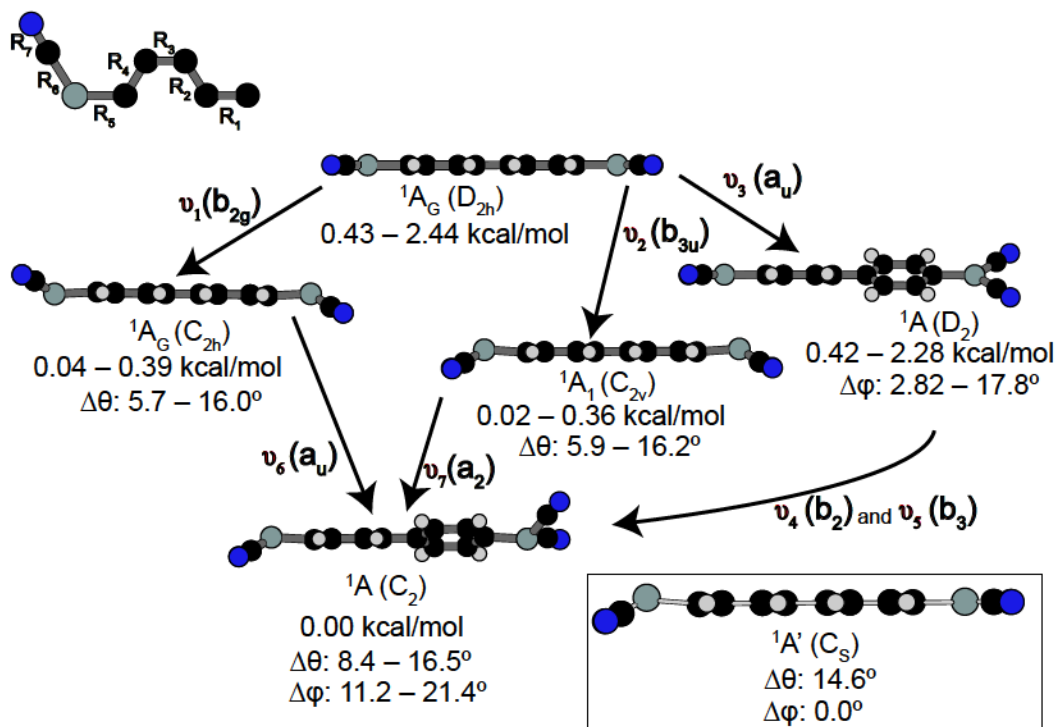


**Figure 7.4:** Representative PES for 2Si TCNDQ with numbering of bond lengths. M06<sup>29</sup> data omitted. Inset box: CAM-B3LYP minimum. Energy values are relative to the surface minima.  $\Delta\theta$  is the amount of Si-pyramidalization and  $\Delta\phi$  is the amount of torsion around  $R_1$ .  $\nu$  indicates an imaginary frequency

### 7.3.1.5 – 2Si TCNP

All functionals except M06-HF predict the planar structure to be a saddle point unstable with respect to *trans*-bending  $b_{2g}$  and *cis*-bending  $b_{3u}$  modes. The saddle point relaxes to *trans*-bent  $C_{2h}$  and *cis*-bent  $C_{2v}$  structures, with the  $C_{2h}$  structure as the lowest energy structure on all surfaces except M06 (**Figure 7.5**). The stabilization ranges from 0.99 to 2.78 kcal/mol. On the M06 surface the  $C_{2v}$  structure is 0.02 kcal/mol more stable than the planar structure (and 0.015 kcal/mol more stable than  $C_{2h}$ ) and is the lowest energy structure. On the CAM-B3LYP surface the  $C_{2h}$  and  $C_{2v}$  structures further relax to a  $C_s$  symmetry structure that is 1.07kcal/mol more stable than the planar structure.

The  $C_{2h}$  and  $C_{2v}$  minima have Si-nuclei that are equally pyramidalized 12.2 to 17.6°. The  $C_s$  minima is pyramidalized 26.0° at one Si-nucleus but planar at the other. In the  $C_{2h}$  and  $C_{2v}$  minima  $R_1$  (0.03 to 0.04%),  $R_2$  (0.11 to 0.27%),  $R_5$  (0.11 to 0.20%),  $R_7$  (1.06 to 1.44%) and  $R_8$  (0.64 to 1.31%) increase and  $R_3$  (0.04 to 0.07%),  $R_4$  (0.06 to 0.16%),  $R_6$  (0.19 to 0.32%) and  $R_9$  (0.03 to 0.14%) decrease. In the  $C_s$  minima the same changes in bond lengths are observed for the half of the molecule attached to the pyramidalized Si. In the other half of the molecule,  $R_7$  (0.16%) and  $R_8$ (0.05%) decrease while all other bond lengths display the same changes as above.

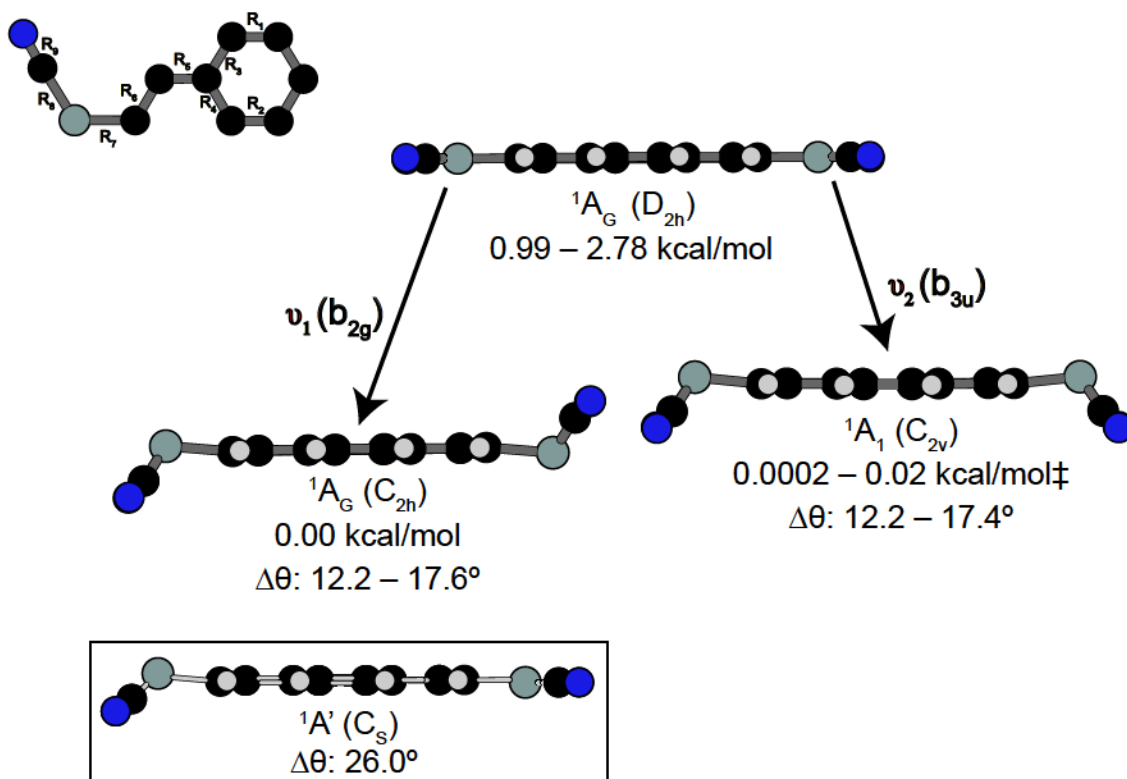


**Figure 7.5:** Representative PES for 2Si TCNP with numbering of bond lengths. ‡ on the M06 surface the  $C_{2v}$  structure is the lowest energy structure ( $\Delta E = 0.02\text{kcal/mol}$ ). Inset box: CAM-B3LYP minimum. Energy values are relative to the surface minimum.  $\Delta\theta$  is the amount of Si-pyramidalization.  $\nu$  indicates an imaginary frequency.

In contrast to the 0Si versions, the 2Si versions prefer geometries that are pyramidalized at the Si-nuclei. This is consistent with experimentally observed disilenes<sup>1</sup> as well as the *p*-disilaquinodimethane synthesized by Sekiguchi *et. al.*<sup>4</sup> In all cases, the amount of pyramidalization and stabilization resulting from symmetry breaking are commensurate with one another (Figure 7.6), consistent with our earlier results (Chapter 5).

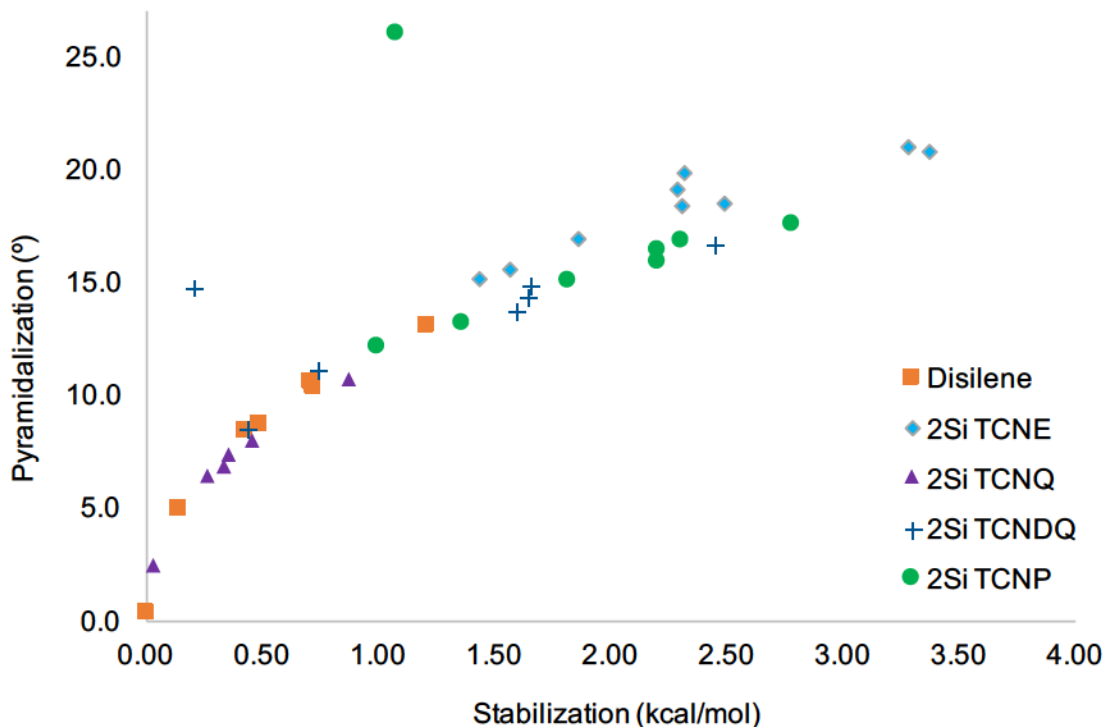


**Figure 7.6:** The amount of pyramidalization as a function of the amount of stabilization (kcal/mol) at the global surface minima for the 2Si molecules. All functionals<sup>29a,b</sup>/Def2TZVPP. The outliers correspond to results obtained using CAM-B3LYP.

### 7.3.2 – Types of Pseudo Jahn-Teller Effect Responsible for Symmetry Breaking

In our analysis, we will focus on the major symmetry breaking modes only, of which three are observed in the  $D_{2h}$  2Si molecules above: *trans* bending, *cis* bending and twisting.<sup>30</sup> The type of pJTE responsible for each can be identified based on symmetry requirements; the product of the irreducible representations of the ground and excited state must produce the irreducible representation of the distorting mode.<sup>7,8</sup> All planar 2Si structures have  $^1A_g$  ground states.  $b_{2g}$ ,  $b_{3u}$  and  $a_u$  modes are responsible for the *trans*-bending, *cis*-bending and twisting distortions, respectively.

A ( $^1A_g + ^1B_{2g}$ )  $\otimes$   $b_{2g}$  pJTE is responsible for the *trans*-bending distortion common to all five 2Si molecules. A ( $^1A_g + ^1B_{3u}$ )  $\otimes$   $b_{3u}$  pJTE is responsible for the *cis*-bending

distortion common to all extended  $\pi$ -systems. The ( ${}^1A_G + {}^1A_U$ )  $\otimes a_U$  pJTE is responsible for the twisting distortion in 2Si TCNDQ.

### 7.3.3 – Evaluating the Pseudo Jahn-Teller Effect Parameters

Using the model vibronic Hamiltonian (7.5) and surface fitting approach described earlier, the pJTE parameters are evaluated for the planar geometries of all molecules:  $K_0$  and  $F$  are obtained by the fitting procedure while  $\Delta$  is directly calculated using TD-DFT. These values, as well as  $K_V$  and the total surface curvature ( $K$ ), are compiled in **Table 7.1** for all three PJTEs. The scans along the APES as well as the coefficients and  $r^2$  values obtained from the fitting are available in Appendix E.

$K_0$  and  $\Delta$  are greater in all 0Si cases.  $F$  is greater in the 2Si cases of TCNQ and  $K_V$  is greater in the 2Si cases of TCNQ and ethene. It is difficult to assign any physical significance to values obtained to the fitting procedure. However, the magnitude of the values can still be compared with values obtained in studies of pJTEs in series of isovalently substituted molecules.<sup>10,31,32</sup>

**Table 7.1:** pJTE parameters assessed using B3LYP/Def2TZVPP for planar 0 and 2Si molecules.

		$K_0$ (eV/Å <sup>2</sup> )	F (eV/Å)	$\Delta$ (eV)	$K_V$ (eV/Å <sup>2</sup> )	K (eV/Å <sup>2</sup> )
		$(^1A_G + ^1B_{2G}) \otimes b_{2g}$				
Ethene	0	29.76	13.62	8.99	20.63	9.13
	2	24.40	11.86	4.98	28.23	-3.84
TCNE	0	47.38	7.16	4.96	10.34	37.04
	2	1.97	3.53	4.00	3.12	-1.15
TCNQ	0	9.47	1.94	4.79	0.79	8.68
	2	2.72	3.16	3.18	3.13	-0.42
TCNDQ	0	775.16	31.18	4.53	214.56	560.60
	2	58.67	15.71	2.85	86.63	-27.96
TCNP	0	25.27	4.72	4.37	5.11	20.16
	2	2.71	3.48	2.77	4.38	-1.67
		$(^1A_G + ^1B_{3U}) \otimes b_{3u}$				
TCNQ	0	23.55	5.68	4.66	6.93	16.62
	2	20.22	9.81	3.07	31.36	-11.14
TCNDQ	0	58.23	8.44	4.51	15.79	42.44
	2	2.87	3.68	2.84	4.77	-1.90
TCNP	0	72.92	9.44	4.38	20.36	52.56
	2	2.84	3.91	2.77	5.52	-2.68
		$(^1A_G + ^1A_U) \otimes a_u$				
TCNDQ	0	11.20	6.58	4.20	10.31	0.89
	2	1.01	2.20	3.93	1.23	-0.21

Liu *et. al.* studied the puckering distortion in  $A_4H_4^{2+}$  (A = C or Si) using a model Hamiltonian fit to MRCI/cc-pvTZ PES cross-sections and reported that the more distorted  $C_4H_4^{2+}$  had a greater vibronic contribution to its ground state curvature ( $K_V$ ).<sup>10</sup> This is not true of our results. For example, 2Si TCNE typically displays the greatest pyramidalization but does not have the largest  $K_V$ .

Ilkhani assessed the pJTE causing puckering in  $C_4AE_5$  (A = N, P, As and E = H, F, Cl)<sup>31</sup> and  $C_2Y_3H_2$  (Y = O, S, Se, Te)<sup>32</sup> at the CASSCF/cc-pvTZ level of theory. The value of F was generally found to increase going down groups 15 and 16. On the other

hand, Liu *et. al.* reported that F was greater in the C version.<sup>10</sup> In all cases, the value of  $\Delta$  decreases going down the periodic table.<sup>10,31,32</sup>

#### 7.3.4 – Suggested Best Practices in Assessing pJTE Problems

There are additional caveats regarding the determination of the pJTE parameters that warrant further discussion. The first is that the excitation energies obtained by TD-DFT may not be accurate. While there are no experimental or post-HF vertical excitation energies to compare to for the  $\pi$ -conjugated OSi molecules or any of the 2Si molecules, there are suitable values to compare to for ethene and TCNE.

Experimentally, the lowest lying  $^1B_{2G}$  excited state of ethene is 7.90eV above the ground state.<sup>33</sup> Our calculated value overestimates this value by 13.8%. There are no experimental studies of the excited states of TCNE, however, at the CCSD and CCSD(T) levels of theory the lowest lying  $^1B_{2G}$  excited state is predicted to be 6.32 and 6.13eV above the ground state.<sup>34</sup> Our value is approximately 20% greater than these.

The second point of discussion is related to the fitting procedure itself, which is based upon fitting a fourth order polynomial to the scans along the APES and equating the coefficients to those of the model vibronic Hamiltonian.

In developing the fitting procedure, the most appropriate choice of Q (x-axis) had to be determined. One option that was tested was using the intrinsic reaction coordinate (IRC) to follow a transition structure (or saddle point) to the surface minimum. This was problematic for our application because the IRC algorithm was unable to follow the APES to the minimum due to the flat nature of the surface (the barriers to non-planarity are less than 5 kcal/mol).

The most commonly used choice of Q in the literature is an arbitrary coordinate where 0 corresponds to the high symmetry configuration and 1 corresponds to full displacement of the distorting mode.<sup>10-12</sup> This choice was also problematic. Following the imaginary (distorting) modes did not lead to the optimized low symmetry geometry. This is due to the fact that the nuclei will optimize differently than the motion of the normal mode. The force constant and non-adiabatic coupling constant have units of energy/distance. Using an arbitrary coordinate results in the constants lacking a distance unit.

Another choice of Q we tested was the amount of pyramidalization of the Si-nuclei, however, this choice cannot be applied to the twisting distortions. Soto *et. al.* used the difference between the coordinates of the high and low symmetry geometries and the scaled difference (in 0.1 increments) to the high symmetry configuration. This results in the x-axis having units of angstroms and the quantities of interest carrying the correct units. We have used this approach throughout this work. However, this approach is still problematic.

The energies of the distorted geometries initially increase and exceed that of the high symmetry configuration (See **Figure 7.7** for example). This is a problem related to the Gaussian09 package. These data points are removed from the scan. The resulting scan along the APES is fit to a fourth order polynomial and the value of the  $a_0$  coefficient is set to the stabilization energy resulting from symmetry breaking.

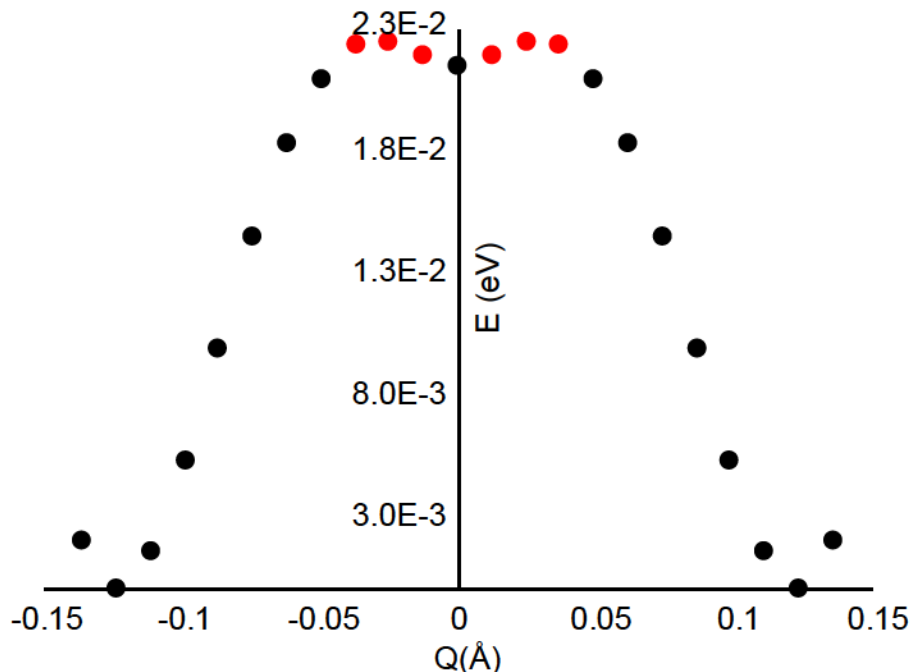


**Figure 7.7:** Example scan along of APES of disilene. The red points correspond to geometries with energies greater than the planar geometry that are removed from the polynomial fit.

There were additional challenges in applying the fitting procedure to the 0Si cases. The normal modes that are responsible for the distortions in the 2Si cases are not normal modes of the 0Si cases. To circumvent this problem, the scaled displacements used for the 2Si versions were used to create the same atomic displacements in the 0Si cases. This approach ensures that the scale of the x-axis is identical between the 0 and 2Si versions. However, the scale of the y-axis is significantly greater (3 to 49 times) in the 0Si cases. This results in coefficients in the polynomial fit that are also significantly larger. This makes a direct comparison of the values obtained for the 0 and 2Si versions difficult.

Finally, the fitting of the scans along the APES in the cases where symmetry breaking is not observed uses a fourth polynomial, despite no fourth order character to the APES. It is likely that this leads to overfitting. However, the fourth order polynomial is

required because the non-adiabatic coupling constant is obtained by equating the fourth order coefficient to the  $Q^4$  term in the model vibronic Hamiltonian.

### 7.3.5 – Changes in the Topology of the Electron Density

As described above the changes in geometry influence changes in the electron density and vice versa. The electron density in the planar versions and the global minima of the 2Si analogs were analyzed using AIMAll. The number of bond and ring critical points do not change upon symmetry breaking. However, with all functionals, disilene and 2Si TCNE exhibit non-nuclear attractors (NNAs)<sup>34</sup> along the Si–Si bond path. The appearance of NNAs on Si-Si bond paths has been previously discussed by Zhikol *et al.*<sup>35</sup> When BLYP is used the NNA in disilene disappears upon symmetry breaking, but persists for the other functionals. In 2Si TCNE the NNA disappears upon symmetry breaking for all functionals except CAM-B3LYP, M06-L and PBE0. Moreover, the atomic energy and electron population of the NNAs decrease upon symmetry breaking while the ellipticity of the Si-NNA critical points decreases in cases where it does not disappear.

The Laplacian of the electron density ( $\nabla^2\rho$ ) reveals areas of local concentration (valence shell charge concentrations (VSCCs)) and depletion (VSCD). The VSCC and VSCD reflect the shell structure of the atom where there is a region of concentration and depletion associated with each quantum shell.<sup>16,17</sup> VSCC are interpreted as lone pairs of electrons and provide an accurate mapping of the localized nature of the electron pair domains described by the valence-shell electron pair repulsion (VSEPR) model. A lone pair of electrons belonging to a nucleus can influence a pyramidalized geometry (e.g., the  $2p_z$  orbital of nitrogen in ammonia).<sup>37</sup>

No VSCC's were detected in any of the molecules considered, however,  $\nabla^2\rho$  can be visualized as an isosurface on top of the molecular graph to visualize how the concentration of  $\rho$  changes due to the pJTE. A representative example is given in **Figure 7.8** for disilene.

In the planar configuration the distribution of  $\nabla^2\rho$  is symmetrically distributed around the Si-nuclei. Upon symmetry breaking, the distribution of  $\nabla^2\rho$  changes such that there is a region of charge density concentrated above the Si-nuclei only. While there are no VSCC's detected it is clear that the pJTE results in changes to the electronic structure beyond the geometry.

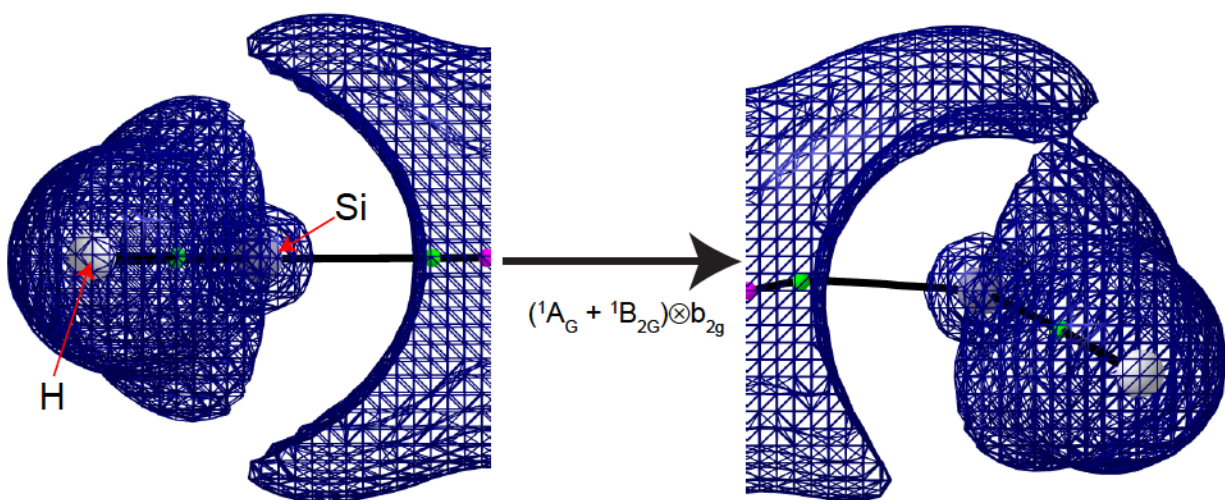


**Figure 7.8:** Changes in  $\nabla^2\rho$  isosurface due to the  $(^1A_g + ^1B_{2g}) \otimes b_{2g}$  pJTE in disilene<sup>38</sup> Only half the molecular graph is visualized for ease of viewing. Green – BCP, Pink – NNA. B3LYP/Def2TZVPP.

Changes in the positions of the nuclei will be accompanied by changes in atomic properties.<sup>16</sup> Interesting atomic properties in which to examine the changes in upon symmetry breaking are the atomic electronic energy and electron populations. Upon symmetry breaking the Si and N nuclei are always stabilized. Any atoms directly bonded

to the Si are destabilized, while all other carbon atoms are stabilized. In **Figure 7.9** the amount of stabilization of the Si-nuclei is plotted as a function of the pyramidalization.

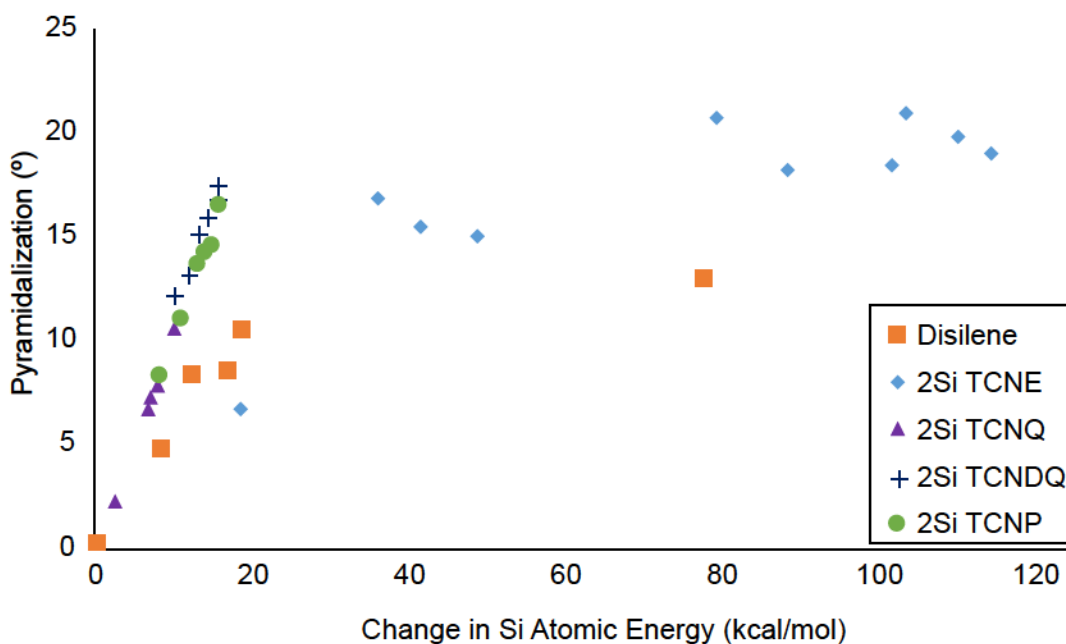


**Figure 7.9:** The amount of pyramidalization at Si-nuclei at the APES global minima as a function of the change in atomic energy calculated using QTAIM. Calculated using all functionals<sup>28</sup> in combination with Def2TZVPP.

The trend in **Figure 7.9** is similar to the one presented in **Figure 7.6**. However, the relationship is not as strong as the one described in **Figure 7.6** and it can be seen that the disilene and 2Si TCNE entries strongly deviate from the trend. A similar trend is observed if the change in atomic electron population is plotted as a function of the pyramidalization as in **Figure 7.10**. Generally, a greater amount of pyramidalization is associated with a greater increase in the atomic electron population. This can be rationalized using a simple electrostatic argument. The deviation of disilene and 2Si TCNE is likely due to the presence of NNA in these systems. When considered separately, the  $\pi$ -conjugated systems display a stronger linear relationship in both plots.

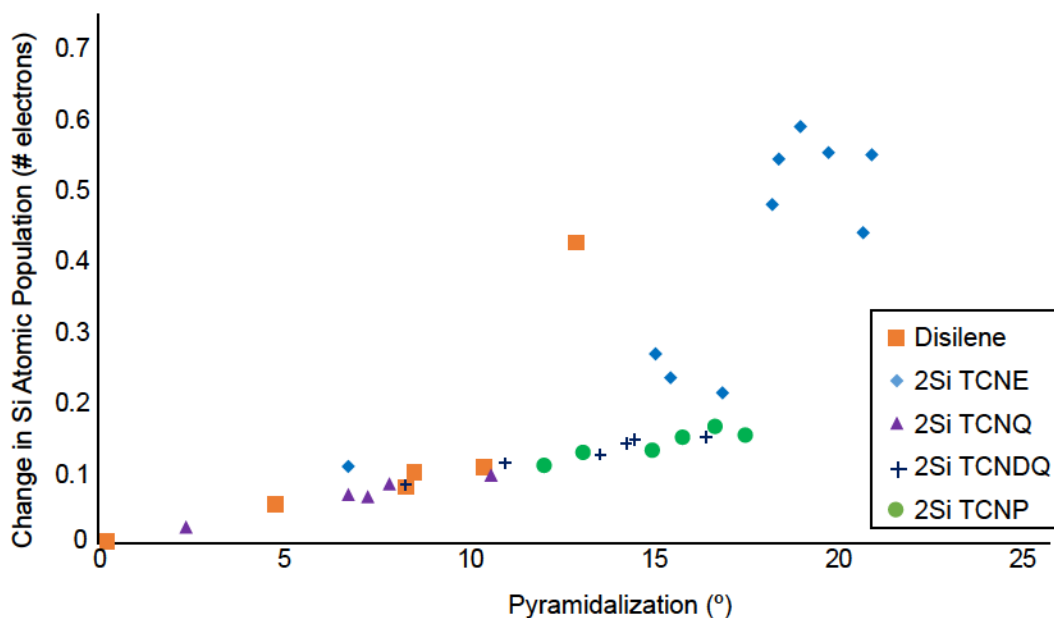


**Figure 7.10:** The change in atomic electron population (# electrons) as a function of the pyramidalization of the Si-nuclei at the APES global minima. Calculated using all functionals<sup>28</sup> in combination with Def2TZVPP.

The symmetry breaking that results from the pJT effect causes changes in the geometries of all 2Si systems which are accompanied by changes in the distribution of the electron density. The pyramidalized geometries result from a shift in the concentration of the electron density at the Si-nuclei which is due to the pJT effect. This is supported by the changes in the Laplacian visualized in **Figure 7.9** as well as the increase in the atomic electron population as shown in **Figure 7.10**. Symmetry breaking is found to have a stabilizing effect on the Si-nuclei.

#### **7.4 – Conclusions**

In contrast to the all carbon versions, the 2Si analogs of ethene and the cyanocarbons prefer non-planar, pyramidalized geometries. The cause of the pyramidalized geometry is the pJTE which is the only source of symmetry breaking in non-electronically degenerate molecules.

QTAIM analysis revealed changes in the electron density. The pJTE results in a redistribution in the concentration of electron density, resulting in a stabilization of the Si-nuclei as well as an increase in its atomic electron population. The pyramidalized geometries can be rationalized on the basis of simple chemical concepts.

The pJTE parameters were assessed by fitting a model vibronic Hamiltonian to cross-sections of the PES calculated using DFT. This is in contrast to previous studies which use post-HF methods (typically CASSCF or MRCI) to generate the cross-sections. The methodology used here does account for the negative curvature of the APES, but raises points about best practices in assessing pJTE problems. It is difficult to state what the controlling factor in the symmetry breaking of hypovalent silicon is based on the results obtained. However, the increased vibronic interaction in the silicon analogs is facilitated by the decrease in vertical excitation energies.

## 7.5 – References

- (1) Fischer, R. C. and Power, P. P. *Chem. Rev.*, **2010**, 110, 3877
- (2) West, R.; Fink, M. J. and Michl, J. *Science*, **1981**, 214(4527), 1343
- (3) Fink, M. J.; Michalczyk, M. J.; Haller, K. J.; West, R. and Michl, J. *Organometallics*, **1984**, 3, 793
- (4) Nozawa, T.; Nagata, M.; Ichinohe, M. and Sekiguchi, A. *J. Am. Chem. Soc.*, **2011**, 133, 5773
- (5) Carter, E. A. and Goddard, W. A. *J. Phys. Chem.*, **1986**, 90(6), 998
- (6) Trinquier, G. and Malrieu J.-P. *J. Am. Chem. Soc.*, **1987**, 109, 5303
- (7) Bersuker, I.B. *Chem. Rev.*, **2013**, 113(3), 1351
- (8) Bersuker, I.B. *The Jahn-Teller Effect*. Cambridge University Press, Cambridge, UK. (**2005**)
- (9) Bersuker, I.B. *Teor. Ekp. Khim.*, **1980**, 66, 161
- (10) Liu, Y.; Bersuker, I.B.; and Boggs, J.E. *Chemical Physics*, **2013**, 417, 26
- (11) Kayi H.; Garcia-Fernandez, P.; Bersuker, I.B. and Boggs, J.E. *J. Phys. Chem. A.*, **2013**, 117, 8671
- (12) Kayi, H.; Bersuker, I.B.; and Boggs, J.E. *J. Mol. Str.*, **2012**, 1023, 108
- (13) Soto, J.R.; Molina, B. and Castro, J.J. *Phys. Chem. Chem. Phys.*, **2015**, 17 7624
- (14) Soto, J.R.; Molina, B. and Castro, J.J. *MRS Advances*, **2016**, 1(22) 1591
- (15) Soto, J.R.; Molina, B. and Castro, J.J. *MRS Advances*, **2017**, 2(29) 1563
- (16) Bader, R.F.W. *Atoms in Molecules: A Quantum Theory*. Oxford University Press Inc. New York, New York (**2003**)
- (17) Matta, C.F. and Boyd, R.J. *The Quantum Theory of Atoms in Molecules: From Solid State to DNA and Drug Design*. Wiley-VCH, Weinheim, Germany (**2007**)
- (18) a) Becke, A.D. *Phys. Rev. A*. **1988**, 38, 3098  
b) Lee, C.; Yang, W. and Parr, R.G. *Phys. Rev. B.*, **1988**, 37, 785

- (19) Zhao, Y. and Truhlar, D.G. *Theor. Chem. Acct.*, **2008**, 120, 215
- (20) Perdew, J.P.; Burke, K. and Ernzerhof, M. *Phys. Rev. Lett.*, **1996**, 77, 3865
- (21) Becke, A.D. *J. Chem. Phys.*, **1993**, 98, 5648
- (22) Ernzerhof, M. and Scuseria, G.E. *J. Chem. Phys.*, **1999**, 110, 5029
- (23) Yanai, T.; Tew, D.P. and Handy, N.C. *Chem. Phys. Lett.*, **2004**, 393 51
- (24) **Gaussian 09, Revision D.01**, Frisch, M. J.; Trucks, G. W.; Schlegel, H. B.; Scuseria, G. E.; Robb, M. A.; Cheeseman, J. R.; Scalmani, G.; Barone, V.; Mennucci, B.; Petersson, G. A.; Nakatsuji, H.; Caricato, M.; Li, X.; Hratchian, H. P.; Izmaylov, A. F.; Bloino, J.; Zheng, G.; Sonnenberg, J. L.; Hada, M.; Ehara, M.; Toyota, K.; Fukuda, R.; Hasegawa, J.; Ishida, M.; Nakajima, T.; Honda, Y.; Kitao, O.; Nakai, H.; Vreven, T.; Montgomery, J. A., Jr.; Peralta, J. E.; Ogliaro, F.; Bearpark, M.; Heyd, J. J.; Brothers, E.; Kudin, K. N.; Staroverov, V. N.; Kobayashi, R.; Normand, J.; Raghavachari, K.; Rendell, A.; Burant, J. C.; Iyengar, S. S.; Tomasi, J.; Cossi, M.; Rega, N.; Millam, J. M.; Klene, M.; Knox, J. E.; Cross, J. B.; Bakken, V.; Adamo, C.; Jaramillo, J.; Gomperts, R.; Stratmann, R. E.; Yazyev, O.; Austin, A. J.; Cammi, R.; Pomelli, C.; Ochterski, J. W.; Martin, R. L.; Morokuma, K.; Zakrzewski, V. G.; Voth, G. A.; Salvador, P.; Dannenberg, J. J.; Dapprich, S.; Daniels, A. D.; Farkas, Ö.; Foresman, J. B.; Ortiz, J. V.; Cioslowski, J.; Fox, D. J. Gaussian, Inc., Wallingford CT, 2009.
- (25) Non-linear regression performed to fit the model vibronic Hamiltonian (Equation 7.5) using GraphPad Prism version 7.00 for Macintosh, GraphPad Software, La Jolla California, USA. [www.graphpad.com](http://www.graphpad.com)
- (26) AIMAll (Version 16.05.18), Todd A. Keith, TK Gristmill Software, Overland Park KS, USA, (2016) ([aim.tkgristmill.com](http://aim.tkgristmill.com))
- (27) Liang C. and Allen L.C. *J. Am. Chem. Soc.* **1990**, 112, 1039
- (28) The pyramidalization of Si-nuclei are slightly different (6.3714° and 6.3772°). When the values are rounded they become equal (6.4°).
- (29) a) Results obtained using M06 are not included. An optimized structure could not be obtained for the C<sub>2v</sub> symmetry structure using default parameters. The Guess=huckel, SCF=QC keywords were used. The energy values are comparable with the values obtained for the other structures on the PES.
- b) The outliers (15.0° and 26.0° pyramidalization) correspond to CAM-B3LYP results

(30) The pJT effects of the further symmetry breaking are as follows

Twisting of  $D_2$  to  $C_2$

$$({}^1A + {}^1B_3) \otimes b_3$$

$$({}^1A + {}^1B_2) \otimes b_2$$

Distortion of  $C_{2h}$  to  $C_2$

$$({}^1A_G + {}^1A_2) \otimes a_2$$

Distortion of  $C_{2v}$  to  $C_2$

$$({}^1A_1 + {}^1A_U) \otimes a_U$$

Distortion of  $C_{2h}$  to  $C_S$

$$({}^1A_G + {}^1B_U) \otimes b_U$$

Distortion of  $C_{2v}$  to  $C_S$

$$({}^1A_G + {}^1B_1) \otimes b_1$$

In these cases, there are a greater number of excited states with the correct symmetry for coupling to the ground state.

(31) Ilkhani A.R. and Monajjemi, M. *Comp. and Theo. Chem.*, **2015**, 1074, 19

(32) Ilkhani A.R. *Quim. Nova*, **2017**, 40(5), 491

(33) Wiberg, K.B.; Hadad, C.M.; Foresman, J.B. and Chupka, W.A. *J. Phys. Chem.* **1992**, 96, 10756

(34) Garcia-Cuesta, I.; Sanchez de Meras, A.M.J and Koch, H. *J. Chem. Phys.* **2003**, 118(18), 8216

(35) Non-nuclear attractors are classified as (3,-3) critical points. They are topologically equivalent to an atom (i.e., they are a local maximum in the electron density) but do not have the same physical interpretation.

(36) Zhikol, O.A.; Oshkalo, A.F.; Shishkin, O.V. and Prezhdo, O.V. *Chemical Physics*, **2003**, 288, 159

(37) Bader, R.F.W.; Gillespie, R.J. and MacDougall, P.J., *J. Am. Chem. Soc.*, **1988**, 110, 7329

(38) All other isosurface plots look like that of disilene around their Si nuclei.

## **Chapter EIGHT**

**Summary, Future Work and Conclusions**

## **8.1 – Overview**

This thesis focused on two topics: symmetry breaking in hypovalent silicon containing compounds, and incongruous descriptions of electronic structure by quantum chemical methods. These were related by catastrophe theory. Another theme that was explored is tuning electronic structure through isovalent substitution. A summary of the results obtained in each chapter will be presented. Following this, recommendations for topics of future study along with the general conclusions of this work will be presented.

## **8.2 – Isothiirane: a molecular structure dilemma resolved**

A congruous description of the electronic structure of isothiirane was obtained using all methods of analysis. It is best described as a hybrid of an acyclic and cyclic structure. This study resolved a long standing question in the literature regarding the electronic structure of isothiirane. QTAIM and NBO/NRT analysis are commonly used tools in computational quantum chemistry and the results presented of this work give further insight into their capabilities.

The quality of the NRT expansions was assessed by building bond order – bond length relationships of the substituted series. This provides a well-defined measure of the quality of the expansion that is external to the NRT module, in contrast to the internal measure, which is somewhat ambiguous.

The usage of  $^{13}\text{C}$  NMR chemical shift shielding tensors to gain additional insight into the electronic structure was also discussed. While this type of analysis is commonly performed, we were able to relate it to the other methods employed and use it to strengthen the overall analysis as exemplified in 3.3.5.5 where the key descriptors of all three modalities of analysis were related to one another to provide a consistent

description of electronic structure. The results highlight how the electronic structure of a molecule can unambiguously be characterized using commonly employed tools and modified to enhance reactivity.

### **8.3 – The Electron Affinities of TCNE and TCNQ: The Effect of Si-Substitution**

A variety of model chemistries were tested for their ability to reproduce the experimental structures and electron affinities of TCNE and TCNQ. DFT was found to be well suited to the study of the structure of cyanocarbons as the experimental structures and the electron affinities (EAs) of both were generally well reproduced. In many cases, the DFT model chemistries outperformed post Hartree-Fock methods reported in the literature for the determination of the EAs. In the case of TCNE BLYP/cc-pvDZ (0.32% dev.) slightly outperformed CASPT2 (0.64% dev.) and in the case of TCNQ M06-L/6-311++g(d,p) (0.15%) outperformed PMP2 (0.81%). Additionally, DFT was found to be well suited to studying Si analogs of small carbon based molecules.

In contrast to the parent compounds which are planar with  $D_{2h}$  symmetry, the reduced 1Si analogs as well as the neutral and reduced 2Si analogs structural symmetry breaking was observed.

Si-substitution generally enhanced the adiabatic electron affinities of both TCNE and TCNQ, improving their function as electron acceptors in charge-transfer complexes. Si-substitution was also found to enhance the singlet diradical character of the ground state of TCNQ, in agreement with previous findings of Fukuda *et. al.*<sup>1</sup>

### **8.4 – How the Amount of Hartree-Fock Exchange Affects the Observation of the pseudo Jahn-Teller Effect**

In chapter 4 it was observed that the nature of the planar stationary point of disilene and neutral 2Si TCNQ (closed-shell singlet) varied with the choice of functional.

Functionals containing higher amounts of Hartree-Fock exchange were found to characterize these stationary points as minima on their PES. Therefore, in developing a DFT based approach to evaluate pseudo Jahn-Teller effect (pJTE) parameters it was important to investigate this discrepancy in further detail.

An expanded selection of basis sets was used in this study to ensure the absence of symmetry breaking was not simply a basis set issue. Moreover, the effect of integration grid used to evaluate the density functional was also tested. Neither of these choices had a significant impact on the observation of symmetry breaking as functionals containing higher amounts of Hartree-Fock exchange still did not display the symmetry breaking effect.

To establish the affect that greater amounts of Hartree-Fock exchange had on the characterization of the stationary points, the amount of exchange was scaled manually using the BXLYPTest functional described. This confirmed that larger amounts of Hartree-Fock exchange resulted in the stationary points being characterized as planar minima. The APES in the direction of the distorting modes of interest were scanned for each increment of Hartree-Fock exchange in BXLYPTest. The APES changed from a double-well potential to a single-well potential. A cusp catastrophe model was then introduced in order to account for this change.

Also in chapter 5 a DFT approach to obtain the pJTE parameters was described. The vertical excitation energy ( $\Delta$ ) was determined using time-dependent DFT. The remaining parameters were obtained by fitting cross-sections of the APES to a fourth order polynomial. The polynomial coefficients were equated to the  $Q^2$  and  $Q^4$  terms of

the model vibronic Hamiltonian to determine the primary force constant ( $K_0$ ) and non-adiabatic coupling constant ( $F$ ).

$\Delta$  increased as the amount of Hartree-Fock exchange was increased. This increase is related to delocalization error present in DFT.<sup>2,3</sup> 2Si TCNQ showed a greater increase which is the result of it having a more delocalized electronic structure.

### **8.5 – Computational Insights in to the Electronic Structure of TCNDQ and TCNP: The Effect of Si-Substitution**

Prior to the results presented in Chapter 6 there were no detailed computational studies of the electronic structure of TCNDQ or TCNP. Moreover, their structures and electron affinities had not been definitively characterized experimentally.

The structures of TCNDQ and TCNP in their neutral and reduced forms were assessed using DFT. TCNDQ, TCNP and  $[\text{TCNP}]^-$  were determined to have planar structures with  $D_{2h}$  symmetry. On the other hand,  $[\text{TCNDQ}]^-$  was predicted to have a twisted structure with  $D_2$  symmetry. Our calculations support the UV-vis analysis of Addison *et. al.* which suggested a twisted type structure for  $[\text{TCNDQ}]^-$ .<sup>4</sup>

Si-substitution resulted in structural symmetry breaking in both TCNDQ and TCNP. The neutral 1Si analogs were generally planar while the reduced 1Si analogs were pyramidalized at the Si-nuclei, and in the case of 1Si TCNDQ, also twisted around the central C–C bond. The neutral and reduced 2Si analogs exhibited non-planar geometries at the global surface minima. Both 2Si TCNDQ and 2Si TCNP displayed pyramidalization of the Si-nuclei. 2Si TCNDQ also displayed twisting around the central C-C bond.

The AEAs of TCNDQ and TCNP were calculated. The AEA of TCNDQ ranged from 3.311 to 4.252eV, and 3.411 to 4.467eV for TCNP. Our results predict that the AEAs of cyanocarbons increase with an extension of the  $\pi$ -conjugation network. This is contrary

to the experimental results of Maxfield *et. al.*<sup>5</sup> Si-substitution was found to enhance the AEAs of both TCNDQ and TCNP.

TCNDQ and TCNP were found to possess quinoidal type structures. Bond length alternation (BLA) and delocalization index alternation (DIA) was found to decrease as the  $\pi$ -conjugation network was extended, with Si-substitution and structural symmetry breaking. These changes in BLA and DIA were also observed in TCNQ and imply an increase in aromaticity.

### **8.6 – What is the Controlling Factor in the Symmetry Breaking of Hypovalent Silicon?**

The potential energy surfaces of the 0 and 2Si versions of ethene and the cyanocarbons were characterized using DFT in combination with the Def2TZVPP basis set. The carbon (0Si) versions of all molecules were predicted to be planar minima with D2h symmetry. Conversely, the planar 2Si versions underwent structural symmetry breaking.

Three separate pJTE types were identified: a trans-bending ( ${}^1A_G + {}^1B_{2G}$ )  $\otimes$   $b_{2g}$  effect, a cis-bending ( ${}^1A_G + {}^1B_{3U}$ )  $\otimes$   $b_{3u}$  effect and a twisting ( ${}^1A_G + {}^1A_U$ )  $\otimes$   $a_u$  effect. In order to ascertain the controlling factor in the pJTE of the Si-analogs the procedure described in chapter 5 was used. As detailed in chapter 7 there were challenges in applying the procedure to the 0Si cases. This made a direct comparison of the pJTE parameters between the 0 and 2Si cases difficult.

### **8.7 – Topics for Future Study**

The interaction of electron acceptors and donors is of interest for materials applications. The interaction of TTF and TCNQ has been studied in the literature using DFT previously.<sup>6,7,8</sup> Of interest is how the nature of the interaction between the donor and

acceptor molecules changes upon isovalent substitution. Additionally, the interaction of the larger  $\pi$ -conjugated cyanocarbons (i.e., TCNDQ or TCNP) with TTF has not been explored. Such studies may be of value in understanding the interactions of such materials.

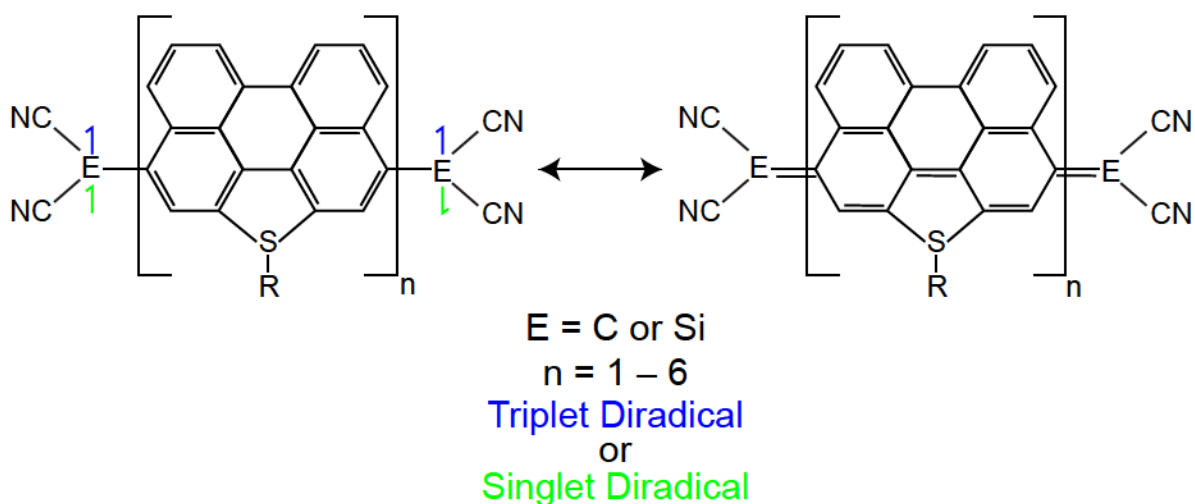
The elliptic umbilic (EU) catastrophe theory model described is of value in the analysis of the electronic structure of any three-membered ring system. By varying the constituent atoms of the ring it is possible to understand how the control parameters of the EU vary in different chemical environments. This would further the understanding of how three-membered ring systems are formed and destroyed. Such information may be of value in understanding how to better control the synthesis of three membered ring systems (e.g., epoxides, cyclopropanes, aziridines).

The cusp catastrophe model has a number of potential applications unrelated to chapter 5. For example, the study of elementary chemical transformations can be modelled and interpreted using the cusp catastrophe. Both  $S_N2$  and elementary steps within a catalytic cycle provide interesting cases to apply the cusp catastrophe model to.

Another application of the cusp catastrophe are molecules with low lying bending modes, NCCNO and XCNO ( $X=Cl$  or  $Br$ ) for example, have ambiguous descriptions with some methods assigning them linear structures while others describe them as bent.<sup>9-12</sup> Another example is  $HC=C-NCO$  and its isomers, some of which are linear while others are bent.<sup>13</sup> These examples provide cases where the **b** control parameter (related to the symmetry of the system) is not equal to 0 and provide a means to further explore the usefulness of the cusp catastrophe as an analysis tool.

Si-substitution was shown to enhance the singlet or triplet diradical character of the  $\pi$ -conjugated cyanocarbons. An interesting follow up to this would be to vary the exocyclic position with other group 12-14 elements to examine how the diradical character, and therefore aromaticity, can be enhanced with substitution. Such a study would provide a means to further apply the BLA and DIA analysis described in chapter 6 and compare them with other common measures of aromaticity (e.g., nucleus independent chemical shift<sup>14</sup>). These analysis methods are also broadly applicable to understanding the material properties of conjugated systems based on polyacetylenes or polythiophenes.<sup>15,16</sup>

Recently, Zeng *et. al.* presented a series of cyanocarbons using N-perylene units as the spacers between the terminal cyanoethylene units instead of *p*-QDM units.<sup>17,18</sup> This strategy enhanced open shell singlet or triplet diradical character depending on chain length. This strategy, in combination with the exocyclic Si-substitution discussed in this work, may provide a method to further enhance the singlet or triplet diradical character of the ground state of cyanocarbons (**Scheme 8.1**).



**Scheme 8.1**

## **8.8 – General Conclusions**

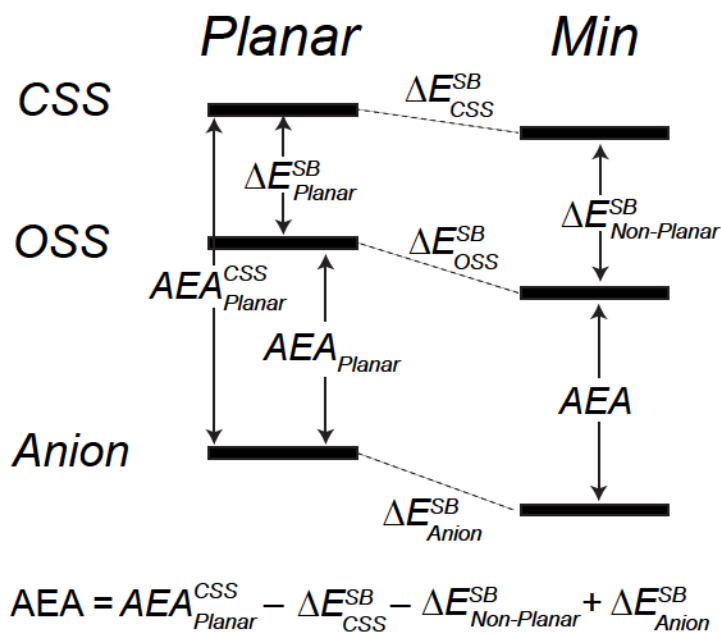
The 2Si versions of the planar cyanocarbons were found to break structural symmetry and prefer pyramidalized geometries at the Si-nuclei. This finding is in agreement with experimentally characterized disilenes.<sup>19</sup> The 2Si analogs of TCNDQ and TCNP are, to the best of our knowledge, the only examples of this effect where the Si nuclei are separated by two phenyl units. The symmetry breaking effects in the planar analogs were studied from the perspective of the pJTE.

The catastrophe theory models presented offer an additional technique for analyzing electronic structure, particularly in cases where incongruous descriptions are obtained by various quantum chemical methods.

A procedure for determining the pJTE parameters using DFT was proposed by fitting scans along the APES in the direction of the distorting mode to a polynomial function. By equating the polynomial coefficients to the model vibronic Hamiltonian it is possible to obtain primary force constant ( $K_0$ ) and non-adiabatic coupling constant ( $F$ ). The vertical excitation energy ( $\Delta$ ) is readily calculable using TD-DFT. As described in chapter 7 there are a number of complications associated with the procedure. To refine the procedure additional methods of scanning along the adiabatic potential energy surface should be explored. Moreover, the normal modes responsible for the distortion of the 2Si cases were absent in their 0Si versions. This peculiarity should also be examined in greater detail.

Si-substitution was found to be an effective strategy for enhancing the electron accepting abilities of the cyanocarbons. In contrast to previous strategies for modifying the cyanocarbons which result in decreased EAs, the strategy presented in this work

generally enhances the EA. The AEA of the planar Si analogs was less than that of the parent compounds, however, structural symmetry breaking resulted in an increase in the AEA (**Scheme 8.2**). Therefore, the enhancement of the AEA with Si-substitution is a geometric effect, driven by the observed pJTEs.



**Scheme 8.2**

## **8.9 – References**

- (1) Fukuda, K *et. al. J. Phys. Chem. C.*, **2015**, 119(2), 1188
- (2) Cohen, A.J.; Mori-Sanchez, P. and Yang, W. *Chem. Rev.*, **2012**, 112, 289
- (3) Cohen, A.J.; Mori-Sanchez, P. and Yang, W. *Science*, **2008**, 321, 792
- (4) Addison, A. W.; Dalal, N. S.; Hoyano, Y.; Huizinga, S. and Weiler, L. *Can. J. Chem.*, **1977**, 55, 4191
- (5) Maxfield, M.; Bloch, A. N. and Cowan, D. O. *J. Org. Chem.*, **1985**, 50(11) 1789
- (6) Sini, G.; Sears J.G. and Bredas, J-L. *J. Chem. Theory Comput.*, **2011**, 7, 602
- (7) Steinmann, S.N.; Piemontesi, C.; Delachat, A. and Corminboeuf, C. *J. Chem. Theory Comput.* **2012**, 8, 1629
- (8) Van Regemorter, T.; Guillaume, M.; Sini, G.; Sears, J.S.; Geskin, V.; Bredas, J-L., Beljonne, D. and Cornil, J. *Theor. Chem. Acc.*, **2012**, 131(1273)
- (9) Lichau, H.; Ross, S.C.; Lock, M.; Albert, S.; Winnewisser, B.P.; Winnewisser, M. and De Lucia F.C. *J. Phys. Chem. A*, **2001**, 105, 10080
- (10) Pasinszki, T. and Westwood, N.P.C *J. Phys. Chem. A*, **1998**, 102, 4939
- (11) Jacek, K. *J. Phys. Chem. A*, **1999**, 103, 2170
- (12) Lichau, H., Gillies, C.W., Gillies, J.Z., Ross, S.C., Winnewisser, B.P. and Winnewisser, M. *J. Phys. Chem. A*, **2001**, 105, 10065
- (13) Pasinszki, T. and Havasi, B. *Phys. Chem. Chem. Phys.*, **2003**, 5, 259
- (14) Chen, Z., Wannere, C.S., Corminboeuf, Puchta, R. and von Rague Schleyer, P., *Chem. Rev.*, **2005**, 105(10), 3842
- (15) Casado, J., Burrezo, P.M., Zafra, J.L. and Navattete, J.T.L. *Angew. Chem. Int. Ed.*, **2017**, 56(9), 2250
- (16) Kaloni, T.P., Giesbrecht, P.K., Schreckenbach, G. and Freund, M.S. *Chem. Mater.* **2017**, 29, 10248
- (17) Zeng, Z., Ishida, M., Zafra, J.L., Zhu, X., Sung, Y.M., Bao, N., Webster R.D., Lee, B.S., Li, R-W., Zeng, W., Li, Y., Chi, C., Navarrete, J.T.L., Ding, J., Casado, J., Kim, D. and Wu, J. *J. Am. Chem. Soc.*, **2013**, 135, 6363

- (18) Zeng, Z. and Wu, J. *Chem. Rec.*, **2015**, 15, 322
- (19) Fischer, R. C. and Power, P. P. *Chem. Rev.*, **2010**, 110, 387

## **Appendices**

APPENDIX A

Supplementary Information for Chapter Three

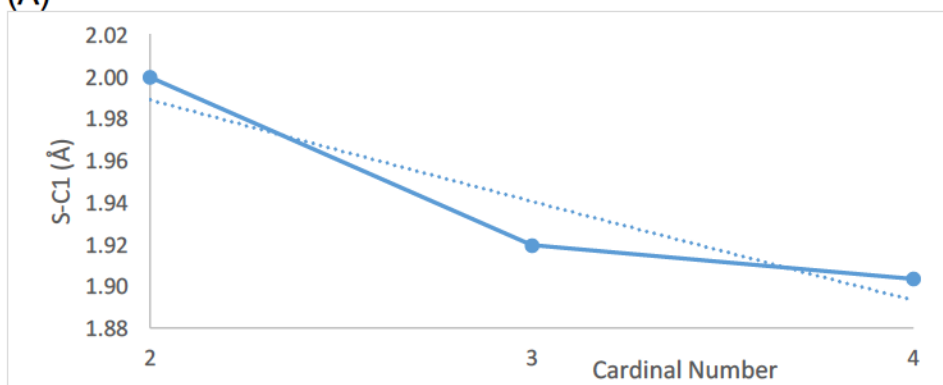
Table A1: Geometric parameters for heavy atoms in isothirane for all model chemistries. a) from reference 7.

		R(S-C <sub>1</sub> )	R(S-C <sub>2</sub> )	R(C <sub>1</sub> -C <sub>2</sub> )	P	A(SC <sub>2</sub> C <sub>1</sub> )	A(C <sub>2</sub> SC <sub>1</sub> )	A(SC <sub>1</sub> C <sub>2</sub> )	Area
B3LYP	BS 1	1.971	1.881	1.468	5.320	70.9	44.7	64.4	1.304
	BS 2	1.944	1.875	1.467	5.286	69.9	45.1	64.9	1.291
	BS 3	1.920	1.865	1.465	5.250	69.2	45.5	65.2	1.277
	TZVP	1.984	1.888	1.465	5.337	71.3	44.4	64.3	1.310
B3PW91	BS 1	1.920	1.865	1.470	5.255	69.4	45.8	64.8	1.284
	BS 2	1.890	1.849	1.470	5.209	68.7	46.2	65.1	1.261
	BS 3	1.870	1.839	1.469	5.178	68.1	46.5	65.3	1.247
	TZVP	1.930	1.863	1.467	5.260	69.7	45.4	62.7	1.280
PBE0	BS 1	1.907	1.847	1.468	5.222	69.1	46.0	64.9	1.267
	BS 2	1.887	1.841	1.470	5.198	68.5	46.4	65.1	1.258
	BS 3	1.866	1.831	1.468	5.165	67.9	46.8	65.3	1.245
PBE	TZVP	1.916	1.877	1.476	5.269	68.5	45.8	65.7	1.289
BP86		1.939	1.888	1.477	5.304	69.1	45.4	65.5	1.303
BLYP		1.989	1.92	1.474	5.383	70.3	44.3	65.4	1.334
CCSD		2.007	1.869	1.473	5.349	72.7	44.5	62.7	1.315
HF	BS 1	2.203	1.856	1.465	5.524	82.2	41.2	56.6	1.347
MP2		1.903	1.846	1.478	5.227	68.8	46.4	64.8	1.272
CISD <sup>a</sup>		1.980	1.849	1.471	5.300	72.2	45.0	62.8	1.294

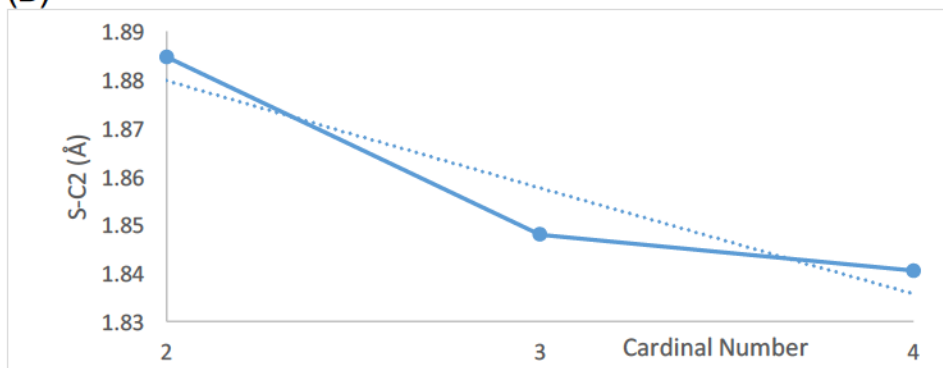
Table A2: Geometric parameters for thiirane

	B3LYP			B3PW91			PBE0		
	BS1	BS2	BS3	BS1	BS2	BS3	BS1	BS2	BS3
S-C	1.836	1.836	1.827	1.820	1.819	1.812	1.813	1.813	1.807
C=C	1.478	1.478	1.478	1.479	1.478	1.477	1.477	1.477	1.476
Perimeter	5.153	5.151	5.133	5.118	5.117	5.102	5.105	5.103	5.090
Area	1.243	1.242	1.235	1.223	1.228	1.222	1.223	1.223	1.217

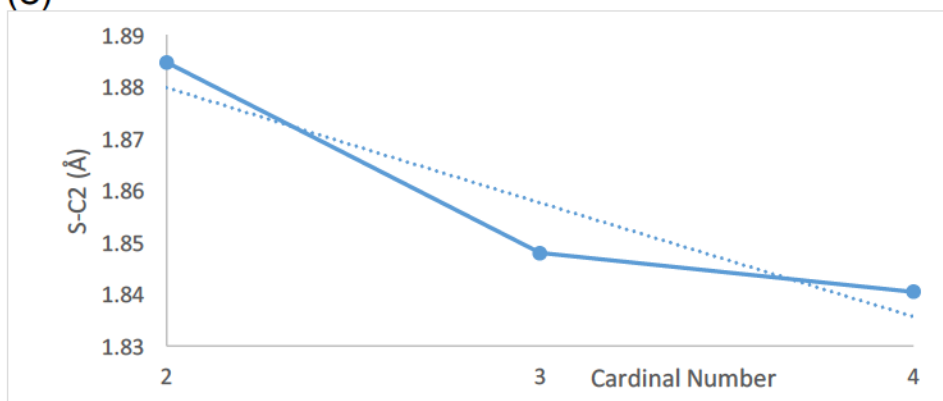
(A)



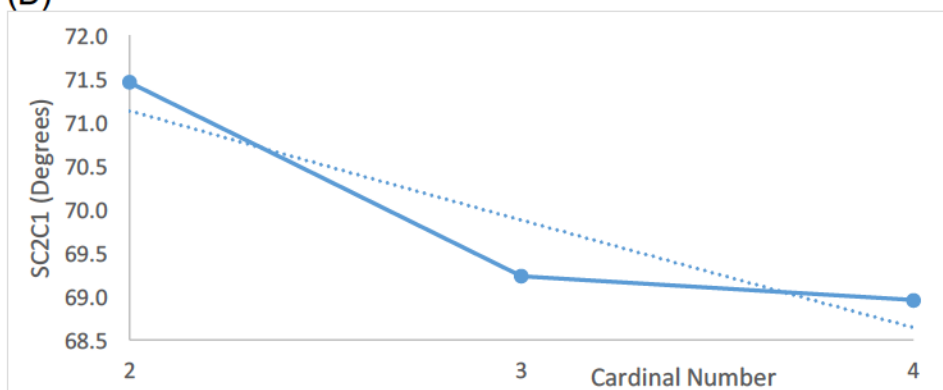
(B)



(C)



(D)



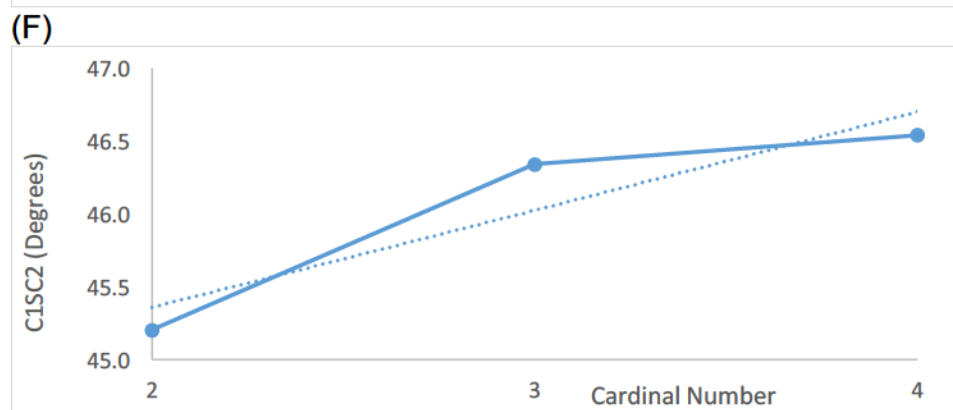
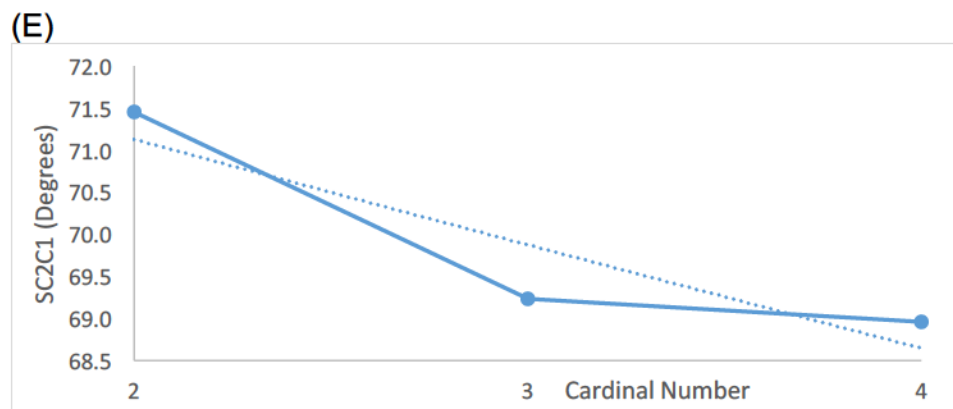


**Figure A1:** CBS Extrapolation plots for (A) S-C<sub>1</sub> Distance (B) S-C<sub>2</sub> Distance (C) C<sub>1</sub>-C<sub>2</sub> Distance (D) SC<sub>2</sub>C<sub>1</sub> angle (E)SC<sub>1</sub>C<sub>2</sub> angle (F) C<sub>1</sub>SC<sub>2</sub> angle

Table A3: RCP Data for Isothiirane and Thiirane

Isothiirane		$\rho$	$\lambda_1$	$\lambda_2$	$\epsilon$	$\lambda_3$
B3PW91	BS2	0.130	-0.153	0.021	6.286	0.262
	BS3	0.140	-0.174	0.011	14.818	0.253
PBE0	BS2	0.133	-0.158	0.027	4.852	0.26
	BS3	0.143	-0.179	0.019	8.421	0.251
MP2	BS1	0.132	-0.173	0.004	42.250	0.248
BP86	TZVP	0.121	-0.157	0.048	2.271	0.249
PBE		0.126	-0.165	0.060	1.750	0.250
Thiirane						
B3LYP	BS1	0.140	-0.193	0.112	0.723	0.219
	BS2	0.136	-0.172	0.113	0.522	0.231
	BS3	0.144	-0.193	0.110	0.755	0.216
B3PW91	BS1	0.145	-0.198	0.116	0.707	0.213
	BS2	0.141	-0.176	0.118	0.492	0.227
	BS3	0.149	-0.197	0.112	0.759	0.211
PBE0	BS1	0.147	-0.202	0.117	0.726	0.209
	BS2	0.143	-0.179	0.119	0.504	0.224
	BS3	0.151	-0.199	0.113	0.761	0.207

Table A4: Frequency of normal mode of interest for isothiirane calculated in this work

		$\omega$ (cm <sup>-1</sup> )
B3LYP	BS1	367
	BS2	392
	BS3	409
B3PW91	BS1	425
	BS2	449
	BS3	465
PBE0	BS1	441
	BS2	465
	BS3	482

Table A5: NRT expansion weights and bond orders of isothiirane for all model chemistries in combination with the default algorithm. a) Ref 7.

	NRT Resonance Structure (%)					Natural Bond Order			
	%B	%C	%D	%I	%O	S-C <sub>1</sub>	S-C <sub>2</sub>	$\Delta BO_{NRT}$	C <sub>1</sub> -C <sub>2</sub>
HF BS1 <sup>a</sup>	87.8	-	8.3	-	3.9	0.920	0.910	-0.010	1.110
MP2 BS1 <sup>a</sup>	78.4	-	3.5	-	18.1	0.980	0.940	-0.040	1.080
CISD BS1 <sup>a</sup>	80.6	-	4.3	-	15.1	0.950	0.930	-0.020	1.100
BP86 TZVP	86.3	-	5.6	-	8.1	0.969	0.944	-0.025	1.112
BLYP TZVP	87.2	-	6.2	-	6.5	0.938	0.938	0.000	1.128
PBE TZVP	86.0	-	5.5	-	8.5	0.973	0.945	-0.028	1.112
B3LYP BS1	87.4	-	6.3	-	6.3	0.950	0.940	-0.010	1.110
B3LYP BS2	94.0	-	5.9	-	0.1	0.959	0.941	-0.018	1.107
B3LYP BS3	87.2	-	5.8	-	7.0	0.963	0.942	-0.021	1.107
B3LYP TZVP	87.3	-	6.2	-	6.5	0.954	0.938	-0.016	1.100
B3PW91 BS1	87.4	-	5.7	-	6.9	0.960	0.940	-0.020	1.100
B3PW91 BS2	94.6	-	5.4	-	-	0.946	0.946	0.000	1.109
B3PW91 BS3	87.3	-	5.2	-	7.5	0.972	0.947	-0.025	1.102
B3PW91 TZVP	87.3	-	5.7	-	7.0	0.962	0.943	-0.019	1.108
PBE0 BS1	87.6	-	5.4	-	7.0	0.966	0.944	-0.022	1.102
PBE0 BS2	94.7	-	5.2	-	0.1	0.970	0.947	-0.023	1.101
PBE0 BS3	87.4	-	5.1	-	7.5	0.974	0.948	-0.026	1.101

Table A6: NRT expansion weights and bond orders of thiirane calculated using default algorithm. "Other" corresponds to a number of low weight ionic structures.

			Other	BO S-C	BO C-C
B3LYP	BS1	92.5	7.5	0.984	1.042
	BS2	92.5	7.5	0.984	1.041
	BS3	92.4	7.6	0.985	1.039
B3PW91	BS1	92.4	7.6	0.986	1.038
	BS2	92.4	7.6	0.987	1.038
	BS3	92.3	7.7	0.987	1.038
PBE0	BS1	92.4	7.6	0.987	1.038
	BS2	92.4	7.6	0.987	1.038
	BS3	92.3	7.7	0.988	1.038

**Table A7:** Bond orders for the S-C distances of isothiirane calculated using Schomaker-Stevenson relationship (See reference 25 for details) and the difference between them for each model chemistry.

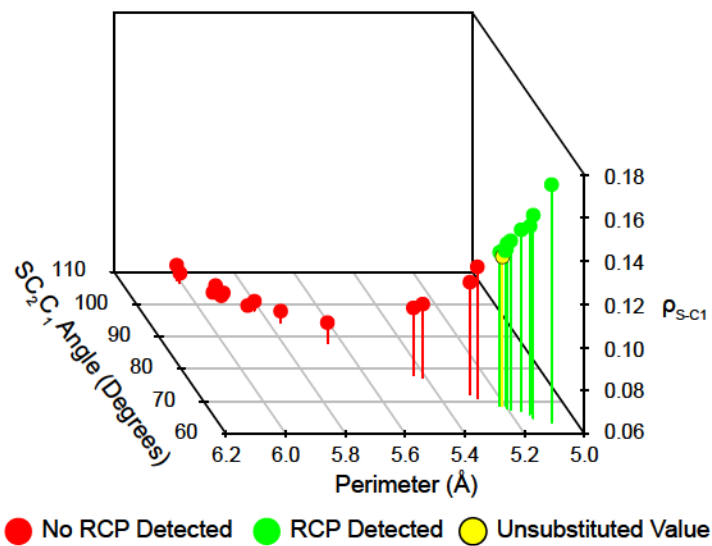
		BO <sub>S-C1</sub>	BO <sub>S-C2</sub>	ΔBO
CCSD(T)	aug-cc-pvDZ	0.538	0.607	0.070
	aug-cc-pvTZ	0.585	0.630	0.045
	aug-cc-pvQZ	0.595	0.635	0.040
	CBSExtrap	0.599	0.636	0.038
B3LYP	BS1	0.553	0.609	0.057
	BS2	0.570	0.613	0.043
	BS3	0.585	0.619	0.035
	TZVP	0.544	0.605	0.060
B3PW91	BS1	0.585	0.619	0.035
	BS2	0.604	0.629	0.026
	BS3	0.616	0.636	0.020
	TZVP	0.578	0.621	0.042
PBE0	BS1	0.593	0.631	0.038
	BS2	0.606	0.635	0.029
	BS3	0.619	0.641	0.022
PBE	TZVP	0.587	0.612	0.025
BP86		0.573	0.605	0.032
BLYP		0.541	0.585	0.043
CCSD		0.530	0.617	0.087
HF	BS1	0.407	0.625	0.219
MP2		0.595	0.631	0.036
CISD		0.547	0.629	0.083

Table A8: Delocalization index (DI) for the S-C distances of isothiirane and the difference between them for each model chemistry.

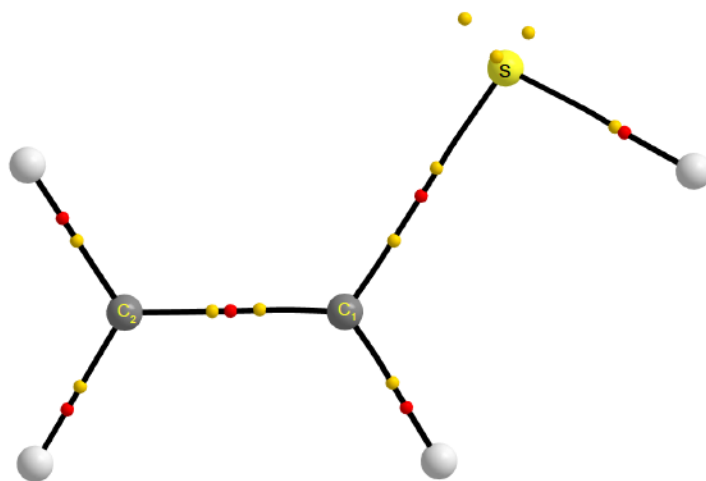
		DI S-C <sub>1</sub>	DI S-C <sub>2</sub>	$\Delta$ DI
CCSD(T)	aug-cc-pvDZ	0.695	0.937	0.242
	aug-cc-pvTZ	0.821	0.982	0.161
	aug-cc-pvQZ	0.839	0.983	0.144
B3LYP	BS1	0.851	0.969	0.118
	BS2	0.909	0.974	0.065
	BS3	0.942	0.989	0.047
	TZVP	0.834	0.964	0.130
B3PW91	BS1	0.908	0.984	0.076
	BS2	0.966	0.993	0.027
	BS3	0.997	1.008	0.011
	TZVP	0.889	0.980	0.091
PBE0	BS1	0.917	0.991	0.074
	BS2	0.975	0.999	0.024
	BS3	1.006	1.015	0.009
PBE BP86 BLYP CCSD	TZVP	0.954	0.982	0.028
		0.927	0.975	0.048
		0.871	0.950	0.079
		-	-	-
HF MP2 CISD	BS1	0.477	0.984	0.507
		0.749	0.813	0.064
		-	-	-

Table A9: Properties of the C<sub>1</sub> VSCC depicted in Figure 1. Magnitude of VSCC in a.u., distance (R) in Bohr, Dihedral in degrees. <sup>1</sup>CF<sub>3</sub><sup>-</sup> is an example carbanion lone pair VSCC. <sup>1</sup>CF<sub>2</sub> is an example carbene lone pair

		$\nabla^2$	R	Dihedral
Cyclic Zwitterion MG				
PBE0	BS2	-1.05	0.885	170.67
	BS3	-1.03	0.886	168.62
B3PW91	BS2	-1.057	0.884	171.08
	BS3	-1.037	0.885	169.11
BP86	TZVP	-1.126	0.868	174.90
PBE		-1.103	0.869	174.14
MP2	BS1	-1.093	0.882	173.20
<sup>1</sup> CF <sub>3</sub> <sup>-</sup>				
B3LYP	BS3	-1.557	0.852	129.02
B3PW91		-1.524	0.854	129.01
PBE0		-1.519	0.855	128.95
Acyclic Carbene MG				
B3LYP	BS1	-1.141	0.875	175.76
	BS2	-1.101	0.879	172.96
	BS3	-1.082	0.880	171.14
	TZVP	-1.238	0.862	175.34
B3PW91	BS1	-1.094	0.880	174.20
	TZVP	-1.175	0.866	174.80
PBE0	BS1	-1.087	0.881	173.85
BLYP	TZVP	-1.193	0.863	175.89
HF	BS1	-1.412	0.865	177.69
CCSD(T)	aug-cc-pvDZ	-1.578	0.854	176.54
	aug-cc-pvTZ	-1.202	0.868	171.17
	aug-cc-pvQZ	-1.322	0.867	171.68
<sup>1</sup> CF <sub>2</sub>				
B3LYP	BS3	-1.571	0.845	180.00
B3PW91		-1.539	0.848	180.00
PBE0		-1.540	0.848	180.00



**Figure A2:** Relationship between ring perimeter (Å),  $SC_2C_1$  angle (degrees) and the minimum electron density along the S- $C_1$  geometric line (a.u) calculated at the B3PW91/BS2 level. Green (red) markers indicate a RCP is (not) detected. Yellow marker indicates unsubstituted value. Isomerized cases are excluded.



**Figure A3:** Example molecular graph of ethenylthiol.

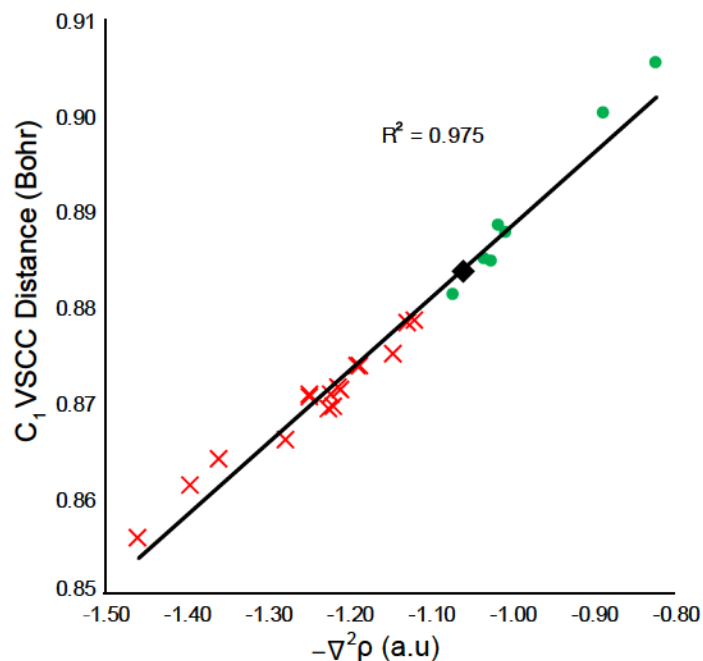


**Figure A4:** Comparison of the value of  $\nabla^2\rho$  VSCC and its distance from  $C_1$  nucleus calculated at the B3PW91/BS2 level. Circles indicate a ring structure. X's indicate an acyclic structure. Diamond marker is the unsubstituted (cyclic) compound.

The VSCC corresponds to the lone pair of a carbanionic centre in the cyclic MG (further from the nucleus, less charge concentration), and a carbene lone pair in the case of the acyclic MG (situated closer to the nucleus, greater charge concentration). Substitution has an effect on the local electronic environment of  $C_1$  as shown in Figure A4. At the B3PW91 / BS2 level, the parent compound exhibits a cyclic structure and the  $C_1$  VSCC has a  $\nabla^2\rho$  value of -1.057 a.u and a distance of 0.884 Bohr from the nuclei.

Table A10: NRT expansion weights and natural bond orders for substituted series using RS-B\* as input. Calculated at the B3PW91 / BS2 level.

RS-B	%B	%C	%D	%I	%O	Bond Order		
						S-C1	S-C2	C1-C2
NH <sub>2</sub> , H	87.95	0.00	4.05	2.31	5.69	1.016	0.937	1.084
H, CHO	92.36	1.37	5.63	0.00	0.64	0.954	0.944	1.088
H, SiH <sub>3</sub>	94.67	0.00	5.33	0.00	0.00	0.981	0.947	1.116
CH <sub>3</sub> , H	94.08	0.00	5.92	0.00	0.00	0.856	0.874	1.137
H, CF <sub>3</sub>	99.49	0.48	0.03	0.00	0.00	0.814	0.874	1.127
PH <sub>2</sub> , H	91.33	1.68	5.80	0.00	1.19	0.938	0.938	1.123
H, CCl <sub>3</sub>	90.04	2.94	5.78	0.00	1.24	1.885	0.808	1.860
H, PH <sub>2</sub>	91.33	1.68	5.80	0.00	1.19	0.925	0.942	1.115
H, CN	89.58	4.53	4.99	0.00	0.90	0.905	0.950	1.084
CH <sub>3</sub> , CH <sub>3</sub>	91.51	1.97	5.96	0.00	0.56	0.921	0.940	1.105
NC, NC	83.82	7.54	5.55	1.68	1.41	0.869	0.928	1.077
H, CH <sub>3</sub>	93.34	1.97	4.32	0.00	0.37	0.914	0.937	1.109
H, Br			n/a				n/a	
H, NC	87.32	5.12	5.87	0.00	1.69	0.876	0.941	1.063
H, Cl	90.62	4.80	4.58	0.00	0.00	0.881	0.940	1.084
H, F	84.99	7.51	6.60	0.00	0.90	0.859	0.934	1.073
OH, OH	77.07	14.13	6.63	2.17	0.00	0.788	0.921	1.090
NCS, NCS	74.69	18.75	0.00	5.90	0.66	0.763	0.941	1.049
H, NCS	72.39	17.03	8.09	0.00	2.49	0.749	0.924	1.082
H, SCN	67.93	22.24	8.06	0.00	1.77	0.688	0.934	1.109
H, OH			n/a				n/a	
SeH, SeH	64.73	24.98	7.17	2.34	0.78	0.671	0.912	1.101
H, SeH	63.08	27.44	8.66	0.82	0.00	0.661	0.927	1.121
H, SH			n/a				n/a	
SCN, SCN			n/a				n/a	
H, NH <sub>2</sub>			n/a				n/a	
NH <sub>2</sub> , NH <sub>2</sub>			n/a				n/a	

n/a: When structures are manually specified, the program first determines a set of corresponding NBO's. If NBO's corresponding to the given resonance structure cannot be found the calculation terminates.

\* RS-B is not suitable for two reasons: 1) in the parent compound it failed to assign the greater bond order to the shorter S-C<sub>2</sub> distance, and 2) a set of NBO's could not be obtained for the 7 of 28 molecules.

Table A11: NRT expansion weights and natural bond orders for substituted series using RS-BC as input. Calculated at the B3PW91 / BS2 level.

RS-BC	%B	%C	%D	%I	%O	Bond Order		
						S-C1	S-C2	C1-C2
NH <sub>2</sub> , H	93.65	0.00	4.05	2.30	0.00	1.016	0.937	1.084
H, CHO	92.36	1.36	5.63	0.00	0.65	0.954	0.944	1.088
H, SiH <sub>3</sub>	94.67	0.00	5.33	0.00	0.00	0.981	0.947	1.116
CH <sub>3</sub> , H	94.88	0.00	5.12	0.00	0.00	0.949	0.949	1.110
H, CF <sub>3</sub>	93.48	0.49	6.03	0.00	0.00	0.935	0.940	1.095
PH <sub>2</sub> , H	84.58	7.43	5.79	2.20	0.00	0.868	0.920	1.116
H, CCl <sub>3</sub>	90.04	2.94	5.78	0.00	1.24	0.913	0.942	1.080
H, PH <sub>2</sub>	82.48	8.64	5.38	2.26	1.24	0.858	0.923	1.107
H, CN	89.58	4.53	4.99	0.00	0.90	0.905	0.950	1.084
CH <sub>3</sub> , CH <sub>3</sub>	82.31	9.57	5.41	1.98	0.73	0.849	0.925	1.095
NC, NC	73.62	16.10	5.27	3.40	1.61	0.786	0.910	1.069
H, CH <sub>3</sub>	79.37	12.84	5.50	2.29	0.00	0.817	0.922	1.099
H, Br			n/a				n/a	
H, NC	72.38	19.39	4.75	1.73	1.75	0.758	0.935	1.051
H, Cl	73.39	19.13	4.82	1.76	0.90	0.759	0.934	1.074
H, F	53.99	38.87	5.78	0.00	1.36	0.545	0.945	1.066
OH, OH	47.97	44.68	6.08	1.27	0.00	0.490	0.932	1.074
NCS, NCS	48.17	46.08	4.11	0.99	0.65	0.493	0.949	1.041
H, NCS	39.78	51.65	5.90	0.00	2.67	0.410	0.943	1.058
H, SCN	38.61	53.89	6.16	0.00	1.34	0.390	0.946	1.091
H, OH	3.81	93.79	2.40	0.00	0.00	0.04	0.98	1.04
SeH, SeH	31.86	59.06	7.99	1.08	0.01	0.330	0.929	1.084
H, SeH	30.07	64.53	5.40	0.00	0.00	0.301	0.952	1.088
H, SH	3.75	93.13	2.52	0.00	0.60	0.04	0.97	1.05
SCN, SCN			n/a				n/a	
H, NH <sub>2</sub>	0.61	96.25	1.79	0.00	1.35	0.01	1.00	1.03
NH <sub>2</sub> , NH <sub>2</sub>	1.43	92.41	3.83	0.00	2.33	0.01	0.97	1.03

n/a: When structures are manually specified, the program first determines a set of corresponding NBO's. If NBO's corresponding to the given resonance structure cannot be found the calculation terminates.

Table A12: NRT expansion weights and natural bond orders for substituted series using RS-BD as input. Calculated at the B3PW91 / BS2 level.

RS-BD	%B	%C	%D	%I	%O	Bond Order		
						S-C1	S-C2	C1-C2
NH <sub>2</sub> , H	80.35	6.73	5.38	7.29	0.25	0.926	0.872	1.109
H, CHO	76.95	4.65	8.22	9.46	0.72	0.889	0.823	1.120
H, SiH <sub>3</sub>	79.26	7.42	7.42	5.80	0.10	0.880	0.867	1.146
CH <sub>3</sub> , H	81.48	6.87	7.49	4.16	0.00	0.856	0.874	1.137
H, CF <sub>3</sub>	77.54	9.62	7.89	4.55	0.40	0.814	0.874	1.127
PH <sub>2</sub> , H	77.64	8.34	8.99	5.02	0.01	0.827	0.860	1.155
H, CCl <sub>3</sub>	74.27	9.88	9.66	5.46	0.73	0.808	0.853	1.117
H, PH <sub>2</sub>	75.38	9.52	8.71	5.38	1.01	0.818	0.859	1.148
H, CN	67.99	17.55	7.87	5.83	0.76	0.806	0.863	1.115
CH <sub>3</sub> , CH <sub>3</sub>	76.12	9.86	8.88	4.62	0.52	0.813	0.865	1.135
NC, NC	68.41	14.31	8.99	6.71	1.58	0.764	0.841	1.111
H, CH <sub>3</sub>	72.96	10.96	9.83	4.26	1.99	0.914	0.937	1.109
H, Br			n/a				n/a	
H, NC	70.00	14.24	10.05	4.10	1.61	0.755	0.857	1.102
H, Cl	70.45	13.41	10.63	4.29	1.22	0.760	0.851	1.126
H, F	67.07	18.88	13.27	0.00	0.78	0.678	0.870	1.131
OH, OH	61.66	23.09	13.85	1.40	0.00	0.631	0.851	1.140
NCS, NCS	43.82	38.71	15.92	0.78	0.77	0.614	0.833	1.135
H, NCS	55.89	24.10	16.87	0.37	2.77	0.587	0.835	1.140
H, SCN	51.44	30.56	16.68	0.00	1.32	0.521	0.844	1.154
H, OH	0.00	56.43	43.57	0.00	0.00	0.000	0.564	1.327
SeH, SeH	49.17	31.44	17.04	2.35	0.00	0.509	0.818	1.153
H, SeH	49.63	31.50	18.87	0.00	0.00	0.493	0.830	1.164
H, SH	0.00	54.92	45.08	0.00	0.00	0.000	0.549	1.280
SCN, SCN			n/a				n/a	
H, NH <sub>2</sub>	0.00	52.33	47.67	0.00	0.00	0.000	0.523	1.255
NH <sub>2</sub> , NH <sub>2</sub>	0.00	52.75	39.62	7.62	0.01	0.000	0.528	1.285

n/a: When structures are manually specified, the program first determines a set of corresponding NBO's. If NBO's corresponding to the given resonance structure cannot be found the calculation terminates.

Table A13: NRT expansion weights and natural bond orders for substituted series using RS-BCD as input. Calculated at the B3PW91 / BS2 level.

RS-BCD	%B	%C	%D	%I	%O	Bond Order		
						S-C1	S-C2	C1-C2
NH <sub>2</sub> , H	80.35	6.73	5.38	7.29	0.25	1.165	0.971	-0.194
H, CHO	76.95	5.78	8.22	8.23	0.82	1.023	0.944	-0.078
H, SiH <sub>3</sub>	79.25	7.42	7.42	5.80	0.11	1.112	0.980	-0.132
CH <sub>3</sub> , H	80.50	6.87	7.49	5.14	0.00	1.850	1.831	-0.019
H, CF <sub>3</sub>	77.54	3.27	8.81	10.10	0.28	0.948	0.968	0.021
PH <sub>2</sub> , H	77.64	8.34	8.99	5.02	0.01	0.996	0.977	-0.019
H, CCl <sub>3</sub>	74.26	12.80	8.95	2.71	1.28	0.905	0.969	0.064
H, PH <sub>2</sub>	75.38	9.52	8.69	5.38	1.03	0.977	0.977	0.000
H, CN	74.00	11.54	7.87	5.82	0.77	0.908	0.971	0.063
CH <sub>3</sub> , CH <sub>3</sub>	76.12	9.86	8.88	4.62	0.52	0.912	0.991	0.079
NC, NC	68.04	14.60	8.86	6.73	1.77	0.773	0.928	0.155
H, CH <sub>3</sub>	73.94	11.59	9.63	4.39	0.45	0.816	0.992	0.176
H, Br			n/a				n/a	
H, NC	68.34	16.26	10.22	4.15	1.03	0.644	1.005	0.360
H, Cl	69.13	15.72	9.96	4.33	0.86	0.673	1.011	0.338
H, F	53.17	35.56	10.28	0.00	0.99	0.429	1.105	0.675
OH, OH	47.23	40.25	10.97	1.27	0.28	0.291	1.029	0.738
NCS, NCS	47.25	38.44	12.89	0.60	0.82	0.240	1.002	0.762
H, NCS	36.65	51.87	11.31	0.00	0.17	0.243	1.057	0.814
H, SCN	37.54	48.54	12.65	0.00	1.27	0.267	1.048	0.782
H, OH	3.45	90.11	6.30	0.00	0.14	0.207	1.075	0.868
SeH, SeH	31.97	53.57	13.03	1.08	0.35	0.219	1.028	0.809
H, SeH	29.66	58.72	11.62	0.00	0.00	0.220	1.057	0.837
H, SH	3.27	88.24	7.87	0.00	0.62	0.205	1.065	0.860
SCN, SCN			n/a				n/a	
H, NH <sub>2</sub>	0.56	92.12	5.82	0.00	1.50	0.137	1.084	0.947
NH <sub>2</sub> , NH <sub>2</sub>	1.30	88.51	8.00	0.00	2.19	0.141	1.074	0.933

n/a: When structures are manually specified, the program first determines a set of corresponding NBO's. If NBO's corresponding to the given resonance structure cannot be found the calculation terminates.

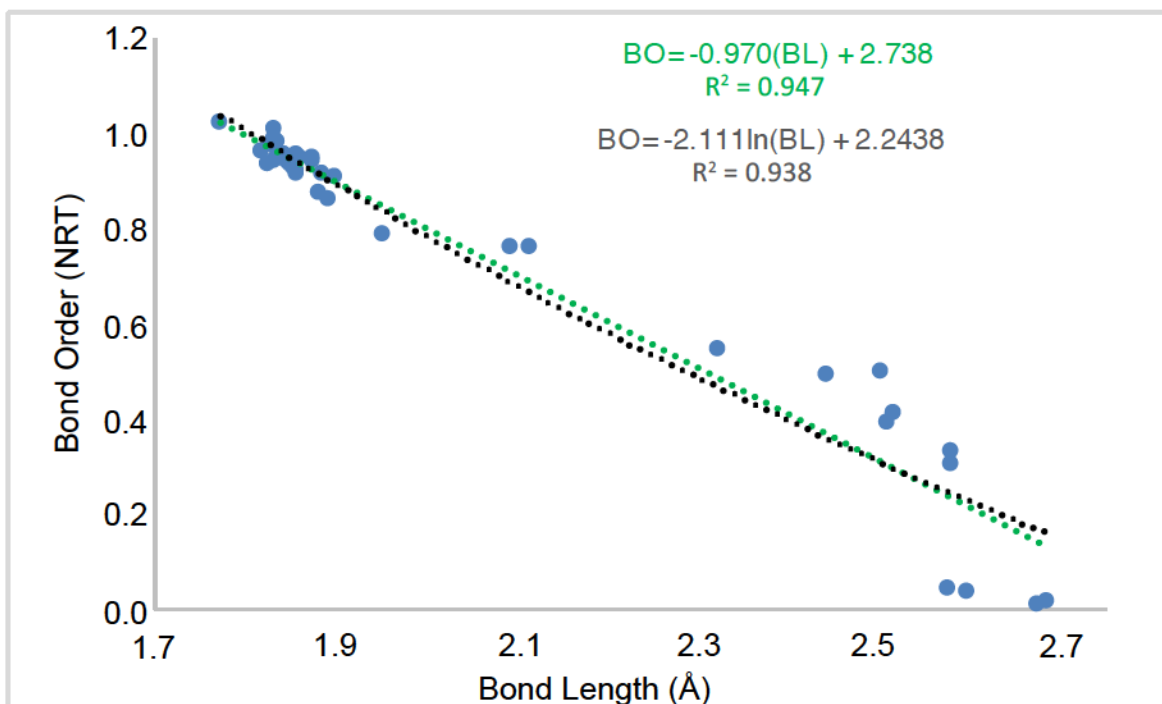


**Figure A5:** Bond length – bond order relationship for substituted series based on RS-BC with linear (green) and logarithmic (black) regressions.

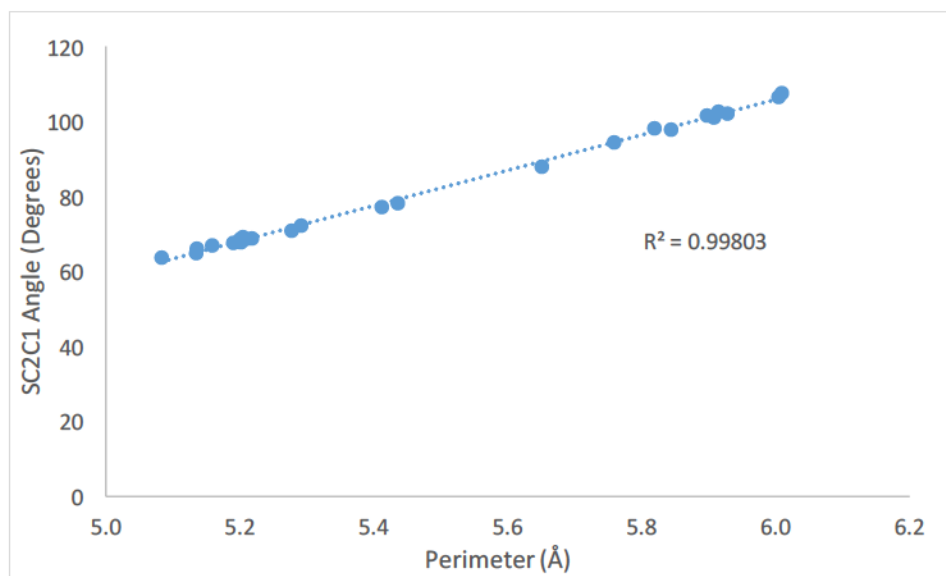


**Figure A6:** Relationship between ring perimeter and SC2C1 angle for substituted series. B3PW91/BS2.

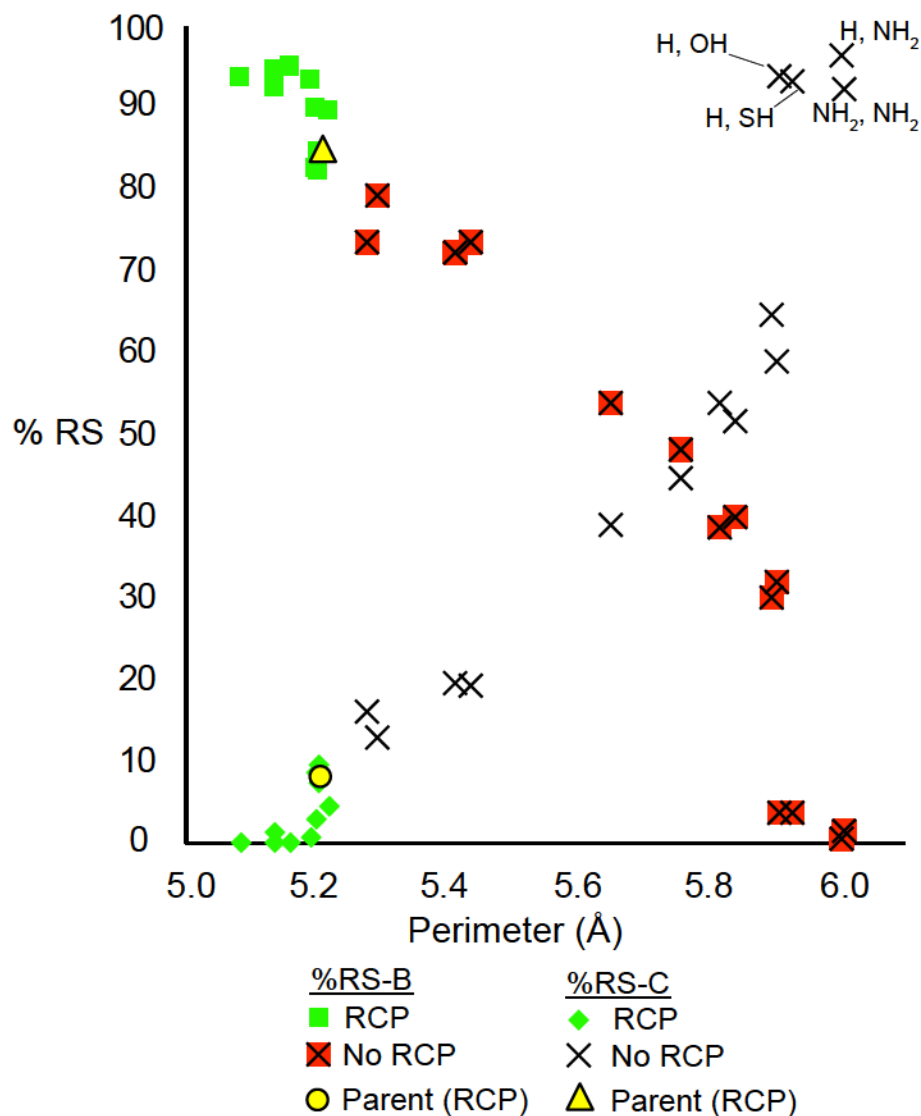


**Figure A7:** Weight of %RS-B (square markers) and %RS-C (diamond markers) as a function of the ring perimeter. Green filled markers – RCP detected. Red filled markers – No RCP detected. Yellow markers indicate the %RS-B and %RS-C of the unsubstituted parent (RCP detected). Calculated at the B3PW91/BS 2 level.

### <sup>13</sup>C NMR Chemical Shielding Tensor Analysis Details

Carbenes exhibit a very distinctive chemical shift.<sup>1</sup> The distinctiveness comes from the fact that a carbene has a unique symmetry and orbital orientation and the resulting tensor components when diagonalized to a principal axis system have a very specific pattern: the  $\sigma_{xx}$  component is strongly deshielded, the  $\sigma_{yy}$  component is less strongly

deshielded and the  $\sigma_{zz}$  component is not very deshielded ( $\sigma_{xx} < \sigma_{yy} < \sigma_{zz}$ ). Orienting isothiirane in this manner (SI-Figure 8), we obtained the  $\sigma_{xx}$  component for the  $C_1$  nucleus and have plotted its value with the perimeter of the ring in Figure A9.

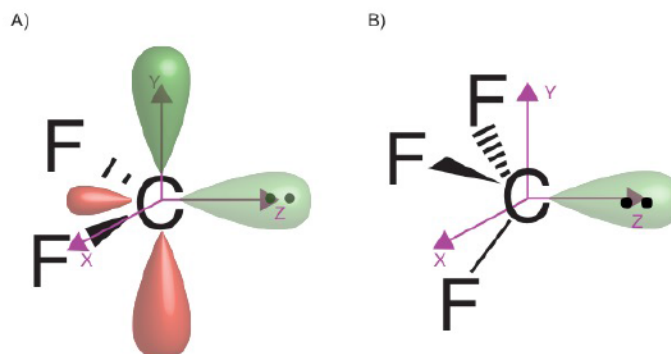


**Figure A8:** Orientation of chemical shift shielding tensor for an example of A) a singlet carbene and B) a singlet carbanion

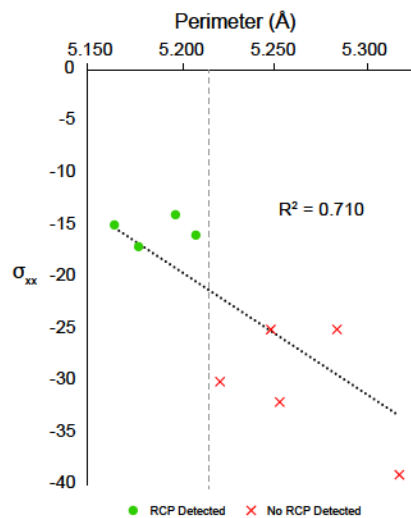


**Figure A9:** Ring perimeter (Å) and  $\sigma_{xx}$  component of the  $^{13}C_1$  NMR chemical shielding tensor for the B3LYP, B3PW91, and PBE0 / BS1-3 levels of theory. Circles – RCP detected. X's – No RCP detected. Dashed line – CCSD(T)/CBS<sub>Extrap</sub> perimeter

It can be seen from Figure A9 that model chemistries predicting a perimeter greater than that of the CCSD(T)/CBS<sub>Extrap</sub> value exhibit  $\sigma_{xx}$  components that are more deshielded than that for the cyclic structures. For comparison, the chemical shielding tensors of  $^1CF_2$  (a stable singlet carbene) and  $^1CF_3^-$  (a carbanion) were calculated and oriented as shown in Figure A8. These values, as well as those of isothiirane are presented in Table A14. In

all cases, the chemical shielding tensor components of isothirane are more comparable with  $^1\text{CF}_2$ , indicating that there is some carbenic character to the  $\text{C}_1$  nucleus.

Table A14: Chemical shielding tensors for isothirane,  $^1\text{CF}_2$ , and  $^1\text{CF}_3^-$  calculated using BS3.

Isothirane	$\sigma_{xx}$	$\sigma_{yy}$	$\sigma_{zz}$
B3LYP	-25	124	198
B3PW91	-16	126	205
PBE0	-15	128	207
$^1\text{CF}_2$			
PBE0	-435	31	35
$^1\text{CF}_3^-$			
PBE0	64	-33	-33

Table A15:  $^{13}\text{C}$  NMR chemical shift shielding tensor components, spans, and skews for  $\text{C}_1$  nuclei of the substituted series calculated at the B3PW91/BS 2 level of theory.

	R1, R2	$\sigma_{xx}$	$\sigma_{yy}$	$\sigma_{zz}$
Acyclic MG	H, H	-16	126	205
	H, Br	-291	-3	96
	H, F	-681	-27	37
	H, Cl	-578	-58	111
	H, $\text{CH}_3$	-202	53	196
	$\text{PH}_2$ , $\text{PH}_2$	-1016	-170	214
	H, $\text{NH}_2$	-526	-82	155
	$\text{NH}_2$ , $\text{NH}_2$	-555	-80	170
	H, OH	-756	-76	95
	OH, OH	-717	-66	107
	H, NC	-567	39	139
	NC, NC	-779	22	148
	H, SCN	-688	-191	191
	SCN, SCN	-766	-209	190
	H, NCS	-1451	-32	131
	NCS, NCS	-1544	-29	141
	H, SH	-1010	-183	197
	H, SeH	-928	-240	173
SeH, SeH	-996	-254	180	
Cyclic MG	$\text{CH}_3$ , H	1	139	203
	$\text{CH}_3$ , $\text{CH}_3$	-133	201	93
	H, $\text{PH}_2$	-58	98	209
	$\text{PH}_2$ , H	73	115	172
	$\text{NH}_2$ , H	36	152	196
	H, CN	-44	126	192
	H, CHO	56	103	142
	H, $\text{SiH}_3$	14	143	233
	H, $\text{CF}_3$	26	123	170
	H, $\text{CCl}_3$	6	106	135

Table A16: Energy (hartree) of molecules studied

Molecule	Model Chemistry	Energy (h)
(HS)(CH <sub>2</sub> )(CH)	B3LYP 6-311++g(d,p)	-476.7289322
	B3LYP 6-311++g(2d,2p)	-476.7386719
	B3LYP 6-311++g(2df,pd)	-476.7427959
	B3LYP TZVP	-476.7287581
	B3PW91 6-311++g(d,p)	-476.6479917
	B3PW91 6-311++g(2d,2p)	-476.658462
	B3PW91 6-311++g(2df,pd)	-476.6627957
	B3PW91 TZVP	-476.648254
	PBE0 6-311++g(d,p)	-476.4707295
	PBE0 6-311++g(2d,2p)	-476.4813885
	PBE0 6-311++g(2df,pd)	-476.4859308
	BLYP TZVP	-476.6670227
	BP86 TZVP	-476.7541936
	HF 6-311++g(d,p)	-475.488331
	MP2 6-311++g(d,p)	-475.4834858
PBE 6-311++g(d,p)	-476.4315769	
(CH <sub>3</sub> S)(CH <sub>2</sub> )(CH)		-515.9776213
(NH <sub>2</sub> S)(CH <sub>2</sub> )(CH)		-532.0127248
(NCS)(CH <sub>2</sub> )(CH)		-568.9944322
(NCSS)(CH <sub>2</sub> )(CH)		-967.2093481
(OHS)(CH <sub>2</sub> )(CH)		-551.9919136
(PH <sub>2</sub> S)(CH <sub>2</sub> )(CH)		-818.6007839
(SHS)(CH <sub>2</sub> )(CH)		-875.070656
(SCNS)(CH <sub>2</sub> )(CH)		-2878.403961
(SeHS)(CH <sub>2</sub> )(CH)		-2878.403961
(HS)(CH <sub>2</sub> )(CCl <sub>3</sub> )		-1894.679071
(HS)(CH <sub>2</sub> )(CCF <sub>3</sub> )	B3PW91 6-311++g(2d,2p)	-813.6964907
(HS)(CH <sub>2</sub> )(CCN)		-568.8941943
(HS)(CH <sub>2</sub> )(CCHO)		-589.9866093
(HS)(CH <sub>2</sub> )(CSiH <sub>3</sub> )		-1894.679071
(HS)(CH <sub>2</sub> )(CCH <sub>3</sub> )		-515.9724988
(HS)(CH <sub>2</sub> )(CF)		-575.9001259
(HS)(CH <sub>2</sub> )(CCI)		-936.2376457
(HS)(CH <sub>2</sub> )(CBr)		-3050.190188
(HS)(CH <sub>2</sub> )(CNH <sub>2</sub> )		-532.059725
(HS)(CH <sub>2</sub> )(HNC)		-568.8569161
(HS)(CH <sub>2</sub> )(HNCS)		-967.0813655

Table A16 Continued:

Molecule	Model Chemistry	Energy (h)
(HS)(CH <sub>2</sub> )(COH)		-551.9066002
(HS)(CH <sub>2</sub> )(CPH <sub>2</sub> )		-818.5897383
(HS)(CH <sub>2</sub> )(CSH)		-874.8503452
(HS)(CH <sub>2</sub> )(CSCN)		-967.0650075
(HS)(CH <sub>2</sub> )(CSeH)		-2878.203935
(CH <sub>3</sub> S)(CH <sub>2</sub> )(CCH <sub>3</sub> )		-555.29022
(NH <sub>2</sub> S)(CH <sub>2</sub> )(CNH <sub>2</sub> )	B3PW91	-587.3979094
(NCS)(CH <sub>2</sub> )(CNC)	6-311++g(2d,2p)	-661.0170837
(NCSS)(CH <sub>2</sub> )(CNCS)		-1457.45975
(OHS)(CH <sub>2</sub> )(COH)		-627.1055253
(PH <sub>2</sub> S)(CH <sub>2</sub> )(CPH <sub>2</sub> )		-1160.530745
(SHS)(CH <sub>2</sub> )(CSH)		-1273.096027
(SCNS)(CH <sub>2</sub> )(CSCN)		-1457.447274
(SeHS)(CH <sub>2</sub> )(CSeH)		-5279.742165

### References

1. D. Tapu, D. Dixon, C. Roe, *Chem. Rev.*, **2009**, *109*, 3385.

APPENDIX B

Supplemental Information for Chapter Four

All percent deviations calculated as:

$$\left[ \frac{(\text{Calculated} - \text{Experimental})}{\text{Experimental}} \right] \times 100\%$$

**Table B1:** Experimental bond lengths (Å) including mean value and standard deviation (S.D.) for neutral and *reduced* TCNE

	R <sub>1</sub>		R <sub>2</sub>		R <sub>3</sub>	
	1.344 <sup>a</sup>	1.392 <sup>c</sup>	1.439 <sup>a</sup>	1.417 <sup>c</sup>	1.153 <sup>a</sup>	1.140 <sup>c</sup>
	1.355 <sup>a</sup>	1.432 <sup>d</sup>	1.431 <sup>a</sup>	1.418 <sup>d</sup>	1.160 <sup>a</sup>	1.155 <sup>d</sup>
	1.357 <sup>b</sup>	1.429 <sup>c</sup>	1.435 <sup>b</sup>	1.406 <sup>c</sup>	1.166 <sup>b</sup>	1.170 <sup>c</sup>
Mean	1.352	1.418	1.435	1.414	1.160	1.155
S.D.	0.006	0.018	0.003	0.005	0.005	0.012

a) Chapter 4 Ref 28

b) Chapter 4 Ref 29

c) Chapter 4 Ref 10

d) Chapter 4 Ref 30

**Table B2A-F:** Deviation of methods from average experimental TCNE bond lengths and mean % deviation. Green – overestimate. Red – Underestimate.

(A)BS1	R1	R2	R3	Mean (%)
BLYP	0.026	-0.003	0.007	0.986
BP86	0.024	-0.006	0.008	0.897
HCTH	0.020	-0.010	0.003	0.413
M06-L	0.015	-0.010	0.001	0.167
PBE	0.024	-0.007	0.008	0.809
TPSS	0.022	-0.007	0.005	0.672
TPSSh	0.015	-0.007	0.000	0.274
B3LYP	0.012	-0.006	-0.005	0.036
PBE0	0.008	-0.008	-0.005	-0.183
M06	0.005	-0.008	-0.006	-0.276
BH&HLYP	-0.003	-0.007	-0.017	-0.925
M06-2X	0.001	-0.002	-0.010	-0.358
CAMB3LYP	0.001	-0.005	-0.011	-0.495
M06-HF	-0.008	0.002	-0.020	-0.865

(B) BS2	R1	R2	R3	Mean (%)
BLYP	0.030	0.001	0.015	1.529
BP86	0.028	-0.002	0.016	1.409
HCTH	0.022	-0.008	0.010	0.825
M06-L	0.017	-0.008	0.008	0.590
PBE	0.027	-0.004	0.015	1.294
TPSS	0.025	-0.003	0.013	1.155
TPSSh	0.019	-0.004	0.007	0.741
B3LYP	0.016	-0.002	0.003	0.557
PBE0	0.012	-0.005	0.002	0.272
M06	0.010	-0.004	0.003	0.279
BH&HLYP	0.001	-0.004	-0.010	-0.448
M06-2X	0.005	0.000	-0.002	0.100
CAMB3LYP	0.005	-0.001	-0.003	0.032
M06-HF	-0.004	0.006	-0.012	-0.325

(C) BS3	R1	R2	R3	Mean (%)
BLYP	0.023	-0.005	0.005	0.760
BP86	0.022	-0.007	0.006	0.690
HCTH	0.017	-0.011	0.001	0.241
M06-L	0.012	-0.012	-0.002	-0.087
PBE	0.021	-0.008	0.006	0.628
TPSS	0.019	-0.008	0.003	0.473
TPSSh	0.013	-0.008	-0.002	0.080
B3LYP	0.009	-0.007	-0.007	-0.170
PBE0	0.006	-0.009	-0.007	-0.351
M06	0.002	-0.009	-0.009	-0.508
BH&HLYP	-0.006	-0.008	-0.020	-1.123
M06-2X	-0.001	-0.004	-0.011	-0.539
CAMB3LYP	-0.002	-0.006	-0.013	-0.687
M06-HF	-0.010	0.001	-0.020	-0.977

(D) BS4	R1	R2	R3	Mean (%)
BLYP	0.023	-0.004	0.004	0.767
BP86	0.022	-0.007	0.005	0.693
HCTH	0.018	-0.011	0.000	0.241
M06-L	0.012	-0.012	-0.002	-0.056
PBE	0.021	-0.008	0.005	0.623
TPSS	0.019	-0.008	0.002	0.448
TPSSh	0.013	-0.008	-0.003	0.050
B3LYP	0.009	-0.007	-0.007	-0.178
PBE0	0.006	-0.009	-0.008	-0.368
M06	0.003	-0.009	-0.009	-0.482
BH&HLYP	-0.006	-0.008	-0.020	-1.140
M06-2X	-0.001	-0.003	-0.012	-0.543
CAMB3LYP	-0.002	-0.006	-0.014	-0.698
M06-HF	-0.010	0.001	-0.022	-1.045

(E) BS5	R1	R2	R3	Mean (%)
BLYP	0.030	0.000	0.015	1.474
BP86	0.028	-0.003	0.015	1.360
HCTH	0.023	-0.008	0.009	0.801
M06-L	0.017	-0.008	0.007	0.525
PBE	0.027	-0.004	0.015	1.259
TPSS	0.025	-0.004	0.012	1.110
TPSSh	0.019	-0.004	0.006	0.694
B3LYP	0.015	-0.003	0.003	0.496
PBE0	0.011	-0.006	0.001	0.227
M06	0.009	-0.005	0.002	0.219
BH&HLYP	0.000	-0.005	-0.011	-0.519
M06-2X	0.004	0.000	-0.003	0.052
CAMB3LYP	0.005	-0.002	-0.003	-0.029
M06-HF	-0.004	0.006	-0.012	-0.351

(F) BS6	R1	R2	R3	Mean (%)
BLYP	0.029	0.001	0.014	1.464
BP86	0.028	-0.002	0.015	1.352
HCTH	0.022	-0.007	0.009	0.800
M06-L	0.017	-0.008	0.007	0.539
PBE	0.027	-0.003	0.014	1.249
TPSS	0.025	-0.003	0.012	1.105
TPSSh	0.018	-0.004	0.006	0.700
B3LYP	0.015	-0.002	0.002	0.497
PBE0	0.011	-0.005	0.001	0.238
M06	0.009	-0.004	0.001	0.211
BH&HLYP	0.000	-0.004	-0.011	-0.492
M06-2X	0.004	0.001	-0.003	0.058
CAMB3LYP	0.004	-0.001	-0.004	-0.026
M06-HF	-0.005	0.006	-0.013	-0.373

Table B3A-F: Deviation of methods from average experimental [TCNE]<sup>-</sup> bond lengths and mean deviation. Green – overestimate. Red – Underestimate.

(A) BS1	R1	R2	R3	Mean (%)
BLYP	0.028	0.001	0.019	1.575
BP86	0.024	-0.001	0.020	1.417
HCTH	0.018	-0.006	0.014	0.880
M06-L	0.016	-0.007	0.012	0.730
PBE	0.022	-0.002	0.019	1.304
TPSS	0.023	-0.002	0.017	1.239
TPSSh	0.018	-0.004	0.012	0.883
B3LYP	0.017	-0.003	0.007	0.716
PBE0	0.012	-0.006	0.006	0.439
M06	0.011	-0.005	0.006	0.384
BH&HLYP	0.008	-0.006	-0.005	-0.119
M062X	0.009	-0.001	0.002	0.336
CAMB3LYP	0.010	-0.003	0.001	0.262
M06-HF	0.011	-0.005	0.006	0.384

(B) BS2	R1	R2	R3	Mean
BLYP	0.030	0.006	0.026	2.094
BP86	0.027	0.004	0.027	1.918
HCTH	0.020	-0.002	0.021	1.294
M06-L	0.018	-0.003	0.019	1.138
PBE	0.025	0.002	0.026	1.787
TPSS	0.025	0.002	0.024	1.716
TPSSh	0.021	0.001	0.019	1.352
B3LYP	0.020	0.002	0.015	1.212
PBE0	0.015	-0.001	0.013	0.886
M06	0.015	-0.001	0.014	0.931
BH&HLYP	0.010	-0.002	0.002	0.337
M062X	0.011	0.002	0.009	0.755
CAMB3LYP	0.013	0.001	0.008	0.760
M06-HF	0.015	-0.001	0.014	0.931

(C) BS3	R1	R2	R3	Mean (%)
BLYP	0.025	-0.001	0.016	1.348
BP86	0.022	-0.002	0.017	1.210
HCTH	0.017	-0.007	0.012	0.704
M06-L	0.014	-0.009	0.009	0.485
PBE	0.020	-0.003	0.017	1.122
TPSS	0.020	-0.003	0.014	1.032
TPSSh	0.016	-0.005	0.009	0.691
B3LYP	0.015	-0.004	0.005	0.501
PBE0	0.010	-0.006	0.004	0.263
M06	0.009	-0.006	0.002	0.171
BH&HLYP	0.005	-0.007	-0.008	-0.337
M062X	0.007	-0.003	0.000	0.148
CAMB3LYP	0.008	-0.005	-0.002	0.054
M06-HF	0.009	-0.006	0.002	0.171

(D) BS4	R1	R2	R3	Mean (%)
BLYP	0.026	-0.001	0.016	1.367
BP86	0.022	-0.002	0.017	1.216
HCTH	0.017	-0.007	0.011	0.717
M06-L	0.015	-0.008	0.009	0.518
PBE	0.021	-0.003	0.016	1.122
TPSS	0.021	-0.004	0.014	1.012
TPSSh	0.016	-0.005	0.009	0.672
B3LYP	0.015	-0.004	0.004	0.504
PBE0	0.011	-0.006	0.004	0.257
M06	0.010	-0.006	0.003	0.201
BH&HLYP	0.005	-0.007	-0.008	-0.342
M062X	0.007	-0.002	0.000	0.150
CAMB3LYP	0.008	-0.005	-0.002	0.060
M06-HF	0.010	-0.006	0.003	0.201

(E) BS5	R1	R2	R3	Mean (%)
BLYP	0.030	0.004	0.026	2.013
BP86	0.027	0.002	0.027	1.838
HCTH	0.021	-0.004	0.020	1.242
M06-L	0.018	-0.005	0.019	1.053
PBE	0.025	0.000	0.026	1.729
TPSS	0.025	0.000	0.024	1.642
TPSSh	0.021	-0.001	0.018	1.275
B3LYP	0.020	0.000	0.015	1.128
PBE0	0.015	-0.003	0.013	0.814
M06	0.014	-0.002	0.014	0.845
BH&H	0.009	-0.003	0.001	0.239
M062X	0.011	0.001	0.009	0.687
CAMB3LYP	0.013	-0.001	0.008	0.674
M06-HF	0.014	-0.002	0.014	0.845

(F) BS6	R1	R2	R3	Mean (%)
BLYP	0.030	0.005	0.026	2.008
BP86	0.026	0.003	0.026	1.837
HCTH	0.020	-0.003	0.020	1.250
M06-L	0.018	-0.004	0.018	1.057
PBE	0.025	0.001	0.026	1.716
TPSS	0.025	0.001	0.023	1.648
TPSSh	0.020	0.000	0.018	1.283
B3LYP	0.019	0.001	0.014	1.141
PBE0	0.014	-0.002	0.013	0.828
M06	0.014	-0.002	0.013	0.843
BH&H	0.010	-0.002	0.001	0.278
M062X	0.011	0.002	0.008	0.701
CAMB3LYP	0.013	0.001	0.008	0.689
M06-HF	0.014	-0.002	0.013	0.843

Table B4:  $\langle S^2 \rangle$  values for [TCNE]<sup>-</sup>

	BS1	BS2	BS3	BS4	BS5	BS6
BLYP	0.754	0.754	0.753	0.754	0.754	0.754
BP86	0.754	0.754	0.753	0.754	0.754	0.754
HCTH	0.755	0.755	0.755	0.755	0.755	0.755
M06-L	0.757	0.757	0.757	0.757	0.757	0.757
PBE	0.754	0.754	0.753	0.754	0.753	0.754
TPSS	0.756	0.756	0.755	0.756	0.756	0.756
TPSSh	0.759	0.759	0.758	0.759	0.759	0.759
B3LYP	0.759	0.759	0.759	0.759	0.760	0.759
PBE0	0.762	0.762	0.761	0.762	0.762	0.762
M06	0.759	0.758	0.758	0.758	0.759	0.758
BHandHLYP	0.775	0.773	0.773	0.775	0.776	0.774
M06-2X	0.761	0.760	0.760	0.760	0.760	0.760
CAM-B3LYP	0.765	0.764	0.764	0.765	0.765	0.764
M06-HF	0.759	0.758	0.758	0.758	0.759	0.758

Table B5: Experimental bond lengths (Å) including mean value and standard deviation (S.D.) for neutral and *reduced* TCNQ

	R <sub>1</sub>		R <sub>2</sub>		R <sub>3</sub>		R <sub>4</sub>		R <sub>5</sub>	
	1.346	1.356 <sup>a</sup>	1.448	1.425 <sup>a</sup>	1.374	1.401 <sup>a</sup>	1.441	1.417 <sup>a</sup>	1.140	1.151 <sup>a</sup>
	–	1.373 <sup>b</sup>	–	1.426 <sup>b</sup>	–	1.420 <sup>b</sup>	–	1.412 <sup>b</sup>	–	1.155 <sup>b</sup>
	–	1.374 <sup>b</sup>	–	1.420 <sup>b</sup>	–	1.420 <sup>b</sup>	–	1.415 <sup>b</sup>	–	1.155 <sup>b</sup>
	–	–	–	–	–	–	–	1.414 <sup>b</sup>	–	1.155 <sup>b</sup>
	–	–	–	–	–	–	–	1.424 <sup>b</sup>	–	1.148 <sup>b</sup>
	–	1.356 <sup>c</sup>	–	1.426 <sup>c</sup>	–	1.402 <sup>c</sup>	–	1.418 <sup>c</sup>	–	1.155 <sup>c</sup>
	–	–	–	1.440 <sup>c</sup>	–	–	–	1.428 <sup>c</sup>	–	1.147 <sup>c</sup>
	–	1.375 <sup>d</sup>	–	1.425 <sup>d</sup>	–	1.438 <sup>d</sup>	–	1.408 <sup>d</sup>	–	1.164 <sup>d</sup>
	–	–	–	–	–	–	–	1.440 <sup>d</sup>	–	1.156 <sup>d</sup>
Mean	–	1.367	–	1.427	–	1.416	–	1.420	–	1.154
S. D.	–	0.009	–	0.006	–	0.014	–	0.009	–	0.005

- a) Chapter 4 Ref 32  
b) Chapter 4 Ref 33  
c) Chapter 4 Ref 34  
d) Chapter 4 Ref 35

Table B6A-F: Deviation of methods from average experimental TCNQ bond lengths and mean % deviation. Green – overestimate. Red – Underestimate.

(A) BS1	R1	R2	R3	R4	R5	Mean (%)
BLYP	0.02	0.00	0.03	-0.01	0.03	1.59
BP86	0.02	0.00	0.03	-0.01	0.04	1.43
HCTH	0.01	-0.01	0.02	-0.01	0.03	0.84
M06-L	0.01	-0.01	0.02	-0.01	0.03	0.62
PBE	0.02	0.00	0.02	-0.01	0.03	1.31
TPSS	0.02	0.00	0.02	-0.01	0.03	1.21
TPSSh	0.01	0.00	0.02	-0.01	0.03	0.85
B3LYP	0.01	0.00	0.01	-0.01	0.02	0.72
PBE0	0.01	0.00	0.01	-0.01	0.02	0.41
M06	0.00	0.00	0.01	-0.01	0.02	0.39
BH&HLYP	0.00	0.00	0.00	-0.01	0.01	-0.16
M06-2X	0.00	0.00	0.00	0.00	0.02	0.34
CAMB3LYP	0.00	0.00	0.00	-0.01	0.02	0.23
M06-HF	0.00	0.01	-0.01	0.00	0.01	0.12

(B) BS2 N/A

(C) BS3	R1	R2	R3	R4	R5	Mean (%)
BLYP	0.02	0.00	0.03	-0.01	0.03	1.52
BP86	0.02	0.00	0.03	-0.01	0.03	1.37
HCTH	0.01	-0.01	0.02	-0.01	0.03	0.80
M06-L	0.01	-0.01	0.01	-0.02	0.03	0.54
PBE	0.02	0.00	0.02	-0.01	0.03	1.26
TPSS	0.02	0.00	0.02	-0.01	0.03	1.15
TPSSh	0.00	-0.01	0.01	-0.01	0.02	0.21
B3LYP	0.01	0.00	0.01	-0.01	0.02	0.65
PBE0	0.01	0.00	0.01	-0.01	0.02	0.36
M06	0.00	0.00	0.01	-0.01	0.02	0.32
BH&H	0.00	0.00	-0.01	-0.01	0.01	-0.24
M06-2X	0.00	0.00	0.00	-0.01	0.02	0.30
CAMB3LYP	0.00	0.00	0.00	-0.01	0.02	0.16
M06-HF	0.00	0.01	-0.01	0.00	0.01	0.10

(D) BS4	R1	R2	R3	R4	R5	Mean (%)
BLYP	0.01	0.00	0.02	-0.01	0.02	0.89
BP86	0.00	0.00	0.00	-0.01	0.02	0.23
HCTH	0.01	-0.01	0.02	-0.02	0.02	0.31
M06-L	0.00	-0.01	0.01	-0.02	0.02	0.00
PBE	0.01	-0.01	0.02	-0.01	0.02	0.69
TPSS	0.01	-0.01	0.02	-0.01	0.02	0.57
TPSSh	0.01	-0.01	0.01	-0.01	0.02	0.23
B3LYP	0.00	0.00	0.01	-0.01	0.01	0.05
PBE0	0.00	-0.01	0.00	-0.01	0.01	-0.16
M06	0.00	-0.01	0.00	-0.01	0.01	-0.32
BH&HLYP	-0.01	0.00	-0.01	-0.01	0.00	-0.78
M06-2X	0.00	0.00	-0.01	-0.01	0.01	-0.23
CAMB3LYP	-0.01	0.00	-0.01	-0.01	0.01	-0.43
M06-HF	-0.01	0.01	-0.02	0.00	0.00	-0.49

(E) BS5	R1	R2	R3	R4	R5	Mean (%)
BLYP	0.02	0.00	0.02	-0.01	0.03	1.14
BP86	0.01	0.00	0.02	-0.01	0.03	1.01
HCTH	0.01	-0.01	0.02	-0.02	0.02	0.50
M06-L	0.01	-0.01	0.01	-0.02	0.02	0.27
PBE	0.01	0.00	0.02	-0.01	0.03	0.90
TPSS	0.01	0.00	0.02	-0.01	0.02	0.81
TPSSh	0.01	0.00	0.01	-0.01	0.02	0.46
B3LYP	0.00	0.00	0.01	-0.01	0.01	0.29
PBE0	0.00	0.00	0.00	-0.01	0.01	0.04
M06	0.00	0.00	0.00	-0.01	0.01	-0.07
M06-2X	0.00	0.00	0.00	-0.01	0.01	-0.02
BH&HLYP	-0.01	0.00	-0.01	-0.01	0.00	-0.55
CAMB3LYP	0.00	0.00	-0.01	-0.01	0.01	-0.20
M06-HF	-0.01	0.01	-0.02	0.00	0.00	-0.31

(F) BS6	R1	R2	R3	R4	R5	Mean (%)
BLYP	0.01	0.00	0.02	-0.01	0.02	0.90
BP86	0.01	0.00	0.02	-0.01	0.02	0.78
HCTH	0.01	-0.01	0.02	-0.02	0.02	0.32
M06-L	0.00	-0.01	0.01	-0.02	0.02	0.04
PBE	0.01	-0.01	0.02	-0.01	0.02	0.70
TPSS	0.01	-0.01	0.02	-0.01	0.02	0.56
TPSSh	0.00	-0.01	0.01	-0.01	0.02	0.21
B3LYP	0.00	0.00	0.01	-0.01	0.01	0.05
PBE0	0.00	-0.01	0.00	-0.01	0.01	-0.17
M06	0.00	-0.01	0.00	-0.01	0.01	-0.29
BH&HLYP	-0.01	0.00	-0.01	-0.01	0.00	-0.78
M06-2X	0.00	0.00	-0.01	-0.01	0.01	-0.23
CAMB3LYP	-0.01	0.00	-0.01	-0.01	0.01	-0.43
M06-HF	-0.01	0.01	-0.02	0.00	0.00	-0.52

Table B7A-F: Deviation of methods from average experimental [TCNQ]<sup>-</sup> bond lengths and mean % deviation. Green – overestimate. Red – Underestimate.

(A) BS1	R1	R2	R3	R4	R5	Mean (%)
BLYP	0.02	0.01	0.02	0.00	0.03	1.50
BP86	0.01	0.00	0.02	0.00	0.03	1.32
HCTH	0.01	0.00	0.01	0.00	0.02	0.72
M06-L	0.01	0.00	0.01	-0.01	0.02	0.53
PBE	0.01	0.00	0.02	0.00	0.03	1.20
TPSS	0.01	0.00	0.02	0.00	0.02	1.12
TPSSh	0.01	0.00	0.01	0.00	0.02	0.79
B3LYP	0.01	0.00	0.01	0.00	0.01	0.68
PBE0	0.00	0.00	0.01	0.00	0.01	0.37
M06	0.00	0.00	0.01	0.00	0.01	0.35
BH&HLYP	0.00	0.00	0.00	0.00	0.00	-0.14
M06-2X	0.00	0.00	0.00	0.00	0.01	0.30
CAMB3LYP	0.00	0.00	0.00	0.00	0.01	0.23
M06-HF	0.00	0.00	0.00	0.01	0.00	0.09

(B) BS2 N/A

(C) BS3	R1	R2	R3	R4	R5	Mean (%)
BLYP	0.02	0.01	0.02	0.00	0.03	1.43
BP86	0.01	0.00	0.02	0.00	0.03	1.26
HCTH	0.01	0.00	0.01	-0.01	0.02	0.68
M06-L	0.01	0.00	0.01	-0.01	0.02	0.44
PBE	0.01	0.00	0.02	0.00	0.03	1.15
TPSS	0.01	0.00	0.02	0.00	0.02	1.06
TPSSh	0.01	0.00	0.01	0.00	0.02	0.73
B3LYP	0.01	0.00	0.01	0.00	0.01	0.61
PBE0	0.00	0.00	0.01	-0.01	0.01	0.31
M06	0.00	0.00	0.01	0.00	0.01	0.28
BH&HLYP	0.00	-0.01	0.00	-0.01	0.00	-0.22
M06-2X	0.00	0.00	0.00	0.00	0.01	0.24
CAMB3LYP	0.00	0.00	0.00	0.00	0.01	0.16
M06-HF	0.04	0.00	0.00	0.00	0.00	0.78

(D) BS4	R1	R2	R3	R4	R5	Mean (%)
BLYP	0.01	0.00	0.02	0.00	0.02	0.81
BP86	0.01	0.00	0.01	-0.01	0.02	0.67
HCTH	0.00	-0.01	0.01	-0.01	0.01	0.19
M06-L	0.00	-0.01	0.01	-0.01	0.01	-0.08
PBE	0.01	0.00	0.01	-0.01	0.02	0.58
TPSS	0.01	0.00	0.01	-0.01	0.01	0.49
TPSSh	0.00	-0.01	0.01	-0.01	0.01	0.18
B3LYP	0.00	0.00	0.01	-0.01	0.00	0.02
PBE0	0.00	-0.01	0.00	-0.01	0.00	-0.21
M06	0.00	-0.01	0.00	-0.01	0.00	-0.34
BH&H	-0.01	-0.01	0.00	-0.01	-0.01	-0.75
M06-2X	0.00	0.00	0.00	0.00	0.00	-0.26
CAMB3LYP	0.00	-0.01	0.00	-0.01	0.00	-0.42
M06-HF	-0.01	0.00	-0.01	0.00	-0.01	-0.51

(E) BS4	R1	R2	R3	R4	R5	Mean (%)
BLYP	0.01	0.00	0.02	0.00	0.02	1.07
BP86	0.01	0.00	0.02	0.00	0.02	0.91
HCTH	0.01	0.00	0.01	-0.01	0.01	0.38
M06-L	0.00	-0.01	0.01	-0.01	0.01	0.19
PBE	0.01	0.00	0.02	-0.01	0.02	0.80
TPSS	0.01	0.00	0.02	0.00	0.02	0.73
TPSSh	0.01	0.00	0.01	-0.01	0.01	0.40
B3LYP	0.00	0.00	0.01	-0.01	0.01	0.27
PBE0	0.00	-0.01	0.01	-0.01	0.01	0.00
M06	0.00	-0.01	0.00	-0.01	0.01	-0.10
BH&HLYP	0.00	-0.01	0.00	-0.01	-0.01	-0.52
M06-2X	0.00	0.00	0.00	0.00	0.00	-0.04
CAMB3LYP	0.00	0.00	0.00	-0.01	0.00	-0.18
M06-HF	0.00	0.00	-0.01	0.00	-0.01	-0.31

(F) BS4	R1	R2	R3	R4	R5	Mean (%)
BLYP	0.99	0.11	1.77	-0.30	1.59	0.83
BP86	0.88	-0.12	1.50	-0.50	1.68	0.69
HCTH	0.34	-0.62	1.07	-0.95	1.16	0.20
M06-L	0.06	-0.81	0.75	-1.11	0.92	-0.04
PBE	0.78	-0.24	1.38	-0.62	1.66	0.59
TPSS	0.66	-0.31	1.33	-0.63	1.38	0.49
TPSSh	0.31	-0.51	0.88	-0.75	0.88	0.16
B3LYP	0.14	-0.46	0.70	-0.68	0.44	0.03
PBE0	-0.09	-0.74	0.29	-0.89	0.38	-0.21
M06	-0.29	-0.81	0.13	-0.87	0.29	-0.31
M06-2X	-0.23	-0.39	-0.16	-0.42	-0.04	-0.25
BH&HLYP	-0.74	-0.92	-0.40	-0.90	-0.81	-0.76
M06-HF	-0.52	-0.18	-0.89	-0.06	-1.01	-0.53
CAMB3LYP	-0.46	-0.62	-0.16	-0.65	-0.17	-0.41

Table B8:  $\langle S^2 \rangle$  values for [TCNQ]<sup>-</sup>

	BS1	BS2	BS3	BS4	BS5	BS6
BLYP	0.753	–	0.753	0.753	0.753	0.753
BP86	0.753	–	0.753	0.753	0.753	0.753
HCTH	0.754	–	0.754	0.754	0.754	0.754
M06-L	0.757	–	0.756	0.757	0.756	0.757
PBE	0.753	–	0.753	0.753	0.753	0.753
TPSS	0.755	–	0.755	0.755	0.755	0.755
TPSSh	0.760	–	0.759	0.760	0.759	0.760
B3LYP	0.762	–	0.761	0.762	0.761	0.762
PBE0	0.767	–	0.766	0.766	0.765	0.766
M06	0.763	–	0.762	0.762	0.762	0.762
BHandHLYP	0.788	–	0.785	0.786	0.785	0.786
M06-2X	0.772	–	0.771	0.772	0.771	0.772
CAM-B3LYP	0.782	–	0.779	0.780	0.779	0.780
M06-HF	0.791	–	0.790	0.790	0.790	0.790

Table B9: AEA's of TCNE (eV) calculated with chosen methods.

	BS1	BS2	BS3	BS4	BS5	BS6	Min	Max	Range	Min x	S. D.
BLYP	2.781	3.248	3.240	3.100	3.266	3.248	2.781	3.266	0.485	2.781	0.173
BP86	3.133	3.498	3.493	3.387	3.523	3.505	3.133	3.523	0.390	3.133	0.137
HCTH	3.142	3.523	3.529	3.402	3.540	3.533	3.142	3.540	0.398	3.142	0.144
M06-L	3.180	3.407	3.393	3.239	3.392	3.376	3.180	3.407	0.227	3.180	0.088
PBE	3.010	3.399	3.398	3.273	3.421	3.407	3.010	3.421	0.411	3.010	0.146
TPSS	2.996	3.330	3.347	3.233	3.365	3.347	2.996	3.365	0.369	2.996	0.130
TPSSh	3.075	3.381	3.397	3.288	3.411	3.394	3.075	3.411	0.336	3.075	0.119
B3LYP	3.095	3.485	3.477	3.360	3.500	3.482	3.095	3.500	0.405	3.095	0.144
PBE0	3.202	3.504	3.504	3.401	3.518	3.507	3.202	3.518	0.316	3.202	0.113
M06	3.245	3.571	3.522	3.302	3.507	3.496	3.245	3.571	0.326	3.245	0.122
BH&HLYP	3.125	3.442	3.432	3.330	3.446	3.430	3.125	3.446	0.321	3.125	0.115
M06-2X	3.110	3.411	3.406	3.396	3.465	3.456	3.110	3.465	0.355	3.110	0.121
CAM-B3LYP	3.135	3.534	3.518	3.409	3.542	3.528	3.135	3.542	0.407	3.135	0.145
M06-HF	-2.948	-2.772	-1.397	-3.189	-1.912	-2.311	-3.189	-1.397	1.792	1.397	0.621
Min	-2.948	-2.772	-1.397	-3.189	-1.912	-2.311					
Max	3.245	3.571	3.529	3.409	3.542	3.533					
Range	6.193	6.343	4.926	6.598	5.454	5.844					
Min x	2.781	2.772	1.397	3.100	1.912	2.311					
S.D.	1.56	1.602	1.247	1.678	1.384	1.483					

Table B10: Percent deviation of TCNE AEA's from Experimental Value ( $3.17 \pm 0.2\text{eV}$ )

	BS1	BS2	BS3	BS4	BS5	BS6	Min	Max	Range	Min x	S.D
BLYP	-12.28	2.46	2.19	-2.23	3.02	2.45	-12.28	3.02	15.3	2.19	5.45
BP86	-1.15	10.34	10.18	6.84	11.13	10.57	-1.15	11.13	12.28	1.15	4.31
HCTH	-0.88	11.12	11.33	7.33	11.68	11.44	-0.88	11.68	12.56	0.88	4.52
M06-L	0.32	7.47	7.02	2.17	7.01	6.51	0.32	7.02	6.70	0.32	2.78
PBE	-5.03	7.22	7.20	3.24	7.61	7.47	-5.03	7.61	12.64	3.24	4.57
TPSS	-5.48	4.72	5.58	1.98	6.15	5.58	-5.48	6.15	11.63	1.98	4.06
TPSSh	-2.99	6.65	7.14	3.72	7.61	7.06	-2.99	7.61	10.60	2.99	3.74
B3LYP	-2.36	9.95	9.69	5.99	10.40	9.83	-2.36	10.4	12.76	2.36	4.54
PBE0	1.01	10.52	10.54	7.28	10.97	10.63	1.01	10.97	9.96	1.01	3.57
M06	2.35	12.65	11.11	4.15	10.62	10.29	2.35	12.65	10.30	2.35	3.84
BH&HLYP	-1.41	8.58	8.27	5.06	8.70	8.19	-1.41	8.70	10.11	1.41	3.64
M06-2X	-1.89	7.60	7.45	7.14	9.31	9.01	-1.89	9.31	11.2	1.89	3.81
CAM-B3LYP	-1.10	11.48	10.97	7.54	11.75	11.3	-1.10	11.75	12.85	1.10	4.59
M06-HF	-	-	-	-	-	-	-	-	-	-	-
Min	-12.28	2.46	2.19	-2.23	3.02	2.45					
Max	2.35	12.65	11.33	7.54	11.75	11.44					
Range	14.63	10.19	9.14	9.77	8.73	8.99					
Min x	0.32	2.46	2.19	1.98	3.02	2.45					
S.D	3.54	2.78	2.55	2.76	2.47	2.52					

Table B11: AEA's of TCNQ (eV) with chosen methods.

	BS1	BS2	BS3	BS4	BS5	BS6	Min	Max	Range	Min x	S.D.
BLYP	-7.30	–	3.89	0.42	4.82	4.28	-7.39	4.82	12.21	0.42	4.53
BP86	3.17	–	11.82	9.24	12.8	12.29	3.17	12.80	9.63	3.17	3.56
HCTH	3.71	–	13.19	9.75	13.49	13.19	3.71	13.49	9.78	3.71	3.74
M06-L	3.83	–	8.88	5.12	9.33	8.68	3.83	9.33	5.50	3.83	2.25
PBE	-0.15	–	9.24	6.04	9.96	9.54	-0.15	9.96	10.11	-0.15	3.80
TPSS	-1.11	–	7.33	4.40	7.93	7.39	-1.11	7.92	9.03	-1.11	3.38
TPSSh	1.41	–	9.15	6.28	6.28	9.06	1.40	9.15	7.75	1.41	2.81
B3LYP	2.27	–	11.61	8.53	12.29	11.73	2.27	12.29	10.02	2.27	3.75
PBE0	5.68	–	13.01	10.14	13.43	12.95	5.68	13.43	7.75	5.68	2.93
M06	6.82	–	13.34	7.81	13.49	12.95	6.82	13.49	6.67	6.82	2.93
BH&HLYP	2.24	–	9.87	6.79	10.17	9.45	2.24	10.17	7.93	2.24	2.98
M06-2X	5.06	–	12.44	11.7	13.85	13.28	5.05	13.85	8.80	5.06	3.19
CAM-B3LYP	4.34	–	13.73	10.59	14.3	13.67	4.33	14.29	9.96	4.34	3.73
M06-HF	4.67	–	13.88	16.03	16.6	16.21	4.66	16.60	11.94	4.67	4.50
Min	-7.30	–	3.89	0.42	4.82	4.28					
Max	6.82	–	13.88	16.03	16.60	16.21					
Range	14.12	–	9.99	15.61	11.78	11.93					
Min x	0.15	–	3.89	0.42	4.82	4.28					
S.D.	3.43	–	2.79	3.60	3.23	3.00					

Table B12: Percent deviation of TCNQ AEA's from Experimental Value ( $3.343 \pm 0.001\text{eV}$ )

	BS1	BS2	BS3	BS4	BS5	BS6	Min	Max	Range	Min x	S.D.
BLYP	-7.30	–	3.89	0.42	4.82	4.28	-7.39	4.82	12.21	0.42	4.53
BP86	3.17	–	11.82	9.24	12.8	12.29	3.17	12.80	9.63	3.17	3.56
HCTH	3.71	–	13.19	9.75	13.49	13.19	3.71	13.49	9.78	3.71	3.74
M06-L	3.83	–	8.88	5.12	9.33	8.68	3.83	9.33	5.50	3.83	2.25
PBE	-0.15	–	9.24	6.04	9.96	9.54	-0.15	9.96	10.11	-0.15	3.80
TPSS	-1.11	–	7.33	4.4	7.93	7.39	-1.11	7.92	9.03	-1.11	3.38
TPSSh	1.41	–	9.15	6.28	6.28	9.06	1.401	9.15	7.75	1.41	2.81
B3LYP	2.27	–	11.61	8.53	12.29	11.73	2.27	12.29	10.02	2.27	3.75
PBE0	5.68	–	13.01	10.14	13.43	12.95	5.68	13.43	7.75	5.68	2.93
M06	6.82	–	13.34	7.81	13.49	12.95	6.82	13.49	6.67	6.82	2.93
BH&HLYP	2.24	–	9.87	6.79	10.17	9.45	2.24	10.17	7.93	2.24	2.98
M06-2X	5.06	–	12.44	11.7	13.85	13.28	5.05	13.85	8.80	5.06	3.19
CAM-B3LYP	4.34	–	13.73	10.59	14.30	13.67	4.33	14.29	9.96	4.34	3.73
M06-HF	4.67	–	13.88	16.03	16.60	16.21	4.66	16.60	11.94	4.67	4.50
Min	-7.30	–	3.89	0.42	4.82	4.28					
Max	6.82	–	13.88	16.03	16.60	16.21					
Range	14.12	–	9.99	15.61	11.78	11.93					
Min x	0.15	–	3.89	0.42	4.82	4.28					
S.D.	3.43	–	2.79	3.60	3.23	3.00					

Table B13: Post-HF AEA's calculated by Milian *et. al.* and their percent deviation from the literature value (TCNE:  $3.17 \pm 0.2\text{eV}$ , TCNQ:  $3.343 \pm 0.001\text{eV}$ )

TCNE	AEA (eV)	% Dev.
MP2/BS1	1.70	-46.37
MP2/BS2	2.17	-31.55
PMP2/BS1	2.18	-31.23
PMP2/BS2	2.65	-16.40
CASSCF/ANO	1.66	-47.63
CCSD/BS2	2.99	-5.68
CCSD/aug-cc-pvDZ <sup>[1]</sup>	3.00	-5.36
CCSD(T)/aug-cc-pvDZ <sup>[1]</sup>	2.94	-7.26
CASPT-2/ANO	3.19	0.63
TCNQ		
CCSD(T)/aug'-cc-pvDZ <sup>[1]</sup>	3.22	-3.68
MP2/6-31G(d)	2.19	-34.49
MP2/6-311G(d,p)	2.46	-26.41
MP2/6-311++G(d,p)	2.69	-19.53
MP2/BS1	2.39	-28.51
MP2/BS2	2.85	-14.75
PMP2/6-31G(d)	2.72	-18.64
PMP2/6-311G(d,p)	3.02	-9.66
PMP2/6-311++G(d,p)	3.23	-3.38
PMP2/BS1	2.94	-12.06
PMP2/BS2	3.37	0.81

[1] single point calculation on B3LYP/aug-cc-pvDZ geometry

Table B14: Percent deviation of chosen methods from experimental bond length of silene

	BS1	BS2	BS3	BS4	BS5	BS6	Min	Max	Min x	S. D.
BLYP	1.48	1.65	1.31	0.92	1.06	0.77	0.77	1.65	0.77	0.31
BP86	1.39	1.51	1.17	0.80	0.92	0.63	0.63	1.51	0.63	0.31
HCTH	1.02	1.14	0.82	0.46	0.54	0.28	0.28	1.14	0.28	0.31
M06-L	0.48	0.52	0.08	-0.20	-0.17	-0.40	-0.40	0.52	0.08	0.34
PBE	1.35	1.47	1.14	0.79	0.89	0.61	0.61	1.47	0.61	0.31
TPSS	1.12	1.24	0.92	0.55	0.67	0.38	0.38	1.24	0.38	0.31
TPSSh	0.80	0.92	0.59	0.24	0.35	0.06	0.06	0.92	0.06	0.30
B3LYP	0.66	0.81	0.48	0.11	0.23	-0.05	-0.05	0.81	0.05	0.30
PBE0	0.49	0.60	0.28	-0.05	0.03	-0.23	-0.23	0.60	0.05	0.30
M06	0.18	0.29	-0.09	-0.46	-0.38	-0.61	-0.61	0.29	0.09	0.33
BHandHLYP	-0.18	-0.05	-0.36	-0.68	-0.59	-0.85	-0.85	-0.05	0.05	0.28
M06-2X	0.10	0.25	-0.08	-0.35	-0.23	-0.50	-0.50	0.25	0.08	0.26
CAM-B3LYP	-0.04	0.12	-0.23	-0.56	-0.45	-0.71	-0.71	0.12	0.04	0.29
M06-HF	-0.12	0.11	-0.11	-0.40	-0.25	-0.58	-0.58	0.11	0.11	0.22
Min	-0.18	-0.05	-0.36	-0.68	-0.59	-0.85				
Max	1.48	1.65	1.31	0.92	1.06	0.77				
Min x	0.04	0.05	0.08	0.05	0.03	0.05				
S. D.	0.56	0.56	0.55	0.53	0.54	0.53				

Table B15: Lengths of a selection of Si=Si bonds from Chapter 5 Reference 39.

	Si=Si (Å)
(Mes) <sub>2</sub> Si=Si(Mes) <sub>2</sub>	2.1433
	2.147
	2.169
	2.145
(Trip) <sub>2</sub> Si=Si(Trip)(Ph)	2.174
1,4-{Trip <sub>2</sub> Si=SiTrip} <sub>2</sub> C <sub>6</sub> H <sub>4</sub>	2.1673
(Dep) <sub>2</sub> Si=Si(Dep) <sub>2</sub>	2.1403
{Trip <sub>2</sub> Si=SiTrip} <sub>2</sub>	2.175
<sup>t</sup> BuMe <sub>2</sub> Si <sub>2</sub> =Si=Si{ <sup>i</sup> Pr <sub>3</sub> Si} <sub>2</sub>	2.201
Avg.	2.163
S.D.	±0.019

Table B16: Percent deviation of chosen methods from CCSD(T)-F12/aug-cc-pv(d+tz) value of disilene

	BS1	BS2	BS3	BS4	BS5	BS6	Min	Max	Min x	S. D.
BLYP	-0.31	-0.27	-0.37	-0.68	-0.56	-0.79	-0.79	-0.27	0.27	0.19
BP86	-0.54	-0.52	-0.65	-0.95	-0.82	-1.07	-1.07	-0.52	0.52	0.21
HCTH	-0.91	-0.83	-0.97	-1.11	-1.06	-1.20	-1.20	-0.83	0.58	0.12
M06-L	-1.54	-1.52	-1.81	-1.91	-1.92	-2.03	-2.03	-1.52	0.58	0.19
PBE	-0.61	-0.58	-0.70	-0.97	-0.84	-1.07	-1.07	-0.58	0.58	0.18
TPSS	-0.89	-0.89	-1.07	-1.23	-1.18	-1.34	-1.34	-0.89	0.89	0.17
TPSSh	-1.16	-1.13	-1.31	-1.51	-1.42	-1.62	-1.62	-1.13	1.07	0.18
B3LYP	-1.11	-1.07	-1.20	-1.46	-1.36	-1.53	-1.53	-1.07	1.07	0.17
PBE0	-1.37	-1.31	-1.48	-1.62	-1.59	-1.74	-1.74	-1.31	1.31	0.15
M06	-1.48	-1.44	-1.64	-1.93	-1.86	-2.07	-2.07	-1.44	1.44	0.23
BHandHLYP	-1.87	-1.79	-1.99	-2.18	-2.13	-2.30	-2.30	-1.79	1.79	0.18
M06-2X	-1.72	-1.66	-1.84	-1.99	-1.95	-2.10	-2.10	-1.66	1.66	0.15
CAM-B3LYP	-1.84	-2.23	-2.38	-2.01	-1.93	-2.28	-2.38	-1.84	1.84	0.20
M06-HF	-1.95	-2.14	-1.91	-2.24	-2.20	-2.34	-2.34	-1.91	1.91	0.15
Min	-1.95	-2.23	-2.38	-2.24	-2.20	-2.34				
Max	-0.31	-0.27	-0.37	-0.68	-0.56	-0.79				
Min x	0.31	0.27	0.37	0.68	0.56	0.79				
S. D.	0.51	0.57	0.56	0.49	0.51	0.50				

Table B17: Percent deviation of chosen methods from experimental Si-CN bond length

	BS1	BS2	BS3	BS4	BS5	BS6	Min	Max	Min x	S. D.
BLYP	2.90	2.94	2.43	2.29	2.38	2.11	2.11	2.94	2.11	0.31
BP86	2.68	2.65	2.16	2.03	2.07	1.82	1.82	2.68	1.82	0.32
HCTH	2.57	2.62	2.13	2.00	2.01	1.78	1.78	2.62	1.78	0.31
M06L	2.10	2.08	1.53	1.46	1.50	1.26	1.26	2.10	1.26	0.32
PBE	2.53	2.55	2.06	1.92	1.95	1.71	1.71	2.55	1.71	0.31
TPSS	2.44	2.48	1.99	1.81	1.87	1.61	1.61	2.48	1.61	0.32
TPSSh	2.32	2.39	1.89	1.73	1.76	1.51	1.51	2.39	1.51	0.32
B3LYP	2.47	2.50	2.00	1.88	1.94	1.69	1.69	2.50	1.69	0.30
PBE0	2.21	2.24	1.76	1.63	1.65	1.42	1.42	2.24	1.42	0.30
M06	2.52	2.51	2.00	1.82	1.87	1.66	1.66	2.52	1.66	0.33
BHandHLYP	2.16	2.19	1.68	1.59	1.62	1.38	1.38	2.19	1.38	0.30
M06-2X	2.47	2.51	2.01	1.86	1.93	1.69	1.69	2.51	1.69	0.31
CAM-B3LYP	1.75	2.26	1.69	1.51	1.81	2.30	1.51	2.30	1.51	0.29
M06-HF	2.74	2.84	2.41	2.02	2.21	1.85	1.85	2.84	1.85	0.36
Min	1.75	2.08	1.53	1.46	1.50	1.26				
Max	2.90	2.94	2.43	2.29	2.38	2.30				
Min x	1.75	2.08	1.53	1.46	1.50	1.26				
S. D.	0.28	0.23	0.25	0.22	0.22	0.27				

Table B18: Percent deviation of chosen methods from experimental SiC-N bond length

	BS1	BS2	BS3	BS4	BS5	BS6	Min	Max	Min x	S.D.
BLYP	0.59	0.52	0.60	-0.43	-0.12	-0.45	-0.45	0.60	0.12	0.46
BP86	0.68	0.58	0.63	-0.32	-0.03	-0.35	-0.35	0.68	0.03	0.44
HCTH	0.09	0.03	0.03	-0.79	-0.51	-0.83	-0.83	0.09	0.03	0.39
M06-L	-0.03	-0.15	-0.11	-0.99	-0.68	-1.02	-1.02	-0.03	0.03	0.42
PBE	0.62	0.55	0.58	-0.32	-0.06	-0.36	-0.36	0.62	0.06	0.43
TPSS	0.38	0.31	0.33	-0.59	-0.30	-0.64	-0.64	0.38	0.30	0.44
TPSSh	-0.09	-0.15	-0.14	-1.02	-0.75	-1.09	-1.09	-0.09	0.09	0.43
B3LYP	-0.45	-0.52	-0.46	-1.42	-1.14	-1.46	-1.46	-0.45	0.45	0.44
PBE0	-0.57	-0.62	-0.61	-1.45	-1.21	-1.50	-1.50	-0.57	0.57	0.41
M06	-0.44	-0.56	-0.50	-1.56	-1.25	-1.53	-1.56	-0.44	0.44	0.48
BHandHLYP	-1.63	-1.68	-1.66	-2.54	-2.27	-2.59	-2.59	-1.63	1.63	0.42
M06-2X	-0.91	-0.95	-0.93	-1.75	-1.55	-1.82	-1.82	-0.91	0.91	0.40
CAM-B3LYP	-1.68	-0.98	-1.94	-1.98	-0.99	-1.05	-1.98	-0.98	0.98	0.44
M06-HF	-1.76	-1.76	-1.67	-2.56	-2.44	-2.66	-2.66	-1.67	1.67	0.42
Min	-1.76	-1.76	-1.94	-2.56	-2.44	-2.66				
Max	0.68	0.58	0.63	-0.32	-0.03	-0.35				
Min x	0.03	0.03	0.03	0.32	0.03	0.35				
S.D.	0.82	0.74	0.84	0.73	0.74	0.72				

Table B19: Energetics of 1Si TCNE anion potential energy surfaces. Values (in kcal/mol) relative to surface minimum.

BS1	C <sub>2v</sub>	C <sub>s</sub>	C <sub>2</sub>	C <sub>1</sub>
BLYP	10.25	0.00	–	–
BP86	9.02	0.00	–	–
HCTH	8.15	0.00	–	–
M06-L	9.42	0.00	–	–
PBE	8.66	0.00	–	–
TPSS	10.25	0.00	–	–
TPSSh	10.44	0.00	–	–
B3LYP	10.50	0.00	–	–
PBE0	9.33	0.00	–	–
M06	10.06	0.00	–	–
BHandHLYP	11.52	0.00	–	–
M06-2X	10.53	0.03	10.43	0.00
CAM-B3LYP	10.789	0.00(1)	10.788	0.000
M06-HF	10.06	0.00	–	–
<b>BS6</b>				
BLYP	8.66	0.00	–	–
BP86	7.64	0.00	–	–
HCTH	6.97	0.00	–	–
M06-L	7.81	0.00	–	–
PBE	7.40	0.00	–	–
TPSS	9.05	0.00	–	–
TPSSh	9.29	0.00	–	–
B3LYP	9.03	0.00	–	–
PBE0	8.19	0.00	–	–
M06	8.50	0.00	–	–
BHandHLYP	10.29	0.00(1)	10.28	0.00
M06-2X	9.02	0.03	8.76	0.00
CAM-B3LYP	9.49	0.00(2)	9.48	0.00
M06-HF	11.13	0.06	8.33	0.00

Table B20: Imaginary frequencies ( $\text{cm}^{-1}$ ) for 1Si TCNE anion PES

BS1	$C_{2v}$		$C_2$
	$b_1$	$a_2$	$b$
BLYP	262 <i>i</i>	–	–
BP86	249 <i>i</i>	–	–
HCTH	252 <i>i</i>	–	–
M06-L	234 <i>i</i>	–	–
PBE	243 <i>i</i>	–	–
TPSS	272 <i>i</i>	–	–
TPSSh	280 <i>i</i>	–	–
B3LYP	275 <i>i</i>	–	–
PBE0	266 <i>i</i>	–	–
M06	229 <i>i</i>	–	–
BHandHLYP	308 <i>i</i>	–	–
M06-2X	337 <i>i</i>	15 <i>i</i>	322 <i>i</i>
CAM-B3LYP	292 <i>i</i>	–	292 <i>i</i>
M06-HF	229 <i>i</i>	–	–
BS6			
BLYP	256 <i>i</i>	–	–
BP86	242 <i>i</i>	–	–
HCTH	246 <i>i</i>	–	–
M06-L	231 <i>i</i>	–	–
PBE	237 <i>i</i>	–	–
TPSS	270 <i>i</i>	–	–
TPSSh	279 <i>i</i>	–	–
B3LYP	270 <i>i</i>	–	–
PBE0	262 <i>i</i>	–	–
M06	228 <i>i</i>	–	–
BHandHLYP	308 <i>i</i>	7 <i>i</i>	305 <i>i</i>
M06-2X	335 <i>i</i>	15 <i>i</i>	314 <i>i</i>
CAM-B3LYP	289 <i>i</i>	5 <i>i</i>	288 <i>i</i>
M06-HF	508 <i>i</i>	15 <i>i</i>	726 <i>i</i>

Table B21: Energetics of [1Si TCNQ]<sup>-</sup> anion potential energy surfaces. Values (in kcal/mol) relative to surface minimum.

BS1	C <sub>2v</sub>	C <sub>s</sub>
BLYP	8.62	0.00
BP86	7.44	0.00
HCTH	6.53	0.00
M06-L	7.80	0.00
PBE	7.11	0.00
TPSS	8.50	0.00
TPSSh	8.63	0.00
B3LYP	8.79	0.00
PBE0	7.47	0.00
M06	8.47	0.00
BHandHLYP	9.24	0.00
M06-2X	8.37	0.00
CAM-B3LYP	8.32	0.00
M06-HF	8.47	0.00
BS6		
BLYP	7.27	0.00
BP86	6.27	0.00
HCTH	5.51	0.00
M06-L	6.53	0.00
PBE	6.02	0.00
TPSS	7.51	0.00
TPSSh	7.65	0.00
B3LYP	7.48	0.00
PBE0	6.45	0.00
M06	7.09	0.00
BHandHLYP	8.08	0.00
M06-2X	6.71	0.00
CAM-B3LYP	7.17	0.00
M06-HF	8.31	0.00

Table B22: Imaginary frequencies ( $\text{cm}^{-1}$ ) for  $[1\text{Si TCNQ}]^-$  PES

		$C_{2v}$
BS1		$b_1$
	BLYP	219 <i>i</i>
	BP86	204 <i>i</i>
	HCTH	204 <i>i</i>
	M06-L	195 <i>i</i>
	PBE	199 <i>i</i>
	TPSS	224 <i>i</i>
	TPSSh	230 <i>i</i>
	B3LYP	228 <i>i</i>
	PBE0	217 <i>i</i>
	M06	189 <i>i</i>
	BHandHLYP	257 <i>i</i>
	M06-2X	285 <i>i</i>
	CAM-B3LYP	241 <i>i</i>
	M06-HF	189 <i>i</i>
BS6		
	BLYP	213 <i>i</i>
	BP86	199 <i>i</i>
	HCTH	200 <i>i</i>
	M06-L	191 <i>i</i>
	PBE	194 <i>i</i>
	TPSS	223 <i>i</i>
	TPSSh	231 <i>i</i>
	B3LYP	226 <i>i</i>
	PBE0	216 <i>i</i>
	M06	188 <i>i</i>
	BHandHLYP	261 <i>i</i>
	M06-2X	286 <i>i</i>
	CAM-B3LYP	242 <i>i</i>
	M06-HF	502 <i>i</i>

**Table B23:** Energetics of 2Si TCNE potential energy surfaces. Values (in kcal/mol) relative to surface minimum.

BS1	D <sub>2h</sub>	C <sub>2h</sub>
BLYP	4.30	0.00
BP86	3.34	0.00
HCTH	2.20	0.00
M06-L	2.49	0.00
PBE	2.93	0.00
TPSS	2.79	0.00
TPSSh	2.46	0.00
B3LYP	3.28	0.00
PBE0	2.10	0.00
M06	4.18	0.00
BHandHLYP	2.20	0.00
M06-2X	3.01	0.00
CAM-B3LYP	2.12	0.00
M06-HF	3.44	0.00
<b>BS6</b>		
BLYP	3.50	0.00
BP86	2.65	0.00
HCTH	1.75	0.00
M06-L	1.92	0.00
PBE	2.36	0.00
TPSS	2.25	0.00
TPSSh	1.94	0.00
B3LYP	2.56	0.00
PBE0	1.58	0.00
M06	3.46	0.00
BHandHLYP	1.56	0.00
M06-2X	2.20	0.00
CAM-B3LYP	1.51	0.00
M06-HF	2.02	0.00

Table B24: Imaginary frequencies ( $\text{cm}^{-1}$ ) for 2Si TCNE PES

BS1	$b_{2g}$
BLYP	150 <i>i</i>
BP86	136 <i>i</i>
HCTH	117 <i>i</i>
M06-L	116 <i>i</i>
PBE	129 <i>i</i>
TPSS	128 <i>i</i>
TPSSh	122 <i>i</i>
B3LYP	134 <i>i</i>
PBE0	114 <i>i</i>
M06	141 <i>i</i>
BHandHLYP	115 <i>i</i>
M06-2X	125 <i>i</i>
CAM-B3LYP	113 <i>i</i>
M06-HF	145 <i>i</i>
BS6	
BLYP	136 <i>i</i>
BP86	123 <i>i</i>
HCTH	107 <i>i</i>
M06-L	101 <i>i</i>
PBE	117 <i>i</i>
TPSS	116 <i>i</i>
TPSSh	111 <i>i</i>
B3LYP	122 <i>i</i>
PBE0	102 <i>i</i>
M06	133 <i>i</i>
BHandHLYP	104 <i>i</i>
M06-2X	109 <i>i</i>
CAM-B3LYP	102 <i>i</i>
M06-HF	127 <i>i</i>

**Table B25:** Energetics of [2Si TCNE]<sup>-</sup> potential energy surfaces. Values (in kcal/mol) relative to surface minimum.

BS1	D <sub>2h</sub>	C <sub>2h</sub>	C <sub>2v</sub>	C <sub>s</sub>	C <sub>2</sub>	D <sub>2</sub>	C <sub>1</sub>
BLYP	26.72	0.00(2)	15.61	0.01	0.00	25.04	–
BP86	24.61	0.00(2)	14.73	0.01	0.00	22.75	–
HCTH	22.98	0.01	13.32	0.02	0.00	21.34	–
M06-L	23.97	0.06	14.36	0.00	14.08	22.33	0.00(01)
PBE	23.92	0.00(1)	14.29	10.16	0.00	22.05	–
TPSS	25.57	0.00(3)	14.77	10.19	0.00	23.48	0.01
TPSSh	26.54	0.00	15.31	10.13	0.00(2)	24.32	0.00(3)
B3LYP	28.25	0.00	16.55	10.54	0.00(01)	26.29	0.01
PBE0	26.47	0.00	15.73	9.69	0.00	24.25	0.01
M06	29.19	0.05	17.64	9.52	17.35	27.09	0
BH&HLYP	31.43	0.00	18.03	10.14	17.70	29.02	0.01
M06-2X	31.82	0.03	18.53	8.45	0.09	28.44	0.00
CAM-B3LYP	30.08	0.00	17.57	9.81	17.25	27.77	0.00(5)
M06-HF	39.57	0.08	21.92	7.07	21.49	33.80	0.00
<b>BS6</b>							
BLYP	24.187	0.000	14.558	0.008	14.030	22.397	–
BP86	22.254	0.000	13.698	0.006	13.076	20.284	0.006
HCTH	20.833	0.010	12.299	0.018	0.000	19.073	–
M06-L	21.889	0.059	13.448	0.000	0.009	20.167	–
PBE	21.751	0.000	13.338	0.006	12.771	19.776	0.007
TPSS	23.474	0.000	13.756	10.011	13.176	21.290	0.005
TPSSh	24.392	0.005	14.225	9.982	0.000	22.094	0.010
B3LYP	25.668	0.000	15.326	0.007	0.007	23.630	–
PBE0	24.121	0.001	14.540	0.006	0.000	21.850	–
M06	27.171	0.043	16.536	0.000	0.008	24.951	–
BH&HLYP	28.727	0.000	16.558	10.074	16.101	26.301	0.004
M06-2X	28.860	0.029	17.117	7.971	0.064	25.648	0.000
CAM-B3LYP	27.434	0.000	16.219	9.781	15.757	25.074	0.003
M06-HF	34.286	0.000	19.486	6.586	0.021	29.314	2.620

Table B26: Imaginary frequencies ( $\text{cm}^{-1}$ ) for  $[\text{2Si TCNE}]^-$  PES (BS1).

	$D_{2h}$			$C_{2v}$		$D_2$	
	$b_{2g}$	$b_{3u}$	$a_u$	$b_3$	$a_2$	$b_3$	$b_2$
BLYP	265 <i>i</i>	185 <i>i</i>	42 <i>i</i>	201 <i>i</i>	24 <i>i</i>	227 <i>i</i>	187 <i>i</i>
BP86	254 <i>i</i>	169 <i>i</i>	43 <i>i</i>	196 <i>i</i>	25 <i>i</i>	213 <i>i</i>	172 <i>i</i>
HCTH	250 <i>i</i>	170 <i>i</i>	39 <i>i</i>	191 <i>i</i>	24 <i>i</i>	204 <i>i</i>	176 <i>i</i>
M06-L	252 <i>i</i>	152 <i>i</i>	37 <i>i</i>	155 <i>i</i>	3 <i>i</i>	206 <i>i</i>	167 <i>i</i>
PBE	249 <i>i</i>	162 <i>i</i>	43 <i>i</i>	193 <i>i</i>	25 <i>i</i>	207 <i>i</i>	167 <i>i</i>
TPSS	259 <i>i</i>	180 <i>i</i>	43 <i>i</i>	203 <i>i</i>	25 <i>i</i>	212 <i>i</i>	184 <i>i</i>
TPSSh	263 <i>i</i>	183 <i>i</i>	45 <i>i</i>	219 <i>i</i>	25 <i>i</i>	213 <i>i</i>	188 <i>i</i>
B3LYP	270 <i>i</i>	187 <i>i</i>	44 <i>i</i>	226 <i>i</i>	25 <i>i</i>	226 <i>i</i>	190 <i>i</i>
PBE0	259 <i>i</i>	172 <i>i</i>	45 <i>i</i>	234 <i>i</i>	25 <i>i</i>	210 <i>i</i>	177 <i>i</i>
M06	258 <i>i</i>	151 <i>i</i>	44 <i>i</i>	682 <i>i</i>	12 <i>i</i>	221 <i>i</i>	157 <i>i</i>
BHandHLYP	285 <i>i</i>	207 <i>i</i>	48 <i>i</i>	279 <i>i</i>	25 <i>i</i>	231 <i>i</i>	208 <i>i</i>
M06-2X	297 <i>i</i>	245 <i>i</i>	62 <i>i</i>	268 <i>i</i>	26 <i>i</i>	231 <i>i</i>	216 <i>i</i>
CAM-B3LYP	277 <i>i</i>	193 <i>i</i>	48 <i>i</i>	273 <i>i</i>	24 <i>i</i>	225 <i>i</i>	193 <i>i</i>
M06-HF	542 <i>i</i>	419 <i>i</i>	93 <i>i</i>	404 <i>i</i>	35 <i>i</i>	313 <i>i</i>	290 <i>i</i>

Table B27: Imaginary frequencies ( $\text{cm}^{-1}$ ) for  $[\text{2Si TCNE}]^-$  PES (BS6).

	$D_{2h}$			$C_{2v}$		$D_2$	
	$b_{2g}$	$b_{3u}$	$a_u$	$b_3$	$a_2$	$b_3$	$b_2$
BLYP	253 <i>i</i>	168 <i>i</i>	43 <i>i</i>	178 <i>i</i>	27 <i>i</i>	215 <i>i</i>	174 <i>i</i>
BP86	242 <i>i</i>	153 <i>i</i>	45 <i>i</i>	176 <i>i</i>	29 <i>i</i>	201 <i>i</i>	159 <i>i</i>
HCTH	240 <i>i</i>	156 <i>i</i>	40 <i>i</i>	177 <i>i</i>	26 <i>i</i>	194 <i>i</i>	162 <i>i</i>
M06-L	248 <i>i</i>	146 <i>i</i>	41 <i>i</i>	139 <i>i</i>	13 <i>i</i>	195 <i>i</i>	154 <i>i</i>
PBE	238 <i>i</i>	148 <i>i</i>	44 <i>i</i>	174 <i>i</i>	28 <i>i</i>	196 <i>i</i>	165 <i>i</i>
TPSS	249 <i>i</i>	166 <i>i</i>	44 <i>i</i>	183 <i>i</i>	27 <i>i</i>	202 <i>i</i>	174 <i>i</i>
TPSSh	253 <i>i</i>	170 <i>i</i>	45 <i>i</i>	196 <i>i</i>	27 <i>i</i>	203 <i>i</i>	177 <i>i</i>
B3LYP	259 <i>i</i>	172 <i>i</i>	45 <i>i</i>	199 <i>i</i>	28 <i>i</i>	214 <i>i</i>	177 <i>i</i>
PBE0	249 <i>i</i>	159 <i>i</i>	46 <i>i</i>	207 <i>i</i>	28 <i>i</i>	199 <i>i</i>	165 <i>i</i>
M06	254 <i>i</i>	147 <i>i</i>	47 <i>i</i>	668 <i>i</i>	21 <i>i</i>	211 <i>i</i>	150 <i>i</i>
BHandHLYP	276 <i>i</i>	192 <i>i</i>	48 <i>i</i>	239 <i>i</i>	28 <i>i</i>	220 <i>i</i>	197 <i>i</i>
M06-2X	280 <i>i</i>	218 <i>i</i>	56 <i>i</i>	294 <i>i</i>	27 <i>i</i>	215 <i>i</i>	200 <i>i</i>
CAM-B3LYP	266 <i>i</i>	178 <i>i</i>	49 <i>i</i>	237 <i>i</i>	28 <i>i</i>	213 <i>i</i>	181 <i>i</i>
M06-HF	317 <i>i</i>	293 <i>i</i>	74 <i>i</i>	1510 <i>i</i>	36 <i>i</i>	237 <i>i</i>	230 <i>i</i>

**Table B28:** Energetics of 2Si TCNQ PES. Values (in kcal/mol) relative to surface minimum.

BS1	D <sub>2h</sub>	C <sub>2h</sub>	C <sub>s</sub>	C <sub>2v</sub>	C <sub>s</sub>
BLYP	1.13	0.00	–	0.30	–
BP86	0.60	0.00	–	0.22	–
HCTH	0.21	0.00	–	0.12	–
M06-L	0.56	0.00	–	0.27	0.02
PBE	0.42	0.00	–	0.18	–
TPSS	0.67	0.00	–	0.22	–
TPSSh	0.38	0.00	–	0.15	–
B3LYP	0.38	0.00	–	0.14	0.01
PBE0	0.01	0.00	–	–	–
M06	0.40	0.01	0.00	0.17	0.00(00126)
BH&HLYP	0.00	–	–	–	–
M06-2X	0.00	–	–	–	–
CAM-B3LYP	0.00	–	–	–	–
M06-HF	0.00	–	–	–	–
<b>BS6</b>					
BLYP	0.94	0.00	–	0.25	–
BP86	0.49	0.00	–	0.18	–
HCTH	0.22	0.00	–	0.12	–
M06-L	0.37	0.00	–	0.20	0.02
PBE	0.37	0.00	–	0.15	–
TPSS	0.67	0.00	–	0.20	–
TPSSh	0.41	0.00	–	0.13	–
B3LYP	0.34	0.00	–	0.12	–
PBE0	0.34	0.00	–	0.12	–
M06	0.29	0.00	0.003	0.12	0.00(3)
BH&HLYP	0.00	–	–	–	–
M06-2X	0.00	–	–	–	–
CAM-B3LYP	0.00	–	–	–	–
M06-HF	0.00	–	–	–	–

Table B29: Imaginary frequencies ( $\text{cm}^{-1}$ ) for 2Si TCNQ PES.

		$D_{2h}$	
BS1		$b_{2g}$	$b_{3u}$
	BLYP	$78i$	$69i$
	BP86	$62i$	$50i$
	HCTH	$44i$	$28i$
	M06-L	$63i$	$49i$
	PBE	$54i$	$41i$
	TPSS	$63i$	$52i$
	TPSSh	$53i$	$41i$
	B3LYP	$55i$	$45i$
	PBE0	$19i$	–
	M06	$65i$	$57i$
	BH&HLYP	–	–
	M06-2X	–	–
	CAM-B3LYP	–	–
	M06-HF	–	–
BS6			
	BLYP	$74i$	$65i$
	BP86	$60i$	$47i$
	HCTH	$45i$	$31i$
	M06-L	$52i$	$35i$
	PBE	$53i$	$40i$
	TPSS	$64i$	$54i$
	TPSSh	$55i$	$44i$
	B3LYP	$54i$	$44i$
	PBE0	$25i$	$11i$
	M06	$60i$	$50i$
	BH&HLYP	–	–
	M06-2X	–	–
	CAM-B3LYP	–	–
	M06-HF	–	–

Table B30: Energetics of [2Si TCNQ]<sup>-</sup>PES. Values (in kcal/mol) relative to surface minimum.

BS1	D <sub>2h</sub>	C <sub>2h</sub>	C <sub>s</sub>	C <sub>2v</sub>	C <sub>s</sub>
BLYP	19.93	0.00	–	0.64	–
BP86	0.86	0.00	–	0.56	–
HCTH	16.58	0.00	–	0.54	–
M06-L	18.72	0.00	–	0.65	–
PBE	17.18	0.00	–	0.58	–
TPSS	19.76	0.00	–	0.60	–
TPSSh	20.65	0.00	–	0.57	–
B3LYP	21.55	0.00	–	0.56	–
PBE0	19.65	0.00	–	0.51	–
M06	21.71	0.03	0.00	0.69	0.69
BH&HLYP	26.01	1.21	0.00	1.67	0.36
M06-2X	24.99	1.61	0.00	2.11	0.43
CAM-B3LYP	24.57	1.47	0.00	1.95	0.35
M06-HF	35.88	8.10	0.00	8.40	0.55
BS6					
BLYP	17.97	0.00	–	0.58	–
BP86	16.02	0.00	–	0.54	–
HCTH	15.08	0.00	–	0.46	–
M06-L	17.05	0.00	–	0.60	–
PBE	15.53	0.00	–	0.53	–
TPSS	18.38	0.00	–	0.54	–
TPSSh	19.31	0.00	–	0.50	–
B3LYP	19.79	0.00	–	0.50	–
PBE0	18.11	0.00	–	0.44	–
M06	20.33	0.03	0.00	0.60	0.60
BH&HLYP	24.51	1.28	0.00	1.67	0.34
M06-2X	23.37	2.11	0.00	2.54	0.38
CAM-B3LYP	22.99	1.59	0.00	2.01	0.34
M06-HF	32.46	8.02	0.00	8.28	0.47

Table B31: Imaginary frequencies ( $\text{cm}^{-1}$ ) for  $[\text{2Si TCNQ}]^-$   
PES. BS1

	$D_{2h}$		$C_{2h}$		$C_{2v}$
	$b_{2g}$	$b_{3u}$	$b_u$	$a_u$	$b_2$
BLYP	225 <i>i</i>	225 <i>i</i>	–	–	–
BP86	211 <i>i</i>	212 <i>i</i>	–	–	–
HCTH	208 <i>i</i>	209 <i>i</i>	–	–	–
M06-L	212 <i>i</i>	213 <i>i</i>	–	–	–
PBE	205 <i>i</i>	207 <i>i</i>	–	–	–
TPSS	225 <i>i</i>	226 <i>i</i>	–	–	–
TPSSh	231 <i>i</i>	232 <i>i</i>	–	–	–
B3LYP	233 <i>i</i>	234 <i>i</i>	–	–	–
PBE0	221 <i>i</i>	223 <i>i</i>	–	–	–
M06	214 <i>i</i>	216 <i>i</i>	31 <i>i</i>	4 <i>i</i>	85 <i>i</i>
BH&HLYP	257 <i>i</i>	258 <i>i</i>	208 <i>i</i>	–	214 <i>i</i>
M06-2X	266 <i>i</i>	266 <i>i</i>	48 <i>i</i>	–	35 <i>i</i>
CAM-B3LYP	244 <i>i</i>	246 <i>i</i>	240 <i>i</i>	–	252 <i>i</i>
M06-HF	368 <i>i</i>	365 <i>i</i>	165 <i>i</i>	–	137 <i>i</i>

Table B32: Imaginary frequencies ( $\text{cm}^{-1}$ ) for  $[\text{2Si TCNQ}]^-$   
PES. BS6

	$D_{2h}$		$C_{2h}$	$C_{2v}$
	$b_{2g}$	$b_{3u}$	$b_u$	$b_2$
BLYP	220 <i>i</i>	220 <i>i</i>	–	–
BP86	206 <i>i</i>	207 <i>i</i>	–	–
HCTH	205 <i>i</i>	207 <i>i</i>	–	–
M06-L	213 <i>i</i>	215 <i>i</i>	–	–
PBE	201 <i>i</i>	202 <i>i</i>	–	–
TPSS	223 <i>i</i>	224 <i>i</i>	–	–
TPSSh	229 <i>i</i>	230 <i>i</i>	–	–
B3LYP	231 <i>i</i>	231 <i>i</i>	–	–
PBE0	219 <i>i</i>	230 <i>i</i>	–	–
M06	213 <i>i</i>	214 <i>i</i>	100 <i>i</i>	156 <i>i</i>
BH&HLYP	258 <i>i</i>	259 <i>i</i>	226 <i>i</i>	227 <i>i</i>
M06-2X	258 <i>i</i>	258 <i>i</i>	71 <i>i</i>	68 <i>i</i>
CAM-B3LYP	244 <i>i</i>	243 <i>i</i>	268 <i>i</i>	274 <i>i</i>
M06-HF	284 <i>i</i>	282 <i>i</i>	352 <i>i</i>	338 <i>i</i>

Table B33:  $\langle S^2 \rangle$  values for  $C_{2v}$  structure 1Si TCNE anion. BS1

	C2v
BLYP	0.753
BP86	0.753
HCTH	0.756
M06-L	0.756
PBE	0.753
TPSS	0.755
TPSSh	0.758
B3LYP	0.758
PBE0	0.760
M06	0.757
BHandHLYP	0.772
M06-2X	0.759
CAM-B3LYP	0.763
M06-HF	0.757

Table B34:  $\langle S^2 \rangle$  values for  $C_{2v}$  structure 1Si TCNE anion.BS6

	C2v
BLYP	0.753
BP86	0.754
HCTH	0.758
M06-L	0.757
PBE	0.754
TPSS	0.755
TPSSh	0.758
B3LYP	0.758
PBE0	0.760
M06	0.757
BHandHLYP	0.770
M06-2X	0.760
CAM-B3LYP	0.763
M06-HF	0.762

Table B35:  $\langle S^2 \rangle$  values for  $C_{2v}$  structure 1Si TCNQ anion. BS1

	C2v
BLYP	0.754
BP86	0.754
HCTH	0.757
M06-L	0.757
PBE	0.754
TPSS	0.756
TPSSh	0.761
B3LYP	0.762
PBE0	0.767
M06	0.762
BHandHLYP	0.785
M06-2X	0.770
CAM-B3LYP	0.778
M06-HF	0.762

Table B36:  $\langle S^2 \rangle$  values for  $C_{2v}$  structure 1Si TCNQ anion. BS6

	C2v
BLYP	0.754
BP86	0.754
HCTH	0.759
M06-L	0.758
PBE	0.754
TPSS	0.756
TPSSh	0.760
B3LYP	0.762
PBE0	0.766
M06	0.761
BHandHLYP	0.782
M06-2X	0.769
CAM-B3LYP	0.776
M06-HF	0.775

Table B37:  $\langle S^2 \rangle$  values for  $D_{2h}$  structure 2Si TCNE anion. BS1

	D2h
BLYP	0.753
BP86	0.753
HCTH	0.756
M06-L	0.756
PBE	0.753
TPSS	0.755
TPSSh	0.758
B3LYP	0.758
PBE0	0.761
M06	0.757
BH&HLYP	0.774
M06-2X	0.759
CAM-B3LYP	0.767
M06-HF	0.761

Table B38:  $\langle S^2 \rangle$  values for  $D_{2h}$  structure 2Si TCNE anion. BS6

	D2h
BLYP	0.753
BP86	0.754
HCTH	0.757
M06-L	0.757
PBE	0.754
TPSS	0.755
TPSSh	0.759
B3LYP	0.759
PBE0	0.762
M06	0.758
BH&HLYP	0.775
M06-2X	0.761
CAM-B3LYP	0.769
M06-HF	0.766

Table B39:  $\langle S^2 \rangle$  values for  $D_{2h}$  structure 2Si TCNQ anion. BS1

	$D_{2h}$
BLYP	0.755
BP86	0.756
HCTH	0.761
M06-L	0.761
PBE	0.756
TPSS	0.758
TPSSh	0.767
B3LYP	0.771
PBE0	0.783
M06	0.773
BH&HLYP	0.826
M06-2X	0.795
CAM-B3LYP	0.826
M06-HF	0.834

Table B40:  $\langle S^2 \rangle$  values for  $D_{2h}$  structure 2Si TCNQ anion. BS6

	$D_{2h}$
BLYP	0.755
BP86	0.757
HCTH	0.764
M06-L	0.764
PBE	0.757
TPSS	0.760
TPSSh	0.769
B3LYP	0.773
PBE0	0.787
M06	0.777
BH&HLYP	0.833
M06-2X	0.804
CAM-B3LYP	0.835
M06-HF	0.848

Table B41: Relative energies of 2Si TCNQ neutral manifold (kcal/mol) BS1.

		CSS	TBR	OSS
BLYP	D <sub>2h</sub>	2.81	11.24	–
	C <sub>2h</sub>	1.68	3.30	0.00
	C <sub>2v</sub>	1.98	3.27	0.33
BP86	D <sub>2h</sub>	2.67	10.04	2.62
	C <sub>2h</sub>	2.07	3.10	0.00
	C <sub>2v</sub>	2.29	3.07	0.28
HCTH	D <sub>2h</sub>	5.34	9.33	3.98
	C <sub>2h</sub>	5.12	2.27	0.00
	C <sub>2v</sub>	5.24	2.26	0.22
M06-L	D <sub>2h</sub>	4.37	9.96	3.53
	C <sub>2h</sub>	3.81	3.06	0.00
	C <sub>2v</sub>	4.09	3.07	0.32
PBE	D <sub>2h</sub>	2.75	9.79	2.67
	C <sub>2h</sub>	2.33	2.95	0.00
	C <sub>2v</sub>	2.51	2.92	0.27
TPSS	D <sub>2h</sub>	5.22	11.58	4.87
	C <sub>2h</sub>	4.55	2.49	0.00
	C <sub>2v</sub>	4.77	2.47	0.28
TPSSh	D <sub>2h</sub>	8.45	12.09	6.45
	C <sub>2h</sub>	8.06	2.14	0.00
	C <sub>2v</sub>	8.21	2.14	0.25
B3LYP	D <sub>2h</sub>	8.42	11.82	6.12
	C <sub>2h</sub>	8.04	2.20	0.00
	C <sub>2v</sub>	8.17	2.21	0.24
PBE0	D <sub>2h</sub>	11.19	11.21	6.31
	C <sub>2h</sub>	11.18	1.96	0.00
	C <sub>2v</sub>	–	1.98	0.20
M06	D <sub>2h</sub>	7.99	10.94	5.21
	C <sub>2h</sub>	7.59	2.50	0.00
	C <sub>2v</sub>	7.76	2.50	0.24
BHandHLYP	D <sub>2h</sub>	18.96	14.88	9.56
	C <sub>2h</sub>	–	1.97	0.00
	C <sub>2v</sub>	–	2.02	0.20
M06-2X	D <sub>2h</sub>	15.90	14.23	9.95
	C <sub>2h</sub>	–	1.38	0.00
	C <sub>2v</sub>	–	1.43	0.21

CAM-B3LYP	D <sub>2h</sub>	42.75	13.49	8.88
	C <sub>2h</sub>	–	1.71	0.00
	C <sub>2v</sub>	–	1.75	0.20
M06-HF	D <sub>2h</sub>	24.76	20.41	16.78
	C <sub>2h</sub>	–	0.98	0.00
	C <sub>2v</sub>	–	1.06	0.20

Table B42: Relative energies of 2Si TCNQ neutral manifold (kcal/mol) BS6. \*Cs minima

		CSS	TBR	OSS
BLYP	D <sub>2h</sub>	0.94	9.25	–
	C <sub>2h</sub>	0.00	1.64	–
	C <sub>2v</sub>	0.25	1.61	–
BP86	D <sub>2h</sub>	2.70	9.80	2.60
	C <sub>2h</sub>	2.20	3.13	0.00
	C <sub>2v</sub>	2.39	3.11	0.26
HCTH	D <sub>2h</sub>	5.98	8.65	3.80
	C <sub>2h</sub>	5.76	2.06	0.00*
	C <sub>2v</sub>	5.88	2.06	0.00*
M06-L	D <sub>2h</sub>	4.52	9.20	3.28
	C <sub>2h</sub>	4.15	2.60	0.00*
	C <sub>2v</sub>	4.35	2.61	0.00*
PBE	D <sub>2h</sub>	2.86	9.60	2.70
	C <sub>2h</sub>	2.49	3.00	0.00
	C <sub>2v</sub>	2.65	2.98	0.25
TPSS	D <sub>2h</sub>	5.66	11.67	5.18
	C <sub>2h</sub>	4.99	2.48	0.00
	C <sub>2v</sub>	5.19	2.47	0.26
TPSSh	D <sub>2h</sub>	8.65	12.02	6.49
	C <sub>2h</sub>	8.24	1.91	0.00*
	C <sub>2v</sub>	8.37	1.92	0.00*
B3LYP	D <sub>2h</sub>	8.11	11.52	5.84
	C <sub>2h</sub>	7.77	1.99	0.00*
	C <sub>2v</sub>	7.88	2.01	0.00*
PBE0	D <sub>2h</sub>	11.08	11.01	6.14
	C <sub>2h</sub>	11.05	1.80	0.00*
	C <sub>2v</sub>	11.08	1.82	0.00*

M06	D <sub>2h</sub>	7.94	10.56	5.06
	C <sub>2h</sub>	7.65	2.23	0.00*
	C <sub>2v</sub>	7.77	2.24	0.00*
BHandHLYP	D <sub>2h</sub>	18.85	15.14	9.90
	C <sub>2h</sub>	–	1.93	0.00
	C <sub>2v</sub>	–	1.99	0.20
M06-2X	D <sub>2h</sub>	16.45	13.20	9.09
	C <sub>2h</sub>	–	1.20	0.00*
	C <sub>2v</sub>	–	1.25	0.00*
CAM-B3LYP	D <sub>2h</sub>	17.43	13.53	8.96
	C <sub>2h</sub>	–	1.71	0.00
	C <sub>2v</sub>	–	1.77	0.21
M06-HF	D <sub>2h</sub>	25.22	18.12	14.60
	C <sub>2h</sub>	–	0.79	0.00*
	C <sub>2v</sub>	–	0.89	0.00*

Table B43:  $\langle S^2 \rangle$  values for open shell singlet structures.

BS1	D <sub>2h</sub>	C <sub>2h</sub>	C <sub>2v</sub>
BLYP	–	–	–
BP86	0.15	0.74	0.71
HCTH	0.58	0.87	0.76
M06L	0.49	0.80	0.88
PBE	0.20	0.77	0.81
TPSS	0.36	0.86	0.78
TPSSh	0.66	0.92	0.86
B3LYP	0.68	0.92	0.93
PBE0	0.82	0.96	0.93
M06	0.72	0.91	0.97
BHandHLYP	0.96	1.02	0.92
M06-2X	0.88	0.98	1.02
CAM-B3LYP	0.93	1.00	0.99
M06-HF	0.95	1.00	1.00
BS6			
BLYP	–	–	–
BP86	0.209	0.750	0.760
HCTH <sup>[1]</sup>	0.666	0.887	–
M06L <sup>[1]</sup>	0.573	0.838	–
PBE	0.264	0.772	0.781
TPSS	0.410	0.865	0.874
TPSSh <sup>[1]</sup>	0.673	0.933	–
B3LYP <sup>[1]</sup>	0.676	0.929	–
PBE0 <sup>[1]</sup>	0.820	0.964	–
M06 <sup>[1]</sup>	0.730	0.916	–
BHandHLYP	0.949	1.015	1.017
M06-2X <sup>[1]</sup>	0.895	0.988	–
CAM-B3LYP	0.921	0.995	0.998
M06-HF <sup>[1]</sup>	0.965	1.005	–

[1] Second-order saddle points where both modes relax to a C<sub>S</sub>-symmetry (pseudo C<sub>2h</sub>) structure.

Table B44:  $\langle S^2 \rangle$  values for TCNQ triplet state. BS1 and BS6

	BS1	BS6
BLYP	2.01	2.01
BP86	2.01	2.01
HCTH	2.02	2.02
M06-L	2.03	2.02
PBE	2.01	2.01
TPSS	2.02	2.02
TPSSh	2.03	2.03
B3LYP	2.03	2.03
PBE0	2.04	2.04
M06	2.04	2.03
BHandHLYP	2.09	2.08
M06-2X	2.03	2.03
CAM-B3LYP	2.05	2.05
M06-HF	2.04	2.04

Table B45:  $\langle S^2 \rangle$  values for triplet 1Si TCNQ molecules. BS1.

	C <sub>2v</sub>	C <sub>s</sub>
BLYP	2.01	2.01
BP86	2.01	2.01
HCTH	2.02	2.02
M06-L	2.02	2.02
PBE	2.01	2.01
TPSS	2.02	2.02
TPSSh	2.03	2.03
B3LYP	2.03	2.03
PBE0	2.04	2.04
M06	2.03	2.03
BHandHLYP	2.08	2.08
M06-2X	2.03	2.03
CAM-B3LYP	2.05	2.05
M06-HF	2.03	2.03

Table B46:  $\langle S^2 \rangle$  values for triplet 1Si TCNQ molecules.  
BS6.

	C <sub>2v</sub>	C <sub>s</sub>
BLYP	2.01	2.01
BP86	2.01	2.01
HCTH	2.02	2.02
M06-L	2.02	2.02
PBE	2.01	2.01
TPSS	2.02	2.02
TPSSh	2.03	2.03
B3LYP	2.03	2.02
PBE0	2.04	2.03
M06	2.03	2.03
BHandHLYP	2.07	2.07
M06-2X	2.03	2.03
CAM-B3LYP	2.04	2.04
M06-HF	2.03	2.03

Table B47:  $\langle S^2 \rangle$  values for triplet 2Si TCNQ molecules.  
BS1.

	D <sub>2h</sub>	C <sub>2h</sub>	C <sub>2v</sub>
BLYP	2.01	2.01	2.01
BP86	2.01	2.01	2.01
HCTH	2.02	2.01	2.01
M06-L	2.02	2.01	2.01
PBE	2.01	2.01	2.01
TPSS	2.02	2.01	2.01
TPSSh	2.02	2.01	2.01
B3LYP	2.02	2.01	2.01
PBE0	2.03	2.01	2.01
M06	2.02	2.01	2.01
BHandHLYP	2.05	2.02	2.02
M06-2X	2.02	2.01	2.01
CAM-B3LYP	2.03	2.01	2.01
M06-HF	2.02	2.01	2.01

Table B48:  $\langle S^2 \rangle$  values for triplet 2Si TCNQ molecules.

BS6.

	D <sub>2h</sub>	C <sub>2h</sub>	C <sub>2v</sub>
BLYP	2.01	2.01	2.01
BP86	2.01	2.01	2.01
HCTH	2.02	2.01	2.01
M06-L	2.02	2.01	2.01
PBE	2.01	2.01	2.01
TPSS	2.02	2.01	2.01
TPSSh	2.02	2.01	2.01
B3LYP	2.02	2.01	2.01
PBE0	2.02	2.01	2.01
M06	2.02	2.01	2.01
BHandHLYP	2.04	2.02	2.02
M06-2X	2.02	2.01	2.01
CAM-B3LYP	2.03	2.01	2.01
M06-HF	2.03	2.01	2.01

Table B49: Global minima AEA's (eV) for TCNE series (BS1). Negative AEA's omitted from statistical information.

	0Si	1Si	2Si
BLYP	2.781	3.122	3.434
BP86	3.133	3.426	3.746
HCTH	3.142	3.406	3.709
M06-L	3.180	3.452	3.754
PBE	3.010	3.297	3.618
TPSS	2.996	3.343	3.672
TPSSh	3.075	3.413	3.763
B3LYP	3.095	3.411	3.770
PBE0	3.202	3.474	3.849
M06	3.245	3.489	3.864
BHandHLYP	3.125	3.434	3.862
M06-2X	3.110	3.440	3.936
CAM-B3LYP	3.135	3.437	3.870
M06-HF	-2.948	-2.258	4.186
Min	2.781	3.122	3.434
Max	3.245	3.489	4.186
Range	0.464	0.367	0.752
S. D.	0.112	0.093	0.127

Table B50: Global minima AEA's (eV) for TCNE series (BS6). Negative AEA's omitted from statistical information.

	0Si	1Si	2Si
BLYP	3.248	3.481	3.721
BP86	3.505	3.714	3.961
HCTH	3.533	3.719	3.942
M06-L	3.376	3.569	3.801
PBE	3.407	3.612	3.860
TPSS	3.347	3.623	3.875
TPSSh	3.394	3.667	3.936
B3LYP	3.482	3.704	3.982
PBE0	3.507	3.716	4.003
M06	3.496	3.676	3.986
BHandHLYP	3.430	3.666	3.996
M06-2X	3.456	3.723	4.126
CAM-B3LYP	3.528	3.437	4.079
M06-HF	-2.311	3.928	4.448
Min	3.248	3.437	3.721
Max	3.533	3.928	4.448
Range	0.285	0.491	0.727
S. D.	0.080	0.114	0.165

Table B51: Global minima AEA's (eV) for TCNQ series (BS1). Negative AEA's omitted from statistical information.

	0Si	1Si	2Si
BLYP	3.099	3.297	3.532
BP86	3.449	3.426	3.721
HCTH	3.467	3.584	3.560
M06-L	3.471	3.620	3.684
PBE	3.338	3.475	3.581
TPSS	3.306	3.505	3.562
TPSSh	3.390	3.592	3.523
B3LYP	3.419	3.618	3.565
PBE0	3.533	3.687	3.475
M06	3.571	3.727	3.683
BHandHLYP	3.418	3.659	3.280
M06-2X	3.512	3.733	3.488
CAM-B3LYP	3.488	3.706	3.378
M06-HF	3.499	-5.854	3.585
Min	3.099	3.297	3.280
Max	3.571	3.733	3.721
Range	0.472	0.436	0.441
S.D.	0.115	0.151	0.116

Table B52: Global minima AEA's (eV) for TCNQ series (BS6). Negative AEA's omitted from statistical information.

	0Si	1Si	2Si
BLYP	3.486	3.596	3.697
BP86	3.754	3.833	3.893
HCTH	3.784	3.844	3.731
M06-L	3.633	3.709	3.705
PBE	3.662	3.733	3.776
TPSS	3.590	3.732	3.721
TPSSh	3.646	3.795	3.672
B3LYP	3.735	3.858	3.758
PBE0	3.776	3.879	3.617
M06	3.776	3.870	3.785
BHandHLYP	3.659	3.844	3.419
M06-2X	3.787	3.952	3.639
CAM-B3LYP	3.800	3.958	3.580
M06-HF	3.885	4.207	3.807
Min	3.486	3.596	3.419
Max	3.885	4.207	3.893
Range	0.399	0.611	0.474
S.D.	0.100	0.138	0.112

Table B53: Planar geometry AEA's (eV) for TCNE series (BS1). Negative AEA's omitted from statistical information.

	0Si	1Si	2Si
BLYP	2.781	2.678	2.462
BP86	3.133	3.035	2.823
HCTH	3.142	3.052	2.808
M06-L	3.180	3.044	2.822
PBE	3.010	2.921	2.708
TPSS	2.996	2.899	2.708
TPSSh	3.075	2.960	2.684
B3LYP	3.095	2.955	2.686
PBE0	3.202	3.070	2.792
M06	3.245	3.053	2.779
BHandHLYP	3.125	2.935	2.595
M06-2X	3.110	2.983	2.687
CAM-B3LYP	3.135	2.969	2.658
M06-HF	-2.948	-2.695	2.619
Min	2.781	2.678	2.462
Max	3.245	3.070	2.823
Range	0.464	0.392	0.361
S. D.	0.112	0.099	0.098

Table B54: Planar geometry AEA's (eV) for TCNE series (BS6). Negative AEA's omitted from statistical information.

	0Si	1Si	2Si
BLYP	3.248	3.106	2.824
BP86	3.505	3.383	3.111
HCTH	3.533	3.417	3.114
M06-L	3.376	3.230	2.935
PBE	3.407	3.291	3.019
TPSS	3.347	3.231	2.955
TPSSh	3.394	3.264	2.962
B3LYP	3.482	3.312	2.979
PBE0	3.507	3.361	3.026
M06	3.496	3.308	2.958
BHandHLYP	3.43	3.220	2.818
M06-2X	3.456	3.332	2.970
CAM-B3LYP	3.528	3.334	2.955
M06-HF	-2.311	3.445	3.049
Min	3.248	3.106	2.818
Max	3.533	3.445	3.114
Range	0.285	0.340	0.296
S. D.	0.080	0.086	0.084

Table B55: Planar geometry AEA's (eV) for TCNQ series (BS1). Negative AEA's omitted from statistical information.

	0Si	1Si	2Si
BLYP	3.099	2.923	2.717
BP86	3.449	3.275	3.064
HCTH	3.467	3.301	3.014
M06-L	3.471	3.282	3.026
PBE	3.338	3.167	2.952
TPSS	3.306	3.136	2.916
TPSSh	3.390	3.218	2.908
B3LYP	3.419	3.236	2.895
PBE0	3.533	3.363	3.896
M06	3.571	3.360	2.967
BHandHLYP	3.418	3.259	2.566
M06-2X	3.512	3.369	2.836
CAM-B3LYP	3.488	3.346	2.698
M06-HF	3.499	-6.221	2.757
Min	3.099	2.923	2.566
Max	3.571	3.369	3.064
Range	0.472	0.447	0.498
S. D.	0.115	0.118	0.137

Table B56: Planar geometry AEA's (eV) for TCNQ series (BS6). Negative AEA's omitted from statistical information.

	0Si	1Si	2Si
BLYP	3.486	3.281	3.033
BP86	3.754	3.561	3.311
HCTH	3.784	3.604	3.242
M06-L	3.633	3.426	3.107
PBE	3.662	3.472	3.219
TPSS	3.590	3.407	3.149
TPSSh	3.646	3.464	3.116
B3LYP	3.735	3.533	3.154
PBE0	3.776	3.600	3.098
M06	3.776	3.562	3.124
BHandHLYP	3.659	3.494	2.785
M06-2X	3.787	3.661	3.020
CAM-B3LYP	3.800	3.647	2.972
M06-HF	3.885	3.847	3.032
Min	3.486	3.281	2.785
Max	3.885	3.847	3.311
Range	0.399	0.566	0.527
S. D.	0.100	0.131	0.124

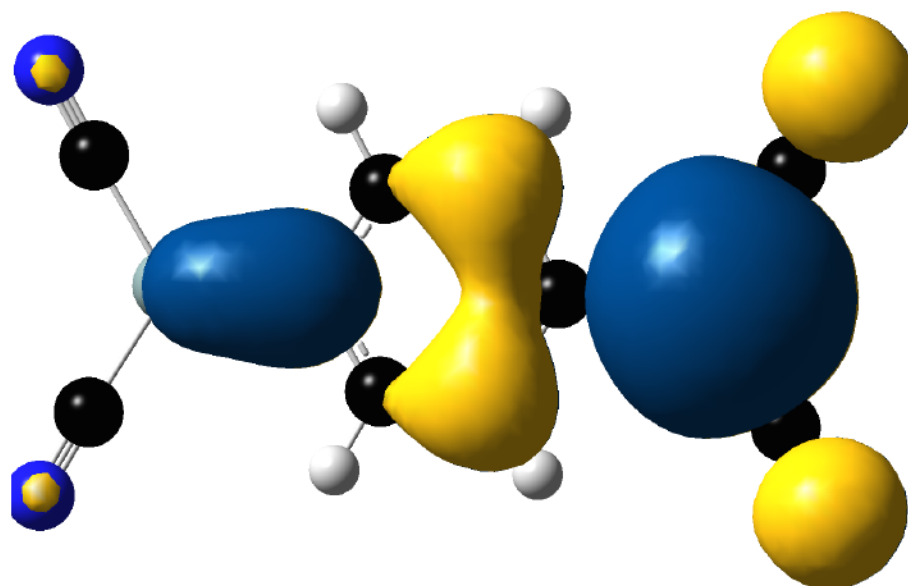


Figure B1: 2Si TCNQ  $\langle S^2 \rangle_{M_S=0}$   $\alpha$ -HOMO. BHandHLYP/6-311++g(2df,pd). 0.001a.u. isosurface

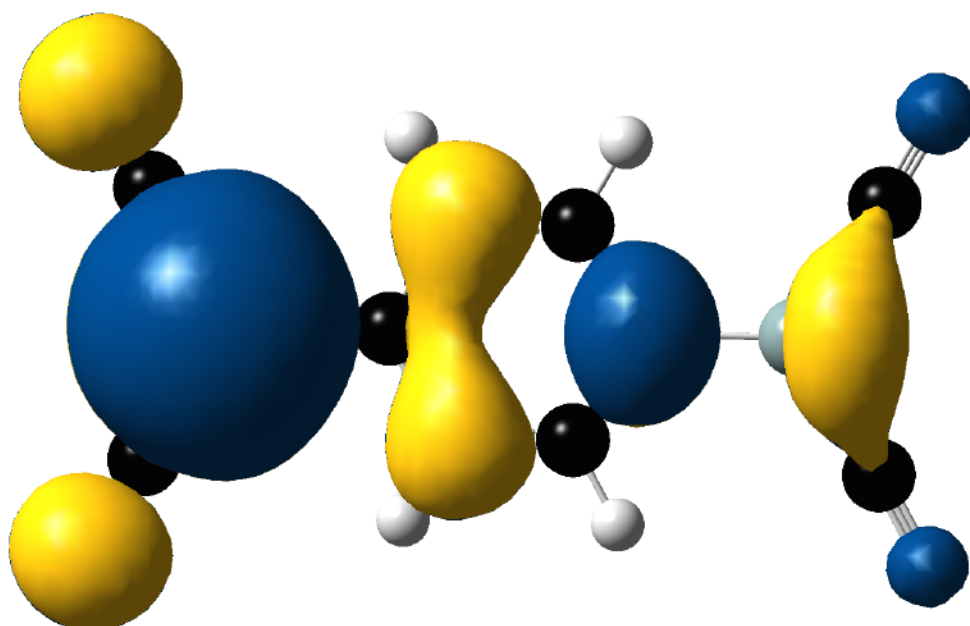


Figure B2: 2Si TCNQ  $\langle S^2 \rangle_{M_S=0}$   $\alpha$ -LUMO. BHandHLYP/6-311++g(2df,pd). 0.001a.u. isosurface

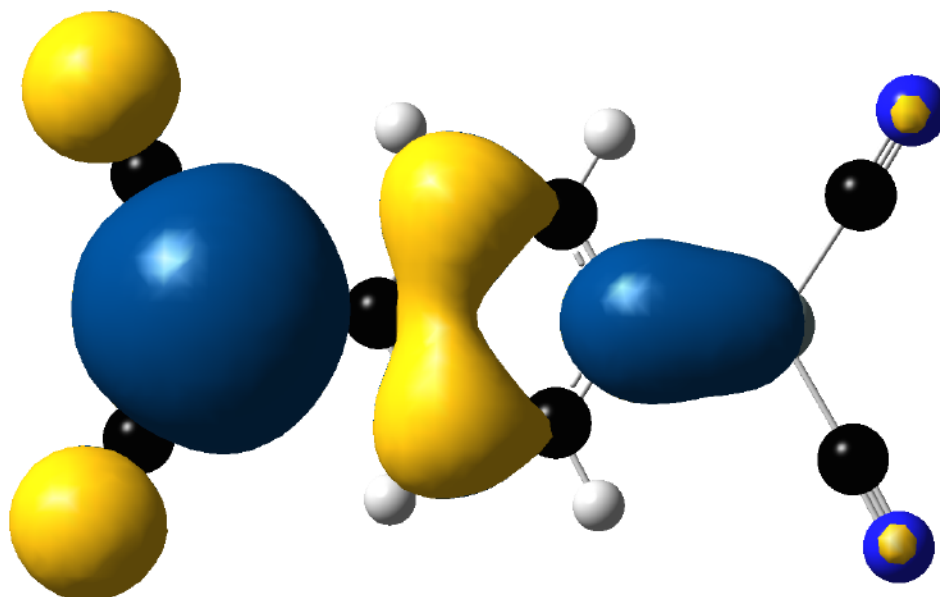


Figure B3: 2Si TCNQ  $\langle S^2 \rangle_{M_S=0}$   $\beta$ -HOMO. BHandHLYP/6-311++g(2df,pd). 0.001a.u. isosurface

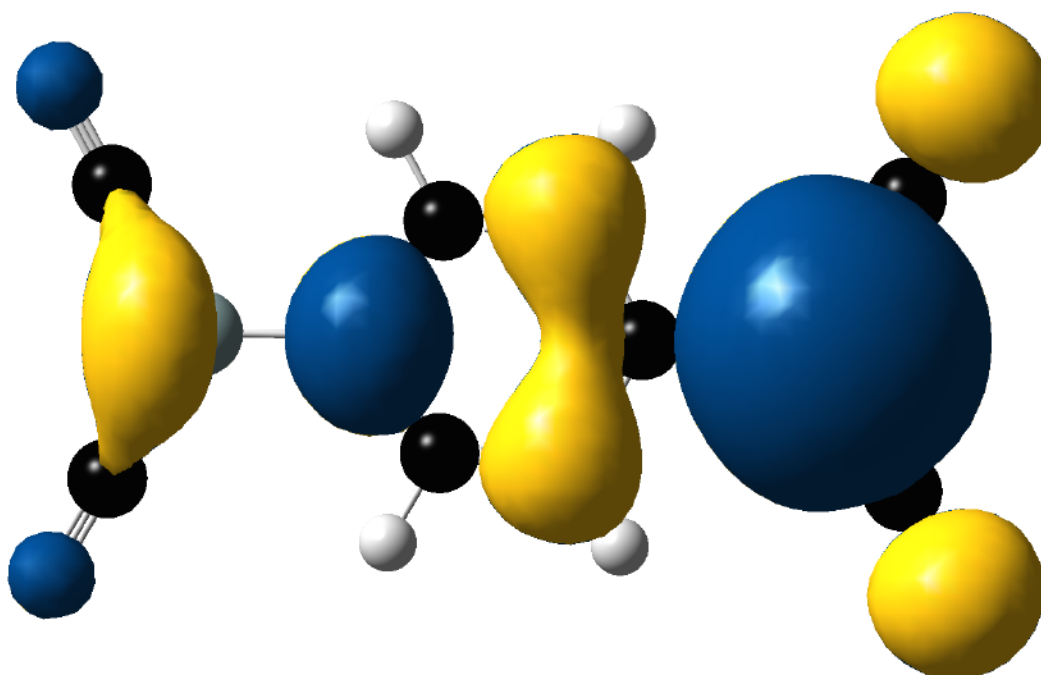


Figure B4: 2Si TCNQ  $\langle S^2 \rangle_{M_S=0}$   $\beta$ -LUMO. BHandHLYP/6-311++g(2df,pd). 0.001a.u. isosurface

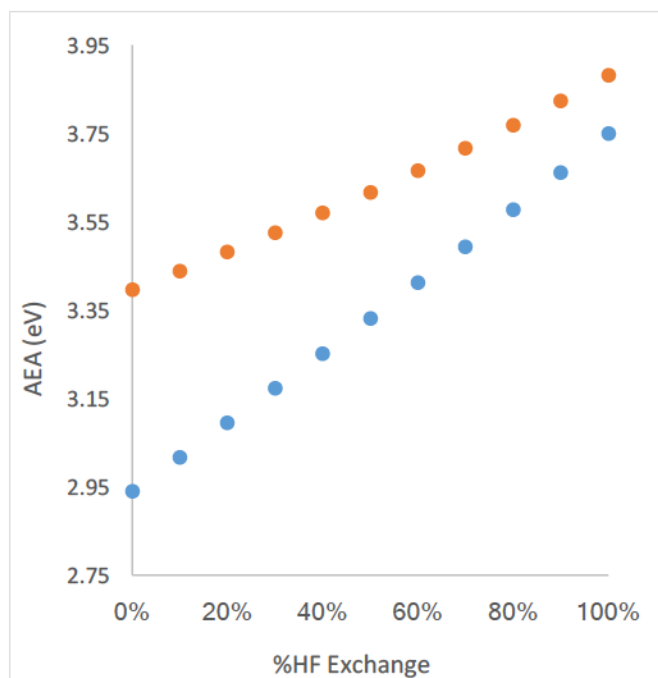


Figure B5: TCNE AEA value as %HF is increased. Blue markers - BS1 (cc-pvDZ). Orange markers - BS6 (6-311++g(2df,pd))

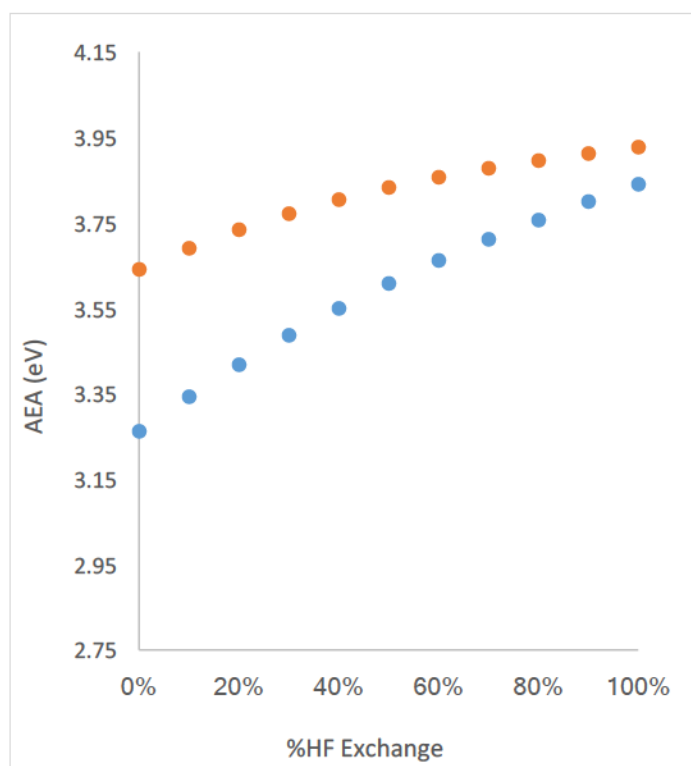
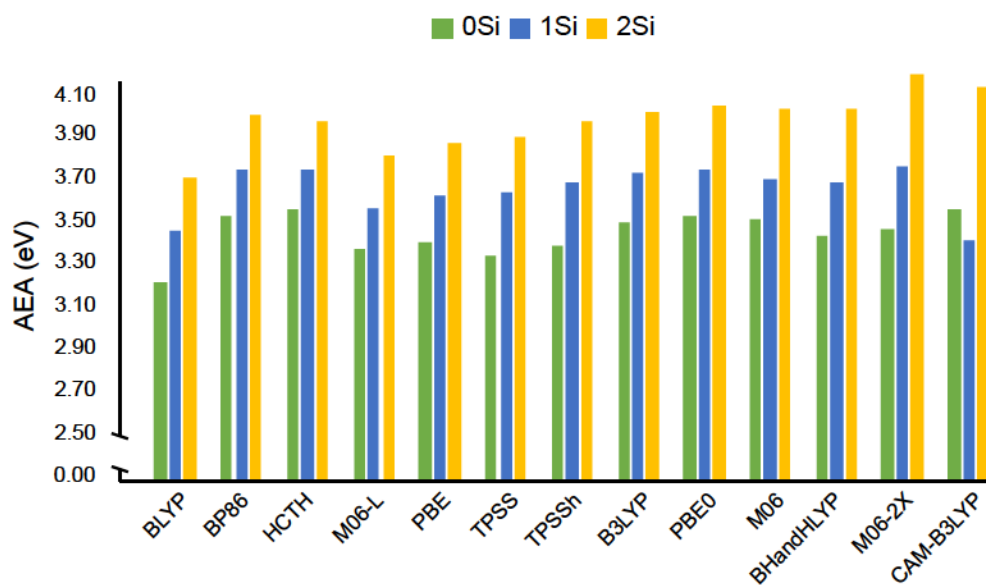


Figure B6: TCNQ AEA value as %HF is increased. Blue markers - BS1 (cc-pvDZ). Orange markers - BS6 (6-311++g(2df,pd))

(A)



(B)

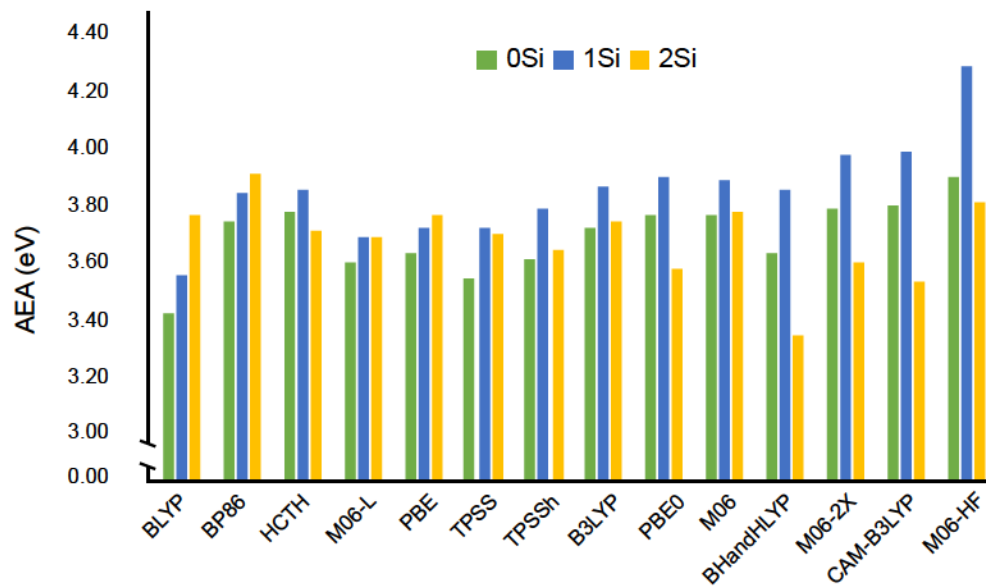


Figure B7: The adiabatic electron affinities (eV) for (a) TCNE series and (b) TCNQ series for BS6.

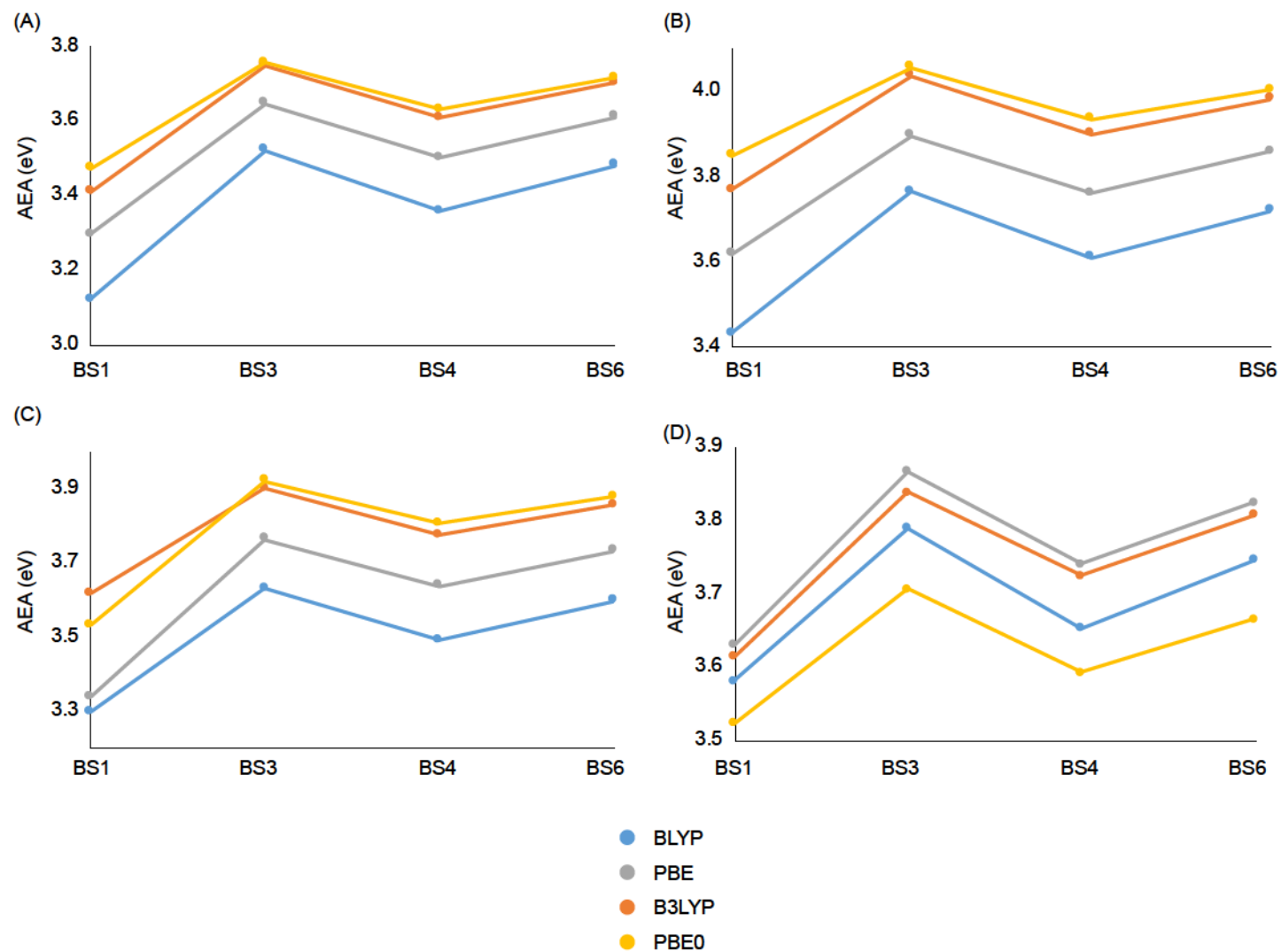


Figure B8: AEA's (eV) for (A) 1Si TCNE (B) 2Si TCNE (C) 1Si TCNQ and (D) 2Si TCNQ calculated using BS1, BS3, BS4 and BS6

Table B57: Relationship between planar AEA, adiabatic AEA and stabilization due to structural symmetry breaking. All values in eV.

		Planar AEA	AEA	$\Delta$ AEA	$\Delta E$ N S.B.	$\Delta E$ A S.B.	$\Delta\Delta E$ S.B.
BS1	BLYP	2.717	3.532	0.815	0.049	0.864	0.815
	PBE	2.952	3.581	0.629	0.116	0.745	0.629
	B3LYP	2.895	3.565	0.669	0.265	0.935	0.669
	PBE0	2.896	3.475	0.578	0.274	0.852	0.578
BS3	BLYP	2.997	3.740	0.743	0.146	0.889	0.743
	PBE	3.234	3.818	0.584	0.147	0.731	0.584
	B3LYP	3.158	3.789	0.631	0.294	0.925	0.631
	PBE0	3.096	3.657	0.561	0.300	0.861	0.562
BS4	BLYP	2.855	3.604	0.749	0.124	0.873	0.749
	PBE	3.125	3.691	0.566	0.127	0.693	0.566
	B3LYP	3.066	3.675	0.609	0.273	0.883	0.610
	PBE0	3.019	3.544	0.525	0.286	0.811	0.525
BS6	BLYP	3.033	3.697	0.664	0.041	0.779	0.738
	PBE	3.219	3.776	0.557	0.117	0.674	0.557
	B3LYP	3.154	3.758	0.605	0.253	0.858	0.605
	PBE0	3.098	3.617	0.519	0.266	0.785	0.519

APPENDIX C

Supplementary Information for Chapter Five

Table C1: Disilene  $b_{2g}$  wavenumber ( $\text{cm}^{-1}$ ) calculated using different grid sizes and tight optimization criteria. BS3.

	Fine	Ultrafine	Superfine	SG-1
SVWN	200 <i>i</i>	202 <i>i</i>	200 <i>i</i>	200 <i>i</i>
BLYP	281 <i>i</i>	280 <i>i</i>	278 <i>i</i>	279 <i>i</i>
PBE	244 <i>i</i>	235 <i>i</i>	236 <i>i</i>	237 <i>i</i>
TPSS	247 <i>i</i>	218 <i>i</i>	223 <i>i</i>	226 <i>i</i>
M06L	249 <i>i</i>	254 <i>i</i>	228 <i>i</i>	221 <i>i</i>
TPSSh	218 <i>i</i>	187 <i>i</i>	194 <i>i</i>	196 <i>i</i>
B3LYP	220 <i>i</i>	222 <i>i</i>	220 <i>i</i>	220 <i>i</i>
PBE0	165 <i>i</i>	154 <i>i</i>	156 <i>i</i>	157 <i>i</i>
M06	262 <i>i</i>	262 <i>i</i>	250 <i>i</i>	246 <i>i</i>
BH&HLYP	103 <i>i</i>	113 <i>i</i>	110 <i>i</i>	110 <i>i</i>
M062X	96	111 <i>i</i>	109 <i>i</i>	109 <i>i</i>
M06-HF	179	224	183	166
CAM-B3LYP	118 <i>i</i>	128 <i>i</i>	123 <i>i</i>	125 <i>i</i>
w-B97XD	112 <i>i</i>	100 <i>i</i>	103 <i>i</i>	79 <i>i</i>

Table C2: 2Si TCNQ  $b_{2g}$  wavenumber ( $\text{cm}^{-1}$ ) calculated using different grid sizes and tight optimization criteria. BS3.

	Fine	Ultrafine	Superfine	SG-1
SVWN	25 <i>i</i>	25 <i>i</i>	25 <i>i</i>	25 <i>i</i>
BLYP	74 <i>i</i>	74 <i>i</i>	74 <i>i</i>	74 <i>i</i>
PBE	53 <i>i</i>	54 <i>i</i>	54 <i>i</i>	54 <i>i</i>
TPSS	64 <i>i</i>	66 <i>i</i>	66 <i>i</i>	66 <i>i</i>
M06L	52 <i>i</i>	53 <i>i</i>	53 <i>i</i>	52 <i>i</i>
TPSSh	55 <i>i</i>	57 <i>i</i>	57 <i>i</i>	57 <i>i</i>
B3LYP	54 <i>i</i>	53 <i>i</i>	53 <i>i</i>	53 <i>i</i>
PBE0	26 <i>i</i>	26 <i>i</i>	26 <i>i</i>	26 <i>i</i>
M06	60 <i>i</i>	49 <i>i</i>	49 <i>i</i>	48 <i>i</i>
BHandHLYP	14	16	16	16
M062X	31	30	24	28
M06-HF	41	35	35	62
CAM-B3LYP	35	36	36	37
w-B97XD	44	41	40	40

Table C3: 2Si TCNQ  $b_{3u}$  wavenumber ( $\text{cm}^{-1}$ ) calculated using different grid sizes and tight optimization criteria. BS3.

	Fine	Ultrafine	Superfine	SG-1
SVWN	<i>6i</i>	<i>5i</i>	<i>6i</i>	<i>6i</i>
BLYP	<i>65i</i>	<i>65i</i>	<i>65i</i>	<i>65i</i>
PBE	<i>40i</i>	<i>41i</i>	<i>40i</i>	<i>40i</i>
TPSS	<i>54i</i>	<i>56i</i>	<i>56i</i>	<i>56i</i>
M06L	<i>35i</i>	<i>37i</i>	<i>38i</i>	<i>37i</i>
TPSSh	<i>44i</i>	<i>47i</i>	<i>46i</i>	<i>47i</i>
B3LYP	<i>44i</i>	<i>43i</i>	<i>43i</i>	<i>43i</i>
PBE0	<i>12i</i>	<i>13i</i>	<i>13i</i>	<i>13i</i>
M06	<i>51i</i>	<i>38i</i>	<i>38i</i>	<i>37i</i>
BHandHLYP	16	17	17	17
M062X	37	37	30	23
M06-HF	45	42	39	33
CAM-B3LYP	26	27	27	27
wB97XD	31	29	28	28

Table C4: Absolute value of stabilization (kcal/mol) and pyramidalization ( $^{\circ}$ ) resulting from symmetry breaking in disilene. Visualized in SI-Figure 1B.

Basis Set	Functional	Stabilization	Pyramidalization
BS1	SVWN	0.563	9.5
	BLYP	1.520	14.2
	M06L	0.791	10.6
	PBE	0.936	11.7
	TPSS	0.786	10.7
	TPSSh	0.543	8.9
	B3LYP	0.785	10.5
	PBE0	0.327	7.1
	M06	1.100	12.1
	BHandHLYP	0.212	5.7
	CAM-B3LYP	0.173	5.3
	w-B97XD	0.132	4.5
BS2	SVWN	0.498	9.1
	BLYP	1.317	13.4
	M06L	0.508	9.0
	PBE	0.784	10.9
	TPSS	0.579	9.4
	TPSSh	0.342	7.3
	B3LYP	0.559	9.2
	PBE0	0.176	5.3
	M06	0.755	10.5
	BHandHLYP	0.041	2.7
	CAM-B3LYP	0.007	0.2
	w-B97XD	0.006	0.2

Continued on next page

Table C4 continued

BS3	SVWN	0.445	8.5
	BLYP	1.285	13.3
	M06L	0.512	8.8
	PBE	0.747	10.6
	TPSS	0.591	9.5
	TPSSh	0.348	7.3
	B3LYP	0.540	9.0
	PBE0	0.159	5.0
	M06	0.790	10.9
	BHandHLYP	0.037	2.6
	CAM-B3LYP	0.006	0.2
	w-B97XD	0.019	1.3
BS4	SVWN	0.418	8.3
	BLYP	1.215	13.1
	M06L	0.427	8.3
	PBE	0.715	10.5
	TPSS	0.550	9.2
	TPSSh	0.317	7.0
	B3LYP	0.495	8.6
	PBE0	0.143	4.8
	M06	0.722	10.3
	BHandHLYP	0.004	0.2
	CAM-B3LYP	0.004	0.2
	w-B97XD	0.003	0.2
BS5	SVWN	0.315	7.2
	BLYP	1.413	13.8
	M06L	0.551	9.1
	PBE	0.716	10.4
	TPSS	0.731	10.3
	TPSSh	0.515	8.6
	B3LYP	0.758	10.4
	PBE0	0.240	6.1
	M06	0.984	11.6
	BHandHLYP	0.294	6.5
	CAM-B3LYP	0.151	4.9
	w-B97XD	0.058	3.3

Table C5: Absolute value of stabilization (kcal/mol) and pyramidalization ( $^{\circ}$ ) resulting from symmetry breaking in 2Si TCNQ ( $b_{2g}$  mode). PBE0/BS3 not visualized in Figure C1B.

BS1	SVWN	0.125	5.1
	BLYP	1.236	12.7
	M06L	0.711	10.3
	PBE	0.587	9.5
	TPSS	0.891	11.3
	TPSSh	0.597	9.5
	B3LYP	0.541	8.8
	PBE0	0.002	4.5
	M06	0.591	9.4
	BHandHLYP	0.016	1.9
	CAM-B3LYP w-B97XD	–	–
BS2	SVWN	0.022	2.5
	BLYP	0.982	11.6
	M06L	0.543	8.9
	PBE	0.358	7.8
	TPSS	0.651	10
	TPSSh	0.384	8
	B3LYP	0.340	7.4
	PBE0	0.008	1.5
	M06	0.387	7.9
	BHandHLYP	–	–
	CAM-B3LYP w-B97XD	–	–
BS3	SVWN	0.034	2.7
	BLYP	0.942	11.1
	M06L	0.373	7.4
	PBE	0.371	7.6
	TPSS	0.666	9.8
	TPSSh	0.410	7.8
	B3LYP	0.342	6.9

Continued on next page

Table C5 Continued

Basis Set	Functional	Stabilization	Pyramidalization
BS3	PBE0	13.697	2.2
	M06	0.293	6.9
	BHandHLYP	–	–
	CAM-B3LYP	–	–
	w-B97XD	–	–
BS4	SVWN	0.038	2.8
	BLYP	0.874	10.7
	M06L	0.455	7.9
	PBE	0.353	7.3
	TPSS	0.678	9.7
	TPSSh	0.43	7.8
	B3LYP	0.329	6.9
	PBE0	0.032	2.4
	M06	0.263	6.4
	BHandHLYP	–	–
	CAM-B3LYP	–	–
	w-B97XD	–	–
BS5	SVWN	0.024	2.1
	BLYP	1.316	13
	M06L	0.955	10.9
	PBE	0.528	8.7
	TPSS	0.96	11.3
	TPSSh	0.615	9.2
	B3LYP	0.522	8.5
	PBE0	0.059	3
	M06	0.579	8.7
	BHandHLYP	0.016	1.6
	CAM-B3LYP	–	–
	w-B97XD	–	–

Table C6: Absolute value of stabilization (kcal/mol) and pyramidalization (°) resulting from symmetry breaking in 2Si TCNQ ( $b_{3u}$  mode). PBE0/BS3 not visualized in Figure C1C.

Basis Set	Functional	Stabilization	Pyramidalization
BS1	SVWN	0.034	2.9
	BLYP	0.946	11.0
	M06L	0.444	8.9
	PBE	0.386	7.7
	TPSS	0.654	9.5
	TPSSh	0.426	7.9
	B3LYP	0.391	7.5
	PBE0	0.059	3.0
	M06	0.422	8.1
	BHandHLYP	0.004	1.0
	CAM-B3LYP	–	–
w-B97XD	–	–	
BS2	SVWN	–	–
	BLYP	0.718	9.9
	M06L	0.305	6.9
	PBE	0.200	5.9
	TPSS	0.450	8.2
	TPSSh	0.249	6.4
	B3LYP	0.224	5.9
	PBE0	–	–
	M06	0.251	6.3
	BHandHLYP	–	–
	CAM-B3LYP	–	–
w-B97XD	–	–	
BS3	SVWN	0.001	0.3
	BLYP	0.689	9.5
	M06L	0.173	4.9
	PBE	0.217	5.8
	TPSS	0.469	8.1

Continued on next page

Table C6 Continued

BS3	TPSSh	0.275	6.3
	B3LYP	0.226	5.7
	PBE0	13.673	0.9
	M06	0.173	5.0
	BHandHLYP	–	–
	CAM-B3LYP	–	–
	w-B97XD	–	–
BS4	SVWN	0.001	0.5
	BLYP	0.630	9.1
	M06L	0.248	5.8
	PBE	0.201	5.5
	TPSS	0.478	8.1
	TPSSh	0.290	6.4
	B3LYP	0.213	5.5
	PBE0	0.006	1.0
	M06	0.154	5.0
	BHandHLYP	–	–
	CAM-B3LYP	–	–
w-B97XD	–	–	
BS5	SVWN	0.0001	0.01
	BLYP	0.979	11.1
	M06L	0.618	9.5
	PBE	0.322	6.8
	TPSS	0.673	9.3
	TPSSh	0.408	7.4
	B3LYP	0.346	6.9
	PBE0	0.014	1.4
	M06	0.362	7.2
	BHandHLYP	0.002	0.4
	CAM-B3LYP	–	–
w-B97XD	–	–	

**Table C7:** Wavenumbers of modes that restore planarity ( $\omega'$ ) to the broken symmetry geometries calculated using BS1.

	Disilene	2Si TCNQ	
	$a_g$	$a_g$	$a_u$
HF	347 <sup>[a]</sup>	_ <sup>[b]</sup>	_ <sup>[b]</sup>
SVWN	292	46	23
BLYP	337	66	33
M06-L	326	60	31
PBE	326	60	29
TPSS	326	64	33
TPSSh	290	62	33
B3LYP	322	62	32
PBE0	257	47	25
M06	342	57	27
M06-2X	242	_ <sup>[b]</sup>	_ <sup>[b]</sup>
BH&HLYP	258	_ <sup>[b]</sup>	_ <sup>[b]</sup>
CAM-B3LYP	_ <sup>[b]</sup>	31	17
w-B97XD	205	_ <sup>[b]</sup>	_ <sup>[b]</sup>

[a] Further relaxes to  $C_s$  minimum

[b] No symmetry breaking observed in planar geometry

**Table C8:** Wavenumbers of modes that restore planarity ( $\omega'$ ) to the broken symmetry geometries calculated using BS2.

	Disilene	2Si TCNQ	
	$a_g$	$a_g$	$a_u$
SVWN	284	31	_ <sup>[b]</sup>
BLYP	337	65	33
M06-L	290	58	30
PBE	318	56	26
TPSS	297	62	32
TPSSh	248	59	31
B3LYP	298	58	31
PBE0	215	25	_ <sup>[b]</sup>
M06	310	51	26
BH&HLYP	158	_ <sup>[c]</sup>	_ <sup>[c]</sup>
CAM-B3LYP	103 <sup>[a]</sup>	_ <sup>[c]</sup>	_ <sup>[c]</sup>
w-B97XD	90 <sup>[a]</sup>	_ <sup>[c]</sup>	_ <sup>[c]</sup>

[a] Further relaxes to  $C_s$  minimum

[b] No symmetry breaking in the direction of the  $b_{3u}$  mode

[c] No symmetry breaking in planar geometry

Table C9: Wavenumbers of modes that restore planarity ( $\omega'$ ) to the broken symmetry geometries calculated using BS3.

	Disilene	2SiTCNQ	
	$a_g$	$a_g^{[a]}$	$a_1^{[b]}$
SVWN	275	35	9
BLYP	336	66	33
M06-L	289	58	30
PBE	316	57	29
TPSS	299	63	33
TPSSh	249	60	32
B3LYP	296	59	31
PBE0	210	65	16
M06	318	54	28
BH&HLYP	154	_ <sup>[d]</sup>	_ <sup>[d]</sup>
CAM-B3LYP	100 <sub>i</sub> <sup>[c]</sup>	_ <sup>[d]</sup>	_ <sup>[d]</sup>
w-B97XD	101	_ <sup>[d]</sup>	_ <sup>[d]</sup>

[a] – Restores planarity to  $C_{2h}$  minimum

[b] – Restores planarity to  $C_{2v}$  minimum

[c] – Further relaxes to  $C_s$  minimum

[d] – No symmetry breaking observed in planar geometry

Table C10: Wavenumbers of modes that restore planarity ( $\omega'$ ) to the broken symmetry geometries calculated using BS4.

	Disilene	2SiTCNQ	
	$a_g$	$a_g$	$a_u$
HF	_ <sup>[a]</sup>	66	_ <sup>[c]</sup>
SVWN	272	36	11
BLYP	336	65	33
M06-L	284	61	29
PBE	310	57	30
TPSS	290	63	33
TPSSh	243	60	32
B3LYP	289	60	31
PBE0	206	65	18
M06	312	53	29
BH&HLYP	80 <sub>i</sub> <sup>[b]</sup>	_ <sup>[a]</sup>	_ <sup>[a]</sup>
CAM-B3LYP	85 <sub>i</sub> <sup>[b]</sup>	_ <sup>[a]</sup>	_ <sup>[a]</sup>
w-B97XD	59 <sub>i</sub> <sup>[b]</sup>	_ <sup>[a]</sup>	_ <sup>[a]</sup>

[a] No symmetry breaking observed in planar geometry

[b] Further relax to  $C_s$  minimum

[c] No symmetry breaking in the direction of the  $b_{3u}$  mode

**Table C11:** Wavenumbers of modes that restore planarity ( $\omega'$ ) to the broken symmetry geometries calculated using BS5.

	Disilene	2SiTCNQ	
	ag	ag	au
HF	219	_[a]	_[a]
SVWN	260	31	4
BLYP	345	67	35
M06-L	293	61	31
PBE	312	59	32
TPSS	321	65	35
TPSSh	286	63	34
B3LYP	321	62	32
PBE0	243	41	21
M06	322	57	23
BH&HLYP	268	31	13
CAM-B3LYP	224	_[a]	_[a]
w-B97XD	168	_[a]	_[a]

[a] No symmetry breaking observed in planar geometry

**Table C12:** Polynomial coefficients and  $R^2$  values obtained from fitting Disilene APES scans. To obtain value of  $a$  for cusp multiply  $a_2$  by 2.

	$a_0$	$a_2$	$a_4$	$R^2$
0%	0.042	-0.281	0.438	0.928
10%	0.032	-0.239	0.409	0.923
20%	0.023	-0.198	0.377	0.917
30%	0.016	-0.158	0.342	0.911
40%	0.010	-0.119	0.304	0.904
50%	0.005	-0.088	0.340	0.899
60%	0.002	-0.050	0.294	0.890
70%	0.0002	-0.015	0.233	0.876
80%	0.000	0.165	3.269	0.999
90%	0.000	0.225	3.315	0.999
100%	0.000	0.283	3.409	0.999

**Table C13:** Polynomial coefficients and  $R^2$  values obtained from fitting 2Si TCNQ  $b_{2g}$  APES scans. To obtain value of  $a$  for cusp multiply  $a_2$  by 2.

	$a_0$	$a_2$	$a_4$	$R^2$
0%	0.0231	-0.4706	2.3640	0.992
10%	0.0192	-0.2226	0.6542	0.982
20%	0.0144	-0.1971	0.6816	0.982
30%	0.0093	-0.1607	0.7012	0.986
40%	0.0045	-0.1593	1.4060	0.892
50%	0.0009	-0.0669	1.2390	0.229
60%	0.0000	0.0458	0.5061	0.999
70%	0.0000	0.0840	0.5249	0.999
80%	0.0000	0.1206	0.5281	0.999
90%	0.0000	0.1552	0.5398	0.999
100%	0.0000	0.1929	0.5637	0.999

**Table C14:** Polynomial coefficients and  $R^2$  values obtained from fitting 2Si TCNQ  $b_{3u}$  APES scans. To obtain value of  $a$  for cusp multiply  $a_2$  by 2.

	$a_0$	$a_2$	$a_4$	$R^2$
0%	0.015	-0.305	0.897	0.873
10%	0.013	-0.293	1.110	0.876
20%	0.010	-0.260	1.235	0.863
30%	0.006	-0.206	1.265	0.869
40%	0.003	-0.099	0.753	0.897
50%	0.0003	-0.031	0.867	0.890
60%	0.000	0.015	0.177	0.999
70%	0.000	0.020	0.104	0.999
80%	0.000	0.023	0.061	0.999
90%	0.000	0.024	0.041	0.999
100%	0.000	0.025	0.026	0.999

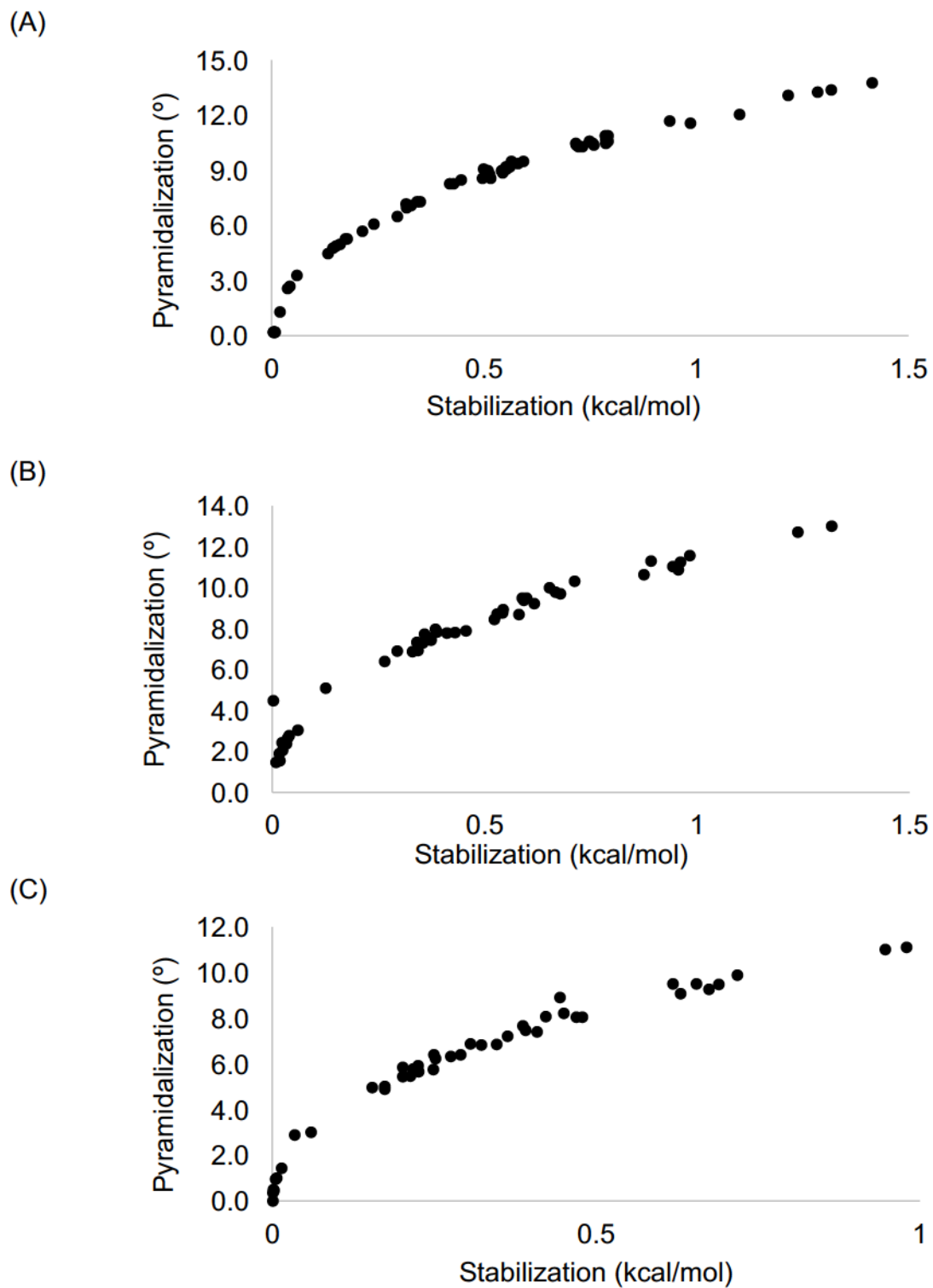


**Figure C1:** The amount of pyramidalization as a function of the absolute value of stabilization predicted by all model chemistries for (A) Disilene (B) 2Si TCNQ ( $b_{2g}$ ) and (C) 2Si TCNQ ( $b_{3u}$ ). Raw data available in Tables C1-3

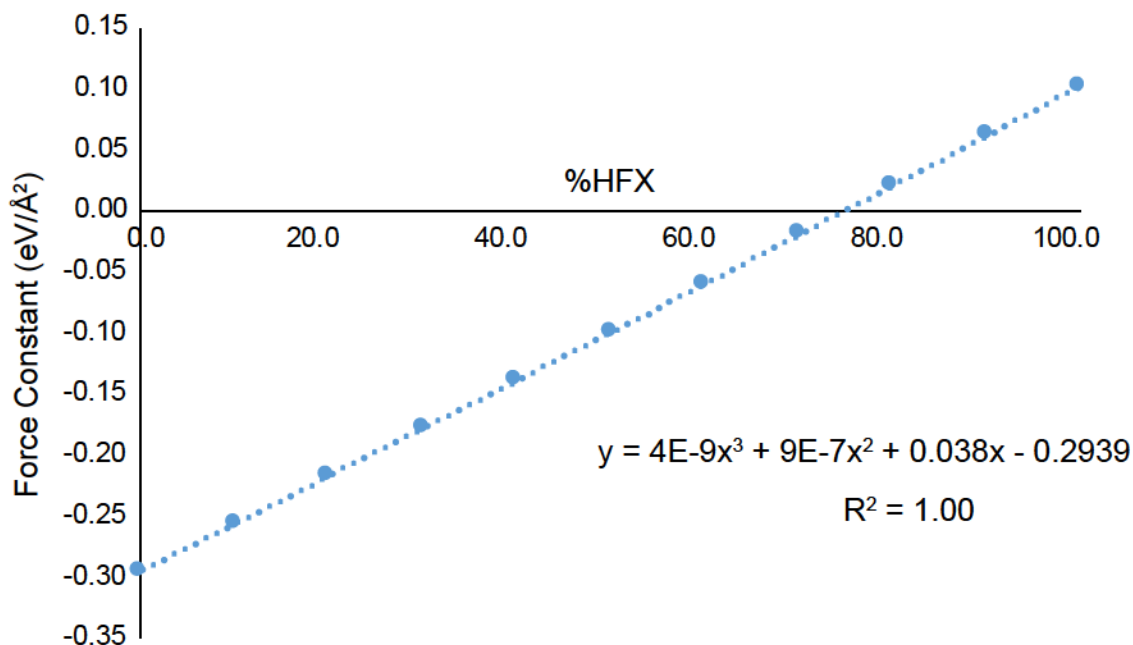


**Figure C2:** Dependence of disilene  $b_{2g}$  force constant (eV/Å<sup>2</sup>) on amount of exact exchange with third order polynomial regression. Root: 77.3%

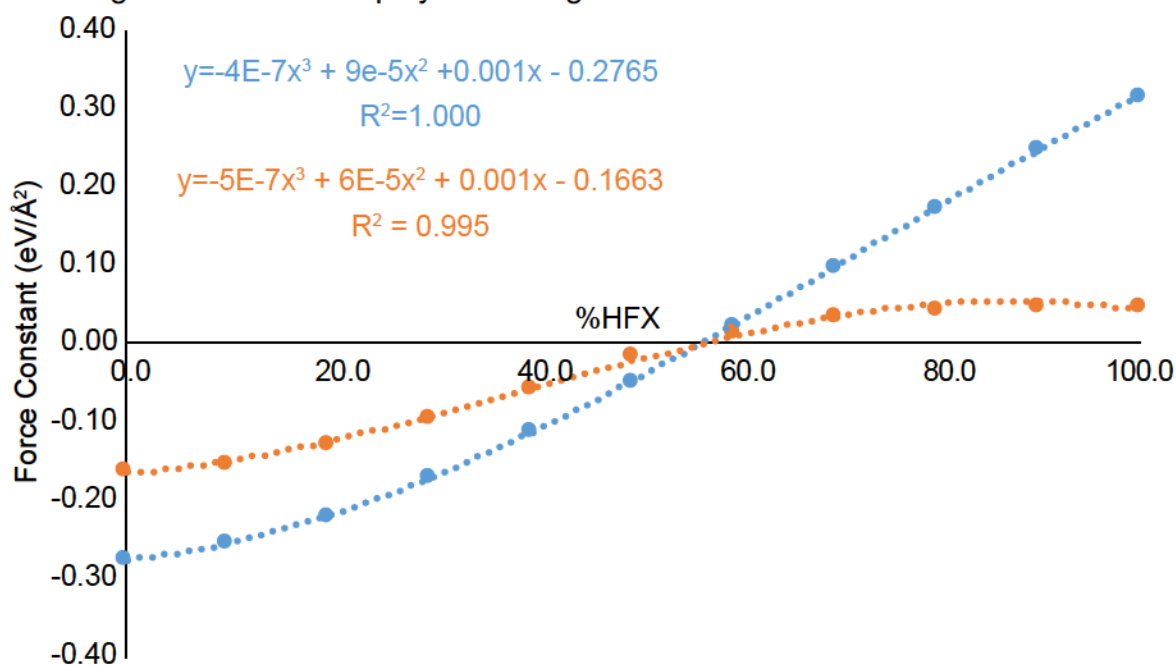
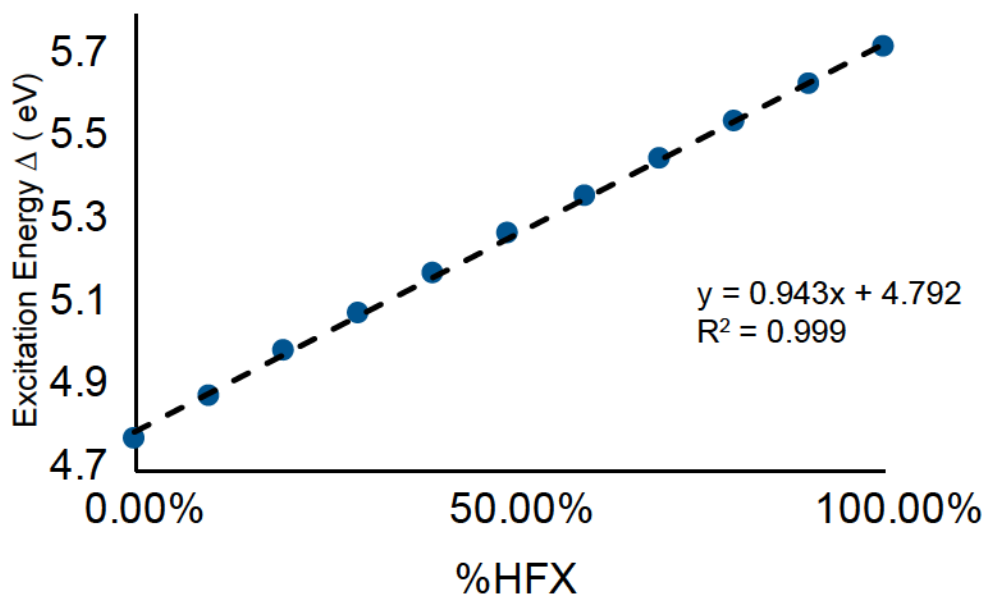


**Figure C3:** Dependence of 2Si TCNQ  $b_{2g}$  (blue) and  $b_{3u}$  (orange) force constants (eV/Å<sup>2</sup>) on amount of exact exchange with third order polynomial regressions. Roots: 57.1% ( $b_{2g}$ ) and 59.4% ( $b_{3u}$ )

(A)



(B)

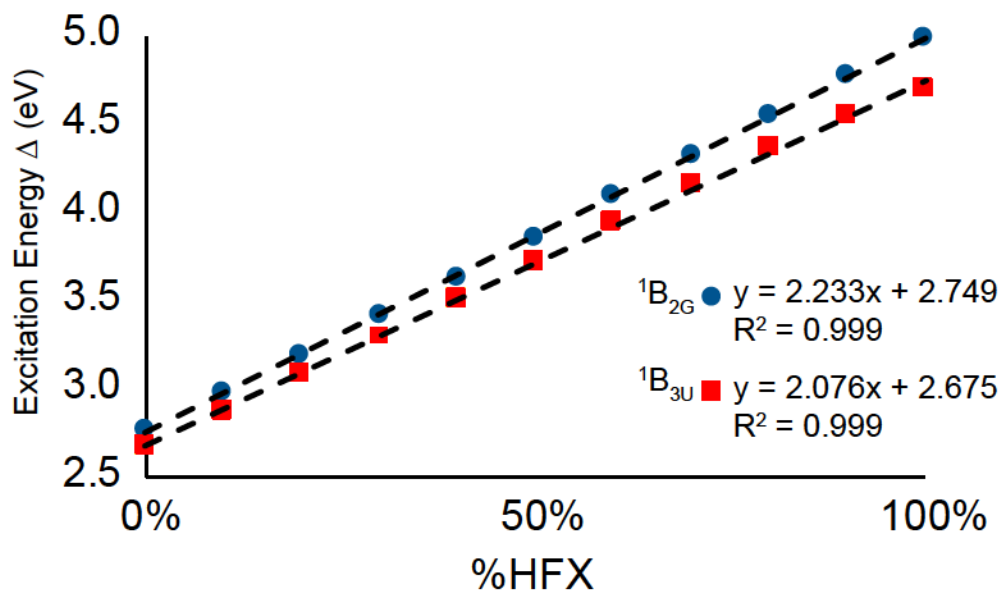


Figure C4: Change in excitation energy  $\Delta$  (eV) for lowest lying (A)  ${}^1B_{2G}$  excited state of Disilene and (B)  ${}^1B_{2G}$  (blue circles) and  ${}^1B_{3U}$  (red squares) excited states of 2Si TCNQ

APPENDIX D

Supplementary Information for Chapter Six

Table D1: Bond lengths (Å) for TCNDQ

		R <sub>1</sub>	R <sub>2</sub>	R <sub>3</sub>	R <sub>4</sub>	R <sub>5</sub>	R <sub>6</sub>	R <sub>7</sub>
B3LYP	BS1	1.423	1.443	1.366	1.440	1.402	1.427	1.163
	BS2	1.422	1.442	1.365	1.440	1.401	1.426	1.167
	BS3	1.418	1.439	1.360	1.437	1.396	1.421	1.158
	BS4	1.414	1.436	1.356	1.434	1.392	1.420	1.155
BLYP	BS1	1.446	1.446	1.381	1.444	1.424	1.431	1.177
	BS2	1.445	1.446	1.380	1.443	1.422	1.430	1.180
	BS3	1.441	1.443	1.374	1.440	1.418	1.424	1.171
	BS4	1.437	1.439	1.371	1.437	1.414	1.423	1.168
CAM-B3LYP	BS1	1.398	1.449	1.353	1.445	1.381	1.430	1.156
	BS2	1.396	1.448	1.352	1.445	1.379	1.429	1.159
	BS3	1.391	1.446	1.346	1.442	1.374	1.424	1.150
	BS4	1.388	1.443	1.343	1.439	1.370	1.423	1.147
M06-L	BS1	1.413	1.439	1.360	1.436	1.393	1.424	1.163
	BS2	1.400	1.450	1.355	1.446	1.382	1.433	1.156
	BS3	1.392	1.445	1.346	1.441	1.372	1.427	1.149
	BS4	1.403	1.432	1.349	1.430	1.382	1.417	1.152
M06	BS1	1.399	1.449	1.354	1.445	1.380	1.431	1.159
	BS2	1.411	1.438	1.358	1.436	1.392	1.423	1.166
	BS3	1.406	1.435	1.352	1.433	1.385	1.418	1.156
	BS4	1.395	1.448	1.350	1.444	1.376	1.427	1.151
M06-2X	BS1	1.379	1.464	1.345	1.459	1.364	1.443	1.145
	BS2	1.379	1.464	1.345	1.459	1.364	1.442	1.148
	BS3	1.374	1.462	1.340	1.456	1.358	1.436	1.139
	BS4	1.371	1.459	1.338	1.454	1.356	1.436	1.138
M06-HF	BS1	1.429	1.433	1.367	1.430	1.407	1.418	1.168
	BS2	1.427	1.432	1.366	1.430	1.406	1.417	1.172
	BS3	1.425	1.430	1.361	1.428	1.402	1.413	1.164
	BS4	1.421	1.426	1.357	1.424	1.398	1.411	1.160
PBE0	BS1	1.417	1.438	1.362	1.436	1.396	1.423	1.162
	BS2	1.415	1.438	1.361	1.435	1.394	1.422	1.165
	BS3	1.411	1.435	1.356	1.433	1.390	1.417	1.157
	BS4	1.408	1.432	1.353	1.430	1.386	1.417	1.154

Table D1 Con't

PBE	BS1	1.442	1.440	1.378	1.438	1.420	1.425	1.177
	BS2	1.440	1.439	1.377	1.437	1.418	1.424	1.181
	BS3	1.436	1.436	1.372	1.434	1.413	1.419	1.172
	BS4	1.433	1.433	1.369	1.431	1.410	1.418	1.169

Table D2: Bond lengths for [TCNDQ]<sup>-</sup> (D<sub>2h</sub>)

		R <sub>1</sub>	R <sub>2</sub>	R <sub>3</sub>	R <sub>4</sub>	R <sub>5</sub>	R <sub>6</sub>	R <sub>7</sub>
B3LYP	BS1	1.459	1.425	1.381	1.425	1.434	1.419	1.168
	BS2	1.452	1.417	1.372	1.418	1.425	1.411	1.159
	BS3	1.454	1.421	1.375	1.421	1.428	1.412	1.162
	BS4	1.472	1.434	1.392	1.433	1.449	1.425	1.181
BLYP	BS1	1.457	1.425	1.379	1.425	1.432	1.419	1.171
	BS2	1.465	1.426	1.383	1.426	1.440	1.416	1.172
	BS3	1.468	1.430	1.387	1.430	1.444	1.417	1.176
	BS4	1.447	1.423	1.372	1.423	1.421	1.420	1.161
CAM-B3LYP	BS1	1.471	1.434	1.391	1.433	1.447	1.425	1.184
	BS2	1.400	1.445	1.350	1.448	1.354	1.540	1.470
	BS3	1.443	1.418	1.367	1.419	1.415	1.412	1.155
	BS4	1.450	1.420	1.375	1.421	1.426	1.416	1.167
M06-L	BS1	1.445	1.422	1.371	1.423	1.419	1.419	1.164
	BS2	1.443	1.412	1.365	1.413	1.417	1.408	1.157
	BS3	1.442	1.418	1.366	1.419	1.412	1.415	1.154
	BS4	1.447	1.424	1.373	1.424	1.417	1.421	1.164
M06	BS1	1.448	1.424	1.374	1.425	1.419	1.422	1.161
	BS2	1.445	1.421	1.370	1.422	1.415	1.416	1.156
	BS3	1.446	1.415	1.369	1.416	1.420	1.409	1.161
	BS4	1.438	1.427	1.368	1.430	1.406	1.429	1.149
M06-2X	BS1	1.449	1.419	1.374	1.420	1.424	1.415	1.170
	BS2	1.432	1.422	1.362	1.424	1.400	1.422	1.143
	BS3	1.435	1.425	1.365	1.427	1.403	1.422	1.144
	BS4	1.455	1.420	1.378	1.419	1.433	1.412	1.172
M06-HF	BS1	1.438	1.429	1.369	1.431	1.405	1.429	1.152
	BS2	1.448	1.412	1.369	1.412	1.425	1.404	1.164
	BS3	1.452	1.416	1.374	1.416	1.429	1.406	1.168
	BS4	1.453	1.421	1.377	1.421	1.428	1.415	1.166

Table D2 Con't

PBE0	BS1	1.454	1.419	1.377	1.418	1.431	1.411	1.176
	BS2	1.446	1.413	1.368	1.414	1.419	1.408	1.158
	BS3	1.449	1.416	1.372	1.417	1.422	1.408	1.161
	BS4	1.465	1.429	1.388	1.428	1.443	1.419	1.181
PBE	BS1	1.451	1.420	1.376	1.420	1.426	1.414	1.169
	BS2	1.464	1.428	1.387	1.428	1.441	1.419	1.184
	BS3	1.462	1.424	1.383	1.424	1.438	1.412	1.176
	BS4	1.459	1.421	1.380	1.421	1.435	1.412	1.173

Table D3: Bond lengths (Å) for [TCNDQ]<sup>-</sup> (D<sub>2</sub>)

		R <sub>1</sub>	R <sub>2</sub>	R <sub>3</sub>	R <sub>4</sub>	R <sub>5</sub>	R <sub>6</sub>	R <sub>7</sub>
B3LYP	BS1	1.458	1.424	1.381	1.425	1.435	1.419	1.168
	BS2	1.457	1.423	1.380	1.425	1.433	1.419	1.171
	BS3	1.454	1.419	1.376	1.422	1.430	1.412	1.162
	BS4	1.451	1.416	1.372	1.418	1.426	1.411	1.159
BLYP	BS1	1.471	1.433	1.393	1.434	1.450	1.425	1.181
	BS2	1.470	1.432	1.392	1.434	1.448	1.424	1.184
	BS3	1.467	1.428	1.387	1.430	1.445	1.417	1.176
	BS4	1.463	1.424	1.384	1.426	1.442	1.416	1.172
CAM-B3LYP	BS1	1.447	1.423	1.372	1.424	1.421	1.420	1.161
	BS2	1.445	1.421	1.371	1.423	1.419	1.419	1.163
	BS3	1.442	1.417	1.367	1.420	1.416	1.412	1.155
	BS4	1.439	1.414	1.363	1.416	1.412	1.411	1.152
M06-L	BS1	1.454	1.419	1.378	1.419	1.434	1.412	1.172
	BS2	1.452	1.418	1.378	1.419	1.432	1.411	1.176
	BS3	1.451	1.415	1.374	1.416	1.430	1.406	1.168
	BS4	1.447	1.412	1.370	1.413	1.426	1.404	1.164
M06	BS1	1.450	1.420	1.375	1.421	1.426	1.416	1.167
	BS2	1.449	1.419	1.374	1.420	1.424	1.415	1.170
	BS3	1.445	1.414	1.369	1.417	1.420	1.409	1.161
	BS4	1.442	1.411	1.365	1.413	1.417	1.408	1.157
M06-2X	BS1	1.447	1.423	1.374	1.425	1.420	1.422	1.161
	BS2	1.446	1.422	1.374	1.425	1.418	1.421	1.164
	BS3	1.444	1.418	1.370	1.422	1.416	1.415	1.156
	BS4	1.440	1.416	1.367	1.419	1.413	1.414	1.154

Table D3 Con't

M06-HF	BS1	1.438	1.427	1.368	1.430	1.406	1.429	1.149
	BS2	1.438	1.428	1.369	1.431	1.406	1.429	1.153
	BS3	1.434	1.422	1.365	1.427	1.404	1.422	1.144
	BS4	1.431	1.421	1.363	1.424	1.401	1.421	1.143
PBE0	BS1	1.452	1.420	1.377	1.421	1.428	1.415	1.166
	BS2	1.450	1.419	1.376	1.420	1.426	1.414	1.169
	BS3	1.448	1.415	1.372	1.417	1.424	1.408	1.161
	BS4	1.445	1.412	1.369	1.414	1.420	1.408	1.158
PBE	BS1	1.464	1.428	1.389	1.428	1.444	1.419	1.181
	BS2	1.463	1.427	1.388	1.428	1.442	1.419	1.184
	BS3	1.460	1.422	1.384	1.424	1.439	1.412	1.176
	BS4	1.457	1.420	1.381	1.421	1.436	1.411	1.173

Table D4: Bond lengths (Å) for TCNP

		R <sub>1</sub>	R <sub>1</sub> '	R <sub>2</sub>	R <sub>3</sub>	R <sub>4</sub>	R <sub>5</sub>	R <sub>6</sub>	R <sub>7</sub>	R <sub>8</sub>
B3LYP	BS1	1.358	1.394	1.449	1.450	1.380	1.435	1.411	1.425	1.164
	BS2	1.357	1.393	1.449	1.450	1.379	1.435	1.409	1.424	1.167
	BS3	1.351	1.388	1.446	1.447	1.374	1.432	1.404	1.419	1.158
	BS4	1.348	1.384	1.443	1.444	1.370	1.429	1.400	1.418	1.155
BLYP	BS1	1.372	1.410	1.454	1.456	1.396	1.439	1.433	1.429	1.178
	BS2	1.371	1.410	1.454	1.456	1.395	1.439	1.431	1.428	1.181
	BS3	1.365	1.404	1.451	1.453	1.390	1.436	1.426	1.422	1.172
	BS4	1.361	1.401	1.447	1.450	1.386	1.433	1.423	1.421	1.169
CAM-B3LYP	BS1	1.347	1.377	1.452	1.452	1.364	1.441	1.389	1.428	1.156
	BS2	1.345	1.376	1.452	1.452	1.363	1.440	1.386	1.428	1.159
	BS3	1.340	1.370	1.450	1.449	1.358	1.438	1.381	1.422	1.150
	BS4	1.336	1.367	1.447	1.446	1.354	1.434	1.378	1.421	1.148
M06-L	BS1	1.358	1.396	1.440	1.443	1.382	1.426	1.415	1.416	1.169
	BS2	1.357	1.395	1.440	1.442	1.381	1.425	1.413	1.415	1.173
	BS3	1.353	1.392	1.438	1.440	1.377	1.423	1.410	1.411	1.165
	BS4	1.348	1.388	1.434	1.437	1.373	1.419	1.406	1.409	1.160
M06	BS1	1.353	1.386	1.445	1.445	1.373	1.432	1.401	1.422	1.163
	BS2	1.351	1.385	1.444	1.445	1.372	1.431	1.399	1.421	1.166
	BS3	1.345	1.380	1.442	1.442	1.366	1.429	1.393	1.416	1.156
	BS4	1.341	1.376	1.438	1.438	1.362	1.425	1.390	1.416	1.153
M06-2X	BS1	1.349	1.380	1.454	1.453	1.367	1.442	1.389	1.431	1.156
	BS2	1.348	1.379	1.453	1.453	1.366	1.441	1.387	1.430	1.160
	BS3	1.343	1.374	1.452	1.451	1.361	1.440	1.383	1.425	1.152
	BS4	1.340	1.371	1.449	1.449	1.358	1.437	1.380	1.425	1.149

Table D4 Con't

M06-HF	BS1	1.340	1.364	1.465	1.463	1.354	1.455	1.369	1.441	1.145
	BS2	1.341	1.364	1.465	1.463	1.354	1.456	1.369	1.441	1.148
	BS3	1.335	1.359	1.463	1.461	1.349	1.453	1.364	1.435	1.139
	BS4	1.333	1.356	1.461	1.459	1.346	1.451	1.361	1.435	1.138
PBE0	BS1	1.354	1.389	1.445	1.445	1.375	1.431	1.404	1.421	1.162
	BS2	1.353	1.388	1.444	1.445	1.374	1.430	1.402	1.420	1.165
	BS3	1.348	1.383	1.442	1.442	1.370	1.428	1.398	1.415	1.157
	BS4	1.345	1.380	1.439	1.439	1.366	1.425	1.395	1.415	1.154
PBE	BS1	1.369	1.407	1.447	1.450	1.393	1.433	1.428	1.423	1.178
	BS2	1.368	1.406	1.447	1.450	1.392	1.433	1.426	1.422	1.181
	BS3	1.363	1.401	1.445	1.447	1.387	1.430	1.422	1.417	1.173
	BS4	1.360	1.398	1.442	1.444	1.384	1.427	1.419	1.416	1.170

Table D5: Bond lengths (Å) of [TCNP]<sup>-</sup>

		R <sub>1</sub>	R <sub>1</sub> '	R <sub>2</sub>	R <sub>3</sub>	R <sub>4</sub>	R <sub>5</sub>	R <sub>6</sub>	R <sub>7</sub>	R <sub>8</sub>
B3LYP	BS1	1.363	1.412	1.445	1.438	1.393	1.422	1.441	1.418	1.168
	BS2	1.362	1.411	1.445	1.438	1.392	1.422	1.439	1.417	1.171
	BS3	1.357	1.407	1.443	1.434	1.388	1.418	1.436	1.411	1.163
	BS4	1.353	1.403	1.439	1.431	1.384	1.415	1.432	1.410	1.160
BLYP	BS1	1.376	1.422	1.451	1.448	1.406	1.430	1.456	1.424	1.181
	BS2	1.375	1.422	1.451	1.448	1.405	1.430	1.454	1.423	1.185
	BS3	1.370	1.418	1.448	1.444	1.401	1.426	1.452	1.416	1.176
	BS4	1.366	1.414	1.445	1.441	1.397	1.423	1.448	1.415	1.173
CAM-B3LYP	BS1	1.353	1.404	1.447	1.433	1.382	1.421	1.427	1.418	1.161
	BS2	1.351	1.403	1.447	1.433	1.381	1.420	1.425	1.418	1.164
	BS3	1.346	1.399	1.444	1.429	1.377	1.417	1.422	1.411	1.155
	BS4	1.343	1.395	1.441	1.426	1.373	1.414	1.418	1.410	1.152

Table D5 Con't

M06-L	BS1	1.363	1.409	1.437	1.434	1.392	1.416	1.440	1.410	1.173
	BS2	1.362	1.408	1.437	1.434	1.391	1.415	1.438	1.410	1.177
	BS3	1.358	1.405	1.435	1.431	1.388	1.413	1.436	1.405	1.169
	BS4	1.353	1.402	1.431	1.427	1.384	1.409	1.432	1.403	1.164
M06	BS1	1.358	1.406	1.441	1.432	1.387	1.418	1.432	1.415	1.167
	BS2	1.356	1.405	1.440	1.432	1.386	1.417	1.430	1.414	1.170
	BS3	1.351	1.400	1.437	1.428	1.381	1.414	1.426	1.408	1.161
	BS4	1.347	1.397	1.434	1.425	1.377	1.410	1.423	1.407	1.157
M06-2X	BS1	1.355	1.405	1.449	1.435	1.384	1.423	1.425	1.421	1.161
	BS2	1.354	1.404	1.448	1.435	1.383	1.422	1.424	1.420	1.164
	BS3	1.350	1.401	1.447	1.432	1.380	1.419	1.421	1.414	1.157
	BS4	1.346	1.397	1.444	1.429	1.376	1.417	1.418	1.414	1.154
M06-HF	BS1	1.347	1.399	1.458	1.436	1.376	1.428	1.411	1.428	1.150
	BS2	1.347	1.398	1.459	1.436	1.376	1.428	1.411	1.428	1.153
	BS3	1.342	1.394	1.456	1.433	1.372	1.425	1.408	1.421	1.144
	BS4	1.340	1.391	1.453	1.431	1.369	1.423	1.405	1.421	1.143
PBE0	BS1	1.359	1.407	1.441	1.433	1.389	1.418	1.435	1.414	1.166
	BS2	1.358	1.406	1.441	1.432	1.388	1.417	1.432	1.413	1.169
	BS3	1.354	1.402	1.438	1.429	1.384	1.414	1.429	1.407	1.162
	BS4	1.350	1.399	1.435	1.426	1.380	1.411	1.426	1.407	1.159
PBE	BS1	1.373	1.418	1.445	1.443	1.402	1.425	1.450	1.418	1.182
	BS2	1.372	1.417	1.445	1.442	1.401	1.425	1.448	1.417	1.185
	BS3	1.367	1.414	1.442	1.439	1.397	1.421	1.445	1.411	1.177
	BS4	1.364	1.411	1.439	1.436	1.394	1.418	1.442	1.410	1.174

Table D6: Twist angles for [TCNDQ]<sup>-</sup> D<sub>2</sub> geometry

	BS1	BS2	BS3	BS4
BLYP	18.5	19.0	21.5	19.9
PBE	18.3	19.0	21.8	19.7
M06-L	15.0	16.3	18.1	14.0
B3LYP	15.2	16.4	19.2	17.5
PBE0	15.0	16.6	19.4	17.4
M06	0.0002	0.015	16.5	12.3
M062X	14.4	17.3	20.9	17.9
M06-HF	1.6	9.6	19.6	14.6
CAM-B3LYP	1.5	11.1	15.5	13.5

Table D7:  $\langle S^2 \rangle$  Values for D<sub>2h</sub> [TCNDQ]<sup>-</sup>

	BS1	BS2	BS3	BS4
BLYP	0.75	0.75	0.75	0.75
M06-L	0.75	0.76	0.76	0.76
PBE	0.75	0.75	0.75	0.75
B3LYP	0.77	0.77	0.75	0.75
PBE0	0.78	0.78	0.77	0.77
M06	0.77	0.77	0.77	0.77
M06-2X	0.79	0.79	0.79	0.79
M06-HF	0.84	0.83	0.83	0.83
CAM-B3LYP	0.81	0.81	0.80	0.80

Table D8:  $\langle S^2 \rangle$  Values for D<sub>2</sub> [TCNDQ]<sup>-</sup>

	BS1	BS2	BS3	BS4
BLYP	0.75	0.75	0.75	0.75
M06-L	0.76	0.76	0.76	0.76
PBE	0.75	0.75	0.75	0.75
B3LYP	0.77	0.77	0.77	0.77
PBE0	0.77	0.78	0.77	0.77
M06	0.77	0.77	0.77	0.77
M06-2X	0.79	0.79	0.79	0.79
M06-HF	0.84	0.83	0.83	0.83
CAM-B3LYP	0.81	0.81	0.80	0.80

Table D9:  $\langle S^2 \rangle$  values for  $D_{2h}$  [TCNP]<sup>-</sup>

	BS1	BS2	BS3	BS4
BLYP	0.75	0.75	0.75	0.75
M06-L	0.76	0.76	0.76	0.76
PBE	0.78	0.75	0.75	0.75
B3LYP	0.77	0.77	0.77	0.77
PBE0	0.77	0.77	0.77	0.77
M06	0.77	0.77	0.77	0.77
M06-2X	0.78	0.78	0.78	0.78
M06-HF	0.83	0.82	0.82	0.82
CAM-B3LYP	0.80	0.80	0.80	0.80

Table D10:  $\langle S^2 A \rangle$  values for  $D_{2h}$  [TCNDQ]<sup>-</sup>

	BS1	BS2	BS3	BS4
M06-2X	0.751	0.751	0.751	0.751
M06-HF	0.753	0.753	0.753	0.753
CAM-B3LYP	0.752	0.752	0.751	0.750

Table D11:  $\langle S^2 A \rangle$  values for  $D_2$  [TCNDQ]<sup>-</sup>

	BS1	BS2	BS3	BS4
M06-2X	0.751	0.751	0.751	0.751
M06-HF	0.753	0.753	0.753	0.753
CAM-B3LYP	0.752	0.752	0.751	0.751

Table D12:  $\langle S^2 A \rangle$  values for  $D_{2h}$  [TCNP]<sup>-</sup>

	BS1	BS2	BS3	BS4
M06-2X	0.751	0.751	0.751	0.751
M06-HF	0.752	0.752	0.752	0.752
CAM-B3LYP	0.751	0.751	0.751	0.751

Table D13: Deviation of all model chemistries from experimental TCNDQ ESR coupling constants (A) H\*, (B) H‡ (C) N

(A)

	BS1	BS2	BS3	BS4
BLYP	-0.29	-0.30	-0.31	-0.36
PBE	-0.26	-0.26	-0.28	-0.34
M06-L	0.37	0.32	0.66	0.57
B3LYP	-0.06	-0.07	-0.08	-0.13
PBE0	0.13	0.11	0.09	0.02
M06	0.28	0.29	0.72	0.67
M06-2X	0.04	0.05	0.15	0.15
M06-HF	-0.24	-0.20	-0.28	-0.17
CAM-B3LYP	0.05	0.03	0.02	-0.03
Min	-0.29	-0.30	-0.31	-0.36
Max	0.37	0.32	0.72	0.67
Min	0.04	0.03	0.02	0.02
Range	0.67	0.62	1.03	1.03

(B)

	BS1	BS2	BS3	BS4
BLYP	-0.18	-0.16	-0.12	-0.14
PBE	-0.19	-0.15	-0.13	-0.15
M06-L	-0.21	-0.18	-0.04	-0.09
B3LYP	-0.31	-0.31	-0.25	-0.26
PBE0	-0.19	-0.24	-0.29	-0.28
M06	-0.15	-0.18	0.00	-0.01
M06-2X	0.00	0.00	0.07	0.14
M06-HF	0.09	0.06	0.05	0.13
CAM-B3LYP	-0.22	-0.27	-0.31	-0.31
Min	-0.31	-0.31	-0.31	-0.31
Max	0.09	0.06	0.07	0.14
Min	0.01	0.00	0.00	0.01
Range	0.40	0.37	0.38	0.45

(C)

	BS1	BS2	BS3	BS4
BLYP	1.48	-0.36	0.61	-0.36
PBE	1.28	0.50	0.50	-0.52
M06-L	3.36	1.64	1.67	1.68
B3LYP	1.92	-0.13	0.90	-0.20
PBE0	1.96	-0.20	0.94	-0.25
M06	2.29	0.56	1.09	0.15
M06-2X	1.49	0.69	0.47	0.90
M06-HF	-0.63	-0.27	-0.61	-0.27
CAM-B3LYP	1.89	-0.22	0.90	-0.29
Min	-0.63	-0.36	-0.61	-0.52
Max	3.36	1.64	1.67	1.68
Min	0.63	0.22	0.61	0.15
Range	3.99	2.00	2.27	2.21

Table D14: Deviation of all model chemistries from experimental TCNP ESR coupling constants (A) H<sup>\*</sup>, (B) H $\ddagger$  (C) N

(A)

	BS1	BS2	BS3	BS4
BLYP	-0.32	-0.33	-0.34	-0.39
M06-L	0.85	0.76	1.28	1.17
PBE	-0.29	-0.30	-0.32	-0.38
B3LYP	-0.11	-0.13	-0.13	-0.18
PBE0	0.06	0.04	0.02	-0.05
M06	0.68	0.66	1.25	1.20
M06-2X	0.32	0.34	0.47	0.47
M06-HF	-0.14	-0.05	-0.14	0.00
CAM-B3LYP	0.01	-0.02	-0.02	-0.08
Min	-0.32	-0.33	-0.34	-0.39
Max	0.85	0.76	1.28	1.20
Min	0.01	0.02	0.02	0.00
Range	1.18	1.09	1.61	1.59

(B)

	BS1	BS2	BS3	BS4
BLYP	-0.17	-0.17	-0.16	-0.17
M06-L	-0.15	-0.15	-0.15	-0.15
PBE	-0.17	-0.17	-0.17	-0.17
B3LYP	-0.17	-0.17	-0.17	-0.17
PBE0	-0.17	-0.17	-0.17	-0.17
M06	-0.16	-0.16	-0.15	-0.15
M06-2X	-0.16	-0.16	-0.15	-0.15
M06-HF	-0.15	-0.16	-0.16	-0.16
CAM-B3LYP	-0.17	-0.17	-0.17	-0.17
Min	-0.17	-0.17	-0.17	-0.17
Max	-0.15	-0.15	-0.15	-0.15
Min	0.16	0.15	0.15	0.15
Range	0.02	0.02	0.02	0.02

(C)

	BS1	BS2	BS3	BS4
BLYP	-0.63	-0.72	-0.84	-0.83
M06-L	-0.60	-0.72	-0.71	-0.71
PBE	-0.65	-0.74	-0.85	-0.85
B3LYP	-0.58	-0.69	-0.81	-0.81
PBE0	-0.58	-0.69	-0.82	-0.81
M06	-0.67	-0.75	-0.81	-0.78
M06-2X	-0.72	-0.79	-0.76	-0.77
M06-HF	-0.88	-0.86	-0.86	-0.83
CAM-B3LYP	-0.59	-0.69	-0.82	-0.82
Min	-0.88	-0.86	-0.86	-0.85
Max	-0.58	-0.69	-0.71	-0.71
Min	0.58	0.69	0.71	0.71
Range	0.30	0.17	0.14	0.13

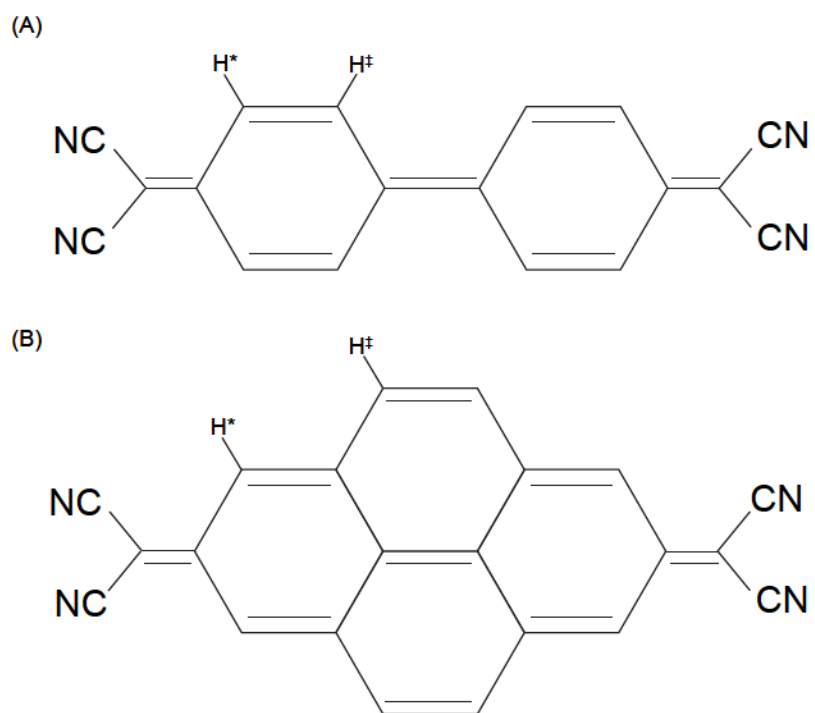


Figure D1: Atom labelling for ESR coupling constants for (A) [TCNDQ]<sup>•-</sup> and (B) [TCNP]<sup>•-</sup>

Table D15: PES energetics (kcal/mol) for 1Si TCNDQ BS1

	C <sub>2v</sub>	C <sub>s</sub>	C <sub>2</sub>	C <sub>1</sub>
BLYP	0.5812	0.089	0.5811	0.00
M06-L	0.12	0.00	–	–
PBE	0.105	0.00	–	–
B3LYP	0.02	0.00	–	–
PBE0	0.00	–	–	–
M06	0.00001	0.00	–	–
M06-2X	0.002	–	0.000	–
M06-HF	0.00	–	–	–
CAM-B3LYP	0.00	–	–	–

Table D17: PES energetics (kcal/mol) for 1Si TCNDQ BS4 (kcal/mol)

	C <sub>2v</sub>	C <sub>s</sub>	C <sub>2</sub>	C <sub>1</sub>
BLYP	0.37	0.08	0.31	0.00
M06-L	0.055	0.00	–	–
PBE	0.134	0.078	0.073	0.00
B3LYP	0.0031	0.002	0.0028	0.00
PBE0	0.00	–	–	–
M06	0.00	–	–	–
M06-2X	0.0001	–	0.00	–
M06-HF	0.00	–	–	–
CAM-B3LYP	0.00	–	–	–

Table D16: Imaginary frequencies (cm<sup>-1</sup>) for 1Si TCNDQ BS1.

	C <sub>2v</sub>		C <sub>s</sub>	C <sub>2</sub>
	b <sub>1</sub>	a <sub>2</sub>	a''	b
BLYP	67 <i>i</i>	6 <i>i</i>	11 <i>i</i>	66 <i>i</i>
M06-L	39 <i>i</i>	–	–	–
PBE	37 <i>i</i>	–	–	–
B3LYP	22 <i>i</i>	–	–	–
PBE0	–	–	–	–
M06	12 <i>i</i>	–	–	–
M06-2X	–	10 <i>i</i>	–	–
M06-HF	–	–	–	–
CAM-B3LYP	–	–	–	–

Table D18: Imaginary frequencies (cm<sup>-1</sup>) for 1Si TCNDQ BS4

	C <sub>2v</sub>		C <sub>s</sub>	C <sub>2</sub>
	b <sub>1</sub>	a <sub>2</sub>	a''	b
BLYP	58 <i>i</i>	22 <i>i</i>	23 <i>i</i>	58 <i>i</i>
M06-L	25 <i>i</i>	–	–	–
PBE	32 <i>i</i>	20 <i>i</i>	22 <i>i</i>	34 <i>i</i>
B3LYP	13 <i>i</i>	7 <i>i</i>	7 <i>i</i>	13 <i>i</i>
PBE0	–	–	–	–
M06	–	–	–	–
M06-2X	–	4 <i>i</i>	–	–
M06-HF	–	–	–	–
CAM-B3LYP	–	–	–	–

Table D19: PES Energetics (kcal/mol) for 2Si TCNDQ BS1

	D <sub>2h</sub>	C <sub>2h</sub>	C <sub>2v</sub>	D <sub>2</sub>	C <sub>2</sub>	C <sub>1</sub>
BLYP	2.82	0.32	0.23	2.76	0.00	–
M06-L	2.22	0.43	0.34	–	0.00	–
PBE	1.70	0.34	0.26	1.64	0.00	–
B3LYP	1.82	0.17	0.10	1.81	0.00	–
PBE0	0.87	0.17	0.12	0.87	0.00	–
M06	1.83	0.07	0.00	–	–	–
M06-2X	0.41	0.10	0.06	0.39	0.00	–
M06-HF	0.00	–	–	–	–	–
CAM-B3LYP	0.35	0.17	0.16	–	0.14	0.00

Table D20: Imaginary frequencies (cm<sup>-1</sup>) for 2Si TCNDQ BS1

	D <sub>2h</sub>			C <sub>2h</sub>	C <sub>2v</sub>	D <sub>2</sub>		C <sub>2</sub>
	b <sub>2g</sub>	b <sub>3u</sub>	a <sub>u</sub>	a <sub>u</sub>	a <sub>2</sub>	b <sub>3</sub>	b <sub>2</sub>	b
BLYP	101 <i>i</i>	103 <i>i</i>	18 <i>i</i>	26 <i>i</i>	25 <i>i</i>	103 <i>i</i>	102 <i>i</i>	–
M06-L	90 <i>i</i>	93 <i>i</i>	–	14 <i>i</i>	12 <i>i</i>	90 <i>i</i>	87 <i>i</i>	–
PBE	77 <i>i</i>	80 <i>i</i>	15 <i>i</i>	22 <i>i</i>	22 <i>i</i>	83 <i>i</i>	80 <i>i</i>	–
B3LYP	84 <i>i</i>	86 <i>i</i>	8 <i>i</i>	19 <i>i</i>	18 <i>i</i>	86 <i>i</i>	84 <i>i</i>	–
PBE0	59 <i>i</i>	62 <i>i</i>	4 <i>i</i>	16 <i>i</i>	16 <i>i</i>	62 <i>i</i>	59 <i>i</i>	–
M06	95 <i>i</i>	97 <i>i</i>	–	–	–	–	–	–
M062X	34 <i>i</i>	35 <i>i</i>	20 <i>i</i>	24 <i>i</i>	24 <i>i</i>	31 <i>i</i>	29 <i>i</i>	–
CAM-B3LYP	37 <i>i</i>	39 <i>i</i>	–	38 <i>i</i>	36 <i>i</i>	38 <i>i</i>	36 <i>i</i>	36 <i>i</i>

Table D21: PES Energetics (kcal/mol) for 2Si TCNDQ BS4

	D <sub>2h</sub>	C <sub>2h</sub>	C <sub>2v</sub>	D <sub>2</sub>	C <sub>2</sub>	C <sub>s</sub>
BLYP	2.44	0.39	0.32	2.28	0.00	–
M06-L	1.87	0.30	0.24	1.83	0.00	–
PBE	1.60	0.41	0.35	1.42	0.00	–
B3LYP	1.65	0.21	0.16	1.64	0.00	–
PBE0	0.91	0.21	0.17	0.87	0.00	–
M06	–	–	–	–	–	–
M06-2X	0.44	0.17	0.15	0.42	0.00	–
M06-HF	0.00	–	–	–	–	–
CAM-B3LYP	0.21	0.07	0.05	–	–	0.00

Table D22: Imaginary frequencies ( $\text{cm}^{-1}$ ) for 2Si TCNDQ BS4

	D <sub>2h</sub>			C <sub>2h</sub>		C <sub>2v</sub>		D <sub>2</sub>	
	D <sub>2h</sub>	C <sub>2h</sub>	C <sub>2v</sub>	D <sub>2</sub>	D <sub>2h</sub>	C <sub>2h</sub>	C <sub>2v</sub>	D <sub>2</sub>	D <sub>2h</sub>
BLYP	97i	99i	29i	36i	–	36i	–	101i	99i
M06L	85i	87i	17i	24i	–	24i	–	86i	84i
PBE	76i	79i	28i	33i	–	34i	–	81i	79i
B3LYP	84i	86i	20i	27i	–	28i	–	86i	84i
PBE0	63i	65i	18i	25i	–	25i	–	67i	65i
M06-2X	30i	31i	18i	25i	–	25i	–	37i	36i
CAM-B3LYP	36i	37i	–	–	26i	–	27i	–	–

Table D23: PES Energetics (kcal/mol) for 1Si TCNP BS1

	C <sub>2v</sub>	C <sub>s</sub>
BLYP	0.65	0.00
PBE	0.19	0.00
M06-L	0.05	0.00
B3LYP	0.08	0.00
PBE0	0.00	–
M06	0.02	0.00
M06-2X	0.00	–
M06-HF	0.00	–
CAM-B3LYP	0.00	–

Table D24: Imaginary frequencies ( $\text{cm}^{-1}$ ) for 1Si TCNP BS1

	C <sub>2v</sub>
	b <sub>1</sub>
BLYP	73i
PBE	45i
M06-L	45i
B3LYP	34i
PBE0	–
M06	21i
M06-2X	–
M06-HF	–
CAM-B3LYP	–

Table D25: PES Energetics (kcal/mol) for 1Si TCNP BS4

	C <sub>2v</sub>	C <sub>s</sub>
BLYP	0.41	0.00
PBE	0.12	0.00
M06-L	0.12	0.00
B3LYP	0.03	0.00
PBE0	0.00	–
M06	0.00	–
M06-2X	0.00	–
M06-HF	0.00	–
CAM-B3LYP	0.00	–

Table D26: Imaginary frequencies (cm<sup>-1</sup>) for 1Si TCNP BS4

	C <sub>2v</sub>
	b <sub>1</sub>
BLYP	67 <i>i</i>
PBE	41 <i>i</i>
M06-L	33 <i>i</i>
B3LYP	27 <i>i</i>
PBE0	–
M06	–
M06-2X	–
M06-HF	–
CAM-B3LYP	–

Table D27: PES Energetics (kcal/mol) for 2Si TCNP BS1

	D <sub>2h</sub>	C <sub>2h</sub>	C <sub>2v</sub>	C <sub>s</sub>
BLYP	3.29	0.00	0.04	–
PBE	2.04	0.00	0.03	–
M06-L	2.58	0.00	0.07	–
B3LYP	2.45	0.00	0.02	–
PBE0	1.37	0.00	0.01	–
M06	2.60	0.00	0.03	–
M06-2X	1.23	0.13	0.14	0.00
M06-HF	0.00	–	–	–
CAM-B3LYP	1.36	0.41	0.40	0.00

Table D28: Imaginary frequencies ( $\text{cm}^{-1}$ ) for 2Si TCNP BS1

	D <sub>2h</sub>		C <sub>2h</sub>	C <sub>2v</sub>
	b <sub>2g</sub>	b <sub>3u</sub>	b <sub>u</sub>	b <sub>2</sub>
BLYP	115 <i>i</i>	115 <i>i</i>	–	–
PBE	92 <i>i</i>	92 <i>i</i>	–	–
M06-L	105 <i>i</i>	106 <i>i</i>	–	–
B3LYP	100 <i>i</i>	101 <i>i</i>	–	–
PBE0	78 <i>i</i>	79 <i>i</i>	–	–
M06	112 <i>i</i>	113 <i>i</i>	–	–
M06-2X	61 <i>i</i>	62 <i>i</i>	14 <i>i</i>	23 <i>i</i>
M06-HF	–	–	–	–
CAM-B3LYP	66 <i>i</i>	67 <i>i</i>	44 <i>i</i>	43 <i>i</i>

Table D29: PES Energetics (kcal/mol) for 2Si TCNP BS4

	D <sub>2h</sub>	C <sub>2v</sub>	C <sub>2h</sub>	C <sub>s</sub>
BLYP	2.78	0.02	0.00	–
PBE	1.81	0.02	0.00	–
M06-L	2.31	0.01	0.00	–
B3LYP	2.20	0.01	0.00	–
PBE0	1.36	0.00	0.00	–
M06	2.22	0.00	0.02	–
M06-2X	0.99	0.00	0.00	–
M06-HF	0.00	–	–	–
CAM-B3LYP	1.07	0.22	0.22	0.00

Table D30: Imaginary frequencies ( $\text{cm}^{-1}$ ) for 2Si TCNP BS4

	D <sub>2h</sub>		C <sub>2h</sub>	C <sub>2v</sub>
	b <sub>3u</sub>	b <sub>2g</sub>	b <sub>u</sub>	b <sub>2</sub>
BLYP	113 <i>i</i>	112 <i>i</i>	–	–
PBE	91 <i>i</i>	91 <i>i</i>	–	–
M06-L	100 <i>i</i>	100 <i>i</i>	–	–
B3LYP	102 <i>i</i>	101 <i>i</i>	–	–
PBE0	83 <i>i</i>	82 <i>i</i>	–	–
M06	107 <i>i</i>	107 <i>i</i>	–	–
M06-2X	61 <i>i</i>	59 <i>i</i>	–	–
M06-HF	–	–	–	–
CAM-B3LYP	68 <i>i</i>	67 <i>i</i>	34 <i>i</i>	34 <i>i</i>

Table D31: PES Energetics (kcal/mol) for [1Si TCNDQ]<sup>-</sup> BS1

	C <sub>2v</sub>	C <sub>s</sub>	C <sub>2</sub>	C <sub>1</sub>
BLYP	8.17	0.44	7.86	0.00
M06-L	7.43	0.21	7.34	0.00
PBE	6.92	0.43	6.62	0.00
B3LYP	8.33	0.37	8.07	0.00
PBE0	7.12	0.36	6.84	0.00
M06	7.68	0.21	7.57	0.00
M06-2X	6.84	0.52	6.30	0.00
M06-HF	9.52	1.14	8.44	0.00
CAM-B3LYP	6.77	0.26	6.84	0.00

Table D32: Imaginary frequencies (cm<sup>-1</sup>) for [1Si TCNDQ]<sup>-</sup> BS1

	C <sub>2v</sub>		C <sub>s</sub>	C <sub>2</sub>
	b <sub>1</sub>	a <sub>2</sub>	a''	b
BLYP	212 <i>i</i>	41 <i>i</i>	45 <i>i</i>	212 <i>i</i>
M06-L	202 <i>i</i>	31 <i>i</i>	28 <i>i</i>	204 <i>i</i>
PBE	193 <i>i</i>	38 <i>i</i>	43 <i>i</i>	194 <i>i</i>
B3LYP	223 <i>i</i>	38 <i>i</i>	42 <i>i</i>	223 <i>i</i>
PBE0	213 <i>i</i>	37 <i>i</i>	40 <i>i</i>	214 <i>i</i>
M06	185 <i>i</i>	31 <i>i</i>	36 <i>i</i>	186 <i>i</i>
M06-2X	288 <i>i</i>	53 <i>i</i>	51 <i>i</i>	293 <i>i</i>
M06-HF	665 <i>i</i>	69 <i>i</i>	77 <i>i</i>	738 <i>i</i>
CAM-B3LYP	237 <i>i</i>	41 <i>i</i>	36 <i>i</i>	237 <i>i</i>

Table D33: PES Energetics (kcal/mol) for [1Si TCNDQ]<sup>-</sup> BS4

	C <sub>2v</sub>	C <sub>s</sub>	C <sub>2</sub>	C <sub>1</sub>
BLYP	9.45	0.36	9.23	0.00
M06-L	8.69	0.29	8.54	0.00
PBE	7.88	0.35	7.69	0.00
B3LYP	9.61	0.31	9.43	0.00
PBE0	8.13	0.31	7.94	0.00
M06	9.38	0.17	–	0.00
M06-2X	8.79	0.42	8.37	0.00
M06-HF	10.18	1.02	9.23	0.00
CAM-B3LYP	8.67	0.34	8.46	0.00

Table D34: Imaginary frequencies ( $\text{cm}^{-1}$ ) for  $[\text{1Si TCNDQ}]^-$  BS4

	$C_{2v}$		$C_s$	$C_2$
	$b_1$	$a_2$	$a''$	$b$
BLYP	214 <i>i</i>	29 <i>i</i>	36 <i>i</i>	215 <i>i</i>
M06-L	196 <i>i</i>	20 <i>i</i>	16 <i>i</i>	198 <i>i</i>
PBE	195 <i>i</i>	25 <i>i</i>	33 <i>i</i>	197 <i>i</i>
B3LYP	223 <i>i</i>	28 <i>i</i>	34 <i>i</i>	223 <i>i</i>
PBE0	211 <i>i</i>	26 <i>i</i>	32 <i>i</i>	212 <i>i</i>
M06	186 <i>i</i>	–	21 <i>i</i>	–
M06-2X	281 <i>i</i>	50 <i>i</i>	43 <i>i</i>	201 <i>i</i>
M06-HF	702 <i>i</i>	70 <i>i</i>	71 <i>i</i>	744 <i>i</i>
CAM-B3LYP	232 <i>i</i>	31 <i>i</i>	37 <i>i</i>	232 <i>i</i>

Table D35: PES Energetics (kcal/mol) for  $[\text{2Si TCNDQ}]^-$  BS1

	$D_{2h}$	$C_{2h}$	$C_{2v}$	$D_2$	$C_2$	$C_1$
BLYP	20.35	0.67	0.65	20.08	0.00	–
M06L	19.32	0.63	0.63	19.11	0.00	–
PBE	17.54	0.70	0.68	17.29	0.00	–
B3LYP	22.17	0.65	0.65	21.94	0.00	–
PBE0	20.24	0.72	0.71	20.01	0.00	–
M06	22.25	0.39	0.40	22.14	0.00	–
M062X	26.93	3.37	3.36	26.60	2.49	0.00
M06-HF	41.40	13.76	13.77	41.27	12.94	0.00
CAM-B3LYP	26.57	3.57	3.57	26.47	3.06	0.00

Table D36: Imaginary frequencies ( $\text{cm}^{-1}$ ) for  $[\text{2Si TCNDQ}]^-$  BS1

	$D_{2h}$			$C_{2h}$		$C_{2v}$		$D_2$		$C_2$
	$b_{2g}$	$b_{3u}$	$a_u$	$a_u$	$b_u$	$a_2$	$b_2$	$b_3$	$b_2$	$b$
BLYP	220 <i>i</i>	220 <i>i</i>	32 <i>i</i>	47 <i>i</i>	–	47 <i>i</i>	–	221 <i>i</i>	221 <i>i</i>	–
M06L	210 <i>i</i>	210 <i>i</i>	28 <i>i</i>	40 <i>i</i>	–	40 <i>i</i>	–	213 <i>i</i>	213 <i>i</i>	–
PBE	201 <i>i</i>	201 <i>i</i>	27 <i>i</i>	44 <i>i</i>	–	43 <i>i</i>	–	203 <i>i</i>	203 <i>i</i>	–
B3LYP	229 <i>i</i>	229 <i>i</i>	30 <i>i</i>	48 <i>i</i>	–	47 <i>i</i>	–	231 <i>i</i>	231 <i>i</i>	–
PBE0	217 <i>i</i>	217 <i>i</i>	28 <i>i</i>	47 <i>i</i>	–	47 <i>i</i>	–	220 <i>i</i>	220 <i>i</i>	–
M06	212 <i>i</i>	211 <i>i</i>	13 <i>i</i>	35 <i>i</i>	–	35 <i>i</i>	–	212 <i>i</i>	212 <i>i</i>	–
M062X	262 <i>i</i>	262 <i>i</i>	48 <i>i</i>	62 <i>i</i>	62 <i>i</i>	60 <i>i</i>	56 <i>i</i>	263 <i>i</i>	263 <i>i</i>	74 <i>i</i>
M06-HF	369 <i>i</i>	369 <i>i</i>	53 <i>i</i>	72 <i>i</i>	453 <i>i</i>	71 <i>i</i>	452 <i>i</i>	371 <i>i</i>	371 <i>i</i>	582 <i>i</i>
CAM-B3LYP	240 <i>i</i>	240 <i>i</i>	23 <i>i</i>	43 <i>i</i>	441 <i>i</i>	43 <i>i</i>	430 <i>i</i>	240 <i>i</i>	240 <i>i</i>	468 <i>i</i>

Table D37: PES Energetics (kcal/mol) for [2Si TCNDQ]<sup>-</sup> BS4

	D <sub>2h</sub>	C <sub>2h</sub>	C <sub>2v</sub>	D <sub>2</sub>	C <sub>2</sub>	C <sub>s</sub>	C <sub>1</sub>
BLYP	18.32	0.77	0.77	17.95	0.00	–	–
M06-L	17.64	0.55	0.55	17.49	0.00	–	–
PBE	15.96	0.77	0.77	17.49	0.00	–	–
B3LYP	20.44	0.74	0.75	20.12	0.00	–	–
PBE0	18.84	0.76	0.76	18.54	0.00	–	–
M06-2X	25.91	4.28	4.28	25.55	3.34	1.40	0.00
M06-HF	38.76	14.01	14.05	38.59	13.12	2.14	0.00
CAM-B3LYP	25.25	4.03	4.05	25.09	3.44	1.06	0.00

Table D38: Imaginary frequencies (cm<sup>-1</sup>) for [2Si TCNDQ]<sup>-</sup> BS4

	D <sub>2h</sub>			C <sub>2h</sub>	C <sub>2v</sub>	D <sub>2</sub>		C <sub>2</sub>
	b <sub>2g</sub>	b <sub>3u</sub>	a <sub>u</sub>	a <sub>u</sub>	a <sub>2</sub>	b <sub>2</sub>	b <sub>3</sub>	b
BLYP	217 <i>i</i>	217 <i>i</i>	44 <i>i</i>	57 <i>i</i>	57 <i>i</i>	218 <i>i</i>	218 <i>i</i>	–
M06-L	221 <i>i</i>	221 <i>i</i>	35 <i>i</i>	47 <i>i</i>	55 <i>i</i>	224 <i>i</i>	224 <i>i</i>	–
PBE	199 <i>i</i>	199 <i>i</i>	41 <i>i</i>	55 <i>i</i>	55 <i>i</i>	201 <i>i</i>	201 <i>i</i>	–
B3LYP	229 <i>i</i>	229 <i>i</i>	41 <i>i</i>	56 <i>i</i>	56 <i>i</i>	231 <i>i</i>	231 <i>i</i>	–
PBE0	218 <i>i</i>	218 <i>i</i>	38 <i>i</i>	55 <i>i</i>	55 <i>i</i>	220 <i>i</i>	220 <i>i</i>	–
M06-2X	258 <i>i</i>	258 <i>i</i>	46 <i>i</i>	61 <i>i</i>	60 <i>i</i>	262 <i>i</i>	262 <i>i</i>	113 <i>i</i>
M06-HF	309 <i>i</i>	309 <i>i</i>	46 <i>i</i>	68 <i>i</i>	68 <i>i</i>	318 <i>i</i>	318 <i>i</i>	27 <i>i</i>
CAM-B3LYP	241 <i>i</i>	241 <i>i</i>	40 <i>i</i>	50 <i>i</i>	50 <i>i</i>	242 <i>i</i>	241 <i>i</i>	593 <i>i</i>

Table D39: PES Energetics (kcal/mol) for [1Si TCNP]<sup>-</sup> BS1

	C <sub>2v</sub>	C <sub>s</sub>	C <sub>1</sub>
BLYP	9.26	0.00	–
PBE	7.67	0.00	–
M06-L	8.54	0.00	–
B3LYP	9.17	0.00	–
PBE0	7.45	0.00	–
M06	8.86	0.00	–
M06-2X	7.25	0.00	–
M06-HF	9.20	0.02	0.00
CAM-B3LYP	8.05	0.00	–

Table D40: Imaginary frequencies ( $\text{cm}^{-1}$ ) for  $[\text{1Si TCNP}]^-$  BS1

	$C_{2v}$	$C_s$
	$b_1$	$a''$
BLYP	216 <i>i</i>	–
PBE	198 <i>i</i>	–
M06-L	194 <i>i</i>	–
B3LYP	223 <i>i</i>	–
PBE0	211 <i>i</i>	–
M06	181 <i>i</i>	–
M06-2X	285 <i>i</i>	4 <i>i</i>
M06-HF	741 <i>i</i>	–
CAM-B3LYP	231 <i>i</i>	–

Table D41: PES Energetics (kcal/mol) for  $[\text{1Si TCNP}]^-$  BS4

	$C_{2v}$	$C_s$
BLYP	7.85	0.00
PBE	6.57	0.00
M06-L	7.31	0.00
B3LYP	7.73	0.00
PBE0	6.34	0.00
M06	6.96	0.00
M06-2X	6.04	0.00
M06-HF	8.37	0.00
CAM-B3LYP	5.99	0.00

Table D42: Imaginary frequencies ( $\text{cm}^{-1}$ ) for  $[\text{1Si TCNP}]^-$  BS4

	$C_{2v}$
	$b_1$
BLYP	214 <i>i</i>
PBE	196 <i>i</i>
M06-L	198 <i>i</i>
B3LYP	224 <i>i</i>
PBE0	214 <i>i</i>
M06	179 <i>i</i>
M06-2X	293 <i>i</i>
M06-HF	700 <i>i</i>
CAM-B3LYP	238 <i>i</i>

Table D43: PES Energetics (kcal/mol) for [2Si TCNP]<sup>-</sup> BS1

	D <sub>2h</sub>	C <sub>2h</sub>	C <sub>2v</sub>	C <sub>s</sub>
BLYP	20.86	0.00	0.10	–
PBE	18.01	0.00	0.089	–
M06-L	19.83	0.00	0.12	–
B3LYP	22.62	0.00	0.09	–
PBE0	20.64	0.00	0.08	–
M06-2X	28.55	3.82	3.94	0.00
M06-HF	0.00	–	–	–
CAM-B3LYP	28.61	4.48	4.55	0.00

Table D44: Imaginary frequencies (cm<sup>-1</sup>) [2Si TCNP]<sup>-</sup> BS1

	D <sub>2h</sub>		C <sub>2h</sub>	C <sub>2v</sub>
	b <sub>2g</sub>	b <sub>3u</sub>	b <sub>u</sub>	b <sub>2</sub>
BLYP	226 <i>i</i>	226 <i>i</i>	–	–
PBE	207 <i>i</i>	207 <i>i</i>	–	–
M06-L	214 <i>i</i>	214 <i>i</i>	–	–
B3LYP	235 <i>i</i>	235 <i>i</i>	–	–
PBE0	223 <i>i</i>	223 <i>i</i>	–	–
M06-2X	267 <i>i</i>	267 <i>i</i>	171 <i>i</i>	167 <i>i</i>
M06-HF	–	–	–	–
CAM-B3LYP	245 <i>i</i>	245 <i>i</i>	851 <i>i</i>	839 <i>i</i>

Table D45: PES Energetics (kcal/mol) for [2Si TCNP]<sup>-</sup> BS4

	D <sub>2h</sub>	C <sub>2h</sub>	C <sub>2v</sub>	C <sub>s</sub>
BLYP	18.71	0.00	0.07	–
PBE	16.34	0.00	0.07	–
M06-L	18.28	0.00	0.09	–
B3LYP	20.80	0.00	0.06	–
PBE0	19.22	0.000	0.06	–
M06	20.94	0.013	0.014	0.00
M06-2X	27.43	4.65	4.71	0.00
M06-HF	25.86	0.00	0.01	–
CAM-B3LYP	27.15	4.74	4.80	0.00

Table D46: Imaginary frequencies ( $\text{cm}^{-1}$ ) for  $[\text{2Si TCNP}]^-$  BS4

	$D_{2h}$		$C_{2h}$	$C_{2v}$
	$b_{2g}$	$b_{3u}$	$b_u$	$b_2$
BLYP	224 <i>i</i>	224 <i>i</i>	–	–
PBE	206 <i>i</i>	205 <i>i</i>	–	–
M06-L	225 <i>i</i>	225 <i>i</i>	–	–
B3LYP	235 <i>i</i>	235 <i>i</i>	–	–
PBE0	224 <i>i</i>	224 <i>i</i>	–	–
M06	218 <i>i</i>	217 <i>i</i>	151 <i>i</i>	155 <i>i</i>
M06-2X	263 <i>i</i>	263 <i>i</i>	221 <i>i</i>	214 <i>i</i>
M06-HF	315 <i>i</i>	315 <i>i</i>	–	–
CAM-B3LYP	246 <i>i</i>	246 <i>i</i>	1233 <i>i</i>	1206 <i>i</i>

Table D47:  $\langle S^2 \rangle$  values for  $[\text{1Si TCNDQ}]^-$  BS2

	$C_{2v}$	$C_s$	$C_2$	$C_1$
BLYP	0.75	0.76	0.75	0.76
M06-L	0.77	0.76	0.76	0.76
PBE	0.78	0.76	0.76	0.76
B3LYP	0.77	0.77	0.77	0.77
PBE0	0.77	0.78	0.78	0.77
M06	0.76	0.77	0.77	0.77
M06-2X	0.78	0.79	0.78	0.78
M06-HF	0.76	0.77	0.77	0.76
CAM-B3LYP	0.79	0.81	0.79	0.80

Table D48:  $\langle S^2 \rangle$  values for  $[\text{1Si TCNDQ}]^-$  BS4

	$C_{2v}$	$C_s$	$C_2$	$C_1$
BLYP	0.75	0.76	0.75	0.76
M06-L	0.76	0.76	0.76	0.76
PBE	0.76	0.76	0.76	0.76
B3LYP	0.77	0.77	0.77	0.77
PBE0	0.78	0.78	0.77	0.78
M06	0.77	0.77	0.77	0.77
M06-2X	0.78	0.78	0.77	0.78
M06-HF	0.77	0.76	0.77	0.76
CAM-B3LYP	0.79	0.80	0.78	0.79

Table D49:  $\langle S^2 \rangle$  values for [2Si TCNDQ]<sup>-</sup> BS2

	D <sub>2h</sub>	C <sub>2h</sub>	C <sub>2v</sub>	D <sub>2</sub>	C <sub>2</sub>	C <sub>1</sub>
BLYP	0.76	0.76	0.76	0.76	0.76	–
M06-L	0.77	0.76	0.83	0.77	0.76	–
PBE	0.76	0.76	0.79	0.76	0.76	–
B3LYP	0.79	0.77	0.77	0.78	0.77	–
PBE0	0.81	0.78	0.76	0.80	0.78	–
M06	0.79	0.76	0.76	0.79	0.76	–
M06-2X	0.84	0.79	0.78	0.83	0.78	0.76
M06-HF	0.95	0.83	0.76	0.93	0.82	0.76
CAM-B3LYP	0.89	0.81	0.81	0.89	0.80	0.77

Table D50:  $\langle S^2 \rangle$  values for [2Si TCNDQ]<sup>-</sup> BS4

	D <sub>2h</sub>	C <sub>2h</sub>	C <sub>2v</sub>	D <sub>2</sub>	C <sub>2</sub>	C <sub>1</sub>
BLYP	0.76	0.76	0.77	0.76	0.76	–
M06-L	0.77	0.77	0.76	0.77	0.76	–
PBE	0.76	0.76	0.76	0.76	0.76	–
B3LYP	0.79	0.77	0.77	0.79	0.77	–
PBE0	0.81	0.79	0.79	0.81	0.78	–
M06	0.80	0.77	0.77	0.80	0.77	–
M06-2X	0.85	0.80	0.80	0.84	0.79	0.77
M06-HF	0.97	0.85	0.85	0.95	0.77	0.78
CAM-B3LYP	0.91	0.82	0.82	0.90	0.81	0.77

Table D51:  $\langle S^2 \rangle$  values for [1Si TCNP]<sup>-</sup> BS2

	C <sub>2v</sub>	C <sub>s</sub>
BLYP	0.75	0.76
M06-L	0.76	0.76
PBE	0.76	0.76
B3LYP	0.77	0.77
PBE0	0.77	0.78
M06	0.77	0.77
M06-2X	0.77	0.78
M06-HF	0.77	0.76
CAM-B3LYP	0.78	0.82

Table D52:  $\langle S^2 \rangle$  values for [1Si TCNP]<sup>-</sup> BS4

	C <sub>2v</sub>	C <sub>s</sub>
BLYP	0.75	0.76
M06-L	0.76	0.76
PBE	0.76	0.76
B3LYP	0.76	0.77
PBE0	0.77	0.78
M06	0.77	0.77
M06-2X	0.77	0.76
M06-HF	0.77	0.76
CAM-B3LYP	0.78	0.77

Table D53:  $\langle S^2 \rangle$  values for [2Si TCNP]<sup>-</sup> BS2

	D <sub>2h</sub>	C <sub>2h</sub>	C <sub>2v</sub>
BLYP	0.76	0.76	0.76
M06-L	0.76	0.76	0.76
PBE	0.76	0.76	0.76
B3LYP	0.78	0.77	0.77
PBE0	0.79	0.77	0.77
M06	0.78	0.76	0.76
M06-2X	0.81	0.78	0.78
M06-HF	0.89	0.82	0.82
CAM-B3LYP	0.85	0.80	0.80

Table D54:  $\langle S^2 \rangle$  values for [2Si TCNP]<sup>-</sup> BS4

	D <sub>2h</sub>	C <sub>2h</sub>	C <sub>2v</sub>
BLYP	0.76	0.76	0.76
M06-L	0.77	0.76	0.76
PBE	0.76	0.76	0.76
B3LYP	0.78	0.77	0.77
PBE0	0.79	0.78	0.78
M06	0.79	0.77	0.77
M06-2X	0.82	0.79	0.79
M06-HF	0.91	0.83	0.83
CAM-B3LYP	0.86	0.81	0.81

Table D55:  $\langle S^2A \rangle$  values for [1Si TCNDQ]<sup>-</sup> BS2

	C <sub>2v</sub>	C <sub>s</sub>	C <sub>2</sub>	C <sub>1</sub>
M06-2X	0.750	0.751	0.750	0.751
M06-HF	0.750	0.750	0.750	0.750
CAM-B3LYP	0.751	0.752	0.751	-

Table D56:  $\langle S^2A \rangle$  values for [1Si TCNDQ]<sup>-</sup> BS4

	C <sub>2v</sub>	C <sub>s</sub>	C <sub>2</sub>	C <sub>1</sub>
M06-2X	0.750	0.750	0.750	0.750
M06-HF	0.750	0.750	0.750	0.750
CAM-B3LYP	0.750	0.751	0.751	0.751

Table D57:  $\langle S^2A \rangle$  values for [2Si TCNDQ]<sup>-</sup> BS2

	D <sub>2h</sub>	C <sub>2h</sub>	C <sub>2v</sub>	D <sub>2</sub>	C <sub>2</sub>	C <sub>1</sub>
M06-2X	0.750	0.750	0.750	0.751	0.750	0.750
M06-HF	0.758	0.752	0.752	0.757	0.751	0.750
CAM-B3LYP	0.756	0.751	0.751	0.755	0.751	0.750

Table D58:  $\langle S^2A \rangle$  values for [2Si TCNDQ]<sup>-</sup> BS4

	D <sub>2h</sub>	C <sub>2h</sub>	C <sub>2v</sub>	D <sub>2</sub>	C <sub>2</sub>	C <sub>1</sub>
M06-2X	0.752	0.750	0.750	0.752	0.750	0.750
M06-HF	0.761	0.752	0.752	0.759	0.750	0.752
CAM-B3LYP	0.756	0.751	0.751	0.756	0.751	0.750

Table D59:  $\langle S^2A \rangle$  values for [1Si TCNP]<sup>-</sup> BS2

	C <sub>2v</sub>	C <sub>s</sub>
M06-2X	0.750	0.751
M06-HF	0.750	0.750
CAM-B3LYP	0.751	0.755

Table D60:  $\langle S^2A \rangle$  values for [1Si TCNP]<sup>-</sup> BS4

	C <sub>2v</sub>	C <sub>s</sub>
M06-2X	0.750	0.750
M06-HF	0.750	0.750
CAM-B3LYP	0.751	0.750

Table D61:  $\langle S^2 A \rangle$  values for  $[2\text{Si TCNP}]^-$  BS2

	D <sub>2h</sub>	C <sub>2h</sub>	C <sub>2v</sub>
M06-2X	0.751	0.750	0.750
M06-HF	0.754	0.751	0.751
CAM-B3LYP	0.753	0.750	0.750

Table D62:  $\langle S^2 A \rangle$  values for  $[2\text{Si TCNP}]^-$  BS4

	D <sub>2h</sub>	C <sub>2h</sub>	C <sub>2v</sub>
M06-2X	0.751	0.750	0.750
M06-HF	0.756	0.751	0.751
CAM-B3LYP	0.753	0.751	0.751

Table D63: Bond lengths (Å) for 1Si TCNDQ PES BS2

C <sub>2v</sub>	R <sub>1</sub>	R <sub>2</sub>	R <sub>3</sub>	R <sub>4</sub>	R <sub>5</sub>	R <sub>6</sub>	R <sub>7</sub>	R <sub>8</sub>	R <sub>9</sub>	R <sub>10</sub>	R <sub>11</sub>	R <sub>12</sub>	R <sub>13</sub>
B3LYP	1.433	1.436	1.372	1.432	1.779	1.816	1.168	1.436	1.369	1.436	1.407	1.424	1.167
BLYP	1.454	1.441	1.386	1.437	1.804	1.822	1.181	1.441	1.383	1.441	1.428	1.429	1.181
CAM-B3LYP	1.408	1.442	1.358	1.437	1.749	1.817	1.160	1.441	1.356	1.440	1.387	1.427	1.160
M06	1.423	1.431	1.365	1.428	1.765	1.816	1.167	1.431	1.362	1.432	1.399	1.421	1.167
M06-2X	1.411	1.442	1.361	1.436	1.751	1.821	1.161	1.441	1.359	1.441	1.387	1.429	1.160
M06-HF	1.389	1.457	1.352	1.449	1.728	1.827	1.149	1.456	1.350	1.454	1.370	1.440	1.148
M06-L	1.436	1.427	1.371	1.425	1.782	1.808	1.174	1.427	1.369	1.427	1.411	1.415	1.173
PBE0	1.427	1.431	1.367	1.428	1.772	1.814	1.166	1.431	1.364	1.431	1.401	1.420	1.166
PBE	1.449	1.434	1.382	1.431	1.799	1.818	1.181	1.435	1.379	1.435	1.423	1.422	1.181
C <sub>s</sub>	R <sub>1</sub>	R <sub>2</sub>	R <sub>3</sub>	R <sub>4</sub>	R <sub>5</sub>	R <sub>6</sub>	R <sub>7</sub>	R <sub>8</sub>	R <sub>9</sub>	R <sub>10</sub>	R <sub>11</sub>	R <sub>12</sub>	R <sub>13</sub>
B3LYP	1.434	1.435	1.372	1.431	1.785	1.821	1.168	1.436	1.369	1.436	1.407	1.424	1.167
BLYP	1.457	1.439	1.388	1.435	1.827	1.841	1.181	1.441	1.383	1.440	1.428	1.428	1.181
M06	1.423	1.431	1.365	1.428	1.765	1.816	1.167	1.431	1.362	1.432	1.399	1.421	1.167
M06-L	1.438	1.426	1.372	1.423	1.795	1.819	1.173	1.427	1.369	1.427	1.411	1.415	1.173
PBE	1.450	1.434	1.383	1.430	1.810	1.827	1.181	1.435	1.379	1.434	1.423	1.422	1.181
C <sub>2</sub>	R <sub>1</sub>	R <sub>2</sub>	R <sub>3</sub>	R <sub>4</sub>	R <sub>5</sub>	R <sub>6</sub>	R <sub>7</sub>	R <sub>8</sub>	R <sub>9</sub>	R <sub>10</sub>	R <sub>11</sub>	R <sub>12</sub>	R <sub>13</sub>
BLYP	1.454	1.441	1.386	1.437	1.804	1.822	1.181	1.441	1.383	1.441	1.428	1.429	1.181
M06-2X	1.411	1.441	1.362	1.436	1.751	1.821	1.161	1.441	1.359	1.441	1.387	1.429	1.160
M06-HF	1.389	1.457	1.352	1.449	1.728	1.827	1.149	1.456	1.350	1.454	1.370	1.440	1.148

Table D64: Bond lengths (Å) for 1Si TCNDQ PES BS4.

C <sub>2v</sub>	R <sub>1</sub>	R <sub>2</sub>	R <sub>3</sub>	R <sub>4</sub>	R <sub>5</sub>	R <sub>6</sub>	R <sub>7</sub>	R <sub>8</sub>	R <sub>9</sub>	R <sub>10</sub>	R <sub>11</sub>	R <sub>12</sub>	R <sub>13</sub>
B3LYP	1.426	1.429	1.363	1.426	1.764	1.800	1.156	1.429	1.360	1.430	1.399	1.417	1.156
BLYP	1.447	1.433	1.377	1.431	1.788	1.805	1.169	1.434	1.374	1.434	1.420	1.421	1.169
CAM-B3LYP	1.400	1.436	1.349	1.431	1.734	1.801	1.148	1.434	1.347	1.434	1.379	1.420	1.148
M06	1.415	1.425	1.356	1.421	1.749	1.800	1.154	1.425	1.353	1.425	1.390	1.415	1.153
M06-2X	1.404	1.437	1.354	1.432	1.738	1.807	1.150	1.437	1.351	1.436	1.380	1.424	1.150
M06-HF	1.382	1.452	1.345	1.444	1.715	1.814	1.139	1.450	1.342	1.449	1.363	1.433	1.139
M06-L	1.430	1.420	1.363	1.419	1.767	1.792	1.162	1.421	1.360	1.421	1.404	1.409	1.160
PBE0	1.420	1.425	1.360	1.422	1.758	1.799	1.155	1.426	1.357	1.426	1.394	1.414	1.155
PBE	1.443	1.428	1.375	1.425	1.784	1.802	1.170	1.429	1.372	1.428	1.416	1.416	1.170

C <sub>s</sub>	R <sub>1</sub>	R <sub>2</sub>	R <sub>3</sub>	R <sub>4</sub>	R <sub>5</sub>	R <sub>6</sub>	R <sub>7</sub>	R <sub>8</sub>	R <sub>9</sub>	R <sub>10</sub>	R <sub>11</sub>	R <sub>12</sub>	R <sub>13</sub>
B3LYP	1.426	1.429	1.363	1.426	1.764	1.801	1.156	1.429	1.360	1.430	1.399	1.417	1.156
BLYP	1.449	1.432	1.379	1.428	1.804	1.818	1.169	1.434	1.374	1.434	1.420	1.421	1.169
M06L	1.431	1.420	1.364	1.418	1.774	1.798	1.161	1.421	1.360	1.421	1.404	1.409	1.160
PBE0	1.444	1.428	1.375	1.424	1.791	1.808	1.170	1.428	1.372	1.428	1.416	1.416	1.170

C <sub>2</sub>	R <sub>1</sub>	R <sub>2</sub>	R <sub>3</sub>	R <sub>4</sub>	R <sub>5</sub>	R <sub>6</sub>	R <sub>7</sub>	R <sub>8</sub>	R <sub>9</sub>	R <sub>10</sub>	R <sub>11</sub>	R <sub>12</sub>	R <sub>13</sub>
B3LYP	1.426	1.429	1.363	1.426	1.764	1.800	1.156	1.429	1.360	1.430	1.399	1.417	1.156
BLYP	1.447	1.433	1.378	1.431	1.789	1.805	1.169	1.433	1.374	1.434	1.420	1.421	1.169
M06-2X	1.404	1.437	1.354	1.432	1.738	1.807	1.150	1.437	1.351	1.436	1.380	1.424	1.150
PBE	1.442	1.427	1.375	1.425	1.784	1.802	1.170	1.428	1.372	1.428	1.416	1.416	1.170

Table D65: Bond lengths (Å) for 2Si TCNDQ PES BS2.

D <sub>2h</sub>	R <sub>1</sub>	R <sub>2</sub>	R <sub>3</sub>	R <sub>4</sub>	R <sub>5</sub>	R <sub>6</sub>	R <sub>7</sub>
B3LYP	1.444	1.430	1.375	1.429	1.788	1.815	1.168
BLYP	1.463	1.437	1.388	1.435	1.811	1.821	1.182
CAM-B3LYP	1.418	1.435	1.361	1.433	1.758	1.816	1.161
M06	1.434	1.426	1.369	1.424	1.775	1.815	1.168
M06-2X	1.424	1.434	1.365	1.432	1.762	1.820	1.161
M06-HF	1.397	1.451	1.355	1.447	1.735	1.828	1.150
M06-L	1.445	1.423	1.374	1.422	1.789	1.807	1.174
PBE0	1.437	1.426	1.371	1.424	1.781	1.812	1.167
PBE	1.457	1.431	1.385	1.429	1.805	1.817	1.182

C <sub>2h</sub>	R <sub>1</sub>	R <sub>2</sub>	R <sub>3</sub>	R <sub>4</sub>	R <sub>5</sub>	R <sub>6</sub>	R <sub>7</sub>
B3LYP	1.452	1.427	1.378	1.425	1.815	1.835	1.168
BLYP	1.470	1.434	1.391	1.431	1.841	1.846	1.181
CAM-B3LYP	1.423	1.432	1.364	1.430	1.772	1.824	1.160
M06	1.442	1.422	1.372	1.419	1.804	1.836	1.167
M06-2X	1.431	1.431	1.368	1.428	1.778	1.829	1.161
M06-HF	1.397	1.451	1.355	1.447	1.735	1.828	1.150
M06-L	1.451	1.420	1.376	1.418	1.815	1.828	1.173
PBE0	1.443	1.423	1.373	1.421	1.800	1.825	1.166
PBE	1.462	1.429	1.387	1.426	1.828	1.835	1.181

C <sub>2v</sub>	R <sub>1</sub>	R <sub>2</sub>	R <sub>3</sub>	R <sub>4</sub>	R <sub>5</sub>	R <sub>6</sub>	R <sub>7</sub>
B3LYP	1.452	1.427	1.378	1.424	1.815	1.835	1.168
BLYP	1.470	1.434	1.391	1.431	1.842	1.846	1.181
CAM-B3LYP	1.424	1.432	1.364	1.430	1.773	1.824	1.160
M06	1.442	1.422	1.372	1.419	1.805	1.836	1.167
M06-2X	1.431	1.431	1.368	1.428	1.779	1.829	1.161

C <sub>2v</sub> con't							
M06-HF	1.397	1.451	1.355	1.447	1.735	1.828	1.150
M06-L	1.450	1.420	1.376	1.418	1.815	1.828	1.173
PBE0	1.444	1.423	1.373	1.421	1.801	1.826	1.166
PBE	1.462	1.429	1.387	1.426	1.829	1.836	1.181

D <sub>2</sub>	R <sub>1</sub>	R <sub>2</sub>	R <sub>3</sub>	R <sub>4</sub>	R <sub>5</sub>	R <sub>6</sub>	R <sub>7</sub>
B3LYP	1.444	1.430	1.375	1.429	1.788	1.815	1.168
BLYP	1.462	1.436	1.389	1.435	1.812	1.821	1.182
CAM-B3LYP	1.418	1.435	1.362	1.433	1.758	1.816	1.161
M06	1.434	1.426	1.369	1.424	1.775	1.815	1.168
M06-2X	1.424	1.434	1.366	1.432	1.762	1.820	1.161
M06-HF	1.397	1.451	1.355	1.447	1.735	1.828	1.150
M06-L	1.444	1.422	1.374	1.422	1.790	1.808	1.174
PBE0	1.437	1.426	1.371	1.424	1.781	1.812	1.167
PBE	1.456	1.430	1.385	1.429	1.806	1.817	1.182

C <sub>2</sub>	R <sub>1</sub>	R <sub>2</sub>	R <sub>3</sub>	R <sub>4</sub>	R <sub>5</sub>	R <sub>6</sub>	R <sub>7</sub>
B3LYP	1.452	1.426	1.379	1.424	1.817	1.835	1.168
BLYP	1.468	1.432	1.392	1.431	1.844	1.847	1.181
CAM-B3LYP	1.424	1.432	1.364	1.430	1.773	1.824	1.160
M06	1.442	1.421	1.373	1.419	1.807	1.836	1.167
M06-2X	1.431	1.430	1.368	1.428	1.779	1.829	1.161
M06-HF	1.397	1.451	1.355	1.447	1.735	1.828	1.150
M06-L	1.449	1.419	1.377	1.419	1.817	1.828	1.173
PBE0	1.443	1.422	1.374	1.421	1.803	1.826	1.166
PBE	1.461	1.427	1.388	1.426	1.831	1.836	1.181

Table D66: Bond lengths (Å) for 2Si TCNDQ PES BS4.

D <sub>2h</sub>	R <sub>1</sub>	R <sub>2</sub>	R <sub>3</sub>	R <sub>4</sub>	R <sub>5</sub>	R <sub>6</sub>	R <sub>7</sub>
B3LYP	1.438	1.423	1.367	1.422	1.773	1.799	1.157
BLYP	1.456	1.429	1.380	1.428	1.795	1.804	1.170
CAM-B3LYP	1.410	1.429	1.353	1.427	1.744	1.801	1.149
M06	1.427	1.419	1.360	1.418	1.759	1.799	1.155
M06-2X	1.417	1.430	1.358	1.427	1.748	1.807	1.151
M06-HF	1.389	1.446	1.348	1.442	1.723	1.815	1.140
M06-L	1.439	1.416	1.366	1.416	1.775	1.791	1.162
PBE0	1.431	1.420	1.363	1.419	1.767	1.798	1.156
PBE	1.451	1.424	1.377	1.423	1.791	1.801	1.171

C <sub>2h</sub>	R <sub>1</sub>	R <sub>2</sub>	R <sub>3</sub>	R <sub>4</sub>	R <sub>5</sub>	R <sub>6</sub>	R <sub>7</sub>
B3LYP	1.445	1.420	1.369	1.418	1.796	1.816	1.156
BLYP	1.463	1.427	1.383	1.424	1.821	1.825	1.169
CAM-B3LYP	1.414	1.427	1.355	1.425	1.755	1.806	1.149
M06	1.435	1.415	1.363	1.413	1.785	1.815	1.154
M06-2X	1.423	1.427	1.360	1.424	1.762	1.814	1.151
PBE0	1.437	1.417	1.366	1.415	1.784	1.809	1.155
PBE	1.456	1.422	1.379	1.420	1.810	1.817	1.170

C <sub>2v</sub>	R <sub>1</sub>	R <sub>2</sub>	R <sub>3</sub>	R <sub>4</sub>	R <sub>5</sub>	R <sub>6</sub>	R <sub>7</sub>
B3LYP	1.445	1.420	1.370	1.418	1.797	1.816	1.156
BLYP	1.463	1.427	1.383	1.424	1.822	1.826	1.169
CAM-B3LYP	1.415	1.427	1.355	1.425	1.755	1.807	1.149
M06	1.435	1.415	1.363	1.413	1.785	1.816	1.154

C <sub>2v</sub> Con't							
M06-2X	1.423	1.427	1.360	1.424	1.763	1.814	1.151
M06-L	1.445	1.414	1.368	1.412	1.798	1.809	1.161
PBE0	1.437	1.417	1.366	1.415	1.784	1.809	1.155
PBE	1.456	1.422	1.379	1.420	1.810	1.817	1.170

D <sub>2</sub>	R <sub>1</sub>	R <sub>2</sub>	R <sub>3</sub>	R <sub>4</sub>	R <sub>5</sub>	R <sub>6</sub>	R <sub>7</sub>
B3LYP	1.438	1.423	1.367	1.422	1.773	1.799	1.157
BLYP	1.456	1.428	1.381	1.428	1.797	1.804	1.170
M06	1.427	1.419	1.360	1.418	1.760	1.799	1.155
M06-2X	1.417	1.429	1.358	1.427	1.749	1.807	1.151
M06-L	1.438	1.416	1.366	1.416	1.775	1.791	1.162
PBE0	1.431	1.419	1.364	1.419	1.768	1.797	1.156
PBE	1.450	1.423	1.378	1.423	1.792	1.801	1.171

C <sub>2</sub>	R <sub>1</sub>	R <sub>2</sub>	R <sub>3</sub>	R <sub>4</sub>	R <sub>5</sub>	R <sub>6</sub>	R <sub>7</sub>
B3LYP	1.445	1.418	1.370	1.418	1.798	1.816	1.156
BLYP	1.462	1.425	1.383	1.424	1.823	1.826	1.169
M06	1.434	1.415	1.363	1.413	1.785	1.816	1.154
M06-2X	1.423	1.426	1.361	1.424	1.764	1.814	1.151
M06-L	1.443	1.413	1.368	1.413	1.798	1.809	1.161
PBE0	1.437	1.416	1.366	1.415	1.786	1.810	1.156
PBE	1.455	1.420	1.380	1.420	1.812	1.817	1.170

Table D67: Bond lengths (Å) for 1Si TCNP PES BS2.

C <sub>2v</sub>	R <sub>1</sub>	R <sub>2</sub>	R <sub>3</sub>	R <sub>4</sub>	R <sub>5</sub>	R <sub>6</sub>	R <sub>7</sub>	R <sub>8</sub>	R <sub>9</sub>	R <sub>10</sub>	R <sub>11</sub>	R <sub>12</sub>	R <sub>13</sub>	R <sub>14</sub>	R <sub>15</sub>	R <sub>16</sub>
B3LYP	1.358	1.400	1.446	1.446	1.386	1.427	1.788	1.815	1.168	1.447	1.445	1.383	1.431	1.417	1.422	1.168
BLYP	1.372	1.415	1.452	1.453	1.402	1.433	1.813	1.821	1.182	1.452	1.453	1.398	1.436	1.437	1.426	1.182
CAM-B3LYP	1.347	1.384	1.449	1.447	1.371	1.431	1.757	1.815	1.160	1.450	1.445	1.368	1.434	1.396	1.424	1.160
M06	1.353	1.393	1.441	1.440	1.379	1.422	1.773	1.815	1.167	1.442	1.439	1.376	1.427	1.408	1.419	1.167
M06-2X	1.350	1.387	1.450	1.447	1.374	1.430	1.760	1.819	1.161	1.451	1.446	1.371	1.435	1.396	1.426	1.161
M06-HF	1.343	1.373	1.461	1.456	1.363	1.443	1.735	1.826	1.149	1.463	1.455	1.360	1.448	1.378	1.437	1.149
M06-L	1.359	1.401	1.438	1.439	1.387	1.420	1.789	1.807	1.174	1.438	1.439	1.384	1.422	1.420	1.413	1.174
PBE0	1.355	1.395	1.442	1.440	1.382	1.422	1.780	1.812	1.166	1.442	1.439	1.378	1.426	1.410	1.417	1.166
PBE	1.369	1.411	1.445	1.447	1.398	1.427	1.807	1.817	1.182	1.446	1.446	1.395	1.430	1.432	1.420	1.182

C <sub>s</sub>	R <sub>1</sub>	R <sub>2</sub>	R <sub>3</sub>	R <sub>4</sub>	R <sub>5</sub>	R <sub>6</sub>	R <sub>7</sub>	R <sub>8</sub>	R <sub>9</sub>	R <sub>10</sub>	R <sub>11</sub>	R <sub>12</sub>	R <sub>13</sub>	R <sub>14</sub>	R <sub>15</sub>	R <sub>16</sub>
B3LYP	1.358	1.401	1.446	1.445	1.387	1.426	1.799	1.824	1.168	1.447	1.445	1.383	1.431	1.417	1.422	1.168
BLYP	1.372	1.416	1.451	1.452	1.403	1.430	1.837	1.842	1.181	1.452	1.453	1.398	1.436	1.437	1.426	1.182
M06	1.353	1.393	1.441	1.440	1.379	1.422	1.774	1.816	1.167	1.442	1.439	1.376	1.427	1.408	1.419	1.167
PBE	1.369	1.411	1.445	1.447	1.399	1.425	1.821	1.829	1.181	1.446	1.447	1.395	1.430	1.432	1.420	1.182

Table D68: Bond lengths (Å) for 1Si TCNP PES BS4.

C <sub>2v</sub>	R <sub>1</sub>	R <sub>2</sub>	R <sub>3</sub>	R <sub>4</sub>	R <sub>5</sub>	R <sub>6</sub>	R <sub>7</sub>	R <sub>8</sub>	R <sub>9</sub>	R <sub>10</sub>	R <sub>11</sub>	R <sub>12</sub>	R <sub>13</sub>	R <sub>14</sub>	R <sub>15</sub>	R <sub>16</sub>
B3LYP	1.350	1.392	1.440	1.439	1.378	1.421	1.772	1.799	1.156	1.441	1.438	1.375	1.424	1.409	1.415	1.156
BLYP	1.363	1.407	1.445	1.446	1.394	1.426	1.796	1.803	1.170	1.446	1.445	1.390	1.429	1.430	1.418	1.170
CAM-B3LYP	1.339	1.376	1.443	1.440	1.362	1.425	1.742	1.800	1.148	1.444	1.439	1.360	1.428	1.389	1.418	1.149
M06	1.344	1.384	1.435	1.434	1.371	1.416	1.757	1.799	1.154	1.436	1.433	1.367	1.420	1.399	1.412	1.154
M06-2X	1.342	1.380	1.445	1.442	1.367	1.426	1.746	1.806	1.150	1.447	1.441	1.364	1.431	1.390	1.421	1.150
M06-HF	1.336	1.366	1.456	1.451	1.356	1.438	1.722	1.813	1.139	1.458	1.449	1.353	1.443	1.371	1.430	1.139
M06-L	1.350	1.393	1.432	1.433	1.379	1.414	1.774	1.791	1.162	1.433	1.432	1.376	1.416	1.414	1.406	1.161
PBE0	1.347	1.388	1.436	1.435	1.374	1.417	1.765	1.798	1.155	1.437	1.434	1.371	1.421	1.403	1.412	1.156
PBE	1.361	1.403	1.439	1.441	1.391	1.421	1.791	1.801	1.171	1.440	1.440	1.387	1.424	1.425	1.414	1.171

C <sub>s</sub>	R <sub>1</sub>	R <sub>2</sub>	R <sub>3</sub>	R <sub>4</sub>	R <sub>5</sub>	R <sub>6</sub>	R <sub>7</sub>	R <sub>8</sub>	R <sub>9</sub>	R <sub>10</sub>	R <sub>11</sub>	R <sub>12</sub>	R <sub>13</sub>	R <sub>14</sub>	R <sub>15</sub>	R <sub>16</sub>
B3LYP	1.350	1.392	1.440	1.439	1.378	1.420	1.778	1.803	1.156	1.350	1.438	1.375	1.424	1.409	1.415	1.156
BLYP	1.363	1.408	1.445	1.446	1.394	1.424	1.814	1.820	1.169	1.363	1.446	1.390	1.429	1.429	1.419	1.169
M06-L	1.350	1.394	1.432	1.432	1.380	1.412	1.786	1.800	1.161	1.350	1.433	1.376	1.416	1.413	1.407	1.161
PBE	1.361	1.404	1.439	1.440	1.391	1.419	1.801	1.809	1.170	1.361	1.440	1.387	1.424	1.425	1.414	1.171

Table D69: Bond lengths (Å) for 2Si TCNP PES BS2.

D <sub>2h</sub>	R <sub>1</sub>	R <sub>2</sub>	R <sub>3</sub>	R <sub>4</sub>	R <sub>5</sub>	R <sub>6</sub>	R <sub>7</sub>	R <sub>8</sub>	R <sub>9</sub>
B3LYP	1.359	1.406	1.445	1.442	1.389	1.424	1.798	1.813	1.169
BLYP	1.373	1.419	1.451	1.451	1.404	1.430	1.821	1.820	1.182
CAM-B3LYP	1.349	1.391	1.448	1.441	1.375	1.427	1.770	1.814	1.161
M06	1.354	1.399	1.440	1.436	1.383	1.419	1.785	1.814	1.168
M06-2X	1.351	1.395	1.448	1.441	1.378	1.426	1.773	1.818	1.162
M06-HF	1.344	1.380	1.460	1.450	1.366	1.439	1.746	1.826	1.150
M06-L	1.359	1.405	1.437	1.436	1.389	1.417	1.798	1.806	1.175
PBE0	1.356	1.401	1.440	1.436	1.385	1.419	1.791	1.811	1.167
PBE	1.370	1.415	1.444	1.445	1.400	1.424	1.815	1.816	1.182

C <sub>2h</sub>	R <sub>1</sub>	R <sub>2</sub>	R <sub>3</sub>	R <sub>4</sub>	R <sub>5</sub>	R <sub>6</sub>	R <sub>7</sub>	R <sub>8</sub>	R <sub>9</sub>
B3LYP	1.360	1.409	1.444	1.440	1.392	1.420	1.826	1.836	1.168
BLYP	1.374	1.422	1.450	1.449	1.407	1.427	1.851	1.848	1.181
CAM-B3LYP	1.349	1.395	1.447	1.439	1.378	1.422	1.793	1.828	1.161
M06	1.355	1.403	1.439	1.434	1.386	1.415	1.815	1.837	1.167
M06-2X	1.352	1.399	1.447	1.439	1.381	1.421	1.796	1.832	1.161
M06-HF	1.344	1.380	1.460	1.450	1.366	1.439	1.746	1.826	1.150
M06-L	1.360	1.408	1.436	1.435	1.392	1.414	1.825	1.830	1.173
PBE0	1.356	1.404	1.440	1.435	1.387	1.416	1.813	1.828	1.166
PBE	1.370	1.417	1.444	1.443	1.402	1.421	1.839	1.837	1.181

C <sub>2v</sub>	R <sub>1</sub>	R <sub>2</sub>	R <sub>3</sub>	R <sub>4</sub>	R <sub>5</sub>	R <sub>6</sub>	R <sub>7</sub>	R <sub>8</sub>	R <sub>9</sub>
B3LYP	1.360	1.409	1.444	1.440	1.392	1.420	1.826	1.836	1.168
BLYP	1.373	1.422	1.450	1.449	1.406	1.427	1.851	1.848	1.181
CAM-B3LYP	1.349	1.395	1.447	1.439	1.378	1.422	1.793	1.828	1.161
M06	1.355	1.403	1.439	1.434	1.386	1.415	1.815	1.837	1.167
M06-2X	1.352	1.399	1.447	1.439	1.381	1.421	1.796	1.832	1.161
M06-HF	1.344	1.380	1.460	1.450	1.366	1.439	1.746	1.826	1.150
M06-L	1.360	1.407	1.436	1.435	1.392	1.414	1.824	1.829	1.173
PBE0	1.356	1.404	1.440	1.435	1.387	1.416	1.813	1.828	1.166
PBE	1.370	1.417	1.444	1.443	1.402	1.422	1.839	1.837	1.181

Table D70: Bond lengths (Å) for 2Si TCNP PES BS4.

D <sub>2h</sub>	R <sub>1</sub>	R <sub>2</sub>	R <sub>3</sub>	R <sub>4</sub>	R <sub>5</sub>	R <sub>6</sub>	R <sub>7</sub>	R <sub>8</sub>	R <sub>9</sub>
B3LYP	1.351	1.399	1.439	1.435	1.382	1.417	1.784	1.798	1.157
BLYP	1.364	1.412	1.444	1.443	1.396	1.423	1.805	1.803	1.171
CAM-B3LYP	1.340	1.383	1.442	1.435	1.366	1.421	1.756	1.799	1.150
M06	1.345	1.391	1.434	1.429	1.374	1.413	1.770	1.797	1.155
M06-2X	1.344	1.388	1.444	1.436	1.371	1.421	1.760	1.805	1.151
M06-HF	1.337	1.372	1.455	1.445	1.359	1.434	1.734	1.813	1.140
M06-L	1.351	1.399	1.431	1.430	1.382	1.411	1.784	1.790	1.163
PBE0	1.348	1.394	1.435	1.430	1.378	1.413	1.777	1.796	1.156
PBE	1.362	1.408	1.439	1.438	1.393	1.418	1.800	1.800	1.171

C <sub>2h</sub>	R <sub>1</sub>	R <sub>2</sub>	R <sub>3</sub>	R <sub>4</sub>	R <sub>5</sub>	R <sub>6</sub>	R <sub>7</sub>	R <sub>8</sub>	R <sub>9</sub>
B3LYP	1.352	1.401	1.438	1.433	1.384	1.413	1.808	1.817	1.156
BLYP	1.365	1.414	1.443	1.442	1.398	1.420	1.831	1.827	1.169
CAM-B3LYP	1.341	1.387	1.441	1.432	1.369	1.416	1.775	1.811	1.149
M06	1.345	1.395	1.433	1.427	1.377	1.408	1.796	1.817	1.154

C <sub>2h</sub> con't									
M06-2X	1.344	1.392	1.443	1.434	1.374	1.417	1.779	1.817	1.151
M06-L	1.351	1.401	1.430	1.429	1.384	1.408	1.807	1.810	1.161
PBE0	1.349	1.397	1.434	1.429	1.380	1.410	1.796	1.811	1.156
PBE	1.363	1.410	1.438	1.437	1.395	1.415	1.820	1.819	1.170

C <sub>2v</sub>	R <sub>1</sub>	R <sub>2</sub>	R <sub>3</sub>	R <sub>4</sub>	R <sub>5</sub>	R <sub>6</sub>	R <sub>7</sub>	R <sub>8</sub>	R <sub>9</sub>
B3LYP	1.351	1.401	1.438	1.433	1.384	1.413	1.808	1.817	1.156
BLYP	1.365	1.414	1.444	1.442	1.398	1.420	1.831	1.827	1.169
CAM-B3LYP	1.340	1.387	1.441	1.432	1.369	1.416	1.775	1.811	1.149
M06	1.345	1.394	1.433	1.427	1.377	1.408	1.796	1.817	1.155
M06-2X	1.344	1.392	1.443	1.434	1.374	1.417	1.780	1.817	1.151
M06-L	1.351	1.401	1.431	1.429	1.384	1.408	1.807	1.810	1.161
PBE0	1.348	1.397	1.434	1.429	1.380	1.410	1.796	1.811	1.156
PBE	1.362	1.410	1.438	1.437	1.395	1.415	1.820	1.818	1.170

Table D71: Bond lengths (Å) for [1Si TCNDQ]<sup>-</sup> BS2.

C <sub>2v</sub>	R <sub>1</sub>	R <sub>2</sub>	R <sub>3</sub>	R <sub>4</sub>	R <sub>5</sub>	R <sub>6</sub>	R <sub>7</sub>	R <sub>8</sub>	R <sub>9</sub>	R <sub>10</sub>	R <sub>11</sub>	R <sub>12</sub>	R <sub>13</sub>
B3LYP	1.462	1.423	1.384	1.419	1.817	1.816	1.171	1.422	1.381	1.425	1.433	1.418	1.172
BLYP	1.473	1.433	1.394	1.429	1.834	1.824	1.185	1.432	1.392	1.434	1.447	1.424	1.185
CAM-B3LYP	1.458	1.417	1.379	1.412	1.807	1.814	1.163	1.415	1.375	1.421	1.425	1.416	1.165
M06	1.453	1.417	1.378	1.413	1.806	1.816	1.171	1.416	1.375	1.420	1.426	1.414	1.171
M06-2X	1.458	1.419	1.381	1.413	1.805	1.819	1.164	1.417	1.377	1.423	1.423	1.418	1.166
M06-HF	1.471	1.414	1.384	1.408	1.810	1.823	1.152	1.412	1.379	1.422	1.422	1.423	1.155
M06-L	1.456	1.418	1.381	1.415	1.813	1.809	1.177	1.418	1.378	1.419	1.432	1.411	1.177
PBE0	1.455	1.418	1.380	1.414	1.812	1.814	1.169	1.417	1.377	1.420	1.427	1.413	1.170
PBE	1.466	1.427	1.391	1.424	1.827	1.819	1.185	1.427	1.388	1.428	1.441	1.418	1.185

Table D71  
Con't

C <sub>s</sub>	R <sub>1</sub>	R <sub>2</sub>	R <sub>3</sub>	R <sub>4</sub>	R <sub>5</sub>	R <sub>6</sub>	R <sub>7</sub>	R <sub>8</sub>	R <sub>9</sub>	R <sub>10</sub>	R <sub>11</sub>	R <sub>12</sub>	R <sub>13</sub>
B3LYP	1.466	1.420	1.387	1.416	1.883	1.887	1.168	1.422	1.381	1.424	1.434	1.419	1.171
BLYP	1.478	1.430	1.398	1.425	1.900	1.895	1.181	1.431	1.392	1.432	1.449	1.424	1.184
CAM-B3LYP	1.461	1.413	1.382	1.409	1.911	1.908	1.162	1.419	1.373	1.420	1.420	1.420	1.162
M06	1.458	1.414	1.381	1.410	1.884	1.895	1.168	1.417	1.375	1.419	1.425	1.415	1.170
M06-2X	1.458	1.417	1.382	1.412	1.879	1.896	1.163	1.420	1.374	1.423	1.419	1.421	1.164
M06-HF	1.471	1.414	1.384	1.407	1.830	1.868	1.150	1.412	1.378	1.422	1.422	1.423	1.155
M06-L	1.460	1.415	1.384	1.411	1.875	1.875	1.174	1.417	1.378	1.418	1.432	1.411	1.176
PBE0	1.459	1.415	1.382	1.411	1.867	1.875	1.167	1.417	1.377	1.419	1.427	1.414	1.169
PBE	1.471	1.424	1.393	1.420	1.885	1.880	1.181	1.426	1.388	1.427	1.442	1.418	1.184

C <sub>2</sub>	R <sub>1</sub>	R <sub>2</sub>	R <sub>3</sub>	R <sub>4</sub>	R <sub>5</sub>	R <sub>6</sub>	R <sub>7</sub>	R <sub>8</sub>	R <sub>9</sub>	R <sub>10</sub>	R <sub>11</sub>	R <sub>12</sub>	R <sub>13</sub>
B3LYP	1.461	1.422	1.384	1.419	1.819	1.816	1.171	1.421	1.381	1.425	1.434	1.418	1.172
BLYP	1.472	1.431	1.395	1.430	1.835	1.823	1.185	1.431	1.393	1.434	1.449	1.424	1.185
CAM-B3LYP	1.457	1.416	1.379	1.412	1.808	1.814	1.163	1.413	1.376	1.421	1.427	1.416	1.165
M06	1.452	1.416	1.379	1.413	1.806	1.815	1.171	1.415	1.376	1.420	1.427	1.414	1.171
M06-2X	1.457	1.416	1.382	1.413	1.807	1.819	1.164	1.414	1.378	1.423	1.425	1.418	1.166
M06-HF	1.471	1.411	1.385	1.408	1.813	1.823	1.152	1.409	1.381	1.422	1.425	1.423	1.155
M06-L	1.454	1.417	1.381	1.416	1.814	1.809	1.177	1.416	1.379	1.419	1.432	1.411	1.177
PBE0	1.454	1.417	1.381	1.414	1.813	1.813	1.169	1.415	1.378	1.421	1.428	1.413	1.170
PBE	1.465	1.426	1.391	1.424	1.828	1.819	1.185	1.425	1.389	1.428	1.443	1.418	1.185

C <sub>1</sub>	R <sub>1</sub>	R <sub>2</sub>	R <sub>3</sub>	R <sub>4</sub>	R <sub>5</sub>	R <sub>6</sub>	R <sub>7</sub>	R <sub>8</sub>	R <sub>9</sub>	R <sub>10</sub>	R <sub>11</sub>	R <sub>12</sub>	R <sub>13</sub>
B3LYP	1.465	1.418	1.387	1.416	1.885	1.887	1.168	1.420	1.382	1.424	1.435	1.418	1.171
BLYP	1.476	1.428	1.398	1.425	1.902	1.895	1.181	1.429	1.393	1.433	1.450	1.424	1.184
CAM-B3LYP	1.461	1.410	1.383	1.409	1.917	1.910	1.162	1.416	1.374	1.420	1.422	1.420	1.162
M06	1.456	1.413	1.382	1.410	1.885	1.895	1.169	1.415	1.376	1.419	1.426	1.415	1.170

C <sub>1</sub> con't														
M06-2X	1.457	1.414	1.383	1.412	1.889	1.900	1.163	1.418	1.375	1.423	1.421	1.421	1.164	
M06-HF	1.470	1.411	1.386	1.407	1.832	1.867	1.150	1.409	1.380	1.422	1.425	1.422	1.155	
M06-L	1.458	1.414	1.384	1.412	1.877	1.875	1.174	1.415	1.379	1.418	1.433	1.411	1.176	
PBE0	1.458	1.414	1.383	1.412	1.870	1.876	1.167	1.415	1.378	1.419	1.429	1.414	1.169	
PBE	1.469	1.423	1.394	1.420	1.887	1.881	1.181	1.424	1.389	1.427	1.444	1.418	1.184	

Table D72: Bond lengths (Å) for [1Si TCNDQ]<sup>-</sup> BS4.

C <sub>2v</sub>	R <sub>1</sub>	R <sub>2</sub>	R <sub>3</sub>	R <sub>4</sub>	R <sub>5</sub>	R <sub>6</sub>	R <sub>7</sub>	R <sub>8</sub>	R <sub>9</sub>	R <sub>10</sub>	R <sub>11</sub>	R <sub>12</sub>	R <sub>13</sub>
B3LYP	1.456	1.416	1.376	1.412	1.802	1.800	1.160	1.415	1.373	1.418	1.427	1.410	1.160
BLYP	1.468	1.425	1.386	1.422	1.818	1.806	1.173	1.424	1.384	1.426	1.441	1.416	1.173
CAM-B3LYP	1.454	1.410	1.371	1.405	1.792	1.798	1.152	1.407	1.368	1.413	1.421	1.408	1.154
M06	1.448	1.410	1.370	1.406	1.791	1.799	1.158	1.408	1.367	1.413	1.419	1.407	1.158
M06-2X	1.456	1.413	1.375	1.406	1.793	1.804	1.153	1.410	1.371	1.416	1.420	1.411	1.156
M06-HF	1.469	1.407	1.378	1.401	1.797	1.809	1.143	1.404	1.374	1.414	1.420	1.414	1.146
M06-L	1.450	1.412	1.373	1.409	1.798	1.793	1.165	1.411	1.370	1.413	1.426	1.403	1.164
PBE0	1.450	1.412	1.373	1.408	1.797	1.798	1.159	1.410	1.370	1.414	1.421	1.406	1.159
PBE	1.461	1.420	1.383	1.417	1.812	1.803	1.174	1.420	1.381	1.422	1.435	1.411	1.174

C <sub>s</sub>	R <sub>1</sub>	R <sub>2</sub>	R <sub>3</sub>	R <sub>4</sub>	R <sub>5</sub>	R <sub>6</sub>	R <sub>7</sub>	R <sub>8</sub>	R <sub>9</sub>	R <sub>10</sub>	R <sub>11</sub>	R <sub>12</sub>	R <sub>13</sub>
B3LYP	1.460	1.413	1.378	1.409	1.855	1.862	1.157	1.414	1.373	1.417	1.427	1.410	1.159
BLYP	1.472	1.422	1.389	1.418	1.874	1.869	1.169	1.424	1.384	1.425	1.442	1.416	1.172
CAM-B3LYP	1.450	1.411	1.370	1.405	1.818	1.847	1.149	1.409	1.366	1.414	1.417	1.409	1.153
M06	1.451	1.407	1.372	1.403	1.851	1.865	1.155	1.409	1.366	1.412	1.418	1.408	1.157
M06-2X	1.454	1.413	1.374	1.406	1.816	1.850	1.151	1.411	1.370	1.417	1.418	1.412	1.155
M06-HF	1.469	1.407	1.379	1.400	1.814	1.851	1.140	1.404	1.374	1.414	1.420	1.414	1.146
M06-L	1.455	1.409	1.375	1.405	1.850	1.850	1.162	1.410	1.370	1.412	1.426	1.403	1.164
PBE0	1.453	1.410	1.375	1.405	1.840	1.852	1.156	1.410	1.370	1.413	1.421	1.407	1.159
PBE	1.465	1.418	1.386	1.413	1.860	1.857	1.170	1.419	1.381	1.421	1.436	1.411	1.173

C <sub>2</sub>	R <sub>1</sub>	R <sub>2</sub>	R <sub>3</sub>	R <sub>4</sub>	R <sub>5</sub>	R <sub>6</sub>	R <sub>7</sub>	R <sub>8</sub>	R <sub>9</sub>	R <sub>10</sub>	R <sub>11</sub>	R <sub>12</sub>	R <sub>13</sub>
B3LYP	1.455	1.414	1.377	1.412	1.803	1.799	1.160	1.413	1.374	1.418	1.428	1.409	1.160
BLYP	1.466	1.423	1.387	1.423	1.819	1.805	1.174	1.423	1.385	1.427	1.442	1.416	1.173
CAM-B3LYP	1.453	1.407	1.372	1.404	1.794	1.797	1.152	1.404	1.369	1.413	1.423	1.407	1.154
M06	1.447	1.409	1.370	1.406	1.791	1.799	1.158	1.407	1.368	1.413	1.420	1.407	1.158
M06-2X	1.454	1.409	1.376	1.406	1.795	1.804	1.153	1.407	1.372	1.416	1.422	1.410	1.156
M06-HF	1.467	1.403	1.380	1.401	1.800	1.809	1.143	1.401	1.376	1.414	1.423	1.414	1.146
M06-L	1.449	1.410	1.373	1.410	1.799	1.793	1.165	1.410	1.371	1.413	1.426	1.403	1.165
PBE0	1.449	1.410	1.374	1.408	1.798	1.798	1.159	1.408	1.371	1.414	1.423	1.406	1.160
PBE	1.459	1.419	1.384	1.418	1.813	1.802	1.174	1.418	1.382	1.422	1.437	1.411	1.174

C <sub>1</sub>	R <sub>1</sub>	R <sub>2</sub>	R <sub>3</sub>	R <sub>4</sub>	R <sub>5</sub>	R <sub>6</sub>	R <sub>7</sub>	R <sub>8</sub>	R <sub>9</sub>	R <sub>10</sub>	R <sub>11</sub>	R <sub>12</sub>	R <sub>13</sub>
B3LYP	1.458	1.411	1.379	1.409	1.858	1.862	1.157	1.412	1.374	1.417	1.429	1.410	1.159
BLYP	1.470	1.420	1.390	1.418	1.876	1.870	1.169	1.421	1.385	1.426	1.444	1.416	1.172
CAM-B3LYP	1.449	1.409	1.371	1.405	1.818	1.846	1.149	1.407	1.367	1.414	1.419	1.409	1.154
M06	1.450	1.406	1.373	1.403	1.854	1.866	1.155	1.408	1.367	1.412	1.419	1.408	1.157
M06-2X	1.453	1.410	1.375	1.406	1.816	1.848	1.151	1.408	1.371	1.417	1.420	1.411	1.155
M06-HF	1.467	1.403	1.380	1.401	1.816	1.850	1.141	1.401	1.375	1.414	1.423	1.414	1.147
M06-L	1.453	1.407	1.376	1.405	1.852	1.851	1.162	1.409	1.371	1.412	1.428	1.403	1.164
PBE0	1.451	1.408	1.375	1.406	1.842	1.852	1.156	1.408	1.371	1.413	1.423	1.407	1.159
PBE	1.463	1.416	1.387	1.414	1.862	1.858	1.170	1.417	1.382	1.421	1.438	1.411	1.173

Table D73: Bond lengths (Å) for [2Si TCNDQ]<sup>-</sup> BS2.

D <sub>2h</sub>	R <sub>1</sub>	R <sub>2</sub>	R <sub>3</sub>	R <sub>4</sub>	R <sub>5</sub>	R <sub>6</sub>	R <sub>7</sub>
B3LYP	1.465	1.421	1.384	1.420	1.819	1.816	1.172
BLYP	1.476	1.432	1.395	1.430	1.835	1.823	1.186
CAM-B3LYP	1.453	1.419	1.376	1.418	1.803	1.815	1.164
M06	1.457	1.416	1.378	1.415	1.808	1.816	1.172
M06-2X	1.457	1.419	1.378	1.418	1.802	1.819	1.165
M06-HF	1.448	1.423	1.375	1.422	1.788	1.827	1.153
M06-L	1.459	1.417	1.381	1.416	1.815	1.809	1.178
PBE0	1.458	1.417	1.380	1.416	1.813	1.813	1.170
PBE	1.469	1.426	1.391	1.425	1.828	1.819	1.186

C <sub>2h</sub>	R <sub>1</sub>	R <sub>2</sub>	R <sub>3</sub>	R <sub>4</sub>	R <sub>5</sub>	R <sub>6</sub>	R <sub>7</sub>
B3LYP	1.476	1.416	1.388	1.414	1.883	1.884	1.168
BLYP	1.487	1.427	1.399	1.423	1.901	1.892	1.181
CAM-B3LYP	1.468	1.412	1.381	1.410	1.867	1.881	1.161
M06	1.467	1.411	1.383	1.408	1.876	1.887	1.168
M06-2X	1.471	1.413	1.384	1.410	1.868	1.885	1.162
M06-HF	1.471	1.414	1.382	1.412	1.858	1.893	1.152
M06-L	1.468	1.413	1.385	1.410	1.875	1.872	1.174
PBE0	1.469	1.412	1.384	1.409	1.872	1.874	1.167
PBE	1.479	1.422	1.395	1.418	1.888	1.880	1.181

C <sub>2v</sub>	R <sub>1</sub>	R <sub>2</sub>	R <sub>3</sub>	R <sub>4</sub>	R <sub>5</sub>	R <sub>6</sub>	R <sub>7</sub>
B3LYP	1.476	1.416	1.388	1.414	1.884	1.884	1.168
BLYP	1.487	1.427	1.399	1.423	1.901	1.892	1.181
CAM-B3LYP	1.468	1.412	1.381	1.410	1.868	1.881	1.161
M06	1.467	1.411	1.383	1.408	1.876	1.886	1.168
M06-2X	1.471	1.412	1.384	1.410	1.868	1.885	1.162

C <sub>2v</sub> con't							
M06-HF	1.471	1.414	1.382	1.412	1.859	1.893	1.152
M06-L	1.468	1.413	1.385	1.410	1.875	1.872	1.174
PBE0	1.469	1.412	1.384	1.409	1.872	1.875	1.167
PBE	1.479	1.422	1.395	1.418	1.888	1.880	1.181

D <sub>2</sub>	R <sub>1</sub>	R <sub>2</sub>	R <sub>3</sub>	R <sub>4</sub>	R <sub>5</sub>	R <sub>6</sub>	R <sub>7</sub>
B3LYP	1.464	1.420	1.385	1.421	1.820	1.816	1.172
BLYP	1.475	1.430	1.396	1.430	1.836	1.823	1.186
CAM-B3LYP	1.453	1.417	1.376	1.418	1.804	1.815	1.164
M06	1.455	1.414	1.379	1.415	1.809	1.815	1.172
M06-2X	1.456	1.416	1.379	1.418	1.804	1.819	1.165
M06-HF	1.449	1.421	1.376	1.422	1.791	1.827	1.153
M06-L	1.457	1.415	1.381	1.417	1.816	1.809	1.178
PBE0	1.457	1.415	1.381	1.416	1.814	1.813	1.170
PBE	1.467	1.424	1.392	1.425	1.830	1.818	1.186

C <sub>2</sub>	R <sub>1</sub>	R <sub>2</sub>	R <sub>3</sub>	R <sub>4</sub>	R <sub>5</sub>	R <sub>6</sub>	R <sub>7</sub>
B3LYP	1.473	1.414	1.389	1.414	1.886	1.884	1.168
BLYP	1.483	1.425	1.400	1.424	1.903	1.892	1.181
CAM-B3LYP	1.466	1.410	1.382	1.410	1.870	1.881	1.161
M06	1.465	1.409	1.384	1.408	1.878	1.886	1.168
M06-2X	1.468	1.410	1.385	1.410	1.871	1.886	1.162
M06-HF	1.469	1.411	1.383	1.412	1.862	1.894	1.152
M06-L	1.465	1.411	1.386	1.410	1.877	1.872	1.174
PBE0	1.467	1.410	1.385	1.410	1.874	1.875	1.167
PBE	1.475	1.420	1.396	1.419	1.890	1.880	1.181

Table D74: Bond lengths (Å) for [2Si TCNDQ]<sup>-</sup> BS4.

D <sub>2h</sub>	R <sub>1</sub>	R <sub>2</sub>	R <sub>3</sub>	R <sub>4</sub>	R <sub>5</sub>	R <sub>6</sub>	R <sub>7</sub>
B3LYP	1.459	1.414	1.376	1.414	1.805	1.799	1.161
BLYP	1.470	1.424	1.387	1.423	1.819	1.805	1.174
CAM-B3LYP	1.447	1.412	1.368	1.411	1.788	1.799	1.153
M06	1.451	1.408	1.370	1.408	1.793	1.799	1.159
M06-2X	1.451	1.414	1.372	1.413	1.789	1.806	1.155
M06-HF	1.442	1.417	1.368	1.416	1.777	1.813	1.144
M06-L	1.453	1.410	1.373	1.410	1.800	1.793	1.166
PBE0	1.452	1.410	1.373	1.410	1.799	1.798	1.160
PBE	1.464	1.419	1.384	1.418	1.813	1.802	1.175

C <sub>2h</sub>	R <sub>1</sub>	R <sub>2</sub>	R <sub>3</sub>	R <sub>4</sub>	R <sub>5</sub>	R <sub>6</sub>	R <sub>7</sub>
B3LYP	1.471	1.409	1.381	1.406	1.862	1.862	1.157
BLYP	1.481	1.419	1.391	1.416	1.879	1.869	1.169
CAM-B3LYP	1.462	1.405	1.373	1.403	1.847	1.861	1.150
M06	1.462	1.403	1.374	1.400	1.855	1.864	1.155
M06-2X	1.467	1.407	1.377	1.404	1.849	1.867	1.152
M06-HF	1.464	1.408	1.375	1.406	1.837	1.874	1.142
PBE0	1.464	1.405	1.377	1.403	1.852	1.855	1.156
PBE	1.474	1.415	1.388	1.412	1.866	1.858	1.170

C <sub>2v</sub>	R <sub>1</sub>	R <sub>2</sub>	R <sub>3</sub>	R <sub>4</sub>	R <sub>5</sub>	R <sub>6</sub>	R <sub>7</sub>
B3LYP	1.471	1.409	1.381	1.406	1.863	1.862	1.157
BLYP	1.481	1.419	1.391	1.416	1.879	1.869	1.169
CAM-B3LYP	1.462	1.405	1.373	1.402	1.847	1.861	1.150
M06	1.462	1.403	1.374	1.400	1.855	1.864	1.155
M06-2X	1.467	1.407	1.377	1.404	1.849	1.867	1.152
M06-HF	1.464	1.408	1.375	1.406	1.838	1.874	1.142

C <sub>2v</sub> con't							
M06-L	1.463	1.406	1.377	1.403	1.856	1.850	1.162
PBE0	1.464	1.405	1.377	1.403	1.852	1.855	1.156
PBE	1.473	1.415	1.388	1.412	1.867	1.858	1.170

D <sub>2</sub>	R <sub>1</sub>	R <sub>2</sub>	R <sub>3</sub>	R <sub>4</sub>	R <sub>5</sub>	R <sub>6</sub>	R <sub>7</sub>
B3LYP	1.458	1.412	1.377	1.414	1.806	1.799	1.161
BLYP	1.469	1.422	1.388	1.423	1.821	1.805	1.174
CAM-B3LYP	1.446	1.410	1.368	1.411	1.790	1.799	1.153
M06	1.449	1.407	1.370	1.408	1.794	1.799	1.159
M06-2X	1.450	1.411	1.373	1.413	1.791	1.805	1.155
M06-HF	1.442	1.414	1.369	1.416	1.779	1.812	1.144
M06-L	1.452	1.409	1.373	1.411	1.801	1.793	1.166
PBE0	1.451	1.408	1.374	1.410	1.800	1.798	1.160
PBE	1.462	1.417	1.384	1.419	1.815	1.802	1.175

C <sub>2</sub>	R <sub>1</sub>	R <sub>2</sub>	R <sub>3</sub>	R <sub>4</sub>	R <sub>5</sub>	R <sub>6</sub>	R <sub>7</sub>
B3LYP	1.468	1.407	1.381	1.407	1.865	1.863	1.157
BLYP	1.477	1.417	1.392	1.417	1.881	1.870	1.169
CAM-B3LYP	1.460	1.402	1.374	1.403	1.850	1.861	1.150
M06	1.459	1.401	1.375	1.401	1.857	1.864	1.155
M06-2X	1.464	1.404	1.378	1.405	1.852	1.867	1.152
M06-HF	1.459	1.401	1.375	1.401	1.857	1.864	1.155
M06-L	1.460	1.404	1.378	1.404	1.857	1.850	1.162
PBE0	1.461	1.403	1.378	1.403	1.855	1.855	1.156
PBE	1.470	1.412	1.388	1.412	1.869	1.859	1.171

Table D75: Bond lengths (Å) for [1Si TCNP]<sup>-</sup> BS2.

C <sub>2v</sub>	R <sub>1</sub>	R <sub>2</sub>	R <sub>3</sub>	R <sub>4</sub>	R <sub>5</sub>	R <sub>6</sub>	R <sub>7</sub>	R <sub>8</sub>	R <sub>9</sub>	R <sub>10</sub>	R <sub>11</sub>	R <sub>12</sub>	R <sub>13</sub>	R <sub>14</sub>	R <sub>15</sub>	R <sub>16</sub>
B3LYP	1.363	1.415	1.443	1.435	1.399	1.413	1.890	1.887	1.168	1.445	1.436	1.394	1.421	1.441	1.417	1.171
BLYP	1.376	1.426	1.449	1.446	1.412	1.422	1.907	1.895	1.181	1.451	1.447	1.406	1.429	1.456	1.423	1.185
CAM-B3LYP	1.354	1.415	1.442	1.424	1.395	1.405	1.932	1.915	1.163	1.443	1.430	1.387	1.415	1.430	1.419	1.162
M06	1.357	1.410	1.438	1.428	1.393	1.407	1.893	1.897	1.169	1.439	1.430	1.388	1.415	1.432	1.414	1.170
M06-2X	1.355	1.413	1.445	1.428	1.394	1.409	1.909	1.910	1.163	1.446	1.433	1.387	1.418	1.428	1.421	1.163
M06-HF	1.351	1.420	1.452	1.425	1.393	1.405	1.834	1.868	1.150	1.455	1.422	1.387	1.420	1.427	1.422	1.155
M06-L	1.362	1.412	1.435	1.431	1.398	1.408	1.882	1.875	1.174	1.437	1.433	1.393	1.414	1.439	1.410	1.176
PBE0	1.359	1.410	1.439	1.430	1.394	1.408	1.873	1.875	1.167	1.440	1.431	1.389	1.416	1.434	1.412	1.170
PBE	1.373	1.421	1.443	1.440	1.407	1.417	1.891	1.880	1.182	1.444	1.441	1.402	1.424	1.450	1.417	1.185

C <sub>s</sub>	R <sub>1</sub>	R <sub>2</sub>	R <sub>3</sub>	R <sub>4</sub>	R <sub>5</sub>	R <sub>6</sub>	R <sub>7</sub>	R <sub>8</sub>	R <sub>9</sub>	R <sub>10</sub>	R <sub>11</sub>	R <sub>12</sub>	R <sub>13</sub>	R <sub>14</sub>	R <sub>15</sub>	R <sub>16</sub>
B3LYP	1.363	1.413	1.443	1.438	1.397	1.416	1.824	1.816	1.171	1.445	1.436	1.393	1.423	1.439	1.417	1.172
BLYP	1.376	1.423	1.450	1.448	1.409	1.426	1.841	1.823	1.185	1.451	1.447	1.406	1.431	1.454	1.423	1.185
CAM-B3LYP	1.354	1.413	1.443	1.429	1.391	1.408	1.815	1.814	1.163	1.444	1.426	1.387	1.418	1.432	1.414	1.166
M06	1.358	1.408	1.438	1.431	1.392	1.410	1.812	1.815	1.171	1.439	1.429	1.388	1.417	1.432	1.413	1.172
M06-2X	1.356	1.413	1.444	1.431	1.393	1.409	1.813	1.818	1.164	1.446	1.428	1.388	1.420	1.429	1.416	1.166
M06-HF	1.351	1.419	1.452	1.425	1.393	1.406	1.816	1.823	1.152	1.454	1.422	1.387	1.420	1.427	1.421	1.155
M06-L	1.362	1.410	1.436	1.433	1.395	1.412	1.820	1.809	1.177	1.437	1.432	1.392	1.416	1.437	1.409	1.177
PBE0	1.359	1.409	1.438	1.432	1.393	1.410	1.818	1.813	1.169	1.440	1.430	1.389	1.418	1.432	1.412	1.171
PBE	1.373	1.419	1.444	1.443	1.405	1.420	1.835	1.818	1.185	1.444	1.441	1.402	1.425	1.447	1.417	1.185

Table D76: Bond lengths (Å) for [1Si TCNP]<sup>-</sup> BS4.

C <sub>2v</sub>	R <sub>1</sub>	R <sub>2</sub>	R <sub>3</sub>	R <sub>4</sub>	R <sub>5</sub>	R <sub>6</sub>	R <sub>7</sub>	R <sub>8</sub>	R <sub>9</sub>	R <sub>10</sub>	R <sub>11</sub>	R <sub>12</sub>	R <sub>13</sub>	R <sub>14</sub>	R <sub>15</sub>	R <sub>16</sub>
B3LYP	1.355	1.406	1.437	1.431	1.390	1.409	1.809	1.799	1.160	1.438	1.428	1.386	1.415	1.433	1.408	1.161
BLYP	1.367	1.416	1.443	1.441	1.401	1.419	1.825	1.805	1.174	1.444	1.440	1.398	1.423	1.448	1.414	1.173
CAM-B3LYP	1.346	1.406	1.436	1.422	1.384	1.401	1.800	1.797	1.152	1.438	1.419	1.380	1.410	1.428	1.406	1.155
M06	1.349	1.401	1.431	1.424	1.384	1.402	1.797	1.799	1.158	1.433	1.422	1.380	1.410	1.426	1.405	1.159
M06-2X	1.349	1.408	1.439	1.425	1.387	1.403	1.801	1.804	1.153	1.441	1.422	1.382	1.414	1.426	1.409	1.156
M06-HF	1.344	1.414	1.447	1.418	1.387	1.399	1.802	1.809	1.143	1.449	1.415	1.381	1.412	1.425	1.413	1.146
M06-L	1.354	1.403	1.430	1.427	1.388	1.405	1.805	1.793	1.165	1.431	1.426	1.384	1.410	1.432	1.402	1.165
PBE0	1.352	1.403	1.433	1.426	1.387	1.404	1.804	1.798	1.159	1.434	1.423	1.383	1.411	1.427	1.405	1.160
PBE	1.365	1.412	1.438	1.436	1.398	1.414	1.819	1.802	1.174	1.439	1.435	1.394	1.419	1.441	1.410	1.174

C <sub>s</sub>	R <sub>1</sub>	R <sub>2</sub>	R <sub>3</sub>	R <sub>4</sub>	R <sub>5</sub>	R <sub>6</sub>	R <sub>7</sub>	R <sub>8</sub>	R <sub>9</sub>	R <sub>10</sub>	R <sub>11</sub>	R <sub>12</sub>	R <sub>13</sub>	R <sub>14</sub>	R <sub>15</sub>	R <sub>16</sub>
B3LYP	1.354	1.408	1.437	1.428	1.391	1.406	1.860	1.861	1.157	1.439	1.429	1.386	1.414	1.435	1.409	1.160
BLYP	1.367	1.418	1.443	1.439	1.403	1.415	1.881	1.869	1.169	1.444	1.440	1.398	1.422	1.450	1.414	1.173
CAM-B3LYP	1.345	1.404	1.437	1.423	1.383	1.401	1.818	1.842	1.149	1.439	1.420	1.379	1.411	1.426	1.406	1.154
M06	1.348	1.402	1.432	1.422	1.384	1.400	1.856	1.865	1.155	1.433	1.423	1.379	1.409	1.425	1.407	1.157
M06-2X	1.349	1.407	1.439	1.425	1.387	1.402	1.818	1.846	1.151	1.441	1.423	1.382	1.414	1.425	1.409	1.156
M06-HF	1.344	1.414	1.446	1.419	1.387	1.399	1.817	1.851	1.140	1.449	1.415	1.381	1.412	1.425	1.413	1.146
M06-L	1.354	1.405	1.429	1.425	1.390	1.402	1.856	1.850	1.162	1.431	1.426	1.385	1.408	1.434	1.402	1.164
PBE0	1.351	1.403	1.433	1.424	1.387	1.403	1.842	1.849	1.156	1.435	1.424	1.382	1.410	1.428	1.405	1.159
PBE	1.365	1.414	1.437	1.434	1.400	1.410	1.866	1.857	1.170	1.439	1.435	1.395	1.417	1.443	1.410	1.174

Table D77: Bond lengths (Å) for [2Si TCNP]<sup>-</sup> BS2.

D <sub>2h</sub>	R <sub>1</sub>	R <sub>2</sub>	R <sub>3</sub>	R <sub>4</sub>	R <sub>5</sub>	R <sub>6</sub>	R <sub>7</sub>	R <sub>8</sub>	R <sub>9</sub>
B3LYP	1.363	1.415	1.444	1.436	1.396	1.417	1.827	1.815	1.172
BLYP	1.376	1.425	1.450	1.447	1.409	1.427	1.843	1.822	1.186
CAM-B3LYP	1.352	1.408	1.445	1.431	1.386	1.415	1.810	1.814	1.165
M06	1.357	1.409	1.439	1.430	1.390	1.412	1.815	1.815	1.172
M06-2X	1.355	1.410	1.446	1.432	1.388	1.415	1.809	1.818	1.165
M06-HF	1.349	1.405	1.456	1.432	1.382	1.420	1.795	1.825	1.153
M06-L	1.362	1.411	1.436	1.432	1.395	1.413	1.822	1.808	1.178
PBE0	1.359	1.410	1.439	1.431	1.392	1.413	1.820	1.812	1.170
PBE	1.373	1.420	1.444	1.442	1.405	1.421	1.836	1.817	1.186

C <sub>2h</sub>	R <sub>1</sub>	R <sub>2</sub>	R <sub>3</sub>	R <sub>4</sub>	R <sub>5</sub>	R <sub>6</sub>	R <sub>7</sub>	R <sub>8</sub>	R <sub>9</sub>
B3LYP	1.363	1.420	1.442	1.433	1.401	1.411	1.890	1.883	1.168
BLYP	1.376	1.430	1.448	1.444	1.413	1.421	1.908	1.892	1.181
CAM-B3LYP	1.353	1.415	1.444	1.426	1.391	1.407	1.873	1.880	1.161
M06	1.358	1.415	1.437	1.427	1.395	1.406	1.880	1.886	1.168
M06-2X	1.356	1.418	1.445	1.427	1.394	1.408	1.874	1.885	1.162
M06-HF	1.349	1.417	1.454	1.426	1.389	1.410	1.863	1.892	1.152
M06-L	1.363	1.416	1.435	1.430	1.399	1.407	1.881	1.872	1.174
PBE0	1.359	1.415	1.438	1.428	1.396	1.407	1.878	1.874	1.167
PBE	1.373	1.424	1.442	1.439	1.409	1.415	1.895	1.880	1.181

C <sub>2v</sub>	R <sub>1</sub>	R <sub>2</sub>	R <sub>3</sub>	R <sub>4</sub>	R <sub>5</sub>	R <sub>6</sub>	R <sub>7</sub>	R <sub>8</sub>	R <sub>9</sub>
B3LYP	1.363	1.420	1.443	1.433	1.401	1.411	1.889	1.883	1.168
BLYP	1.376	1.429	1.449	1.444	1.413	1.421	1.908	1.892	1.181
CAM-B3LYP	1.353	1.415	1.444	1.426	1.391	1.407	1.873	1.880	1.161
M06	1.358	1.414	1.437	1.427	1.395	1.405	1.881	1.886	1.168
M06-2X	1.356	1.417	1.445	1.427	1.394	1.408	1.873	1.885	1.162

C <sub>2v</sub> con't									
M06-HF	1.349	1.417	1.454	1.426	1.389	1.410	1.862	1.892	1.152
M06-L	1.363	1.415	1.435	1.430	1.399	1.407	1.881	1.872	1.174
PBE0	1.359	1.415	1.438	1.428	1.396	1.407	1.878	1.874	1.167
PBE	1.373	1.424	1.443	1.439	1.409	1.415	1.895	1.880	1.182

Table D78: Bond lengths (Å) for [2Si TCNP]<sup>-</sup> BS4.

D <sub>2h</sub>	R <sub>1</sub>	R <sub>2</sub>	R <sub>3</sub>	R <sub>4</sub>	R <sub>5</sub>	R <sub>6</sub>	R <sub>7</sub>	R <sub>8</sub>	R <sub>9</sub>
B3LYP	1.354	1.408	1.438	1.429	1.389	1.411	1.812	1.798	1.161
BLYP	1.367	1.418	1.443	1.440	1.401	1.420	1.828	1.804	1.174
CAM-B3LYP	1.344	1.400	1.439	1.424	1.378	1.408	1.796	1.798	1.154
M06	1.348	1.402	1.433	1.423	1.382	1.405	1.801	1.798	1.159
M06-2X	1.348	1.404	1.442	1.426	1.382	1.410	1.796	1.805	1.155
M06-HF	1.342	1.398	1.451	1.427	1.376	1.414	1.783	1.811	1.144
M06-L	1.354	1.405	1.430	1.426	1.387	1.407	1.808	1.792	1.167
PBE0	1.351	1.404	1.434	1.424	1.385	1.407	1.806	1.797	1.160
PBE	1.365	1.413	1.438	1.435	1.398	1.415	1.821	1.801	1.175

C <sub>2h</sub>	R <sub>1</sub>	R <sub>2</sub>	R <sub>3</sub>	R <sub>4</sub>	R <sub>5</sub>	R <sub>6</sub>	R <sub>7</sub>	R <sub>8</sub>	R <sub>9</sub>
B3LYP	1.355	1.413	1.436	1.426	1.393	1.404	1.869	1.863	1.157
BLYP	1.368	1.422	1.442	1.437	1.405	1.413	1.886	1.870	1.169
CAM-B3LYP	1.345	1.408	1.437	1.419	1.383	1.400	1.853	1.861	1.150
M06	1.349	1.407	1.431	1.420	1.387	1.398	1.859	1.864	1.155
M06-2X	1.348	1.411	1.440	1.422	1.387	1.402	1.855	1.867	1.152
M06-HF	1.342	1.410	1.449	1.420	1.382	1.404	1.843	1.874	1.142
M06-L	1.355	1.409	1.429	1.423	1.392	1.400	1.861	1.850	1.162
PBE0	1.352	1.409	1.432	1.421	1.389	1.400	1.858	1.855	1.156
PBE	1.366	1.417	1.437	1.432	1.402	1.409	1.874	1.859	1.171

C <sub>2v</sub>	R <sub>1</sub>	R <sub>2</sub>	R <sub>3</sub>	R <sub>4</sub>	R <sub>5</sub>	R <sub>6</sub>	R <sub>7</sub>	R <sub>8</sub>	R <sub>9</sub>
B3LYP	1.355	1.413	1.436	1.426	1.393	1.404	1.868	1.863	1.157
BLYP	1.368	1.422	1.442	1.437	1.405	1.413	1.886	1.869	1.169
CAM-B3LYP	1.345	1.408	1.437	1.419	1.383	1.400	1.853	1.861	1.150
M06	1.349	1.407	1.431	1.420	1.387	1.398	1.860	1.863	1.155
M06-2X	1.348	1.411	1.440	1.422	1.387	1.402	1.854	1.867	1.152
M06-HF	1.343	1.409	1.449	1.420	1.382	1.405	1.841	1.873	1.142
M06-L	1.354	1.409	1.429	1.423	1.391	1.400	1.862	1.850	1.162
PBE0	1.352	1.408	1.432	1.421	1.389	1.400	1.858	1.855	1.156
PBE	1.365	1.417	1.437	1.432	1.401	1.409	1.873	1.859	1.171

Table D79: Delocalization indices (DI) for TCNDQ series. B3LYP/Def2TZVPP

		R <sub>1</sub>	R <sub>2</sub>	R <sub>3</sub>	R <sub>4</sub>	R <sub>5</sub>	R <sub>6</sub>	R <sub>7</sub>	R <sub>8</sub>	R <sub>9</sub>	R <sub>10</sub>	R <sub>11</sub>	R <sub>12</sub>	R <sub>13</sub>
0Si	D <sub>2h</sub>	1.293	1.181	1.566	1.166	1.344	1.110	2.309	–	–	–	–	–	–
1Si	C <sub>2v</sub>	1.244	1.211	1.523	1.267	0.837	0.559	2.446	1.205	1.543	1.183	1.312	1.119	2.298
	C <sub>s</sub>	1.243	1.211	1.522	1.268	0.836	0.559	2.445	1.205	1.542	1.183	1.312	1.119	2.298
	C <sub>2</sub>	1.244	1.211	1.523	1.267	0.837	0.559	2.445	1.205	1.543	1.184	1.312	1.119	2.298
	C <sub>1</sub>	1.243	1.211	1.522	1.268	0.836	0.559	2.445	1.205	1.542	1.184	1.312	1.119	2.298
2Si	D <sub>2h</sub>	1.202	1.232	1.503	1.281	0.821	0.575	2.431	–	–	–	–	–	–
	C <sub>2h</sub>	1.178	1.245	1.487	1.297	0.774	0.559	2.431	–	–	–	–	–	–
	C <sub>2v</sub>	1.178	1.245	1.486	1.297	0.773	0.558	2.431	–	–	–	–	–	–
	D <sub>2</sub>	1.201	1.233	1.503	1.281	0.821	0.575	2.431	–	–	–	–	–	–
	C <sub>2</sub>	1.169	1.249	1.483	1.300	0.768	0.558	2.431	–	–	–	–	–	–

Table D80: Delocalization indices (DI) for [TCNDQ]<sup>-</sup> series. B3LYP/Def2TZVPP

		R <sub>1</sub>	R <sub>2</sub>	R <sub>3</sub>	R <sub>4</sub>	R <sub>5</sub>	R <sub>6</sub>	R <sub>7</sub>	R <sub>8</sub>	R <sub>9</sub>	R <sub>10</sub>	R <sub>11</sub>	R <sub>12</sub>	R <sub>13</sub>
0Si	D <sub>2h</sub>	1.165	1.258	1.488	1.238	1.222	1.152	2.258						
	D <sub>2</sub>	1.158	1.261	1.484	1.240	1.219	1.152	2.258						
1Si	C <sub>2v</sub>	1.149	1.270	1.462	1.325	0.784	0.650	2.390	1.268	1.480	1.242	1.214	1.159	2.248
	C <sub>s</sub>	1.138	1.280	1.449	1.339	0.683	0.558	2.388	1.269	1.479	1.242	1.213	1.153	2.257
	C <sub>2</sub>	1.140	1.274	1.458	1.327	0.781	0.650	2.390	1.272	1.476	1.245	1.209	1.160	2.247
	C <sub>1</sub>	1.128	1.284	1.446	1.341	0.679	0.558	2.388	1.274	1.473	1.246	1.208	1.154	2.256
2Si	D <sub>2h</sub>	1.139	1.275	1.461	1.319	0.796	0.661	2.375	–	–	–	–	–	–
	C <sub>2h</sub>	1.107	1.296	1.437	1.348	0.665	0.558	2.387	–	–	–	–	–	–
	C <sub>2v</sub>	1.106	1.296	1.437	1.348	0.665	0.558	2.387	–	–	–	–	–	–
	D <sub>2</sub>	1.130	1.279	1.457	1.322	0.793	0.663	2.374	–	–	–	–	–	–
	C <sub>2</sub>	1.093	1.301	1.432	1.352	0.659	0.557	2.387	–	–	–	–	–	–

Table D81: Delocalization indices (DI) for TCNP series. B3LYP/Def2TZVPP

		R <sub>1</sub>	R <sub>2</sub>	R <sub>3</sub>	R <sub>4</sub>	R <sub>5</sub>	R <sub>6</sub>	R <sub>7</sub>	R <sub>8</sub>	R <sub>9</sub>	R <sub>10</sub>	R <sub>11</sub>	R <sub>12</sub>	R <sub>13</sub>	R <sub>14</sub>	R <sub>15</sub>	R <sub>16</sub>
0Si	D <sub>2h</sub>	1.616	1.375	1.139	1.134	1.456	1.187	1.309	1.116	2.302	–	–	–	–	–	–	–
1Si	C <sub>2v</sub>	1.605	1.338	1.150	1.154	1.414	1.293	0.811	0.561	2.443	1.147	1.151	1.432	1.209	1.272	1.127	2.289
	C <sub>s</sub>	1.605	1.337	1.151	1.155	1.412	1.296	0.802	0.558	2.441	1.147	1.151	1.432	1.208	1.273	1.126	2.290
2Si	D <sub>2h</sub>	1.598	1.310	1.155	1.168	1.397	1.307	0.793	0.582	2.426	–	–	–	–	–	–	–
	C <sub>2h</sub>	1.594	1.297	1.158	1.174	1.385	1.322	0.743	0.558	2.428	–	–	–	–	–	–	–
	C <sub>2v</sub>	1.594	1.297	1.158	1.174	1.385	1.322	0.743	0.558	2.428	–	–	–	–	–	–	–

Table D82: Delocalization indices (DI) for [TCNP]<sup>-</sup> series. B3LYP/Def2TZVPP

		R <sub>1</sub>	R <sub>2</sub>	R <sub>3</sub>	R <sub>4</sub>	R <sub>5</sub>	R <sub>6</sub>	R <sub>7</sub>	R <sub>8</sub>	R <sub>9</sub>	R <sub>10</sub>	R <sub>11</sub>	R <sub>12</sub>	R <sub>13</sub>	R <sub>14</sub>	R <sub>15</sub>	R <sub>16</sub>
0Si	D <sub>2h</sub>	1.595	1.291	1.159	1.179	1.391	1.256	1.198	1.156	2.254	–	–	–	–	–	–	–
1Si	C <sub>2v</sub>	1.587	1.278	1.167	1.187	1.364	1.346	0.768	0.651	2.393	1.163	1.185	1.384	1.259	1.193	1.166	2.243
	C <sub>s</sub>	1.589	1.272	1.166	1.192	1.359	1.355	0.670	0.558	2.389	1.162	1.186	1.383	1.261	1.188	1.159	2.252
2Si	D <sub>2h</sub>	1.588	1.273	1.165	1.189	1.369	1.337	0.781	0.668	2.372	–	–	–	–	–	–	–
	C <sub>2h</sub>	1.583	1.252	1.169	1.201	1.348	1.364	0.653	0.558	2.386	–	–	–	–	–	–	–
	C <sub>2v</sub>	1.583	1.252	1.169	1.201	1.349	1.364	0.653	0.558	2.387	–	–	–	–	–	–	–

Table D83: TCNDQ Triplet PES  $\langle S^2 \rangle$  values BS2

	D <sub>2h</sub>	D <sub>2</sub>
BLYP	2.01	2.02
M06-L	2.03	2.03
PBE	2.02	2.02
B3LYP	2.04	2.05
PBE0	2.06	2.06
M06	2.05	2.06
M06-2X	2.04	2.04
M06-HF	2.05	2.06
CAM-B3LYP	2.08	2.09

Table D85: 1Si TCNDQ Triplet PES  $\langle S^2 \rangle$  values BS2

	C <sub>2v</sub>	C <sub>s</sub>	C <sub>2</sub>	C <sub>1</sub>
BLYP	2.01	2.01	2.01	2.01
M06-L	2.03	2.02	2.03	2.02
PBE	2.01	2.04	2.01	2.01
B3LYP	2.03	2.03	2.04	2.03
PBE0	2.05	2.04	2.05	2.04
M06	2.04	2.04	2.04	2.04
M06-2X	2.03	2.03	2.04	2.03
M06-HF	2.04	2.04	2.04	2.04
CAM-B3LYP	2.07	2.06	2.07	2.06

Table D84: TCNDQ Triplet PES  $\langle S^2 \rangle$  values BS4

	D <sub>2h</sub>	D <sub>2</sub>
BLYP	2.01	2.02
M06-L	2.03	2.03
PBE	2.01	2.02
B3LYP	2.04	2.04
PBE0	2.06	2.06
M06	2.05	2.05
M06-2X	2.04	2.04
M06-HF	2.05	2.06
CAM-B3LYP	2.08	2.08

Table D86: 1Si TCNDQ Triplet PES  $\langle S^2 \rangle$  values BS4

	C <sub>2v</sub>	C <sub>s</sub>	C <sub>2</sub>	C <sub>1</sub>
BLYP	2.01	2.01	2.01	2.01
M06-L	2.20	2.02	2.03	2.02
PBE	2.01	2.01	2.01	2.01
B3LYP	2.03	2.03	2.03	2.03
PBE0	2.05	2.04	2.05	2.04
M06	2.04	2.03	2.04	2.03
M06-2X	2.03	2.03	2.04	2.03
M06-HF	2.04	2.04	2.04	2.04
CAM-B3LYP	2.06	2.05	2.06	2.05

Table D87: 2Si TCNDQ Triplet PES  $\langle S^2 \rangle$  values BS2

	D <sub>2h</sub>	C <sub>2h</sub>	C <sub>2v</sub>	D <sub>2</sub>	C <sub>2</sub>
BLYP	2.01	2.01	2.01	2.01	2.01
M06-L	2.02	2.01	2.01	2.02	2.01
PBE	2.01	2.01	2.01	2.01	2.01
B3LYP	2.02	2.01	2.01	2.03	2.01
PBE0	2.03	2.02	2.02	2.03	2.02
M06	2.03	2.01	2.01	2.03	2.01
M06-2X	2.02	2.01	2.01	2.03	2.01
M06-HF	2.03	2.01	2.01	2.03	2.01
CAM-B3LYP	2.04	2.02	2.02	2.04	2.20

Table D89: TCNP Triplet PES  $\langle S^2 \rangle$  values BS2

	D <sub>2h</sub>
BLYP	2.01
M06-L	2.03
PBE	2.01
B3LYP	2.04
PBE0	2.05
M06	2.04
M06-2X	2.04
M06-HF	2.04
CAM-B3LYP	2.07

Table D88: 2Si TCNDQ Triplet PES  $\langle S^2 \rangle$  values BS4

	D <sub>2h</sub>	C <sub>2h</sub>	C <sub>2v</sub>	D <sub>2</sub>	C <sub>2</sub>
BLYP	2.01	2.01	2.01	2.01	2.01
M06-L	2.02	2.01	2.01	2.02	2.01
PBE	2.01	2.01	2.01	2.01	2.01
B3LYP	2.02	2.01	2.01	2.02	2.01
PBE0	2.03	2.02	2.02	2.03	2.02
M06	2.02	2.01	2.01	2.03	2.01
M06-2X	2.03	2.01	2.01	2.03	2.01
M06-HF	2.03	2.01	2.01	2.03	2.01
CAM-B3LYP	2.04	2.02	2.02	2.04	2.02

Table D90: TCNP Triplet PES  $\langle S^2 \rangle$  values BS4

	D <sub>2h</sub>
BLYP	2.01
M06-L	2.03
PBE	2.01
B3LYP	2.03
PBE0	2.05
M06	2.04
M06-2X	2.04
M06-HF	2.05
CAM-B3LYP	2.06

Table D91: 1Si TCNP Triplet PES  $\langle S^2 \rangle$  values BS2

	C <sub>2v</sub>	C <sub>s</sub>
BLYP	2.01	2.01
M06-L	2.03	2.02
PBE	2.01	2.01
B3LYP	2.03	2.03
PBE0	2.04	2.04
M06	2.04	2.04
M06-2X	2.03	2.03
M06-HF	2.04	2.03
CAM-B3LYP	2.06	2.06

Table D93: 2Si TCNP Triplet PES  $\langle S^2 \rangle$  values BS2

	D <sub>2h</sub>	C <sub>2h</sub>	C <sub>2v</sub>
BLYP	2.01	2.01	2.01
M06-L	2.02	2.01	2.01
PBE	2.01	2.01	2.01
B3LYP	2.02	2.01	2.01
PBE0	2.03	2.01	2.01
M06	2.02	2.01	2.01
M06-2X	2.02	2.01	2.01
M06-HF	2.02	2.01	2.01
CAM-B3LYP	2.04	2.02	2.02

Table D92: 1Si TCNP Triplet PES  $\langle S^2 \rangle$  values BS4

	C <sub>2v</sub>	C <sub>s</sub>
BLYP	2.01	2.01
M06-L	2.03	2.02
PBE	2.01	2.01
B3LYP	2.03	2.03
PBE0	2.04	2.04
M06	2.04	2.03
M06-2X	2.03	2.03
M06-HF	2.04	2.03
CAM-B3LYP	2.06	2.06

Table D94: 2Si TCNP Triplet PES  $\langle S^0 \rangle$  values BS4

	D <sub>2h</sub>	C <sub>2h</sub>	C <sub>2v</sub>
BLYP	2.01	2.01	2.01
M06-L	2.02	2.01	2.01
PBE	2.02	2.01	2.01
B3LYP	2.02	2.01	2.01
PBE0	2.03	2.01	2.01
M06	2.02	2.01	2.01
M06-2X	2.02	2.01	2.01
M06-HF	2.03	2.01	2.01
CAM-B3LYP	2.03	2.02	2.02

Table D95: AEA (eV) of TCNDQ series. BS2

	0Si	1Si	2Si
BLYP	3.311	3.530	3.672
PBE	3.553	3.708	3.840
M06-L	3.674	3.857	4.001
B3LYP	3.674	3.910	4.134
PBE0	3.803	3.990	4.222
M06	3.831	4.046	4.253
M062X	3.855	4.141	4.617
M06-HF	3.883	4.395	5.367
CAM-B3LYP	3.811	4.122	4.604

Table D97: AEA (eV) of TCNP series. BS2

	0Si	1Si	2Si
BLYP	3.411	3.607	3.724
PBE	3.660	3.789	3.900
M06-L	3.790	3.947	4.068
B3LYP	3.812	4.014	4.198
PBE0	3.954	4.103	4.296
M06	3.985	4.163	4.322
M062X	4.038	4.281	4.753
M06-HF	4.121	4.653	5.572
CAM-B3LYP	3.997	4.309	4.757

Table D96: AEA (eV) of TCNDQ series. BS4

	0Si	1Si	2Si
BLYP	3.608	3.745	3.836
PBE	3.794	3.887	3.973
M06-L	3.699	3.819	3.932
B3LYP	3.913	4.076	4.254
PBE0	3.975	4.115	4.299
M06	3.910	4.053	–
M062X	4.050	4.286	4.756
M06-HF	4.196	4.749	5.584
CAM-B3LYP	4.042	4.270	4.742

Table D98: AEA (eV) of TCNP series. BS4

	0Si	1Si	2Si
BLYP	3.694	3.806	3.879
PBE	3.884	3.953	4.020
M06-L	3.805	3.901	3.992
B3LYP	4.036	4.166	4.308
PBE0	4.111	4.216	4.364
M06	4.049	4.170	4.300
M062X	4.218	4.453	4.889
M06-HF	4.418	4.983	5.171
CAM-B3LYP	4.213	4.440	4.886

Table D99: AEA (eV) of TCNDQ calculated using planar geometries. BS2

	0Si	1Si	2Si
BLYP	3.304	3.121	2.912
M06-L	3.670	3.480	3.259
PBE	3.547	3.366	3.153
B3LYP	3.670	3.493	3.251
PBE0	3.798	3.638	3.382
M06	3.831	3.640	3.367
M06-2X	3.850	3.760	3.467
M06-HF	3.880	3.953	3.572
CAM-B3LYP	3.810	3.746	3.467

Table D100: AEA (eV) of TCNDQ calculated using planar geometries. BS4

	0Si	1Si	2Si
BLYP	3.598	3.391	3.148
M06-L	3.696	3.497	3.249
PBE	3.784	3.587	3.346
B3LYP	3.905	3.715	3.439
PBE0	3.967	3.806	3.522
M06	3.908	3.720	3.417
M06-2X	4.043	3.989	3.651
M06-HF	4.193	4.336	3.903
CAM-B3LYP	4.027	3.976	3.657

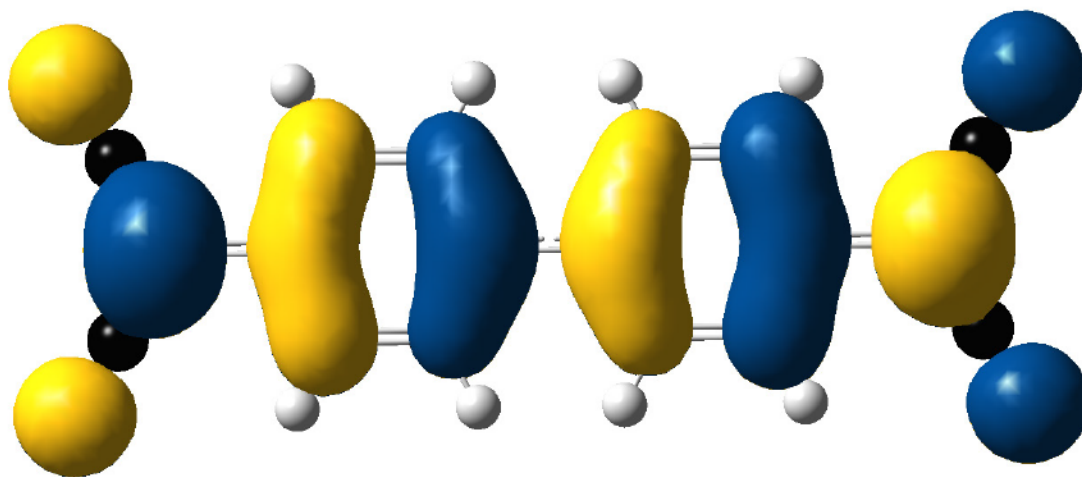
Table D101: AEA (eV) of TCNP calculated using planar geometries. BS2

	0Si	1Si	2Si
BLYP	3.411	3.206	2.963
M06-L	3.790	3.577	3.320
PBE	3.660	3.456	3.207
B3LYP	3.812	3.616	3.323
PBE0	4.064	3.779	3.460
M06	3.985	3.779	3.448
M06-2X	4.038	3.967	3.568
M06-HF	4.121	4.254	3.731
CAM-B3LYP	4.099	3.960	3.575

Table D102: AEA (eV) of TCNP calculated using planar geometries. BS4

	0Si	1Si	2Si
BLYP	3.694	3.466	3.188
M06-L	3.805	3.585	3.299
PBE	3.884	3.668	3.389
B3LYP	4.036	3.831	3.501
PBE0	4.172	3.940	3.590
M06	4.049	3.869	3.488
M06-2X	4.218	4.191	3.743
M06-HF	4.418	4.620	4.049
CAM-B3LYP	4.280	4.180	3.755

(A)



(B)

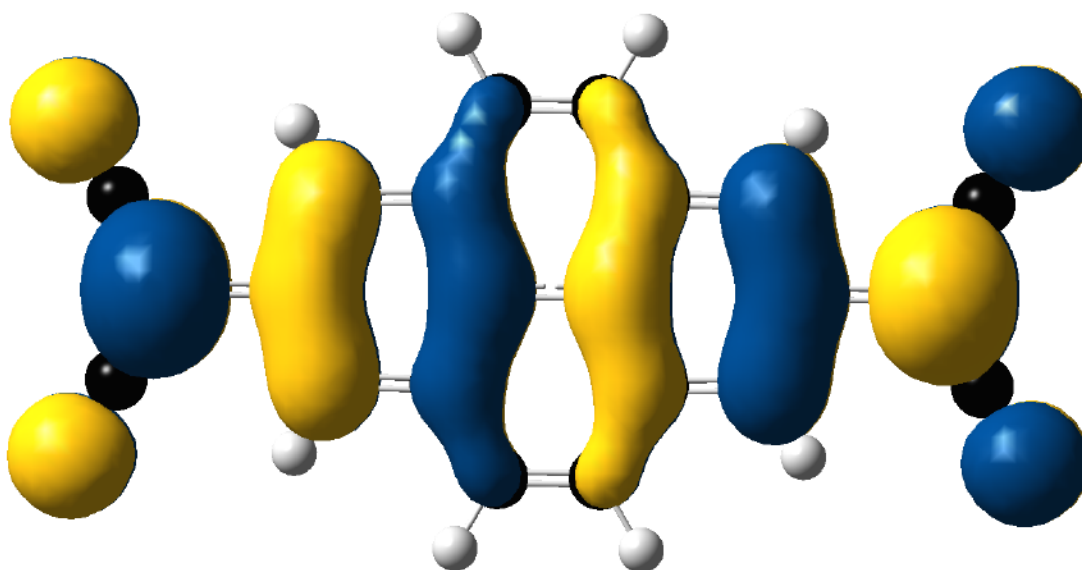
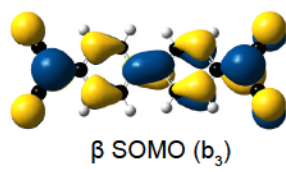
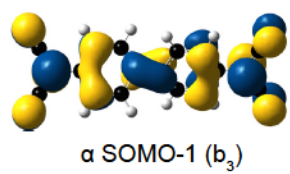
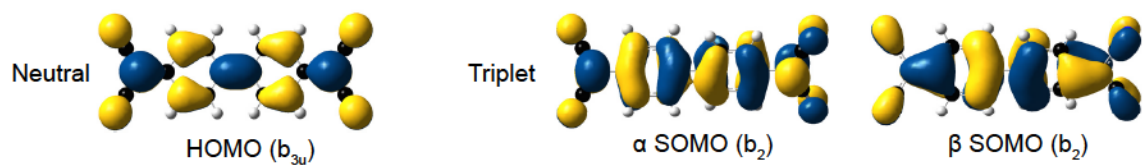
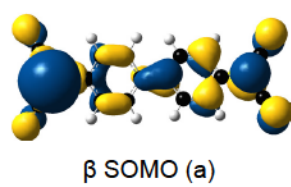
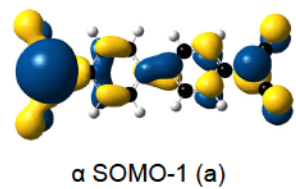
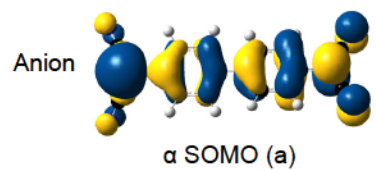
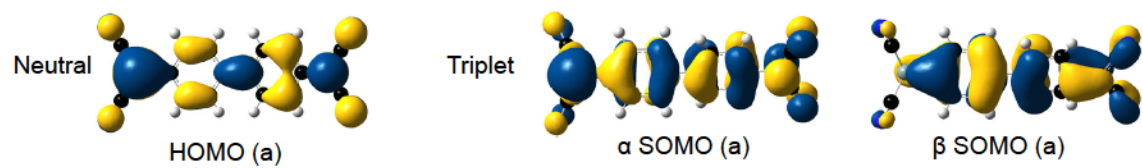


Figure D2: LUMO of (A) TCNDQ and (B) TCNP. B3LYP/BS4 isovalue: 0.02 a.u. The MOs are consistent with those reported by Gerson *et. al.*<sup>17</sup>

(A)



(B)



(C)

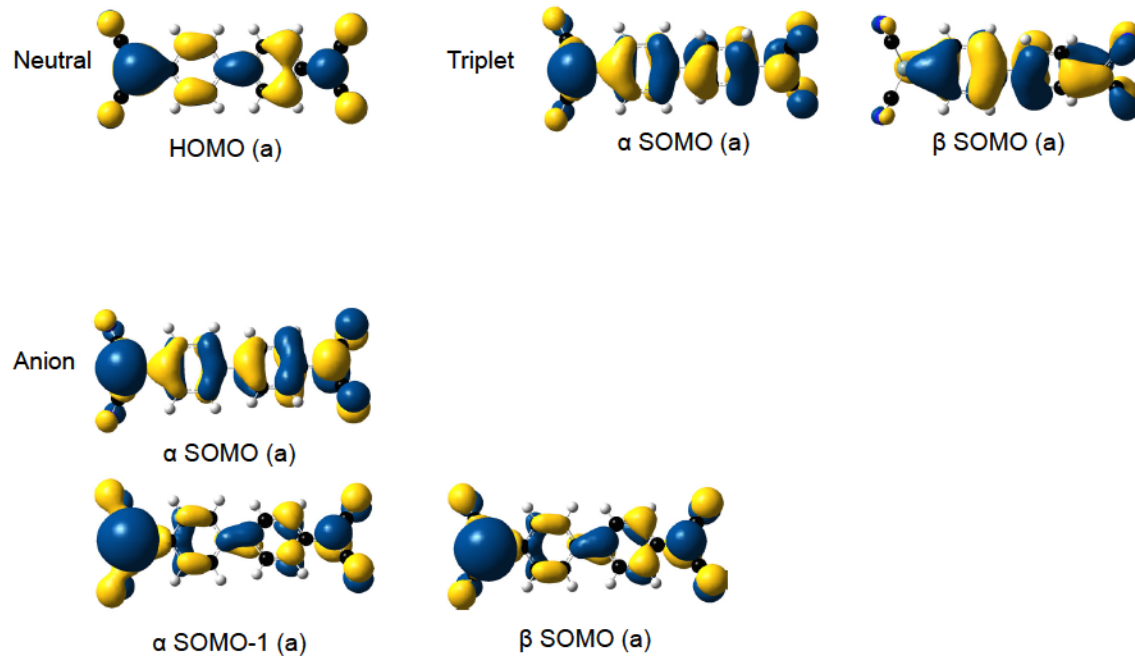
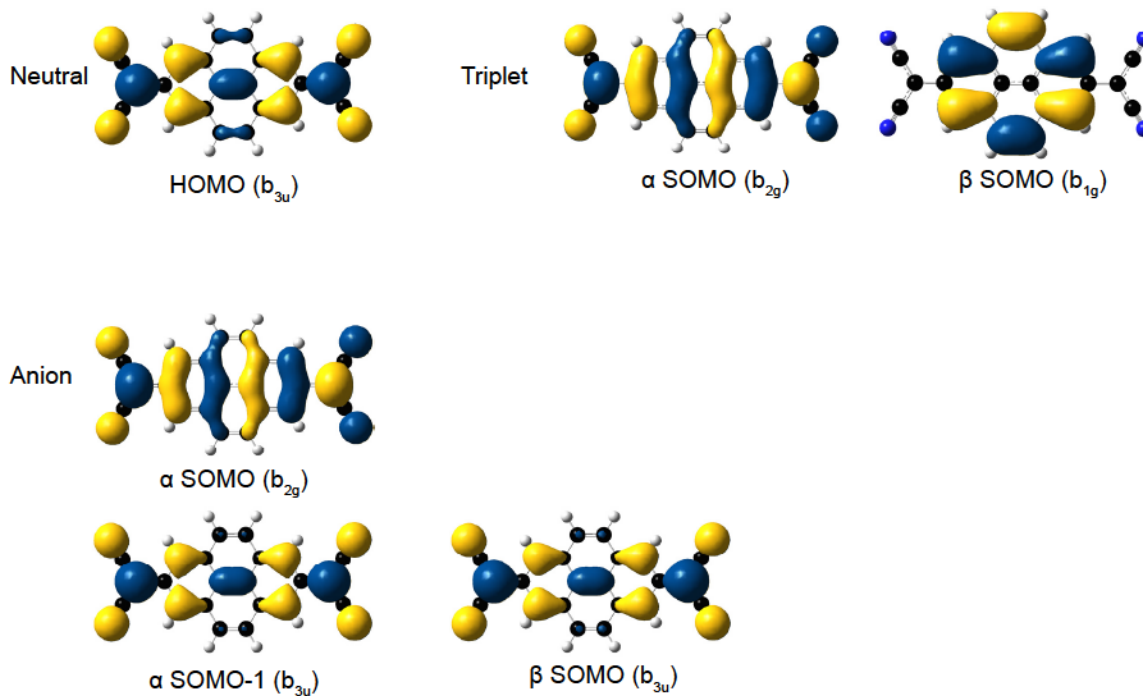


Figure D3: Molecular orbitals of interest for (A) TCNDQ (B) 1Si TCNDQ and (C) 2Si TCNDQ. B3LYP/BS4. Isovalue=0.02

(A)



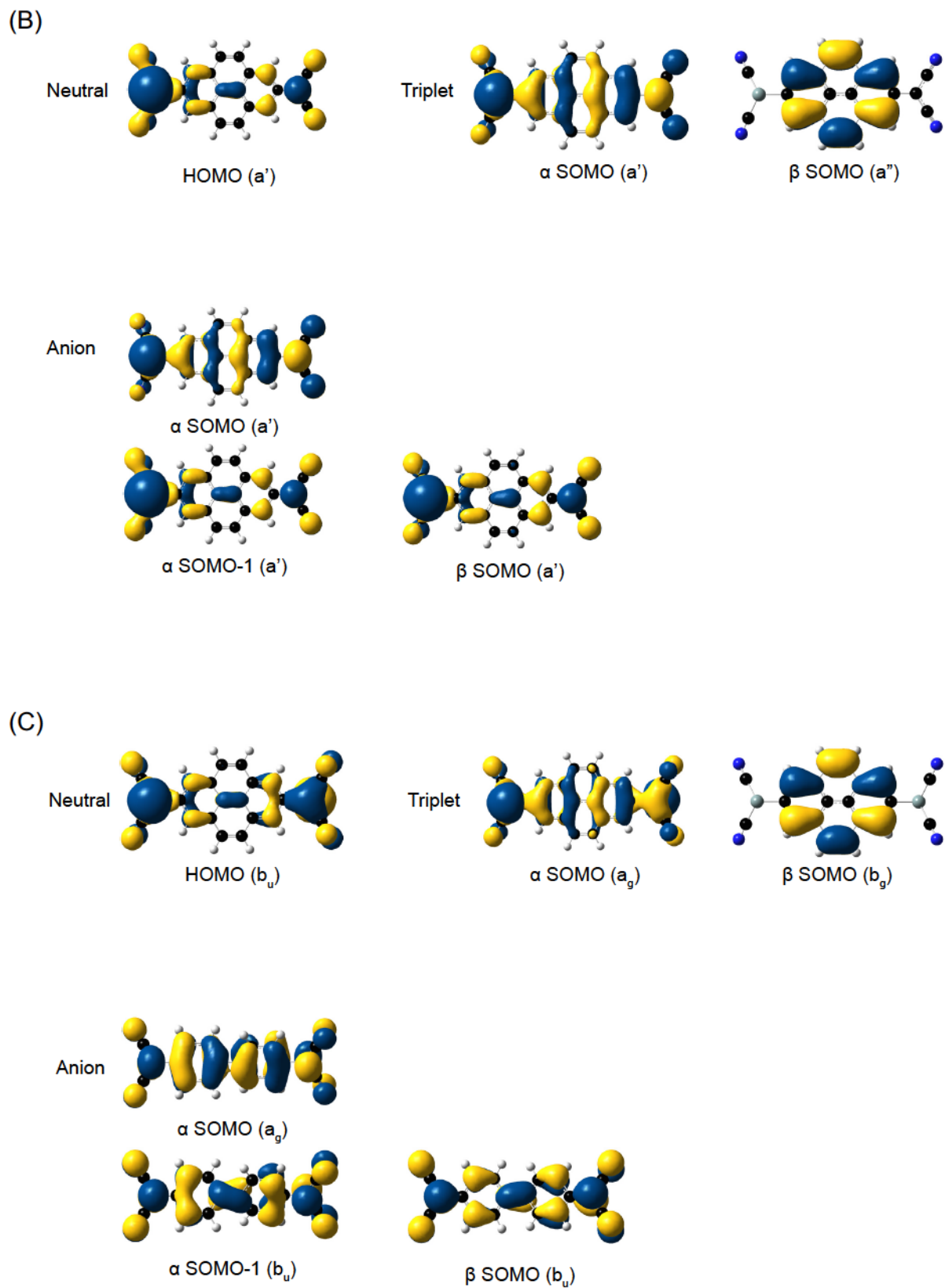
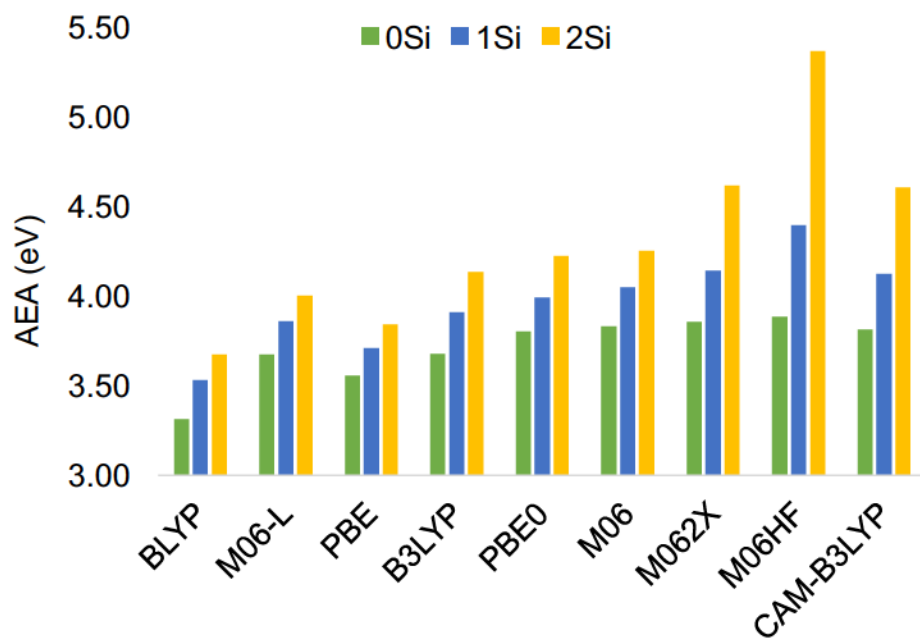


Figure D4: Molecular orbitals of interest for (A) TCNP (B) 1Si TCNP and (C) 2Si TCNP. B3LYP/BS4. Isovalue=0.02

(A)



(B)

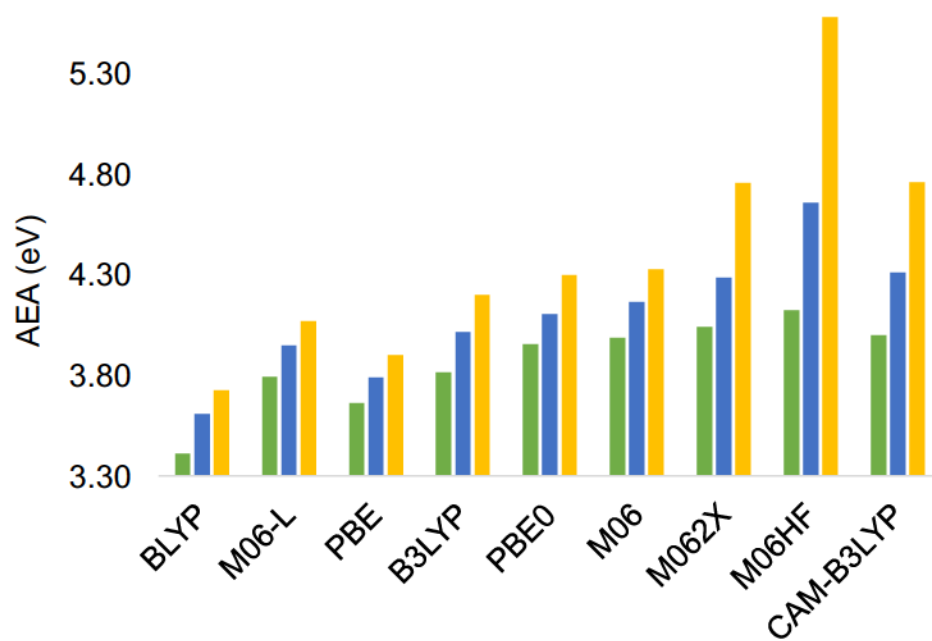


Figure D5: Adiabatic electron affinities (eV) calculated using BS2 for (A) TCNDQ series and (B) TCNP series. Green – 0Si, Blue – 1Si and Yellow – 2Si.

APPENDIX E

Supplemental Information for Chapter Seven

Table E1: Vibrational modes ( $\text{cm}^{-1}$ ) of disilene potential energy surfaces

	D <sub>2h</sub>
	b <sub>2g</sub>
BLYP	272i
M06-L	256i
PBE	234i
B3LYP	214i
PBE0	156i
M06	271i
M06-2X	-
M06-HF	-
CAM-B3LYP	78i

Table E2: Energies (relative to surface minimum in kcal/mol) of structures on disilene potential energy surface

	D <sub>2h</sub> ( <sup>1</sup> A <sub>G</sub> )	C <sub>2h</sub> ( <sup>1</sup> A <sub>G</sub> )
BLYP	1.21	0.00
M06-L	0.43	0.00
PBE	0.72	0.00
B3LYP	0.49	0.00
PBE0	0.14	0.00
M06	0.72	0.00
M06-2X	0.00	-
M06-HF	0.00	-
CAM-B3LYP	0.003	0.00

Table E3: Normal modes ( $\text{cm}^{-1}$ ) of 2Si TCNE potential energy surfaces

	D <sub>2h</sub>
	b <sub>2g</sub>
BLYP	137i
M06-L	102i
PBE	119i
B3LYP	123i
PBE0	105i
M06	127i
M06-2X	113i
M06-HF	137i
CAM-B3LYP	101i

Table E4: Energetics (kcal/mol) of 2Si TCNE potential energy surface relative to surface minimum

	D <sub>2h</sub> ( <sup>1</sup> A <sub>G</sub> )	C <sub>2h</sub> ( <sup>1</sup> A <sub>G</sub> )
BLYP	3.37	0.00
M06-L	1.86	0.00
PBE	2.30	0.00
B3LYP	2.49	0.00
PBE0	1.56	0.00
M06	3.28	0.00
M06-2X	2.29	0.00
M06-HF	2.32	0.00
CAM-B3LYP	1.44	0.00

Table E5: Normal modes (cm<sup>-1</sup>) of 2Si TCNQ potential energy surfaces

	D <sub>2h</sub>		C <sub>2v</sub>
	b <sub>2g</sub>	b <sub>3u</sub>	b <sub>2</sub>
BLYP	74 <i>i</i>	65 <i>i</i>	–
M06-L	59 <i>i</i>	44 <i>i</i>	–
PBE	54 <i>i</i>	40 <i>i</i>	–
B3LYP	55 <i>i</i>	45 <i>i</i>	–
PBE0	24 <i>i</i>	13 <i>i</i>	–
M06	58 <i>i</i>	48 <i>i</i>	30 <i>i</i>
M06-2X	–	–	–
M06-HF	–	–	–
CAM-B3LYP	–	–	–

Table E6: Energetics (kcal/mol) of 2Si TCNQ potential energy surfaces relative to surface minimum

	D <sub>2h</sub>	C <sub>2h</sub>	C <sub>2v</sub>	C <sub>s</sub>
BLYP	0.87	0.00	0.24	–
M06-L	0.45	0.00	0.21	–
PBE	0.35	0.00	0.15	–
B3LYP	0.33	0.00	0.12	–
PBE0	0.03	0.00	0.028	–
M06	0.27	0.004	0.11	0.00
M06-2X	0.00	–	–	–
M06-HF	0.00	–	–	–
CAM-B3LYP	0.00	–	–	–

Table E7: Normal modes ( $\text{cm}^{-1}$ ) of 2Si TCNDQ potential energy surfaces relative to surface minimum

	D <sub>2h</sub>			C <sub>2h</sub>	C <sub>2v</sub>	D <sub>2</sub>	
	b <sub>2g</sub>	b <sub>3u</sub>	a <sub>u</sub>	a <sub>u</sub>	a <sub>2</sub>	b <sub>3</sub>	b <sub>2</sub>
BLYP	97i	99i	29i	37i	36i	101i	99i
M06-L	87i	84i	17i	24i	24i	86i	84i
PBE	76i	79i	28i	34i	33i	81i	79i
B3LYP	84i	86i	20i	28i	28i	86i	84i
PBE0	65i	63i	16i	25i	25i	67i	65i
M06	87i	89i	11i	17i	17i	87i	84i
M06-2X	30i	31i	18i	25i	26i	37i	36i
M06-HF	–	–	–	–	–	–	–
CAM-B3LYP	36i	37i	–	27i	26i	–	–

Table E8: Energetics (kcal/mol) of 2Si TCNDQ potential energy surfaces relative to surface minimum

	D <sub>2h</sub>	C <sub>2h</sub>	C <sub>2v</sub>	D <sub>2</sub>	C <sub>2</sub>	C <sub>s</sub>
BLYP	2.444	0.388	0.321	2.281	0.000	–
M06-L	1.873	0.302	0.236	1.828	0.000	–
PBE	1.599	0.413	0.352	1.422	0.000	–
B3LYP	1.648	0.211	0.163	1.643	0.000	–
PBE0	0.914	0.208	0.169	0.867	0.000	–
M06	1.452	0.052	0.000	1.450	0.067	–
M06-2X	0.435	0.175	0.154	0.417	0.000	–
M06-HF	0.000	–	–	–	–	–
CAM-B3LYP	0.210	0.067	0.053	–	–	0.000

Table E9: Normal modes ( $\text{cm}^{-1}$ ) of 2Si TCNP potential energy surfaces relative to surface minimum

	D <sub>2h</sub>		C <sub>2v</sub>	C <sub>2v</sub>
	b <sub>2g</sub>	b <sub>3u</sub>	b <sub>u</sub>	b <sub>2</sub>
BLYP	112i	112i	–	–
M06-L	101i	101i	–	–
PBE	91i	91i	–	–
B3LYP	101i	102i	–	–
PBE0	82i	83i	–	–
M06	107i	107i	–	–
M06-2X	59i	61i	–	–
M06-HF	–	–	–	–
CAM-B3LYP	67i	68i	34i	34i

**Table E10: Energetics (kcal/mol) of 2Si TCNP potential energy surfaces relative to surface minimum**

	D <sub>2h</sub>	C <sub>2h</sub>	C <sub>2v</sub>	C <sub>s</sub>
BLYP	2.78	0.00	0.02	–
M06-L	2.31	0.00	0.01	–
PBE	1.81	0.00	0.02	–
B3LYP	2.20	0.00	0.01	–
PBE0	1.36	0.00	0.004	–
M06	2.22	0.02	0.00	–
M06-2X	0.99	0.00	0.0002	–
M06-HF	0.00	–	–	–
CAM-B3LYP	1.07	0.23	0.22	0.00

**Table E11: Polynomial coefficients obtained from APES fit for 0Si molecules**

		a <sub>0</sub>	a <sub>2</sub>	a <sub>4</sub>	R <sup>2</sup>
Ethylene	b <sub>2g</sub>	0.000	4.566	11.830	1.000
TCNE	b <sub>2g</sub>	0.000	18.520	5.388	0.999
TCNQ	b <sub>2g</sub>	0.000	4.339	0.032	1.000
	b <sub>3u</sub>	0.000	8.308	2.578	1.000
TCNDQ	b <sub>2g</sub>	0.000	280.3	2540.0	0.999
	b <sub>3u</sub>	0.000	21.220	13.830	0.999
	a <sub>u</sub>	0.000	0.444	6.324	0.999
TCNP	b <sub>2g</sub>	0.000	10.080	1.492	0.999
	b <sub>3u</sub>	0.000	26.280	23.690	0.999

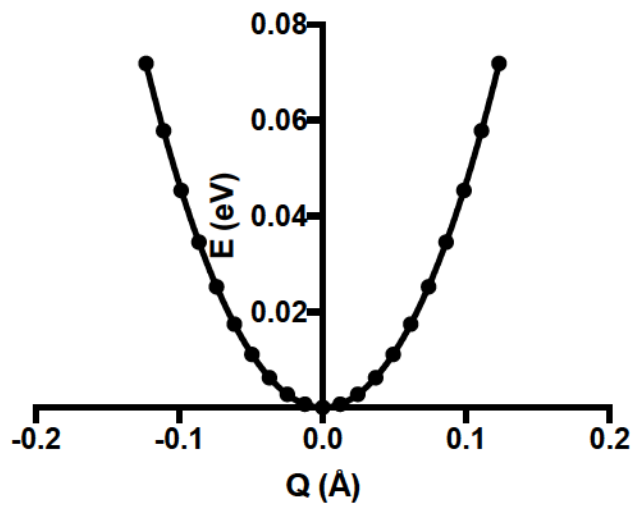


**Figure E1:** Ethylene polynomial fit

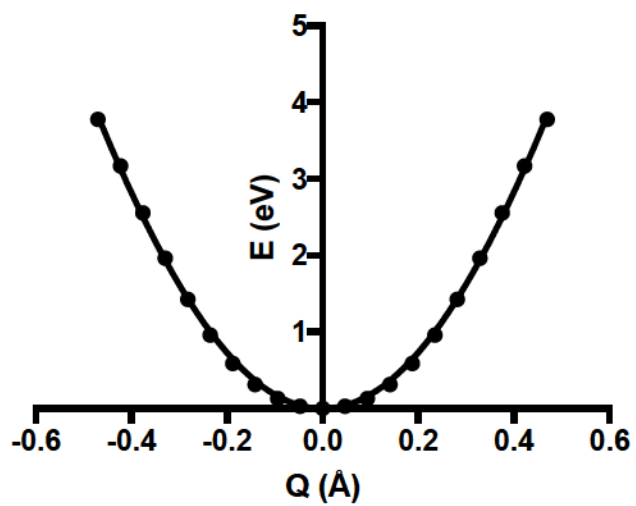


**Figure E2:** TCNE polynomial fit

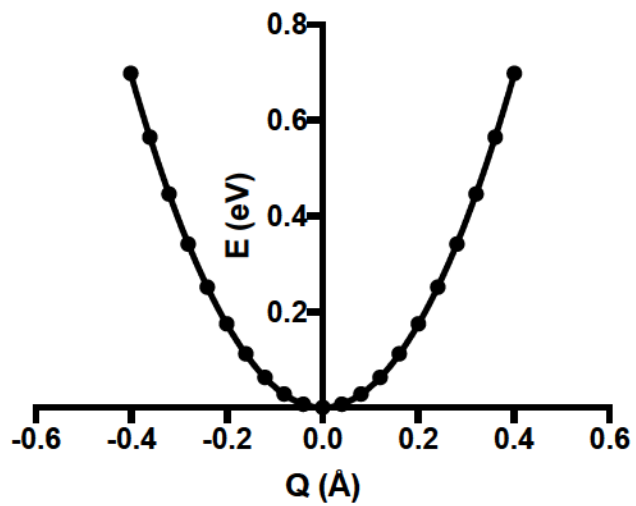


**Figure E3:** TCNQ  $b_{2g}$  polynomial fit

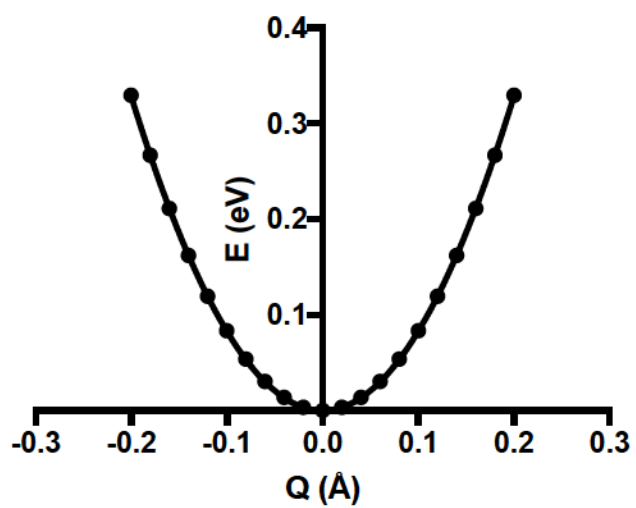


**Figure E4:** TCNQ  $b_{3u}$  polynomial fit

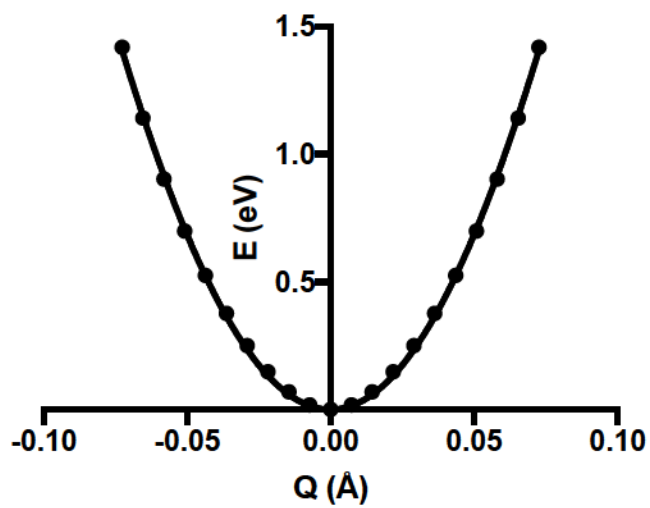


**Figure E5:** TCNDQ  $b_{2g}$  polynomial fit

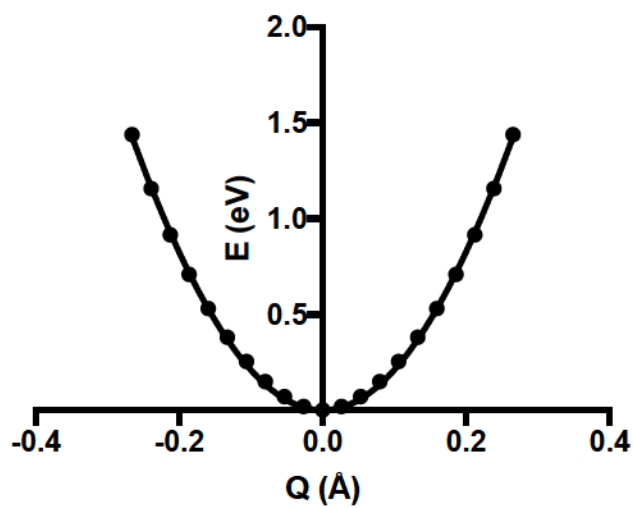


**Figure E6:** TCNDQ  $b_{3u}$  polynomial fit

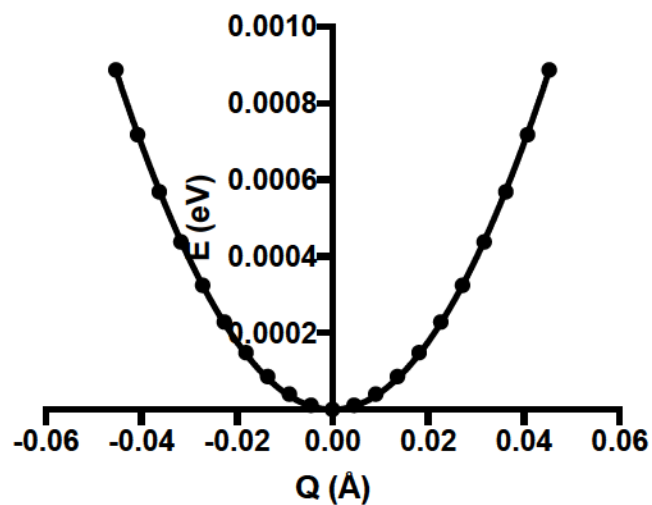


**Figure E7:** TCNDQ  $a_u$  polynomial fit

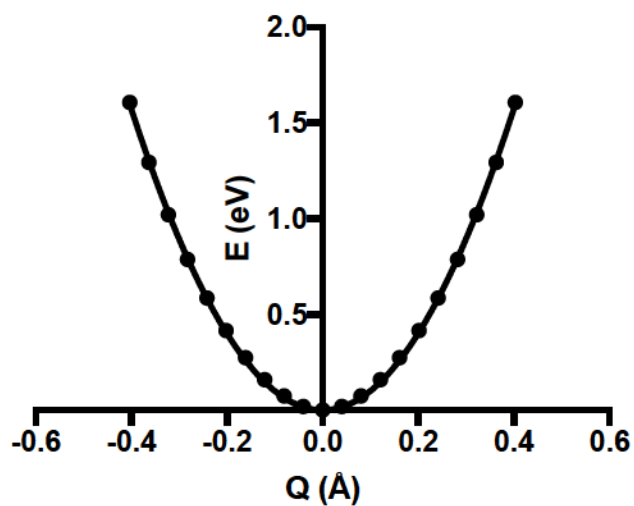


**Figure E8:** TCNP  $b_{2g}$  polynomial fit

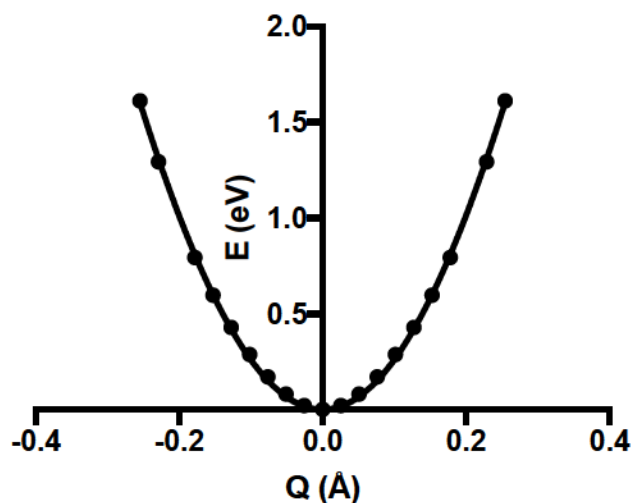


**Figure E9:** TCNP  $b_{3u}$  polynomial fit – missing a data point, will correct before submitting

**Table E12:** Polynomial coefficients obtained from APES fit for 2Si analogs

		$a_0$	$a_2$	$a_4$	$R^2$
Disilene	$b_{2g}$	0.021	-1.918	40.000	0.918
2Si TCNE	$b_{2g}$	0.108	-0.574	0.609	0.858
2Si TCNQ	$b_{2g}$	0.014	-0.209	0.772	0.989
	$b_{3u}$	0.091	-5.568	80.120	0.920
2Si TCNDQ	$b_{2g}$	0.062	-13.980	658.300	0.861
	$b_{3u}$	0.064	-0.952	2.002	0.850
	$a_u$	0.000	-0.107	0.096	
2Si TCNP	$b_{2g}$	0.095	-0.833	1.733	0.947
	$b_{3u}$	0.095	-1.338	2.747	0.882

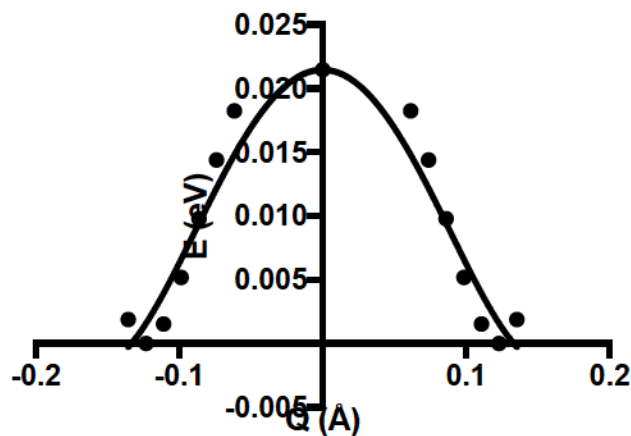


**Figure E10:** Disilene  $b_{2g}$  polynomial fit

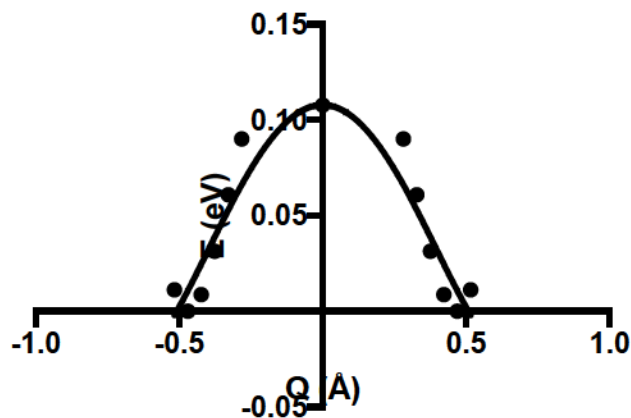


**Figure E11:** 2Si TCNE  $b_{2g}$  polynomial fit

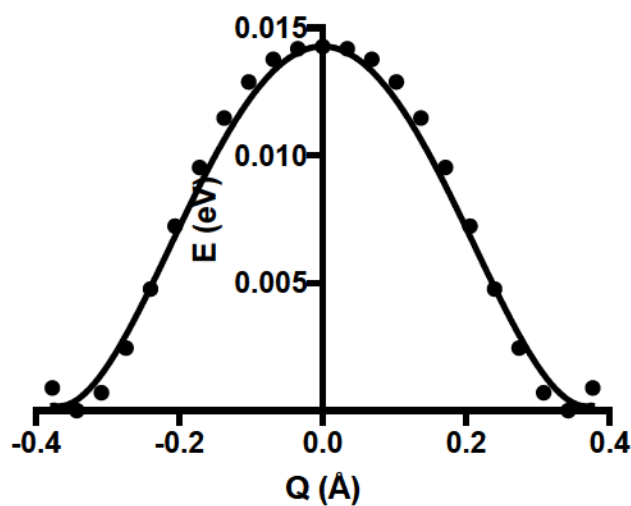


**Figure E12:** 2Si TCNQ  $b_{2g}$  polynomial fit

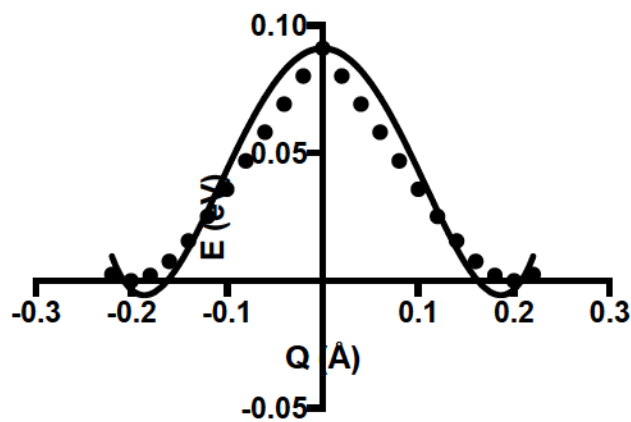


**Figure E13:** 2Si TCNQ  $b_{3u}$  polynomial fit

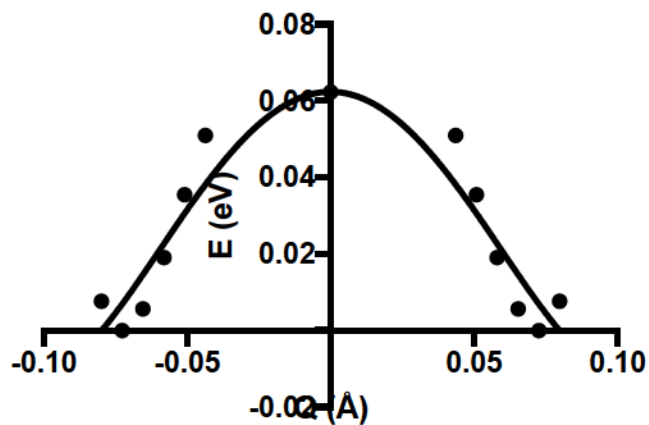


**Figure E14:** 2Si TCNDQ  $b_{2g}$  polynomial fit

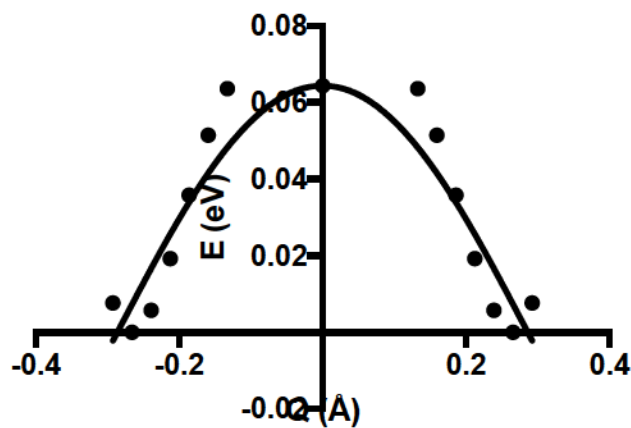


**Figure E15:** 2Si TCNDQ  $b_{3u}$  polynomial fit

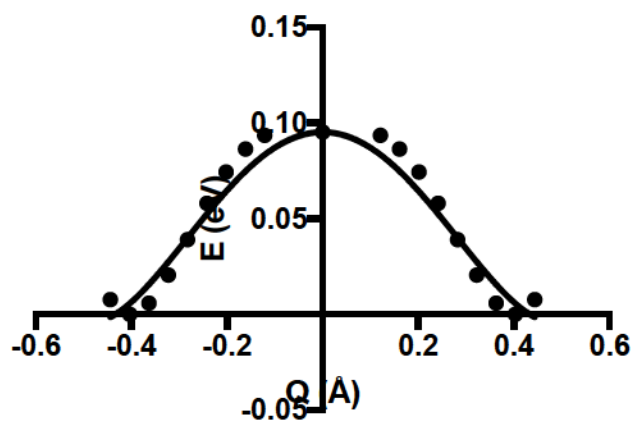


**Figure E16:** 2Si TCNP  $b_{2g}$  polynomial fit

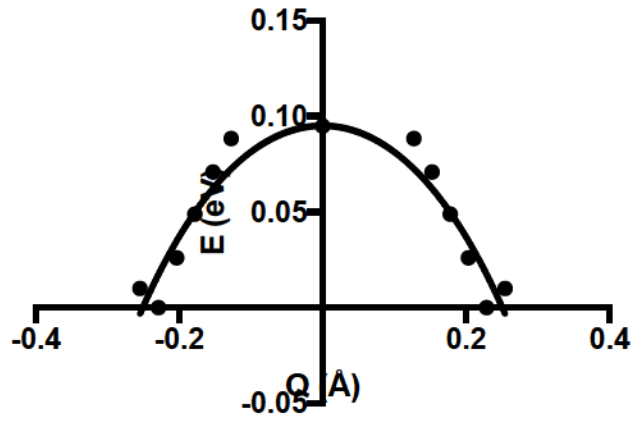


**Figure E17:** 2Si TCNP  $b_{3u}$  polynomial fit